D. 187

[illegible]

1,080
10-11-79

CERAMICS IN NUCLEAR WASTE MANAGEMENT

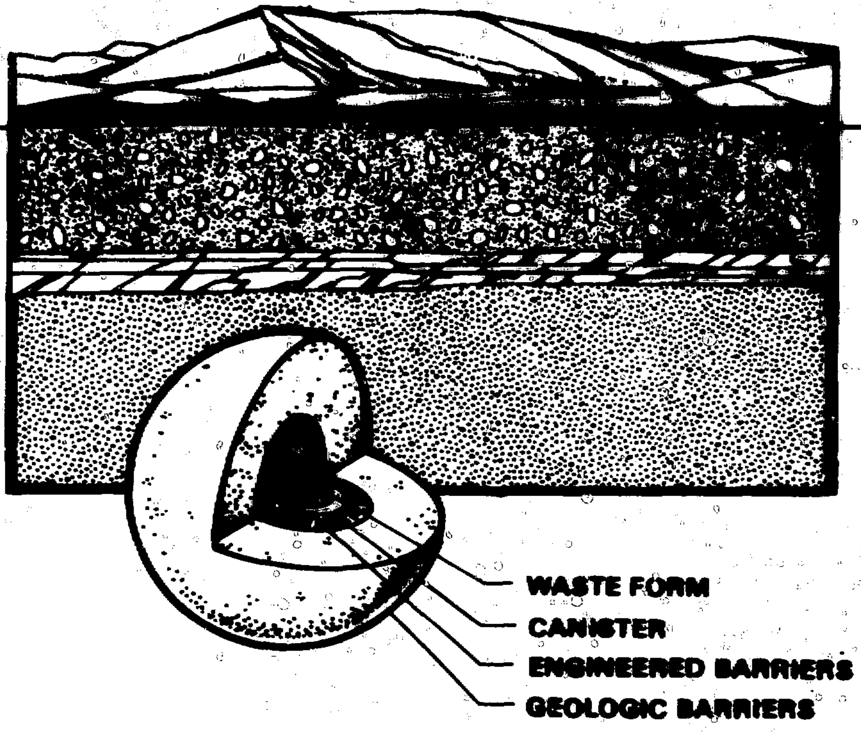
WASTE FORM
CANISTER
ENGINEERED BARRIERS
GEOLOGIC BARRIERS

DISTRIBUTION OF THIS DOCUMENT IS UNLIMITED

Technical Information Center
UNITED STATES DEPARTMENT OF ENERGY

CONF-790420
Distribution Category UC-70

CERAMICS IN NUCLEAR WASTE MANAGEMENT

PROCEEDINGS OF AN INTERNATIONAL SYMPOSIUM HELD IN
CINCINNATI, OHIO, APRIL 30–May 2, 1979

Sponsored by

The Nuclear Division
of the American Ceramic Society
and the
U. S. Department of Energy

DISCLAIMER

Edited by

Thomas D. Chikalla and John E. Mendel
Pacific Northwest Laboratory
Richland, Washington

Work Performed Under Contract No. EY-76-C-06-1830

Published by

Technical Information Center
United States Department of Energy

PREFACE

The International Symposium on Ceramics in Nuclear Waste Management was held April 30 May 2, 1979, in Cincinnati, Ohio. The symposium was held in conjunction with the 81st annual meeting of the American Ceramic Society and was cosponsored by the Nuclear Division of the American Ceramic Society and the U. S. Department of Energy.

The interest in the materials aspects of nuclear waste management and the timeliness of the symposium are evidenced by the large number of registrants, approximately 350. The symposium participants included international representatives from industry, national laboratories, universities, and government agencies. Seventy-four papers were presented in eight technical sessions. Thirteen countries were represented, including Australia, Austria, Belgium, Canada, England, France, Germany, Italy, Japan, Russia, Scotland, Sweden, and the United States.

The scope of the meeting included invited reviews of the materials aspects of national programs in six different countries. Technical sessions were devoted to glass processing, ceramic processing, waste form stability and characterization, leaching, waste form properties, and immobilization of special wastes. Recent developments and research highlights were described for many processes and waste form types. The informal technical discussions and the opportunities to make new acquaintances and renew old ones were a valuable part of the meeting. Hopefully a continuing exchange of technical information, both on a formal and informal basis, will take place as a result of contacts made at this symposium.

This proceedings will provide a permanent record of the state of the technology in ceramic materials for nuclear waste management as of the spring of 1979. Many people contributed to the success of the symposium and the issuance of the proceedings. We should like to acknowledge the contributions of the session chairmen, A. M. Platt, J. Kelley, C. Sombret, W. Lutze, R. D. Walton, H. W. Godbee, A. Marples, and M. J. Smith, in running a smooth meeting. A large effort was put forth in a short time period by the technical review committee, J. L. McElroy, J. Plodinec, D. M. Strachan, G. Strathdee, W. J. Weber, G. L. McVay, L. R. Bunnell, and J. M. Berreth, which has contributed greatly toward the quality and timeliness of the proceedings. The publications group at the Technical Information Center did an excellent job in typesetting the proceedings and arranging for printing. We are grateful for the assistance of Mr. J. L. Harrison of the Babcock and Wilcox Company and Mr. Clarence Seeley of the American Ceramic Society in the program and meeting arrangements and to the U. S. Department of Energy for financial assistance in publication. Finally, the dedicated efforts of Carol Parks from day one of the symposium planning through the symposium proper and the issuance of this proceedings are gratefully acknowledged.

T. D. Chikalla
J. E. Mendel
Symposium Cochairmen

Pacific Northwest Laboratory
Richland, Washington
May 1979

TABLE OF CONTENTS

Preface iii

List of Acronyms and Abbreviations ix

I. NATIONAL PROGRAMS FOR THE DISPOSAL OF RADIOACTIVE WASTES

DOE Materials Program Supporting Immobilization of Radioactive Wastes 1
G. K. Oertel and W. S. Scheib, Jr., U. S. Department of Energy, Washington, D. C.

Materials Aspects of Nuclear Waste Disposal in Canada 4
D. J. Cameron and G. G. Strathdee, AECL, Whiteshell Nuclear Research Establishment, Pinawa, Manitoba, Canada

Use of Glasses and Ceramics in the French Waste Management Program 9
Yves Sousselier, Commissariat à l'Energie Atomique, Paris, France

The Concept for the Treatment and Disposal of Radioactive Wastes in the German Entsorgungszentrum 13
C. Salander and P. Zühlke, Deutsche Gesellschaft für Wiederaufarbeitung von Kernbrennstoffen mbH, Hannover, Federal Republic of Germany

The UK Program—Glasses and Ceramics for Immobilization of Radioactive Wastes for Disposal 17
K. D. B. Johnson, United Kingdom Atomic Energy Authority, Harwell, United Kingdom

Principal Trends of Investigations Carried on in the USSR on Incorporation of Highly Active Wastes into Glass and Ceramic Type Materials 25
A. S. Polyakov, State Committee for the Utilization of Atomic Energy, Moscow, USSR

II. WASTE FORM STABILITY AND CHARACTERIZATION

The Influence of System Considerations on Waste Form Design 27
A. A. Bauer, S. C. Matthews, and R. W. Peterson, Office of Nuclear Waste Isolation, Columbus, Ohio

The IAEA Coordinated Research Program on the Evaluation of Solidified High-Level Radioactive Waste Products 33
J. R. Grover, Atomic Energy Research Establishment, Harwell, United Kingdom, and K. J. Schneider, International Atomic Energy Agency, Vienna, Austria

Development of Comprehensive Waste Acceptance Criteria for Commercial Nuclear Waste 36
F. A. O'Hara, N. E. Miller, B. S. Ausmus, K. R. Yates, J. L. Means, R. N. Christensen, and F. A. Kulacki, Battelle Columbus Laboratories, Columbus, Ohio

An Approach Towards Long Term Prediction of Stability of Nuclear Waste Forms 41
E. Lue Yen-Bower, D. E. Clark, and L. L. Hench, University of Florida, Gainesville, Florida

Glassy and Crystalline High-Level Nuclear Waste Forms—An Attempt at Critical Evaluation 47
W. Lutze, Hahn-Meitner-Institut für Kernforschung Berlin GmbH, Berlin, Germany

A Comparison of Glass and Crystalline Waste Materials 52
W. A. Ross, R. P. Turcotte, J. E. Mendel, and J. M. Rusin, Pacific Northwest Laboratory, Richland, Washington

Glasses as Materials Used in France for Management of High-Level Wastes 57
R. A. Bonniaud, N. R. Jacquet Francillon, F. L. Laude, and C. G. Sombret, Commissariat à l'Energie Atomique, Marcoule, France

Characterization of Borosilicate Glasses Containing Simulated High-Level Radioactive Wastes from PNC 62
R. Terai, K. Eguchi, and H. Yamanaka, Government Industrial Research Institute, Osaka, Japan

Characterization and Evaluation of Multibarrier Nuclear Waste Forms 66
J. M. Rusin, R. O. Lokken, and J. W. Wald, Pacific Northwest Laboratory, Richland, Washington

III. IMMOBILIZATION OF RADIOACTIVE WASTES—GLASS PROCESSING

Operational Experience of the First Industrial HLW Vitrification Plant 73
M. M. Chotin, Compagnie Générale des Matières Nucléaires, and R. A. Bonniaud, A. F. Jouan, and G. E. Rabot, Commissariat à l'Energie Atomique, Marcoule, France

Compatibility Tests of Materials for a Prototype Ceramic Melter for Defense Glass-Waste Products 82
G. G. Wicks, Savannah River Laboratory, Aiken, South Carolina

Vitrification of High-Level Radioactive Waste in a Continuous Liquid-Fed Ceramic Melter 86
S. Weisenburger, W. Grünewald, and H. Koschorke, Karlsruhe Nuclear Research Center, Karlsruhe, Federal Republic of Germany

Vitrification of Hanford Radioactive Defense Wastes 93
M. J. Kupfer, Rockwell Hanford Operations, Richland, Washington

Solidification of HLW Solutions with the PAMELA Process 97
W. Heimerl, Deutsche Gesellschaft für Wiederaufarbeitung von Kernbrennstoffen mbH, Mol, Belgium

Development of Engineering Scale HLLW Vitrification Technique at PNC 102
H. Nagaki, N. Oguino, N. Tsunoda, and T. Segawa, Power Reactor and Nuclear Fuel Development Corporation, Tokai-mura, Japan

A Review of Continuous Ceramic-Lined Melter and Associated Experience at PNL 107
J. L. Buelt, C. C. Chapman, S. M. Barnes, and R. D. Dierks, Pacific Northwest Laboratory, Richland, Washington

Progress in Fission Product Solidification and Characterization Utilizing the Jülich FIPS Process . . . 114
S. Halaszovich, E. Merz, and R. Odoj, Institute for Chemical Technology, Jülich, Federal Republic of Germany

A Laboratory-Scale Glass Melter for Testing Defense Waste Glass 118
D. Gombert II, Allied Chemical Corporation, Idaho Falls, Idaho

The Influence of Heat Transfer on the Pot Vitrification Process 122
J. B. Morris, Atomic Energy Research Establishment, Harwell, United Kingdom

IV. IMMOBILIZATION OF RADIOACTIVE WASTES—CERAMIC PROCESSING

Recent Developments in Low- and Intermediate-Level Waste Fixation by Cement 127
H. O. Witte, NUKEM GmbH, Hanau, Germany, and R. Köster, Kernforschungszentrum Karlsruhe GmbH, Karlsruhe, Germany

FUETAP (Formed Under Elevated Temperatures and Pressures) Concretes as Hosts for Radioactive Wastes 132
J. G. Moore, G. C. Rogers, J. H. Paehler, and H. E. Devaney, Oak Ridge National Laboratory, Oak Ridge, Tennessee

A Low Temperature Ceramic Radioactive Waste Form 136
D. M. Roy, B. E. Scheetz, M. W. Grutzeck, A. K. Sarkar, and S. D. Atkinson, Materials Research Laboratory, The Pennsylvania State University, University Park, Pennsylvania

Solidification of HLLW by Glass–Ceramic Process 143
N. Oguino, S. Masuda, and N. Tsunoda, Power Reactor and Nuclear Fuel Development Corporation, Tokai-mura, Japan, and T. Yamanaka, M. Ninomiya, T. Sakane, S. Nakamura, and S. Kawamura, Nippon Electric Glass Co., Ltd., Otsu, Japan

Coating of Waste Containing Ceramic Granules . . . 150
W. Neumann and O. Kofler, Österreichische Studiengesellschaft für Atomenergie GmbH, Vienna, Austria

Solidification of HLLW into Sintered Ceramics . . . 155
K. O-Oka and T. Ohta, Toshiba Corporation, Kawasaki, Japan, and S. Masuda and N. Tsunoda, Power Reactor and Nuclear Fuel Development Corporation, Tokai-mura, Japan

Embedding Methods of Solidified Waste in Metal Matrices 160
W. Neumann, Österreichische Studiengesellschaft für Atomenergie GmbH, Vienna, Austria

Development of Cermets for High-Level Radioactive Waste Fixation 164
W. S. Aaron, T. C. Quinby, and E. H. Kobisk, Oak Ridge National Laboratory, Oak Ridge, Tennessee

Densification of Calcines and Direct Containment of Spent Nuclear Fuel in Ceramics by Hot Isostatic Pressing 169
H. T. Larker, High-Pressure Laboratory, ASEA, Robertsfors, Sweden

Immobilization of High-Level Wastes in SYNROC Titanate Ceramic 174
A. E. Ringwood and S. E. Kesson, Australian National University, Canberra, Australia

Use of the Natural Aluminosilicates and Porous Ceramic Materials for the Inclusion of Radioactive Wastes 179
L. N. Lazarev, E. A. Shashukov, Yu. V. Kuznetsov, and R. I. Lyubtsev, V. G. Khlopin Radium Institute, Leningrad, USSR

V. IMMOBILIZATION OF RADIOACTIVE WASTES—CERAMIC AND GLASS PROCESSING

Vitrification of ICPP High-Level Zirconia Calcine . . 183
J. R. Berreth, D. Gombert II, and H. S. Cole, Allied Chemical Corporation, Idaho Falls, Idaho

Development and Characterization of the Glass-Ceramic VCP 15 for Immobilization of High-Level-Liquid Radioactive Waste 188
W. Guber, M. Hussain, L. Kahl, W. Müller, and J. Saidl, Kernforschungszentrum Karlsruhe GmbH, Karlsruhe, Germany, and *Pakistan Atomic Energy Commission*

Phase Separation in Nuclear Waste Glasses 193
M. Tomozawa, G. M. Singer, Y. Oka, and J. T. Warden, Rensselaer Polytechnic Institute, Troy, New York

Compatibility of Actinides with HLW Borosilicate Glass: Solubility and Phase Formation 198
C. T. Walker, European Institute for Transuranium Elements, and U. Riege, Nuclear Research Center, Karlsruhe, Federal Republic of Germany

An Investigation of Crystallization in Glasses Containing Fission Products 203
G. Malow, Hahn-Meitner-Institut für Kernforschung Berlin GmbH, Berlin, Federal Republic of Germany

Viscosity and Electrical Conductivity of Glass Melts as a Function of Waste Composition . . . 210
M. J. Plodinec and J. R. Wiley, Savannah River Laboratory, Aiken, South Carolina

Effects of Composition on Waste Glass Properties 213
G. B. Mellinger and L. A. Chick, Pacific Northwest Laboratory, Richland, Washington

Phase Boundary Effects in Metal Matrix Embedded Glasses 218
E. Schiewer, Hahn-Meitner-Institut für Kernforschung Berlin GmbH, Berlin, Federal Republic of Germany

A Pelleted Waste Form for High-Level ICPP Wastes . . 224
K. M. Lamb, S. J. Priebe, H. S. Cole, and B. D. Taki, Allied Chemical Corporation, Idaho Falls, Idaho

The Use of Glass–Ceramic Materials for the Fixation of Radioactive Wastes 229
A. A. Minaev, S. N. Oziraner, and N. P. Prokhorova, State Committee on Peaceful Use of Atomic Energy, Moscow, USSR

VI. LEACHING OF WASTE MATERIALS

Relative Leach Behavior of Waste Glasses and Naturally Occurring Glasses 233
P. B. Adams, Corning Glass Works, Corning, New York

Evaluation of Long-Term Leaching of Borosilicate Glass in Pure Water 238
F. Lanza and E. Parnisari, Joint Research Centre, Ispra, Italy

Development of Aluminosilicate and Borosilicate Glasses as Matrices for CANDU High-Level Waste . . 243
G. G. Strathdee, N. S. McIntyre, and P. Taylor, Atomic Energy of Canada, Ltd., Whiteshell Nuclear Research Establishment, Pinawa, Canada

The Leaching of Radioactive Waste Storage Glasses 248
K. A. Boult, J. T. Dalton, A. R. Hall, A. Hough, and J. A. C. Marples, Atomic Energy Research Establishment, Harwell, United Kingdom

Corrosion Behavior of Zinc-Borosilicate Simulated Nuclear Waste Glass 256
D. E. Clark, E. Lue Yen-Bower, and L. L. Hench, University of Florida, Gainesville, Florida

Chemical Durability of Nuclear Waste Glasses . . . 263
J. H. Simmons, A. Barkatt, P. B. Macedo, P. E. Pehrsson, C. J. Simmons, A. Barkatt, D. C. Tran, H. Sutter, and M. Saleh, Catholic University of America, Washington, D. C.

Chemical Durability and Characterization of Nuclear Waste Forms in a Hydrothermal Environment 269
J. W. Braithwaite and J. K. Johnstone, Sandia Laboratories, Albuquerque, New Mexico

Hydrothermal Stability of Spent Fuel and High-Level Waste Ceramics in the Geologic Repository Environment 274
G. J. McCarthy, W. B. White, S. Komarneni, B. E. Scheetz, W. P. Freeborn, and D. K. Smith, The Pennsylvania State University, University Park, Pennsylvania

Devitrification and Leaching Effects in HLW Glass—Comparison of Simulated and Fully Radioactive Waste Glass 277
J. W. Wald and J. H. Westsik, Jr., Pacific Northwest Laboratory, Richland, Washington

Long-Term Leach Rates of Glasses Containing Actual Waste 284
J. R. Wiley and J. H. LeRoy, Savannah River Laboratory, Aiken, South Carolina

VII. PROPERTIES OF NUCLEAR WASTE FORMS

Simulations of Radiation Damage in Glasses 289
M. Antonini, F. Lanza, and A. Manara, Joint Research Centre, Ispra, Italy

Radiation Effects in Vitreous and Devitrified Simulated Waste Glass 294
W. J. Weber, R. P. Turcotte, L. R. Bunnell, F. P. Roberts, and J. H. Westsik, Jr., Pacific Northwest Laboratory, Richland, Washington

Effects of Irradiation on Structural Properties of Crystalline Ceramics 300
F. W. Clinard, Jr., and G. F. Hurley, Los Alamos Scientific Laboratory, Los Alamos, New Mexico

The Metamict State Radiation Damage in Crystalline Materials 305
R. F. Haaker and R. C. Ewing, University of New Mexico, Albuquerque, New Mexico

Radiation Damage Studies on Synthetic NaCl Crystals and Natural Rock Salt for Waste Disposal Applications 310
R. W. Klaffky, K. J. Swyler, and P. W. Levy, Brookhaven National Laboratory, Upton, New York

Crystalline Chemistry of the Synthetic Minerals in Current Supercalcine-Ceramics 315
G. J. McCarthy, J. G. Pepin, and D. E. Pfoertsch, The Pennsylvania State University, University Park, Pennsylvania, and D. R. Clarke, Rockwell Science Center, Thousand Oaks, California

Porous Glass Matrix Method for Encapsulating High-Level Nuclear Wastes 321
P. B. Macedo, D. C. Tran, J. H. Simmons, M. Saleh, A. Barkatt, C. J. Simmons, N. Lagakos, and E. DeWitt, Catholic University of America, Washington, D. C.

The Effect of Impact Energy on Solid-Waste Composites of Brittle and Ductile Materials 327
W. J. Mecham, L. J. Jardine, and M. J. Steindler, Argonne National Laboratory, Argonne, Illinois

Stress Analysis of Glass–Canister Interaction: A Study of Residual Stresses and Fracturing 333
F. A. Simonen and J. R. Friley, Pacific Northwest Laboratory, Richland, Washington

VIII. IMMOBILIZATION OF SPECIAL RADIOACTIVE WASTES

Utilization of Borosilicate Glass for Transuranic Waste Immobilization 338
J. A. Ledford and P. M. Williams, Rockwell International, Golden, Colorado

Crystallochemical Stabilization of Radwaste Elements in Portland Cement Clinker 342
C. M. Jantzen and F. P. Glasser, University of Aberdeen, Old Aberdeen, Scotland

Iodide and Iodate Sodalites for the Long-Term Storage of Iodine-129 349
D. M. Strachan and H. Babad, Rockwell Hanford Operations, Richland, Washington

Processes for Immobilization of High-Level Solid Wastes by Glass and Ceramic Matrices 354
K. H. Lin, W. E. Clark, and W. B. Howerton, Oak Ridge National Laboratory, Oak Ridge, Tennessee

Incorporation of Precipitate from Treatment of Medium Level Liquid Radioactive Waste into Glass Matrix or Ceramics Together with High Level Liquid Waste 359
M. Hussain, Pakistan Atomic Energy Commission, and L. Kahl, Kernforschungszentrum Karlsruhe GmbH, Karlsruhe, Federal Republic of Germany

Characteristics of Stored High-Level ICPP Waste Calcine 365
B. A. Staples, G. S. Pomiak, and E. L. Wade, Allied Chemical Corporation, Idaho Falls, Idaho

Stabilization of High-Level Waste from a Chloride Volatility Nuclear Fuel Reprocessing System . . . 370
L. A. Smith and T. A. Thornton, Babcock and Wilcox Company, Lynchburg, Virginia

Glass-Crystalline Materials for Active Waste Incorporation 374
V. V. Kulichenko, N. V. Krylova, V. I. Vlasov, and A. S. Polyakov, State Committee for the Utilization of Atomic Energy, Moscow, USSR

LIST OF ACRONYMS AND ABBREVIATIONS

AES-IM	Auger electron spectroscopy-ion milling
ANL	Argonne National Laboratory
ASTM	American Society for Testing Materials
BNL	Brookhaven National Laboratory
BONI	Borosilicate glass neutron irradiation
COGEMA	Compagnie Générale des Matières Nucléaires
CORA	Kratos transmission electron microanalyzer
CVD	Chemical vapor deposition
DOE	U. S. Department of Energy
dpa	Displacement per atom
DTA	Differential thermal analyses
DWK	Deutsche Gesellschaft für Wiederaufarbeitung von Kernbrennstoffen mbH
EDAX, EDX	Energy dispersive X-ray fluorescence
EDS	Energy dispersive spectroscopy
EMA	Electron microprobe analysis
ESR	Electron spin resonance
FP	Fission product
Gwdt^{-1}	Gigawatt days/ton
HIP	Hot isostatic pressing
HLLW	High-level liquid waste
HLSW	High-level solid waste
HLW	High-level waste
HTGR	High temperature gas-cooled reactor
IAEA	International Atomic Energy Agency
ICM	In-can melting
ICP	Induction coupled plasma
ICPP	Idaho Chemical Processing Plant
INEL	Idaho National Engineering Laboratory
IRRS	Infrared reflection spectroscopy
ISO	International Standards Organization
KfK	Kernforschungszentrum
LASL	Los Alamos Scientific Laboratory
LLL	Lawrence Livermore Laboratory
LimRPB	Limited reaction product buildup
MLLW	Medium-level liquid waste
MTU	Metric ton uranium
MWD/MTM	Megawatt days/metric ton metal
NFS	Nuclear Fuel Services
ORNL	Oak Ridge National Laboratory
PGM	Porous glass matrix process
PNL	Pacific Northwest Laboratory
PyC	Pyrolytic carbon
SA	Surface area
SEM	Scanning electron microscope
SigRPB	Significant reaction product buildup
SIMS	Secondary ion mass spectroscopy
SNWG	Simulated nuclear waste glass
SRP	Savannah River Plant
SRL	Savannah River Laboratory
STEM	Scanning transmission electron microscopy
TGA	Thermal gravimetric analysis
TRU	Transuranic
WCF	Waste calcining facility
WIPP	Waste Isolation Pilot Plant
XPS	X-ray photoelectron spectroscopy

I. NATIONAL PROGRAMS FOR THE DISPOSAL OF RADIOACTIVE WASTES

DOE MATERIALS PROGRAM SUPPORTING IMMOBILIZATION OF RADIOACTIVE WASTES

GOETZ K. OERTEL and WALTER S. SCHEIB, JR.
Division of Waste Products, U. S. Department of Energy, Washington, DC

ABSTRACT

A summary is presented of the DOE program for developing waste-form criteria, immobilization processes, and generation and evaluation of performance characterization data. Interrelationships are discussed among repository design, materials requirements, immobilization process definition, quality assurance, and risk analysis as part of the National Environmental Policy Act and regulatory processes.

The ultimate objective of radioactive waste management is the isolation of waste to prevent its dispersal into the biosphere. DOE is pursuing a number of alternative means of accomplishing this objective in compliance with the procedures of the National Environmental Policy Act. A summary of these options is presented in the Draft Report of the Interagency Review Group on Nuclear Waste Management and in the reports of IRG Subgroups on Waste Disposal Alternatives and on DOE Waste Management. With respect to high-level waste, the options for Savannah River's waste management are detailed in the Report on Alternatives for Long-Term Management of Defense High-Level Radioactive Waste, ERDA 77-42. Many of the options involve a system of barriers—stable geologic matrix, remote location, capsule overpacking, engineered containment, and the immobilized waste form. A successful system is one in which the combination of barriers prevents dispersal of radioactive materials into the biosphere in accordance with criteria reflecting specified exposure levels and reliability against specified risks.

Because one of the barriers is the waste form itself, waste-form performance under a range of repository and transport conditions must be predictable and reliable. As summarized in Table 1, the features of a materials-development program to provide performance data include statistically planned experiments covering the full spectrum of interactions between material capability and imposed requirements; certification and categorization of data in accordance with the quality and relevance of the tests; test results in a form amenable to risk and reliability analyses; support of repository transport and immobilization process engineering design; and development of production standards and quality-control procedures.

Several candidate waste forms have been advocated for further characterization and process development (glass, supercalcine, cement, cermets and crystalline materials). Although repository waste-acceptance criteria are still under development, the expected repository environments are understood sufficiently well to define preliminary materials-performance experiments, and a great deal of valuable data has already been published. The source of test samples has ranged from materials prepared in laboratory scoping studies to materials from operation of cold and hot engineering components. Attributes which should be measured to characterize waste forms fully were proposed several years ago by Battelle Pacific Northwest Laboratories

TABLE 1

Features of Waste-Materials Characterization Program

- Support selection and development of immobilization processes
- Support selection and development of repository options
- Provide repository engineering design with reliable materials data
- Provide risk and reliability data to DOE, NRC, EPA
- Identify quality-control sampling, inspection, measurement techniques
- Foster new initiatives and product/process improvement
- Support DOE decisions in NEPA and regulatory proceedings
- Provide basis for materials codes and standards

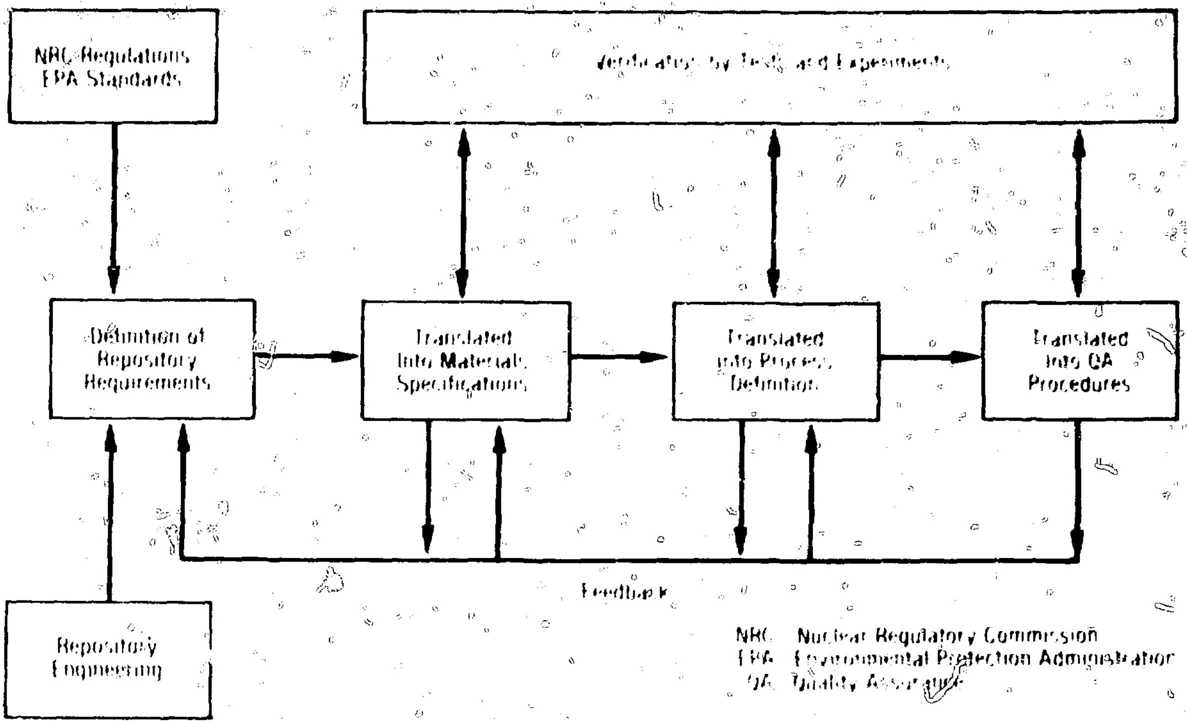
NRC Regulations
EPA Standards
Verification by Tests and Experiments
Definition of Repository Requirements
Translated Into Materials Specifications
Translated Into Process Definition
Translated Into QA Procedures
Feedback
Repository Engineering
NRC Nuclear Regulatory Commission
EPA Environmental Protection Administration
QA Quality Assurance

Fig. 1 Interaction between repository development and materials data program

in "A Program for Comprehensive Characterization of Solidified High-Level Wastes," BNWL-1940, December 1975. Most-recent data describe the performance of vitreous forms of waste. Greater emphasis will be placed on measuring the performance and processing of alternative forms. The variety of papers which are to be presented in this symposium reflect the wide-ranging interests of the U. S. program.

Looking ahead, we expect the materials development program to continue to mature through additional cold and hot engineering component development, prototype demonstration, and design of production-scale immobilization processes and components. While this work is proceeding, repository engineering will continue to define the requirements and criteria which must be met by the waste forms, up to and including capsule and in-situ system tests. To the extent that licensing is required, the regulatory safety and environmental analyses will be a source of further definition of materials performance requirements.

As repository development, engineering, and design mature, the interplay among repository requirements and materials property and performance data will be a major objective of the waste-management program. Figure 1 expresses this interplay schematically. The end point is a compatible set of repository designs, waste-acceptance criteria, materials specifications, waste-immobilization processes, and product quality-control techniques. Although this interplay is evident upon a little reflection, it is important to assure its proper implementation. Ideally documented requirements must be in place at all times, tentative if necessary, to guide the development program. As early as possible, tentative specifications should be documented and preliminary reference processes established, with identified trade-offs and options. The purpose of the test program is to verify that the design and development choices are valid in terms of demonstrated product performance.

We are presently emphasizing the role of systematic materials development and data evaluation in waste-management systems definition. Although considerable materials data have been published, the variety of presumed requirements have led to a situation where few data points have been evaluated systematically for their value in repository and process design. Test conditions and procedures often have no firm basis in engineering needs, and documentation is frequently incomplete in terms of test conditions, sample characterization, and experimental planning. A degree of program maturity has been reached where tests of a standardized nature should be applied to all candidate waste forms to allow valid evaluations and conclusions. Preferably, the standard test should be conducted under the direction of a single competent center, with the objective of fair and even-handed evaluation of all waste-form candidates. For high-level waste, we have developed functional needs for acquisition of data and release into a data bank for controlled engineering applica-

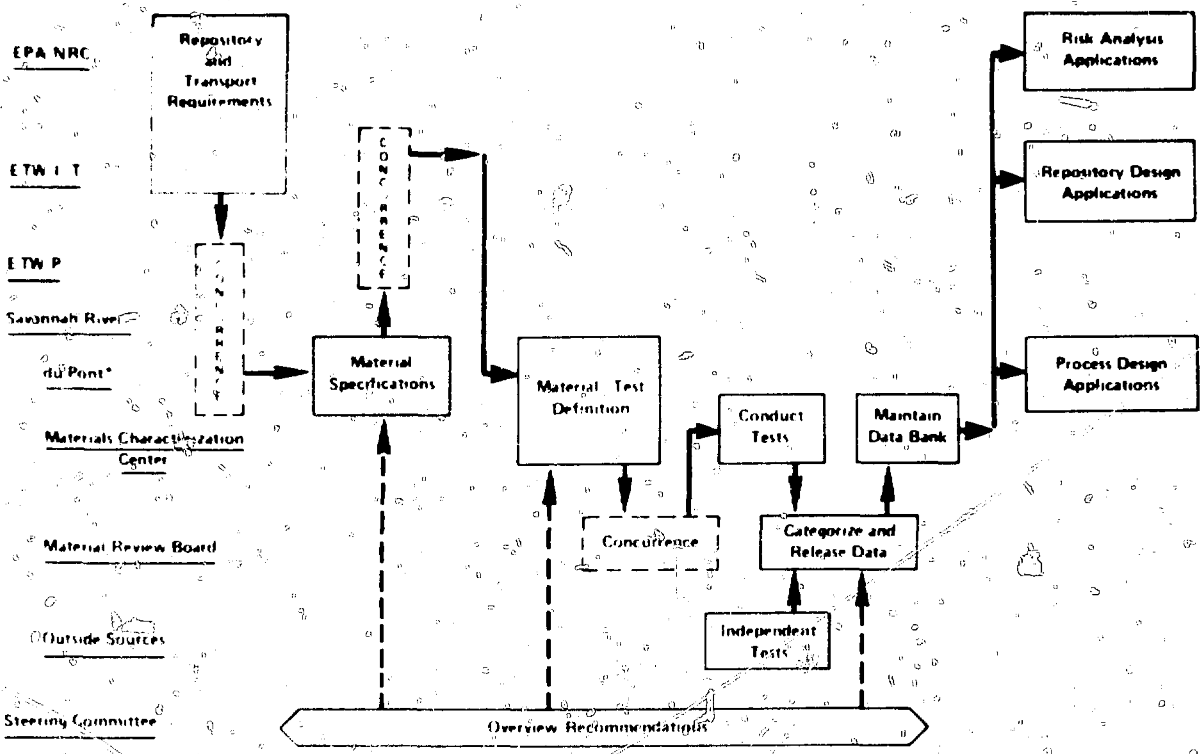
EPA NRC
ETW I T
ETW P
Savannah River
du Pont*
Materials Characterization Center
Material Review Board
Outside Sources
Steering Committee
Repository and Transport Requirements
CONCURRENCE
Material Specifications
CONCURRENCE
Material Test Definition
Concurrence
Conduct Tests
Categorize and Release Data
Independent Tests
Maintain Data Bank
Risk Analysis Applications
Repository Design Applications
Process Design Applications
Overview Recommendations

*Lead Field Office Contractor for Long Term HLW Management

Fig. 2 High-level waste planned materials-characterization program.

tion. Figure 2 shows the actions from establishment of requirements and specifications, through to definition of tests, conduct of tests, release of data, and independent overview, all laid out by the organizational elements performing each function. Please note that the procedure also provides for evaluation of data generated independently of the materials characterization center and outside of DOE sponsorship.

This concept is being discussed with DOE field office organizations involved in preparation for final agreement and identification of all participants in the organization. We will then define test activities, review and categorize existing data, and establish a data bank for engineering application. Continuing interaction with the Environmental Protection Administration and Nuclear Regulatory Commission will be emphasized to determine needs for statistically based data for risk analyses and reliability evaluations.

As the technical papers are presented in these sessions, I hope that the audience will bear in mind the need for a strong, well-planned, systematic materials program which accepts and fosters new ideas and concepts in meeting the evolving waste-management system requirements.

MATERIALS ASPECTS OF NUCLEAR WASTE DISPOSAL IN CANADA

D. J. CAMERON and G. G. STRATHDEE
Chemical Technology Branch, Atomic Energy of Canada Limited
Whiteshell Nuclear Research Establishment, Pinawa, Manitoba ROE 1L0 Canada

ABSTRACT

The concept of disposal of nuclear waste in a deep, hard-rock vault raises a number of questions concerning the behavior of materials. The man-made materials under consideration are the waste form, engineered containment, and the buffer and backfill materials. Our general approach to developing each of these barriers is presented.

INTRODUCTION

The Canadian program for the management of high-level radioactive waste is directed, primarily, to the concept of disposal in a vault excavated deep within a hard-rock body located in the Province of Ontario. The Precambrian Shield area of this province contains many igneous, intrusive geological formations, known as plutons, which we believe will be found to be suitable for this purpose. A general outline of the current and projected waste disposal program has recently been published.[1]

It is assumed that water will be present in the rock formation. Therefore dissolution and transport is the principal mechanism whereby radioactivity might reach the biosphere from such a disposal vault. To counteract this, a multiple-barrier approach is being adopted to provide isolation of the waste and retardation of transport of any material which might be dissolved if containment should break down. The barriers in the disposal scheme are: a low solubility waste form, an engineered barrier built around the waste, buffer and backfill materials to retard migration, the massive geological formation and, finally, the surrounding geosphere. Fig. 1 shows schematically one example of how the waste might be emplaced in the disposal vault. The approach is very similar to that adopted in the conceptual study of waste disposal in Sweden, described in the KBS series of reports.[2,3] Studies of similar hard-rock disposal concepts have been in progress in Canada since 1974.

Of the barriers present, the waste form, the engineered containment, and the buffer and backfill materials are man-made and thus under the control of the materials scientist and engineer. The challenge for us is to develop these man-made barriers into a system which, together with the geologic barriers, best meets the objective of nuclear waste isolation. The use of the word "system" is deliberate. The individual components cannot be developed independently, since it is necessary to consider the effect of one barrier on the performance of another. For example, some buffer materials, with desirable permeability and ion-exchange properties, might lead to water chemistry conditions conducive to corrosion of the engineered barrier or an accelerated dissolution rate of the waste form. Conversely, if the engineered barrier is subject to general corrosion, even at a slow rate, the corrosion products may substantially reduce the ion-exchange capacity of the buffer material.

A major target in the Canadian program is to put into operation a demonstration waste disposal vault by 1989. This target has a significant impact on the selection of waste forms and development activities concerned with the engineered barrier.

THE WASTE FORM

Currently no decision has been made concerning fuel recycle in Canada. It is, therefore, the mandate of AECL to

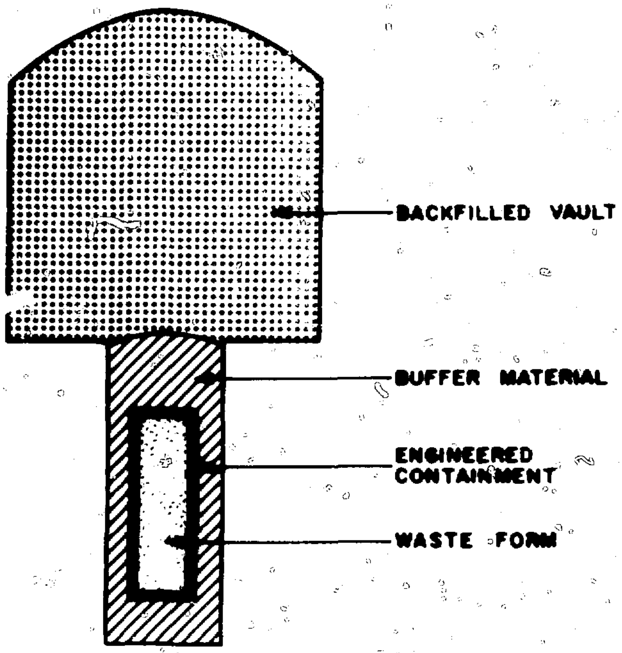

Fig. 1 Schematic representation of one concept of waste emplacement in the disposal vault.

develop the technology by which to immobilize and isolate both separated fission product wastes and irradiated fuel. Given the time scales of the waste management program, the demonstration vault will be loaded, predominantly, with irradiated fuel. This is because there are no streams of fission product waste available in Canada which would allow the development of waste immobilization on a large scale for this disposal demonstration program. Several containers of fission product waste will be included in the demonstration vault, but the major heat and radiation source will be supplied by up to 500 containers of immobilized fuel, each containing approximately 0.8 to 1.4 Mg of UO_2.

Fuel Waste

The geometry of the CANDU* fuel bundle, 100 mm diameter by 495 mm long, is a potential advantage if irradiated fuel is to be considered as waste. The bundles can be handled relatively easily and will fit conveniently into a number of packing arrangements. In view of this, a major consideration in fuel immobilization is whether to treat the intact irradiated bundle itself as the waste form or whether the fuel should be mechanically reduced, or even dissolved, as a prelude to making an alternative product.

This decision is not viewed as a materials science judgment on whether a more dissolution-resistant waste product than UO_2 can be made from the fuel. We must consider the impact of this approach on the total environmental and safety assessment. It is possible that adoption of an alternate waste form could lead to a small improvement in an already large safety factor for future generations and add to the potential hazard incurred by the current generation, due to the selection of more complex process technology and the generation of secondary waste streams.

To date, the major emphasis of the work on fuel immobilization is concerned with taking intact fuel bundles and building packaging containment around them. However, the potential benefits of altering the form of fuel waste will be assessed. Mechanical reduction of the fuel may allow it to be incorporated heterogeneously into a matrix of metal, glass or ceramic or, if the fuel is dissolved or reduced to a fine powder, it could perhaps be incorporated homogeneously into a vitreous or ceramic product.

UO_2 fuel is a complex waste form. Penetration of the Zircaloy fuel sheath exposes three main sources of activity: a portion of the fission product gases which have been released during irradiation, small amounts of compounds of relatively volatile fission products which migrate to the fuel pellet/cladding interface, and the UO_2 matrix which still contains the majority of fission and transmutation products.

About 10% of the fission product Kr and Xe gases, perhaps 20% of I and Cs, and about 1% of the Sr may be released from the fuel matrix during the irradiation of CANDU fuel.[4] Cubicciotti et al.[5] have found these fission products, together with Te and a range of others in smaller concentrations, on the inside of the sheath of light-water-reactor fuel. Evidence was presented that some of the Cs and I coexist as CsI, a readily leachable source of two important fission products.

The majority of the fission products and actinides will still be bound up in the UO_2 matrix. Some, including Zr, the rare earths, and the actinides, should exist as oxides which form dilute solid solutions with UO_2. Others such as Ba and Sr may form separate oxide phases, while Pd, Ru, Rh and Tc are expected to be present in their reduced form under the conditions of oxygen potential which exist in the fuel. These will still be incorporated in the UO_2 matrix, but perhaps heterogeneously.

---

*_CANada Deuterium Uranium._

Release of fission and transmutation products from the UO_2 will depend on the dissolution rate of the UO_2 matrix. The dissolution of UO_2 was reviewed recently by Holland.[6] In essence, UO_2 is a low-solubility waste form under reducing conditions but is significantly more soluble in an oxidizing environment. It is expected that the naturally occurring groundwaters in a deep, hard-rock formation of the type which interests us will have a very low oxygen content.

There is need for data on the dissolution of irradiated UO_2 at elevated temperatures to aid the assessment of this material as a waste form. Such measurements, as well as more basic electrochemical studies of dissolution kinetics in unirradiated UO_2, have commenced in the WNRE laboratories.

Fission Product Waste Forms

The initial specifications for the reference package of high-level waste are shown in Table I. Note that the glass product is expected to incorporate a relatively small amount of fission product waste from either natural UO_2 or ThO_2-based fuels. This dilute-waste composition has been selected for two reasons: first, to keep the temperature increase in the waste and vault relatively low and, second, to minimize the number of different solidified waste types which may be produced at a fuel recycle facility. This can be done by combining the medium- and high-level waste streams.

TABLE I

Initial Specifications for Reference Immobilized Waste

Container dimensions	diameter	0.46 m
	length	3.03 m
Waste glass	volume	0.43 m^3
	mass	1.08 Mg
	fission product content	1 to 3%
Decay heat at 10 years	UO_2 fuel waste	0.2 kW/Mg
	ThO_2 fuel waste	0.3 kW/Mg

By fabricating a dilute waste glass and emplacing the containers in the floor of a hard-rock vault in boreholes spaced with centers about 1.5 m apart, we intend to limit waste package surface temperatures to 150°C and volume-average vault temperatures to 100°C. Under these conditions, our reference container centerline temperatures will remain below 200°C, and the thermal stability of the glass will greatly reduce the possibility of anhydrous devitrification processes in that disposal environment. If the waste is exposed to groundwater as a result of corrosion of the steel container, hydrothermal alteration of the glass product would occur. However, the comparatively low temperature of the waste form in the disposal zone is expected to minimize the extent of chemical reaction. If necessary, an additional engineered barrier or an overpack will be provided to prevent groundwater corrosion of the primary waste package during the thermal period of the vault.

The dilute-waste reference waste package which has been adopted is the result of our decision to evaluate the merits of combining the high- and medium-level liquid waste streams prior to solidification at a fuel recycle facility. A significant fraction of the radionuclides which create the potential long-term waste hazard will be present in the medium-level waste stream. In particular, this waste stream will contain a major fraction of the plutonium which is not extracted. We believe that this should be immobilized in a waste form of comparable integrity to that used for high-level waste. Combination of high- and medium-level waste necessarily means that waste-glass formulation is constrained by the concentration of sodium arising from the medium-level waste stream, and the fission product/sodium ratio of the combined waste stream. To maintain acceptable durability of the final high-level waste-glass product, it is essential to limit the Na_2O content to 20 wt%. For our case this means that fission-product loading will be $<$ 3 wt%. Up to 1 Mg of waste-containing glass will be produced per Mg of irradiated fuel recycled.

Although the early development work in Canada between 1955 and 1960 was concentrated upon nepheline syenite-based glass of the type:

$$\text{Waste}-(Na,K)_2O-CaO-Al_2O_3-SiO_2$$

current product research has been focussed upon borosilicate glasses, particularly of the classes:

$$\text{Waste}-Na_2O-B_2O_3-SiO_2$$

$$\text{Waste}-Na_2O-ZnO-B_2O_3-SiO_2$$

$$\text{Waste}-Na_2O-CaO-B_2O_3-SiO_2$$

The borosilicate glasses are of particular importance because they form the basis of technology being developed in most other countries.

Initial laboratory materials studies have dealt primarily with the thermal stability and the mechanisms of ion-exchange and dissolution of dilute-waste glasses. For example, ZnO substitution for Na_2O has been shown to markedly influence the extent of liquid-liquid phase separation, and the type of alteration products of hydrothermal reaction of $Na_2O-ZnO-B_2O_3-SiO_2$ glasses. These studies are related closely to the expected environment within a hard-rock vault for high-level waste. Some details of this research are reported in another paper at this conference by G. G. Strathdee and co-workers.

TABLE 2

Approximate Timescales for Some Potential Targets of Engineered Containment

Containment target	Fission product waste	Irradiated fuel
Storage and transportation package after immobilization	~5 yrs	~5 yrs
Elevated temperature phase of repository operation	~100 yrs	~5,000 10,000 yrs
Period of high fission product toxicity	300 1,000 yrs	300 10,000 yrs
Very long-term isolation	$>10^5$ yrs	$>10^5$ yrs

ENGINEERED CONTAINMENT

All our work on engineered containment is being performed as part of the fuel immobilization program for handling intact bundles. The majority of this technology will be equally applicable to devising engineered containment for fission product waste forms.

There are several potential targets for engineered containment, as has been pointed out by Braithwaite and Molecke.[7] Our estimates of these targets for the two types of waste are shown in Table 2. These numbers are approximate but do illustrate some important differences between fission product waste and fuel. A vault containing fuel will be hot for a longer period than one containing fission product waste. Also, there are order-of-magnitude differences in relative toxicity in the period 500 to 10^4 years, although it should be noted that after 300 years the toxicity of both forms is quite low (see reference 1 for a more detailed discussion of relative toxicities). A significant observation is that any engineered containment which meets realistic objectives for fuel isolation should be adequate for the disposal of processed fission product waste.

For the disposal of fuel it has been proposed in the KBS study[3] that massive copper containers be used to meet the objective of indefinite isolation, while, for fission product waste, a 100-mm thick layer of lead and a 6-mm thick outer skin of titanium has been suggested for containment through the high-toxicity phase.[2]

We expect to start, next year, the detailed design of a pilot plant to produce up to 500 containers of immobilized fuel for the vault demonstration phase. Isolation for the duration of the high-toxicity phase has been chosen as the target for this containment. The final form of this containment has not been defined, but it is expected that the major barrier will be provided by a shell of corrosion-resistant metal. The three major candidate materials which have been selected[8] for intensive study are: 316L stainless steel, Inconel 625, and titanium grade 2. The stainless steel would only be suitable for very benign vault environments and has been included primarily to facilitate the development and testing programs. Inconel 625 should resist corrosion by the groundwater generally found in the Precambrian Shield which contains 10 to 400 ppm of chloride ion. However, during exploratory drilling into the pluton on which our research center is located, water with very high salinity, 5600 ppm of chloride ion, was encountered,[9] which may be characteristic of disposal-zone groundwater. Titanium would provide the maximum corrosion resistance in this environment.

The possibility of adding additional barriers, perhaps by coating, casting lead or another low-melting point metal within the container, or by packing the container with a medium such as clay or MgO which swell on contact with moisture, is also being investigated. The packed materials will provide a diffusion barrier which could also provide additional retardation by sorption. If needed, other materials could be included which would react with certain nuclides to form new stable compounds. All of these alternatives are under investigation.

For very long-term containment, copper has considerable merit as do some ceramic materials, including the hot isostatic pressed alumina containers developed in the Swedish program.[10] Currently, our approach to very long-term containment is to review the potential of a variety of materials for this purpose, with relatively little emphasis on how they may be employed. For example, alumina has very good resistance to dissolution, but can display slow crack propagation phenomena[11] which might impose stringent inspection requirements on an alumina container. Clearly the effect of environment on crack propagation is of concern. Another ceramic material which interests us is graphite. Graphite has the advantage that it is very resistant to oxidation in water at the temperatures of interest and can be fabricated in rather large sizes. On the negative side there is the problem of permeability. We expect to spend the next year reviewing materials before selecting a concept for very long-term containment; we will then initiate a program to demonstrate a feasible system.

BUFFER AND BACKFILL MATERIALS

The buffer material has a relatively low volume compared to the total amount of backfill and is emplaced immediately around the waste form. It should have a very low permeability, be plastic, and swell when wetted so that fissures will close, yet be sufficiently load bearing to maintain the waste in a fixed position, and also have good sorption and retention properties for the nuclides which may be leached, eventually, from the waste. An additional function which might be desirable is that of water chemistry control. In particular, the beneficial effects of maintaining reducing conditions to control UO_2 dissolution and the corrosion of potential containment materials, such as copper and lead, are most significant. Reducing agents may be incorporated into the buffer (and backfill materials) to react with the oxygen and other oxidizing species which will be trapped in the vault at the time of sealing.

There are many natural materials which act as cation sorbers, including some clays which might be used in a buffer material. However, anions are not as easily retarded, and some of the more problematic species such as iodine, technetium, and plutonium could be released in an anionic form. We are evaluating materials which might be incorporated in the buffer and/or backfill to selectively retard anions if required.

The buffer material could be formed as prefabricated blocks to be emplaced in the vault. The selection, development, and fabrication of this material with good dry strength, adequate load bearing and rheological properties, together with high density and low permeability, will likely draw heavily on the science and technology developed in the ceramics industry.

The backfill material will be used to fill the excavated chambers and tunnels within the repository and will be required in much larger volumes. Many of the required properties of the backfill will be similar to those of the buffer material. Ideally, the backfill should contain a high percentage of crushed rock excavated in forming the vaults, but other components will be required. One of these will probably have some swelling capability on contact with water to counteract any tendency for the backfill to slump after emplacement.

SUMMARY AND CONCLUSIONS

The nature of the Canadian program for disposal of high-level nuclear waste in a deep geological vault dictates that many of the technological problems to be explored, identified, and solved are those of ceramic materials. At every step of our system of multibarrier containment there is considerable scope, not only for imaginative application of existing ceramics technology, but also for creative research into basic processes which limit the physical and chemical durability of synthetic and natural materials.

All our preliminary evidence suggests that the concept of disposal of nuclear waste in a hard-rock vault is realistic and achievable. It will now require a major effort to prove the validity of the concept both to ourselves as scientists and to the general public. The elements of technology exist today by which we can process either high-level fuel recycle waste or irradiated nuclear fuel for disposal, construct a hard-rock vault, modify it to accept the waste packages, and close and seal it. All the components for success are available. With our final goal clearly defined, we expect that the supporting research and development programs will verify in a detailed manner that the concept of deep underground disposal is safe.

REFERENCES

1. J. Boulton (Ed.), *Management of Radioactive Fuel Wastes: The Canadian Disposal Program*, Atomic Energy of Canada Limited Report, AECL-6314, 1978.
2. *Handling of Spent Nuclear Fuel and Final Storage of Vitrified High Level Reprocessing Waste*, Vols. I-IV, prepared by KBS, Stockholm, Sweden, 1977.
3. *Handling and Final Storage of Unreprocessed Spent Nuclear Fuel*, Vols. I and II, prepared by KBS, Stockholm, Sweden, 1978.
4. W. C. Harrison and M. J. F. Notley, Atomic Energy of Canada Limited, unpublished data.
5. D. Cubicciotti, J. E. Sanecki, R. V. Strain, S. Greenberg, L. A. Neimark, and C. E. Johnson, EPRI Project, No. RP 455-1, 1976.
6. H. D. Holland, Uranium Oxides in Ores and Fuels, in Proceedings of *High-Level Radioactive Solid Waste Forms*, Denver, NUREG/CP-0005, National Technical Information Service, Springfield, VA, 1979.
7. J. W. Braithwaite and M. A. Molecke, High-Level Waste Canister Corrosion Studies Pertinent to Geologic Isolation, to be published in *Nuclear Waste Management and Technology*, 1(1): 1979.
8. K. Nuttall and V. F. Urbanic, *An Assessment of Container Materials for Fuel Immobilization*, to be published as Atomic Energy of Canada Limited Report, AECL-6323.
9. *Chemical Analysis of the Initial Groundwater Samples from the Lac du Bonnet Batholith*, Atomic Energy of Canada Limited, Technical Record TR-21, 1979.
10. H. Larker, Hot Isostatic Pressing for Consolidation and Containment of Radioactive Waste, in Proceedings of *Scientific Basis for Nuclear Waste Management*, Boston, G. J. McCarthy (Ed.), Plenum, NY, 1979.
11. A. G. Evans, A Method for Evaluating the Time-Dependent Failure Characteristics of Brittle Materials and Its Application to Polycrystalline Alumina, *J. Mat. Sci.*, 7: 1137 (1972).

USE OF GLASSES AND CERAMICS IN THE FRENCH WASTE MANAGEMENT PROGRAM

YVES SOUSSELIER
Commissariat à l'Energie Atomique, Boite Postale N°6 92260 Fontenay-aux-Roses, Paris, France

ABSTRACT

In order to reduce the dependence of energy, the French nuclear policy consists of reprocessing irradiated fuels discharged from PWR's which are in operation, under construction and planned, and in reusing the separated plutonium in LMFBR. The transuranium solid wastes which will arise from PWR and LMFBR reprocessing and fabrication plants – and among them the vitrified reprocessing first cycle raffinates – will be disposed of in geological formations. In order to improve the disposal safety, several processes have been developed in France, e.g., vitrification for HLW. It seems that it will be possible to use this process also for embedding ^{129}I and also for embedding cladding hulls. Development of a ceramic container as a *second barrier is in progress.*

FRENCH NUCLEAR ENERGY PROGRAM

The specific properties of glasses and ceramics have been regarded by French experts as very interesting for solving some problems of radioactive waste management. The choice of glass as a matrix for high-level wastes has been made for twenty years. Such a choice is part of the French waste management policy and, more generally speaking, a part of the French nuclear energy policy.

The French nuclear energy program has experienced a rapid growth since 1970 because nuclear power plants are economically competitive as a source of electricity and because of the French government's decision to reduce progressively the share of France's energy balance held by imported fossil fuels. This program began with construction of some gas graphite reactors (2300 MW(e) are now in operation), and since 1970 all reactor orders but one have been pressurized water reactors. Total orders and program authorization currently represent about 35,000 MW(e). By 1985 electricity generated by nuclear power plants will represent nearly 20% of France's total energy consumption and nearly 50% of electricity production.

Uranium resources are available in France (about 4% of free world resources) but taking into account the excellent performance of the Phenix breeder reactor and the evident interest of breeder reactors to decrease uranium consumption, the French nuclear program foresees an important development of breeder reactors through the end of the century. The first breeder reactor of industrial scale [1200 MW(e)] is now under construction with start-up scheduled for 1983.

Such a policy implies, as a consequence, the need for reprocessing. Two reprocessing plants are in operation. The Marcoule plant specializes in the processing of natural uranium fuels. The La Hague plant, which has been modified to process oxide fuels including Phenix fuels, has been working for two years on an experimental program with irradiated oxide fuels from light water reactors. More than 100 T have been reprocessed, and the capacity of the plant will be increased gradually to 800 T/yr. It is important to point out that we consider reprocessing as having another advantage: it decreases substantially the plutonium content in the wastes, roughly by a factor of 50.

FRENCH WASTE MANAGEMENT POLICY

The choice of the reprocessing option leads to the production of several categories of wastes such as high-level waste and cladding hulls. The general safety and environmental objectives of the French waste management policy are quite similar to those defined in the O.E.C.D. Nuclear Energy Agency's report "Objectives, Concepts and Strategies for the Management of Radioactive Wastes," September 1977, which are:

- to comply with general radiological protection objectives and principles, notably to keep radiation exposure from waste management activities, including disposal, as low as is reasonably achievable.
- to minimize, to the greatest extent practicable, any potential impact on future generations.
- to avoid preempting present or future exploitation of natural resources.

In order to implement such objectives, we consider that it is necessary:

- to dispose of all radioactive wastes except low-level waste without long-lived emitters in geological formations.
- to follow, for such disposal schemes, the concept of multibarrier isolation.

The first barrier is the matrix in which the waste is embedded (e.g., glass or bitumen). The second is the container. The third is an artificial barrier, made with materials having good sorption properties for radionuclides. The fourth is the geological formation itself in which wastes will be deposited. Two different modes of action are possible for the last two barriers: either providing total isolation (it will be the case for salt formations) or providing an important factor for retardation and retention of waste substances (the case for some rocks like granite and shale). In France, we think it is important, at least in the first analysis, to consider each barrier as such and, for that reason, to make each barrier as efficient as possible independently of the others. It is especially important to have efficient barriers for high activity and transuranic wastes.

For disposal of radioactive wastes in geological formations, the main risk which we have to take into account is migration of radionuclides due to the circulation of groundwater. And, consequently, one of the most important properties for the first barrier, if not the most important, is its leaching rate, which should be as low as possible. For the second barrier, an important property is to have a high degree of corrosion resistance. In both cases, the use of ceramic or glass materials makes it possible to offer a good solution.

USE OF GLASSES IN THE FIRST BARRIER

Vitrification of HLW

Research for solidification of raffinates of the first extraction cycle on reprocessing plants began in France in 1957. As a matter of fact, we never thought that storage of high-active waste as a liquid was desirable, though we consider that storage made with double wall stainless steel tanks, as is actually the case, is entirely safe for several decades.

From the beginning, we concentrated our efforts on borosilicate glass. The atoms in this glass are not arranged in an orderly fashion as in crystalline substances, since atoms of a certain size can be incorporated in a crystalline structure. Glass, on the other hand, is able to embed the different atoms of varying size which occur in high-level waste. In addition, the structure of glass can adjust to the radioactive disintegration which takes place in the fission products and actinides and which results in their conversion to new elements. The first radioactive glasses were made in 1959 and were then compared with synthetic materials such as micas, which already had been prepared at that time. Similar leaching rates, the ease of the glassmaking process, and the more flexible use of the product led to the definitive choice for vitrification. Borosilicate glass is composed of silicon dioxide, sodium dioxide, and boron oxide. The advantages of borosilicate glass are:

- good chemical resistance to leaching in water
- good mechanical resistance to rapid temperature fluctuations
- low crystallization rate
- little increase of leaching rate if the glass crystallizes
- good resistance to radiation damage

The first glass blocks weighing 5 to 15 kg and having specific activities of about 1000 Ci/l were made in 1963 by a gel technique in a graphite crucible. Glasses stored since then have been retrieved after 15 years for examination — no changes have occurred.

A pot vitrification technique has been developed in the Piver pilot plant at Marcoule. In this process a pot made of Inconel, heated by induction, was fed with the fission-product solution and a slurry containing glassmaking chemicals. Drying and calcination were continued until the pot was 80% full. The material was then melted by increasing the temperature to 1180°C and the glass poured, after refining, through a drain tube heated by induction. The empty pot was used again for another run. In 1969, the Piver pilot plant, using this process, was operated under active conditions. Its operation was continued until 1973, processing waste solutions from spent natural uranium fuels. Twelve metric tons of glass with a maximum activity of 3000 Ci/l were produced in this plant. During each run, using a 250-mm diameter pot, 200 liters of solution could be vitrified to produce 90 kg of glass.

An experimental area was built to store the Piver glasses. It consists of 32 pits, 10 m deep, enclosed in a concrete structure equipped with forced-air cooling. A total of 164 containers and 8 used pots are stored in the facility.

Because of the successful operation of Piver, it was decided in 1972 to build an industrial vitrification plant at Marcoule, and economic studies were carried out to compare the pot process with a more advanced continuous vitrification technique that had been developed in the meantime. The continuous process was chosen in preference to the pot process for the Marcoule vitrification plant because it was found to be more flexible, it had lower investment and operating costs, and it was easier to scale up for higher throughputs. This plant started up in active operation in June 1978, and results obtained until now are quite satisfactory. A plant, using the same technique, will be built in La Hague and will be capable of processing 500 m^3/yr of waste solutions. The start-up is scheduled for 1984 to 1985.

Vitrification of Iodine

It is not possible to use the borosilicate glass technique for immobilization of ^{129}I, owing to the volatility of this element. But, taking into account the very interesting characteristics of glass products, we tried to incorporate iodine in a glass network.

Two different methods have been studied:

- The first is the use of oxide glass with a low melting point, such as $PbO\text{-}B_2O_3\text{-}SiO_2$ or $PbO\text{-}Na_2O\text{-}SiO_2$. As iodine is trapped in the reprocessing plant as PbI_2, some lead is brought in by this compound itself. The first results show it is possible to incorporate 10 wt.% of iodine in glass. But, at the present time, the retention of iodine is only 50% and research continues to increase this proportion.
- The second is the use of glass with fluorides without oxygen. This study is made under contract with the Commission of European Communities and is in its early stage. The first results seem to show that it is possible to incorporate about 3% of iodine.

Embedding of Hulls with Glass

One of the most interesting aspects of vitrification is that radionuclides constitute a part of the lattice; thus the process is not an embedding but a vitrification one.

With the very good characteristics of glass, especially in the conditions for geologic disposal, interesting uses of glass as an embedding material for other categories of wastes are possible. In France, we began studies in this direction for cladding hulls. Several goals have been defined:

- voids completely filled with glass
- complete elimination of air trapped in the chopped hulls
- avoiding glass fracture after cooling
- enamel the Zircaloy surfaces with glass

The technology employed is simple: A perforated basket is filled with hulls and introduced into a steel container with a 2-cm gap between the container and the basket. The container is heated to 800°C by a furnace, the temperature of the hulls being about 750°C. The basket is fitted with a central chimney into which a melted glass frit (55% silica, 1150°C) is poured. The first tests indicate that in all cases the glass does not crack after cooling. If the glass is poured at atmospheric pressure, small air bubbles are trapped in the glass block. In order to completely eliminate the presence of small air bubbles on an industrial scale, tests will be performed while pouring the melted glass under negative pressure.

USE OF CERAMICS FOR THE SECOND BARRIER

Glass constitutes a first barrier which gives high performance, such as very low leaching rate (10^{-7} to 10^{-8} g/cm^2 · d for Ce, Ru, actinides) and very high corrosion resistance to groundwater. However, the results can be less favorable if the temperature increases and for some values of pH. For these reasons, it is desirable to have, in a geological repository, a second barrier which will be able to delay leaching of glass blocks by groundwater, especially during the period in which the temperature will be relatively high. It is important for such a barrier to use materials offering good conductivity, buffer characteristics, and of course very high water resistance. Some ceramics are capable of providing these characteristics.

The French program is in its first phase but there is no hurry because we do not plan to dispose of glass blocks in a geologic repository until after 30 years of cooling.

In evaluating materials for the second barrier, we began with a general review of ceramics and selected some materials for further studies among them: electromelt refractories and vitroceramics. We have had good experience with some electromelt refractories for the realization of some furnaces, especially a product named Z–A–C. Its composition is about 50% Al_2O_3, 32% ZrO_2, 16% SiO_2, with some quantities of Na_2O, Fe_2O_3, TiO_2, etc. Its porosity is very low (less than 3%) and its permeability is zero. This product also has very good mechanical properties. A first container will be made this year with this product.

For vitroceramics, we considered the possibility of using a by-product from the steel industry somewhat similar to basalt with a composition of 45% SiO_2, 18% Fe_2O_3, 24% CaO, with some quantities of Al_2O_3, Na_2O, MgO. This product has very good mechanical and thermal properties, and its cost is low. We plan to continue research under this program for the next few years and especially to develop a welding technique for the container lid.

CONCLUSION

An important consequence of the French nuclear program, including breeder reactors, yields to the production of several categories of wastes. For all categories, except LLW, geologic disposal will be used; safety being achieved by the multibarrier concept.

We have developed adequate conditioning processes for different categories of wastes, especially vitrification for HLW. However, the development of the geologic repository is less advanced. But we are not in a hurry, and we prefer to study very carefully the possibilities offered by different geologic formations. As we now have very good conditioning suitable for engineered surface storage it is possible to store the wastes without creating any hazard for many decades.

The development of ceramic containers, which will provide a second barrier and reduce the possibility of migration of radionuclides from a geological repository, will ensure adequate long-term safety after disposal and make the French nuclear and waste management program perfectly coherent.

THE CONCEPT FOR THE TREATMENT AND DISPOSAL OF RADIOACTIVE WASTES IN THE GERMAN ENTSORGUNGSZENTRUM*

C. SALANDER and ZÜHLKE
Deutsche Gesellschaft für Wiederaufarbeitung von Kernbrennstoffen mbH (DWK),
Bünteweg 2, D-300 Hannover 71, Federal Republic of Germany

ABSTRACT

The concept for treatment and disposal of radioactive wastes in the planned German Entsorgungszentrum is presented. HLLW will be converted to borosilicate glass. Medium- and low-level-liquid waste concentrates will be fixed by cementation. The products will be finally disposed of in a salt dome just below the Entsorgungszentrum.

INTRODUCTION

According to the concept of the German Federal Government for closing of the nuclear fuel cycle, the electricity generating utilities have accepted responsibility for waste management of the German nuclear power plants within the framework of the "polluter pays principle"; the ultimate storage of radioactive waste remains a responsibility of the government. The duties of industry mainly include planning, construction, and operation of the facilities for fuel element storage, reprocessing, and waste treatment, and for refabricating the recovered fissile material. The German utilities operating and planning nuclear power plants have set up the Deutsche Gesellschaft für Wiederaufarbeitung von Kernbrennstoffen mbH (DWK), which is to build and operate the Entsorgungszentrum. One of the main characteristics of the concept is that all facilities will be co-located at one area. Thus, the distances for transport of radioactive materials are minimized, and the protection as well as the surveillance of fissile materials is largely facilitated.[1]

RADIOACTIVE WASTE TREATMENT

The overall principle is that all radioactive wastes generated within the Entsorgungszentrum will be transformed on site to products suitable for final disposal.

High Level Waste

From the first extraction cycle of the Purex process, high-level-liquid waste (HLLW) is obtained by concentration of the HAW-stream. Some data of this waste are given in Table 1. Per ton of spent fuel, a volume of about 450 l of HLLW is finally generated. That means that for the Entsorgungszentrum, with its capacity of reprocessing 1,400 T U of spent fuel per year, 600 m^3 of HLLW have to be conditioned annually for subsequent final disposal. It is planned to solidify the HLLW by vitrification six years after reactor discharge of the fuel. As the reference process for vitrification, DWK plans to acquire and adopt the French continuous vitrification process known as AVM[2] because of its advanced stage of development. As a back-up solution the PAMELA process[3] is under advanced development in Germany and Belgium. Both processes shall be tested and demonstrated before their possible use in demonstration plants in the Entsorgungszentrum. At Karlsruhe, Federal Republic of Germany, a demonstration plant called "HOVA"† using the AVM process is planned to be realized at the earliest possible date under a licensing agreement with the French CEA. This plant shall work up the HLLW of the German reprocessing plant (WAK). A PAMELA demonstration plant shall be built at Mol/

---

*Center for the reprocessing of spent nuclear fuel including treatment and disposal of the generated radioactive waste.

†Hochaktiv-Verglasungsanlage = HLLW Vitrification Plant.

TABLE 1

Some Data of The High-Level-Liquid Waste (HLLW) To Be Processed

Origin: spent LWR-fuel, burnup	36,000 MWd/TU
Volume prior to solidification	450 l/TU
Acidity	2–5 m HNO_3
Salt content	200–250 g/l
Fission-product nitrates	160–170 g/l
Gd-nitrate (if homogeneous poisoning is to be used)	50 g/l
Corrosion products (Fe, Co, Ni)	8 g/l
Solids	12 g/l
Plutonium	85 g/m^3
Uranium	4.5 kg/m^3
Specific activity (at time of solidification)	~10^6 Ci/m^3
Specific heat generation (at time of solidification)	4.2×10^3 W/m^3

Belgium to solidify the Eurochemic LWR–HLLW. Both plants have a similar capacity of 30 l/hr liquid feed, and the scale-up factor for the facility needed at the Entsorgungszentrum is less than five. The HLLW-solidification plant of the Entsorgungszentrum shall have two independent lines with a capacity of 600 m^3/yr. The solidification process comprises four main steps:

- HLLW pretreatment
- Vitrification
- Block handling
- Off-gas treatment

Three of the steps are similar for both the AVM and the PAMELA process. The main difference lies in the equipment for the vitrification step.

1. HLLW Pretreatment

The HLLW shall first undergo a chemical denitration with formaldehyde. However, the need for this process step is still under investigation. The denitration is aimed at minimizing ruthenium volatilization during the melting step (formation of volatile RuO_4 by oxidation). The denitration is carried out batchwise.

2. Vitrification

a. AVM

The pretreated HLLW is first calcined in a tilted rotary kiln. The calcine together with borosilicate glass frit then is fed into a metallic melter which is heated by induction. The glass is drained periodically into stainless steel canisters.

b. PAMELA

The pretreated HLLW is mixed with borosilicate glass frit and vitrified in a liquid fed Joule heated ceramic melter. The melt either is drained periodically to manufacture borosilicate glass blocks or it is drained continuously in the form of droplets which solidify to glass beads. These beads then will be incorporated in a lead matrix (Vitromet-product).

3. Block-Handling

The stainless steel canisters will have the following dimensions: open diameter = 0.3 m, height = 1.2 m, net volume = 70 l. Four to five canisters per day will be manufactured. The canisters are closed by welding a cap on top of each of them. After controlled cooling and subsequent decontamination, the blocks are transferred to an intermediate storage facility (air-cooled vaults). In total, about 1,800 blocks will be produced per year.

4. Off-Gas Treatment

After a pretreatment (sieve grid column for the denitrator and wet scrubber for the melter) the off-gases pass a main off-gas system where a decontamination level is reached which allows sending the remaining off-gas to the stack.

Low and Medium Level Liquid Waste

It is the aim to recycle low- and medium-active liquid effluents to the maximum extent possible after adequate pretreatment. For the remaining reduced quantity of waste, DWK recently decided upon the fixation by cementation in the Entsorgungszentrum after a thorough study of the experiences with bituminization and cementation. The main reasons are that cement is not inflammable, has better radiation resistance and higher thermal stability than bitumen. A further point is the simplicity of the cementation process. After concentration by evaporation, solidification is carried out in the following steps:

- Filling of a 400-l drum with a definite amount of cement
- Mixing of cement and liquid waste
- Setting of the mixture
- Closing of the drum

The fixation of organic medium-level waste (mainly TBP) is actually proposed to be used, although development is underway for processes which avoid organic material as final waste product.

Solid Wastes

Solid radioactive wastes will be treated by adequate mechanical means such as compacting followed by cementation. A survey of the amounts of radioactive wastes conditioned for final disposal per year in total is given in Table 2.

DISPOSAL OF RADIOACTIVE WASTES

Techniques which shall be used for the disposal of radioactive wastes generated within the Entsorgungszentrum are based on procedures which have been developed

TABLE 2

Throughput of Treated Radioactive Waste in the German Entsorgungszentrum

Low-level waste	
Liquid LLW solidified by cementation	2,400 drums/yr (400 l)
Solid LLW after cementation	7,850 drums/yr (400 l)
Intermediate-level waste	
Liquid MLW solidified by cementation	11,150 drums/yr (400 l)
Liquid MLW fixed in PVC	500 drums/yr (400 l)
Solid MLW after cementation	5,000 drums/yr (400 l)
High-level waste	
Liquid high-level waste after vitrification	1,750 blocks/yr (70 l)

Fig. 1 Dumping of LLW-drums in the Asse salt mine.

Fig. 2 Lost concrete shielding container.

and tested at the Asse test disposal facility since 1967 (Ref. 4). The disposal shall be carried out in a salt dome just below the site.

The repository itself will be located in the Gorleben salt dome at a depth of about 800 to 1,000 m in the older halite deep in the core of the salt dome. Before operation starts, the whole area of the future repository will be investigated by drilling actions and with the help of geophysical methods. This is to assure that there is enough homogeneous halite to dispose of all wastes generated during the lifetime of the Entsorgungszentrum. In the present state of site-independent planning of the repository, the following techniques for the disposal of all kinds of radioactive waste generated within the Entsorgungszentrum are foreseen.

1. Low-Level Radioactive Waste (LLW)

The 400-l drums with solidified LLW will be dumped on a salt ramp from the ceiling of a chamber and then covered with crushed salt (Fig. 1). When the end of the chamber is reached, a second layer will be brought in back to the entrance. The free volume of the chamber is then filled with crushed salt which is blown in. The 400-l drums of different kinds of low-level radioactive waste are inserted into so-called "lost concrete shielding containers" (Fig. 2) in order to reduce the dose rate at the surface. These lost concrete shielding containers will be piled up in large rooms and covered with crushed salt. The open space left will be refilled in the same way as described earlier.

2. Intermediate-Level Radioactive Waste (MLW)

Using a technique proven at the Asse test facility since 1972, the 400-l drums with the solidified MLW will be lowered from a shielding container at a gallery through a horizontal shaft into the disposal chamber, thus providing full radiation protection during the whole operation. Following the present concept of waste conditioning and disposal, part of the solidified intermediate-level radioactive waste, for instance solidified sludge from the feed clarification step, produces minor amounts of heat at the time it is to be disposed of. Because of the short-time heat production, a borehole technique shall be applied for the disposal of the wastes. From a shielding container the wastes contained in 400-l drums will be lowered into boreholes, each about 50 m deep. The arrangement of the boreholes is chosen in such a way as not to affect the disposal medium by the generated heat.

3. High-Level Radioactive Waste

Vitrified high-level radioactive waste canned in stainless steel canisters with an effective volume of 70 l will be disposed of in boreholes following the same technique as described above. The arrangement of the boreholes with a depth of 50 m is chosen in a way that a good dissipation of the released heat is guaranteed. A maximum temperature of 200°C (in the center of the disposal area) will not be exceeded. Tests at the Asse test facility using electrical heaters show that this requirement can be fulfilled by the present disposal concept.

Generally, it has to be stated that in the repository, only areas in which disposal actions take place will be kept open. Thus, after finishing disposal operations in a chamber or gallery these will be refilled at once leaving the waste within an almost homogeneous and compact rock salt mass. After finishing operations in the repository, all open space within the repository and also the shafts will be refilled with suitable material leaving the radioactive wastes disposed of in a stable geologic medium far from the biosphere.

REFERENCES

1. C. Salander, The Concept for the Disposal of Spent Fuel Elements from Nuclear Power Plants in the Federal Republic of Germany, in *International Conference on the Nuclear Fuel Cycle AIF BNF*, London, September 1978, and paper B 1 at Nuclex, Bale, October 1978.
2. A. Jouan, C. Sombret, Developpement actual du procedé de vitrification continue des solutions de produits de fission, in *Symp on Management of Radioactive Wastes from the Nuclear Fuel Cycle*, IAEA-SM 207/27, Vienna March 22-26, 1976.
3. W. Heimerl, *A Usable Method for the Management of High Level Waste from Nuclear Fuel Reprocessing, Annals of Nuclear Energy*, Vol. 4, p. 273, Pergamon Press, 1977.
4. K. Kuhn, J. Hamstra, Geologic Isolation of Radioactive Waste in the Federal Republic of Germany and the Respective Program of the Netherlands, in International Symposium of USERDA, *Management of Waste from the LWR-Fuel Cycle*, Denver, Colorado, 1976.

THE UK PROGRAM—GLASSES AND CERAMICS FOR IMMOBILIZATION OF RADIOACTIVE WASTES FOR DISPOSAL

K. D. B. JOHNSON
United Kingdom Atomic Energy Authority, Harwell, United Kingdom

ABSTRACT

The UK Research Program on Radioactive Waste Management includes the development of processes for the conversion of high-level-liquid-reprocessing wastes from thermal and fast reactors to borosilicate glasses. The properties of these glasses and their behavior under storage and disposal conditions have been examined. Methods for immobilizing activity from other wastes by conversion to glass or ceramic forms are described. The UK philosophy of final solutions to waste management and disposal is presented.

EARLY WORK

The earliest studies were commenced in 1948 and the use of civilian nuclear power on a large scale was looked forward to. Disposal onto ice caps, rocket ejection into space, and total disposal to the enviroment was rejected and the advantages of putting the radioactivity into small bulk to save shielding were identified. The problems appeared to be soluble, and a salt-free fuel reprocessing flow sheet was adopted so that most of the fission product radioactivity could be evaporated down to a small bulk.

The early experimental work identified methods of packaging low-level wastes in cement for disposal to the seafloor but began to concentrate upon the fixation of the expected high-level wastes. This early work identified adsorption upon clays or waste mixed with clays and fired at 1000°C (Refs. 1 and 2). The products were friable and had to be melted[3,4] at about 1500°C to produce a bubble-free glass. Adding fluxes,[1,2] such as $NaNO_3$, Na_2CO_3, Na_2HPO_4 or borax, lowered the founding temperature to 1000°C. Consideration of the potential industrial technology and long-term storage brought the work in 1958 to a search for glass compositions with high-fission product contents (to save plant and storage size), preparation temperatures below 1100°C (to ensure plant reliability and to control volatilization), and good leach resistance (because the potential routes back to man were seen to be by waterborne routes).

These principles were applied first to wastes from Materials Testing Reactors and defense wastes[5] and involved glasses based upon the $CaO-SiO_2-B_2O_3-(WO)$ system or the $Na_2O-SiO_2-B_2O_3-(WO)$ system, where (WO) is a waste oxide mixture which was high in alumina in the first case and high in uranium, iron, and alumirium oxides in the second case.

Many other glass systems have been examined[6] in the UK at one time or another. They include:

Nepheline syenite–$CaO-B_2O_3-(WO)$
$Na_3PO_4-CaO-SiO_2-(WO)$
$PbO-B_2O_3-SiO_2-(WO)$
$Na_3PO_4-PbO-B_2O_3-(WO)$
$Na_3PO_4-PbO-SiO_2-(WO)$
$Na_3PO_4-SiO_2-(WO)$
$Na_3PO_4-Na_2SiO_3-(WO)$
$BPO_4-Na_2O-SiO_2-(WO)$

All the phosphate glasses are very corrosive to steel, had no other real advantages over borosilicate glasses, and were rejected during the 1960s.

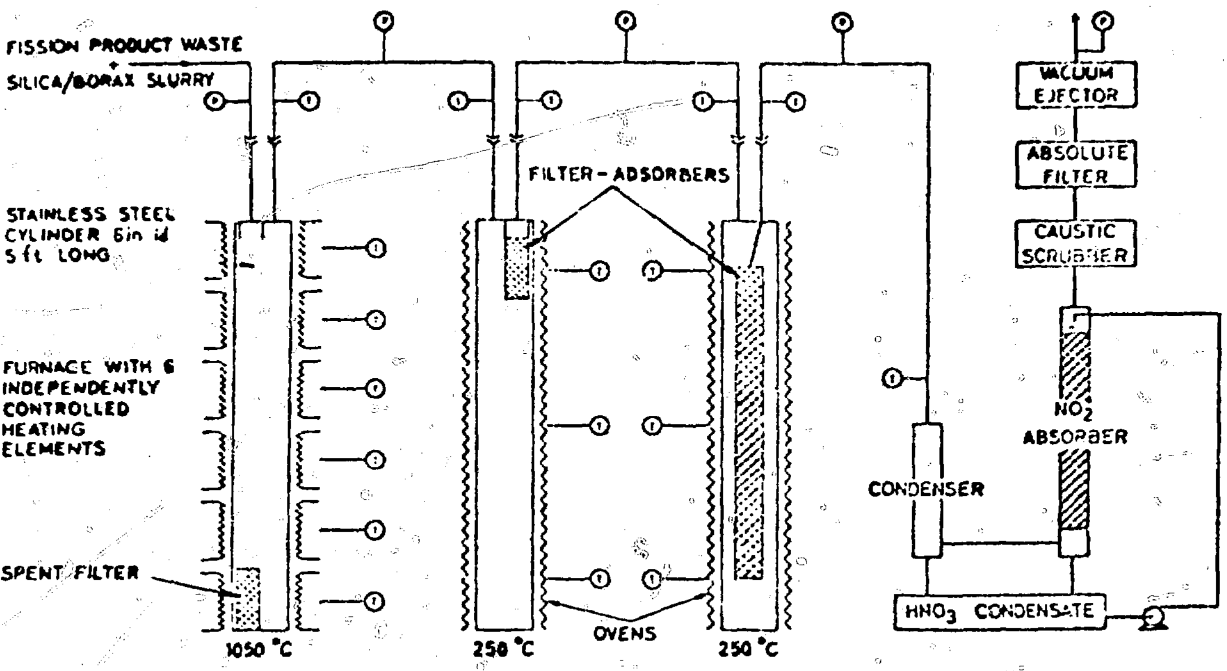

Fig. 1 FINGAL process.

FINGAL

These studies confirmed the technological concept we called FINGAL, which involved the evaporation, denitration, and melting in a single process vessel which became the disposal vessel. The concept included internal filters so that there was virtually no effluent of any kind (Fig. 1). This has been described in detail elsewhere.[6] The "glasses" produced have the properties usually associated with glasses but are very dark in color and contain separate crystalline material in dispersion in a glassy matrix. The coordinated program in support of that concept included glass composition studies, highly active pilot-plant studies, the effect of irradiation and heat on glasses, volatilization of active species during formation and storage, compatibility of glasses with metals, safety analyses of process operations and storage operations compared to tank storage of liquid, and leaching studies. It culminated during 1966 in the production of blocks of vitrified waste made from the highest specific activity reprocessing waste then produced in the UK. It was soon paralleled by similar studies overseas, particularly in the USA and France. International cooperation was very close.

DURABILITY OF FINGAL GLASSES

The preferred glass compositions were of borosilicate glasses made at 1050°C. They were optimized for a waste composition which consisted of 45.8% of fission product mixed oxides, 20% Fe_2O_3, 19% Al_2O_3, 13% U_3O_8, 1% MgO, 0.5% Cr_2O_3, and 0.4% NiO. The glasses were tolerant of variations in waste composition in the sense that mixes of a range of compositions around the selected optimum had durabilities almost the same as the optimum. This is extremely important from the practical plant operator's point of view and from the point of view of confidence analysis of storage and disposal schemes. The principal conclusions from this work[7] were as follows.

Leaching

There was virtually no difference in leaching at ambient temperatures by distilled water or seawater. The actual leach rates were of the same order as those of domestic glass ovenware.

Leached Species

The leachability of different atoms varied in the sequence $Na > Si > B > Cs > Sr \gg Ce > Tb$. In some cases strontium was rather more labile than cesium. This was generally consistent with the explanation that lower valencies and smaller ion sizes are more easily exchangeable with protons.

Radiation Effects

Gamma irradiations to a total dose of 10^{11} rads at ambient temperature had no discernable effect on FINGAL glasses. Earlier work with other glasses had shown that the effect of high doses of radiation upon all the glasses had generally been small.[8] In some cases irradiation improved leach resistance; in no case did it fall dramatically. Irradiations were of two kinds, γ irradiation adjacent to fresh spent fuel elements[9] and reactor irradiation using reactions such as B(n,α)Li reaction. The latter technique had taken doses up to 5.7×10^{11} rads or 3.3×10^{19} alphas/cm^3.

These latter levels of irradiation were comparable to about 10,000 years storage of Magnox-type waste, or 1,000 years of LWR-type waste. One effect was to reduce the discernable crystallinity of the glasses somewhat.

Heating Effects

For the FINGAL glasses the effects of heat treatments were widely studied. Long periods above ambient temperature might be expected to increase crystallinity and devitrification. In a waste fixation strategy based on vitrification, the "glass" will in fact remain at elevated temperatures for many years, particularly on the centerline of the proposed cylindrical vessels, due to the decay heat which must be released. This might be expected to produce a devitrified crystalline solid rather than a supercooled liquid. Various heat treatments were applied.

a. For borosilicate glasses, various annealing treatments for periods of up to 16 weeks at various temperatures in the range 950°C-400°C produced no effect on durability. Slow cooling treatments, for example, during 80 days from 1000°C to 200°C, produced either no change or up to a fivefold improvement in durability.[10]

b. For phosphate-based glasses, a deterioration of about a factor of 10 arose from several weeks heat treatment at 550°C (Ref. 9).

Combined Effects of Heat and Radiation

Radiation tends to cause disorder, heat treatment to cause order. In storage these trends conflict. A large series of empirical trials were carried out on borosilicate glasses irradiated at fixed temperatures between 350°C and 780°C to doses up to 10^{11} rads over a period of a year. Again there was very little effect on durability,[11] such small effects as were observed being generally related to the effect of heat alone.

Variation of Leach Factor with Time

The prediction of leaching or dissolution by groundwater over very long periods of time is very complex. Does the surface area change due to devitrification or fracture of massive glass blocks? Do ions migrate to the leach water through a silica-based network which dissolves only very slowly or does the network dissolve with the radioactive cations? What is the effect of dissolved ions and pH in groundwater, and if it is saturated with silicates does that protect the glass? What predictive models are best to be used in confidence analyses of the long-term future?

Work in the 1960s examined the leach rate variation with time. One clear conclusion[12] was that the rates fall from their initial values during the first 80 days (the duration of the experiments).

Volatilization

Storage at too high a temperature can lead to cesium volatilization to the inner upper walls of the steel container. If this is breached, the solubility of part of the total cesium load could be high. Experiments showed[12] that, provided the surface temperature did not exceed 400°C, the volatilization effect would be no greater than leaching of the bulk glass.

Physical Properties

Thermal conductivity[14] and interaction rates with steels at high temperatures were measured with sufficient accuracy for use in predictive modelling of safety and storage conditions.

RECENT STUDIES OF GLASSES

Eleven years after its production, one of the high-level waste blocks prepared in the FINGAL pilot plant was trepanned.[15] The glass block has apparently not fractured appreciably. The glass produced under industrial conditions and aged in storage had the same leach properties as an inactive freshly prepared material of the same chemical composition and has apparently not deteriorated.

The higher burnup of modern nuclear fuels gives rise to higher α-active transuranic element contents in fuel reprocessing wastes. The radiation dose involved has been modeled by incorporating ^{238}Pu in borosilicate glasses.[16] Those materials have so far accumulated the accelerated dose equivalent to $\gg$100,000 years storage of Magnox reactor waste, 100,000 years storage of AGR reactor waste, and 50,000 years storage of PWR reactor waste. In making this estimate, the essential assumptions were that vitrification occurs two years after fuel removal from the reactor; about 0.5% of the plutonium and 0.25% of the uranium goes to highly active waste. Fuel burnup reaches 3,500 MWd/T for Magnox, 18,000 MWd/T for AGR, and 33,000 MWd/T for PWR, and 12 wt.% of fission product elements are incorporated in the glass. There are no serious effects upon durability so far.

Lithium additions to replace half the sodium in borosilicate glasses reduce the formation temperature from 1050°C to 900°C. Glasses with some added lithium are currently favored in the UK. Leach rates of these better glasses are low,[17] ranging from about 5×10^{-5} g/cm^2 · d at 100°C to 10^{-7} g/cm^2 · d at 0°C.

UK STRATEGY FOR HIGHLY ACTIVE WASTES

After the success of FINGAL, the UK Highly Active Waste Vitrification Program was abandoned for about five years. Meanwhile British Nuclear Fuels Limited and the United Kingdom Atomic Energy Authority have relied quite safely on tank storage for fuel processing wastes.

The UK vitrification program began again in 1972 under the name of HARVEST. The chief differences from FINGAL are:

a. The scale. It was clear that with the expanded size of the reprocessing program and several years' liquid storage before vitrification the waste cylinder diameter should be increased from 25 to 45 or 60 cm. For very young wastes on a large scale, annular vessels are advantageous to dissipate heat, but this is in the future.

b. Waste composition. With higher fuel burnup (though still modest by LWR standards) the waste composition has changed partly because a more efficient uranium extraction is being achieved, and partly because Magnox can material is imperfectly separated from the fuel. A comparison follows:

	FINGAL, %	Current waste, %
Al_2O_3	19.2	20.0
MgO	0.8	24.8
Fe_2O_3	20.0	10.6
U_3O_8	13.3	0.2
NiO	0.4	1.4
Cr_2O_3	0.5	2.2
FPO_X	45.8	39.1
ZnO		1.7

c. Filter. The internal filter in the "next" cylinder of FINGAL was abandoned in favor of more conventional scrubbers.

An almost full-scale nonactive HARVEST pilot plant has been running at Harwell, using simulated waste, for the past three years. It makes about 1 ton per batch of glass. This is being used to investigate the chemical engineering parameters of the system: feed rates, evaporation carry-over, the depth of the working zone in which the glass forms, ruthenium behavior and the like. It is designed to study large annular vessels at a later stage of the program.

At Windscale, four HARVEST plants are in operation or are being considered, two active and two nonactive. A small-scale (5 kg) nonactive plant has been in operation for about a year as a prototype for a similar active plant which it is intended to commission in 1981. These will be followed by nonactive and active demonstration plants at full-scale to be commissioned in about 1983 and 1988 at Windscale. Although this latter plant will vitrify a worthwhile amount of waste, it will not be sufficient to deal with the anticipated waste projections. We will need in the late 1980s, using 50 cm vessels:

- Three operating lines to deal with anticipated Magnox arisings
- Two operating lines to catch up on the backlog
- Six operating lines for THORP, the new reprocessing plant due in the 1980s

An alternative strategy would be to adopt the French AVM technology. We also have longer term research programs on alternative vitrification technologies, all based on borosilicate systems.

DISPOSAL STRATEGY[18]

In the 1960s we designed long-term stores for construction in hard rock or above ground.[19] They were to be air-cooled but were not built. Most of the recent UK work is devoted to assessing the problems of hard-rock disposal, although disposal in clay is also considered. Salt disposal is not favored, largely because the salt deposits found in the UK are of industrial significance. Much of the disposal R&D is undertaken in very close conjunction with other countries of the European Economic Community.

Two possible schemes for a repository are of particular interest. The first conceives of bored blind holes below a system of galleries. The second conceives of raise-bored holes joining two galleries to form a pattern of vertical deposition holes. In the latter case the system could take relatively short-cooled waste and be air-cooled for a few decades (with surveillance) before backfilling and sealing the holes. For backfilling, the excavated granite mixed with a more absorbant clay material or magnesium oxide is preferred.

One of the critical parameters in repository design is the permissible rock temperature. Air cooling in early years can reduce the temperature which the repository must withstand. Once the repository is closed, whether it be early or late, heat dissipation by conduction is relatively poor. One area deserving more study is the effect of temperature upon rocks and the associated moisture in them, and the prediction of the host environment around emplaced waste in terms germane to the desired longevity of the waste.

Many of us feel, therefore, that air-cooled storage of vitrified waste for some decades is advisable whether it be in a separate store or a repository intended to be sealed off at a later stage. Others advocate water-cooled storage. Either will work well. The UK also favors research on the possibility of disposal of all levels of waste into the deep ocean floor.

CONFIDENCE ANALYSIS OF PROPOSED SYSTEMS

A preliminary assessment (albeit 75 pages long) of the health aspects of disposal into geological formations has been made by the National Radiological Protection Board.[20] The study included the effects of unlikely events such as meteoric impact, but the study particularly examined the effect of water entering the repository, leaching radionuclides out of the glass, and transporting them to a source of drinking water. This is the most significant potential route back to future man. The assumptions used were essentially:

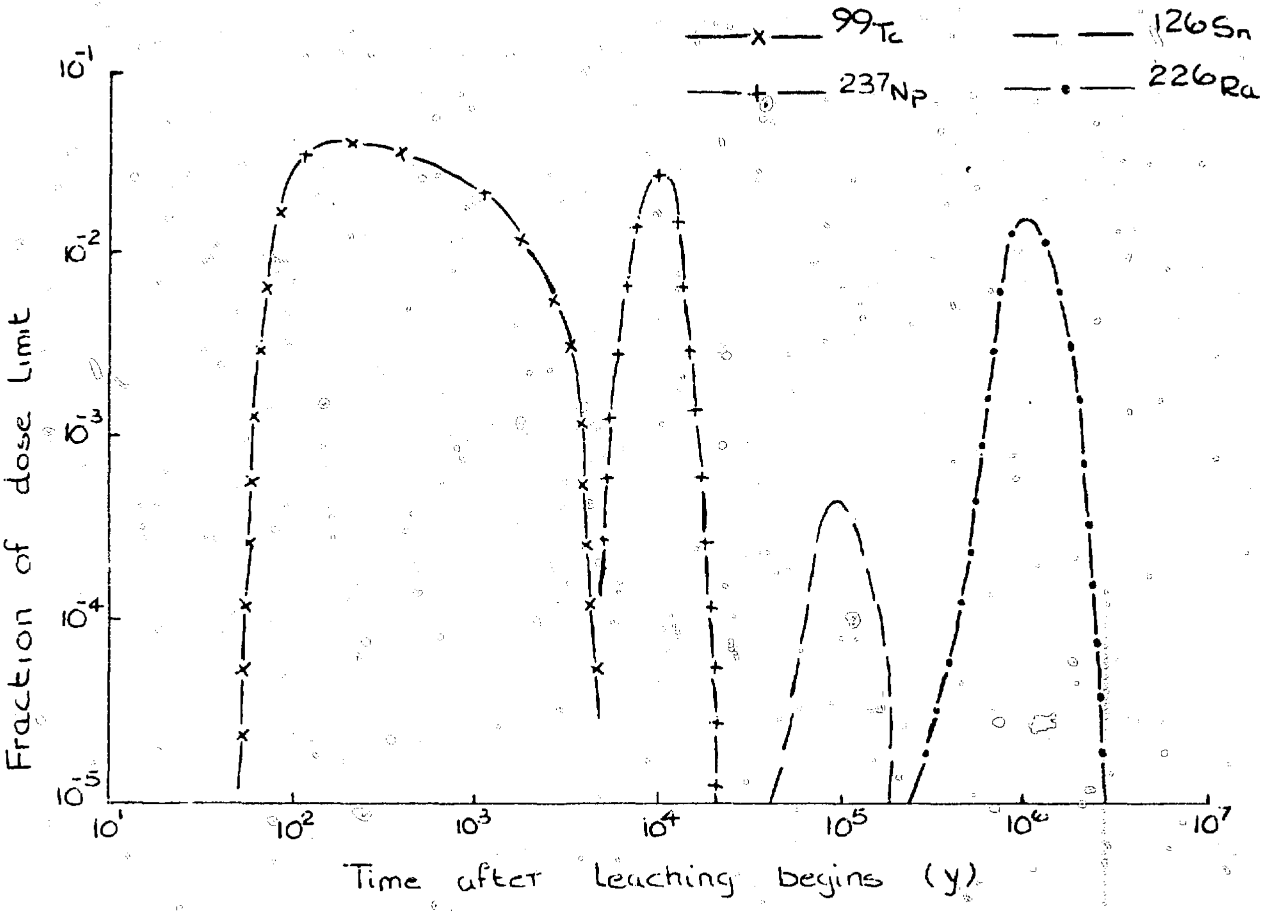

Fig. 2. Doses to individuals from drinking water.

- First groundwater ingress to glass begins after 1000 y
- Glass will be in lumps of average diameter 10 cm
- A leach rate of 10^{-5} g/cm^2 day
- The flow path is one-dimensional
- The path length is 10 km to potable water
- Groundwater velocity 0.3 m per day
- Dispersion coefficient 10 m^2 per day
- Surface stream 0.3 m^3/sec flow rate

The fractions of the maximum permissible level for radioactivity in drinking water for members of the public that result from these assumptions are given in Fig. 2. Interestingly, the critical isotope is ^{99}Tc because it is poorly absorbed on rocks. The radioactivity level of this isotope is particularly sensitive to the assumption that no leaching takes place for the first 1000 years.

An interesting point is that the toxic potential of the uranium (and daughters) in the granite over a 300-m deep repository is higher than that which the waste will have in 10,000 years' time. Thus any radiological hazard likely to arise from glaciation will be from the increased rate of uranium release from the granite.

Two isotopes that may require more careful management in the future are ^{129}I and ^{85}Kr. These are presently released to the environment at the nuclear fuel dissolution stage. If reprocessing increases worldwide, something more positive may have to be done next century. Iodine-129 has a very long half-life (1.6 x 10^7 years) and is difficult to fix permanently. Dilution seems to be the best ultimate solution in this case by localizing the isotope temporarily in concrete to ensure a slow release and to achieve a reasonably even dilution to negligible levels in the world's oceans. Krypton-85 has a half-life of 11 years and work is in progress to fix it into a metallic matrix by an ion bombardment technique.

INTERMEDIATE-LEVEL WASTES

Waste Types

Many other wastes besides the highly active fission product wastes arise in a fully developed civil nuclear power program. Figure 3 indicates both types of radioactive material which arise in the UK and our current policy on disposal form of the conditioned waste.

Low-Level Disposal

The UK disposes of low-level solidified waste, set in concrete or cement, to the deep ocean floor of the North

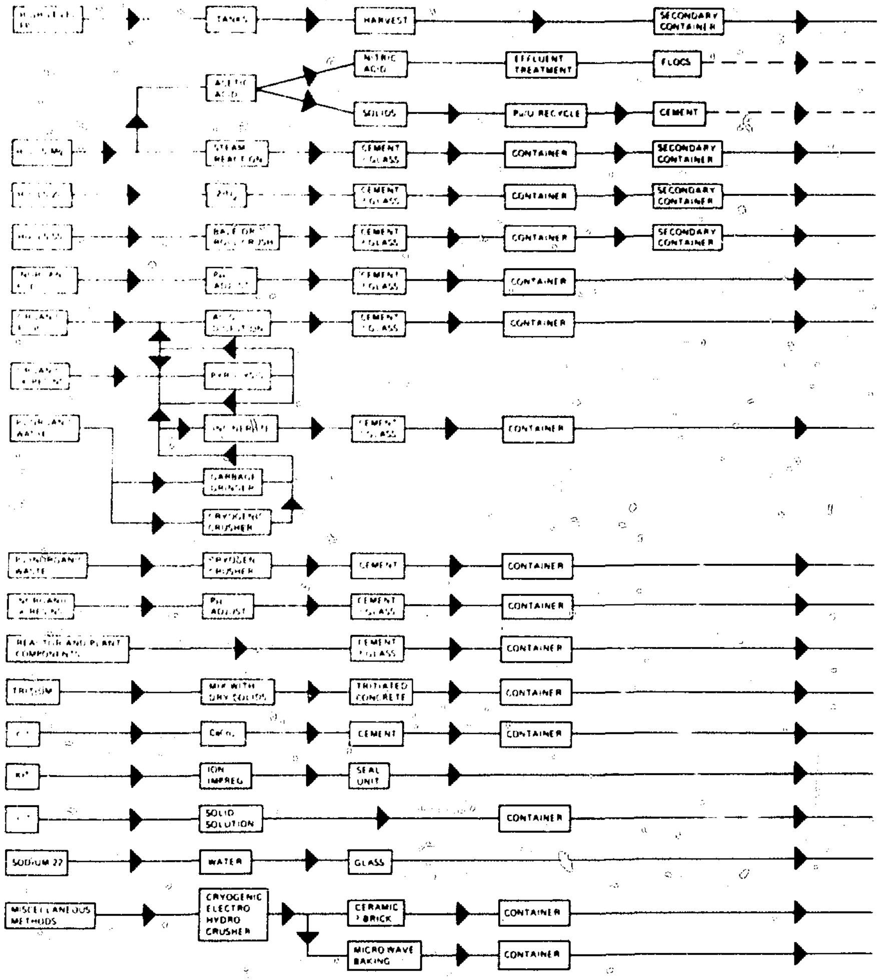
TANKS
HARVEST
SECONDARY CONTAINER
NITRIC ACID
EFFLUENT TREATMENT
FLOCS
ACETIC ACID
SOLIDS
Pu/U RECYCLE
CEMENT
STEAM REACTION
CEMENT /GLASS
CONTAINER
SECONDARY CONTAINER
CEMENT /GLASS
CONTAINER
SECONDARY CONTAINER
BALE OR ROLL CRUSH
CEMENT /GLASS
CONTAINER
SECONDARY CONTAINER
PH ADJUST
CEMENT /GLASS
CONTAINER
ACID DIGESTION
CEMENT /GLASS
CONTAINER
PYROLYSIS
INCINERATE
CEMENT /GLASS
CONTAINER
GARBAGE GRINDER
CRYOGENIC CRUSHER
WASTE
CRYOGEN CRUSHER
CEMENT
CONTAINER
PH ADJUST
CEMENT /GLASS
CONTAINER
REACTOR AND PLANT COMPONENTS
CEMENT /GLASS
CONTAINER
TRITIUM
MIX WITH DRY SOLIDS
TRITIATED CONCRETE
CONTAINER
CEMENT
CONTAINER
ION IMPREG
SEAL UNIT
SOLID SOLUTION
CONTAINER
SODIUM 22
WATER
GLASS
MISCELLANEOUS METHODS
CRYOGENIC ELECTRO HYDRO CRUSHER
CERAMIC / BRICK
CONTAINER
MICRO WAVE BAKING
CONTAINER

Fig. 3 Radioactive waste categorized by type.

Atlantic Ocean. This is done annually to the agreed package designs, package specifications, and radioactivity limits under the eyes of internationally appointed observers, and within a mile or two of an internationally specified spot. One of our development programs concerns the possible disposal of larger packages than our current 40-gallon drum packages. We think in terms of international freight container dimensions of an 8-ft cube. The 1-ft thickness of concrete containment is much more economically achieved on large packages. This appears to us to be a possible route also for disposal of low-level activity reactor components from dismantled nuclear reactors, but much will depend upon international political attitudes.

Plutonium Contaminated Wastes

Plutonium contaminated waste from reprocessing plants can also be converted to solid "conditioned" waste forms. In the UK, we have tried pyrolysis, acid digestion, and incineration of organic materials. The ashes produced from incineration can be leached to recover the low levels of plutonium present, and the ash can be converted to ceramic. For example, we know that:

a. Recovery of plutonium from ash is sharply reduced if the incineration temperature goes above 700°C.

b. Three and four valent metals, if present, reduce plutonium recovery.

c. Multiple leaching is more efficient than single leaching.

d. Hydrochloric acid leachant is more effective than nitric acid, but the latter is preferred for industrial plants.

e. Adding fluoride, as CaF_2, assists the release of plutonium.

f. 50 wt.% incinerator ash with 40% high-alumina cement and 10% clay, mixed with 40 vol.% water is cast, dried, and fired at 1000°C. The briquette is glazed and fired again at 1020°C.

g. The leach rate of plutonium through the glaze is excellent at 5×10^{-8} g/cm^2 day at 40°C. The leach rate of a sectioned briquette face is itself quite good at

Waste	Isotope/Half-life	Form	Bulk leachability (25°C) (g/cm²/day) (8)
HAW	Various (^{90}Sr/^{137}Cs)	Glass	10^{-6} (1)
ZrO_2 (+3% fuel)	Various (UO_2/PuO_2/FPs) (6)	Concrete/Glass	3×10^{-4} (2)
MgO (+3% fuel)	Various (UO_2/PuO_2/FPs) (6)	Concrete/Glass	3×10^{-4} (2)
Tritium	12y	PITC (4)/Polyacetylene/ZrH_2	1.7×10^{-4} 1.8×10^{-8}
^{14}C	5736y	$CaCO_3$ (concrete)	?
^{85}Kr	10.8y	Kr/Cu	5×10^{-4} (3)
^{129}I	1.6×10^7y	Solid solution	(5) ?
^{22}Na	2.6y	Glass (7)	10^{-6}

1. *Extrapolated value.*
2. Polymer-impregnated cement is x 10 better.
3. A worst-value; control of water pH in the environment improves the figure, more refractory metal improves the figure and the cost.
4. Polymer-impregnated tritiated concrete.
5. Prediction over such long periods very difficult.
6. ZrO_2 glass or cement will probably incorporate 3% UO_2 or PuO_2 by substitution solid solution. There should be less than 1%. Zirconium glasses tend to be rather high-melting.
7. Probably quite unnecessary.
8. Data are for pure water at room temperature, and imply continued leaching by a replenished water flow.

Fig. 4 Fixation media.

6×10^{-5} g/cm² day at 60°C. These briquettes themselves may be set in large blocks of cement for disposal.

Other Wastes

The UK has, at various stages of development, methods for the conditioning of *all* gaseous, liquid, or solid wastes to solids. This can be done if society requires it, though we do not recommend extremes which go far beyond the safety of other human activities. Our general specification is that such materials should be:

a. Chemically and biologically stable and resistant to heat and radiation
b. Insoluble
c. Massive
d. Of small volume
e. Involve no toxic dust hazard
f. Have no surface contamination which is easily disturbed
g. Non-inflammable and heat-resistant in fires
h. Free of criticality risk

Ceramics are the obvious candidates. The leach properties of these solids (Fig. 4) are generally sufficient to be comparable, in terms of environmental significance, to the more highly active, but more resistant, borosilicate glasses developed for FINGAL and HARVEST.

AREAS OF FUTURE RESEARCH

The areas which, in my judgment, would benefit from further study by ceramicists are:

a. The search for geologically stable solids whose properties meet the specifications above, but which can also be manufactured very reliably in a high-activity plant with no subsidiary effluents.

b. A good fixation medium for ^{129}I (half-life 1.6×10^7 years) which will probably be a solid solution ceramic form.

c. Understanding of chemical and physical effects of heat on geological materials likely to be encountered in repositories.

d. Better understanding of the chromatographic movement of each radioisotope species in geological media, and particularly the implication of nonlinear movement paths.

e. Better understanding of the leaching or dissolution mechanisms for glasses over very long periods of time in geological environments.

FOOTNOTE

My final conclusion is a personal judgment. I have no doubt that adequate management of radioactive waste has been possible for many years. No one in the UK has suffered any radiological injury from radioactive waste, ever. Their emplacement in respositories where they will do no harm is certainly possible. Adequate techniques already exist. The current standards of safety are already far higher than almost all other human industrial enterprises and, in particular, are higher than the standards of management of other nondecaying toxic materials of "infinite half-life." However, that is another subject.

Data pertinent to this paper were too extensive for inclusion. They will be included in the form of about 25 tables and figures in AERE R-9417 of the same title and authorship for those who need detail. I acknowledge gratefully the assistance of J. A. C. Marples.

REFERENCES

1. C. B. Amphlett, *Treatment and Disposal of Radioactive Wastes*, Pergamon Press, Oxford, p. 76, 1961.
2. C. B. Amphlett, Conversion of Highly Active Wastes to Solid Products, *Atomic Energy Waste*, Chapter 4.4, E. Glueckart (Ed.), Butterworth, London, p. 282, 1961.
3. C. B. Amphlett and D. T. Warren, *Fixation of Activity in Solid Form by Absorption of Soils – Part 1: Firing and Leaching Tests*, AERE-C/R-1686, 1956.
4. C. B. Amphlett and D. T. Warren, *Fixation of Activity in Solid Form by Absorption of Soils – Part 2: Final Report*, AERE-C/R-2202, 1957.
5. J. R. Grover and B. E. Chidley, *Glasses Suitable for the Long-Term Storage of Fission Products*, AERE-R3178, 1960.
6. K. D. B. Johnson, J. R. Grover, and W. H. Hardwick, Work in the UK on Fixation of Highly Radioactive Wastes in Glass, in *Third Geneva Conference on Peaceful Uses of Atomic Energy*, p. 188, 1965.
7. M. N. Elliot and D. B. Auty, *The Durability of FINGAL Glass, Part 1: Discussion of Method and Effect of Leaching Conditions*, AERE-R-5151, 1967.
8. M. N. Elliot, J. R. Grover, W. H. Hardwick, and A. D. Jones, *Fixation of Radioactive Wastes in Glass, Part II: The Experimental Evaluation of Phosphate and Borosilicate Glasses*, AERE-R-4098(Part II), 1962.
9. J. R. Grover and D. Walmsley, *The Durability of FINGAL Glass, Part 2: The Effect of Irradiation at Ambient Temperature*, AERE-R-5376, 1967.
10. J. R. Grover and D. Walmsley, *The Durability of FINGAL Glass, Part 3: The Effect of Heat Treatment*, AERE-R-5583, 1968.
11. J. R. Grover and D. Walmsley, *The Durability of FINGAL Glass, Part 4: The Effect of Irradiation at Elevated Temperatures*, AERE-R-5776, 1969.
12. J. R. Grover, Glasses for the Fixation of High-Level Radioactive Wastes, in *IAEA Symposium on Management of Radioactive Wastes from Reprocessing*, Paris, 1972.
13. D. Walmsley, B. A. Sammons, and J. R. Grover, *Volatility Studies of Glasses for the FINGAL Process*, AERE-R-5777, 1969.
14. D. B. Auty and J. R. Grover, *Thermal Conductivity of a Borosilicate Glass Suitable for Fission Product Wastes*, AERE-R-4685, 1964.
15. J. B. Morris et al., Durability of Vitrified Highly Active Waste from Nuclear Reprocessing, *Nature*, 273(5659): 215 (May 1978).
16. J. A. C. Marples, private communication, 1978.
17. K. A. Boult, J. T. Dalton, A. R. Hall, A. Hough and J. A. C. Marples, The Leaching of Radioactive Waste Storage Glasses, in Proceedings of *Ceramics in Nuclear Waste Management*, Cincinnati, CONF-790420, U. S. Department of Energy, Technical Information Center, Oak Ridge, 1979.
18. L. E. J. Roberts, Radioactive Waste Policy and Perspectives, *BNES Lecture*, London, 1978.
19. D. W. Clelland, A. D. W. Corbet and R. F. Coles, Design of a Plant for the Incorporation of Highly Active Wastes into Glass, in *AIChE Symposium*, New York, 1967.
20. M. D. Hill and P. D. Grimwood, *Preliminary Assessment of the Radiological Protection Aspects of Disposal of High-Level Waste in Geologic Formations*, NRPB-R69, 1978.

PRINCIPAL TRENDS OF INVESTIGATIONS CARRIED ON IN THE USSR ON INCORPORATION OF HIGHLY ACTIVE WASTES INTO GLASS AND CERAMIC TYPE MATERIALS

A. S. POLYAKOV
State Committee for the Utilization of Atomic Energy, Moscow, USSR

ABSTRACT

Studies in the USSR on incorporation of high level waste into glass and ceramic materials are described.

INVESTIGATIONS

Reprocessing one ton of spent fuel from APP results in 3 to 5 m^3 of highly active wastes which, after concentration by evaporation, may be reduced to one m^3 or less. In this state wastes must be transported to special sites for temporary storage and reprocessed to solids for safe burial for ages. The most documented and mastered technical solution of such reprocessing is solidification of highly active liquid waste with conversion to glass-like products in which radionuclides are bound in compounds of low solubility. Based on these principal propositions as well as on the solution of a problem of safe burial of solidified highly active wastes, a program of work has been developed by scientific research and development organizations in the Soviet Union engaged in solidification and burial of highly active wastes in geological formations.

In the USSR, investigations are being carried out and different materials are being developed suitable for the incorporation of highly active wastes. Along with phosphate and borosilicate glasses, glass-like materials with different contents of the most thermodynamically stable crystalline phases and major radionuclides included in these phases are being studied. In addition to this, research work is being carried out to produce ceramic compositions incorporating highly active wastes and to estimate the suitability of materials produced for long-term and safe storage under different conditions. Investigations are also being performed on the preparation of glass-like granules containing highly active wastes and their incorporation into metallic, ceramic-metal, and other solid compositions.

To solidify highly active wastes from reprocessing fast reactor fuel elements, study is made of basalt-like compositions having high chemical and thermal stabilities. Work associated with the search for optimum forms of solidified wastes involves the study of thermal, chemical, and irradiation stability of solid wastes of different types. It also involves the determination of phase separation and devitrification on storage, thermal conductivity and thermal expansion, homogeneity of wastes in the process of storage, variation of mechanical strength, and delocalization of radionuclides in the process of storage, on contact, or without contact of the solidified wastes with water. Special attention is paid to the influence of radiation emitters on the variation of properties of solidified wastes.

In the Soviet Union the following process is carefully checked using simulators. It is carried out in one unit --a ceramic direct electrical furnace. Concentrated highly active solutions with 50% phosphoric acid as a flux and 10 to 15% molasses as a reducing agent to retain ruthenium in a glass mass are fed directly to the surface of a melt in this furnace. In parallel with the above process borosilicate glasses are being developed. Compared to phosphate glasses the borosilicate glasses have a higher thermal endurance but require a higher temperature to carry out the process. The work is performed on an enlarged laboratory scale and in pilot plants using simulants. In addition to this, work is performed to improve corrosion resistance of structural furnace materials, to find materials for electrodes of higher corrosion resistance, to improve the furnace design and the remote filling of the containers with glass that are intended for burial. Some other problems associated with the remote control process are also studied. Vitrified wastes produced by plants are assumed to be temporarily stored in surface storage with arranged air cooling.

Pilot-plant work is planned to be carried out in two stages:

Stage 1—the process of natural waste solidification to produce phosphate glasses. This solution is dictated by milder temperature conditions under which the process is carried out and a more simple solution of a flux supply control.

Stage 2—the process of natural waste solidification to produce borosilicate glasses.

Apart from this, work is continued to study and master a two-stage process of vitrification of highly active wastes. At the first stage calcination is performed. At the second stage vitrification is accomplished which can substantially reduce the size of an electric melting furnace or permit the use of other methods of heating, in particular, induction heating required for high-temperature processes (1200°C and higher). This work is conducted on an enlarged laboratory plant scale and in pilot plants having a capacity up to 100 l/hr of feed solution.

So far as the safety of final burial of solidified active wastes is concerned, the lithosphere is most promising. Of particular interest are its regions of low permeability that permit the localization of wastes within a fixed contour. It is essential to investigate regions of this kind to determine the main conditions for underground burial of solidified wastes, i.e., mine-geological and mine-engineering problems should be studied. Apart from this, it is necessary to solve questions of the hydrogeology of possible geochemical and physicochemical transformations of various rocks under high pressure, high temperature, and a high radiation load on contact with highly active wastes. A number of questions arise associated with the development of a construction design for storage under various mine-geological and mine-engineering conditions for different types of wastes to be buried. These and a number of other problems that arise in connection with the underground burial of solidified highly active wastes in geological formations made it necessary to develop a complex program of scientific research and development work involving theoretical investigation and laboratory simulation of large-scale bench and field tests.

In summary this program can be reduced to the following:

- Development of criteria for estimating geological structures suited for burial of solidified active wastes in salt deposits, clays, and rocks.
- Study of mechanical, thermophysical, and filtration properties of a mountain mass intended for burial of solidified active wastes.
- Development of scientifically grounded requirements for properties of solidified wastes (specific activity, melting temperature, type of packing, etc.) and radiation load on underground storage of different designs for various types of accommodating rocks.
- Development of mine-technical bases for underground storage of solidified active wastes in different geological formations, reasonable schematics and designs of installations, and methods of their calculation and substantiation.
- Development of equipment and automated control systems at storage sites and areas in the region of waste burial.
- Development of sanitary, hygienic bases for arrangement of final burial of solidified active and alpha active wastes in deep geological formations.
- Study of the interaction between solidified wastes and different rocks at high temperatures and pressures and in the presence of humidity.
- Development of methodical bases of the conditions of stability of solidified wastes in the form of glass blocks and crystalline alloys in different geological formations.

Investigations are planned with the aim of finding accommodating rocks which, after melting with glass-like wastes (due to the heat resulting from radiation-induced decay), would form chemically stable materials that could be stored for many hundreds of years without any change. One must not neglect the chemical stability of wastes as a barrier to the pathway of radionuclide propagation as it is practically impossible to ensure absolute hydro-isolation for hundreds of years.

The main characteristic feature of the program is that it does not prefer a certain flow sheet for burial or its modification, since at present there is no basis for any choice to be made; neither is it possible to choose any geological formation (rock salt, clay, rocks). For shipping wastes to possible sites of burial into geological formations, designs are being developed of shipping containers for solidified wastes.

II. WASTE FORM STABILITY AND CHARACTERIZATION

THE INFLUENCE OF SYSTEM CONSIDERATIONS ON WASTE FORM DESIGN

A. A. BAUER, S. C. MATTHEWS, and R. W. PETERSON
Battelle's Project Management Division, Office of Nuclear Waste Isolation, Columbus, Ohio

ABSTRACT

The design of waste forms is constrained by waste management system considerations imposed during generation, treatment, packaging, transportation, storage, and isolation. In the isolation phase, the waste form provides one of the barriers to release in a multibarrier system that includes the natural geologic and hydrologic barriers as well as other engineered barriers.

INTRODUCTION

The objective of the U.S. Waste Management Program is the disposal of radioactive waste in a manner that provides an acceptable risk to man. Often it is overlooked that this includes current as well as future generations and operational personnel as well as the general public. Consequently, in evaluating the risk to man one must consider the total system which encompasses the generation, transportation, treatment, packaging, storage, and, finally, isolation of the waste. Since various options exist for each of these elements, the risk will be determined by the particular path selected to define the system. Cost, while of secondary importance, exhibits the same dependence.

From the viewpoint of waste form design, the system objective is to produce the form, place it in a canister, transport it to a storage or disposal site, and there emplace it for isolation. There are specific functional steps which must be taken to meet this objective, and each step may impact and constrain the waste form design in some manner. Nevertheless, it must be recognized that the method selected for ultimate disposal and isolation entails several unique and dominating considerations. First, as a result of the hazards associated with the waste and the persistence of these hazards over extended periods of time, virtually all isolation concepts, including geologic, rely on nature for assistance. Consequently, isolation options largely deal with existing natural systems, and the constraints imposed by these systems are generally fixed and unchangeable by man. Second, and as a corollary to the first consideration, the isolation element is a complex subsystem of the waste management system with which it must interact. Since the isolation element is primarily natural, the basic problem becomes one of determining if requirements imposed by the remainder of the system match the isolation requirements. Thus the preisolation part of the waste management system must accommodate constraints imposed by the isolation element of the system. That is not to say, however, that the limiting constraint may not occur at some point in the system other than isolation.

The isolation element, as noted above, is a complex subsystem that includes the repository set in a system of geologic, geochemical, and hydrologic barriers to inhibit or prevent release of radionuclides to the biosphere. While it appears probable that the selection of a repository site will require that the natural barriers alone exhibit the potential for accomplishing the waste isolation function, these natural barriers will be supplemented by engineered barriers. The choice of these engineered barriers, one of which is waste form, is widely recognized as being site dependent, tailored to the needs of the disposal system, and acting, if required, to overcome potential deficiencies inherent in a particular geosystem.

WASTE MANAGEMENT SYSTEM

The basic elements of the waste management system are illustrated in Fig. 1. The waste, following generation at

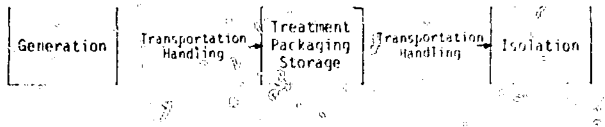

Fig. 1 Schematic of waste management system.

either a reactor or fuel processing plant, is packaged and then emplaced in a repository, either retrievably or permanently. This involves transportation to and handling at various facilities in the system. Optional operations in the system are treatment, either for resource recovery or to produce a more stable waste form, and storage, either prior to or following treatment.[1]

At each step in the system there is a potential environmental impact, and associated cost, that is a function of the particular waste form. Conversely, each step involves operations that may impose requirements on the waste form design. Since there are a number of paths by which the ultimate goal of isolation may be reached, the overall system impact, in terms of risk and cost, is the sum from all the steps over the particular path chosen.

This is illustrated by the relationships shown in Fig. 2. Thus at each step there is a change either in the form of the waste, its position, or environment from W_i to W_{i+1} requiring an input, P_i, and with a resultant environmental impact, E_i, and cost, C_i. The environmental impact and cost for each step are functions of the input waste characteristic, with cost further dependent on the operational requirements associated with the particular step.

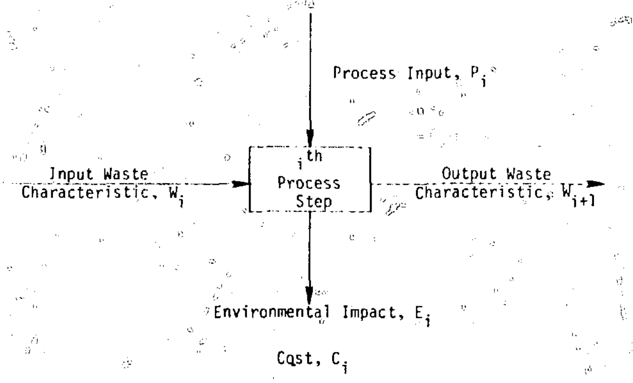
Process Input, P_i
Input Waste Characteristic, W_i
i^{th} Process Step
Output Waste Characteristic, W_{i+1}
Environmental Impact, E_i
Cost, C_i

$$W_{i+1} = f_i\ (W_i)$$

$$E_i = g_i\ (W_i)$$

$$C_i = h_i\ (W_i, P_i)$$

$$\text{Total System Environment Impact, } E = \sum_{i=1}^{n} g_i\ (W_i)$$

$$\text{Total Economic Cost, } C = \sum_{i=1}^{n} h_i\ (W_i, P_i)$$

Fig. 2 System impact and cost relationship to processing step options.

WASTE SOURCES

Waste form design begins with definition of the generated waste that must be considered for disposal. Current policy calls for the indefinite deferral of reprocessing spent fuel from commercial reactors. Under this policy, the major types of waste that must be considered in the waste management system are:

- Commercial waste
  - LWR spent fuel
- Defense waste
  - High-level waste
  - Low- and intermediate-level TRU waste

Other wastes that must be considered for disposal include HTGR and FBR fuel and wastes from decommissioning and decontaminating operations.

In the event a policy change occurs and commercial fuels are reprocessed, the following types of commercial wastes will be generated:

- High-level waste
- Low- and intermediate-level TRU waste
- Cladding waste
- Gaseous fission products

The TRU wastes can be generally characterized as transuranic-contaminated trash and process waste. The cladding waste includes the fuel rod cladding and assembly hardware -- grids, channels and end fittings.

Current programming is aimed at providing the required capability for the disposal of spent fuel while at the same time proceeding with the technology development required for disposal of waste from reprocessed fuel in the event reprocessing policy is changed. Consequently, waste form development is proceeding in response to the characteristics of all the waste types mentioned above.

DESIGN CHARACTERISTICS

The objective of waste form design is to produce a combination of characteristics that, in combination with other elements of the waste management system, satisfy the objective of waste isolation at an acceptable level of risk to man. A number of characteristics are important for this purpose, although their level of significance may vary at different stages in the waste management system.

Perhaps the most pervasive characteristics with respect to the system are the waste composition (fissile and fission-product concentration) and the resultant waste form heat content and radiation level. The fissile composition and concentration will determine criticality control, while radiation levels due to the fission products will dictate essential shielding requirements at various points in the system. The heat content may have to be tailored, in combination with the design of the waste container and repository spacing, to provide repository thermal loadings that are compatible with the thermophysical properties of specific geologic media. Such temperature-dependent characteristics as leachability, volatility, thermal stability, and compatibility are also influenced by heat content and waste form conductivity.

Radiation stability and leachability are of particular importance in the isolation phase as are waste–rock and waste–container compatibility. However, possible waste–container reactions at the treatment/packaging stage also require evaluation.

Characteristics such as combustibility, dispersibility, and volatility assume particular importance during transportation and handling because of the potential for accidents and the necessity to consider fire in connection with them. Volatility is also a consideration during waste processing because of the potential for loss of radioactive species from the waste.

WASTE FORMS

A wide variety of waste forms are being developed and evaluated for potential use. A number of these are shown in Table I along with an indication of their relative advantages and disadvantages. This listing should not be considered as complete.

In general, specific waste forms are considered for specific waste types, although there is considerable overlap. The trend is to place the more radioactive waste in the more stable waste forms. Thus, high-level waste forms include glasses, ceramics, cermets, coated particles, and synthetic minerals. In the case of defense high-level wastes, because of their lower specific activity level as compared with commercial high-level waste, principal emphasis is on glass as a waste form.

At the other end of the activity scale, cement is the principal waste form receiving consideration, along with bitumen, for the immobilization of low-level transuranic wastes. Both glasses and cement are considered in connection with intermediate-level TRU waste.

A major point to be made in presenting Table I is that, while each waste form exhibits certain advantages, there are also notable disadvantages. For some of the forms, the disadvantages may not be readily apparent because of an inadequate data base. It is quite normal for the advantages to be emphasized by early research, while problems are discovered only as a result of detailed study. Also, depending upon the system in which the waste is employed, some of the advantages and disadvantages may lose weight or significance. These require evaluation within the context of a specific system.

SYSTEM CONSIDERATIONS

Generation

The waste form characteristics are subject to constraints imposed by the waste history. This is particularly true of spent fuel and high-level waste where the heat content and radiation level are functions of operating parameters and the decay period. Operating parameters of importance are specific power of operation and fuel burnup. Increases in either of these parameters will lead to a relative increase in heat content and radiation level for any specific period of decay, with burnup playing a dominant role.[2] In this connection it might be noted that high-level defense waste exhibits a significantly lower heat content and radiation level than would waste from commercially reprocessed LWR fuel because of the difference in operating parameters.

Additional constraints may arise as a result of changing fuel-cycle considerations. Current waste form concepts assume the disposal of either spent fuel or of uranium–plutonium fuel-cycle generated reprocessing waste. However, the thorium–uranium cycle is one of the options being examined in the INFCE studies. Changes in fission product spectrum have a relatively minor effect on near-term heat generation and radiation levels. The major effect of a change in fuel cycle will be seen in the actinide content of the waste. Although effects related to actinide content are expected to be minor,[3] their influence on waste form design and long-term waste performance will require evaluation.

Treatment and Packaging

An important consideration in waste form selection at the waste treatment stage is the effluent and by-product waste stream associated with the particular waste treatment process. A criterion of any treatment is that the impact due to processing not result in a greater risk to the public than if the waste were left untreated. From a practical viewpoint it is desirable that the processing not result in large volumes and a great variety of by-product waste because of the added cost and complexity that would result to the waste management system.

In general, processing technologies that employ low temperatures are preferable to those involving elevated temperatures. Simpler processes also are preferable for adaptation to remote operation and for increased reliability. Elevated temperature operations generally impose more stringent materials equipment requirements and result in higher energy costs and the need for increased maintenance. In addition, volatilization of several radioactive species becomes increasingly probable as the processing temperature is increased. Species subject to potential volatilization include cesium, iodine, and ruthenium in the case of fuel waste, and tritium in the case of cladding waste. Ruthenium and iodine may be evolved during calcination, a preliminary step for most waste forms derived from fuel.

In those cases where treatment and packaging operations are combined, the potential for waste–container reactions must be considered. In-can melting of glass[4] and in-can solidification of cement are operations that require controls to limit such reactions.

TABLE I

Waste Form Considerations

Waste type	Waste form	Advantages	Disadvantages
Spent fuel	Assembly + He	Simplicity Leak testing	No added barrier
	Assembly + Pb	Mechanical support Criticality control Corrosion barrier	Resource use Toxicity
	Chemical dissolution and resolidification	Waste form control Potential volume reduction Loading flexibility	Cladding breached Added waste streams Cost Loss of identification
HLW	Calcine	Simple processing High waste loading	Low leach resistance Ease of dispersibility Low thermal conductivity
	Borosilicate glass	Well developed technology Moderate waste loading Improved leach resistance	Thermal instability High-temperature processing
	Phosphate glass	Increased solubility for some waste constituents	Highly corrosive melt Decreased thermal stability High-temperature processing
	Glass ceramics	Improved thermal stability Thermal shock resistant Improved leach resistance	More complex processing Cost High-temperature processing
	Supercalcine	Increased thermal stability High waste loading	More complex processing Uncertain radiation stability High-temperature processing
	Synthetic mineral	Potentially excellent leach resistance Increased thermal stability	High-temperature processing Reduced waste loading Cost
	Coated particles	Excellent leach resistance Added barrier	Complex processing Reduced waste loading Cost
	Metal matrix	High thermal conductivity High waste loading Good impact resistance	Complex processing Cost
Cladding waste	As is	Simplicity	Leachable Fines ignitable Maximum volume
	Compaction	Simple processing Reduced volume	Leachable Presorting may be necessary
	Melting	Reduced volume Leach resistant Possible Zr recycle	Complex processing Tritium release
	Glass matrix	Combine with HLW or ILW Reduce leachability	Complex processing
TRU*	Solid, as is	Simplicity Low dose rate	Large volume Combustible Dispersible Leachable Chemical instability
	Incineration	Chemically stable Reduced volume	Secondary waste streams Dispersible Radionuclide concentration

(Table continues on the next page.)

TABLE 1 (Continued)

Waste type	Waste form	Advantages	Disadvantages
	Cement immobilization	Simple processing Provides shielding	Thermal dewatering Radiolytic gas evolution
	Bitumen immobilization	Improved leach resistance	Fire processing risk Radiolytic decomposition
	Glass and slag	Improved leach resistance Radiation stability	High-temperature processing

In general, it is considered desirable to reduce the volume of waste that must be handled. However, the increased specific activity and heat content associated with the more concentrated waste form may have undesirable side effects from the viewpoint of shielding and heat dissipation requirements. If the waste form is subject to decomposition, concentrating the waste increases the amount of gas generated per unit volume of waste, increasing any container or repository pressurization problems. Volume reduction may also change the waste category. Consequently, volume reduction must be evaluated by considering its impact at a number of points in the total system.

Transportation and Handling

The current focus of state and local officials and the public in general is on the perceived hazards associated with transportation of radioactive materials.[5] A burden is therefore placed on both the waste form and the transportation equipment designers to respond to this concern.

Studies of accident reports show that container-vehicle systems must withstand severe vibration, impact, piercing, and dynamic crushing and shearing loads along with severe fire and water immersion conditions either separately or in various sequential orders. To maintain containment integrity the transportation system designer requires a dry, stable, noncombustible solid waste form in a container that will withstand shock, vibration, and impact loads and exposure to a wide range of temperatures without decomposing, burning, generating internal pressure, or releasing any gases, particularly explosive or flammable gases. While it is quite possible that a safe transportation system could be provided for waste forms that do not have the above desirable characteristics, the design complexity, licensing, construction, and operational problems might become prohibitive.

These same considerations apply to handling operations at the various facilities where the possibility of accidents, which could lead to personnel exposure and facility contamination, dictates the desirability of a waste form that is noncombustible, nondispersible, nonvolatile, and thermally stable.

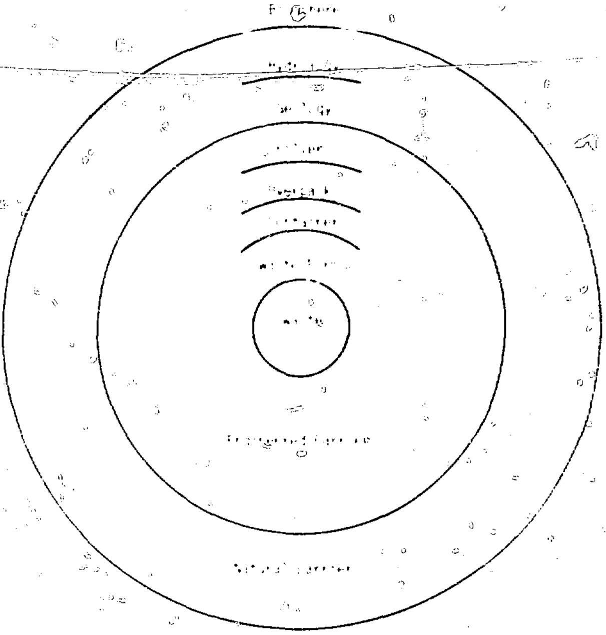

Fig. 3 Schematic of isolation system.

Isolation

Isolation of nuclear waste from the biosphere will be provided by a system of engineered and natural barriers that are judged to be required to achieve that objective. This multibarrier concept is illustrated in Fig. 3. As shown, the waste form is one element that might be designated to form an engineered barrier system.

In such a system, an important concern in selecting barriers is that they be compatible, i.e., one barrier does not have a detrimental effect on the performance of another. Thus it is desirable that the waste form have a low solubility in water, a low leach rate, and be stable both thermally and with respect to irradiation. As noted in the introduction, however, the natural barrier system will be expected to provide the primary line of defense in isolating the waste. Consequently, it is imperative that the waste form not impair this function. Thus, the waste form should not include additives that might adversely affect the absorption characteristics of the host geologic medium.

Also, excessive thermal loadings that could damage the mechanical integrity of the repository must be avoided. Similarly, the effect of temperature on waste rock container interactions and on filler material functions must be evaluated both in design of the waste form and in selection of these other barrier materials. These considerations will vary significantly with change in the geologic medium selected for isolation. Therefore, a careful tailoring of waste form to the specific geologic host and any contained liquid, as well as a matching of the engineered barriers to optimize their performance, is necessary in order to optimize the waste isolation system.

SUMMARY

The IRG report to the President states "a systems approach should be used to select the geologic environment, repository site, and waste form. A systems approach recognizes that, over a thousand years, the fate of the radionuclides in a repository will be determined by the natural geologic environment, the physical and chemical properties of the medium chosen for waste emplacement, the waste form itself, and other engineered barriers. If carefully selected, these factors can and should provide multiple, and to some extent independent, natural and engineered barriers to the release of radionuclides to the biosphere." While this passage provides an adequate statement of the benefits to be realized from application of the system approach to the isolation system, it does not speak to the equally important need to extend the systems approach to the complete waste management system. There are multiple paths that can be followed in the waste management system. The waste form must be responsive to constraints introduced at various points along these paths in order to arrive at the final goal of nuclear waste disposal in a manner that provides an acceptable risk to man, both today and in the future.

REFERENCES

1. *Alternatives for Managing Wastes from Reactors and Post-Fission Operations in the LWR Fuel Cycle,* U. S. Energy Research and Development Administration, ERDA-76-43, Volumes 1–5, May 1976.
2. R. T. Anderson et al., *Current Status and Future Considerations for a Transportation System for Spent Fuel and Radioactive Waste,* Y/OWI-77/42513, Office of Waste Isolation, Columbus, February 1978.
3. T. H. Pigford, Fuel Cycle Alternatives for Nuclear Power Reactors, *Ind. Eng. Chem. Fundam.*, 16(1) 75 (1977).
4. J. E. Mendel, *The Storage and Disposal of Radioactive Waste as Glass in Canisters,* PNL-2764, Pacific Northwest Laboratory, Richland, December 1978.
5. Nuclear Transportation Pullout, *Critical Mass Journal,* p. 5, January 1979.

THE IAEA COORDINATED RESEARCH PROGRAM ON THE EVALUATION OF SOLIDIFIED HIGH-LEVEL RADIOACTIVE WASTE PRODUCTS

J. R. GROVER* and K. J. SCHNEIDER
International Atomic Energy Agency, Vienna, Austria

ABSTRACT

A coordinated research program on the evaluation of solidified high level radioactive waste products has been active with the IAEA since 1976. The program's objectives are to integrate research and to provide a data bank on an international basis in this subject area. Results and considerations to date are presented.

INTRODUCTION

The long-term management of the high-level wastes from the reprocessing of irradiated nuclear fuel is receiving world-wide attention. While the majority of the aqueous high-level waste solutions from the reprocessing of commercial fuels are currently being stored in stainless steel tanks, increasing effort is being devoted to the development of the technology for the conversion of these wastes into stable solids. In October 1977, the International Atomic Energy Agency (IAEA, or the Agency) issued a technical report[1] which surveyed the international state of the art of the many solidification processes being developed.

Many solidified product† forms are being investigated. Because of the long half-lives of some of the radioactive isotopes, it is essential that the solidified products have certain desirable properties initially and that they retain desirable properties for the necessary periods of time (in the order of centuries or perhaps longer). If there are major undesirable changes in these properties with time, they must be understood and shown not to lead to a premature deterioration of the solid product.

This development work on solidified waste forms is taking place in many laboratories around the world. The IAEA's program and budget provide for the placing of research contracts or agreements with laboratories, research centers, and other institutions in member states on problems of direct interest to the Agency's work.[2] In 1976, the Agency initiated a coordinated research program to bring together the workers in these laboratories to analyze and compare their results and, where possible, to coordinate future plans and actions in this field. The overall objective of the program is to integrate research and prepare a comprehensive data bank of the solidified products of interest together with their properties. This will provide important background information necessary for the future preparation by the Agency of codes of practice and standards for the management of high-level wastes.

Participation in the program was invited from the following countries and institutes: Canada, Federal Republic of Germany (Karlsruhe and Hahn-Meitner-Institute), France (Marcoule), India, Japan, Sweden, UK (Harwell), USA (Battelle, Pacific Northwest Laboratories), Eurochemic, Commission of European Communities (observer), and Nuclear Energy Agency (observer).

The first meeting of the representatives from the various institutes was held at the Battelle Memorial Institute, Pacific Northwest Laboratories, Richland, Washington, USA, from June 20–24, 1977. All aspects of possible solid waste forms and their properties were discussed. The information presented at that meeting was compiled by J. R. Grover into an IAEA technical report which was recently published by the Agency.[3]

---

*Present address: Atomic Energy Research Establishment, Harwell, Oxon, UK.

†In this report, a solidified product is defined as the final solid form of the waste ready for disposal (e.g., glass, ceramic, etc.).

Further meetings of the participants in this program will be held periodically to exchange current information to attempt to compare results from standardized test procedures. An updated technical report may be issued as the program progresses.

The rest of this paper summarizes the information derived from that program to date and indicates the future trends in the overall coordinated research program. In general, the format in the existing IAEA technical report[3] is followed.

BACKGROUND

The desirable properties and factors to be assessed in the choice of a solidified waste product are considered individually. The time scale of interest for the waste forms is divided into five general periods:

1. During the manufacturing process of the solid waste product and transfer to storage; at this time the effects due to high temperatures from self-heating will be at their greatest.
2. During the first ten years or so of interim storage; during this period, about 90% of the fission products will decay and maximum temperatures will drop significantly, but stability at high temperature will still be essential.
3. From about 10 to 100 years; during this time the solid wastes will cool somewhat and the accumulated radiation dose will build up; stability to radiation and in the storage disposal environment becomes important; resistance to high temperature is still important.
4. From about 100 to 1000 years; during this period, most of the remaining fission products will decay, further effects from high temperatures and from beta and gamma radiation will become insignificant, but chemical and mechanical stability will remain important.
5. From about 1000 to 100,000 years; during this period, the waste should be stable to the important amount of integrated alpha decay and to chemical degradation in order to minimize releases of wastes to the environment.

TYPES AND COMPOSITIONS OF WASTE PRODUCTS

There are three generic considerations in this field. First, the wide variety of aqueous waste compositions are examined together with the influence of the various constituents that can affect the choice of final solid waste form. Second, the various types of solid waste forms are examined with illustrations of the range of compositions. These alternative solid waste forms include calcines, glasses (e.g., phosphate and borosilicate systems), glass–ceramics, ceramics, supercalcines, coated particles, metal matrix forms, and other miscellaneous forms. The data from the coordinated research program include an appendix with the detailed compositions of the currently preferred forms from some of the laboratories. Third, the flexibility of the various waste forms for incorporating different waste compositions is considered.

PHYSICAL STATE OF THE PRODUCTS AND THERMAL EFFECTS

After reviewing the physical state of the various groups of products, the phenomenon of phase separation is considered, particularly during the initial formation of the product. The long-term stability to thermal effects is examined, specifically with respect to glasses and their potential for crystallization and devitrification as the glasses cool.

PHYSICAL AND MECHANICAL PROPERTIES

Many physical and mechanical properties of the products must be measured in order to understand and control the production process of the final waste form and to define preferred conditions for storage and disposal.

During the actual production of the final waste form, it is necessary to know the influence of the composition of the product and the additives to be used on the formation temperature. It is also necessary to understand the effect of temperature on viscosity, particularly in those processes in which glass is poured into a final container. Selected typical viscosity values have been collected, together with techniques for measurement.

A knowledge of electrical conductivity is required for the design and operation of Joule-heated melters. This is very temperature dependent and can also be influenced by the chemical composition. Density, thermal conductivity, and thermal expansion coefficient are all important in defining container and storage conditions, and typical values are given in the report.

In general, physical property measurements are comparatively easy to make and present few surprises. However, the measurement of mechanical properties is difficult to carry out due to the nature of many of the products. Attempts have been made to study both the impact behavior and thermal fracture behavior of containers of glass and to develop a crack test. While such tests give relative information for a series of products, no one has produced a satisfactory method of interpreting the results relative to the actual conditions that may prevail in practice. Homogeneity is another important property for which no routine test is currently available. In the majority of processes it is not clear what action could be taken if inhomogeneity is suspected or found.

RELEASE OF RADIOACTIVITY

This work is devoted primarily to leaching by water, which represents the main mechanism whereby radioactivity can be released to the environment over long periods of time. The techniques for the measurement of leach rate are considered in the program. The current leach tests employed in member states are described together with the proposed IAEA test[4] published in 1971 and the ISO draft standard leach tests[5,6] proposed in 1977, which are based on the earlier IAEA tests mentioned above but take into account the working experience and shortcomings of the IAEA test. It is hoped that the final ISO test procedures might become the accepted world standard leach tests to enable leach results to be comparable between organizations.

Currently, the comparison of leach results obtained by different groups of workers must be done with caution. However, the program reviews the leaching studies carried out and has summarized the mechanism of leaching.

Finally, the release of radioactive materials by volatilization is considered. This effect requires consideration only if temperatures rise to above approximately 400°C.

EFFECTS OF RADIATION

Solidified waste products will be subjected to intense alpha, beta, and gamma radiation as well as to lesser amounts of neutron radiation. In addition, the radioactive isotopes will decay to different stable elements, in many cases with a change in chemical valence. The program concentrates on the study of the effect of alpha radiation and ways of simulating and accelerating the effects by incorporating up to 5 wt.% of actinide elements. Possible deleterious effects that the alpha decay might cause include volume changes, an accumulation of stored energy which could be spontaneously released later (giving a significant temperature rise), helium generation, increases in leach rate, and cracking of the solid waste form. Each effect is considered in turn. Measurements of the effects of beta and gamma radiation are also considered and summarized in the program. Tests of the effects of radiation take into account a draft standard test being developed by ISO.[7]

FUTURE CONSIDERATIONS OF THE COORDINATED RESEARCH PROGRAM

The IAEA's coordinated research program will continue to study those aspects described above as well as some new ones. The future activities will generally lie in the following areas:

1. Regular exchanges of results between participants, with further compilations of data into one or more technical reports.
2. The use of the ISO standard leach test universally so that leach results are more comparable between different laboratories. More recently, the ISO is now considering a draft Soxhlet test for accelerated leach rate measurements.
3. The development of suitable tests for mechanical strength and homogeneity of solid waste forms.
4. The use of round robin tests for intercomparisons of samples.
5. The preparation and evaluation of fully radioactive samples and their comparison with nonradioactive simulated samples.
6. The development of means of evaluating and predicting the long-term stability of solid waste products from accelerated tests.
7. The development of tests to simulate more accurately the possible conditions in different disposal environments.

It is believed that IAEA's Coordinated Research Program has contributed significantly to the worldwide dissemination of technology regarding evaluation of high-level waste forms. It is expected that the program will continue that function in the future as well as coordinate the related developments on an international basis.

REFERENCES

1. *Techniques for the Solidification of High-Level Wastes,* IAEA Technical Reports Series, No. 176, Vienna, Austria, 1977.
2. *Coordinated Research Programs on the Management of Radioactive Wastes,* IAEA Bulletin, Vol. 19 (2), p.7, April 1977.
3. *Characteristics of Solidified High-Level Waste Products,* IAEA Technical Reports Series, No. 187 (1979).
4. IAEA Leach Test, *Atomic Energy Review,* 9(1): 195(1971).
5. Draft ISO Leach Test, ISO/TC 85/SC 5/WG 5–N37 (1979).
6. Draft ISO Leach Test, ISO/TC 85/SC 5/WG 5–N38 (1979).
7. Draft Irradiation Stability Test, ISO/TC 85/SC 5/WG 5–N39 (1979).

DEVELOPMENT OF COMPREHENSIVE WASTE ACCEPTANCE CRITERIA FOR COMMERCIAL NUCLEAR WASTE

F. A. O'HARA, N. E. MILLER, B. S. AUSMUS, K. R. YATES, J. L. MEANS, R. N. CHRISTENSEN,*
and F. A. KULACKI*
Battelle Columbus Laboratories, 505 King Avenue, Columbus, Ohio

ABSTRACT

A detailed methodology is presented for the identification of the characteristics of commercial nuclear waste which may require criteria. This methodology is analyzed as a six-step process which begins with identification of waste operations and proceeds until the waste characteristics affecting the potential release of radionuclides are determined. All waste types and operations were analyzed using the methodology presented. Several illustrative examples are included. It is found that thirty-three characteristics can be identified as possibly requiring criteria.

INTRODUCTION

Waste management planning has as its objective "to provide assurances that existing and future nuclear waste from military and civilian activities (including discarded spent fuel from the once-through nuclear power cycle) can be isolated from the biosphere and poses no significant threat to public health and safety."[1] Waste management criteria are useful in obtaining this objective. These criteria comprise a hierarchy of criteria, consisting of system, performance, acceptance, and design criteria. This hierarchy describes a sequential response by which the waste management system meets the waste management objectives.[2]

The waste acceptance criteria, as a subset of the criteria hierarchy, are the limits on "the measurable indicators of the waste package performance for acceptability in the waste management system."[2] These acceptance criteria serve as a means of assuring that the wastes are prepared, treated, transported to the repository, and disposed of in a geologic formation in such a manner that the risk to workers and the general public will be minimized before and after placement in the disposal medium. The waste acceptance criteria will generally be determined by the most restrictive of the waste management operations. Two steps underlie the development of all waste acceptance criteria. They are the definition of the characteristics of the waste which may require criteria and the definition of the limits to be placed on these characteristics. This paper presents in a detailed fashion the methodology involved in the first step of the development of waste acceptance criteria. Examples are given to illustrate the methodology.

Methodology

The methodology for the identification of the waste characteristics which may require criteria is a six-step process. In general, each step of the process is aimed at either a qualitative or quantitative delineation of properties, characteristics, or transport mechanisms associated with a given waste type in one or more waste management operations. These steps are:

1. Identify the operations of the waste management system.
2. Identify the waste types to be considered.
3. Identify potential release mechanisms.
4. Determine radiation release scenarios/paths.
5. Determine rate-limiting step for radiation transport.
6. Determine waste characteristics that influence the release mechanism.

These steps are explained and expanded in the following sections. Examples are presented which illustrate steps 4, 5, and 6.

---

*Department of Mechanical and Nuclear Engineering, The Ohio State University, Columbus, Ohio.

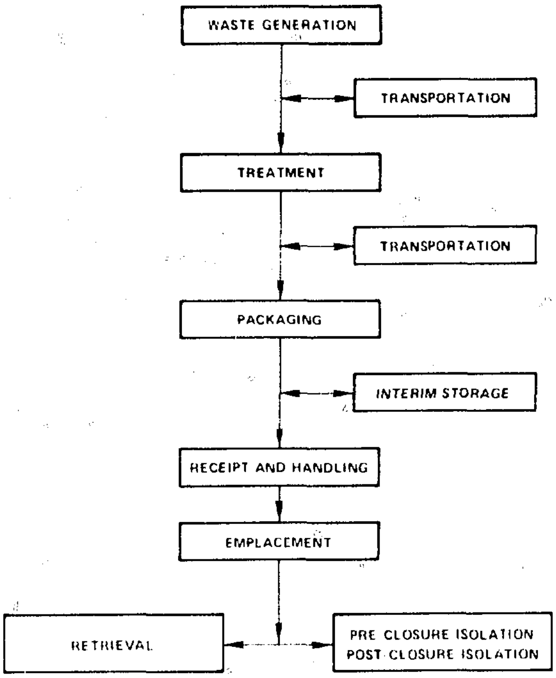

Fig. 1 Waste management operations.

WASTE MANAGEMENT OPERATIONS

The waste acceptance criteria must govern the waste types during all the waste management operations shown in Fig. 1. It should be noted that transportation is a waste management operation that can take place between almost every other waste management operation shown.

WASTE TYPES

The wastes considered in this study are those wastes generated in the closed and once-through commercial nuclear fuel cycles. The waste types are the following.

Remote-Handled Waste

- *Spent Fuel Waste (SF).* SF consists of assemblies of fuel rods discharged from light-water reactors that have not been processed.
- *High-Level Waste (HLW).* HLW includes waste resulting from first-stage solvent-extraction and concentrated waste from subsequent extraction cycles in a spent fuel reprocessing plant.
- *Cladding Waste (CW).* CW consists of solid pieces of Zircaloy or stainless steel cladding and other rod and structural materials which remain in the dissolving vessel after the fuel has been dissolved.
- *Remote-Handled Transuranic (RHT) Waste.* RHT waste is defined as those materials, generally solids, that contain alpha-emitting actinides at a concentration of 10 nCi/g and whose surface dose rate prohibits safe, direct handling.

Contact-Handled Waste

- *Contact-Handled Transuranic (CHT) Waste.* CHT waste is materials, usually solids, containing alpha-emitting actinides at a concentration of 10 nCi/g whose surface dose rate is sufficiently low to permit direct handling.

The following could be either Contact-Handled or Remote-Handled TRU waste:

- *Fission Product Gaseous Waste (FP).* FP includes the noble-gas fission products, especially krypton and xenon, the fission products, iodine and tritium, and carbon-14.
- *Contaminated Equipment (CE) Waste.* CE waste is obsolete, failed, or unwanted equipment or machinery and dismantled structures that result from maintenance or decommissioning of reactors, reprocessing plants, and refabricated plants which are contaminated with TRU materials.

RELEASE MECHANISMS

Several mechanisms that lead to a release of radioactivity have been identified. These are:

- Combustion of the waste
- Volatilization of the waste
- Leaching of the waste into groundwater
- Chemical interactions of the waste with the surroundings
- Loss of physical integrity of the waste
- Attaining a critical configuration by the waste
- Direct exposure to the waste

Each of these mechanisms may be the first step in a succession of events that lead to radiation dose to man and, hence, risk to man. In order to limit the risk to man, one must limit the rate of release of radioactive materials that occur through these mechanisms.

PATHWAYS TO THE ENVIRONMENT

Limiting the rate of release of radioactive materials to the environment requires a knowledge of the possible sequence of events that leads to radiation dose to man. This sequence of events was outlined for each of the seven release mechanisms for all waste management operations. Two of the outlines presented are leaching of the waste into the groundwater in Fig. 2 and volatilization of the waste in Fig. 3. Both of these outlines deal with preclosure and postclosure isolation. For the outlines to be applicable to other waste management operations, modifications would need to be made.

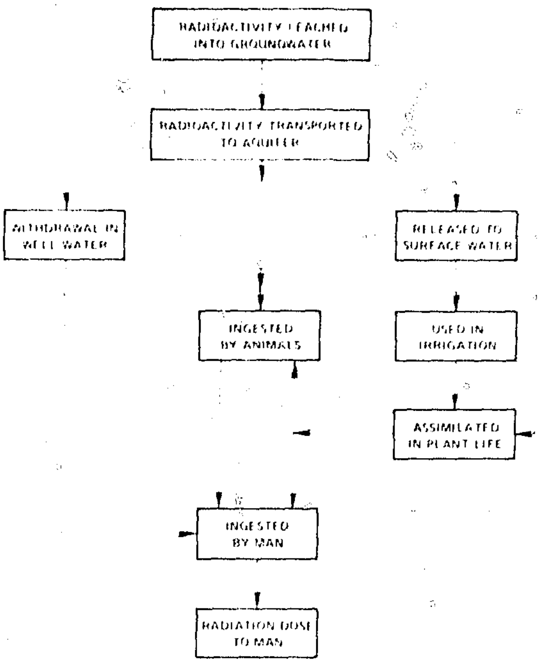
RADIOACTIVITY LEACHED INTO GROUNDWATER
RADIOACTIVITY TRANSPORTED TO AQUIFER
WITHDRAWAL IN WELL WATER
RELEASED TO SURFACE WATER
INGESTED BY ANIMALS
USED IN IRRIGATION
ASSIMILATED IN PLANT LIFE
INGESTED BY MAN
RADIATION DOSE TO MAN

Fig. 2 Leaching of radioactivity into the groundwater.

IDENTIFICATION OF RATE-LIMITING STEPS

In general, the most restrictive step in the succession of events leading to a breach of the repository determines the rate of tolerable radioactivity release. The examples presented above are used to identify the rate-limiting steps. The first of these deals with the leaching of the waste by groundwater. As stated previously, Fig. 2 indicates the succession of events that starts with leaching of the waste into the groundwater and eventually results in dose to man. Several of these events could be the rate-limiting step: (1) the leaching of radioactivity to the groundwater, (2) the groundwater transport of the radioactivity to the aquifer, or (3) the rate of ingestion of radioactivity by man. Since the acceptance criteria apply only to the waste package performance, leaching of radioactivity into the groundwater is the only restrictive step associated with the waste form.

The second example is that of volatilization of the waste form. The succession of events in this case is illustrated in Fig. 3. It should be noted that path A, the overpressure path, can only occur after the repository has been backfilled and sealed. The explosive mixture path, path B, and the flammable mixture path, path C, are paths

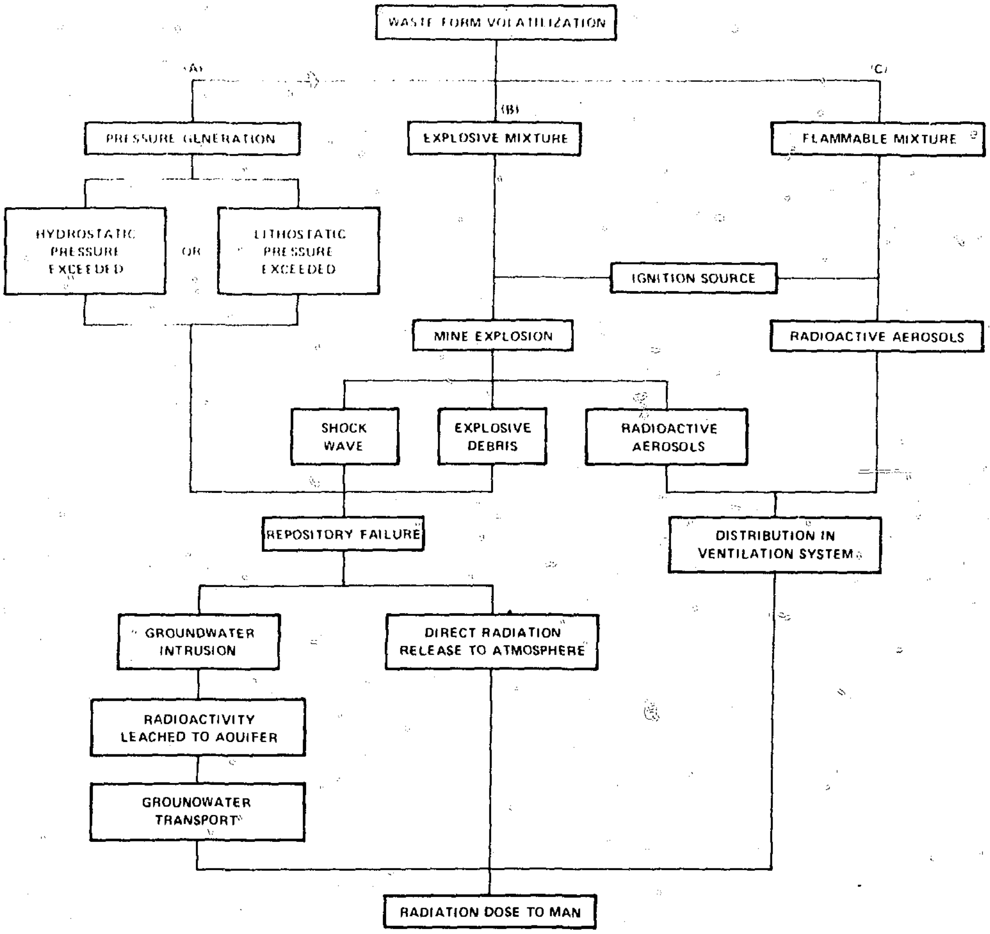
WASTE FORM VOLATILIZATION
(A)
(B)
(C)
PRESSURE GENERATION
EXPLOSIVE MIXTURE
FLAMMABLE MIXTURE
HYDROSTATIC PRESSURE EXCEEDED
OR
LITHOSTATIC PRESSURE EXCEEDED
IGNITION SOURCE
MINE EXPLOSION
RADIOACTIVE AEROSOLS
SHOCK WAVE
EXPLOSIVE DEBRIS
RADIOACTIVE AEROSOLS
REPOSITORY FAILURE
DISTRIBUTION IN VENTILATION SYSTEM
GROUNDWATER INTRUSION
DIRECT RADIATION RELEASE TO ATMOSPHERE
RADIOACTIVITY LEACHED TO AQUIFER
GROUNDWATER TRANSPORT
RADIATION DOSE TO MAN

Fig. 3 Waste from volatilization.

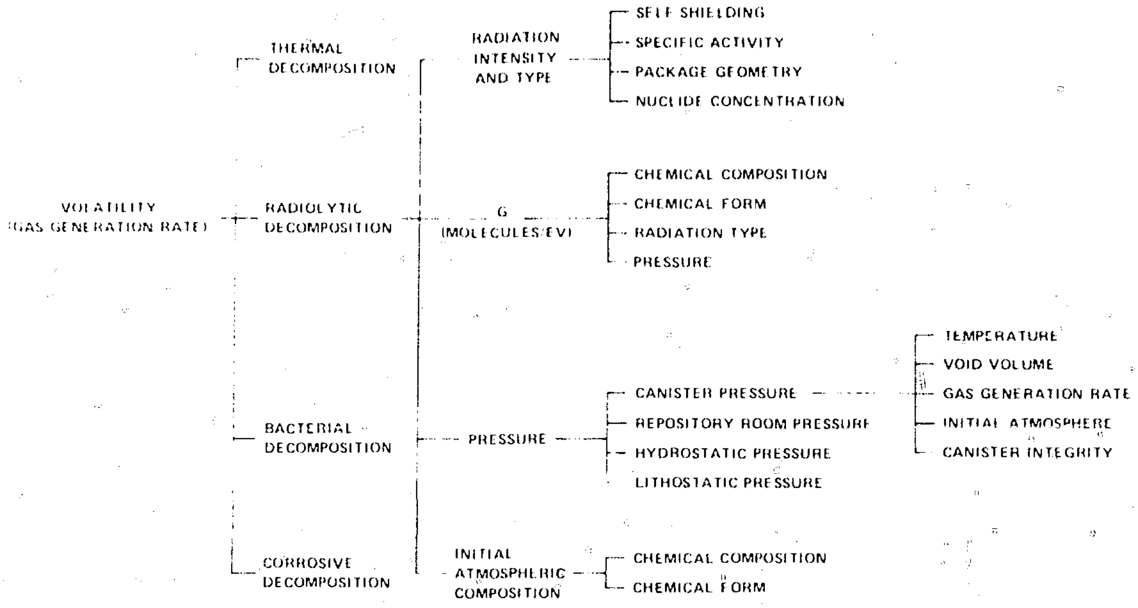
VOLATILITY
(GAS GENERATION RATE)
THERMAL DECOMPOSITION
RADIOLYTIC DECOMPOSITION
BACTERIAL DECOMPOSITION
CORROSIVE DECOMPOSITION
RADIATION INTENSITY AND TYPE
SELF SHIELDING
SPECIFIC ACTIVITY
PACKAGE GEOMETRY
NUCLIDE CONCENTRATION
G (MOLECULES/EV)
CHEMICAL COMPOSITION
CHEMICAL FORM
RADIATION TYPE
PRESSURE
PRESSURE
CANISTER PRESSURE
REPOSITORY ROOM PRESSURE
HYDROSTATIC PRESSURE
LITHOSTATIC PRESSURE
TEMPERATURE
VOID VOLUME
GAS GENERATION RATE
INITIAL ATMOSPHERE
CANISTER INTEGRITY
INITIAL ATMOSPHERIC COMPOSITION
CHEMICAL COMPOSITION
CHEMICAL FORM

Fig. 4 Derivation of factors affecting volatility.

that could only occur before the shaft is backfilled and plugged. If an explosion were to occur after the mine was backfilled and the borehole plugged, the explosion would result in an overpressure, which would then revert back to path A. Further examination of Fig. 3 will reveal that the rate-limiting steps are the waste form volatilization and the leaching of the waste form activity to the aquifer. The many steps that take place between the leaching of the radioactivity in the groundwater and the dose to man are not duplicated in Fig. 3.

IDENTIFICATION OF CONTROLLING CHARACTERISTICS

The rate for the most restrictive step (i.e., the rate-limiting step) is determined by the characteristics of the waste (either derived or fundamental) that can control or influence the rate of the release mechanism. One must therefore determine what properties of the waste control or influence these release mechanisms. This procedure is illustrated by using the volatilization of the waste during the postclosure isolation. As can be seen in Fig. 4, the rate of the volatilization of the waste, or the gas generation rate, is controlled by the rate of thermal decomposition and the rate of corrosive decomposition. In this example, we choose to determine which waste properties control the rate of radiolytic decomposition; however, it should be noted that the rates of thermal decomposition, bacterial decomposition, and corrosive decomposition would be expanded in the same way that radiolytic decomposition is expanded.

As can be seen in Fig. 4, the rate of radiolytic decomposition is a function of the radiation intensity and type, the G value (molecules of gas that are generated per 100 electron volts of radiation that is absorbed in the material), the pressure, and the initial atmosphere composition. The radiation intensity and type are determined by the amount of self-shielding contained in the waste form, the specific activity of the waste form, the waste form package geometry, and the nuclide concentration. Of these four, only the nuclide concentration and the package geometry are fundamental characteristics. Self-shielding and specific activity are characteristics that can be derived from other fundamental characteristics of the waste.

It is also interesting to note that the G value is a function of chemical composition and chemical form; however, it is also a function of radiation type and pressure. Chemical composition and chemical form are fundamental properties, whereas radiation type and pressure are dependent properties that are functions of the other properties, both fundamental and derived, that are listed in Fig. 4. Pressure is dependent on so many variables that we have chosen not to show that dependency. However, several characteristics are of interest: the canister pressure, the repository room pressure, the hydrostatic pressure, and the lithostatic pressure. The initial atmospheric composition is only a function of two properties, chemical composition and chemical form, which are fundamental properties.

The fundamental and derived properties that determine the release mechanisms are categorized as to whether they are chemical, mechanical, nuclear, or thermal in nature. These are given in Table 1, which is a compilation of all characteristics that may require criteria.[3] We have included both derived properties and fundamental properties in this listing of characteristics. In some cases, it may be easier to set a limit on a derived property than to set a limit on a fundamental property. In other cases, however, it may be easier to set a limit on a fundamental property than it would be to set a limit on a derived characteristic.

TABLE I

Fundamental and Derived Characteristics Which May Require Criteria

- Nuclear characteristics
  - Fundamental characteristics
    - Nuclide concentration
    - Fissile concentration
    - Specific activity
    - Lattice geometry
  - Derived characteristics
    - Fissile load
    - Surface contamination
    - Surface dose rate
    - Shielding
    - Radiation damage
- Chemical characteristics
  - Fundamental characteristics
    - Chemical composition and form
    - Atmospheric composition
  - Derived characteristics
    - Gas generation rate
    - Flash point
    - Ignition temperature
    - Corrosion rate
    - Phase change
    - Leach rate
- Physical/mechanical characteristics
  - Fundamental characteristics
    - Canister material properties
    - Package geometry
    - Void volume
    - Emplacement configuration
  - Derived characteristics
    - Structural integrity
    - Weight
    - Surface area
    - Internal pressure and overpressure
    - Leak rate
    - Stress cracking
    - Particle size
    - Dispersibility
- Thermal characteristics
  - Fundamental characteristics
    - Thermal conductance
  - Derived characteristics
    - Surface temperature
    - Bulk temperature
    - Thermal load

All of the factors noted in Table I have been classified as characteristics of the waste. Although we realize that, in essence, temperature is not a characteristic of the waste, but it is an effect of the heat generation and dissipation within the package. There are other characteristics of the waste that appear in other release mechanisms which fall into this same category, for example, surface dose rate. Surface dose rate is not a property of the waste, but it is a manifestation of the specific activity of the waste, the isotopic composition of the waste, the self-shielding, and other factors. However, we classify it as a derived characteristic, and, therefore, we have included it in our final tabulation as a nuclear characteristic of the waste.

SUMMARY

All release mechanisms that lead to radiation dose to man during any of the waste management operations for all waste types were analyzed using the methodology presented. The final result is shown in Table I. These thirty-three characteristics are those characteristics of the waste that may require criteria in order to limit the rate of release of radioactive and chemically toxic substances to the environment and, hence, to man.

ACKNOWLEDGMENT

This work was performed under Subcontract E516-001-1 with Battelle Memorial Institute, Project Management Division, under contract EY-76-C-06-1830 with the United States Department of Energy.

REFERENCES

1. *Report to the President by the Interagency Review Group on Nuclear Waste Management*, DOE Report TID-29442, Technical Information Center, Oak Ridge, Tenn., 1979.
2. *Waste Management System and Package Performance Criteria*, to be published by Criteria Developers Group Working Committee, Office of Nuclear Waste Isolation, 1979.
3. F. A. O'Hara et al., *Preliminary Report Waste Acceptance Criteria Study, Phase I Identification of Characteristics*, ONWI Report ONWI-6(1), Battelle Columbus Laboratory, 1978.

AN APPROACH TOWARDS LONG TERM PREDICTION OF STABILITY OF NUCLEAR WASTE FORMS

E. LUE YEN-BOWER, D. E. CLARK, and L. L. HENCH
Department of Materials Science and Engineering, University of Florida,
Gainesville, Florida

ABSTRACT

An experimental method for predicting long-term stability of nuclear waste encapsulants uses various ratios of surface area to the solution volume exposed to the encapsulant. A graphical technique, involving leaching indices and exposure times, illustrates how predictions can be made based on laboratory experiments, field trials, and museum artifacts.

INTRODUCTION

Evaluation of the corrosion kinetics and mechanisms of complex glasses, i.e., ternary systems or greater, is not a simple matter nor is the interpretation of leach rates. The problem is further aggravated by the inability to do real-time experiments to understand long-term storage behavior. It therefore becomes necessary to use data obtained from short-term laboratory experiments to make predictions concerning the long-term storage stability of glasses. Predictions of this kind are essential for glasses which have been proposed as encapsulants for nuclear wastes. The validity and usefulness of such extrapolations are, of course, heavily dependent on accurate data and even more on their accurate interpretation.

Two types of accelerated tests are used in the study of glass durability. A high-temperature test is one means by which glass corrosion kinetics may be hastened. For this test, long exposure times at low temperatures are simulated in the laboratory by studying the system for short times at high temperatures. High-temperature tests (>100°C) require autoclave conditions which often change the mechanisms from those known to occur at the lower temperature conditions being modelled.

A second type of accelerated glass durability test uses a high ratio of surface area of glass (SA) to volume of leaching medium (V). The high SA/V accelerates the rate at which ions that are leached from the glass accumulate in solution, thus reducing the time needed for characterizing glass durability. This method also has the advantage that it does not affect the corrosion kinetics unless the concentration of leached species in solution exceeds their solubility limits or the pH of the solution increases to a value which alters the corrosion mechanisms.[2,3]

The experimental parameter, SA/V, is one that has been generally ignored in the past. The work of El-Shamy[4] and others[5] have shown that SA/V has a significant effect on glass corrosion kinetics. However, only recently has a systematic evaluation of this important corrosion parameter been developed by Ethridge et al.[6]

The major objective of this report is to present an approach for predicting the long-term stability of nuclear waste forms. We propose to use information derived from observing the effect of varying SA/V values on corrosion kinetics and mechanisms as an aid in this prediction. Preliminary studies are conducted with simple binary alkali silicate glasses so that a thorough understanding may first be developed. An extension to more complicated borosilicate systems containing simulated nuclear wastes is also presented. The results reported are acquired from studies of glasses, but if the same or similar assumptions can be made for other nuclear waste forms (NWF), then corresponding conclusions can be drawn for these.

THEORETICAL CONSIDERATIONS

In the initial stages of surface attack by an aqueous solution, glass constituents are selectively leached into solution. This diffusion controlled ion exchange process results in an increase in the pH of the leaching medium due to the depletion of H^+ from the solution. In high pH solutions a second corrosion process which causes the attack of glass network formers becomes more important. Both modes of corrosion can be expressed with the kinetic equation

$$Q = kt^{\alpha} \tag{1}$$

where Q = quantity of glass constituent extracted or pH of the solution
k = reaction rate constant
t = reaction time

At short corrosion times in acidic and neutral solutions, the exponent, α, has a value of approximately 0.5 for both selective leaching and for the extraction of silica indicating diffusion controlled mechanisms for all species at short times.[2,7] After some time, the corrosion process eventually becomes linearly dependent with time, i.e., $\alpha \rightarrow 1$. This change in kinetics is attributed to the increased solubility of silica in solutions of higher pH values.[2,3,8] The time at which the predominant mode of corrosion changes from a diffusion controlled mechanism to network dissolution is designated, t_c, the changeover time, and the corresponding pH is labelled pH_c.

The term relating the surface area of the glass to volume of leachant (SA/V) is usually incorporated in either Q or k in Eq. 1. However, as shown in detail in a recent publication,[6] by assuming a constant flux of leaching glass constituents into solution per unit surface area, the kinetics equation can be written as

$$C_i = (SA/V)\, kt^{\alpha} \tag{2}$$

where C_i is the concentration of the leached species i in the solution or pH of the solution. The constant k in this equation is assumed to be independent of SA/V.

Equation 2 can be simplified in two ways. If the corrosion time is held constant, it can be shown[6] that

$$\log C_t = \log (SA/V) + c_1 \tag{3}$$

where C_t = concentrations of glass constituent in solution at the given time, t
c_1 = a constant equal to $(\log k + \alpha \log t)$

Equation 3 indicates that a logarithmic plot of the concentration of a specific glass constituent in solution after a given corrosion time versus SA/V should give a straight line with a slope of unity.

The second simplification of Eq. 2 is derived from the time, t_c, required to reach a specific concentration of glass constituent in solution,[6] a specific pH of the solution, or a maximum thickness of surface reaction layer.

$$\log t_c = -\frac{1}{\alpha}\left(\log \frac{SA}{V} - c_2\right) \tag{4}$$

where c_2 is a constant equal to $(\log k - \log C)$.

According to Eq. 4 a logarithmic plot of t_c versus SA/V should theoretically[6] yield a straight line with a slope equal to the negative reciprocal of the reaction rate exponent, α. Both Eqs. 3 and 4 are based on the assumption that the reaction rate constant, k, is not changed by varying SA/V, i.e., the net flux of glass constituents from a unit area of surface is independent of the effective SA/V.

METHODS OF ANALYSIS

It is obvious that the quantities of substances leached, as well as the effect of corrosion on the surface of materials, are required to determine the extent of corrosion. Solution ion concentrations are determined using atomic absorption and emission spectroscopy, and UV-visible absorption spectrophotometry. The pH of the solution is also monitored to determine the pH at which total dissolution of the glass occurs. Surface information is acquired using Auger electron spectroscopy with Ar ion beam milling (AES-IM), infrared reflectance spectroscopy (IRRS) accompanied with a sequential polishing technique,[9] and, occasionally, scanning electron microscopy (SEM).

RESULTS

Binary Alkali Silicate Glasses

For the 33 mol % Li_2O–67 mol % SiO_2 glass (33L), a plot of pH values versus log time shows two distinct portions. In Fig. 1, the slope of the curve at shorter times is approximately 0.5 and agrees favorably with the previous theoretical discussion, i.e., Eq. 1. At longer times the slope of the curve increases to a value of approximately unity. This also is in agreement with theory. The pH values at which the slope (kinetic rate) changes from 0.5 to 1 is between 9.5 and 11.5, and the time at which this occurs is designated t_c. Generally, for binary alkali silicate glasses the value of α changes from 0.5 to 1 when the pH of the solution is between 9 and 10 (Refs. 2, 7, 8). This change, t_c, is often quite sharp when determined for bulk glass surfaces.[2] However, as shown in Fig. 1 the t_c for glass powders varies over a significant range.

A curve for the case of a binary 33 mol % Na_2O–67 mol % SiO_2 glass analog of 33L is also shown in Fig. 1. Note that the corrosion rate for the soda-containing glass is sufficiently more rapid than the lithia glass that the solution temperature must be decreased by 35°C to obtain the same pH versus time behavior.

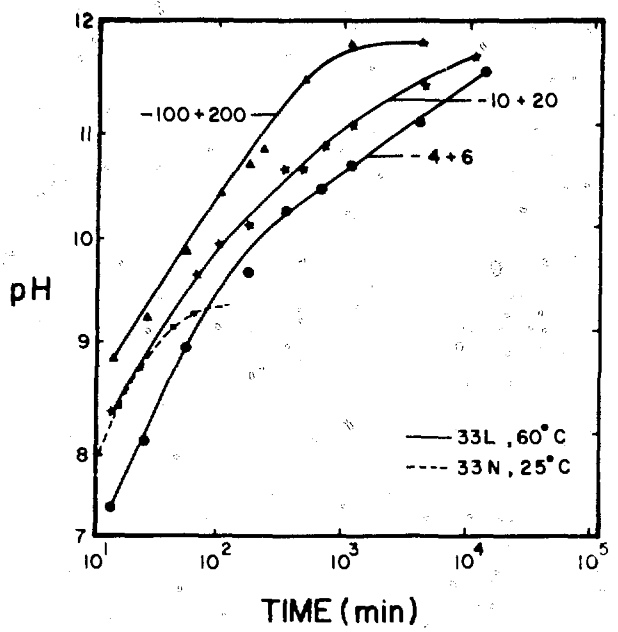

Fig. 1 pH of the corrosion solutions versus log corrosion time (min) for 33L glass grains and 33N glass.

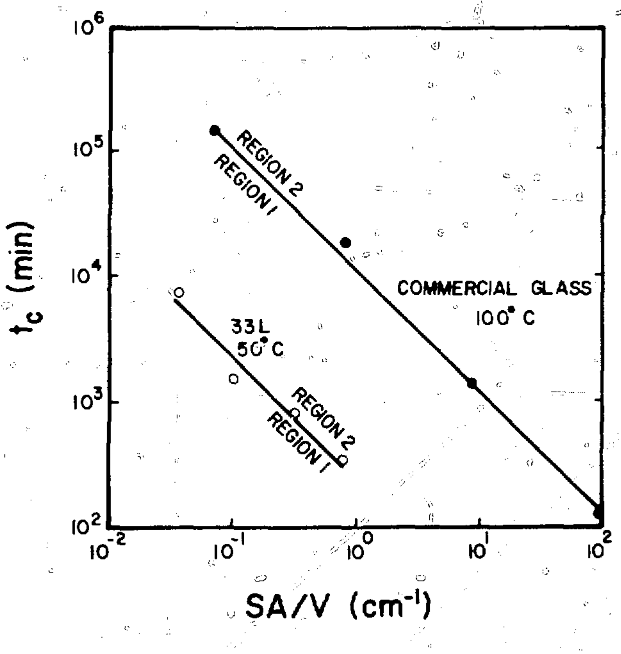

Fig. 2 Changeover time, t_c, versus SA/V plots for 33L glass at 50°C and for a commercial soda-lime-silica glass at 100°C.

If a series of t_c values are obtained in this manner for various SA/V conditions for a particular temperature, the plot shown in Fig. 2 is obtained. Extrapolation of the curve for 33L to low SA/V values, e.g., SA/V = 10^{-2}, reveals that it would take approximately 21 days for the glass to be corroding primarily by total (network) dissolution.

Similar data are also presented in Fig. 2 for a commercial soda-lime-silica container glass corroded at 100°C. The t_c versus SA/V curve for this glass at 50°C would be shifted to the upper right of the figure and parallel to the 100°C curve. *In this case, t_c is the time* necessary to reach a pH of 9. By extrapolation, the soda-lime glass, which is a much more durable glass, would not go into a total dissolution mode until after 23 months if stored so that SA/V = 10^{-2}. This method of analyzing data appears to be a *reasonable* one for the comparison of glasses that exhibit a very wide range of durabilities.

Borosilicate Glasses with Simulated Nuclear Wastes

Laboratory tests under static corrosion conditions for several simulated borosilicate-based nuclear waste glasses (SNWG) give results similar to those obtained for the binary alkali silicate glasses. Figure 3 shows an identical trend for the changes in pH of the solution with time for the SNWG composition 72-68(PW-4b-7(2.8)73.L) obtained from Pacific Northwest Laboratories (PNL).

In order to determine at which pH range the change in *corrosion mechanism* occurs, pH_c, AES-IM is used to provide a depth compositional profile of the corroded glasses. The elements calcium, boron, and potassium are used to monitor surface changes with time. At short reaction times of 2 to 5 hours, a silica-rich layer 500 to 600 Å depleted of calcium, boron, and potassium is developed as shown in detail in another publication.[11] The concentration of the heavy elements is significantly increased in the leached surface layer in comparison to the bulk composition. After 14 hours of exposure time the thickness of the depleted layer has decreased to 200 Å which is evidence that network dissolution is dominant. This time closely approaches the t_c extracted from analysis of the reaction solutions and *corresponds to* $pH_c \cong 8.5$. *In* this case, either solution analysis or surface analysis is sufficient to extract t_c information. However, it is strongly recommended that both analyses be carried out to avoid any misinterpretation.

An example of the importance of doing both solution and surface analyses is seen in Fig. 4 for SNWG [77-260(PW-7c4(1:2)77-269) w/o UO_2] also obtained from PNL. There appears to be no change in the kinetics of the reaction for the time period studied when only solution analysis of the change in solution pH is employed. However, AES-IM of the surface after various times of corrosion shows that the surface network begins to break down and t_c occurs when the pH of the solution is approximately 8.5.

If t_c is chosen as the time when pH = 8.5 for the nuclear waste glasses examined, a logarithmic plot of t_c versus SA/V gives a straight-line curve as shown in Fig. 5. *For a particular glass composition, increasing the exposure* temperature from 75°C to 135°C reduces the time required to reach t_c for all SA/V values by a factor of 15. This type of graphical representation is extremely valuable for

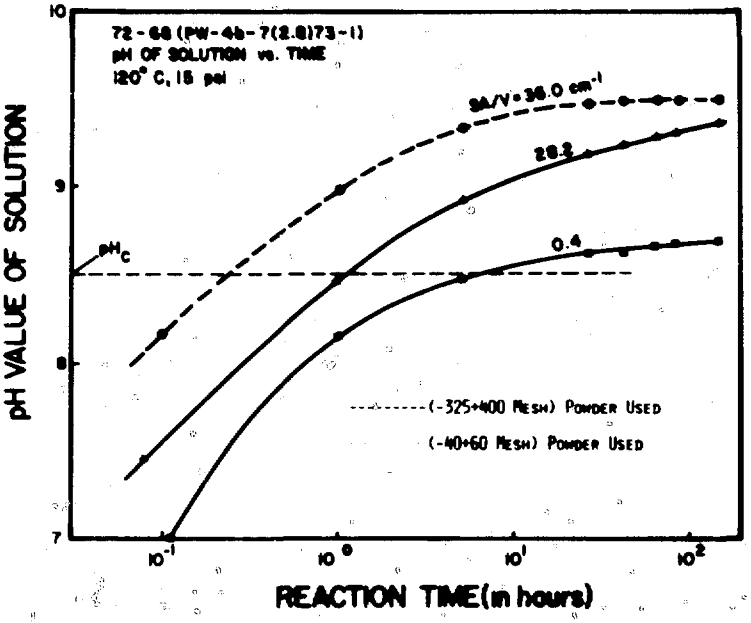

Fig. 3 pH of the corrosion solutions versus log reaction time for SNWG 72-68.

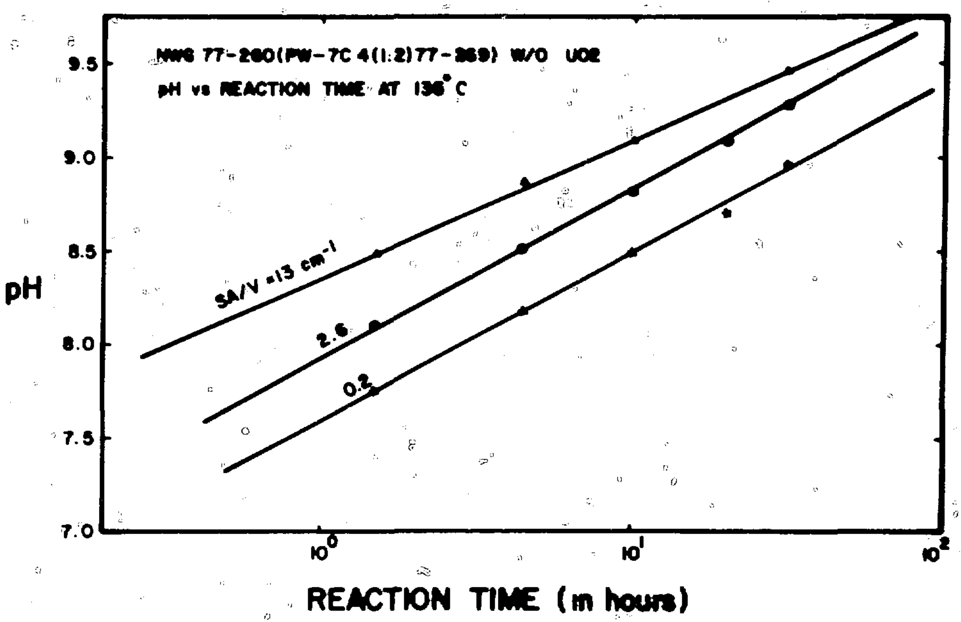

Fig. 4 pH of the corrosion solutions versus log reaction time for SNWG 77-260.

predicting t_c for very low SA/V conditions which are difficult to analyze in the laboratory because of the prohibitively long times involved.

If storage involves continuous removal of the attacking medium such as flowing groundwater, this would effectively provide a very low SA/V ($\ll 10^{-3}$ cm^{-1}). Such conditions would discourage the formation of surroundings with a high pH and serve to extend t_c beyond that observed under static corrosion conditions.

Proposed Approach for Long-Range Predictions of the Stability of Nuclear Waste Forms

Short-term laboratory experiments can be carried out to provide t_c information as discussed previously and as shown in Figs. 1 to 5. Graphical representations such as those shown in Figs. 2 and 5 can be used to predict the time required for a glass to enter a network dissolution mode with a fair degree of reliability. At times below the t_c

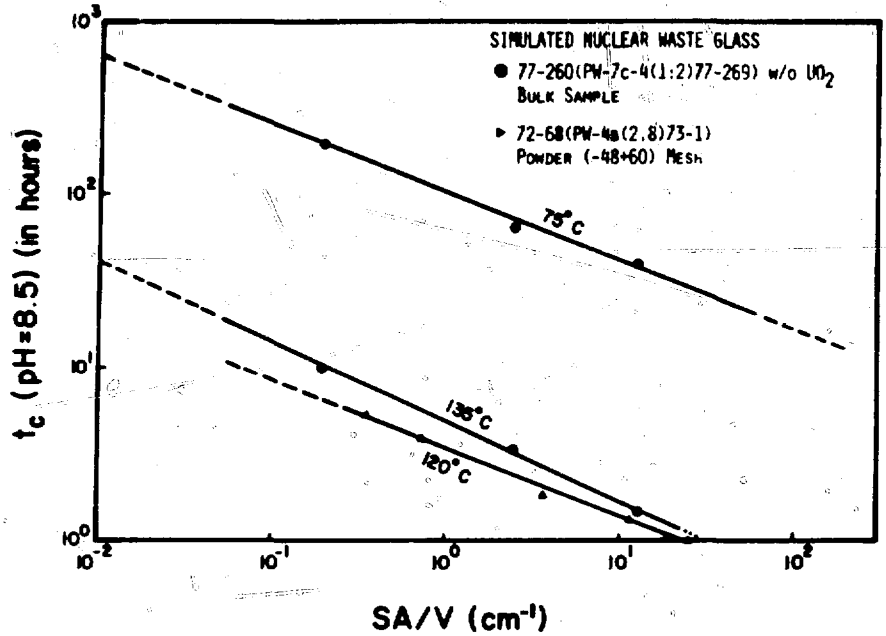

Fig. 5 Changeover time, t_c, versus SA/V plots for SNWG 72-68 and 77-260.

versus SA/V plot for a particular temperature, the slower root time diffusion controlled selective leaching is rate controlling. At greater times, i.e., times above the line, linear extraction rates dominate and network dissolution is rate controlling. Prevention of network dissolution is especially important for glass encapsulants because of the tendency for the radioactive heavy elements to be trapped within surface films that form on the glasses during the selective leaching, diffusion controlled period of attack.[9] From this type of analysis one can set maximum limits on SA/V storage conditions which are critical to prevent network attack from occurring before radioactivity of the nuclear wastes subsides.

In combination with the SA/V versus t_c analysis, we also present a further consideration for long-range predictability. If it can be ascertained that selective leaching is the principal mode of attack, a prediction curve such as the one shown in Fig. 6 may be developed.[10]

The thickness, d, of a leached surface or the concentration, C_i, of a specific ion leached into solution are examples of measurable leaching indices. Although weight change is a widely used leaching index, it is not recommended since reprecipitation on the surface may yield misleading information. Also, extensive leaching of radioactive species may be accompanied by insignificant weight losses.

The use of this graphical method for predicting long-term leaching behavior of nuclear waste forms is based on several assumptions:

- That materials which are similar or related in composition will corrode via similar mechanisms.
- That extrapolations can be made to times longer than those actually measured assuming no change in kinetics. A good guide would involve determining t_c as discussed earlier.
- Laboratory simulations or field trials of varied geologic storage conditions of candidate NWF materials can be made.
- Leaching indices from short-term studies of the NWF materials and analog materials can be compared with the measured indices from the long-term burial of the analog materials to obtain "worst case" and "best case" storage acceleration factors.

If the above assumptions are valid, margins of safety can be dictated as a result of the kinetic extrapolations and comparisons with analog materials.

In Figure 6, A and A′ represent a range of leach rates measured on analog materials. Data for leach indices of analog materials can easily be obtained in the laboratory over a large range of times up to 10^{-1} year. For longer experimental times burial in geologic sites can be conducted. For the time range from tens of years to 10^3 years, results can be obtained from accurately dated museum and archeological samples assuming certain ranges of temperature and groundwater pH based upon the local geology.

It is obvious that the environments of the buried analog materials are by no means equivalent to those to be encountered in the long-term storage of NWF materials. If storage environment simulations are based upon geochemistry computer modelling studies, then perhaps the best case and worst case extremes can lead to B and B′ in Fig. 6.

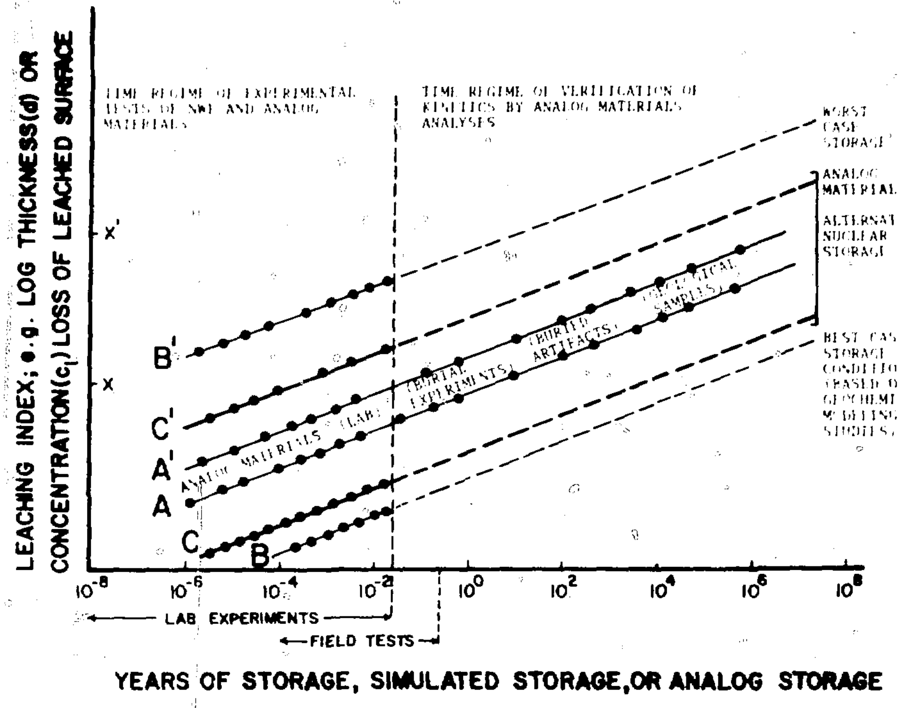

Fig. 6 A methodology for predicting long-term stability of nuclear waste storage forms.

As long as reaction mechanisms do not change in the more severe environment, the curves B-B′ remain parallel to A-A′ and the extrapolations of B-B′ are valid. If there is a potential for a change in mechanism to occur, it is assumed that the changes can be induced during the laboratory range of experiments and can be derived from t_c versus SA/V graphs or their extrapolations.

Finally, laboratory leaching results of NWF materials, C and C', can be extrapolated to long times if a valid comparison is made with the analog materials. It should then be possible to specify an acceptable safety level of cumulative loss of radioactive species from a NWF based on biological tolerances and other relevant concerns.

Figure 6 can be used to predict the time required for the chosen safety level to be reached using the intersection of the appropriate leaching curves. If this results in an unacceptable storage period, an acceptable extension in safety storage time can be achieved by addition of a passivating overpack or could lead to the selection of a different and more suitable NWF material.

ACKNOWLEDGMENTS

The authors thank Pacific Northwest Laboratories for partial financial support and especially Wayne Ross for providing the glass samples. They also thank the Nuclear Regulatory Commission for partial financial support for this work under contract NRC-04-78-252.

REFERENCES

1. D. E. Clark, C. G. Pantano, and L. L. Hench, *Glass Corrosion*, Glass Industry, New York, in press.
2. E. C. Ethridge, *Mechanisms and Kinetics of Binary Alkali Silicate Glass Corrosion*, Ph.D. dissertation, University of Florida, 1977.
3. C. R. Das and R. W. Douglas, Studies on the Reaction Between Water and Glass, Part 3, *Phys. Chem. Glass*, 8: 178 (1967).
4. T. M. El-Shamy and R. W. Douglas, Kinetics of the Reactions of Water and Glass, *Glass Tech.*, 13: 77 (1972).
5. V. Dimbleby and W. E. S. Turner, The Relationship Between Chemical Composition and Resistance of Glasses to the Action of Chemical Reagent, *J. Soc. Glass Tech.*, 10: 304 (1926).
6. F. C. Ethridge, D. E. Clark, and L. L. Hench, Effects of Glass Surface Area-to-Solution Volume Ratio on Glass Corrosion, accepted for publication by *Phys. Chem. Glass*, April 1979.
7. M. A. Rama and R. W. Douglas, The Reaction Between Glass and Water, Part 2, Discussion of Results, *Phys. Chem. Glass*, 2: 196 (1965).
8. T. M. El-Shamy, J. Lewins and R. W. Douglas, The Dependence on the pH of the Decomposition of Glasses by Aqueous Solutions, *Glass Tech.*, 13: 81 (1972).
9. D. E. Clark, E. Lue Yen-Bower, and L. L. Hench, Corrosion Behavior of a Zinc Borosilicate Simulated Nuclear Waste Glass, in Proceedings of *Ceramics in Nuclear Waste Management*, Cincinnati, CONF-790420, U. S. Department of Energy, Technical Information Center, Oak Ridge, 1979.
10. L. L. Hench, D. E. Clark, and E. Lue Yen-Bower, Surface Leaching of Glasses and Glass Ceramics, to be published in *J. Nucl. Wastes & Tech.*
11. F. Ohuichi, D. E. Clark, and L. L. Hench, Chemical Durability of Simulated Nuclear Waste Glass, submitted to *Phys. Chem. Glass*.

GLASSY AND CRYSTALLINE HIGH-LEVEL NUCLEAR WASTE FORMS—AN ATTEMPT AT CRITICAL EVALUATION

W. LUTZE
Hahn-Meitner-Institut für Kernforschung Berlin GmbH, Department of Nuclear Chemistry and Reactor,
Berlin, Germany

ABSTRACT

Pros and cons of glassy and crystalline nuclear waste forms are discussed. An evaluation is given in terms of technological simplicity and safety-relevant product properties, i.e., thermal, chemical, mechanical and radiation stability, showing that glasses are the first choice and alternatives are either the backup solution or second-generation products.

INTRODUCTION

A technology has been developed during the past two decades to solidify HLLW in glass. The potential of alternative final forms has been considered as well, but with less effort. Of these at least one form, a metal-matrix glass composite, has reached technological maturity. Consolidated, fully ceramic waste forms have also been given attention, but the technical feasibility, in terms of remote handling in hot cells, has frequently been questioned. Ceramic forms, therefore, were ranked as second-generation final waste forms. The potential increase in the product's stability has been realized.[1]

Repository concepts were undeveloped until a few years ago. Therefore high-level solidified waste (HLSW) forms could only be tested under the physical and chemical conditions set by the repository during the last two or three years. Geologic formations such as shale, granite, basalt, and salt have been considered and are presently under investigation. These rocks exhibit very different geologic and hydrologic properties with respect to containment of HLW and possible waste–rock interactions, and currently only glass can be offered as a feasible waste form. Glass (blocks) cannot be expected to be *the* universal waste form compatible with any geologic formation and fitting into all assumed waste management systems. There may be more appropriate products than glass blocks if, for example, short-cooled, high-burnup waste is to be disposed of shortly after solidification. In this case, a metal-matrix composite may be highly recommended and salt may not be the best repository. As yet, a comprehensive evaluation of the still-growing number of proposed alternatives to glass and its variants cannot be performed. This paper, however, critically discusses the facts and the options set within a waste management and repository concept when choosing glass as the final waste form.

WASTE FORMS AND TECHNICAL ASPECTS

The short-term storage of HLLW in tanks is today a mature technique. It is clear, however, that this kind of storage cannot be prolonged indefinitely. The fission products in solution must not only be solidified but must be immobilized by incorporation in a stable host material suitable for disposal in a geologic formation. For this reason, a calcined waste is definitely not a final form. Incorporation of the highly radioactive fission products in a host material, however, calls for rather sophisticated processing at high temperature and/or high pressure, both being undesirable in terms of remotely handled equipment. There seems to be no way of processing the waste under both low temperature and pressure.

Present technology[2] provides a high-temperature process, vitrification, where a glass frit or glass formers are added to the waste prior to melting at 1320 to 1470°K. The waste is dissolved in a glass at concentrations up to 30 wt.%. However, half of this quantity could be more desirable, so that the glass properties are not determined by the waste. Monolithic blocks (both simulated and full-scale radioactive) of considerable length (up to 3 m) and thickness (40 cm) as well as small beads (0.5 cm in diameter) have been produced in pilot plants.

Special glasses have been developed in order to make glass ceramics as the final waste product in the form of blocks and beads. In this case, the glass is taken through a carefully programmed thermal treatment to promote controlled nucleation and crystallization and accommodate radionuclides of concern in tailor-made host phases.[3-5] A disadvantage of glass ceramics made from borosilicate glasses is the low chemical durability of their residual glass phase. Very recently, glasses and glass ceramics free of boron and alkali have been developed at the HMI which exhibit increased chemical durability.

In addition to the concept of dissolving the waste in a glass matrix, the fabrication of fully ceramic materials has been envisaged.[6,7] As yet, moderate R&D efforts have been made, and it is already clear that the various product formulations yield final products which may be as stable as glasses or exhibit even better properties, at least under laboratory conditions. Processing is characterized by adding various mineral-forming species to the waste, as in the case of supercalcine[6] and Synroc,[8] or by adding inorganic ion exchangers, as in the Sandia titanate process.[9] The mixtures are chemically reacted at low or moderate temperatures (≤400°K) yielding precursors that have to be consolidated in a second step using further additives. Subsequently sintering, hot pressing, and/or other consolidation techniques are required. Table 1 lists various proposed methods and materials. As can be seen from the table, the final product may be fully ceramic, a glass ceramic, or a metal-matrix composite.

The HLSW is contained in a canister for transport and intermediate storage. This canister is not considered here because the use of a distinct material is not necessarily typical of, or dependent on, the production of a distinct waste form. There seems to be no severe corrosion problem at the waste form/canister interface, and the canister has never been assigned a long-term barrier function in the repository.

From a review of the literature[2,10] related to processing of HLW, the following emerged:

- Processing of glass is currently adequate for the full-scale demonstration of solidification and disposal.
- It is rather unlikely that ceramic (crystalline) waste forms and/or related composites can be processed with simple techniques as to maintenance, repair, off-gas systems, and radiation exposure of personnel.

Glass does not necessarily mean glass blocks. The large-scale production of glass beads has been demonstrated with phosphate glass[11] and is also straightforward with borosilicate glass. A German pilot plant to be built in Belgium at the EUROCHEMIC site provides for the production of both glass blocks and metal-matrix-embedded glass beads. In principle, an additional thermal cycle would be necessary if the matrix-embedded beads (of the properly designed glass) were converted into a glass ceramic. Hence, the options for composites were left open when a decision was made in favor of glass.

CHARACTERISTICS OF HLSW FORMS

Solidified waste is characterized by some typical properties in relation to potential hazards which might occur during transport, storage, and emplacement. These are:

a. Long distance transport and intermediate storage	fragility, dispersibility, solubility
b. Emplacement (operation phase of the repository) c. The sealed repository	stability of the insoluble form in contact with rock and aqueous solutions under the related physical and chemical conditions

Long distance transport of HLSW can be excluded if reprocessing is performed on the repository site; the respective quality criteria listed above are then irrelevant.

Intermediate storage increases the flexibility of radioactive waste management by providing for heat decay, thereby lowering the heat load of the geologic repository. Great Britain[12] presently envisages 50 years of storage prior to ultimate disposal. This may lead to a drastic decrease of the maximum temperature (below 370°K) to be expected after emplacement in the repository.

Attention must be given to possible changes of the final waste form during the period of interim storage. Storage conditions may be different from those to be met in the repository. The temperature of the waste form will probably be higher under engineered storage conditions. This could conceivably affect the integrity of the HLSW form. Adverse effects on glasses may be more likely here than on ceramic waste forms. Glasses can crystallize when subjected to elevated temperatures for long periods of time. This point has been extensively studied as part of a joint EEC program at the HMI. To date, it has been shown that glasses can be formulated without influencing their durability[13] (within one order of magnitude).

Investigations on a celsian glass ceramic revealed recrystallization, crystal growth, appearance of new phases, and some loss of mechanical integrity.[5] Similar instabilities were reported for the Sandia titanate ceramic.[9] These nonequilibrium phenomena led, in the case of glass ceramics, to the formulation of a fresnoite type that shows no phase instabilities up to 100 days at 1000°K, a temperature well above any reasonable value for storage.

Another adverse effect of temperature on the waste form is thermal stress, which may affect the integrity of glass or fully ceramic products, but affects metal-matrix composites to a much lesser extent because the temperature gradients are lower. As yet, little information is available on mechanical stability of glass and ceramic HLW forms under the influence of an internal thermal gradient. It is, however, rather unlikely that nonreinforced glass blocks of the

TABLE 1

Glass and Ceramic Nuclear Waste Forms

Precursor	Waste forms Consolidated	 Composites	State of development
Calcine of HLLW	Glass		Technical scale "hot"
	Glass	Glass ceramic	Lab scale "hot"
	Glass	Glass beads/metal matrix	Pilot plant "hot" and technical scale "cold"
	Glass	Glass ceramic beads/ metal matrix	Lab scale "cold"
Supercalcine	Ceramic (sintered hot pressed)	Sintered glass ceramic and supercalcine/glass	Lab scale "cold"
Calcine	Calcine/metal matrix	Coated supercalcine in a continuous phase	Lab scale "cold"
Waste loaded titanate, zeolite and sludge	Ceramic	Ceramic/metal matrix	Lab scale "cold"
Calcine from low burnup waste		Cement and concrete compositions	Lab scale "cold"
Synroc	Hot pressed ceramic		R&D

presently designed sizes will remain as unfractured monoliths. An increase of surface by at least a factor of ten has to be anticipated. Information on large monoliths of fully ceramic material could not be found in the literature.

The problems associated with emplacement of the HLSW form (as received from the interim storage site) have to be identified and carefully assessed. The question is whether an appropriately designed system can provide satisfactory conditions in terms of waste/rock interaction, e.g., salt in West Germany, which is being referred to in more detail in this context. Such an interaction is inevitable and independent of the waste form beginning with the dissipation of heat and subsequent rise in temperature and induced stress in the vicinity of the waste. In view of adverse effects on the mechanical stability of the rock and, in the case of salt, on the hydrology beyond the boundary of the rock formation, stress and temperature may already be the limiting performance factors for waste/rock interaction. Peak temperatures of the salt and of the waste/salt boundary of <470°K are presently assumed.

During the operation period of the repository, ingress of water and its contact with the waste form are very unlikely but cannot be completely excluded. If the container fails, the waste form will come into contact with a salt brine. This solution will presumably be saturated with NaCl and $KCl \cdot MgCl_2 \cdot 6H_2O$ (carnallite). The brine will be heated but the temperature will remain well below 470°K. The local hydrostatic pressure 700 m below sea level may be on the order of ten bars for a fully flooded repository.

WASTE/ROCK INTERACTION: EXPERIMENTAL

Simulation of hydrothermal waste/rock interaction is being performed with autoclave leach tests. Some results obtained for a series of European waste glasses and a celsian glass ceramic are summarized in Table 2. The samples were in the form of beads. It is noted that, in the case of borosilicate glasses, the interaction started with the formation of a reaction zone on the glass surface which reached a maximum thickness of 50 to 100 μm. Thereafter the incremental weight loss was essentially zero up to 60 days, as yet the maximum period of time. This finding is similar to results reported on glass by Westsik and Turcotte[14] at 530°K in NaCl solution. As seen in Table 2, only phosphate glass does not withstand brine attack; i.e., the glass disintegrated and crystallized. Long-term experiments are necessary to further evaluate the reactivity of the borosilicate glass and glass ceramic/brine interface. Quantitative analyses of the crystallized phases and the mobilized constituents of the glass are under way to provide a data base for extrapolation of waste form behavior over 100 to 200 years when the temperatures are at their highest. As yet, the quantity of remobilized radionuclides cannot be inferred from the weight loss data for borosilicate glass and glass ceramic. This will be possible as soon as the results of ongoing experiments with doped radioactive glasses are available.

The results of hydrothermal experiments are also relevant to characterize the glass/salt interaction after the repository has been sealed. This is characterized by the access of very little or no brine and somewhat higher pressures whose effect may be simulated by a slightly increased temperature in hydrothermal experiments.

The typical waste form criteria for fully ceramic materials, i.e., their chemical, thermal, mechanical and radiation stability, have not been characterized as extensively as for glasses. However, it is evident that such materials can be developed so that they are closer than glasses to equilibrium in a geochemical environment, except

TABLE 2

Leaching Data in Brine (Weight Loss in Percent)

		Temperature						
		120°C,	150°C,	200°C†				
Waste form	Number*	*3 d*	*3 d*	*3 d*	*15 d*	*30 d*	*60 d*	*90 d*
European borosilicate glasses	UK-209	0.02		1.5				
	UK-189	0.06		0.8				
	VG-98/3	0.08		2.0				
	C-31-3		0.3	2.3	2.5	2.3	2.3	2.6
Glass ceramic	C-31-3		0.8	1.5	1.8	1.5	2.5	1.7
Phosphate glass	78/7		3.0	20		Crystallized		

*Information from Ref. 15.

†At 200°C: 3 d values measured at 15 to 100 bars and 15 through 90 d values at 20 bars.

for salt. This is of particular importance if the repository is susceptible to water which might subsequently find its way to the biosphere.

Experiments to evaluate the stability of alternative ceramic waste forms as related to realistic repository conditions are still lacking. The evidence of the product's "stability" under *unrealistic conditions*, *e.g.*, exceedingly high temperatures[8] that will not be encountered (longer periods of interim storage will avoid this), is of little help for the further development of nonglassy waste forms.

CONCLUSIONS

1. The technical issue of this paper is that up to repository emplacement none of the ceramic products listed in Table 1 can be given preference when compared to glass, either in terms of ease of processing or minimizing the potential hazards which might arise from remobilization of radionuclides.
2. After repository emplacement, the stability of any waste form is determined by the waste/rock interaction during the first 200 years, which is typical of any kind of repository. Silicate glass and/or derived alternatives are likely to be compatible with salt because maximum salt temperatures will have to be limited to below 470°K.
3. Fully ceramic waste forms need further characterization to demonstrate their effective stability in geomedia other than salt. R&D should be enhanced to further develop and evaluate the potential safety increase which alternative HLSW forms might offer within a given waste management system.

REFERENCES

1. E. Ewest and H. W. Levi, Evaluation of Products for the Solidification of High-Level Radioactive Waste from Commercial Reprocessing in the Federal Republic of Germany, in *International Symposium on the Management of Radioactive Waste from the Nuclear Fuel Cycle*, Vienna, Austria, March 22–26, 1976.
2. *Techniques for the Solidification of High-Level Wastes*, Technical Report Series No. 176, International Atomic Energy Agency, 1978.
3. A. K. De, B. Luckscheiter, W. Lutze, G. Malow and E. Schiewer, Development of Glass Ceramics for the Incorporation of Fission Products, *Ceramic Bulletin*, 55: 500 (1976).
4. A. K. De, B. Luckscheiter, W. Lutze, G. Malow, E. Schiewer, and S. Tymochowicz, Fixation of Fission Products in Glass Ceramics, in *International Symposium on the Management of Radioactive Wastes from the Nuclear Fuel Cycle*, Vienna, Austria, March 22–26, 1976.
5. W. Lutze, J. Borchardt, and A. K. De, Characterization of Glass and Glass Ceramic Waste Forms, in Proceedings of *Scientific Basis for Nuclear Waste Management*, Boston, G. J. McCarthy (Ed.), Plenum, NY, 1979.
6. J. M. Rusin, M. F. Browning, and G. J. McCarthy, Development of Multibarrier Nuclear Waste Forms, in Proceedings of *Scientific Basis for Nuclear Waste Management*, Boston, G. J. McCarthy (Ed.), Plenum, NY, 1979.
7. G. J. McCarthy, High Level Waste Ceramics: Materials Considerations, Process Simulation, and Product Characterization, *Nucl. Technology*, 32: 92 (1977).
8. A. E. Ringwood, Incorporation of High-Level Radwaste in Synrock, in Proceedings of *Scientific Basis for Nuclear Waste Management*, Boston, G. J. McCarthy (Ed.), Plenum, NY. 1979.
9. J. K. Johnstone, T. J. Headley, P. F. Hlava, and F. V. Stohl, Characterization of a Titanate Based Ceramic for High Level Nuclear Waste Solidification, in Proceedings of *Scientific Basis for Nuclear Waste Management*, Boston, G. J. McCarthy (Ed.), Plenum, NY, 1979.
10. *Characteristics of Solidified High-Level Waste Products*, Technical Report Series No. 187, International Atomic Energy Agency, 1979.
11. J. Van Geel, H. Eschrich, W. Heimerl, and P. Grziwa, Solidification of High-Level Liquid Wastes to Phosphate Glass–Metal Matrix Blocks, in *International Symposium on the Management of Radioactive Wastes from the Nuclear Fuel Cycle*, Vienna, Austria, March 22–26, 1976.
12. R. Shepherd, Britain to Test Synroc High-Level Waste Technique, *Nucleonics Week*, 11: 12 (1978).
13. G. Malow, Investigation of Crystallization in Glasses Containing Fission Products, in *Ceramics in Nuclear Waste Management*, Cincinnati, CONF-790420, U. S. Department of Energy, Technical Information Center, Oak Ridge, 1979.

14. J. H. Westsik and R. P. Turcotte, *Hydrothermal Reactions of Nuclear Waste Solids: A Preliminary Study*, PNL-2759, Pacific Northwest Laboratories, 1978.
15. G. Malow, V. Beran, W. Lutze (HMI), J. A. C. Marples, J. T. Dalton, A. R. Hall, A. Hough, and K. A. Boult (UKAEA), *Testing and Evaluation of the Properties of Various Potential Materials for Immobilizing High Activity Waste*, First Annual Report, EUR-6213-EN, 1977.

A COMPARISON OF GLASS AND CRYSTALLINE WASTE MATERIALS

W. A. ROSS, R. P. TURCOTTE, J. E. MENDEL, and J. M. RUSIN
Pacific Northwest Laboratory, Richland, Washington

ABSTRACT

Either glass or crystalline materials can be shown to have some advantage when a single property is considered. However, the differences are small and each material has both assets and liabilities. With proper design, either type of waste form can almost certainly be utilized to solidify and contain radioactive waste.

INTRODUCTION

Investigation of methods to convert liquid radioactive wastes to inert solids began over twenty years ago. The goal was to increase safety during storage, transportation, and ultimate disposal. As this investigation has proceeded, a large number of waste forms have been studied in United States and foreign laboratories. There is general agreement from these studies that glass is a satisfactory waste form for first-generation waste solidification plants. In fact, a high-level waste vitrification plant is operating routinely in France, and plans are well advanced for such plants to be operating within the next 5 to 15 years in several countries.

However, glass is a metastable material not widely found in nature, and the possibility exists that more thermodynamically stable crystalline waste forms could provide an improved second-generation waste form, particularly if they can be tailored to be compatible with the host rock. This paper examines some of the major considerations involved in the comparison of glass and crystalline waste forms.

EASE OF FABRICATION

The ease of fabrication is considered in two parts: (1) the flexibility of the waste material and (2) the complexity of the process.

Flexibility refers to the ability of the waste form to incorporate the many diverse components characteristic of a radioactive waste stream and the ability of the waste solidification process to operate effectively with an ill-defined, frequently fluctuating waste stream composition. Glass has the required processing flexibility because it is a nonstoichiometric material that accepts most cations in a random atomic network. Relatively large compositional variations in the waste streams are readily accommodated.

Crystalline materials would appear to have less process flexibility because of their requirements of certain stoichiometries to achieve the desired properties. Solid solutions yield some processing flexibility within given crystals. Another route to processing flexibility would be to reduce the waste concentration in the waste form, as in the proposed *Synroc* process.[1]

Process complexity should include consideration of process cell size and remote mechanical operations, as each involves major cost impacts. The latter are particularly important, since remote operations must be carried out behind five ft of concrete. This remote design requirement makes it essential that the equipment be reliable, have a long life expectancy, and be maintainable by remote means. Clearly, the more complex the equipment, the more difficult it is to meet design operation and maintenance requirements. A recent comparison of waste form processes shows that glass processes are generally less complex than crystalline waste form options.[2]

CHEMICAL DURABILITY

The primary mechanism considered for release of radioactivity from waste solids involves water leaching and then groundwater transport to the biosphere.

TABLE 1

Leach Rate Comparison of Materials

Material	99°C Distilled water, g/cm² /d	250°C Salt brine,[4] g/cm² /d
Al_2O_3	1×10^{-6} (Ref. 5)	2×10^{-4}
Supercalcine	8×10^{-6} (Ref. 6)	1×10^{-4}
Waste glass	9×10^{-6} (Ref. 5)	7×10^{-4}
Granite	1×10^{-5} (Ref. 5)	6×10^{-4}
Soda-lime glass	5×10^{-5} (Ref. 5)	3×10^{-3}

Studies of release rates from waste forms have identified temperature, solution type, time of contact, flow rate of solution, approach to solubility limits, surface area and waste form type as important variables in determining release or leaching rates. Temperature is a major consideration, and testing at high temperatures and associated pressures has demonstrated that waste forms can be rapidly attacked.[3,4] A comparison of leach rates of potential waste forms and other materials in both high-temperature (250°C) brine and moderate-temperature (99°C) distilled water is shown in Table 1. These results are based on weight loss and indicate the relative behavior of materials. Note that the maximum difference at one temperature is a factor of 50. The comparisons indicate that, while differences between materials exist, those differences are relatively small and are not likely to make the difference in acceptance of a waste management system. It is recognized that weight loss measurements such as shown in Table 1 do not tell the complete story. For instance, selective displacement of Cs by Na can occur without significant weight loss. If one waste form were much more susceptible to such reactions than others, it would modify the preceding conclusion somewhat.

The effects of flow or solution-to-volume ratio upon potential leach rates are important to consider. Many room-temperature tests on glass are being done with an IAEA-type procedure which calls for replacement of solutions after set time periods. As a comparison to this, a set of tests has been run without changing the solution but with regular minor withdrawals of solution to analyze cesium and strontium concentrations. These concentrations have been converted to a total depletion layer or penetration depth and are shown in Fig. 1. It can be noted that *flow* and *non-flow* behave similarly in the early parts of the test, but after the concentrations build up in the non-flow or static system, the rate drops to a much lower value. Measurements of leach rate for the past two years show values of 3 to 5×10^{-9} g/cm²/day, which are 100 times lower than the average for the first 10 days.

Most autoclave tests have been run in sealed systems at high enough temperatures that equilibrium concentrations are approached. Data from Pacific Northwest Laboratory (PNL) and Pennsylvania State University on concentrations of fission product ions in solution after testing are shown in Table 2. The general agreement is quite good, considering the differences in testing periods and analysis methods. It is important to note that the differences in solution concentration between glass and supercalcine are not large. Glass is lower in some cases and supercalcine in others. This implies that differences in thermodynamic stability are not very important from a solubility point of view. A more important consideration is the difference in solution types and the effects of repository material on the allowable chemical equilibrium. This can be observed by comparison of the fission product ion concentrations in salt, distilled water and basalt for glass in Table 2, and the recognition that ion concentrations decrease in that order. A further interesting comparison reveals the nearly equal strontium concentration in the non-flow IAEA test and the distilled water autoclave tests. Even though different glass compositions are compared, it suggests that the approach to equilibrium may be responsible for the decrease in leach rate observed in these long-term tests.

This review indicates that solution flow and the interactions of solution and surrounding media on waste form are probably more important than are the differences between waste forms.

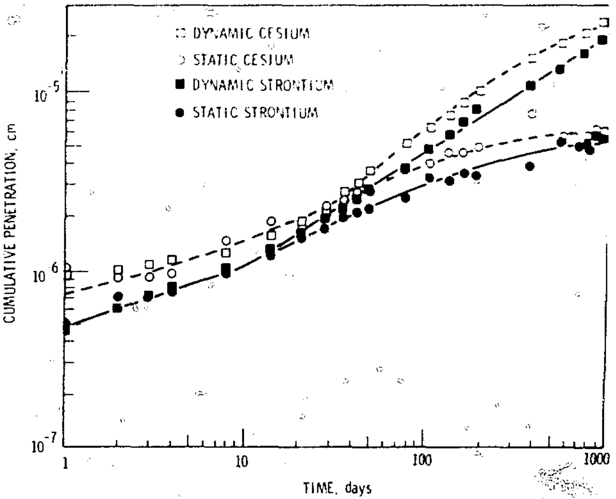

Fig. 1 Static versus dynamic leaching of a 72-68 waste glass composition.

Development of overpacks and engineered barriers is under way which can reduce the importance of waste form behavior in hydrothermal environments. This importance can also be reduced by means of repository design, with reduced thermal loading resulting in lower storage temperatures.

THERMAL STABILITY

The effects of temperature during processing, storage, or potential accident conditions on waste forms need to be evaluated for changes in phases and for volatility. Hydro-

TABLE 2

Concentration of Fission Products Leached from Glass and Supercalcine Materials (ppm)

Element	PNL* (WIPP brine) Glass (76-68), 7 days	PNL* (WIPP brine) Super-calcine (SPC-4), 3 days	Penn State* (USGS NBT-6a brine)[7] Glass (76-68), 28 days	Penn State* (USGS NBT-6a brine)[7] Super-calcine (SPC-4), 28 days	Penn State* (distilled water)[7] Glass (76-68), 28 days	Penn State* (distilled water)[7] Super-calcine (SPC-4), 28 days	PNL* (distilled water) Glass (76-68), 21 days	PNL* (distilled water) Super-calcine (SPC-4), 21 days	PNL* (basalt) Glass (76-68), 21 days	PNL Long-term static test† Glass (72-68), 3 years
Cs	650	2210	500	1600	49	22	37	20	0.8	1.30
Rb	87	487	64	470	10	41	24	11	0.15	
Sr	12	53	160	1300	0.64	1.4	1.3	4.8	0.31	1.04
Ba					0.5	6.9				
Mo	830	40	45	22	1110	540	940	34	1.6	

*Autoclave tests at 350°C.
†Room-temperature tests.

thermal reactions have already been considered in this paper in the discussion of leach behavior.

Phase Stability

For well-designed glasses, effects of anhydrous thermal treatment upon major properties (e.g., leach rate) have been shown to be small. A study by Turcotte and Wald has been presented[8] that gives details of the approach used, which now includes both isothermal and constant cooling rate studies and anneal times of up to one year. Other specific data have been reported in annual reports.[9,10]

Partial crystallization of glasses must be expected at temperatures near the softening point and up to the melting temperature. Devitrification, however, can mean formation of a glass-ceramic-like product without much change in properties. Because most waste glasses have been formulated to have viscosities of >200 poise at 1050°C, ion diffusivities are probably not very different in glasses studied to date. As a result, kinetics of devitrification have not been found to vary greatly in glass compositions studied so far. With respect to physical integrity, we find formation of large crystals can cause microcracking in either glass or ceramics. This is avoided in glasses by maintaining temperatures at less than 650°C.

Crystalline waste forms have already been reacted at high temperatures to give products stable at the preparation temperatures, which are much higher than any likely storage or accident conditions. Consequently, there have been fewer studies done on thermal stability of glass–ceramics, supercalcines, or Synrocs than on waste glasses. Tests on supercalcines have been made at 900°C which indicate that the phases do not recrystallize or that new phases do not form even though solid-solution regions are reduced.[6] Grain growth which should be avoided to prevent microcracking in polycrystalline materials will generally require temperatures in excess of 1000°C.

Volatility

Volatility studies in our work rely upon thermogravimetric methods with cold finger collection of vaporized species (for subsequent chemical analyses). Some results have already been reported by Gray.[11] As expected, the mobile alkali elements are major contributors—especially important because cesium is a major biohazard. Results for cesium are summarized in Fig. 2 for several glasses, for a Purex-type calcine composition (PW-4b), and for several hot-pressed supercalcine formulations. Also, some single-point data are shown for $CsAlSi_2O_6$ and $CsAlSiO_4$. It is important to recognize that the fractional losses shown reflect the sample size and the time period used in the experiments. In a comparative sense, the results clearly show crystalline forms have volatility losses 10 to 100 times

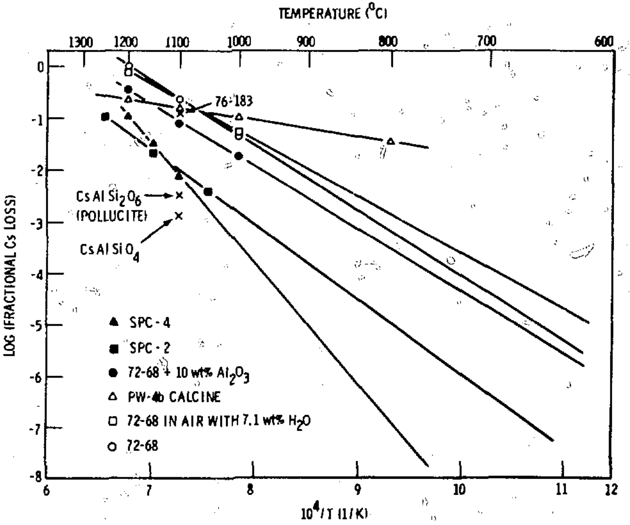

Fig. 2 Cesium loss from waste materials in four hr at various temperatures.

lower than typical waste glasses. For glasses, the presence of water has a small effect, and addition of alumina reduces cesium volatility, probably by simple increase of the viscosity. It is of note that unconsolidated calcine PW-4b shows high losses at 800°C.

For waste glasses and for supercalcines, vaporization appears to follow an *Arrhenius temperature dependence* with activation energies such that volatility at 1100°C decreases to lower rates by a factor of 10^5 or more at 600°C and can be considered negligible at lower temperatures.

RADIATION STABILITY

It is well recognized that the intense radiation fields within solidified nuclear wastes cause measurable property changes. All materials under serious consideration, including glasses, glass ceramics, supercalcines and cements, have been or are being studied. Waste glasses have been the most thoroughly studied, with specific reports available concerning stored energy,[12] helium diffusion,[13] and more general discussions.[9,10,14]

Although experiments are in progress to evaluate gamma field and transmutation effects (Cs → Ba) on both glasses and crystalline waste forms, the major interest has been in evaluating damage from alpha decay of the actinide elements, which is the major source of atomic displacement in solid wastes.[12] Most of the experimental work involves use of ^{244}Cm or ^{238}Pu as dopants to accelerate dose rates by factors of 10^3 to 10^5. Radiation effects in glasses have been simulated to $>10^5$ years for commercial HLW and to $>10^6$ years for lower-activity defense wastes. The work on supercalcines and on glass-ceramics has been undertaken to simulate times of $\sim 10^3$ years.

In studies of waste solids, saturation effects are usually observed at doses in the range of 2 to 5×10^{18} α/cm^3. For glasses major changes are not expected, since glass is a structurally disordered material and, in fact, only small changes have been observed. Depending upon the structure type, crystalline phases are expected to become X-ray amorphous or there may be no loss of structure (especially for simple, cubic oxides). In our work with partially devitrified glasses, glass-ceramics and supercalcines, some of the actinide-containing phases (silicates, titanates) do, in fact, become X-ray amorphous.

Figure 3a summarizes the volumetric changes determined by density measurement for a variety of waste glasses (number coded), supercalcine and a glass–ceramic. In Fig. 3b, results obtained by X-ray diffraction for several actinide compounds are given, either from our own studies or from the literature. The density changes for waste solids are small and can be negative for some glasses. An individual crystalline material, even when contained within a waste as for (1)* RE apatite in supercalcine or (2)* RE titanite in glass ceramics, can have much larger changes, which will introduce stress into the solid.

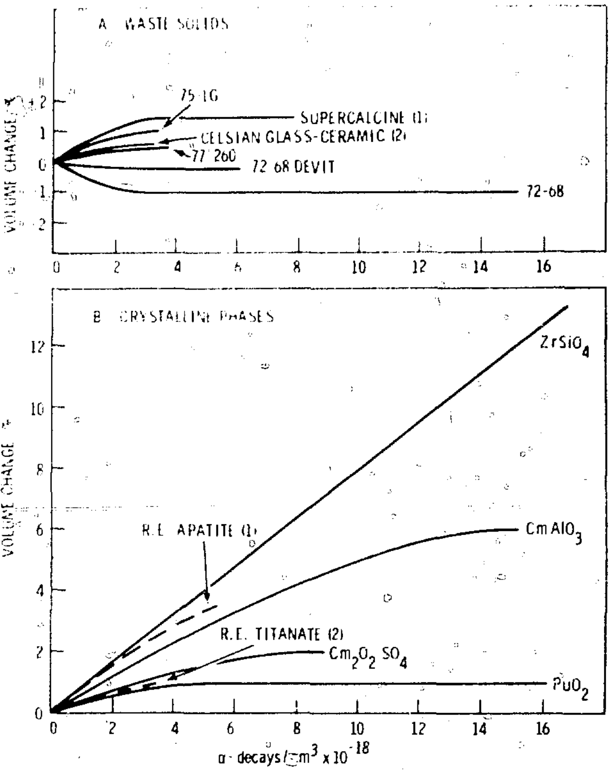

Fig. 3 Effects of radiation on the density of (a) waste solids and (b) crystalline phases.

Measurements of stored energy, impact strength, helium diffusivity, and leach rate have been made on waste glasses, and they show minor radiation-induced changes that do not significantly alter the initial properties. For crystalline waste forms, much less information is available. It is clear that arguments of improved stability for crystalline structures (i.e., lower free energy than in disordered glasses) must be tempered by a recognition that many structures are not stable in the presence of the radioactive elements they are meant to contain. The importance of structural stability is still to be established, since it is also recognized that amorphous (metamict) zircon is commonly found in nature—indicating that this radiation-altered crystal retains a high degree of chemical stability.

MECHANICAL BEHAVIOR

The mechanical behavior of waste materials is important, since both crystalline and glass forms are brittle at normal storage temperatures and mechanical impact will fracture waste forms into particles of various sizes. Fine particles are of most concern, since the <10-μm-size fraction is respirable. The rate of radioactive release by leaching may also increase with increased surface area. The comparison of waste forms indicates that glass forms may produce a greater fraction (~4×) of fine particles upon impact, but will have lower surface areas (~100×) than will sintered crystalline forms. If crystalline materials are hot pressed under proper conditions, surface areas will be similar to those of glass. Massive forms of glass or crystalline materials will be susceptible to thermal-shock fracturing. Glasses are only thermal-shock prone below 550°C; crystalline materials, however, can also be thermally shocked at much higher temperatures.

---

*Numbers correspond to designation in Fig. 3.

CONCLUSIONS

Glass waste forms have been under development for many years and are considered the waste form of choice for near-term utilization. Recently glass has been criticized for its metastable nature and its potential for rapid reaction in a hydrothermal environment. Crystalline forms have been suggested as being more durable in a repository environment. A comparison of glass and potential crystalline forms shows that they have comparable solubilities. A review of the other factors indicates that glass waste forms offer advantages in ease of processing and radiation stability, and that crystalline materials exhibit better thermal stability. To date, tests have shown that differences between glass and ceramic waste form properties are small. With proper design, either glass or crystalline forms can almost certainly be utilized to solidify and contain radioactive waste.

ACKNOWLEDGMENTS

This work was supported by the U. S. Department of Energy under contract EY-76-C-06-1830.

There are many contributions to the work reviewed in this paper. We would like to acknowledge major collaborators: J. H. Westsik, Jr., chemical durability; W. J. Gray and J. W. Wald, thermal stability; F. P. Roberts and W. J. Weber, radiation stability; and L. R. Bunnell, mechanical behavior.

REFERENCES

1. A. E. Ringwood, *Safe Disposal of High-Level Nuclear Reactor Wastes A New Strategy*, Australian National University Press, Canberra, Australia, 1978.
2. W. A. Ross, J. M. Rusin, and J. L. McElroy, Processes for Production of Alternative Waste Forms, *Proceedings of the Symposium on Waste Management*, Tucson, Arizona, February 1979.
3. G. J. McCarthy et al., Interactions Between Nuclear Waste and Surrounding Rock in Geologic Disposal, *Nature*, 273. 216 (1978).
4. J. H. Westsik, Jr., and R. P. Turcotte, *Hydrothermal Reactions of Nuclear Waste Solids – A Preliminary Study*, PNL-2759, Pacific Northwest Laboratory, 1978.
5. J. E. Mendel and W. A. Ross, The Chemical Durability of Glasses Containing Radioactive Fission Product Waste, 76th Annual American Ceramic Society Meeting, Chicago, April 1974.
6. G. J. McCarthy, High-Level Waste Ceramics: Materials Considerations, Process Simulation, and Product Characterization, *Nucl. Tech.*, 32(1): 101, January 1977.
7. G. J. McCarthy et al., Hydrothermal Interaction Among Nuclear Wastes, Containment and Hot Rocks in Geologic Repositories, in Proceedings of *Scientific Basis for Nuclear Waste Management*, Boston, G. J. McCarthy (Ed.), Plenum, NY, 1979.
8. R. P. Turcotte and J. W. Wald, *Devitrification Behavior in a Zinc Borosilicate Nuclear Waste Glass*, PNL-2247, Pacific Northwest Laboratory, 1978.
9. J. E. Mendel et al., *Annual Report on the Characteristics of High-Level Waste Glasses*, BNWL-2252, Pacific Northwest Laboratory, 1977.
10. W. A. Ross et al., *Annual Report on the Characteristics of High-Level Waste Glasses*, PNL-2625, Pacific Northwest Laboratory, 1978.
11. W. J. Gray, *Volatility of a Zinc Borosilicate Glass Containing Simulated High-Level Radioactive Waste*, BNWL-2111, Pacific Northwest Laboratory, 1976.
12. F. D. Roberts, G. H. Jenks, and C. D. Bopp, *Radiation Effects in Solidified High-Level Wastes – Part I, Stored Energy*, BNWL-1944, Pacific Northwest Laboratory, 1976.
13. R. P. Turcotte, *Radiation Effects in Solidified High-Level Wastes – Part 2, Helium Behavior*, BNWL-2051, Pacific Northwest Laboratory, 1976.
14. J. E. Mendel, *The Storage and Disposal of Radioactive Wastes as Glass in Canisters*, PNL-2764, Pacific Northwest Laboratory, 1978.

GLASSES AS MATERIALS USED IN FRANCE FOR MANAGEMENT OF HIGH-LEVEL WASTES

R. A. BONNIAUD, N. R. JACQUET FRANCILLON, F. E. LAUDE, and C. G. SOMBRET
Commissariat à l'Energie Atomique, Marcoule, France

ABSTRACT

Sodium borosilicate and sodium aluminoborosilicate glasses have been selected as final materials in the field of the solidification of high-level radioactive wastes. The properties related to long-term storage are reviewed. The effects of alpha emission upon the structure and of aqueous leaching upon radioactive release are emphasized.

HISTORICAL BACKGROUND

The research and development of the solidification of high-level radioactive wastes have been under investigation in France for over 20 years. In the very beginning emphasis was on the preparation of synthetic minerals as it was thought that crystals seemed to be more stable than the vitreous state and therefore more relevant to the fixation of radionuclides. As a matter of fact, some micas, mainly phlogopites, were prepared successfully.[1,2] But it was soon apparent that the minerals were too specific to fix the whole spectrum of fission products. A cesium mica which displayed a good retention of cesium, for instance, had a rather high water-leaching rate with regard to the other elements. It would have been necessary to perfect a multiple mineral that was quite impossible owing to the large range of nuclides involved in the wastes. Such a mineral does not exist in nature. Since the vitreous network is more suitable to bond the various radioactive ions, glasses were investigated; moreover, the temperatures needed to make glasses are generally lower than temperatures used for the synthesis of minerals.

FRENCH HIGH-LEVEL WASTE SOLUTIONS

The commercial spent fuels presently reprocessed in the French nuclear plants are mainly made of natural uranium (graphite gas reactor system). The subsequent fission products solutions are concentrated to 30 l/T according to the burn-up rate. The highly concentrated defense wastes generated by the reprocessing of the same type of fuel, but with a lower burn-up rate, give rise to glass containing a maximal amount of fission product oxides of 6.4% corresponding to about 7.5 liters of glass per ton of spent fuel. The above-mentioned commercial waste solutions are mixed with defense wastes. Their vitrification generates 11 to 15 liters of glass per ton of spent fuel with a maximum fission product content of 10.8%. All these wastes can be vitrified in the A.V.M. vitrification plant at Marcoule.[3]

Vitrification plants, already under design, will make it possible to vitrify solutions coming from the reprocessing of higher burn-up spent fuel from light water and fast breeder reactors. The investigations carried out to determine suitable glasses take into account the following:

- The solutions will be vitrified 4 years after the LWR fuel discharge and at least 2 years after the FBR fuel discharge.
- The fission products content of the glass will be assigned an upper limit in order to decrease the temperature during storage.
- The most alpha-contaminated caustic solutions resulting from the solvent washing process and the liquids generated by the decontamination of some equipment will be added to the fission products solution and therefore vitrified.

- The content of the total waste in the glass must not be in excess of 25 wt.%.
- The total content of the network former oxides has to be higher than 60 wt.%.

In addition, the technological investigations will be directed toward a higher glass melting point. It applied to 500 l/T concentrated LWR solutions (see example in Table 1), this procedure will produce 94 liters of glass per ton of spent fuel with a 27 W/l specific power. Applied to 1000 l/T concentrated FBR solution (see Table 1), 235 liters of glass with a 26 W/l specific activity will be made per ton of fuel.

TABLE 1

Characteristics of French High-Level Wastes Generated by the Reprocessing of Commercial Oxide Fuels

Reactor system	Type of fuel	Burnup, MWd/T	Concentration rate, l/T	Acidity, N	Approximate chemical composition, g/l Al	Na	Fe	Ni	Cr	P	Gd	Actinides	F.P.
LWR	UO_2	33,000	500	1.8	1	20	20	1	1.5	1	0 or 25	4	67
FBR	UO_2/PuO_2	66,000	1000	2.0		19	15	Low	Low	1	27	4.8	25

TABLE 2

Example of Glass Compositions

Reactor system	Weight composition, % SiO_2	Na_2O	B_2O_3	Al_2O_3	Fe_2O_3	Gd_2O_3	$NiO + Cr_2O_3$	Fission products and actinides oxides	Volume reduction rate	Volume of glass per ton of spent fuel, l
LWR	47.6	12.4	18.6		6.4		Low	15.0	5.5	94
FBR	46.0	15.0	17.9	6.3	3.6	5.2	0.3	6.0	4.9	205

COMPOSITION AND PROPERTIES OF SUITABLE GLASSES

The composition selected for a given radioactive waste glass is governed by three factors: (1) the constituents of the radioactive waste to be immobilized, (2) the vitrification process to be used, and (3) the properties desired for the immobilized waste product.

Silicates are the most stable glasses and have been chosen to be the basic products. An example of glass composition is given in Table 2. The final selection of the glass composition will not take place before 1984 1985. It will be a compromise between the technological requirements and the needed chemical and physical properties.

EFFECT OF THE CONSTITUENTS OF THE WASTES

The range of compositions initiating or not initiating the so-called "yellow phase" has been determined previously for waste solutions free of iron.[4] The occurrence of ferric nitrate in the new wastes made it necessary to repeat the study for these liquids. It appears that the effect of iron is negligible. It is even possible to minimize the region of yellow-phase-containing glasses by substituting CaO for a part of the Na_2O (Fig. 1).

PROCESS REQUIREMENTS

The properties of the vitrification process must be investigated with respect to:

- Corrosion of the vessels
- Volatility of ruthenium
- Viscosity low enough to allow the glass to be transferred into canisters

Many investigations of corrosion make it possible to predict the lifetime of vessels made of various metals. The volatilization of ruthenium, which could cause a blockage in the off-gas line due to a RuO_2 deposit, can be reduced by the use of sugar.[5] The maximum viscosity of the glass which is allowed for the French vitrification process is 600

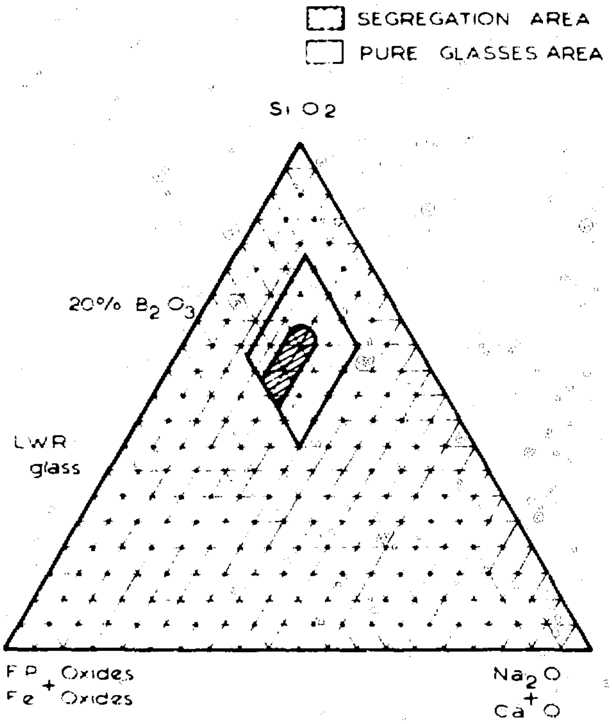

Fig. 1 Composition range of phase segregation in LWR waste glass.

poises at 1100°C. This is easily achieved owing to the boron content of the various compositions.

PROPERTIES CONNECTED WITH DISPOSAL

The main properties to be investigated in relation to long-term glass disposal are:

- Leach rate of the nuclides
- Effect of beta irradiation
- Behavior of the materials under thermal conditions
- Effect of alpha irradiation

The knowledge of these properties is essential to evaluate the quality of the glasses and to predict their behavior in the course of time. A maximum chemical inertness coupled with an adequate mechanical resistance is needed to make te and ineffective a possible way back to man for the contained radioactivity.

The leach rates measured in a shielded cell from 2 kg glass blocks containing 100 to 1000 beta gamma curies activity and leached by tap water at room temperature were found to be 1 to 5 x 10^{-8} g/cm²·d for ruthenium and cerium and ~5 x 10^{-7} g/cm²·d for cesium and strontium after an apparent steady state was reached.[6]

Figure 2 shows the leach rate values versus time. This long-term leaching test demonstrated an apparent steadiness of the leach rate after the 40th day. The leach rate values do not seem to be affected by the presence of a yellow phase in a high boron content glass (Table 3). The effect of temperature upon the leach rates is important with regard to the more diffusible ions (cesium and strontium). Factors of the increase are approximately 3 if temperature goes from 25 to 50°C, 10 if temperature goes from 25 to 70°C, 33 if temperature goes from 25 to 100°C, and 180 if temperature goes from 25 to 150°C.

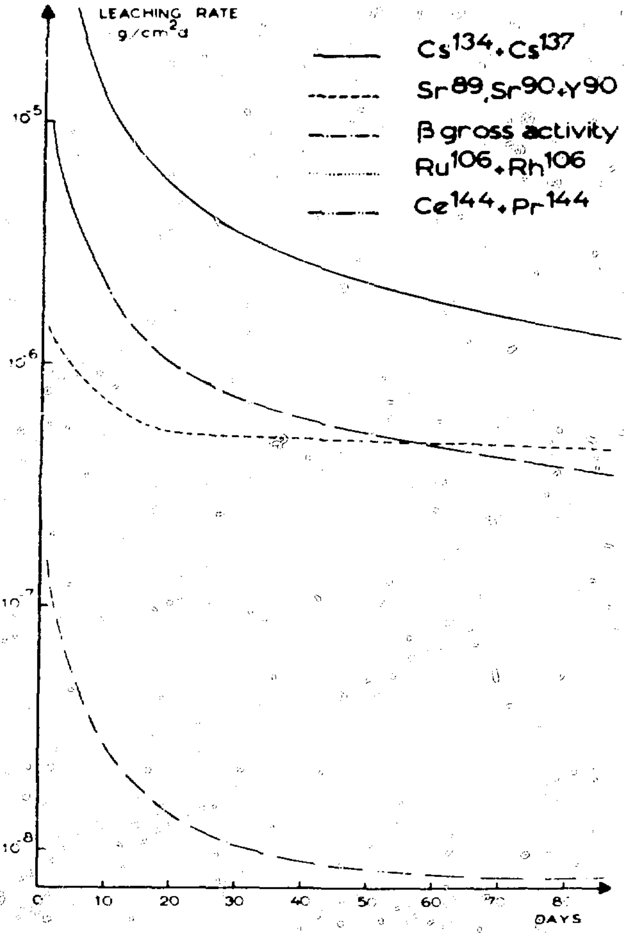

Fig. 2 Long-time leaching rate of a LWR glass.

TABLE 3

Compared Leach Rate Values

	β	Cs	Sr	Ru	Ce
			20% B_2O_3 glass		
With Mo*	2×10^{-7}	2×10^{-7}	3×10^{-7}	9×10^{-7}	3×10^{-8}
Free of Mo	1.5×10^{-7}	3×10^{-7}	3×10^{-7}	1×10^{-7}	3×10^{-7}
			14% B_2O_3 glass		
With Mo*	5×10^{-6}	2×10^{-5}	2×10^{-6}	1×10^{-7}	4×10^{-7}
Free of Mo	2×10^{-7}	7×10^{-7}	2×10^{-7}	1×10^{-7}	1×10^{-7}

*Presence of a yellow phase.

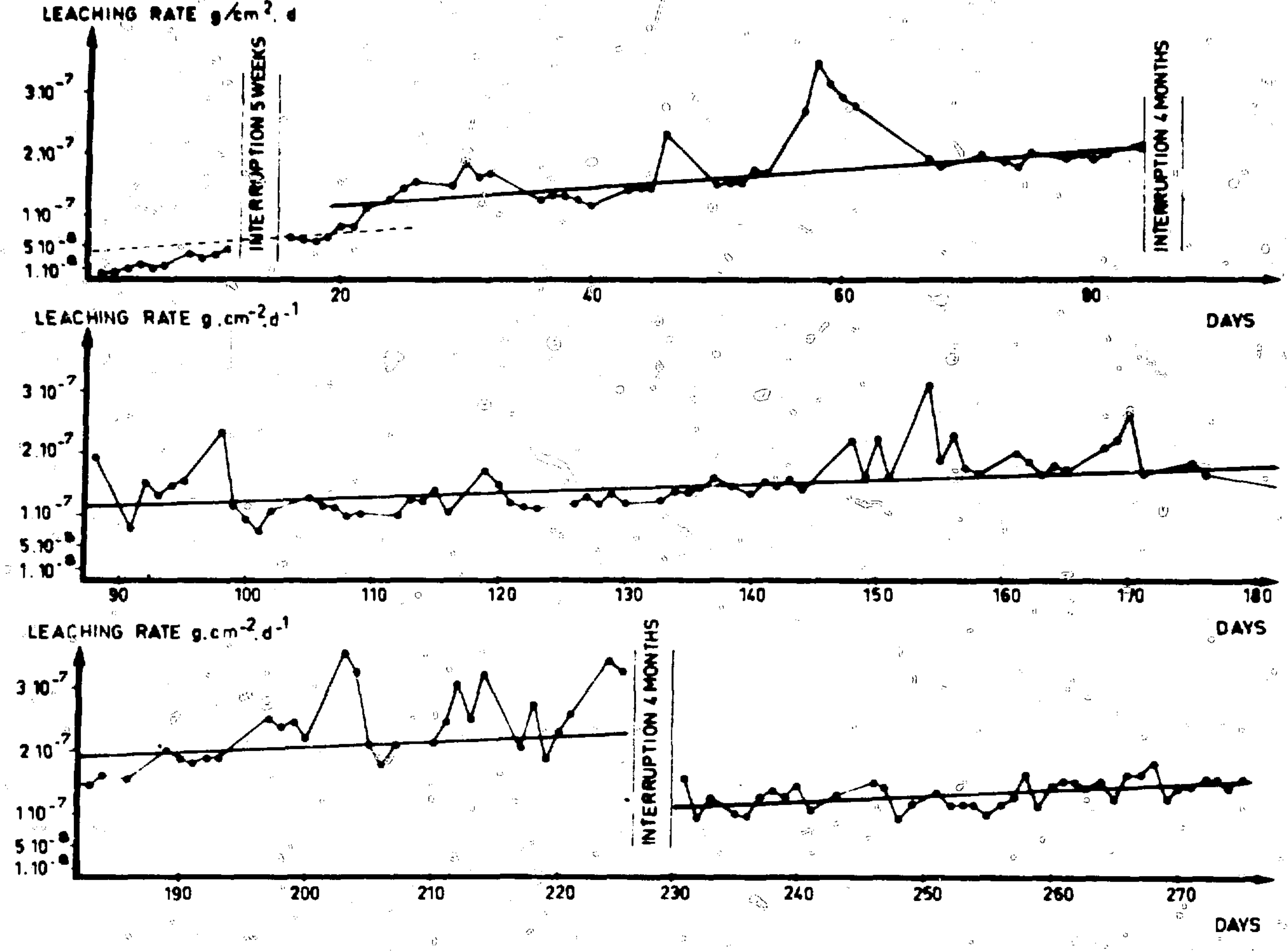

Fig. 3 Leaching curve of ^{238}Pu.

The leach rate of plutonium increases slightly with time. If the leaching process is interrupted and resumed months later, the starting value is lower than the previous one (Fig. 3), but the rate is still increasing. Nevertheless, the increment does not make up for the loss due to the radioactive decay. The effect of beta irradiation is of no importance.[7] However, alteration of the glass structure may occur after heat treatments. The results of tests in which glass samples were kept at a constant temperature of 700 and 800°C confirmed the results of previous tests made at 500 and 600°C (Ref. 8); namely, the glasses containing more than 40% silica behave well.

TABLE 4

Number of Alpha Disintegration/g of Glass

	1 year	2 years	3 years	4 years
^{241}Am glass	9.36×10^{16}	1.87×10^{17}	2.8×10^{17}	3.7×10^{17}
^{238}Pu glass	1.4×10^{17}	2.84×10^{17}	4.24×10^{17}	5.64×10^{17}
^{244}Cm glass	1.04×10^{18}	2.06×10^{18}	3.04×10^{18}	4.01×10^{18}

TABLE 5

Evolution of Density in Relation to Time

^{241}Am glass	Time, days	870	966	1058	1152	1240	1329
	Density	2.818	2.819	2.817	2.817	2.817	2.818
^{238}Pu glass	Time, days	794	892	982	1076	1162	1253
	Density	2.666	2.665	2.666	2.667	2.666	2.667

The effect of actinides is being investigated using alpha-doped glasses. The composition of these glasses has already been given.[9] The cumulative disintegration events versus time are given in Table 4.

The densities of the various glasses appear to be constant (Table 5). The mechanical resistance evaluated in terms of microhardness (Knoop test) seems to be decreasing slightly (Table 6). Until now, no crystallization has been observed by SEM investigation on alpha-doped glasses irradiated at 4 x 10^{17} alpha disintegrations per gram of glass.

TABLE 6

Evolution of Microhardness in Relation to Time

^{241}Am glass	Time, days	163	327	503	653	1109	1348
	Kgf/mm^2	500	420	420	477	420	380*
^{238}Pu glass	Time, days	427	577	1037	1272		
	Kgf/mm^2	527	510	450	430		

*Mean value.

CONCLUSIONS

Glass blocks in long-term disposal will have to withstand for decades the thermal wave due to the radioactive decay of fission products. It is also necessary to know their state later when the alpha emitters play a leading part. The effect of the actinides is not yet investigated enough to permit recommendations about storage conditions. Work related to this topic must be emphasized, but as long as we do not know more, the following steps should be taken to set up a safe geological repository:

- Do not dispose of the blocks in the ultimate place before 30 years in order that the maximum temperature is not in excess of 150°C.
- Surround the glass canister with a container which can act as a complementary barrier against water intrusion during the time required for the glass to be cooled.

REFERENCES

1. R. Bonniaud, P. Cohen, and C. Sombret, Solidification of Concentrated Residual Solutions of Fission Products, *Second International Conference of the United Nations on the Utilization of Atomic Energy for Peaceful Uses,* A/CONF 15P/1176, Geneva, May 1958.
2. R. Bonniaud, P. Cohen, and C. Sombret, *Essay on the Incorporation of Concentrated Solutions of Fission Products in Glasses and Micas,* CEA 1759 (1958).
3. R. Bonniaud, A. Jouan, and C. Sombret, Large Scale Waste Glass Production, in Proceedings of *High Level Radioactive Solid Waste Forms,* Denver, NUREG/CP-0005, National Technical Information Service, Springfield, VA, 1979.
4. R. Bonniaud and C. Sombret, Statement of the Research in the Field of Solidification of High Level Radioactive Wastes in France, *77th Annual Meeting of the American Ceramic Society,* Washington, DC, May 1975.
5. R. Bonniaud, A. Jouan, and C. Sombret, in Symposium Proceedings of *Status of the French AVM Vitrification Facility Waste Management 79,* Tucson, February 1979.
6. R. Bonniaud, A. Jouan, and C. Sombret, *The VULCAIN Series of Reports on Glasses,* Note CEA-1341 (1971).
7. R. Bonniaud, F. Pacaud, and C. Sombret, Some Bearings About the Behaviour of Ultimate Stored Radionuclides in the Form of Glass or Glassy Matrix Product, in Symposium Proceedings of *Congrès de la Société Française de Radioprotection,* Versailles, VII, SFRP/I, May 1974.
8. R. Bonniaud, F. Laude, C. Sombret, and G. Rabot, Containment of Radioactivity in Glasses, *International Symposium on the Management of Radioactive Wastes from the Nuclear Fuel Cycle,* IAEA/OECD, Vienna, IAEA SM 206/36, March 1976.
9. R. Bonniaud, Actinides in Glasses, *Bulletin on the Information of Sciences and Techniques,* 217, September 1976.

CHARACTERIZATION OF BOROSILICATE GLASSES CONTAINING SIMULATED HIGH-LEVEL RADIOACTIVE WASTES FROM PNC

R. TERAI, K. EGUCHI, and H. YAMANAKA
Government Industrial Research Institute, Osaka, Midorigaoka 1, Ikeda-City, Osaka-Pref., Japan

ABSTRACT

The characterization of borosilicate glasses containing simulated HLW from PNC has been carried out. Phase separation of molybdates, volatilization, viscosity, electrical resistivity, thermal conductivity, elastic modulus, chemical durability, and devitrification of these glasses have been measured, and the suitability of the glasses for the vitrified solidification processes is discussed from the viewpoint of safety.

INTRODUCTION

Development of vitrified solidification processes of HLW in Japan is mainly carried out at Power Reactor and Nuclear Fuel Development Corporation (PNC) and the characterization of the glasses is investigated at GIRIO and PNC. This report is concerned with the investigation of the chemical compositions of glasses suitable for the containment of HLW.

EXPERIMENTS AND RESULTS

Properties of Molten Glasses

Phase Separation of Molybdates. In order to elucidate fundamentally the phase separation of molybdates from borosilicate glasses, the absorption capacity for MoO_3 in silicate, borate, and phosphate melts has been measured at 1400°C for silicate and at 1000°C for borate and phosphate, using 250 ml high-alumina clay crucibles with lid. The solubility of MoO_3 in melts was defined as the weight of MoO_3 dissolved in 100 g of base glass for one hr without phase separation. Table 1 shows that the magnitudes of solubility of MoO_3 are the order of phosphate > borate > silicate melts and that the phosphate can dissolve so much larger quantities of MoO_3 that it may be called a molybdate glass rather than a phosphate glass. In the system Na_2O–B_2O_3, a very huge maximum on the solubility curve was observed at $Na_2O \cdot 4B_2O_3$, and a small maximum at $Na_2O \cdot 2B_2O_3$, as shown in Fig. 1, which corresponded to the compositions of the compounds formed in the Na_2O–B_2O_3 phase diagram. Although borate and phosphate glasses exhibit large solubility of MoO_3, these melts are not suitable for containment of HLW because of their very poor durability to water. Thus the incorporation of fission products in borosilicate glasses is limited by the silica contents. However, some ions in a certain range of cationic field strength, such as Mg, Zn, Al, and Zr, were effective in preventing the precipitation of molybdates from borosilicate glasses. In Table 2 the glass compositions suitable for the incorporation of HLW have been listed on the basis of investigations carried out on the phase separation of molybdates.

The effects of melting time and temperature on the phase separation of molybdates were also investigated using glasses containing about 5% more wastes than the glasses listed in Table 2. It was found that the absorption capacity for MoO_3 in melts could be increased by holding the glasses at a higher temperature or for a longer time. The stirring of molten glass and the addition of silicon powders as reducing reagents also improved considerably the phase separation.

Volatilization. Most of the volatilization processes of borosilicate glasses were apparently zero-order reaction at temperatures of 900 to 1300°C, which seems to suggest that the rate-controlling step is the simple escape of volatile components from the surface of melts.[1] Activation energies calculated from an Arrhenius plot of the volatilization rates, as shown in Fig. 2, were about 60 kcal/mole, similar

TABLE 1

Solubility of MoO_3 in Silicate, Borate, and Phosphate Melts

Base glass	Solubility of MoO_3, g of MoO_3/100 g of base glass
$Na_2O \cdot 2SiO_2$	4 (Melted at 1400°C)
$Na_2O \cdot 2B_2O_3$	30 (Melted at 1000°C)
$Na_2O \cdot 2P_2O_5$	500 (Melted at 1000°C)

to the evaporation heats of various kinds of meta-alkali borates which roughly corresponded to the preferential volatile constituents determined by chemical analysis.[1] The volatilization from glasses with the ratio of $Na_2O/B_2O_3 > 1$ was not affected by the concentration of water vapor in the atmosphere, while the volatilization from glasses with $Na_2O/B_2O_3 < 1$ was enhanced by the formation of various metaboric acids.

Viscosity. Viscosity was measured by a rotary cylinder method in the range of 700 to 1400°C. Low melting temperature glasses had very low viscosity at the elevated temperature, and the activation energies for viscous flow also showed very low values, about 20 to 30 kcal/mole.

Electrical resistivity. The measurement was carried out by a bridge with compensative condenser. The activation energies for electrical conductivity above 1000°C were about 15 kcal/mole, suggesting that the sodium ions in the melts were predominantly responsible for the electric current.

Properties of Solid Glasses

Thermal Conductivity. Thermal conductivity was measured by the laser-flash method from room temperature to 500°C.[2] A laser-absorbing film consisting of silicon was deposited on the surface of the specimen by RF-sputtering. Figure 3 shows that thermal conductivity of glasses increases with temperature, depending upon the change of the heat capacity of glasses. The values obtained by the hot-wire method agree with those obtained by the laser-flash method at room temperature.

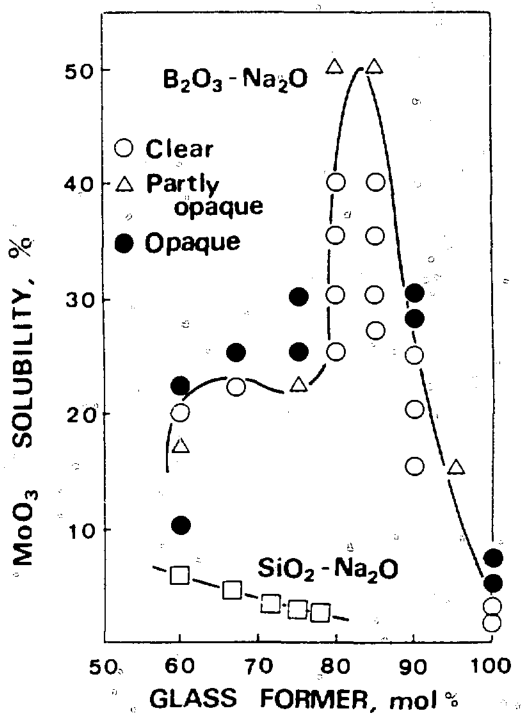

Fig. 1 Solubility of MoO_3 in Na_2O–B_2O_3 and Na_2O–SiO_2 systems.

TABLE 2

Chemical Compositions and Physical Properties of Typical Glasses Containing Simulated High-Level Radioactive Wastes

Glass	LB-I	LB-II	LB-II'	MB-I	MB-II	MB-II'	HB-II'	HB-II'
Melting temperature (°C)	1150–1200	1150–1200	1150–1200	1300–1350	1300–1350	1300–1350	1450–1500	1450–1500
Composition (wt.%)								
SiO_2	38.1	40.8	40.0	43.1	46.0	41.5	59.3	42.6
B_2O_3	14.3	15.3	17.7	11.2	12.0	15.5	9.3	8.3
Li_2O	5.6	5.4	3.0	2.6	2.8		1.2	1.2
Na_2O	4.5	4.8		2.7	2.9			1.2
MgO			3.0			5.0		7.5
CaO	4.8	5.1	3.0	2.6	2.8			
ZrO_2								2.5
Al_2O_3	12.0	5.3	6.1	13.6	6.1	7.0	5.3	6.7
Waste oxides	21.3	23.3	27.2	23.9	27.2	31.0	23.3	30.0
Density (g/cm^3)	2.70	2.74	2.74	2.68	2.73	2.70	2.56	2.75
Thermal expansion coefficient ($\times 10^7$/°C)	105	117	91	95	97	77	72	89
Transition point (°C)	483	462	492	498	500	566	543	556

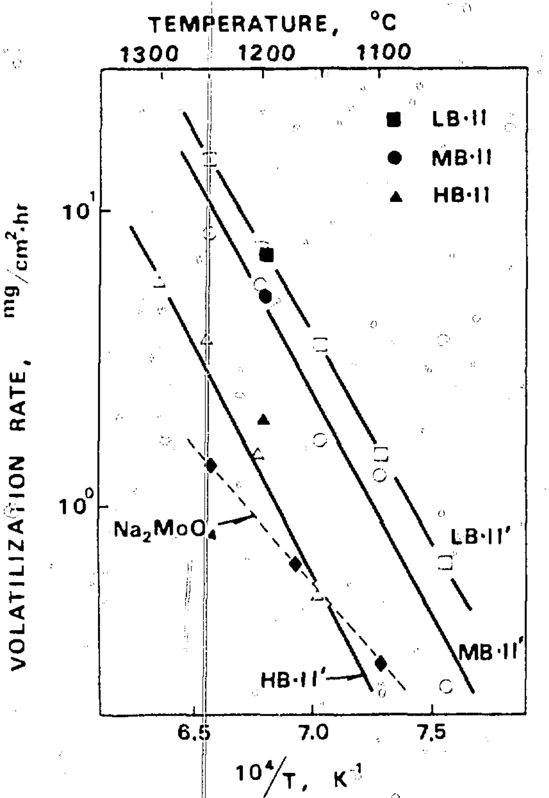

Fig. 2 Arrhenius plots of volatilization rates from the molten glasses.

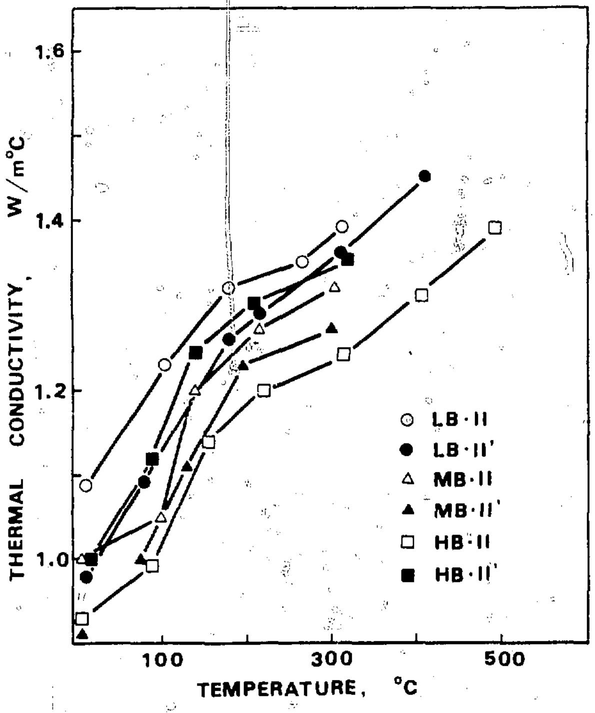

Fig. 3 Variation of thermal conductivity with temperature for various glasses.

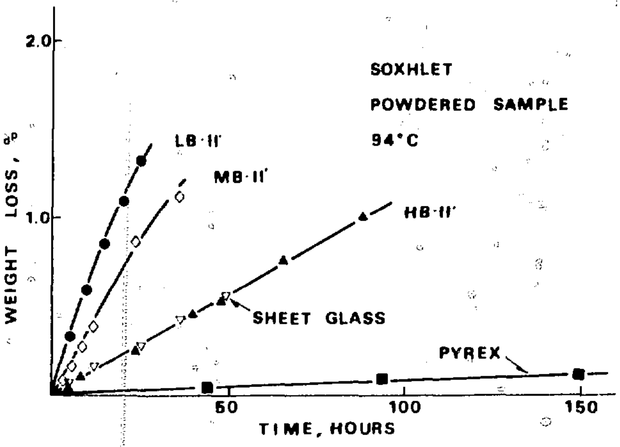

Fig. 4 Variation of weight loss at Soxhlet leaching test with time for various glasses containing the simulated HLW, sheet glass, and Pyrex glass.

Elastic Modulus. Longitudinal and shear sound velocities in glass were measured by the ultrasonic interference method.[3] Elastic properties estimated from the sound velocities, that is, Young's modulus, shear modulus, bulk modulus, and Poisson's ratio, are almost the same as normal silicate glasses.

Chemical Durability, Leachability. (1) Soxhlet leaching method. Figure 4 shows the variation of weight loss with time for various glass powder samples at 94°C. The weight loss revealed slightly parabolic curves, which could be expressed by the square root law in a certain range. Activation energies calculated from the rates at various temperatures below 100°C were about 10 to 12 Kcal/mole, which seems to indicate that the rate-controlling step in the reaction between glass and water may be related to the hydration on the glass surface, especially to the diffusion of protons in hydrated layer. (2) Continuous leaching method. In this method, about 30 g of powdered sample is put in the cell and distilled water flows through the cell at the rate of 250 ml/day. Figure 5 shows the variation of Na_2O extracted into water at 20°C with time for various glasses. There are two types of leaching curves: almost linear curves and saturated ones. The former are thought to be caused by the congruent glass dissolution, and the latter reveal that a resistant layer is formed on the surface.[4] The leach rates calculated from the data in Fig. 5 were on the order of 10^{-6} to 10^{-7} g of $Na_2O/cm^2/day$; the values for SiO_2, SrO, and Cs_2O were also approximately the same order as for Na_2O.

Crystallization Behavior. Borosilicate glasses containing about 30% of the simulated HLW were devitrified easily when the glasses were held above the temperature of upper annealing points. Most of the crystals appearing were various molybdates as shown in Table 3. It seems to prove that the molybdates are not intrinsically compatible with borosilicate glasses, even though the molybdates apparently

TABLE 3

Main Crystals in Glasses Heat Treated at Various Conditions

Glass	600°C, 1 month	700°C, 2 weeks	800°C, 2 weeks
LB-I	$Na_2Ca_2Al_6Si_6O_{24}(MoO_4)_2$ $NaAlSiO_4$	$Na_2Ca_2Al_6Si_6O_{24}(MoO_4)_2$ $NaAlSiO_4$	$Na_2Ca_2Al_6Si_6O_{24}(MoO_4)_2$ $NaAlSiO_4$
LB-II	None	Uncertainty	Uncertainty
LB-II′	None	$NaNd(MoO_4)_2$ $LiNd(MoO_4)_2$	$NaNd(MoO_4)_2$ $LiNd(MoO_4)_2$
MB-I	$LiNd(MoO_4)_2$ $CaMoO_4$	$LiNd(MoO_4)_2$ $(Ca,Na)MoO_4$	$LiNd(MoO_4)_2$ $CaMoO_4$
MB-II	$NaNd(MoO_4)_2$ $LiNd(MoO_4)_2$	$NaNd(MoO_4)_2$ $LiNd(MoO_4)_2$	$NaNd(MoO_4)_2$ $CaMoO_4$
MB-II′	None	Uncertainty	$NaLa(MoO_4)_2$ $CaMoO_4$
HB-II	$NaLa(MoO_4)_2$	$NaLa(MoO_4)_2$ $(Ca,Sr)MoO_4$	$NaLa(MoO_4)_2$
HB-II′	None	$NaCaAlSi_5O_{16}$	Rb_2CrO_4 $Ca_3Si_3O_9$

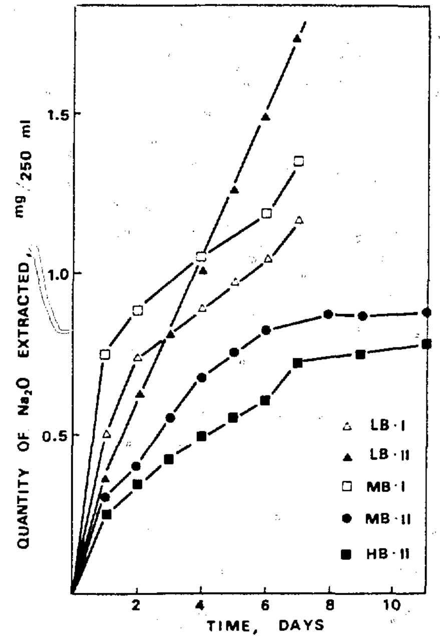

Fig. 5 Variation of quantity of Na_2O extracted into water at continuous leaching test with time for various glasses.

once dissolved in melts. Crystallinity was calculated from the change of halo height at $2\theta = 12°$, $21°$, and $25°$ of X-ray diffraction patterns.[5] The results show that crystallinity in glasses is very small, several percent, and seem to relate closely to the molybdate content in glasses. The effect of crystallization on the chemical durability, therefore, was practically undetected after heat treatment of 600 to 800°C for less than one month.

REFERENCES

1. R. Terai and E. Kosaka, Volatilization of Low Temperature Borosilicate Glasses for High-Level Radioactive Wastes at Elevated Temperatures, *Bull. Gov. Ind. Res. Inst. Osaka*, 27(3): 150 (1976).
2. R. Terai and M. Hori, Measurement of Thermal Conductivity of Borosilicate Glasses by Laser-Flash Method, *J. Ceram. Soc. Japan*, 85(3): 140 (1977).
3. R. Ota, N. Soga, and M. Kunugi, Elastic Properties of As–Se Glasses, *J. Ceram. Soc. Japan*, 81(4): 156 (1973).
4. L. L. Hench and D. E. Clark, Physical Chemistry of Glass Surface, *J. Non-Cryst. Solids*, 28: 83 (1978).
5. L. Červinka, Determination of Crystallinity in Crystallized Glasses by X-Ray Diffraction, *J. Non-Cryst. Solids*, 21: 125 (1976).

CHARACTERIZATION AND EVALUATION OF MULTIBARRIER NUCLEAR WASTE FORMS

J. M. RUSIN, R. O. LOKKEN, and J. W. WALD
Pacific Northwest Laboratory, Richland, Washington

ABSTRACT

Four multibarrier concepts using coatings and metal matrices were developed and demonstrated on a 1-liter scale. The effect of volatility, leachability, and impact resistance on product integrity is discussed. Results of radiation stability tests are also included.

INTRODUCTION

The Radioactive Waste Immobilization Program conducted by the Pacific Northwest Laboratory (PNL) for the United States Department of Energy (DOE) has as one of its objectives the development of processes for converting high level liquid waste (HLLW) from alternative fuel cycles and U. S. defense programs to solid forms demonstrated to be physically, chemically, and radiolytically stable and inert. A major part of this program has been directed towards development of low-melting (1000 to 1150°C) borosilicate glasses.[1,2] However, to provide for waste streams not readily vitrifiable and to ensure that other options for encapsulation of fission product waste were considered, an effort was initiated to develop alternative waste forms based upon a multibarrier concept (Fig. 1). The multibarrier concept aims to separate the radionuclide-containing inner core material and the environment by the use of coatings and metal matrices. The resultant composite waste form exhibits enhanced inertness due to improved thermal stability and mechanical strength, and the added barriers greatly improve leach resistance.

Four 1-liter stainless steel canisters have been produced to demonstrate the multibarrier concept. The concepts, in order of increasing technological complexity, were:

- Simulated waste-glass marbles encapsulated in a Pb–10Sn vacuum-cast matrix
- Uncoated sintered supercalcine pellets encapsulated in an Al–12Si vacuum-cast matrix
- Glass-coated sintered supercalcine pellets encapsulated in an Al–12Si vacuum-cast matrix
- PyC/Al_2O_3 chemical vapor deposited (CVD) coated supercalcine encapsulated in a Cu sintered matrix

Development of these multibarrier waste forms and process technology has been previously described.[3-6] In this paper, the characterization and evaluation of multibarrier samples are discussed. Three waste form stability parameters were used to determine product integrity: volatility, impact resistance, and Soxhlet leachability. The effect of radiation upon waste form integrity was studied by doping with ^{244}Cm.

BULK PROPERTIES

A summary of the pertinent bulk properties of multibarrier waste foms is presented in Table 1. Thermal conductivity measurements were determined using the comparative method. The "maximum use temperature" reported for the different multibarrier waste forms is based on either melting points or temperatures where reactions could occur between multibarrier components.

THERMAL STABILITY

Component Reactions

Reactions between the inner core and the matrix during encapsulation were observed only for uncoated supercalcine in sintered 316 stainless steel (SS). Using scanning electron microscope analysis (SEM), no reactions were detected for

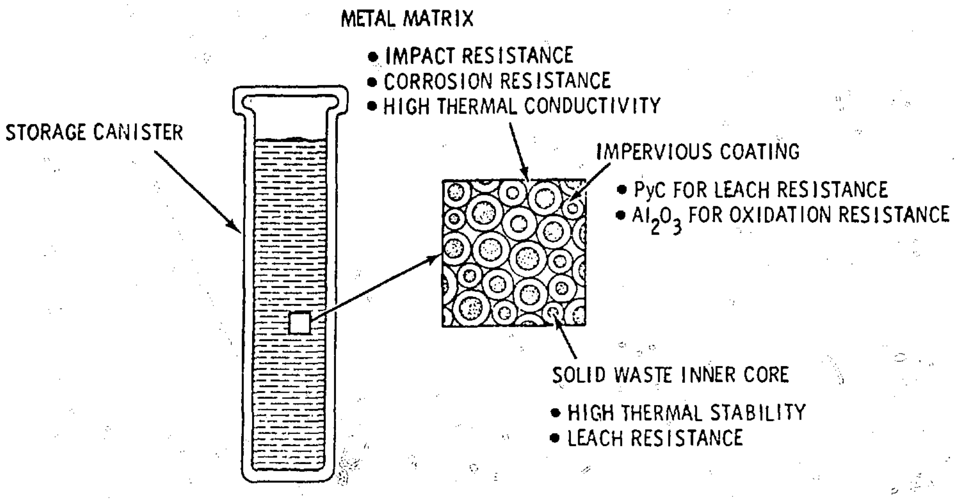

Fig. 1 Multibarrier concept for isolating nuclear waste.

TABLE I

Bulk Properties of Multibarrier Waste Forms

Inner core	Coating	Matrix	Bulk density, g/cm^3	Thermal conductivity, W/m °K	Maximum use temperature, °C
Waste glass	None	None	3.42	0.84	550
Marble (10 mm)	None	Pb–10Sn (vacuum cast)	6.20	8.3	250
Supercalcine					
Hot pressed	None	None	4.88	0.91	1200
Pellet (6 mm)	Glass (1 mm)	Al–12Si (vacuum cast)	3.40	45.0	550
Pellet (2 mm)	PyC (40 μm)/ Al_2O_3 (60 μm)	Cu (sintered)	3.48	24.0	1000

uncoated supercalcine encapsulated in cast Pb–10Sn and Al–12Si and sintered Cu or for coated supercalcine encapsulated in cast Al–12Si and sintered Cu and 316 SS.

The sintered 316 SS sample had a reaction zone around the SS particles. A phase containing high Mo, Cr, and Fe content and a phase containing primarily Cr were identified in the reaction zone, using energy dispersive X-ray analyses (EDAX). Samples of coated supercalcine encapsulated in sintered 316 SS do not contain any of the above observed phases. This, along with vaporization studies that show that a considerable amount of Mo is vaporized, leads to the conclusion that the observed reaction products may be caused by supercalcine vaporization. Thus, if supercalcine is to be encapsulated at higher temperatures, a coating may be necessary.

No apparent reactions between the PyC coating and supercalcine have been observed by optical microscopy or SEM analysis. X-ray diffraction results indicate possible formation of Mo_2C and the solid solution phase $(Sr,Ba)C_2$, as well as an absence of scheelite reflections. Supercalcine cores CVD-coated with 32 μm PyC and 50 μm Al_2O_3 have lost only 0.16 wt.% after heat treatment at 750°C for 27 hr. Complete loss of PyC coating due to oxidation would have given a weight loss of 2.8%.

Glass marble–metal matrix reaction were not observed for Al–12Si and Pb–10Sn matrices after heat treatment for 10 days at 300 and 500°C. The Pb–10Sn sample heat treated at 500°C contained a phase that appeared to nucleate from the glass marbles. From EDAX it was determined that phases of Sn and Sn–Cu had precipitated out of the Pb–10Sn alloy. No elements from the waste glass were observed in the matrix.

Reaction zones were observed for the Pb-encapsulated glass marbles after heat treatment for 10 days at 300 and 500°C. The reaction at 300°C appeared to be due to Pb oxidation. At 500°C the Pb matrix is molten, and the reaction occurs as a continuum between the Pb matrix and the glass marble. At least two phases were observed: a needle-like phase with high Zn and Pb content along with trace amounts of rare earths and a phase of high Pb content (probably lead oxide). The rest of the reaction zone contained both Pb and elements from the glass marble.

TABLE 2

Weight Loss of Supercalcine SPC-4 After 1 hr Sintering at 1200°C

Element	Absolute weight loss,* mg	Weight loss,† %
Na	0.52	12.9
Rb	0.91	6.1
Mo	8.23	5.2
Ru	2.53	24.4
Ag	0.16	4.3
Cd	0.39	9.7
Cs	12.29	9.9

*Pellets were 2.8 g with 3.5 cm^2 exposed surface area.

†Percentage weight loss based on the amount of element originally present.

Volatility

The volatility of waste calcine and zinc borosilicate glasses containing simulated HLLW has been well documented.[7] Studies on supercalcine volatility were conducted using the same thermogravimetric apparatus as that used for calcine and glasses. Initial volatility studies on supercalcine were conducted on powder samples of spray-calcined material. The volatility data on supercalcine powder were influenced by the degree of sintering; therefore, pressed and sintered pellets were used so that the surface areas were the same in all cases.

Two supercalcine formulations[5] were studied: SPC-2 and SPC-4. The SPC-2 pellets were sintered for 1 hr at 1100°C during which time they lost <1 mg. The SPC-4 pellets were sintered for 1 hr at 1200°C and lost 31 mg (Table 2).

Gross weight-loss data for SPC-2 and SPC-4 pellets are shown in Fig. 2 along with 72-68 glass as a reference. The total volatility of supercalcine is less than that of 72-68 waste glass. Depending upon which formulation (SPC-2 or SPC-4) and temperature are selected, there is a decrease in volatility of between 3 to 30 times over that of glass. Since Cs is the major contributor, this also applies to Cs volatility, but the improvement is at least one order of magnitude. The volatility of supercalcine is dependent upon formulation as illustrated by the differing slopes of SPC-2 and SPC-4. Supercalcine SPC-4 has much lower volatility than SPC-2 at low temperatures, whereas above 1100°C SPC-2 demonstrates reduced volatility over SPC-4. This illustrates the possible effect of waste stream variations on supercalcine volatility.

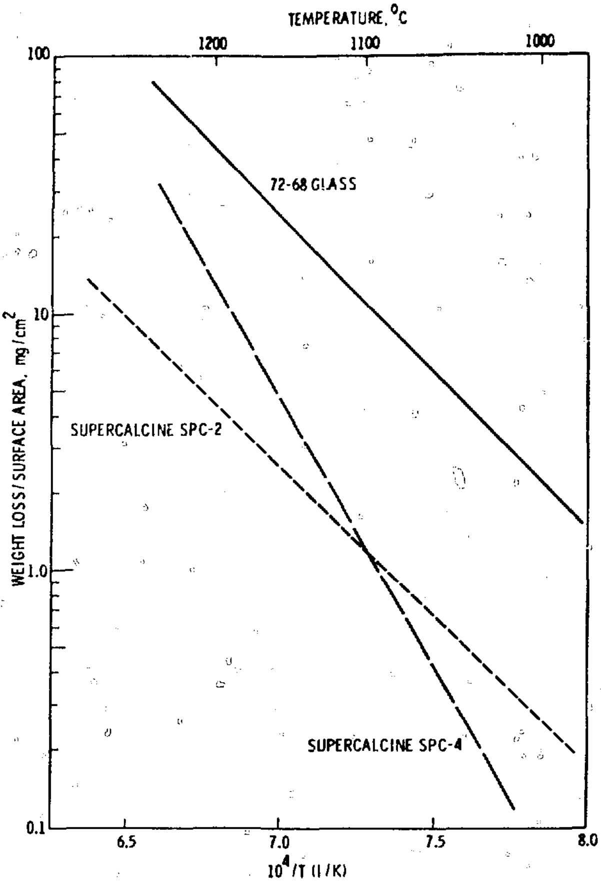

Fig. 2 Gross weight loss of waste forms after 4 hr in dry air.

LEACHABILITY

Several leachability tests are available for determination of leach resistance. A common test for scoping determinations is the Soxhlet apparatus, which is an accelerated test involving recirculated distilled water at 95°C normally for 72 hr. Other tests commonly used at PNL for leach resistance evaluation are conducted at ambient temperatures with buffer solutions of pH 9 and pH 4. Leach resistance is discussed in this paper on a scoping basis. Leaching tests which emphasize elemental analyses rather than Soxhlet weight loss are in progress and will provide for a more detailed leachability analysis (e.g., hydrothermal testing[8,9]). A comparison of Soxhlet leach rates of multi-barrier materials is presented in Table 3.

From the Soxhlet test data, one can conclude that supercalcine may not offer significant increase in leach resistance over waste glasses. Similar conclusions were obtained from hydrothermal tests under equilibrium conditions.[8,10] Coatings appear to offer improved leach resistance, especially in the case of CVD PyC and Al_2O_3 coatings. Coatings could provide a barrier for a finite period of time during which the hazard index of the inner core would be decreasing. For example, a 1 mm glass coating with a leach resistance of 10^{-6} g/cm²/d would provide a barrier for over 600 years. Recent studies at PNL using graphite in deionized water at 95°C have suggested that the leach resistance of PyC is between 10^{-10} to 10^{-11} g/cm²/d. Thus a 50 μm coating of PyC could

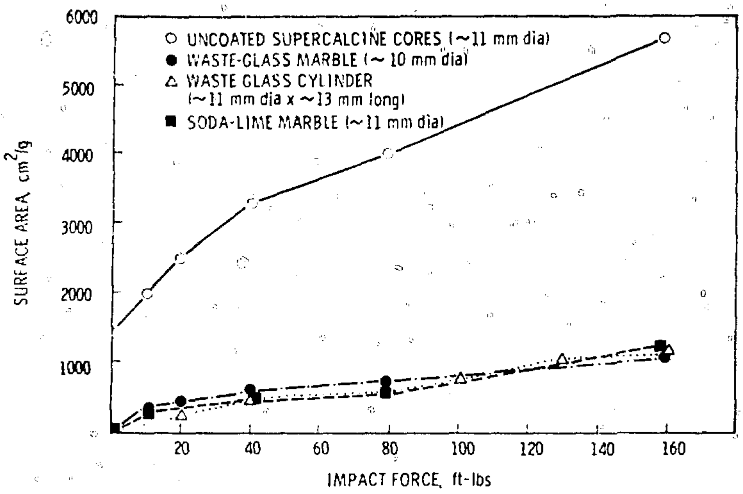

Fig. 3 Surface area of supercalcine and other waste forms after impact tests at various forces.

TABLE 3

Comparison of Soxhlet Leach Rates of Multibarrier Materials

Material	% Weight change over 72 hr
Waste glass†	0.30 to 1.45*
Waste glass marble (10 mm)	0.02 to 0.04
Supercalcine cores (6 mm)	0.3 to 1.90
PyC CVD coated supercalcine (2 mm)	+0.01 to +0.77
Al_2O_3 CVD coated supercalcine (2 mm)	+0.04 to +0.86
Glass coated supercalcine core (6 mm)	0.08 to 0.86

*24-hr period for the high value.
†Ground to 40 + 60 mesh.

provide thousands of years of protection. Hydrothermal studies have indicated no release of waste ions from PyC and Al_2O_3 CVD coated supercalcine cores in either deionized water or brine at 400°C.[11,12]

IMPACT RESISTANCE

Impact resistance is an important parameter in risk analysis because it indicates the potential for air dispersion. A laboratory-scale impact test was used to compare multibarrier waste forms to previously tested reference waste glass specimens.[2] It is difficult to produce multibarrier samples for impact testing equivalent to those used for the reference glass process. The reference glass samples were produced by diamond core drilling of larger solid specimens. The composite nature of multibarrier waste forms makes core drilling difficult because the drilling cuts through the inner cores and their protective coating. Also, since the radionuclides are contained only in the core of the multibarrier waste form, impact damage to the core is of major concern, rather than the complete composite. The approach to determine impact behavior was to first consider the matrix and inner core independently. The entire inner core-matrix composite was then impacted, and the inner core was separated from the matrix for analysis.

The surface area of impacted samples is plotted in Fig. 3. Although the total surface area of supercalcine cores is much greater than that of waste glass or soda-lime marbles, the actual increase in surface area with impact is less. The surface area for supercalcine cores, waste glass marbles, and soda-lime glass marbles increases upon impact at 158.4 ft-lb by a factor of 4, 556, and 521, respectively. The impact results for soda-lime marbles, waste glass marbles, and waste glass right-circular cylinders do not significantly differ on a surface area/g basis.

Since the supercalcine cores contained considerable porosity, additional impact tests were conducted on hot-pressed supercalcine, which represents a product of optimum density. To determine the best possible impact resistance of a ceramic product, tests were also conducted on a sample of Al_2O_3 grinding media. The results for both samples after impact at 158.4 ft-lb are compared with the previous waste glass cylinder in Fig. 4. The dense supercalcine resulted in a factor of 2 reduction in production of fines <37 μm as compared to glass. The impact resistance of the Al_2O_3 grinding media illustrates that a factor of 5 reduction in fines <37 μm could possibly be obtained with use of ceramic products instead of glass.

As mentioned, it is difficult to compare the impact resistance of composite waste forms. Sample size variations and material collection are two examples of the problems encountered. The results in Table 4 are presented in a manner to illustrate the fraction of nuclear waste released per unit volume of waste form. It has been suggested that these release rates be multiplied by the total volume of

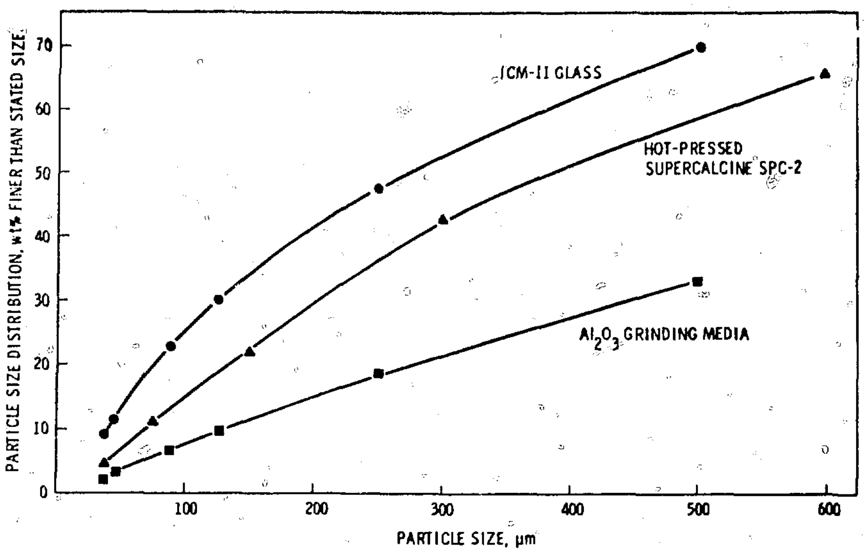

Fig. 4 Particle size distribution of waste forms after impact of 158.4 ft-lb.

waste form required per MTU to determine total risk. For example, the calculated waste release for glass marbles in a metal matrix is 13 times less than that for monolithic glass, but 1.7 times more canisters will be required. Thus the actual improvement may only be a factor of 8.

RADIATION STABILITY

Supercalcine composition SPC-2 was doped with Cm_2O_3 at a 3 wt.% level. X-ray diffraction, stored energy, and density measurements were made initially and later at approximately three-month intervals to assess the effects of the α-recoil damage. Dose levels in excess of 1.4×10^{18} α/g have been reached. For reference, a dose of 1.2×10^{18} α/g is equivalent to 200 years for supercalcine with 80% waste loading.

By comparison of the diffraction angles measured with no dopant and at dose = 0 (with dopant), it was determined that the curium may have gone into both the apatite and the tetragonal supercalcine phases. Both of these phases shifted in diffraction angle by over 0.10 to 2θ while the fluorite phase seems to have remained constant. All three of the potential Cm containing phases exhibited some peak broadening, but, again, those that shifted in diffraction angle seemed to broaden the most. As α-dose increases, the apatite phase shifts towards lower angles, and by a dose of 5.0×10^{17} α/g shifts approximately 0.10 to 2θ from the initial 2θ value. Both the fluorite phase and the tetragonal phase remain at their initial 2θ values up to a dose of 5.0×10^{17} α/g.

Since the fluorite phase does not appear affected by radiation damage and also since initial measurements indicated essentially no change after doping, the (220)

TABLE 4

Calculated Nuclear Waste Release After Impact at 158.4 ft-lb

Material	Sample size, diameter	Length, in.	Coating	Matrix	Waste, vol.%	Particle size after impact, % 37 µm	Nuclear waste released, g/cm³ x 10^{-4}
Supercalcine							
Hot pressed	0.44	0.50	None	None	75	4.4	1600
Cores*	0.50	0.50	PyC/Al_2O_3	410 SS	34	2.0	200
Cores†	0.50	0.50	PyC/Al_2O_3	410 SS	23	0.4	28
ICM-11 glass	0.44	0.50	None	None	35	9.0	1100
ICM-11 glass	1.25	1.25	None	None	35	1.0	120
ICM-11 glass*	1.25	1.25	None	Pb–10Sn	21	0.1	9

*60 vol.% packing.
†40 vol.% packing.

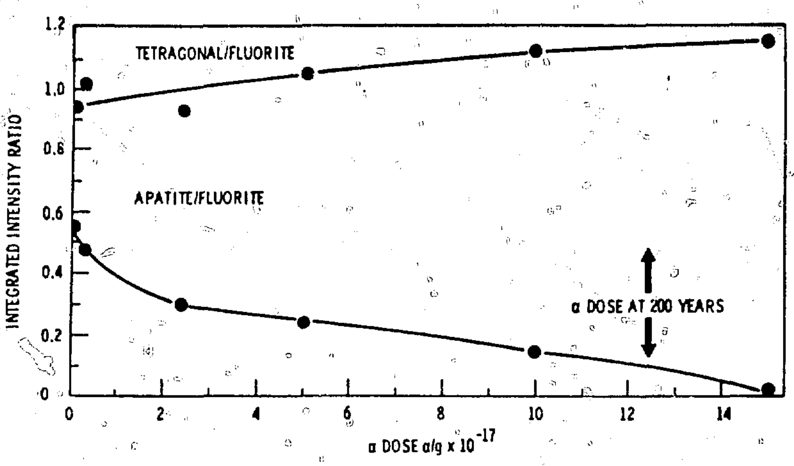

Fig. 5 Ratios of integrated intensities (apatite/fluorite and tetragonal/fluorite).

fluorite peak was used as an internal standard. The ratios of integrated intensities (i.e., apatite/fluorite and tetragonal/fluorite) are given in Fig. 5. There is a decrease in the intensity of the apatite peak while the tetragonal phase shows a slight increasing tendency. After a dose of 1.5×10^{18} α/g, the apatite peak (213) has completely disappeared. Other reflections are barely detectable.

The lattice constants, a_0 and c_0, for the apatite phase were calculated using the (213) and the (211) apatite peaks. The apatite unit cell was found to expand the basal plane as a_0 goes from 9.59 Å initially to 9.70 Å after 1.5×10^{18} α/g. Along with this expansion is a corresponding contraction in the c direction from 7.03 Å to 7.01 Å. It was not possible to calculate lattice constants for the tetragonal cell because of overlaps and weak secondary reflections. The results indicate that in supercalcine SPC-2 the apatite phase will become amorphous with radiation damage while the fluorite and tetragonal phases will remain relatively unaffected.

Stored energy and density measurements were determined in addition to the X-ray diffraction data. The energy release reaches a maximum of about 10 cal/g near 5×10^{17} α/g dose and then decreases. Also the release curve indicates that complete annealing is not attained at 600°C (the upper limit of the calorimeter) and that a substantial energy release may occur at temperatures above 600°C.

The measured bulk density decreased from 4.18 to 4.12 g/cm^3 at a dose of 1.7×10^{18} α/g. This corresponds to a density decrease or volume expansion of 1.4%. The theoretical concentration of apatite in supercalcine is 12.5%. A volume expansion of 3.6% can be estimated for apatite from X-ray diffraction data, which suggests that other phases besides apatite may be contributing to the overall expansion. Although leaching of radiation-damaged supercalcine was not studied, recent work on a devitrified glass by Weber et al.[13] suggests that amorphization of apatite may not significantly affect leach rates.

CONCLUSIONS

The volatility, Soxhlet leachability, and impact resistance have been determined for various multibarrier components and concepts. The effect of alpha irradiation on supercalcine was also studied. The results of these multibarrier characterization studies can be summarized as follows:

- The weight loss of supercalcine ceramics after 4 hr in dry air ranges between 0.01 and 1.6 wt.% from 1000 to 1200°C and is dependent upon composition.
- Glass marbles in a cast lead alloy offer approximately an order of magnitude decrease in the wt.% fines <37 μm released after impact as compared to a glass monolith. CVD coated supercalcine in a sintered 410 SS matrix offers up to two orders of magnitude decrease.
- Hot-pressed supercalcine ceramics may offer no increase in impact resistance or leach resistance over that of a glass monolith.
- Glass and PyC/Al_2O_3 coatings provide effective inert leaching barriers.
- After an equivalent exposure to alpha radiation of 200 years, supercalcine ceramics have maintained their physical integrity but show crystalline phase instability as the apatite phase crystalline structure becomes X-ray amorphous due to radiation damage.

Further characterization of alternative nuclear waste forms is continuing on a more detailed scale, especially with reference to leaching (e.g., time–temperature dependence and hydrothermal conditions). The waste form must be viewed in terms of the total waste management system (i.e., canister, overpack barriers, repository). Based upon results to date, it is recommended that the development of coatings and metal matrices be continued to provide one of the inert barriers in the waste management system.

ACKNOWLEDGMENTS

[illegible] E. P. B[illegible] and W. E. G[illegible] [illegible] State Department of [illegible]

REFERENCES

1. [illegible] Report [illegible] BNWL-[illegible] Pacific Northwest Laboratory, Richland, WA [illegible]
2. [illegible] Report on the Characterization of [illegible] PNL-[illegible] Pacific Northwest Laboratory, Richland, WA [illegible]
3. J. M. R[illegible], Multibarrier Waste Forms, Part [illegible] PNL-[illegible] Pacific Northwest Laboratory, Richland, WA, September [illegible]
4. J. M. Rusin [illegible] "Development of Multibarrier Nuclear Waste Forms," in Proceedings of Scientific Basis for Nuclear Waste Management, G. J. McCarthy (Ed.), Plenum [illegible]
5. J. M. Rusin, R. O. Lokken, and J. W. Wald, Multibarrier Waste Forms, Part [illegible]: Characterization and Evaluation, PNL-[illegible] Pacific Northwest Laboratory, Richland, WA [illegible]
6. W. A. Ross, J. M. Rusin, and J. L. McElroy, "Processes for Production of Alternative Waste Forms," in Proceedings of the [illegible]

[illegible]

[illegible] "Reactive Diffusion [illegible]" [illegible] Management [illegible] CONF-[illegible] U.S. Department of Energy, Technical Information Center, Oak Ridge, [illegible]

III. IMMOBILIZATION OF RADIOACTIVE WASTES—GLASS PROCESSING

OPERATIONAL EXPERIENCE OF THE FIRST INDUSTRIAL HLW VITRIFICATION PLANT

M. M. CHOTIN, R. A. BONNIAUD, A. L. JOUAN, and G. J. RABOT
Compagnie Générale des Matières Nucléaires and Commissariat à l'Energie
Atomique, Etablissement de Marcoule, France

ABSTRACT

Marcoule Vitrification Plant which started up in active operation in June 1978 converts high-level radioactive liquid wastes into glass. The French vitrification process is a continuous technique involving a calcination step. The glass is cast in stainless steel containers. After the lids are welded, a decontamination stage is operated prior to disposal.

HISTORICAL BACKGROUND

Research and development on the solidification of high-level radioactive wastes has been under investigation in France for over 20 years. The first radioactive glasses and synthetic micas were made in 1958.[1] Glass blocks weighing 5 to 15 kg and having a specific activity of about 1000 Ci/l were produced in 1963 for examination purposes using a gel technique in graphite crucibles. Meanwhile, processes of industrial interest, both batch and continuous, were under development.[2-8] The first in operation was a batch process. It used a pot vitrification technique in which drying, calcination, and vitrification were performed in the same vessel, a metallic pot heated by induction. In 1969 a pilot plant called PIVER, using this process, began operation under fully active conditions at the Marcoule Nuclear Center. By 1973 solutions resulting from the reprocessing of spent natural uranium fuel had been processed to yield 12 tons of glass with a maximum activity of 3000 Ci/l.

Because of the successful operation of PIVER, it was decided in 1972 to build an industrial vitrification plant at Marcoule. The continuous process was chosen in preference to the pot technique, as it could cope with various feed solutions and was flexible, cheaper, and easier to scale up for higher throughputs. A plant called AVM was built and started in active operation in June 1978.

BASIC PROCESS

The vitrification process consists of two stages (Fig. 1). The first stage is calcination. The feed solution is introduced to a rotary kiln where it is converted to a calcine solid. The calcine product is mixed with suitable raw materials in an electric furnace to make the desired glass.

The glass is poured at predetermined intervals into canisters which are transferred to a storage facility. The off gases released during the fabrication are processed in special off-gas treatment equipment.

GLASSES INVOLVED IN THE MARCOULE PROCESS

The waste liquids to be vitrified at Marcoule fall into three main types related to the reprocessing of MTR spent fuel, military spent fuel, and commercial natural uranium spent fuel (graphite gas reactor system).

Table 1 gives the characteristics of these wastes. As it is impossible to use any single glass composition to deal with the various compositions of the wastes, three different groups of glass compositions, all of borosilicate type, have been selected after research carried out in cold and hot laboratories.[3,4,6,10-13]

The characteristics of the glasses are shown in Table 2. Examination of the glasses was carried out to determine (1) their behavior under irradiation and thermal conditions, (2) how their physical and chemical properties related to the

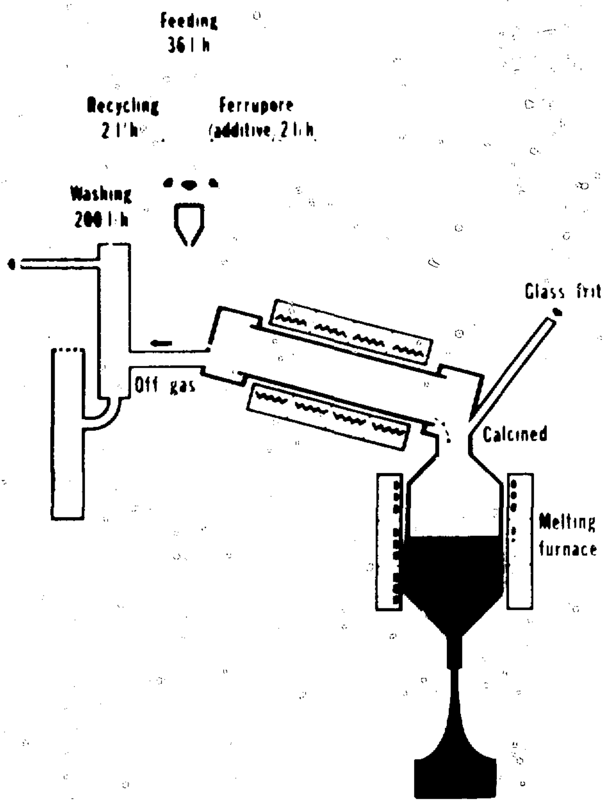

Fig. 1 Continuous vitrification process.

TABLE 1

Characteristics of Marcoule HLW

	Commercial GG spent fuels	Military GG spent fuels	MTR spent fuels
Burn up	4000–5000 MWd/T	1000–1200 MWd/T	500 MWd/kg
Chemical composition, g/l			
Fission product	35–40	20–25	very low
U	2.5–3.5	1.5–2.5	very low
Np	≃0.2	≃0.1	very low
Pu	≃0.02	≃0.02	very low
Al	8–12	30–35	81
Cr	≃0.4	≃1.5	<0.5
Fe	6–10	15–17	0.5–2
Ni	≃0.3	≃1	<0.5
Na	4–6	19–23	1–3
F		≃8	≃12
Mg	2–3	4–5	
Acidity	1.0 Molar	2.0 Molar	–1.8 Molar (depleted)
Specific activity after 2 yr cooling time, Ci/l	1600–1700	500–1000	low
Specific power after 2 yr cooling time, W/l	4–5	2–3	low
Concentration, l/T	≃100	30–40	12,000

TABLE 2

Characteristics of Marcoule Glasses

	Commercial GG spent fuels	Military GG spent fuels	MTR spent fuels
[illegible]			
SiO_2	42.5	40.6	[illegible]
Al_2O_3	8.5	15.0	[illegible]
B_2O_3	16.5	16.0	16.5
Na_2O	14.0	17.0	19.5
MgO	1.0	2.0	
Fe_2O_3	1.6	5.0	<0.2
F	1.4	2.0	1.8
NiO + Cr_2O_3	0.5	1.0	<0.2
Fission product oxides	13.0	4.0	1.[illegible]
Current volume reduction (related to the concentrated liquid)	7.0	5.4	3.5
Volume of glass per ton of fuel	13–15 l	5–6 l	3.4 m^3
Specific gravity of the glass	2.50	2.61	2.43
Viscosity at 1100°C (poise)	150	100	430
Thermal conductivity at 100°C (W/m)	1.25	1.25	1.25
Range of the leaching rate,* $g/cm^2/d$	10^{-7} to 10^{-6}	10^{-7} to 10^{-6}	10^{-7} to 10^{-6}

*Leaching operated at room temperature with tap water.

technology of fabrication, and (3) how their characteristics affected radioactive hazards in final disposal.

THE PLANT

The vitrification plant, designed jointly by C.E.A. and S.G.N., was built by Compagnie Générale des Matières Nucléaires (COGEMA) to solidify all the solutions of fission products generated by the Marcoule reprocessing plant, including those already in storage for over 20 years.

AVM is located close to the storage tanks. The construction which started in the summer of 1974 ended in January 1977 when the first nonradioactive run was made. Actual radioactive operation started in June 1978.

Description

The plant is made up of two different parts—the vitrification facility and a close-coupled storage facility. The facility has been described previously,[14] so the following description is short.

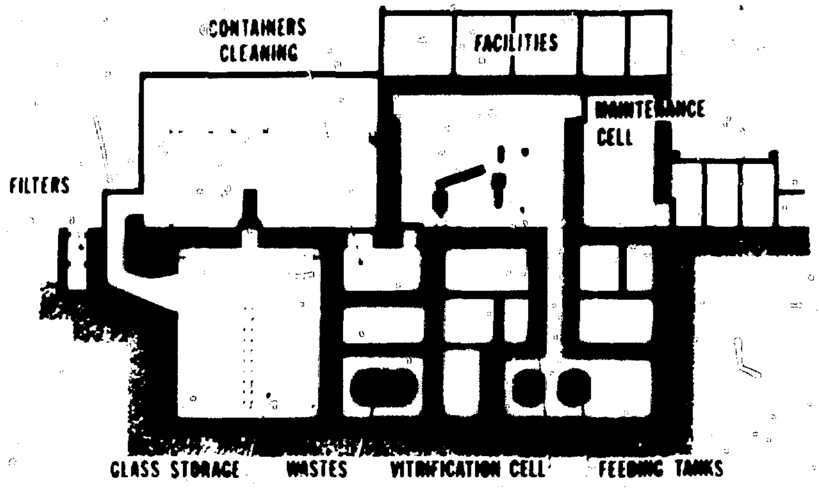
CONTAINERS CLEANING
FACILITIES
MAINTENANCE CELL
FILTERS
GLASS STORAGE
WASTES
VITRIFICATION CELL
FEEDING TANKS

Fig. 2 AVM vertical section.

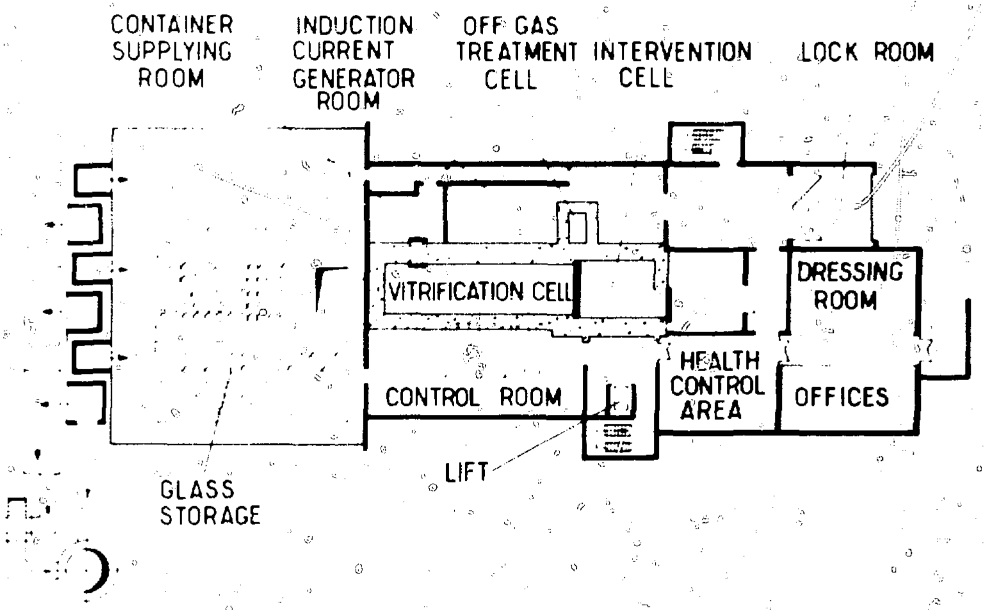
CONTAINER SUPPLYING ROOM
INDUCTION CURRENT GENERATOR ROOM
OFF GAS TREATMENT CELL
INTERVENTION CELL
LOCK ROOM
VITRIFICATION CELL
DRESSING ROOM
HEALTH CONTROL AREA
CONTROL ROOM
OFFICES
LIFT
GLASS STORAGE

Fig. 3 AVM horizontal section.

Figures 2 and 3 show vertical and horizontal cross-sections of the plant. The main part is the vitrification cell, which is totally lined with stainless steel. This cell encloses the vitrification equipment, the device for welding lids on the canisters, and the head part of the off-gas treatment system (scrubber and condenser).

All of the equipment located inside the cell was designed to be *remotely dismantled* for maintenance or replacement (as an example, see Fig. 4, picturing the dismantling of the calciner).

The storage facility is attached to the vitrification building (Fig. 5). It is made up of three engineered underground vaults made of concrete. The canisters (1 m high, 50 cm in diameter) are stacked in 10-m high vertical pits fitted in the vaults. There are 220 pits which will meet the need until the year 2000. A further extension is available.

Operation

The details of the operation have been presented previously.[14] A brief review follows.

Waste solution is injected into the calciner through an upper end-fitting at a flow rate which varies from 30 to $36\,\mathrm{l\,hr^{-1}}$, depending on the concentration of the waste. The barrel of the calciner rotates at 30 rpm. It is heated by a 4-zone furnace.

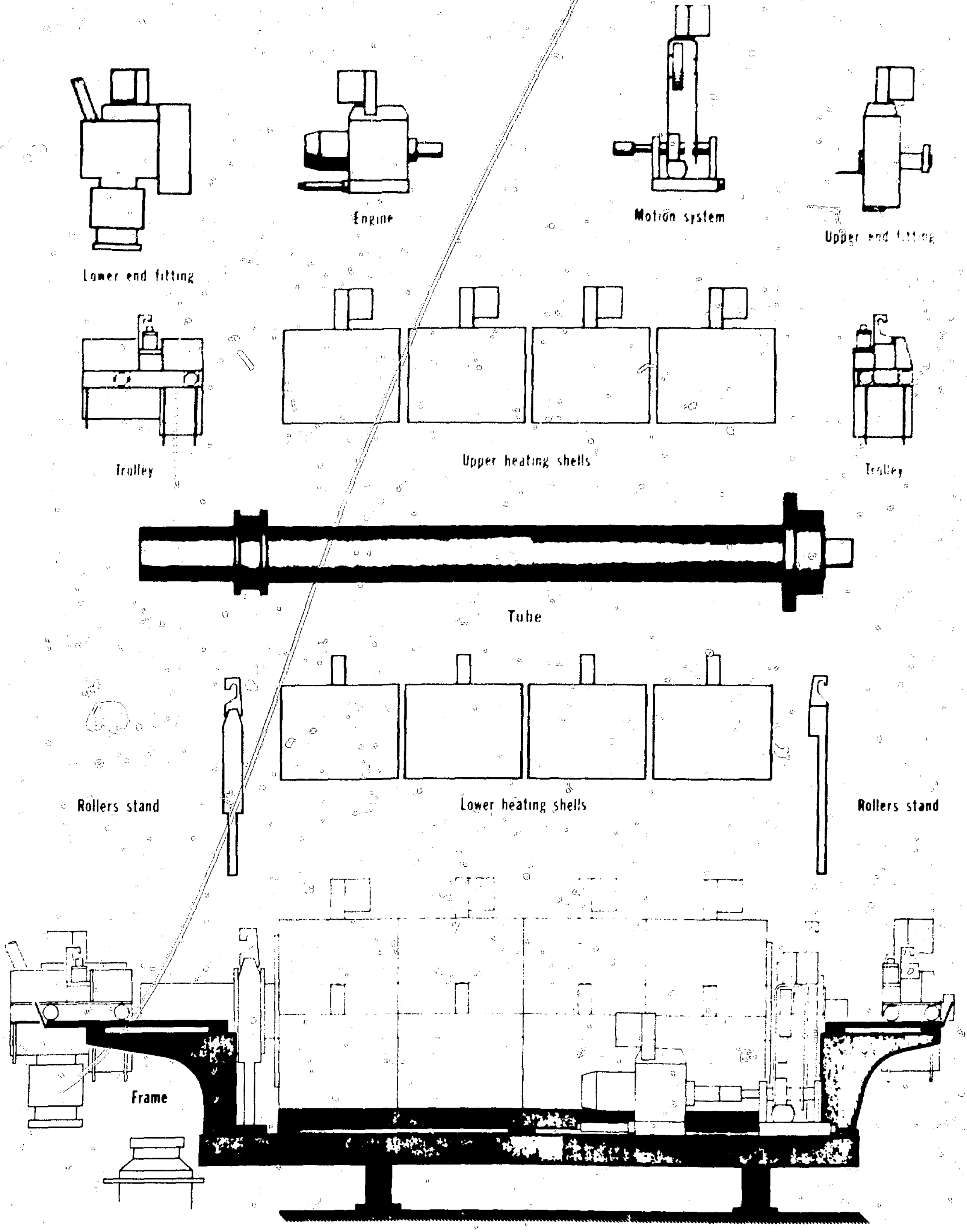
Lower end fitting
Engine
Motion system
Upper end fitting
Trolley
Upper heating shells
Trolley
Tube
Rollers stand
Lower heating shells
Rollers stand
Frame

Fig. 4 Calciner dismantling principle.

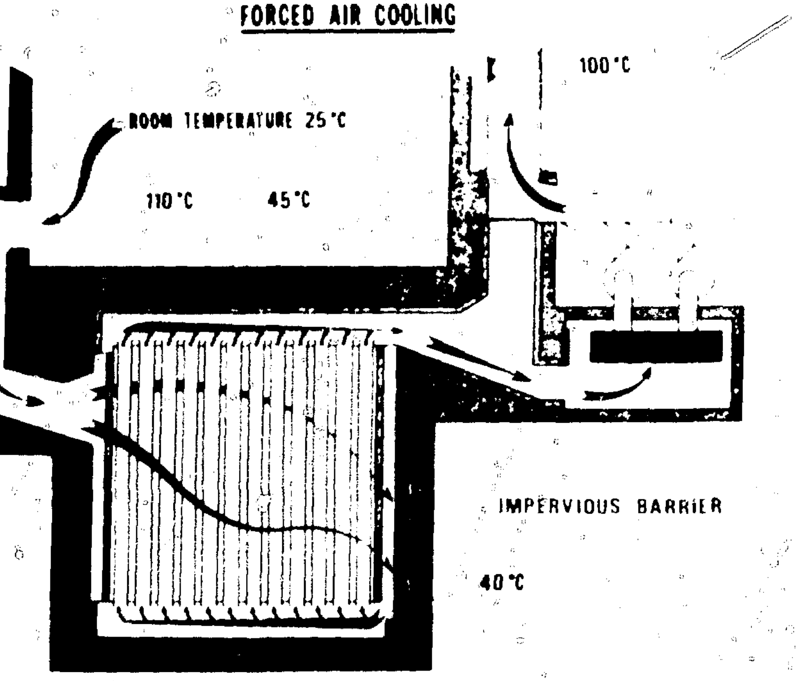

Fig. 5 AVM glass storage.

The resultant calcined product (8 to 9 kg corresponds to 30 l of solution) falls into the melting furnace through a lower end-fitting, simultaneously with the raw material, which is in the form of a primary glass (frit). The frit is fed at a mean rate of 9 to 12 kg hr^{-1} at stated intervals in 400- to 600-g batches. The throughput of the melting furnace is about 15 kg hr^{-1} of glass melted at 1100 to 1150°C. Every 8 hours 120 kg of glass is cast in a canister, which gets three successive casts.

Some hours after filling, the canister is shifted to the welding area where it is sealed by welding on a lid with a plasma torch. The canister is cleaned one day later by washing the surface with high pressure (200 bars) water.

The flow sheet for the off-gas treatment is shown in Fig. 6.

OPERATIONAL EXPERIENCE

The nonradioactive tests were carried out from January 1977 to April 1978. Four radioactive campaigns were scheduled afterwards. The first one lasted 746 hours at a feed rate of 30 l hr^{-1}. The second campaign lasted 994 hours and was stopped to remove the vitrification pot. A third campaign involving solutions of about 300 Ci/l lasted 1124 hours. The fourth is still running with a feed flow rate of 36 l hr^{-1}. During the first three campaigns, 360 casts were performed in 120 canisters. A total volume of 87.7 m^3 was processed during 2864 hours of operating time. This corresponds to 2000 tons of spent fuel yielding 40.6 tons of glass. The volume reduction factor was 5.4. On April 9, 23 more canisters had been filled, and an additional volume of 19.1 m^3 of fission products solution had been vitrified (Table 3).

Running Experience

Apart from a valve, all of the equipment has performed satisfactorily. The metering wheel has provided very accurate liquid feeding. The linear expansion of the calciner barrel has kept the same value, and the differential pressure (15 cm water) has been very stable.

The temperature of the pot wall is kept below 1130°C during melting of the glass. The casts, initiated every 8 hours, have routinely drained out 110 to 120 kg of glass in 15 to 20 minutes, viz., at a mean flow rate of 350 kg/hr.

There have been no difficulties in the welding of the lids on the canisters, except in two cases when a rewelding had to be done due to improper positioning of the lid.

Off-Gas Treatment Experience

The efficiency of the recombination of nitric acid and nitrates reached over 90% in the condenser and over 82% in the first column. This agrees with the data from the nonradioactive campaign. No insolubles could be seen in the liquid from the first scrubber. Chemical analysis of this liquid and of the condensate indicated an average carry-over of 3 to 4% and a trapping efficiency of 96 to 98%. This also agrees with the results of the nonradioactive runs.[14] The data related to the volatilization of the radionuclides and the various decontamination factors are listed in Table 4. Volatilization of ruthenium, the main volatile element, varied from 39% (57% of which was recycled) for the first

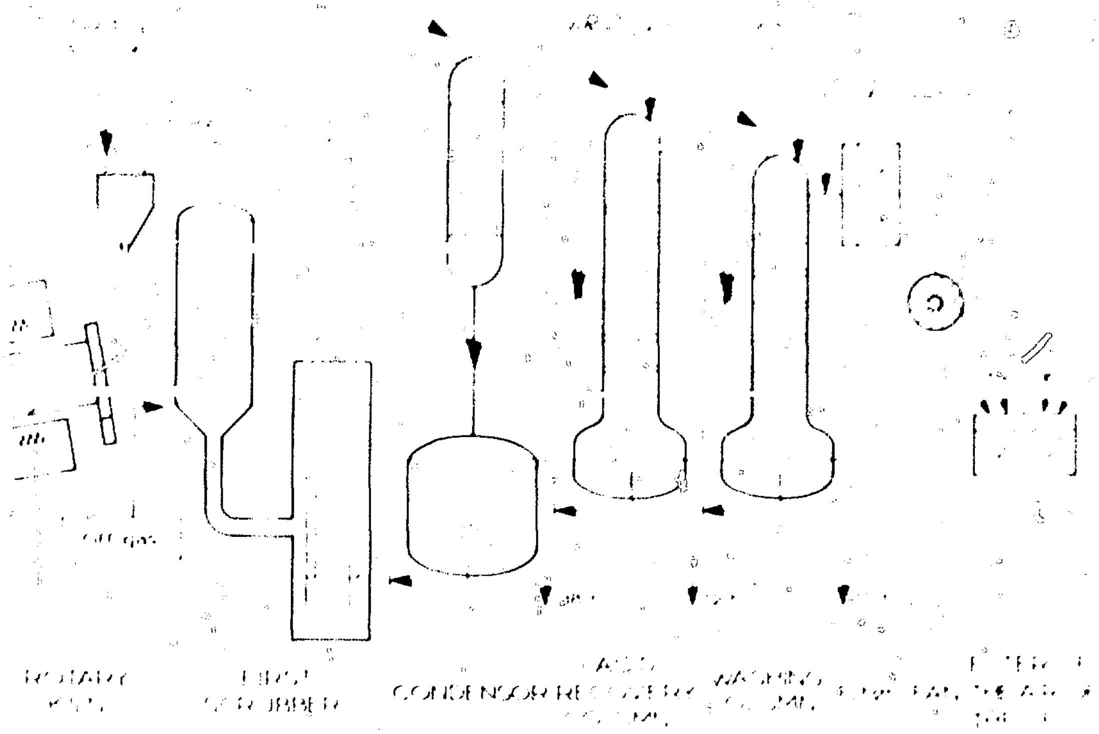

Fig. 6 Off-gas treatment of the AVM

TABLE 3

AVM Hot Run Data

Campaign reference	Working time, hr	Volume of treated solution, m³	Weight of glass, t	Number of glass canisters filled
First	746	21.6	10.11	31
Second	994	31.0	14.44	42
Third	1124	35.1	16.06	47
Fourth*	552	19.1	7.86	23
Total	3416	106.8	48.5	143

*Still in progress - assessment on April 9, 1979.

campaign to 20% (65% of which was recycled) for the second one.

The Ru decontamination factor for every part of the equipment increased perceptibly as operation continued. So, Ru volatilization should not be considered as a shortcoming. Similar values related to the release of Ru were obtained in the pilot plant ATLAS, which has half-scale AVM equipment. In this pilot plant, attempts were made to reduce the Ru volatilization by adding sugar to the feed solution. Figure 7 shows the marked effect of this procedure on the volatilization rate, which is reduced to 2% out of the calciner and <1% in the condensate.

Liquid Wastes

The liquid wastes are

- The condenser condensate and the bottoms from the acid recovery column are assumed to be highly radioactive liquids and are returned to the fission product solution concentration unit for recycle and vitrification.
- The spent liquids from the washing column and canister decontamination (500 l/d) have an activity below 1 mCi/m³. They are transferred to the low-level waste treatment plant. They are the only significant liquid wastes released by AVM. The activity of the spent washing column liquid from the first two campaigns is shown in Table 5.

The average generation rate for this waste is 10 l hr⁻¹. The level of activity in this stream is considered satisfactory and demonstrates the good decontamination factors of the condenser and the acid recovery column.

Solid Wastes

The solid wastes are generated by equipment failure or by the removal of implements or vessels with predetermined lifetimes. The latter include especially the vitrification pots which have to be removed every 2000 hours. The solid wastes can be decontaminated in the vitrification cell by soaking them in a special tank. It is also possible to cut them up partially to shorten their overall

TABLE 4

Efficiency of the Gas Treatment for One Curie of Each Isotope

[illegible]

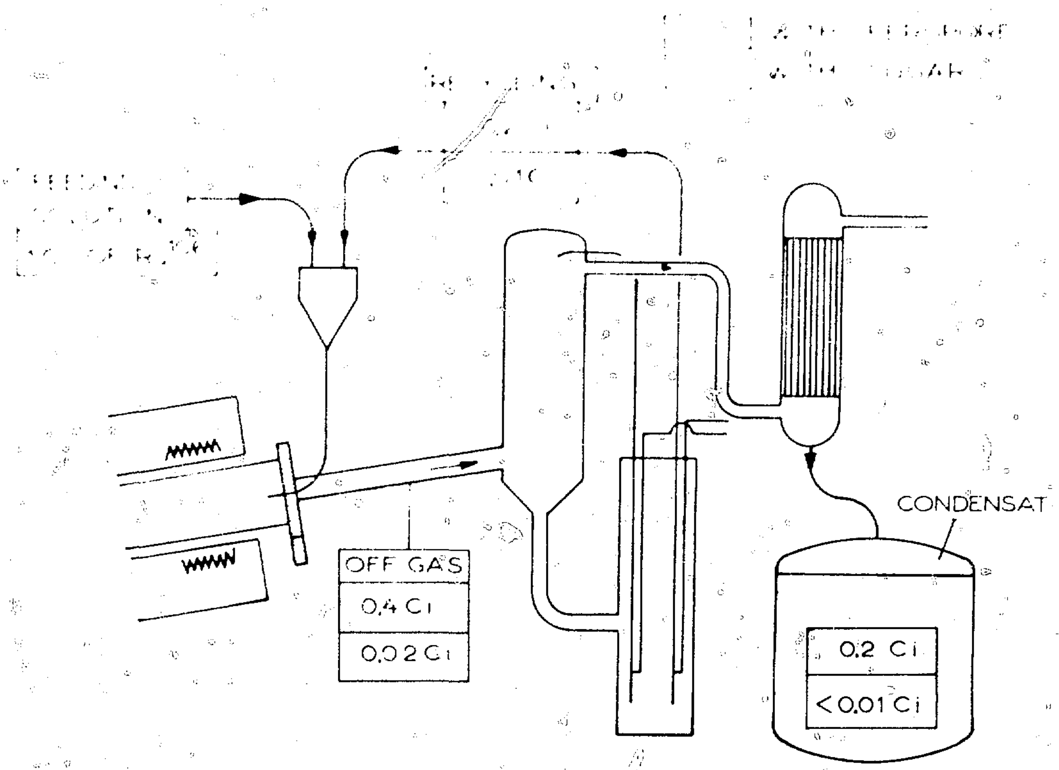

Fig. 7 Effect of the addition of sugar on the Ru volatility.

size. They are then either transferred to the maintenance cell to be encased in concrete in drums or, in the case of the vitrification pots, put in canisters similar to those used for waste glass. The canisters containing the vitrification pots are welded and stored in a particular storage pit. At some time in the future the vitrification pot may be further conditioned by melting, as the major part of metallic wastes will be later on. AVM has yielded only two vitrification pots as solid waste so far (assessment on April 9, 1979).

Gaseous Wastes

In order to evaluate the efficiency of the off-gas treatment equipment, some samples were taken from various locations in the line. The activity in the samples was below analytical detection limits. Based on detection limits, minimum decontamination factors were calculated prior to the final absolute filter. The decontamination factors were 1.2×10^7, 1.2×10^9, and 2×10^7 for Ru, Cs, and Ce, respectively. (These data are related to the first

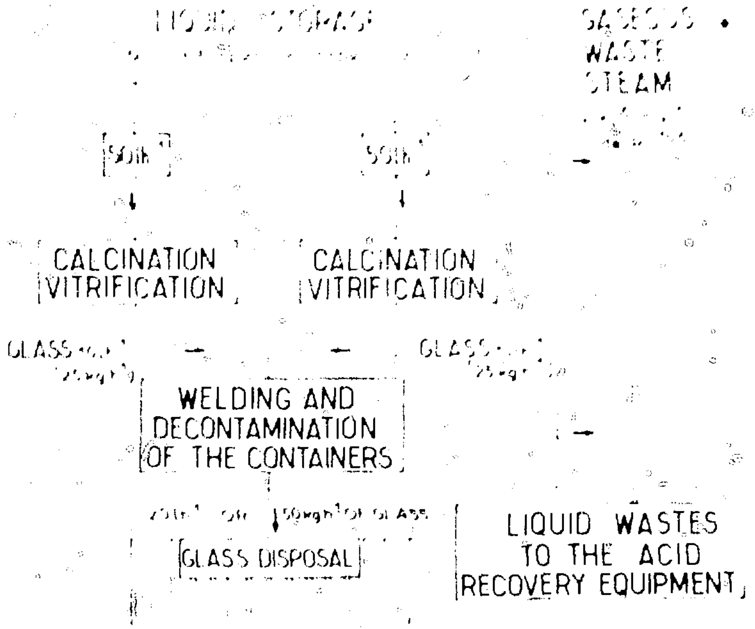

Fig. 8 Diagram of La Hague vitrification plant

TABLE 5

Activity in AVM Off-Gas Washing Column Liquid

	First campaign	Second campaign
^{106}Ru	15.0×10^{-6}	0.7×10^{-6}
^{137}Cs	0.5×10^{-6}	1.9×10^{-6}
^{90}Sr	0.3×10^{-6}	0.4×10^{-6}
^{144}Ce	1.1×10^{-6}	0.3×10^{-6}

campaign; analyses for the next campaign are presently in progress.)

Contamination of the vitrification cell is very low. The activity level in the cell varies from 0 to 60 counts per second.

CONCLUSION

Commissioning of AVM has opened the industrial development era for continuous high-level waste vitrification processing.

Due to the excellent results up to now, a plant to vitrify fission product solutions from the present La Hague reprocessing plant is now in design. Another one for the next reprocessing plant, which will be located on the same site (Fig. 8), is also in design. Each plant will be scaled up from AVM in order to deal with the needs of an 800 T/yr reprocessing plant.

REFERENCES

1. R. Bonniaud, P. Cohen, and C. Sombret, Essays on the Incorporation of Concentrated Solutions of Fission Products in Glasses and Micas, in *Second International Conference of the United Nations on the Utilization of Atomic Energy for Peaceful Uses*, A/CONF 15P/1176, Geneva, May 1958.
2. R. Bonniaud, C. Sombret, and D. Rancon, Vitrification of Concentrated Solutions of Fission Products Technological Studies, in *Symposium on Treatment and Storage of High Level Radioactive Wastes*, IAEA, Vienna, October 1962.
3. R. Bonniaud and C. Sombret, Radioactive Effluent Aspects of Vitrification, *J. Refractories*, 25(2), 1971.
4. R. Bonniaud, F. Laude, and C. Sombret, Experience Acquired in France on the Vitrification of Concentrated Solutions of Fission Products, in *Symposium on the Management of Radioactive Wastes from Fuel Reprocessing*, OECD, Paris, November 1972.
5. A. Jouan and C. Sombret, Continuous Vitrification of Concentrated Solutions of Fission Products, in *1st Conference of the European Nuclear Society "Nuclear Energy Maturity,"* Paris, April 1975.
6. R. Bonniaud and C. Sombret, Statement of Research in the Field of Solidification of High Level Radioactive Wastes in France, in *77th Annual Meeting of the American Ceramic Society*, Washington, D.C., May 1975.
7. R. Bonniaud, R. Cartier, A. Jouan, and C. Sombret, Current Development of the Continuous Vitrification Process for Solutions of Fission Products, in *International Symposium on the Management of Radioactive Wastes from the Nuclear Fuel Cycle*, IAEA/OECD, Vienna, IAEA SM 207/27, March 1976.
8. R. Bonniaud, J. Moulin, J. Reboux, and C. Sombret, New Developments in the Electric Melting of Refractory Glasses, *J. Refractories*, 26(4): 5 (1972).
9. R. Bonniaud, C. Sombret, and A. Barbe, French Industrial Plant "AVM" for Continuous Vitrification of High Level Radioactive Wastes, AIChE meeting, Los Angeles, November 1975, *AIChE (Am. Inst. Chem. Eng.) Symp. Ser.*, 72: 154 (1975).

R. B[illegible], C. S[illegible], and F. L[illegible], [illegible] Storage [illegible] French [illegible] Studies [illegible] Glasses and [illegible] *[illegible] Treatment [illegible] High-Level Radioactive Waste*, IAEA, Vienna, [illegible]

11. R. B[illegible] and F. L[illegible], R. [illegible] [illegible] S[illegible] [illegible] French [illegible] *International Symposium on the Management of Radioactive Waste from the Nuclear Fuel Cycle*, IAEA/OECD, Vienna, IAEA-SM-207 [illegible] March 1976.

12. R. Bonniaud, [illegible] P[illegible] and C. S[illegible] [illegible] Bearings [illegible] the Behavior of [illegible] Stored [illegible] Information *[illegible]* [illegible] [illegible] Metal Products [illegible] Laboratory [illegible] [illegible] Nevada [illegible] May 1974.

13. R. Bonniaud, A. [illegible] and C. S[illegible] [illegible] Application of [illegible] Glass [illegible] the Management of French Radioactive Waste, [illegible] *Conference on Radioactive [illegible]* [illegible] New York [illegible] 197[illegible]

14. R. Bonniaud, A. [illegible] and C. S[illegible] Large Scale [illegible] Glass Production, in: Proceedings of *High Level Radioactive Solid Waste Forms*, Denver, NUREG/CP[illegible] National Technical Information Service, Springfield, VA, 1979.

COMPATIBILITY TESTS OF MATERIALS FOR A PROTOTYPE CERAMIC MELTER FOR DEFENSE GLASS-WASTE PRODUCTS

G. G. WICKS
E. I. du Pont de Nemours & Co., Savannah River Laboratory, Aiken, South Carolina

ABSTRACT

The corrosion-erosion resistance of potential electrode and refractory materials was evaluated by static and dynamic tests in simulated glass-waste. Based on corrosion-erosion, physical, thermal and electrical properties, and cost and availability, *Monofrax K-3* (Carborundum Co.) and *Inconel 690* (International Nickel Co.) were selected as the contact refractory and electrode materials, respectively, for a prototype ceramic melter.

[illegible] candidates were *Monofrax K-3* (registered trademark of the Carborundum Co.) and *Inconel 690* (registered trademark of the International Nickel Co.), respectively. Based on these results, analyses in industrial practice, and at other sites such as Battelle Northwest Laboratory, the lifetime of these components in the remote Savannah River Plant ceramic melter is estimated to be two to ten years.

INTRODUCTION

The primary objective of Savannah River Laboratory's Melter Materials Compatibility Program is to evaluate the corrosion-erosion resistance of melter materials. The experimental program will be used to recommend electrode and refractory candidates for use in a joule-heated ceramic melter and consists of three phases:

- Statically and dynamically performed finger tests in simulated glass-waste compositions
- Evaluation of corrosion resistance in actual glass waste
- Simulated service tests to evaluate the wear and operating performance of construction materials

The final selection of materials for electrode and refractory components will depend not only on their corrosion-erosion resistance but also on electrical resistivity, thermal shock resistance, thermal expansion and conductivity, fabricability, and the cost and availability of the material.

Phase I of the Melter Materials Compatibility Program has been completed. The corrosion-erosion resistance of a variety of electrode and refractory materials was evaluated in simulated glass-waste compositions at various temperatures.

CORROSION RESISTANCE

Static Finger Tests

The static finger test (Fig. 1) severely tests a material's corrosion resistance. Melter components in normal operation are not subjected to molten glass on both sides as in the static finger test, and in most cases one side is significantly cooler than the other. Hence, improved corrosion behavior of the material would be expected under actual service conditions. Although there is no substitute for evaluating materials under service conditions, the finger tests do provide a good qualitative comparison of corrosion resistance of materials in the appropriate media and temperature ranges.

The static finger test used in this study is a modification of a standard ASTM test "Static Corrosion of Refractories by Molten Glass" (ASTM-C621-68, revised 1973). Refractory and electrode candidate materials were cut into rectangular samples approximately 0.25 in. x 0.30 in. x 2.0 in. and notched on one side (except for platinum for which wire was used). The samples were then fixed into cement crucible tops and placed in crucibles containing simulated glass-waste compositions (Table 1). The sample

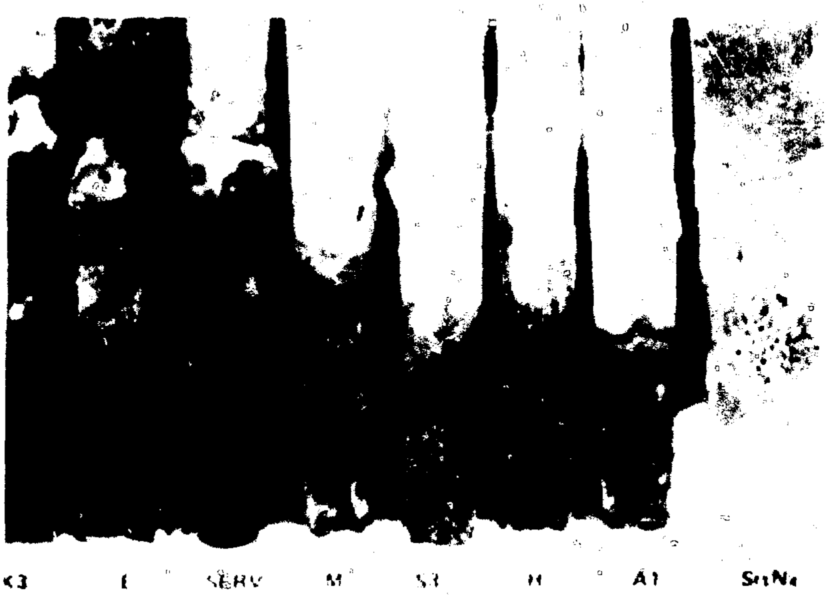

Fig. 1 [illegible]

TABLE 1

Simulated Glass Waste
(72.5 Type 21 Frit 27.5 Sludge)

Metal oxide	Average composition,	High iron composition,	High aluminum composition,
SiO_2	[illegible]	[illegible]	[illegible]
B_2O_3	[illegible]	[illegible]	[illegible]
Na_2O	[illegible]	[illegible]	[illegible]
Li_2O	[illegible]	[illegible]	[illegible]
CaO	[illegible]	[illegible]	[illegible]
TiO_2	[illegible]	[illegible]	[illegible]
Fe_2O_3	12.[illegible]	[illegible]	1.65
Al_2O_3	[illegible]	[illegible]	[illegible]
MnO_2	3.2	[illegible]	1.3
[illegible]	[illegible]	[illegible]	[illegible]
NiO	1.4	2.9	0.25

crucible units were then heated in a furnace for six days at temperatures of 1100, 1200, and 1300 C. The corrosion results are summarized in Table 2.

Corrosion Results

Corrosion effects were characterized by microscopy and dimensional changes. The dimensional measurements were taken every 0.4 in. along the length of the specimens before and after each corrosion test. The extent of corrosion or penetration at the *metal line* (interface of molten glass and air) for each material is given in Table 2.

The most corrosion resistant refractories were Monofrax K3 and E and the best performing electrode materials were Inconel 690 and platinum. *Serv* (registered trade-[illegible] Large Ruby [illegible] performed well. The [illegible] of performance below.

Ranking	Refractory	Electrode
1	Monofrax K3	Inconel 690
	Monofrax E	Platinum
2	Serv	Tin oxide
3	Monofrax AJ	Molybdenum (oxidized away above the metal line)
	Monofrax H	
	Monofrax M	
4	Monofrax S3	Titanium diboride (dissolved)
	Ruby	
5	Type #80 Firebrick* (dissolved)	
	Silicon nitride (dissolved)	

*Registered trademark of Babcock & Wilcox.

EROSION RESISTANCE

Dynamic Finger Tests

Electrode and refractory materials degrade from erosion by flowing molten glass as well as from corrosion by molten glass and its vapors. Refractories can also degrade by a phenomenon called upward drilling. The best method for studying erosion behavior is by a simulated service test, which will be used when melters become available. In the meantime, erosion behavior was qualitatively evaluated and leading refractory or electrode material candidates studied for any unusual wear.

A dynamic finger test was developed in which samples were suspended in molten glass (average composition,

TABLE 2

Metal Line Corrosion of Refractory and Electrode Candidates (Inches)

	Average waste, type 21 frit			High Al, type 21 frit		High Fe, type 21 frit	
	1100 C	1200 C	1300 C	1200 C	1300 C	1200 C	1300 C
Monofrax K3	[illegible]	[illegible]	[illegible]	[illegible]	[illegible]	[illegible]	[illegible]
Monofrax E	[illegible]	[illegible]	0.004	[illegible]	[illegible]	[illegible]	[illegible]
Serv	[illegible]	[illegible]	[illegible]	[illegible]	[illegible]	[illegible]	[illegible]
[illegible]	0.002	[illegible]	[illegible]	[illegible]		[illegible]	[illegible]
[illegible]	0.044	[illegible]	[illegible]	[illegible]			
[illegible]	[illegible]	0.049	0.041	0.016			
[illegible]	[illegible]	[illegible]	[illegible]				
Si_3N_4		Dissolved					
[illegible]			0.050				
Inconel 690	0.001	0.002	[illegible]	0.001	0.001	0.002	0.002
SnO_2	0.012	[illegible]	0.049	[illegible]	[illegible]	0.040	0.045
Pt	0.001	0.001	0.002			0.002	0.001
TiB_2	[illegible]	[illegible]	Dissolved				
Molybdenum	Dissolved above metal line						

simulated glass waste (Table 1) and rotated at 100 rpm. The test was performed at 1,200 C for 4 hours. Although not a standard ASTM testing procedure, the dynamic finger test provides qualitative comparison of erosion resistance that is helpful in making preliminary recommendations on melter materials.

Erosion Results

Erosion of candidate electrode and refractory materials was characterized by changes in area, which were determined by dimensional measurements and by planimetering specimens after dynamic testing. Three samples of each leading material were evaluated. The relative erosion rankings of the materials were similar to their corrosion performance. The measured amounts of erosion are given below:

	Amount erosion (in.)
Refractory	
Monofrax K3	0.002
Monofrax E	0.004
Serv	0.011
Monofrax M	0.050
Electrode materials	
Inconel 690	0.002
Tin oxide	0.030

Microstructures

While the corrosion–erosion resistance of electrode and refractory materials provides considerable insight into the compatibility of these materials with molten glass waste, the interaction zones were also studied. For example, although Monofrax K3 exhibited very little wear, an appreciable interaction zone was formed. This reaction zone consisting of glass and precipitates probably is created due to the molten glass dissolving oxides near the surface of the refractory and reprecipitating a chromium-iron rich phase. These chromium-rich precipitates would most likely retard further corrosion and, along with the absence of a glassy phase in the refractory, contribute to the very good corrosion resistance of this material. The microstructures of the Inconel 690 electrode candidate contained precipitation products and a surface scale, both above and below the melt line. This scale, which was rich in chromium content, would also serve to retard subsequent attack by the molten glass and its gases.

Microstructures for leading refractory and electrode materials were studied by optical and scanning electron microscopy, X-ray energy spectroscopy and X-ray diffraction.

ADDITIONAL CONSIDERATIONS

A qualitative rating of the leading candidates based on corrosion erosion resistance, electrical and thermal properties, and cost and availability of materials is given below. Based on these ratings Inconel 690 is the leading electrode material and Monofrax K3 the leading refractory candidate.

Material	Corrosion resistance	Erosion resistance	Electrical properties	Thermal shock	Cost and availability
Monofrax K3	A	A	A	B	B
Monofrax E	A	A	D	B	B
Serv	B	A	A	B	B+
Inconel 690	A	A	A	A	B
Platinum	A	A	A	A	C–
Tin oxide	C	B	A	D	B

MELTER LONGEVITY

Design Features

[illegible] and (2) design [illegible]. Even the [illegible] material [illegible] conditions [illegible] perform well [illegible]. Thus [illegible] important design [illegible].

Estimated Melter Lifetime

Electric glass melters normally operate about [illegible] yrs in commercial operation, but under special conditions life times have been extended to 5 and 4 yrs. For the melting of SRP glass waste, the lifetime would be somewhat longer. Even [illegible] maintenance can be used, other advantages offset the remote operability limitation to provide a longer potential life. These include (1) much lower processing temperature where corrosion erosion will be reduced, (2) ability to use highly corrosion resistant materials because of the unimportance of product discoloration, (3) low throughputs, minimizing erosion effects, and (4) use of coolants in high wear areas. Thus, an estimated lifetime of a defense waste melter is in the range of 2 to 10 yrs.

ACKNOWLEDGMENT

The author is indebted to [illegible], Jr., for his aid in conducting the compatibility tests. The information contained in this article was developed during the course of work under contract AT(07-2)-1 with the U.S. Department of Energy.

VITRIFICATION OF HIGH-LEVEL RADIOACTIVE WASTE IN A CONTINUOUS LIQUID-FED CERAMIC MELTER

S. WEISENBURGER, W. GRÜNEWALD and H. KOSCHORKE
Karlsruhe Nuclear Research Center, P. O. Box 3640, 7500 Karlsruhe 1, Federal Republic of Germany

ABSTRACT

The vitrification of simulated high-level liquid waste (HLLW) from the nuclear fuel cycle in a ceramic lined waste melter is described. Particular reference is given to the present status of the melter technology. Some features are discussed arising from direct liquid feeding of the waste solution into the melter. Also presented are results concerning the entrainment of particulates as well as the loss of volatilized material into the melter off-gas. Ruthenium behavior in a liquid-fed ceramic melter is reported, and the extent of ruthenium volatility suppressed by predenitration of the waste solution is discussed. The 1500 hr operation experience gained since 1976 with the pilot-scale vitrification unit is outlined, and the construction of an advanced melter having the potential for remote operation is given. The work described here is part of a German cooperative research and development program among seven institutions. One of the major objectives of this program is to provide a vitrification technology for the solidification of the LEWC waste stored at the Eurochemic site in Mol/Belgium.

INTRODUCTION

Ceramic-lined waste melter with direct electrical heating of the glass melt for vitrification of HLLW from the nuclear fuel cycle has received increased attention in the past five years. The principles of electric melting of glass are well known and widely used in the conventional glass industry. The first adaption of this method of glass melting to HLLW vitrification was made in the USA[1] in 1974. Similar development work was started in Germany[2,3] in 1976 and in Japan[4] in 1978. The primary objective in developing ceramic-lined and direct electrically heated waste melters is to achieve a significant improvement of the melting technology for HLLW vitrification. Compared to continuous metallic melters, both longer melter life and higher melting rates are expected by this melting technique. The potential of longer melter life is given by the use of high-temperature, highly corrosion-resistant ceramic refractories for the melter walls. Higher melting rates which are desired for industrial application of HLLW vitrification can be more adequately achieved by direct electrical heating of the melt. The basic principles applied for a conventional electric glass melter and a direct electrically heated HLLW melter are the same. However, several major differences exist between these melters, especially in respect to the size, the glass throughput, the outside containment, and remote operation requirements. In Table I typical design features and essential parameters are compared between a conventional and a HLLW melter system. The glass throughput required for a HLLW melter is two orders of magnitude below that for a typical conventional melter; thus the energy input and the outside dimensions are also appreciably lower. Furthermore the outside containment of a ceramic-lined waste melter and the requirements for its draining and off-gas system are significantly different. Nevertheless the experiences and design criteria known in the conventional glass industry for electric glass melting systems have been helpful in development and optimization of Joule heated ceramic-lined HLLW melters.

STATUS OF MELTER DEVELOPMENT AT KARLSRUHE NRC

The fundamental components of a waste melter are the melting cavity made of ceramic refractories, the electrodes made of metallic or ceramic refractories, and the draining system. Further major components are suitable heat in-

TABLE 1.

Typical Parameters and Design Features of a Ceramic Lined HLLW Melter Compared to Conventional Electric Glass Melters

Parameter or design feature	Ceramic lined waste melter	Conventional electric glass melter
[illegible]	[illegible]	[illegible]

[illegible] of the conventional glass [illegible] with temperatures [illegible] 1600 C [illegible]. Another reason to maintain the glass temperature at 1200 C is the need to suppress the volatility of [illegible] constituents of the glass melt.

The key elements of the melter are the electrodes and the draining system. The shape of the electrodes, the material of which they are made and their location in the furnace are essential. Generally the density of electric power in the glass pool is highest in the immediate neighborhood of the immersed electrode surface. Consequently, if the whole electrical power is introduced through an electrode surface which is too small, then overheating phenomena can occur in the glass melt surrounding the electrode. The layout of the electrodes assures that overheating is as low as possible by providing a sufficiently large electrode surface and that the overheated glass can flow away from the electrode surface by natural convection. Otherwise, the electrode material is strongly attacked by the increased corrosiveness of the overheated

[illegible] HLLW [illegible]

A [illegible] has been tested [illegible] R[illegible] N[illegible] Research Centre (NRC) [illegible] represented in Fig. 1. [illegible] about 2500 h and was [illegible] at [illegible] about 1200 [illegible]. The [illegible] experience and a detailed description of the melter [illegible] Ref. [illegible] of the melter 14 heating elements made of MoSi₂ are used which are located in the upper part of the melter behind the melter walls. The electric power is supplied by two pairs of molybdenum electrodes in the form of cylindrical rods (48 mm in diameter and 580 mm immersed length) under a voltage of about 40 V and an electrical current of 500 amp. The electrodes are air-cooled at the point where they are no longer immersed in the glass. The melter has a draining

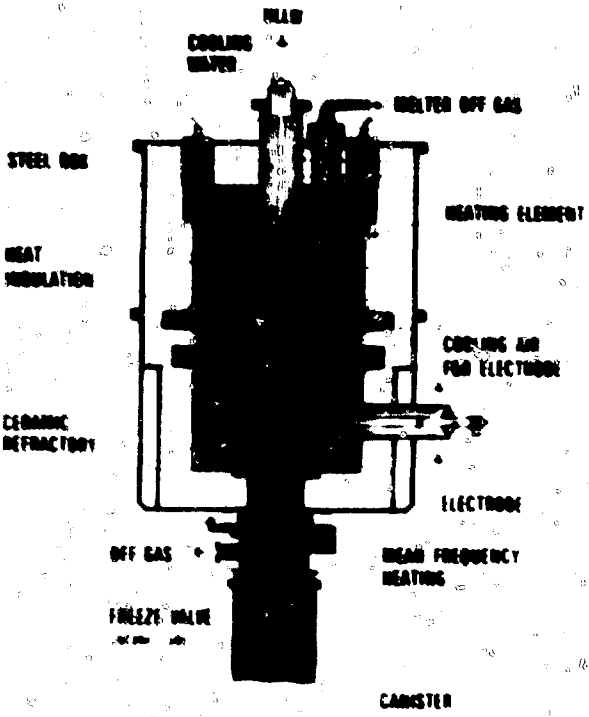
HLLW
COOLING WATER
MELTER OFF GAS
STEEL BOX
HEATING ELEMENT
HEAT INSULATION
COOLING AIR FOR ELECTRODE
CERAMIC REFRACTORY
ELECTRODE
OFF GAS
MEDIUM FREQUENCY HEATING
FREEZE VALVE
CANISTER

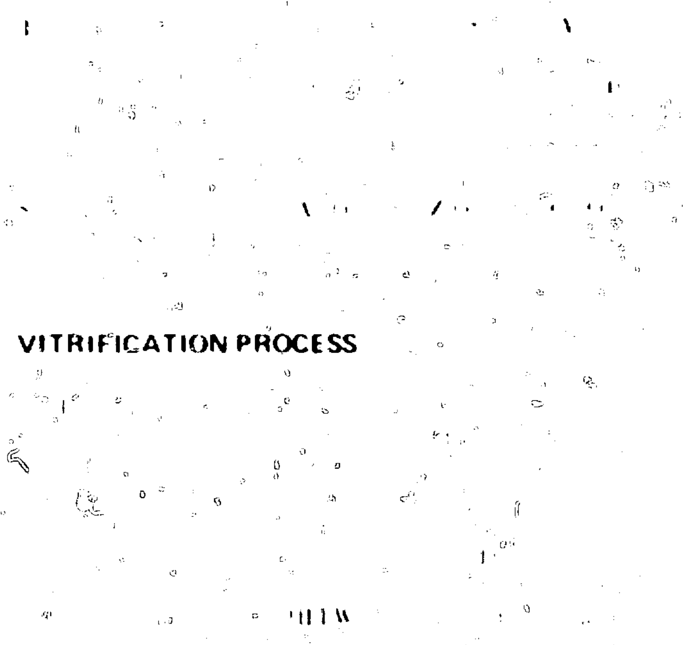
VITRIFICATION PROCESS
HLLW

Fig. 1 [illegible]

[illegible] Inconel 600. To start the glass flow, the Inconel 600 is medium-frequency heated and the glass in the ceramic part of the outlet is heated by passing electrical current through it using the Inconel tube and a power electrode in the melting cavity as the electrodes. To terminate the glass flow, the medium-frequency heating of the Inconel tube and the direct heating of the glass in the outlet channel are switched off. The glass flow rate is 240 kg/hr. Presently 130 glass blocks have been produced with this draining system.

Based on the operation experience gained with the melter, an advanced melter unit, shown in Fig. 2, has been constructed and will be installed at the Karlsruhe NRC in 1979. This melter is capable of containing 700 kg of glass and has a maximum electric power input of 50 kW. The glass pool surface is 0.6 m². The glass pool is heated by four electrodes made of molybdenum. The cylindrical rods, 80 mm in diameter, are provided with an inner cooling

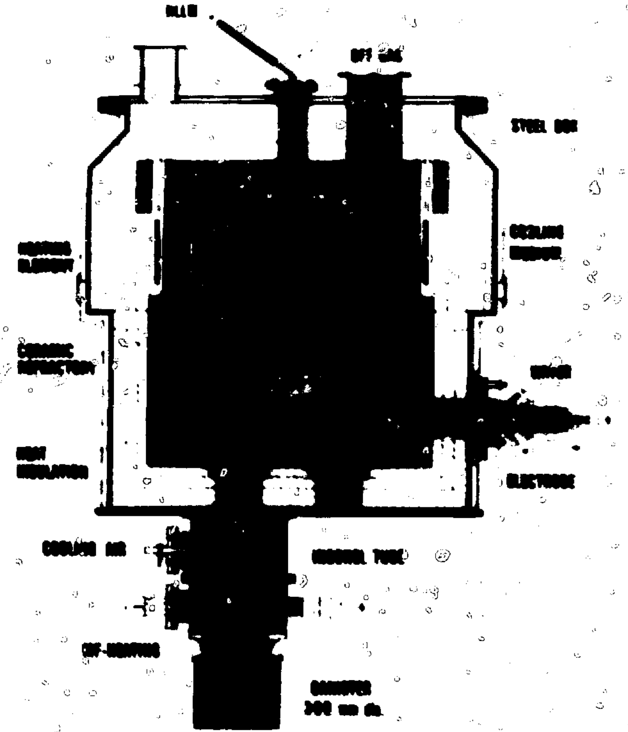
HLLW
OFF GAS
STEEL BOX
HEATING ELEMENT
COOLING WINDOW
CERAMIC REFRACTORY
HEAT INSULATION
ELECTRODE
COOLING AIR
INCONEL TUBE
CANISTER
300 mm dia.

Fig. 2 Advanced ceramic-lined waste melter to be installed at Karlsruhe Nuclear Research Center in 1979.

Outside dimensions	1.6 m × 1.6 m × 1.85 m
Glass-pool surface	0.64 m^2
Glass-containing capacity	700 kg
Power input	150 kW
Melting rate	100 kg/hr (expected)

[illegible]

Fig. 3 illustrates the inactive vitrification plant at Karlsruhe NRC including the feed transfer system by airlifts and the simplified off-gas cleanup system. The plant has been operated with liquid feeding for about 1500 h with a waste rate between 18 and 33 l/h. The glass is continuously introduced into the melter as a fine-powdered borosilicate glass frit together with the waste solution. The advantage is that the oxide residues at the glass pool surface are well mixed with the frit and can therefore react more rapidly with the frit and melt into the glass pool.

In a liquid-fed ceramic waste melter there is neither a significant dust generation associated with drying and calcining nor the need to transfer a fine-powdered calcine into the melter. The solid material contained in the waste solution is dried and calcined at the surface of the glass melter under a layer of boiling liquid. Thus the off-gas stream leaving the melter can be assumed to carry over only a minimum amount of materials contained in the waste solution, and a wet off-gas cleanup system may be adequate. The simplified off-gas system shown in Fig. 3 consists of a dust removal wet scrubber (with an airlift to recycle the scrub solution), a condenser, and a chemical wet-scrubbing system. The ruthenium filter shown in Fig. 3 will be included in the future. The melter off-gas of a liquid-fed ceramic melter includes water vapor, NO_x, particulate material, aerosols, leakage air, oxygen and nitrogen, and volatilized material, preferably cesium and [illegible] cesium [illegible] volatilized by evaporation of Cs_2O [illegible] and the loss of ruthenium may [illegible] gaseous RuO_4 by [illegible] from melter to the [illegible] cesium and [illegible] feeding of the [illegible]

AMOUNT AND REMOVAL OF MATERIAL IN THE MELTER OFF GAS SYSTEM

[illegible] the overall loss of [illegible] melter into the off-gas line and then [illegible] 280 h continuous [illegible] investigation of the trapped [illegible] components of the off gas system [illegible] liquid feeding there is an [illegible] leaving the melter. However, [illegible] dust removal wet scrubber [illegible] with the scrub solution.

Typical results of cesium and ruthenium loss are given in Tables 3 and 4 respectively. The results obtained for cesium indicate that in a liquid-fed ceramic melter Cs_2O evaporation is practically suppressed because the results show that cesium loss does not exceed the overall loss of material given in Table 2. This fact may be caused by the cold cap present at the glass pool surface in a liquid-fed ceramic melter. Ruthenium behavior as shown in Table 4 depends on whether or not the waste solution is denitrated because the oxidizing condition in the melter is influenced by this. The total average ruthenium loss was measured to be 12.8% during vitrification of a 3.4M HNO_3 waste solution and 3.4% for a denitrated waste solution having 0.7M HNO_3 rest molarity. Obviously the decomposition of relatively large amounts of nitrates generates a sufficient amount of oxygen to enhance ruthenium volatilization in a liquid-fed ceramic waste melter. However, most of the lost ruthenium is removed in the dust removal wet scrubber and can be recycled with the scrub solution too. The ruthenium content in the components following the dust scrubber is expected to be significantly lower when the silica-gel based ruthenium filter is used as shown in Fig. 3.

SUMMARY

Progress has been achieved in electric melting of HLLW borosilicate glass in a ceramic-lined melter. Practical experience of 1500 h with liquid feeding shows simple process performance but requires careful control in respect to accumulation of liquid at the glass-pool surface. The overall loss of material from melter into the off-gas cleanup system is an average of 4.5%. Cesium loss was approximately 4%. Ruthenium loss was an average of 12.8% and could be suppressed to 3.4% when the waste solution was predenitrated.

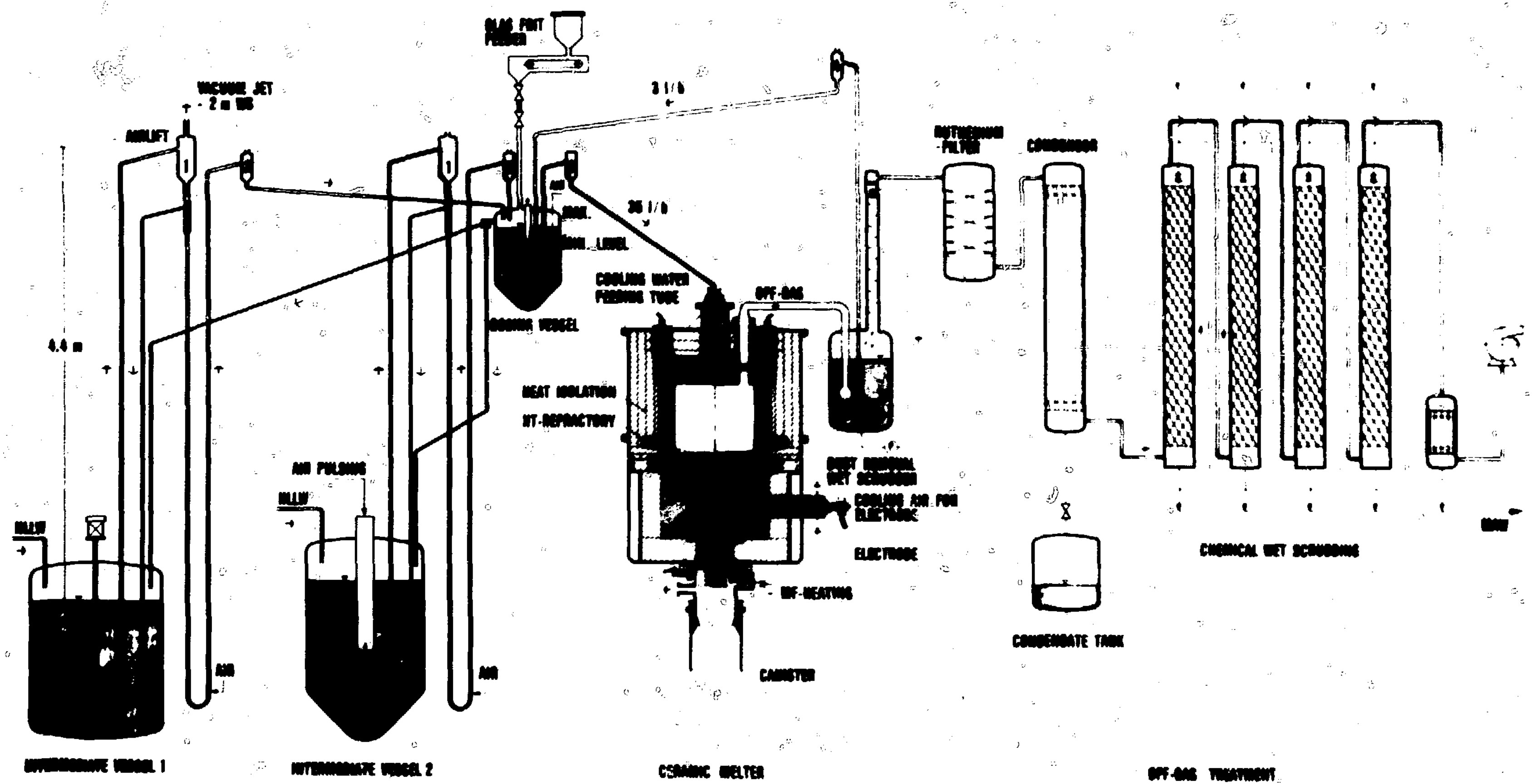
GLASS FRIT FEEDER
VACUUM JET
- 2 m WS
AIRLIFT
3 l/h
35 l/h
AIR
MAX.
MIN. LEVEL
DOSING VESSEL
4.4 m
HLLW
HLLW
AIR PULSING
AIR
AIR
INTERMEDIATE VESSEL 1
INTERMEDIATE VESSEL 2
COOLING WATER FEEDING TUBE
OFF-GAS
HEAT ISOLATION
HT-REFRACTORY
DUST REMOVAL WET SCRUBBER
COOLING AIR FOR ELECTRODE
ELECTRODE
HF-HEATING
CANISTER
CERAMIC MELTER
RUTHENIUM -FILTER
CONDENSOR
CONDENSATE TANK
CHEMICAL WET SCRUBBING
OFF-GAS TREATMENT

Fig. 3 Inactive vitrification plant operated at Karlsruhe Nuclear Research Center.

TABLE 2

Material Loss in a Liquid-Fed Ceramic Waste Melter into the Off-Gas Stream in Wt.% of the Amount (As Oxides) Fed to the Melter with the HLLW

Time, hr	Material loss, %						
	Overall total	Found in the off-gas tube*	Found in dust removal wet scrubber			Found in condenser	Found in chemical wet scrubber
			Suspended†	Dissolved‡	Total in scrubber		
12	8.79		3.90	4.42	8.32	0.08	0.39
28	5.52		1.14	4.18	5.32	0.16	0.04
44	4.36		0.77	3.30	4.07	0.20	0.09
60	3.24		0.55	2.33	2.88	0.22	0.14
76	2.49		0.25	1.91	2.16	0.24	0.09
92	2.52		0.14	1.98	2.12	0.26	0.14
108	2.71		0.21	2.03	2.24	0.30	0.17
132	2.79		0.27	2.06	2.33	0.29	0.17
156	3.03		0.28	2.24	2.52	0.30	0.21
180	2.81		0.26	2.16	2.42	0.26	0.13
204	2.57		0.25	1.96	2.21	0.27	0.09
228	2.71		0.32	2.06	2.38	0.25	0.08
252	2.80		0.36	2.11	2.47	0.25	0.08
280	2.72	1.05	0.38	2.01	2.39	0.25	0.08
Average	3.51 4.56§	1.05	0.65	2.48	3.13	0.24	0.14

*Material deposited in the off-gas tube between melter and dust removal wet scrubber (measured after run termination)

†Suspended material in the scrub solution of the dust removal wet scrubber.

‡Dissolved material in the scrub solution of the dust removal wet scrubber.

§Including the amount deposited in the off-gas tube (1.05%).

TABLE 3

Cesium Loss in a Liquid-Fed Ceramic Waste Melter into the Off-Gas Stream in Wt.% of the Amount Fed to the Melter with the HLLW

Time, hr	Cesium loss, %					
	Overall total*	Found in dust removal wet scrubber			Found in condenser	Found in chemical wet scrubber
		In the removed particulates	Dissolved in the scrub solution	Total in scrubber		
12	2.43		1.90	1.90	0.15	0.38
38	2.78		2.25	2.25	0.31	0.22
44	2.97	0.02	2.35	2.37	0.36	0.24
60	2.86		2.15	2.15	0.41	0.30
76	3.16		2.14	2.14	0.61	0.41
92	3.72		2.54	2.54	0.73	0.45
108	3.82	0.01	2.51	2.52	0.78	0.52
132	4.63		3.05	3.05	0.86	0.72
156	4.96		3.24	3.24	0.94	0.78
180	4.56		2.95	2.95	0.92	0.69
204	4.08		2.58	2.58	0.89	0.61
228	3.91		2.48	2.48	0.86	0.57
252	3.86	0.01	2.48	2.49	0.84	0.53
280	3.75	0.02	2.35	2.37	0.84	0.54
Average	3.68	0.015	2.50	2.50	0.68	0.50

*Amounts deposited in the off-gas tubes are not included. After run termination it was found that approximately 0.3% was deposited in the off-gas tube between melter and dust removal wet scrubber.

TABLE 4

Ruthenium Loss in a Liquid-Fed Ceramic Waste Melter into the Off-Gas Stream in Wt.% of the Amount Fed to the Melter with the HLLW

Time, hr	Ruthenium loss, %											
			Found in dust removal wet scrubber									
	Overall* total		In the removed particulates		Dissolved in the scrub solution		Total in scrubber		Found in condenser		Found in chemical wet scrubber	
	a†	b‡	a	b	a	b	a	b	a	b	a	b
12	10.8	2.8	5.9	0.8	4.8	1.4	10.7	2.2	0.1	0.5	0.04	0.13
20	8.8	3.0	2.6	0.7	5.9	1.7	8.5	2.4	0.3	0.5	0.04	0.11
28	8.6	2.9	2.4	0.8	5.9	1.5	8.3	2.3	0.3	0.5	0.04	0.10
36	10.5	3.5	3.3	0.9	6.8	2.1	10.1	3.0	0.4	0.4	0.03	0.10
44	16.3	3.2	2.8	1.0	13.0	1.7	15.8	2.7	0.5	0.4	0.03	0.11
52	13.1	4.1	1.2	1.5	11.0	2.0	12.2	3.5	0.9	0.5	0.03	0.10
60	15.4	1.9	4.2	0.6	10.3	0.7	14.5	1.3	0.9	0.5	0.03	0.10
68	13.3	3.8	2.5	1.5	10.0	1.7	12.5	3.2	0.8	0.5	0.03	0.10
76	13.5	4.1	2.5	1.7	10.2	1.8	12.7	3.5	0.8	0.5	0.03	0.09
84	13.6	3.2	2.8	1.2	10.0	1.4	12.8	2.6	0.8	0.5	0.03	0.09
92	15.8	3.0	2.4	1.1	12.4	1.3	14.8	2.4	1.0	0.5	0.03	0.09
100	13.7	4.0	2.3	1.5	10.4	1.8	12.7	3.3	1.0	0.6	0.03	0.08
Average	12.9	3.4	2.9	1.1	9.2	1.7	12.1	2.8	0.8	0.5	0.03	0.10

*Ruthenium plated out on the off-gas tubes is not included.

†a, Waste solution 3.4M HNO_3, containing 1 g/l Ru.

‡b, Denitrated waste solution 0.7M HNO_3 (rest molarity), denitrated by HCOOH in a denitration plant, containing 1 g/l Ru.

REFERENCES

1. C. C. Chapman, *Joule Heated Ceramic Melter,* Quarterly Report, BNWL-1871, Pacific Northwest Laboratory, Nov. 1974.
2. W. Heimerl, New Ways for Vitrification of High Level Waste, *Chemie-Technik,* Vol. 10 (1976).
3. S. Weisenburger, Non-Radioactive Operation Experience with a Joule Heated Ceramic Melter for Vitrification of HLLW, in Proceedings of *Scientific Basis for Nuclear Waste Management,* Boston, G. J. McCarthy (Ed.), Plenum, NY, 1979.
4. *HLLW Solidification and Storage,* Power Reactor and Nuclear Development Corporation Report No. N-651-78-05, Tokai, Japan, 1978.

VITRIFICATION OF HANFORD RADIOACTIVE DEFENSE WASTES

M. J. KUPFER
Rockwell Hanford Operations, Richland, Washington

ABSTRACT

Hanford defense waste sludges and residual liquids are effectively immobilized by conversion to borosilicate glasses. The effects of composition on various properties such as chemical durability, viscosity, and devitrification are discussed.

INTRODUCTION

One option for long-term management of the Hanford defense wastes involves retrieval of the radioactive wastes from underground storage tanks and subsequent removal of the long-lived radionuclides ($t_{1/2} > 10$ years) from the water-soluble portion of these wastes.[1] Resulting concentrated radionuclides would then be combined with the water-insoluble waste (sludge) and converted to an insoluble silicate glass form suitable for long-term storage or disposal.

Sludges are the mixtures of hydrated metal oxides, hydroxides, and phosphates that precipitated when highly acid process wastes were made alkaline for storage in mild steel underground tanks. The principal radionuclides in sludges are ^{239}Pu and ^{90}Sr. The bismuth phosphate, uranium recovery, Redox and Purex processes[2] generated sludges characteristic of their different process chemistries. Chemical compositions of such wastes are thus highly varied (Table 1) and pose unique problems to development of suitable glass formulations for their fixation.

A highly radioactive salt solution, residual liquid, will be the most significant volume of liquid waste in the Hanford inventory in the 1980's (most of the waste will be in solid form, e.g., sludge and salt cake). Residual liquid is the highly alkaline solution that remains when neutralized salt solutions in Hanford tanks are evaporated using large evaporator–crystallizer units. The residual liquids contain large concentrations of $NaOH$, $NaNO_3$, and $NaAl(OH)_4$, as well as ^{137}Cs, ^{99}Tc, and ^{90}Sr. Because of the potential mobility of this liquid, another long-term waste management option is to convert residual liquid to a solid form prior to processing the solid sludges and salts. Thus, the residual liquid could be converted directly to glass, or it could be treated to remove the radionuclides which could subsequently be converted to glass. Because the chemical compositions of residual liquids will be quite uniform, they should be somewhat less challenging to vitrify than the sludges.

Results of scouting tests on conversion of Hanford sludges and residual liquids to glasses were reported earlier.[2-4] These test results and more extensive vitrification tests completed recently are summarized in this report.

EXPERIMENTAL

Batches of freshly precipitated synthetic sludges were prepared by duplicating actual process flow-sheet conditions. The wastes were washed three times with water to remove most of the water-soluble salts. The compositions of these wastes are those shown in Table 1. Since only small amounts of these sludges could be prepared from large quantities of the waste solutions, simulated sludges for the vitrification tests were also prepared by simply mixing the appropriate metal oxides, carbonates, phosphates, etc.

The composition of synthetic residual liquid wastes and of the concentrated waste stream that would result if the radionuclides were removed from residual liquid are shown in Tables 2 and 3, respectively. For convenience, these wastes are identified as wo/rr (without radionuclide removal and w/rr (with radionuclide removal).

TABLE 1

Typical Hanford Sludge Compositions*

Component	Separations process				
	$BiPO_4$†	$BiPO_4$ (3rd cycle)	Uranium recovery	Redox	Purex
Al				30-75	8
Bi	28	30			
Cr	2	8		1-20	
Fe	16		30	5-10	16
La		16			
Mn		11		1-2	3
Na	9	8	7	3-10	5
Ni			4		
Si	7			2-5	4
Sr			14		
U			4		
CN			8		
F	0.3	3			
NO_3^-	1	1	1	1	1
PO_4^{3-}	8	13	14		
SO_4^{2-}	0.2	0.5	0.5	0.2-1	0.5
H_2O	7	7	8	25	22.5
O_2	21	3	10	28	38

*Average compositions (in wt.%) based on washed and dried (120°C) synthetic and, in some cases, actual sludges.

†Average compositions of sludges from 1st and 2nd cycle $BiPO_4$ process streams.

Well-mixed glass batches contained in platinum gold alloy nonwettable crucibles were melted in resistance heated furnaces. The melts were maintained for 1 hr at the temperature where viscosity was 50 to 250 poise and then were removed from the furnace and allowed to cool. The 50- to 250-poise viscosity range is considered satisfactory for pouring molten glass from a continuous melter into a final storage container.

The durabilities of crushed test products in distilled water, 1*M* HNO_3 and 1*M* NaOH at 100°C were determined using equipment and methods described earlier.[3] Equipment and methods for determining the percentage of cesium that volatilized from the crucible-scale melts were also described earlier.[3]

The expected cooling rate of molten glass after it is poured into a storage canister is approximately 12°C/hr. The effect on devitrification behavior of slow-cooling glass at a conservative rate of 3°C/hr was determined. The slow-cooled samples were analyzed for crystallinity using X-ray diffraction and optical microscopy techniques. Their durabilities in water, acid, and alkali were also measured.

RESULTS AND DISCUSSION

Borosilicate-type glass formulations were evaluated for fixation of synthetic sludges. Sodium–borosilicate and soda–lime compositions were evaluated for fixation of residual liquid wastes. Because of the superior leach resistance of most high-melting glasses, high-temperature (1200 to 1400°C) as well as low-temperature (1000 to 1200°C) glass formulations were tested. Tables 4 and 5 list conditions and results of selected vitrification experiments.

TABLE 2

Residual Liquid Waste (WO/RR)

Composition*	Molarity
NaOH	5.5
$NaAlO_2$	2.0
$NaNO_2$	2.0
$NaNO_3$	2.0
Na_2CO_3	0.1
Na_2CrO_4	0.1
Na_2SO_4	0.05
Cs_2CO_3	0.055†

*Expressed as metal oxides in wt.%: 74.1 Na_2O; 20.3 Al_2O_3; 1.5 Cr_2O_3; 3.1 Cs_2O; 1.0 SO_3.

†Added to facilitate leach rate determinations.

TABLE 3

Residual Liquid Waste (W/RR)

Composition*	Wt.%
Na_2CO_3	67.5
$NaNO_3$	19.1
NaOH	2.4
$NaAlO_2$	3.9
$NaTi_2O_5H$	3.3
SrO	1.5†
Cs_2CO_3	1.5†

*Expressed as metal oxides in wt.%: 86.5 Na_2O; 4.1 Al_2O_3; 4.5 TiO_2; 2.6 SrO; 2.2 Cs_2O.

†Added to facilitate leach rate determination.

Sludge Glasses

In many cases, satisfactory sludge glasses are prepared by melting a mixture of the sludge and a frit of the composition (in wt.%) 13 Na_2O, 11 B_2O_3, and 76 SiO_2 (Table 4). However, because of the high variability of the compositions of Hanford sludges, additions of other components are often necessary to help optimize glass viscosity and chemical durability. Thus a 1 to 5 wt.% addition of Li_2O effectively reduces the viscosity of sludge glasses and is generally a necessary batch ingredient if glass melting at <1200°C is desired (particularly when immobilizing highly refractory Redox process sludge). An addition of ~5 wt.% ZrO_2, TiO_2 or Al_2O_3 is also often desirable to increase leach resistance. The amount of sludge (wt.%) that

TABLE 4

Vitrification of Hanford Sludges

Sludge type	Waste oxides	Composition, wt.% Frit*	 Li_2O	 ZrO_2	 Al_2O_3	Temperature (for viscosity 50–250 poise), °C	Soxhlet leach rate, 10^{-4} g/cm² d†	Loss, wt.% Soxhlet	 Acid	 Alkali
Purex	30	70				1250	0.9	2.2	0.40	1.2
	30	68	2			1150	1.6	4.5	0.83	1.2
Redox	25	73	2			1400	0.1	0.90	2.1	0.90
	25	70	5			1200	0.6	2.2	5.4	1.4
$BiPO_4$	50	45		5		1300	2.8	2.0	0.08	1.1
	50	43	2	5		1200	3.6	3.0	0.19	1.4
$BiPO_4$	30	65			5	1350	0.7	0.81	0.14	1.5
(3rd cycle)	30	60	5		5	1150	2.0	1.8	0.21	1.8
Uranium	30	70				1300	5.2	12.0	0.40	1.0
recovery	30	63	2	5		1200	2.2	5.9	0.42	1.4
						Total for: Commercial borosilicate glass		0.20	0.08	2.4
						Commercial soda-lime glass		4.1	0.10	0.6

*Frit composition, wt.%: 13 Na_2O; 11 B_2O_3; 76 SiO_2.

†Leach rate @ 100°C based on cesium. The crushed glass particles used for the Soxhlet test are assumed to be spherical which leads to a calculation of minimum surface area. Thus, leach rates noted in the table are believed to be maximum values.

TABLE 5

Vitrification of Hanford Sludges

Waste oxides	Ingredients, wt.% SiO_2	 B_2O_3	 Li_2O	 TiO_2	 CaO	 Al_2O_3	Temperature (for viscosity 50–250 poise), °C	Soxhlet leach rate, 10^{-4} g/cm² d*	Loss, wt.% Soxhlet	 Acid	 Alkali
Vitrification of residual liquid (wo/rr)											
25	60	10		5			1200	0.4	0.60	0.07	2.3
25	58	10	2	5			1100	0.9	1.3	0.14	1.5
Vitrification of radionuclide removal—processed residual liquid (w/rr)											
20	65	10				5	1300	0.5	1.2	0.08	0.71
20	65	10	2			5	1200	0.9	2.4	0.37	2.3
20	63		2		10	5	1300	1.3	2.5	0.15	0.50

*Leach rate @ 100°C based on cesium. The crushed glass particles used for the Soxhlet test are assumed to be spherical which leads to a calculation of minimum surface area. Thus, leach rates noted in the table are believed to be maximum values.

can be successfully loaded into the glass structure is also highly dependent on the waste origin.

As expected, the chemical durability of sludge glasses increases markedly as the melting temperatures, hence, SiO_2 : alkali ratio increases (Table 4). Generally, these glasses are all quite resistant to attack by alkaline solutions at 100°C. Glasses incorporating Purex process waste that is high in iron are also adequately durable in water and acids. Glasses incorporating Redox process sludge are quite durable in water because of the significant amounts of Al_2O_3 in the sludge. For this same reason, however, these glasses exhibit rather poor durability in acids. (It is highly unlikely, however, that a waste form in a nuclear waste repository would encounter acid solutions.)

Glasses containing bismuth (from $BiPO_4$ and uranium recovery process sludges) are highly acid-resistant. A high waste oxide loading (~50%) is possible with $BiPO_4$ process sludge without significant sacrifice in product leachability. The relatively poor resistance of uranium recovery sludge glasses in water is attributed to the significant quantities of nickel ferrocyanide in the waste. Substitution of 2 to 5 wt.% ZrO_2 or Al_2O_3 for silica in these glasses improves water resistances substantially.

Residual Liquid Glasses

Glasses made from residual liquid (w/rr and wo/rr) contain higher SiO_2 content and lower waste oxide loadings than those made from sludges (Table 5). These glasses are about as durable as commercially available soda lime glasses in water, acid, and alkali at 100°C if the $Na_2O + Li_2O$ content is maintained below ~20 wt.%. As with some of the sludge glasses, additions of Li_2O reduce viscosity and TiO_2, ZrO_2, or Al_2O_3 additions increase the chemical durability. Generally, the borosilicate residual liquid glasses are more durable in water than those made using the soda lime formulations. The borosilicate glasses are, however, less durable than the soda lime glasses in alkaline media. A B_2O_3 content in excess of 10 wt.% reduces considerably the chemical durability of borosilicate glasses.

Devitrification Behavior

Glasses made from residual liquid and Purex process sludges do not devitrify when cooled slowly (3°C/hr) from 1000°C to 400°C.

Redox sludge glasses that have been cooled by air quenching normally contain inclusions (~2 vol.%) of Cr_2O_3. When cooled slowly, however, β-spodumene ($LiAlSi_2O_6$) is a primary devitrification product that forms by nucleating on the Cr_2O_3 particles. Leach rates of the devitrified specimens are no higher, however, than those of the original glasses.

Waste forms incorporating $BiPO_4$ and uranium recovery process sludges devitrify when cooled slowly but are vitreous if cooled rapidly. Although devitrification of these glasses may be promoted by the presence of the durability additive ZrO_2, they also devitrify when ZrO_2 is deleted from the formulations. The primary crystalline phase in the devitrified products is SiO_2 (tridymite). Although other phases are present, they have not yet been identified. Leach rates of the devitrified samples in water (100°C) are about five- to tenfold higher than those for the vitreous specimens.

Volatility

About 0.5 to 2.0% and 0.02 to 0.5% of the cesium in residual liquid and sludge wastes, respectively, volatilizes when the waste-glass batches are melted in crucibles.[2,3] Because of the high content of nitrites and nitrates in residual liquid (wo/rr) waste, considerable foaming occurs during melting. In a full-scale residual liquid vitrification plant, foaming should be anticipated and planned for in the melter design or a processing step such as calcination should be used.

Fixation of Sulfate-Bearing Wastes

Residual liquids (wo/rr) and some Hanford sludges will likely contain small amounts of sulfate (Tables 1 and 3). The presence of excessive amounts of sulfate in some glass formulations can result in the formation of an undesirable water-soluble sulfate phase that is rich in cesium and strontium. Sulfate concentrations that are typically present in residual liquids and washed sludges are readily incorporated into the silicate glass matrix. The sulfate solubility limit in these waste glasses is about 0.5 to 1.0 wt.%.

Tests with Actual Wastes

Vitrification tests with actual Redox and Purex process sludges and residual liquids have been performed.[2,3] The products have exhibited properties similar to those prepared from synthetic wastes.

CONCLUSIONS

Hanford sludges and residual liquids can be effectively immobilized by conversion to silicate glasses. Because of the high variability of the compositions of Hanford wastes, glass formulations must be tailored somewhat to provide glasses exhibiting the desired physical and chemical properties. Some compromise in chemical durability must be made to obtain low-melting glasses. Future work will be centered on further refinements of glass compositions and detailed physical and chemical characterization of the products. Compatibility of the glasses with melter electrode and refractory materials will be determined. Methods for reducing the propensity of $BiPO_4$ and uranium recovery process sludge glasses to devitrify will be a prime objective.

REFERENCES*

1. W. W. Schulz, *Removal of Radionuclides from Hanford Defense Waste Solutions*, RHO-SA-51, Rockwell Hanford Operations, Richland, Washington, to be published.
2. J. M. Cleveland, *The Chemistry of Plutonium*, p. 500, Gordon and Breach Science Publishers, New York, New York, 1970.
3. M. J. Kupfer and W. W. Schulz, *Fixation of Hanford Sludge by Conversion to Glass*, ARH-SA-285, Atlantic Richfield Hanford Company, Richland, Washington, March 1977.
4. M. J. Kupfer, *Fixation of Hanford Alkaline Waste Liquors by Conversion to Glass*, RHO-SA-20, Rockwell Hanford Operations, Richland, Washington, April 1978.
5. M. J. Kupfer, *Vitrification of Hanford Bismuth Phosphate and Uranium Recovery Process Sludges*, RHO-LD-60, Rockwell Hanford Operations, Richland, Washington, September 1978.

---

*Both RHO and ARH documents may be obtained by writing to Document Control, Rockwell Hanford Operations, Richland, Washington 99352.

7

SOLIDIFICATION OF HLW SOLUTIONS WITH THE PAMELA PROCESS

WILFRIED HEIMERL
Deutsche Gesellschaft für Wiederaufarbeitung von Kernbrennstoffen mbH (DWK),
c/o Eurochemic, B-2400 Mol, Belgium

ABSTRACT

A revised concept for the PAMELA process for the solidification of HLW solutions is described. The reasons for some changes, e.g., future use of borosilicate glass instead of phosphate glass, manufacture of glass blocks as well as blocks of glass beads in metal matrix, are discussed. Plans for a PAMELA demonstration plant to be built at Mol, Belgium, are presented.

INTRODUCTION

In the Federal Republic of Germany it was decided in 1977 to focus all activities on the development of one German process for HLLW solidification. This process shall be the back-up system for the French continuous vitrification process (AVM), which has been selected by DWK because of the advanced stage of development to be the reference process for HLLW solidification in the German Entsorgungszentrum (national fuel cycle center for spent nuclear fuel elements).

Three German processes are under development.[1-4] A decision was made to take the PAMELA process as the basis for the concentrated efforts and to build a PAMELA demonstration plant at the Eurochemic site at Mol, Belgium. In 1978, the PAMELA technology was taken over from Gelsenberg by DWK. At the same time, the original PAMELA concept was modified in some points.

SHORT REVIEW OF THE HISTORICAL DEVELOPMENT OF THE PAMELA PROCESS

In 1969, the German company Gelsenberg started some R&D activities in the field of HLLW vitrification within a program supported by the government. Originally, this work was aimed at the development of a vitrification process suitable for HLLW from the thorium fuel cycle. Based on the U.S. work at Hanford at that time, a phosphate glass process called PHOTHO (*pho*sphate glass solidification of HLLW from the *tho*rium-fuel cycle) was developed. Final products were blocks of phosphate glass.

In 1973 a collaboration with Eurochemic/Belgium began. During the next years, on the basis of the PHOTHO process and on work at Eurochemic on metal incorporation, the PAMELA process was developed. The original PHOTHO process was extended by two steps: (1) production of glass beads instead of glass blocks and (2) incorporation of the glass beads into a metal matrix.

From 1974 to 1978, the process was tested and demonstrated in a hot-cell installation. During this time, about 200 l of HLLW from LWR fuel reprocessing with a total activity of about 100 KCi have been processed. This operation was followed by cold testing of components on a larger scale and the beginning of the planning of a hot PAMELA demonstration plant. On October 1, 1978, the Gelsenberg part of the PAMELA development was taken over by DWK.

RECENT MODIFICATIONS OF THE PAMELA CONCEPT

As the new owner, DWK introduced some modifications which mainly concern the final product. Originally, a phosphate glass composition was favored, whereas now a borosilicate glass is preferred.

Instead of producing only glass-metal products ("Vitromets"), in the future the manufacture of glass block as well as that of Vitromets will be demonstrated with the PAMELA process. The following [illegible] led to these decisions:

1. Worldwide, borosilicate glass is favored for HLLW solidification. Knowledge of and experience in the use of this product are growing much faster than in that of the phosphate system, which was followed only by Gelsenberg, Eurochemic, and some workers in the Soviet Union. In order to participate in this growing international knowledge, it seemed desirable to switch over from phosphate to borosilicate glass.

2. Some recent leach tests under very hard conditions (quinary brine at 200 C and [illegible] bar) showed that the phosphate glass (which up to 100 C has an excellent leach resistance) has a higher tendency to disintegrate than borosilicate glass under the same conditions.

3. The standard product today as concerns HLLW solidification is the borosilicate glass block.

4. The reference system for HLLW vitrification for DWK is the French continuous vitrification process. The final product of this process is a borosilicate glass block. In order to avoid a complication of the licensing procedure, the back-up process (PAMELA) should deliver a similar product.

5. The Vitromet product is seen to be a product with a great potential on a long-term basis, but at present the manufacture of a glass block seems to have some advantages from the processing side. That is why the option for both of the products should be kept open.

CONCEPT OF THE PAMELA DEMONSTRATION PLANT

A PAMELA demonstration plant will be built at the Eurochemic site at Mol, Belgium. There, from former reprocessing operations, among other kinds of waste about 64 m^3 of HLLW originating from spent LWR fuel are stored in two tanks (Table 1). The main purpose of the plant shall be the [illegible] of the PAMELA process [illegible] On the other hand, the existing HLLW at Eurochemic [illegible] blocks [illegible] The experience [illegible] operation of the PAMELA [illegible] will be helpful for the planning of the HLLW vitrification plant within the German Entsorgungszentrum.

The PAMELA process [illegible] the following steps:

1. Chemical denitration with formaldehyde
2. Vitrification to borosilicate glass [illegible] Joule heated ceramic melter
3. Manufacture of either glass blocks or Vitromet
4. Off-gas cleaning

The throughput of the plant will be 30 l/hr of HLLW. Some additional data are given in Table 2. The schematic flow sheet (Fig. 1) shows the several steps of the process.

TABLE 1

HLLW to be Solidified by the PAMELA Demonstration Plant

Amount of HLLW: 64 m^3, stored in two stainless steel tanks with a capacity of 40 m^3 each.
Type of waste: Purex type HLLW from the reprocessing of spent LWR fuel (average burnup: 16,500 MWd/T)
Concentration: ~500 l/T of fuel
Age (average time since reactor release): 8.5 years
Specific activity: ~200 Ci/l
Specific heat release: 0.7 w/l
Fission product oxide and actinide content: ~40 g/l
Process chemicals:
  Na^+: 10 g/l
  Fe^{3+}: 8 g/l
  SO_4^{2-}: 7 g/l
  F^-: 2.5 g/l

TABLE 2

The PAMELA Demonstration Plant Planned to be Built at Mol

Capacity
  Denitrator: 60 l/hr, 12 hr/d (720 l/d)
  Melter: 30 l/hr continuously (720 l/d)
  Factor of volume reduction HLLW: [illegible]
  Amount of borosilicate glass [illegible] 48 [illegible]
  Frit to waste ratio: 80:20
  Glass production rate: 6 kg/hr

Dimensions of canisters

Net volume	24 l	70 l
Open diameter	20 cm	30 cm
Wall thickness	0.8 cm	0.8 cm
Height	100 cm	120 cm

Production rate
  2 glass blocks of 24 l/d or 1 glass block of 70 l/36 hr
  3 Vitromet blocks of 24 l/d or 1 Vitromet block of 70 l/d
Total production
  110 glass blocks and 110 Vitromets (24 l) or 37 glass blocks and 37 Vitromets (70 l)
Operation time
  Cold testing period: 1 to 1.5 years
  Hot operation: about 2500 hrs with 30 l/hr (several runs within a period of 2 years)
Start of hot operation
  Scheduled for 1985–1986

Denitration

The HLLW is coming in via a pipe connection into two reception tanks of 5 m^3 each. The liquid can then be transferred to the denitration area via airlifts or steam jets. By chemical denitration with formaldehyde, a destruction of nitric acid and part of the nitrates is obtained. Thus the

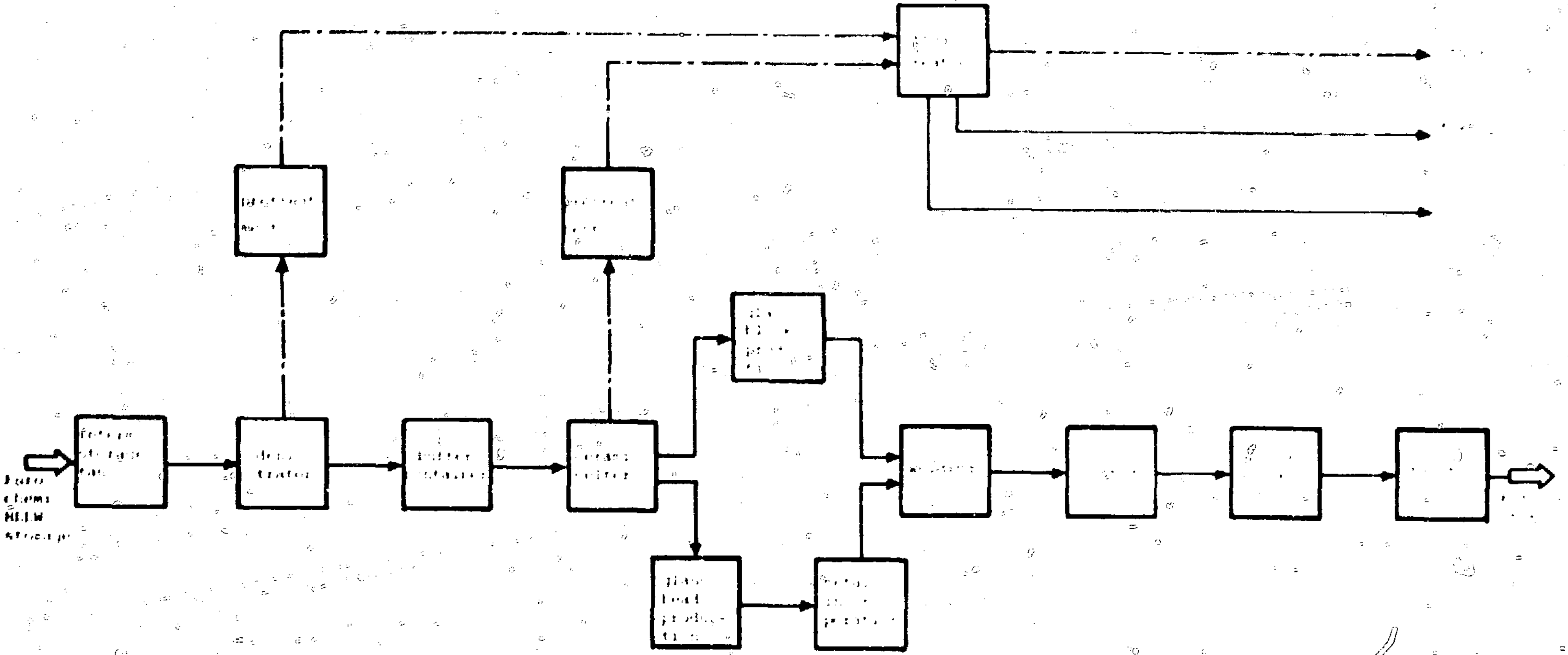

Fig. 1 Simplified block flowsheet of the PAMELA process

oxidation potential of the liquid is lowered, which will help to reduce ruthenium volatilization during melting (the formation of volatile RuO_4 by oxidation will be suppressed). The effectiveness of the denitration step (especially without the support of phosphoric acid, which was used formerly) has not yet been proven in detail. Investigations are under way within a joint R&D program (see Research and Development Activities). A final decision as to whether the effect of chemical denitration is high enough to justify the efforts will be made when clear results are available. Denitration will be performed in batches of 720 liters. Formaldehyde will be used as a 37 wt % solution in water. The capacity of the denitrator shall be one batch per day.

Vitrification

Vitrification is carried out in a Joule-heated ceramic melter, a prototype of which is shown in Fig. 2. The melter has a liquid feeding system. The pretreated HLLW is mixed with borosilicate glass frit in a mixing vessel (about 140 g of frit per liter HLLW). This mixture is fed in just on top of the melt surface. The surface area of the melt is 0.8 x 0.8 m and the depth of the glass bath is 0.4 m. The feed rate is 30 l hr continuously.

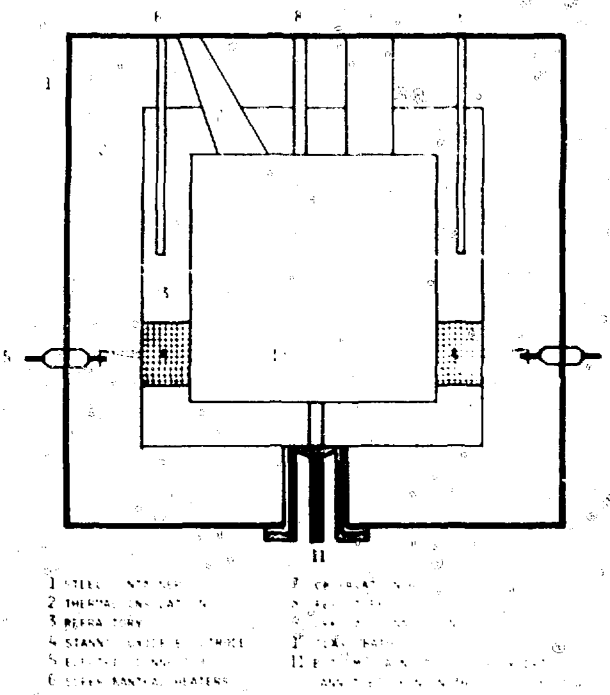

Fig. 2 Joule-heated ceramic melter

The feed is drying, calcining, and melting. The inner chamber of the melter is a cube with an edge length of 0.8 meter. The inside walls including the top part of the melter and the electrodes are all [illegible] of the electrodes will [illegible] wall thickness with thermal insulation [illegible] operation temperature is [illegible]

Manufacture of Glass Blocks

For glass blocks [illegible] drained periodically from the melter [illegible] This bottom drain uses [illegible] frequency induction heating [illegible] cooling. The glass is cast into [illegible] (Table 2). The cooling of the blocks [illegible] by thermal insulation [illegible] controlled cooling.

Manufacture of Vitromets

Here [illegible] flow rate [illegible] will be [illegible] [illegible] glass beads [illegible] from the [illegible] [illegible]

Off Gas Treatment

The [illegible] ment system. [illegible] and [illegible] is a wet scrubbing system. [illegible] off gas streams are [illegible] and sent through the main [illegible] system where [illegible] purification is [illegible] remaining gas [illegible] up the stack.

RESEARCH AND DEVELOPMENT ACTIVITIES

A joint R&D program is under way to support the PAMELA project and [illegible] to optimize the process. This program is financed mainly by the German Ministry of Research and Technology. Partners are DWK, Eurochemic, the Nuclear Research Centers of Karlsruhe and Jülich, Hahn-Meitner-Institute Berlin, Nukem Co., and the Belgian Nuclear Research Center. Within this program, the main components (ceramic melter, denitrator, off-gas system, remote handling systems, respectively) will be tested in a cold mock-up. An important point will be a long test of continuous operation of the equipment. After construction of the PAMELA plant at Mol is completed, these tests will be continued with the equipment built into the hot cells. A cold testing period of at least one year will help to detect and improve any troublesome parts of the system before hot operation is begun.

REFERENCES

[illegible]

DEVELOPMENT OF ENGINEERING SCALE HLLW VITRIFICATION TECHNIQUE AT PNC

HIROSHI NAGAKI, NAOHIKO OGUINO, NAOMI TSUNODA, and TAKESHI SEGAWA
Power Reactor and Nuclear Fuel Development Corporation, Tokai-mura, Ibaraki-ken, 319-11, Japan

ABSTRACT

Some processes have been investigated to develop the technology of solidification of the high-level radioactive liquid waste generated from the nuclear fuel reprocessing plant operated by the Power Reactor and Nuclear Fuel Development Corporation (PNC) at Tokai-mura. This report covers the present state of development of a Joule-heated ceramic melter and a direct megahertz induction-heated melter. Engineering-scale tests have been performed with both melters. The Joule-heated melter could produce 45 kg or 16 liters of glass per hour. The direct-induction furnace was able to melt 5 kg or 1.8 liters of glass per hour. Both melters were composed of electrofused cast refractory brick. Thus it was possible to melt the glass at above 1200°C. Glass produced at higher melting temperatures is generally superior.

INTRODUCTION

The high-level liquid waste generated from PNC's reprocessing plant is assumed to have a rather high concentration of sodium nitrate. About 1 mole/liter comes from the solvent regeneration cycle. If it is desired to produce glass containing 30 wt.% waste oxides, the concentration of sodium oxide might be 10% in the glass product. About 15 wt.% of sodium oxide in borosilicate glass is considered to be a limit based on quality considerations, especially on resistance to leaching by water.

The glass compositions used were as follows:

First and third campaign
SiO_2 43, B_2O_3 14, Al_2O_3 4, Li_2O 3, CaO 2, ZnO 2, and waste 30 wt.%
Second campaign
SiO_2 54 to 50, B_2O_3 9 to 12, Al_2O_3 5, Li_2O 2, and waste 30 wt.%

The waste composition was as follows:

Rh_2O 0.204, Cs_2O 1.3684, SrO 0.5474, BaO 0.907, Y_2O_3 0.337, La_2O_3 0.784, Ce_2O_3 1.529, Nd_2O_3 3.833, mixture of other rare-earth oxide 2.608, ZrO_2 2.6754, MoO_3 2.66, TeO_2 0.343, MnO_2 0.39, Fe_2O_3 1.792, Cr_2O_3 0.172, NiO 0.513, CoO 0.157, Na_2O 9.18, Total 30 wt.%

In the early stages of waste solidification processing, HLLW may be calcined and combined with glass raw materials before being fed to the melter. For this purpose calcination processes such as fluidized bed and spray are being developed in other programs. In the fluidized-bed calcination process, alumina would be added to stabilize the calcination behavior. Silica could also be mixed with the fluidized-bed material. These added components, as well as soda from the waste, can be considered as necessary raw materials for glass melting.

For a homogeneous glass, it is preferable to select a comparatively high temperature melting process, e.g., a ceramic melter. An engineering-scale direct Joule-heated ceramic melter was demonstrated. A megahertz direct-induction-heated ceramic melter was also operated. Through these operations the design goals were realized, and the performance of refractories and electrodes was evaluated.

JOULE-HEATED CERAMIC MELTER

Since Joule heating produces heat in the glass melt, the highest temperatures exist between the electrodes in the molten glass. The covered layer of batch reduces heat dissipation. The batch layer may also trap volatiles from the batch and the glass melt. At the same time, since the

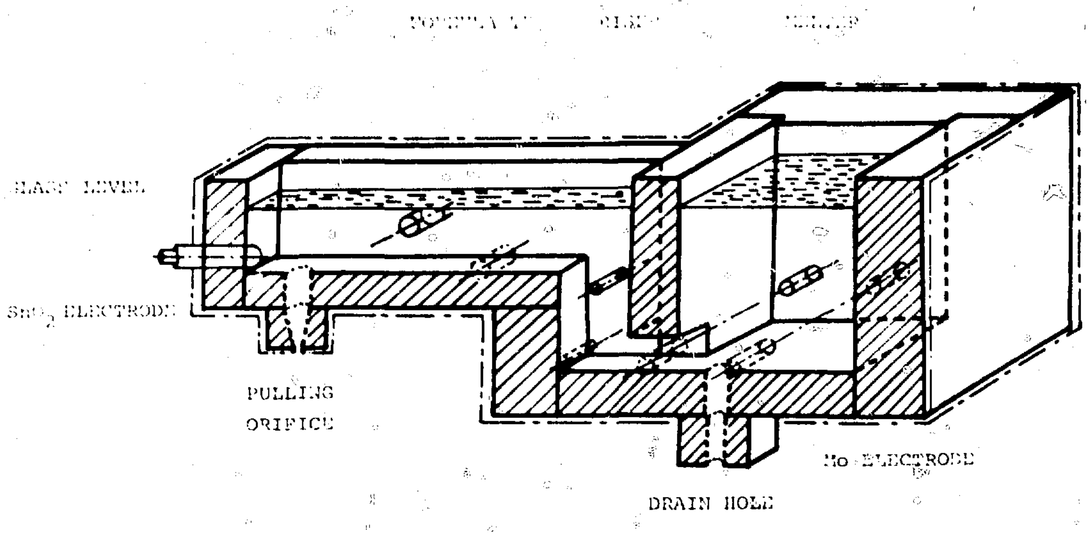

Fig. 1 Schematic of Joule-heated ceramic melter

refractory blocks may be kept at a lower temperature than the glass melt, side wall corrosion can be reduced.

Glass containing waste is very dark in color. Therefore melting by conventional radiation heating is difficult because the infrared rays are absorbed only on the glass surface and do not reach into deeper layers. This fact limits the glass melting depth to only a few centimeters, thus it is impossible to carry out a large-scale melting of waste glass by radiation heating. Joule heating with submerged electrodes avoids the problem.[1]

Metallic molybdenum electrodes endure strong thermal shocks and high electric current density. The problem of using molybdenum is its easy oxidation and sublimation as MoO_3 at temperatures higher than 800°C.

We used both molybdenum and tin oxide electrodes in this experiment. Figure 1 shows the design of the direct Joule-heated ceramic melter, which has the following specifications:

1. Molybdenum electrodes are used in the melting zone. Two pairs of electrodes 50 mm in diameter are connected to a 75 kW electric power supply.
2. A pair of molybdenum electrodes 32 mm in diameter are used in the riser behind the throat. Their role is to control the temperature of the glass prior to pouring. The molybdenum electrodes are protected with water-cooled jackets.
3. Tin oxide electrodes 63 mm in diameter are used in the forehearth, where they might be exposed to air above the glass level.
4. Total holding capacity for glass is 200 liters. The minimum glass holding volume required to maintain Joule heating is 100 liters.

Start-Up and Steady-State Operation

The furnace was heated up to 1200°C in 3 days by a SiC heater of 38 kW in the melter and a $MoSi_2$ heater of 15 kW in the forehearth, both of which were suspended from the superstructure. The heat-up rate was 15°C/hr. After the temperature reached 1200°C, glass cullet and raw material were charged to the melter. Water-cooled molybdenum electrodes were positioned behind the side wall until the glass rose above the electrode levels. Then the electrodes were inserted into their final position (Fig. 2).

The electric resistance R between electrodes was calculated according to Gailhbaud.[2] The relation of R and specific resistivity of molten glass P was $R/P = 0.0552\ cm^{-1}$ for the geometrical arrangement of the melter in Fig. 2.

Calcined raw batch material was supplied by an automatic vibrational feeder which moved cyclically back and forth and charged the raw powder over the entire surface. The feed rate of dry raw batch averaged 45.3 kg glass equivalent per hr and 54 kg/hr maximum. Electrical power supplied to the melter was 35 to 50 kW.

Start-up and steady-state run conditions are tabulated in columns 2–5 of Table 1. The conditions when the glass is held at a constant and the melter is idling without any raw material being fed are shown in columns 6–9 of Table 1.

Slurry Feeding

Slurry feeding experiments were conducted for a week during the third campaign. Simulated high-level liquid waste mixed with glass frit was supplied as a slurry slip directly into the melter by pumping with a peristaltic pump. The feed rate was 30 to 60 l/hr, where 3 liters of waste with glass additives converted to 1 kg glass. After the slurry addition to the melter was under way, the surface was a violently bubbling liquid. There was a sintered layer underneath the liquid and over the molten glass. When the glass level descended, the sintered layer would often form bridges or vacant domes between the batch and molten

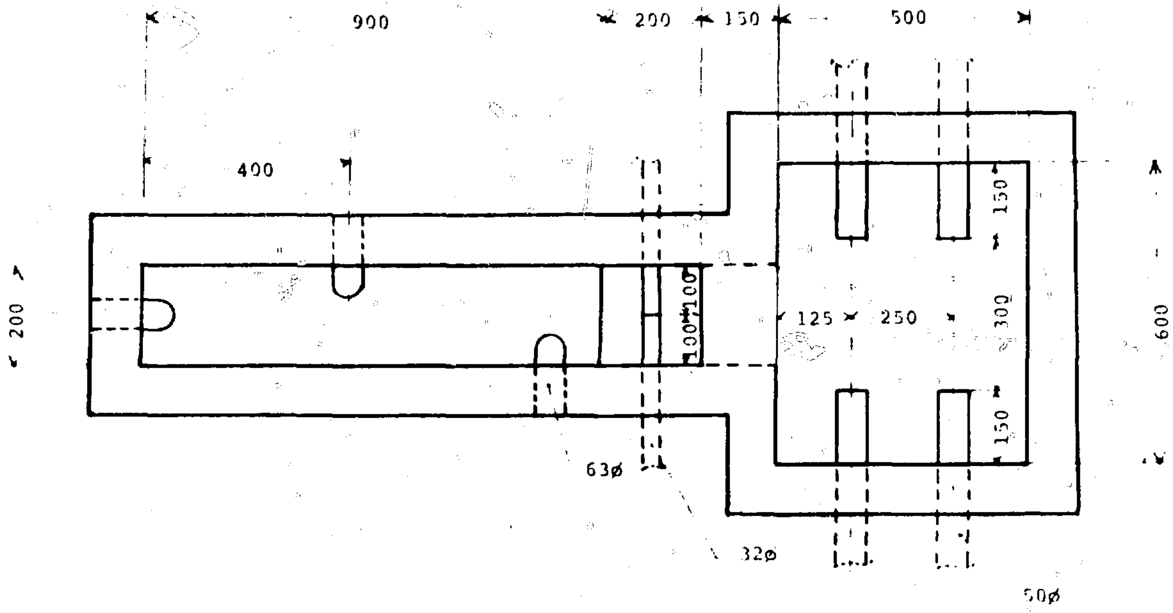

Fig. 2 Plan view of engineering-scale ceramic melter.

glass. By raising the glass level, the slurry could be supplied at a rate of 60 l/hr without any bridge formation. A stable feeding rate to the 0.3 m^2 melting surface was determined to be 50 l/hr, or 167 l/m^2 hr.

Observed Performance

During the first campaign, the furnace operated at 1200°C for 3 weeks and produced about 2.5 tons of glass cast in 13 canisters. The depth of corrosion on the refractories was quite low. However, after the second campaign in which 4.8 tons of glass were melted at 1350°C in 4 weeks, the electro-fused cast aluminozirconium silica (AZS) refractories were corroded to a maximum depth of 12 mm. Corrosion of the chrome zirconia brick (S 216) has not been determined. The corrosion profiles formed inverted arches above the electrodes. The maximum corrosion depth occurred 5 to 10 cm above the electrode level, where the maximum temperature region existed.

Upward drilling 10 to 12 mm in depth was found at the throat. The operating results indicate AZS fused cast block may be corroded at a rate of 0.25 mm/day during the initial stages of operation. There were several cracks on the surface of the refractories. These cracks were concentrated near the glass line where several thermal shocks often occurred due to temporary interruptions in the supply of wet slurry.

Reduction and oxidation reactions between the molybdenum electrodes and molten glass were observed. Thermodynamically, molybdenum is oxidized in the waste glass at high temperature, and nickel, tellurium, cobalt, and other oxides are reduced to metal. Therefore, metallic precipitation must be expected in waste glass melts in contact with molybdenum. In fact, metallic precipitates did appear on the bottom of the melter and on the surface of the molybdenum electrodes, but actual consumption of the electrodes has been almost negligible in these campaigns.

Compared with the long life of the refractory melter, the superstructure which is equipped with electric sensors, heaters, and flow-controlling mechanisms can be expected to be less long lived. Therefore periodical maintenance and parts substitution will be needed under hot operating conditions. So the superstructure must be designed for substitutional repair. Further development on the design of the total waste glass furnace is expected.

Concepts of Hot Operation

After cold (nonradioactive) testing of the furnace is completed, all operations will be completely remote controlled, and the furnace will be run under hot (radioactive) conditions. Once the furnace is operated hot, the ceramic bricks will be severely contaminated by radioisotopes diffusing from the glass; therefore Joule-heated ceramic melters must have a long life. They may be continuously operated for more than a year. The melting capacity is large enough to treat the HLLW generated from a several tons equivalent per day reprocessing plant. At times the melter may be kept idling with a low glass level and a diluted level of activity. The temperature must be maintained high enough to keep the glass molten.

MEGAHERTZ INDUCTION FURNACE

High frequency induction melting comprises both direct and indirect heating of glass. The former represents the

TABLE 1

Stable Operation Conditions of Ceramic Melter

	Operating mode				Idling mode			
	Power, kW	Volts	Amps	Temperature, °C	Power, kW	Volts	Amps	Temperature, C
Melter	46.8	85	550	1150	40.9	95	430	1140
Riser	6.0	63	95	980	3.2	45	70	1020
Forehearth	0.5	21	23	1100				
Orifice	2.1	41	50	800	0.4	13	28	
Forehearth super	8.4	43	195	1030	9.9	44	225	980
Bowl super	6.5	33	197	850	4.2	24	172	940

heating of glass itself by high frequency induction; the latter is the induction heating of a metal pot. Direct induction melting permits the use of a ceramic pot as the melting container, thus providing for high-temperature and long-term melting.

The authors have performed test operation of direct induction melting with an intermediate-scale pilot plant for two years.

Intermediate-Scale Pilot Plant and Its Operation

Figure 3 illustrates the intermediate-scale pilot plant assembly. Raw material consisting of simulated waste calcine and glass frit was supplied to the ceramic pot by a constant-rate feeder located under a hopper. A starting rod made of SiC was suspended at the center of the ceramic pot. To initiate the melting operation, the starting rod was heated by applying a high-frequency current to a work coil installed around the pot. A 4 MHz, 65 kW high-frequency generator supplied the high-frequency power to the coil. After sufficient raw material was melted and the high frequency could couple to the glass melt, the starting rod was pulled up above the glass line. Melting of the raw material then proceeded as it was supplied by the continuous feeder. After the melt reached the 80% level in the pot, the nozzle installed at the bottom of the pot was heated by indirect induction heating of a SiC ring. A 15 kW high-frequency (300 kHz) generator was provided for this indirect heating. The melt was collected in a metal canister located under the nozzle of the pot. The off-gas pipe installed in the furnace cover was connected to dust filters and a duct. Another pipe was also installed at the furnace cover. Measurement of the melt temperature was by a radiation pyrometer.

The output power and work-coil current were controlled and recorded at a control panel. Table 2 shows operational data for the direct induction melting. Start-up was easily performed with 6 kg of the raw material by indirect heating of the SiC rod with about 30 kW anode output. The time required for start-up depends on the thermal shock resistance of the pot material. When a silica pot is used, the start-up can be accomplished within one hour.

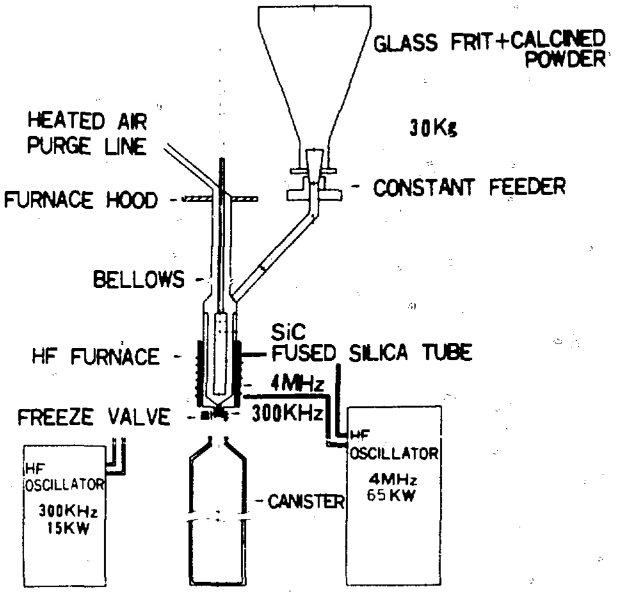

Fig. 3 Middle-scale direct induction melter.

The capacity of the direct induction melting with a 35- to 40-kW anode output was about 6 kg of glass/hr when the inside diameter of the pot was 200 mm. The capacity depends upon the pot size and temperature of the melt. The preceding value was obtained when the melt temperature was kept at 1200°C. The melting capacity increased to 7.5 kg of glass/hr when the inside diameter of the pot was 230 mm.

The process can operate continuously. Thus, the melting capacity of this pilot plant is estimated to be 50 to 60 l/day, depending on the pot size. Test operation of the pilot plant proved the above capacity, except the actual capacity was reduced to 40 to 50 l/day because of the time consumed in melt pouring.

Performance of the Furnace

One of the important factors to consider in the melting process is the life of refractory, in this case the ceramic pot.

TABLE 2

Operational Data of Direct Induction Melting

Pot size		
Inside diameter, mm	200	230
Outside diameter, mm	230	260
Height, mm	550	550
Start-up with SiC rod		
Frequency, MHz	2.8	2.5
Anode output, kW	20	22
Anode current, A	3.7	3.5
Anode voltage, kV	5.3	6.0
Work coil current, A	160	180
Raw material to start, kg	10	14
Time for start-up, min	60	70
Melt temperature, °C	1150	1150
Direct induction melting		
Frequency, MHz	2.8	2.5
Anode output, kW	39	42
Anode current, A	5.6	6.0
Anode voltage, kV	7.0	7.5
Work coil current, A	120	120
Melt temperature, °C	1200	1200
Melting efficiency, kg/hr	5.5	7.5
Melt pouring		
Frequency, kHz	300	300
Anode output, kW	6.3	6.3
Anode current, A	0.9	0.9
Anode voltage, kV	7.0	7.0

Various pots made of sintered silica, fire clay, or fused cast zirconium–aluminate were used in long (10 days) continuous test operations. Sintered silica corroded considerably, and the pot life is assumed to be around 10 days. Pots made of fire clay or fused cast refractories showed no sign of corrosion. Considering the corrosion of those refractories experienced in the glass industry, the life of those pots is estimated to be more than six months.

Possibility of a Full-Scale Radioactive Plant

Direct-induction melting was performed successfully in an intermediate-scale pilot plant. Advantages of the process are the simple furnace structure, ease of operation, and remote control. Many problems, however, still remain in order to scale-up this process to a full-scale active plant.

Remote control and remote maintenance are major subjects for future work. Also, the off-gas system and methods of supplying raw material to the melting process need further consideration.

CONCLUSIONS

A Joule-heated ceramic melter was operated in three campaigns for a total of 58 days. Eight tons of glass containing 30 wt.% equivalent simulated HLLW were produced at an average rate of 45 kg/hr. A slurry feeding experiment was also performed. Performance of the melter was evaluated over more than a year including idling time.

A direct megahertz induction furnace was constructed and used to successfully melt waste glass at a rate of 5 to 7.5 kg/hr. The life of the ceramic melting pot will be longer than a half year. The glass products obtained from both processes were shown to have good homogeneity and to be of high quality.

REFERENCES

1. E. V. Tooley (Ed.), *Hand Book of Glass Manufacture*, Vol. 2, Ogden Publishing Co., New York, 1960.
2. J. Gaillbaud, *Glastechn. Ber.*, 45: 56-67 (1972).

A REVIEW OF CONTINUOUS CERAMIC-LINED MELTER AND ASSOCIATED EXPERIENCE AT PNL

J. L. BUELT, C. C. CHAPMAN, S. M. BARNES, and R. D. DIERKS
Pacific Northwest Laboratory, Richland, Washington

ABSTRACT

Development of continuous, ceramic-lined melters applicable to immobilization of radioactive wastes began at PNL in 1973. A comprehensive program is currently in progress. The melters constructed at PNL have incorporated remote and reliable design features necessary for radioactive use. The extensive experience with vitrification of simulated wastes has proven the continuous melter's applicability to radioactive waste immobilization.

BACKGROUND HISTORY OF CERAMIC MELTER DEVELOPMENT

In 1973 development work began at Pacific Northwest Laboratory (PNL) utilizing ceramic-lined melters for solidification of nuclear wastes. A ceramic melter continuously converts nuclear waste and glass formers into a stable glass product. Molten glass in a ceramic-lined melting cavity is heated electrically by an alternating voltage between a pair of submerged electrodes. This is known as Joule heating. In operation, dried nuclear waste, or calcine, and glass formers are fed onto the molten glass pool, forming a cold cap of solid (unmolten) material. Molten waste glass is then poured from an overflow section into a receiving canister for disposal.

Since the beginning of ceramic melter development at PNL, all the laboratory-scale and full-scale melters have been operated with simulated, nonradioactive nuclear wastes. Each of these melters has a specific purpose as listed below:

1. Mark Series. Five successive short-lived laboratory-scale melters for testing design concepts and construction materials.
   a. Mark I, for testing molybdenum electrode and common firebrick as the glass contact refractory
   b. Mark II, for testing alumina as glass contact refractory, an underflow weir for glass drainage, and a hot plate over the crown of the melter for initial start-up
   c. Mark III, use of molybdenum disilicide electrodes and zircon refractory
   d. Mark IV, use of resistance heater coil (for start-up), connected between molybdenum electrodes
   e. Mark V, use of Inconel* 690 electrode and partial Monofrax* E refractory wall construction.

2. Engineering Scale Ceramic Melter (ESCM). Long-lived pilot scale unit for testing candidate materials and remote operating features such as off-gas containment and glass drainage.

3. Liquid Fed Ceramic Melter (LFCM). Full-scale unit for calcine and liquid feeding of simulated wastes.

4. Calcine Fed Ceramic Melter (CFCM). Full-scale units for direct coupling to spray calcination equipment.

5. Bench Scale Ceramic Melter (BSCM). Pilot-scale design for 1400°C glass temperatures using tin oxide electrodes.

6. Remote Ceramic Melter (RCM). Remotely operable melter being mocked up in cold test facilities prototypic for in-cell use.

Table 1 lists these melters with some operating history.

---

*Monofrax is a registered trademark of Carborundum Corp., Falconer, NY; Inconel is a registered trademark of Huntington Alloys, International Nickel Co., Huntington, WV.

TABLE I

Operating History of Ceramic Melter

Melter	Melting cavity dimensions	Period of operation	Glass produced	Demonstrated maximum feed rate	Melting flux
Typical Mark Series	0.20m x 0.23m x 0.11m deep	8/73 to 10/74			
ESCM	0.36m x 0.76m x 0.15m deep	1/75 to 11/75 1/76 to 1/77		60 kg/hr 29 l/hr	220 kg/hr/m^2 106 l/hr/m^2
LFCM	0.86m x 1.22m x 0.48m deep	2/77 to present	40,000 kg	160 kg/hr 100 l/hr	155 kg/hr/m^2 95 l/hr/m^2
CFCM	0.71m x 1.07m x 0.25m deep	4/78 to 10/78	10,000 kg	50 kg/hr (limited by lid)	66 kg/hr/m^2
BSCM	0.20m x 0.61m x 0.22m deep	11/78 to present	100 kg	14 kg/hr	115 kg/hr/m^2
RCM	0.37m x 0.66m x 0.20m deep	Start-up in 6/79			

REFRACTORY CONSTRUCTION

Many of the different glass contact refractory materials for the Mark melters such as porous alumina were chosen because of material availability and convenience. The Monofrax E, a high chromia-content fused-cast refractory used in Mark V, offered excellent corrosion resistance, whereas the zircon left a zirconium slag on the floor of the melter. However, because of Monofrax E's electrical conductivity relative to the glass at high temperatures,[1] the present melter construction uses a higher alumina fused-cast refractory, known as Monofrax K-3. This refractory has also proven to be highly corrosion resistant.

Greatest wear is expected in the throat through which the glass flows, shown in Fig. 1. Although 40,000 kilograms of glass have been produced in the LFCM, no throat wear has been detected. However, after a 10-day continuous run, where 9,000 kg were produced in the CFCM, erosive penetration of as much as 0.25 in. was measured after shutdown.[2] This is probably attributable to the 16 hours of operation with an extremely corrosive, noncalcine loaded frit at the beginning of the run.

Monofrax K-3 has been subjected to heat-up and cool-down rates greatly exceeding the recommended 20°C/hr without serious detrimental effects.[3] Thermal gradients as high as 300°C/hr during initial liquid feeding in the LFCM have caused some minor cracks of the K-3 at the glass surface, but this can be avoided when the feed rate is slowly increased to the maximum.

Back-up refractory behind the K-3 is required for thermal insulation. Other materials have been tested but a dense, high alumina castable refractory, known as Alfrax* 66, is very good for stopping glass leaks past the K-3. The glass is believed to react with the alumina, creating a viscous, nonflowable residue. Therefore, higher insulative refractory can be used behind the Alfrax since it protects the insulation very well. This composite refractory construction eliminates containment-box water cooling, originally designed to freeze glass leaks, so that fewer in-cell service connections and higher glass temperatures can be attained.

ELECTRODES

Molybdenum was the first electrode material tested in the laboratory melters. It can withstand high glass temperatures but oxidizes rapidly in air above 600°C. Reliable and remotely maintainable cooling connectors were necessary for keeping areas exposed to air below oxidation temperatures. Also, molybdenum and moly-disilicide sometimes corroded, probably due to the oxidizing nature of some high-level waste glasses.[3] Their use, however, is still being investigated.

Inconel 690 has excellent oxidation resistance in glass and air environments but has a continuous operational temperature limit of about 1050°C in glass. However, after the engineering-scale melter was operated at this temperature for two years, less than 10% weight loss of the electrodes was measured. Thus higher operating temperatures are likely.

Flat plate electrodes at the end walls are commonly used in the melters. However, the LFCM has two sets of side-entering electrodes with separate power control.[4] The lower set is used to help increase floor temperatures during idling conditions. The upper set is used to shift the power distribution toward the upper part of the 19-in. deep tank where heat loads are high during liquid feeding.

Higher glass temperatures, and thus greater capacities, are obtained through electrode cooling. A water jacket behind five inches of dense refractory indirectly cools the LFCM electrodes. The temperature difference between the electrodes and the maximum temperature in the center of the tank is nominally 150°C. Glass temperatures as high as 1290°C have been attained while the electrodes were maintained at 1050°C. Similar results have been experienced with the CFCM, which is equipped with air-cooling channels directly on the back side of the electrodes. After the electrodes were cooled, higher glass temperatures and thus higher maximum melting capabilities were measured.[2]

---

*Alfrax is a registered trademark of the Carborundum Co., Falconer, N.Y.

The high-temperature melter, which has been at operating temperature for four months, uses tin oxide as the electrode material. The 2- x 4- x 8-in. tin oxide blocks, which compose the end walls, are air-cooled to prevent glass leakage to the copper bus connector. Expected difficulties with tin oxide are thermal shock and lower current density limits.

DRAIN CONTROL

Molten glass falls by gravity from an externally heated overflow into a receiving canister (Fig. 1). Glass flows through a Monofrax K-3 throat near the floor, through a riser and trough section, and down the pouring tip constructed of Inconel 690. However, in the high temperature melter, the use of Inconel 690 was precluded, so a refractory pouring tip was designed and has worked well. Glass flow may be controlled with a tilt-to-interrupt concept. The entire melter rests on a pivot point and rotates slightly, thus starting or stopping glass flow.

Because the tilt-to-interrupt concept will not completely drain the melter, a bottom drain must also be incorporated into the design for shutdown. The calcine-fed melter successfully demonstrated the use of a remotely operated freeze valve, shown in Fig. 2 (Ref. 2). Cooling air maintained a frozen glass plug in the drain hole when the melter was not in use. After the cooling air was discontinued, power was applied to internal plate heaters, and the temperature of the freeze valve increased. Glass soon began to flow at rates up to 130 kg/hr. It even allowed a viscous, crystalline layer of slag which had accumulated on the floor of the melter to pass.

START-UP TECHNIQUES

Because glass is electrically nonconductive at room temperatures, an external heat source must be supplied for remote start and restart of a continuous melter. The engineering-scale melter utilized a method tested in the Mark Series where a resistance wire was embedded in glass frit and connected between the electrodes.[1] Electrical current generated heat until the frit became molten and conductive. The resistance wire was eventually consumed within the molten glass. The disadvantage of this technique is the difficulty in remote restarting and the undetermined effect that the consumed resistance wire will have on the glass properties.

The LFCM was started using radiant heaters around the lid of the melter. The melting cavity was filled with a crushed, premelted waste glass with a tunnel of 100 pounds of sodium hydroxide placed between the electrodes. Since the melting temperature of sodium hydroxide is 320°C, the tunnel melted first, establishing a conductive path for Joule heating. It then reacted with the premelted waste glass in the rest of the tank.

Both the CFCM and the BSCM started successfully when radiant heaters were used in the lid with nothing but simulated calcine and frit in the melting cavity. This technique is very promising for remote start and restart capabilities.

OPERATING EXPERIENCE WHILE CALCINE FEEDING

A large number of short- and long-term runs, up to ten continuous days of operation, have been carried out with a variety of defense and power reactor simulated waste glass compositions. Table 1 shows some capacity data with these glasses. The melting flux helps determine the size of a continuous melter designed for specific production rates. The melting flux is the amount of material that can be vitrified per unit time per unit of exposed glass surface area. Although no two glass compositions melt at the same rates, melting fluxes, and thus scaled-up capacity predictions, agree very well between the engineering-scale and full-scale units.[3,5]

Limitations other than surface area, however, can play a governing role in melting capacities. One such limitation is the plenum height above the glass level. During feeding, conically shaped cold cap piles up on the glass surface. If the height above the glass surface is insufficient, the top of the cone will approach the feed entry point. The LFCM, which has just enough plenum height for high capacity tests, has 38 inches above the glass surface. The plenum height problem can also be minimized by mechanical distribution of the cold cap, which has been successfully tested in the LFCM. However, this is an extra mechanical operating device not desirable in hot cell operation.

Another melting capacity limit can be the maximum electrode current density. Current densities that are too high at the surface of the electrodes can create interfacial resistance between electrodes, cause corrosion, and dramatically reduce the life of the electrode. The melter must be designed with adequate operating current densities for a range of glass resistivities.

Another limiting factor in production rates is foaming, the entrapment of gases of decomposition in molten glass. The voluminous glass foam can rise and engulf the entire floating cold cap. This will cause rapid melting and decomposition from the increased heat transfer, which will increase the foam production rate. Foaming can be con-

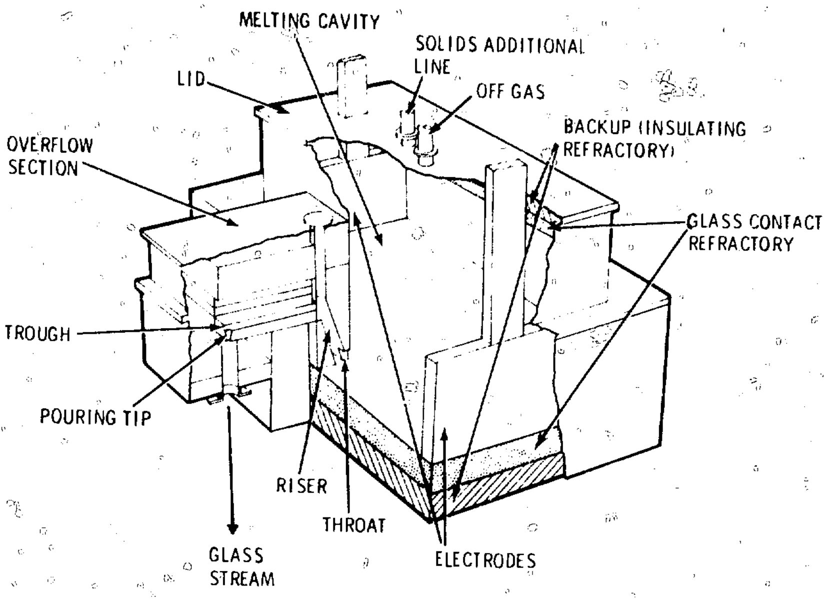
MELTING CAVITY
SOLIDS ADDITIONAL LINE
LID
OFF GAS
BACKUP (INSULATING REFRACTORY)
OVERFLOW SECTION
GLASS CONTACT REFRACTORY
TROUGH
POURING TIP
RISER
THROAT
GLASS STREAM
ELECTRODES

Fig. 1 Typical ceramic melter.

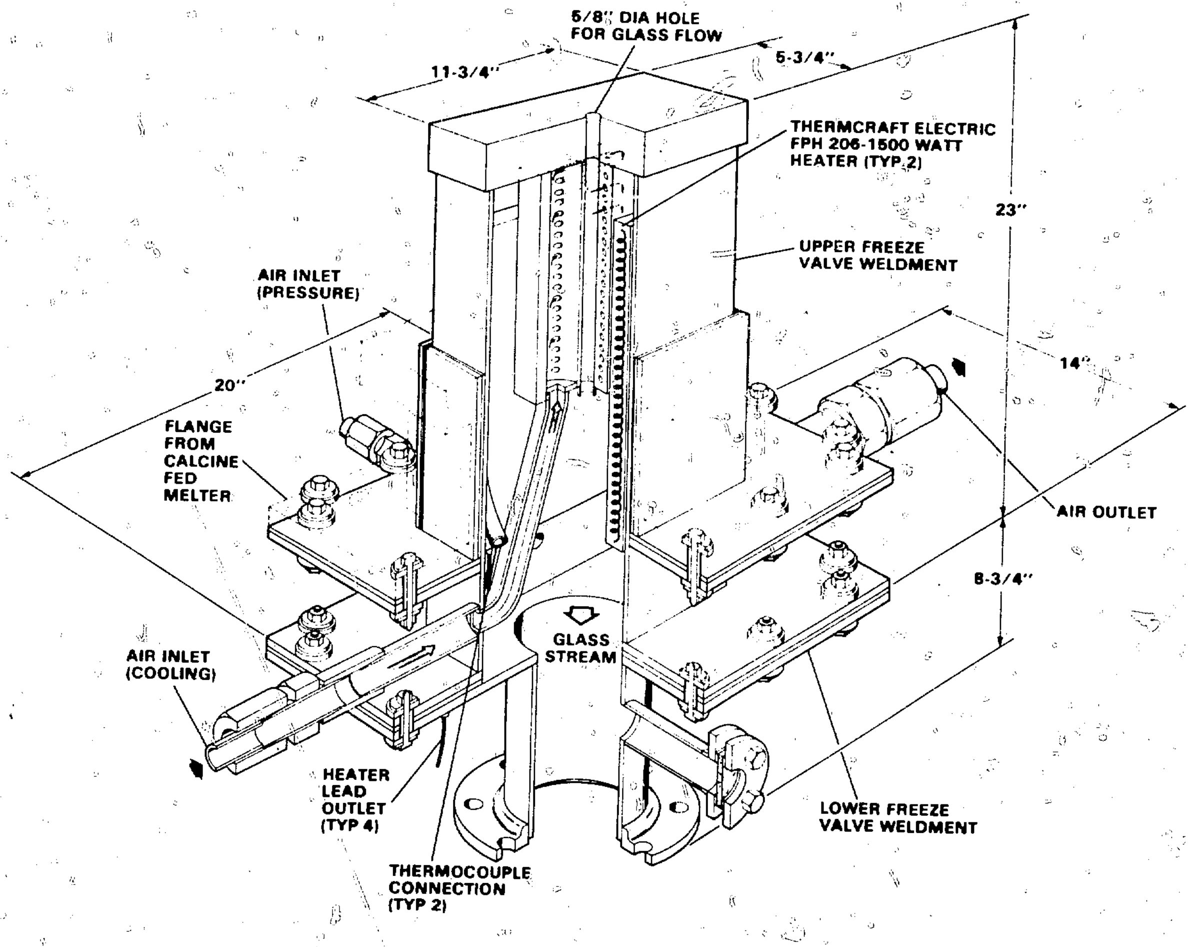
5/8" DIA HOLE FOR GLASS FLOW
11-3/4"
5-3/4"
THERMCRAFT ELECTRIC FPH 206-1500 WATT HEATER (TYP 2)
23"
UPPER FREEZE VALVE WELDMENT
AIR INLET (PRESSURE)
14"
20"
FLANGE FROM CALCINE FED MELTER
AIR OUTLET
8-3/4"
GLASS STREAM
AIR INLET (COOLING)
HEATER LEAD OUTLET (TYP 4)
LOWER FREEZE VALVE WELDMENT
THERMOCOUPLE CONNECTION (TYP 2)

Fig. 2 Ceramic melter bottom drain.

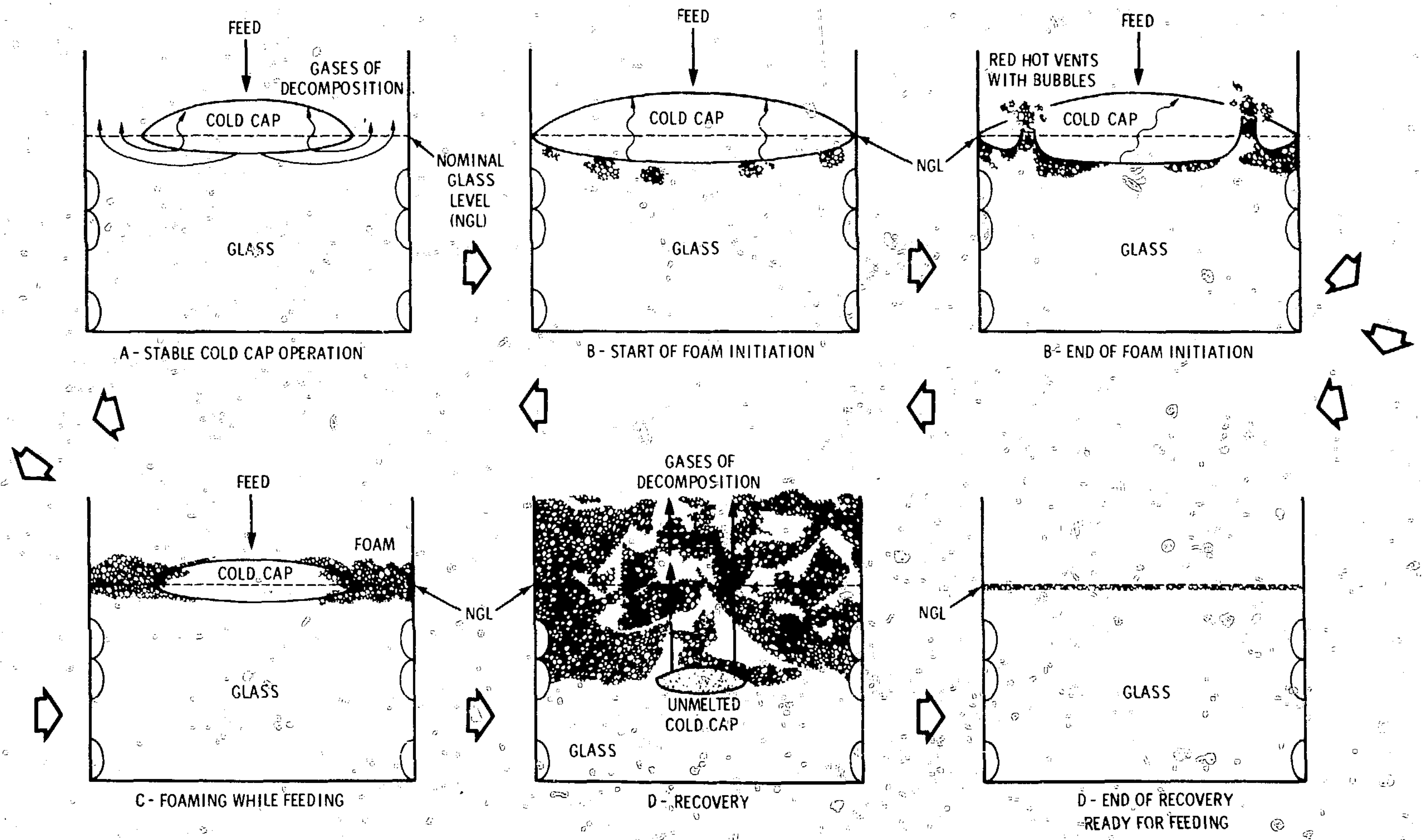
FEED
GASES OF DECOMPOSITION
COLD CAP
NOMINAL GLASS LEVEL (NGL)
GLASS
A - STABLE COLD CAP OPERATION
FEED
COLD CAP
NGL
GLASS
B - START OF FOAM INITIATION
FEED
RED HOT VENTS WITH BUBBLES
COLD CAP
GLASS
B - END OF FOAM INITIATION
FEED
FOAM
COLD CAP
NGL
GLASS
C - FOAMING WHILE FEEDING
GASES OF DECOMPOSITION
UNMELTED COLD CAP
GLASS
D - RECOVERY
NGL
GLASS
D - END OF RECOVERY READY FOR FEEDING

Fig. 3 Sequence of cold cap behavior during foaming.

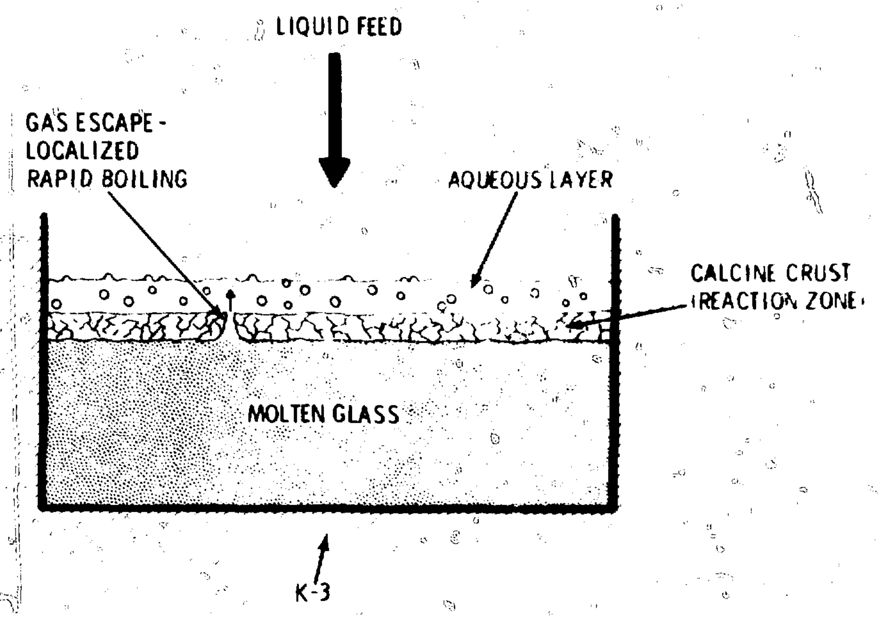
LIQUID FEED
GAS ESCAPE - LOCALIZED RAPID BOILING
AQUEOUS LAYER
CALCINE CRUST (REACTION ZONE)
MOLTEN GLASS
K-3

Fig. 4 Liquid feeding process.

trolled by stopping the feed and reducing power. It can be detected instrumentally through the use of thermocouples throughout the plenum and the glass tank.

A number of causes of foaming have been discovered. In one instance, a premelted frit of very low alkali content recrystallized during melting, at about the same temperature that the gases of decomposition were released. This caused foaming of the very viscous frit. This situation was reduced dramatically when unreacted chemicals were used in place of premelted frit.[5] Doing so increased the melting rate by at least a factor of three. For another waste type, glass former chemicals were used that produced large amounts of gases when melted. In this situation, the cold cap was stable until its edges reached the walls of the melter, blocking the vent path for the escaping gases, as shown in Fig. 3. When the chemicals were replaced with premelted frit which releases no gas when melted, the foaming situation was eliminated and nearly twice the feed rate was demonstrated. Foaming can also be caused by large amounts of sodium nitrate (>40%), which would make the cold cap electrically conductive. This work shows that foam can be prevented with the proper choice of glass and batch compositions.

OPERATING EXPERIENCE DURING LIQUID FEEDING

The engineering-scale melter demonstrated the use of directly feeding slurried waste materials mixed with the glass formers onto the molten glass surface. Heat from the glass transfers through a dried cold cap to the aqueous zone, where the water boils. The promising results experienced in the ESCM led to the construction of the full-scale liquid-fed ceramic melter, which has demonstrated the ability to handle high-level waste generated from the operation of more than 50 power reactors.

To date, the LFCM has vitrified 10,000 liters of liquid waste. Direct observation shows that gases of decomposition are released periodically through the penetrable crust between the glass and aqueous layers, as shown in Fig. 4. This usually exposes molten glass to the aqueous zone momentarily, thus causing some rapid localized boiling about 2 to 3 times the normal rate. The off-gas system must be designed to accommodate these surges and maintain a proper vacuum.

Experiments and demonstrations have been carried out on the merits of using premelted frits and unreacted chemicals for the glass formers. Generally, chemicals and acid soluble frits have proven to be advantageous in allowing a penetrable reaction layer for off-gas release. Premelted frits that are not soluble in the aqueous solution tend to form a viscous layer in the reaction zone. This makes the release of gases of decomposition much more difficult and creates much greater surges in off-gas flow.

IDLING EXPERIENCES

During operation of a vitrification plant, very often a melter will be put into an idling or nonglass-producing state because of process shutdown or melter maintenance. The melter would be kept in an idling state where the glass is held near operating temperatures to avoid restart of the melter. The hot glass surface temperatures require internal lid insulation to reduce heat losses and lid warpage. During the shift from idling to operating states, the temperature rise can cause a release of gases from within the glass.

[illegible] as "reboil." If the amount of gas being released from a [illegible] condition is sufficient, a glass foam can be created. Although the definite cause for reboil has yet been determined, we know that different glasses exhibit different potential for reboil at identical temperature rate increases. [illegible] development and control of temperature increases will prevent reboil. Reboil is an even [illegible] problem in liquid feeding. Foam generated [illegible] can cause instabilities in the liquid cold cap and [illegible] heat transfer to the [illegible] zone, resulting in high [illegible] rate. An off-gas system should be designed [illegible] liquid feeding.

CONCLUSIONS

Developmental work at PNL has provided [illegible] experience [illegible] melters [illegible] high-level [illegible] waste. [illegible] melters [illegible] and, above all, vitrification experience. Currently, work is directed toward higher temperature designs, completely remote operation, and more full-scale testing of calcine and liquid feeds.

REFERENCES

1. C. C. Chapman, *Experience with a Joule Heated Ceramic Melter While Converting Simulated High-Level Waste to Glass*, BNWL-2071, Pacific Northwest Laboratory, August 1976.
2. R. [illegible] DeDiemar, *The Performance of the Calcine Fed Ceramic Melter During Prolonged Normal Operating Conditions—Experiment CFCM-*[illegible], PNL-29[illegible], Pacific Northwest Laboratory, January 1979.
3. C. C. Chapman and J. L. Buelt, *Vitrification of High-Level Waste in a Joule Heated Ceramic Melter*, 70th Annual AIChE Meeting, New York, November 1977.
4. J. L. Buelt and C. C. Chapman, *Liquid Fed Ceramic Melter: A* [illegible] *Design for Reference*, PNL-27[illegible], Pacific Northwest Laboratory, October 1978.
5. C. C. Chapman and J. L. Buelt, *The* [illegible] *Continuous Melter* [illegible] *Radioactive Defense Waste*, Pacific Northwest Laboratory, submitted for publication in *Nucl. Tech.*, [illegible] August 1978.

PROGRESS IN FISSION PRODUCT SOLIDIFICATION AND CHARACTERIZATION UTILIZING THE JÜLICH FIPS PROCESS

S. HALASZOVICH, E. MERZ, and R. ODOJ
Institute for Chemical Technology, Kernforschungsanlage
Jülich, Federal Republic of Germany

ABSTRACT

The FIPS process for solidifying high-level fission product solutions [illegible] is briefly presented. Its main characteristics [illegible] process and product control are discussed. A newly developed [illegible] system of a thermobalance and a mass spectrometer is described. Possible effects of the results of the thermodynamic [illegible] on [illegible] and processing are discussed.

GENERAL LAYOUT

The FIPS process (*Fission Product Solidification*) is one of the processes for the solidification of highly radioactive fission product solutions which have been developed in the Federal Republic of Germany (FRG) during the last ten years. In principle, in all waste vitrification processes the waste is subjected to the same steps, i.e., evaporation, decomposition of nitrates, addition of glass-forming additives, drying, calcination and melting. Significantly in the FIPS process almost every one of these steps is carried out in a separate unit. Thus the steps are uncoupled to a great extent. This is in contrast with the present trend of development favoring a combined assembly consisting of a spray calciner and a Joule-heated ceramic melter or a liquid-fed ceramic melter.

The FIPS process consists of these steps, shown in Fig. 1:

- Preconcentration of the solution as far as required to adjust the concentration of nitric acid to about 5 mol per liter
- Denitration of the solution with formaldehyde and simultaneous concentration
- Addition and homogenization of the glass-forming additives
- Drying of the slurry using a drum dryer
- Melting of the dry product by rising level in-pot melting

Two promising advantages result from this method. First, each step is relatively simple and control of the product passing through each step ensures against substandard glasses. Second, volatility of fission products will be minimized.

PROCESS CONTROL AND QUALITY ASSURANCE

The licensing authorities are paying growing attention to the quality of the final product, i.e., quality control. The criteria for quality in the FRG have been defined to include leachability, macroscopic homogeneity, integrity, mechanical and thermal stability, and radiation resistance, but no quantitative limits have been established as yet.

Direct testing of the final product can be carried out immediately after processing to meet the first four criteria. For leachability, however, this would mean partially destroying the product blocks. Obviously it is absurd to treat a great number of blocks this way. If indirect methods of control turn out to yield unmistakable and reproducible results, the number of direct examinations could be reduced to a minimum. Such an indirect control can be performed by proving the quality of the product passing through the process step by step. It begins with the analysis of the feed in the storage tank. Then it includes examination of the intermediate product after each step and holding to the limits set for operating conditions. Such a

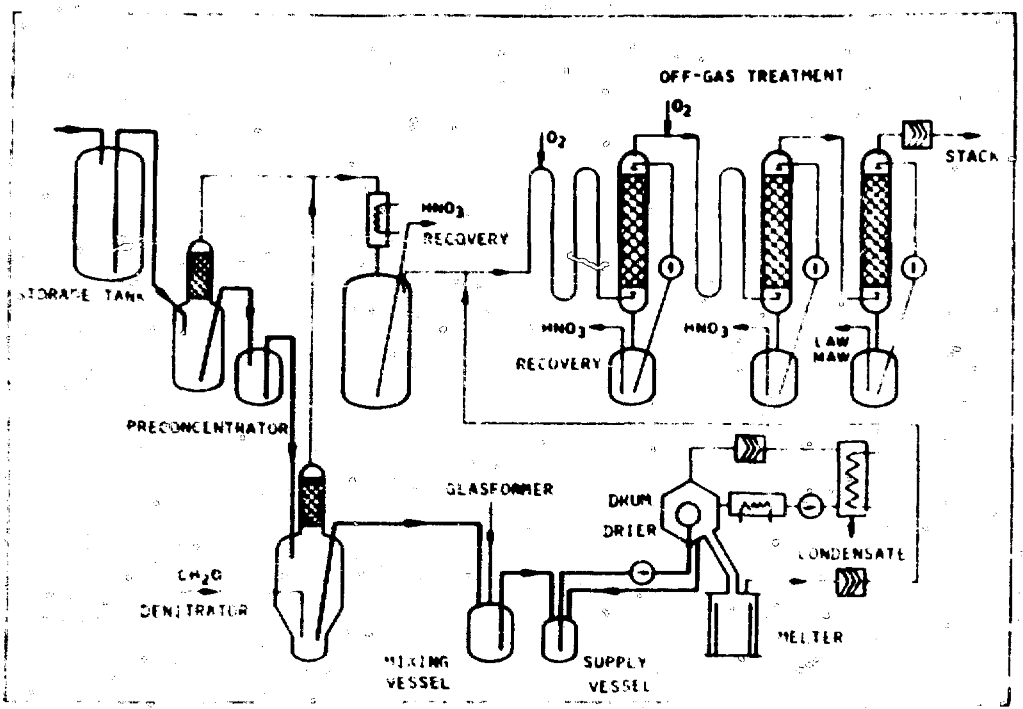

Fig. 1 Flow sheet of the FIPS process

procedure is efficient in a multistep process like the FIPS process, obviously it is far less efficient in pot-processes in which the whole solidification takes place in a single vessel.

Installation of the improved FIPS-II hot experimental facility is in progress and will be finished at the end of the year. Demonstration of the method of control outlined above will start then. To reduce the expense of hot analysis, cold experiments will be performed first to find out whether or not the detection of acid concentration, solids content, specific radioactivity, and organic content characterizes the feed sufficiently. In addition to temperature and pressure indicators, the denitration will be monitored by an infrared analyzer with constant wavelength to continuously measure the CO_2, NO and NO_2 contents in the off-gas. Due to the stoichiometry, these are the components generated during the reaction. Carbon dioxide content, for example, compares with the feed rate of formaldehyde, and the NO and NO_2 contents indicate the rate of reaction, the efficiency and the end of reaction as well.

Before adding the glass-forming additives, the residual nitrate, solids content and organic content in the denitrated concentrated solution will be determined and the viscosity of the solution will be measured. However, the organic content may turn out to be insignificant because only a small quantity is expected. For the succeeding step of drying, it is essential to know the solids content and the viscosity of the slurry. The solids content is known by material balance and by the factor of concentration. Viscosity is measured with a modified flow viscosimeter. Both influence the thickness of the layer on the drum and, therefore, the drying process, particle size of the dry product, and the residual moisture content in it.

In the course of drying and melting, temperature will be controlled to ensure permissible residual moisture content and optimal melting conditions. It is important to note that the glass-forming additives and the fission product solution will have already been well mixed before drying. By this means a well homogenized product is fed into the melter providing the proper precondition for a homogeneous melt.

Admittedly it is difficult to control the highly radioactive product after each step, and the effort should be limited to a minimum, but the procedures described above are a suggested alternative to direct quality control on the final product. It should be emphasized that high accuracy is not demanded concerning the measured data. It is sufficient to maintain the conditions within a certain range. No product whose properties are narrowly limited will be suitable for the incorporation of the multitude of fission products.

VOLATILITY OF FISSION PRODUCTS

In addition to the quality of the product, control of the volatility of the fission products during solidification is essential. Attention has particularly been paid to the volatility of ruthenium. Every process for the solidification of fission products developed in the FRG starts with a denitration step, or at least a reducing agent will be added before melting to suppress the volatility of ruthenium as

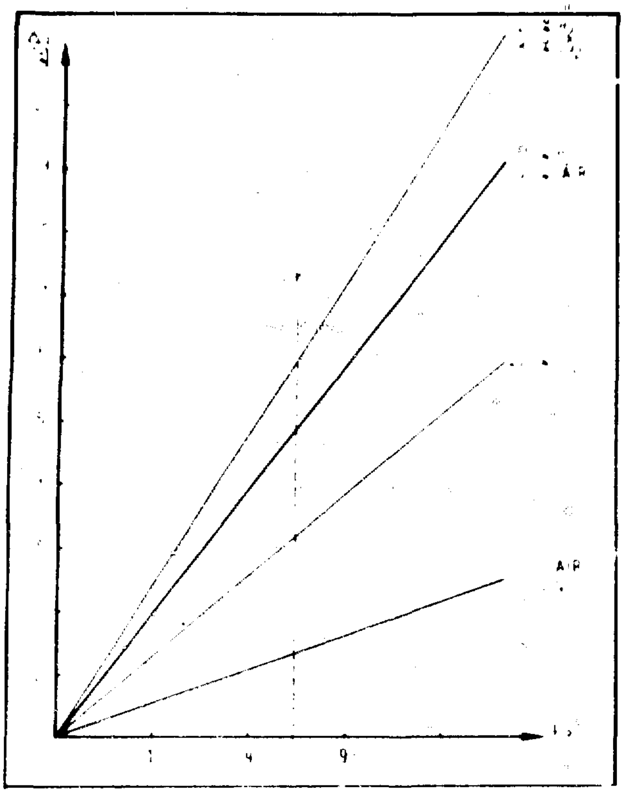

Fig. 2 Weight loss of a sodium boron silicate glass at 1100°C depending on the atmosphere

ruthenium tetroxide. Thermodynamic measurements indicate that the greatest success can be achieved by reducing the ruthenium compound to metallic ruthenium. Its vapor pressure at 1200°C, the usual melting temperature of glasses, amounts to 1×10^{-12} torr.[1] This value corresponds to the detection sensitivity of mass spectrometry. The volatility of ruthenium in this order of magnitude could be neglected.

In the first step of the FIPS process the fission product solution is boiled with formaldehyde to destroy the nitrate anion of the acid and the salts. Formaldehyde has been chosen out of a number of reducing agents because of technical considerations, i.e., to achieve easier process control. Cold laboratory experiments have been started to obtain detailed knowledge of the efficiency of different reducing agents and the efficiency of the denitration itself. Up to now nitric acid solutions of both individual and groups of fission products have been denitrated with formaldehyde. It appears that the nitrate anion of the acid can be completely destroyed, but not the nitrate anions of the alkaline and alkaline earth metals, using the present method of denitration in which the formaldehyde and the solution are fed simultaneously into the denitration vessel.

The volatility of the individual fission products during the melting procedure has not yet been investigated in detail. However, water is known to increase the volatility of the components of glass generally. For this reason, the slurry should be dried before feeding into the hot crucible. Drying is carried out at 150°C on a drum dryer. The temperature is comparatively low, the open surface of the product on the dryer is small, and there is no need for auxiliary propellent gases. Due to these facts hardly any volatility of fission products occurs in this step. During earlier hot experiments the decontamination factor was 10. The contamination of the condensate could be explained by discharge of fines; no selective volatility of any individual fission product was detected.

The separation of the low temperature step of drying from the melter is one of the main characteristics of the FIPS process. In contrast to several other processes with direct liquid feed into the melter a dry product is fed into the preheated crucible. This kind of operation has a fundamental influence on the volatility of fission products in this step. The melting temperature of present glasses ranges from 1100 to 1200°C. The high temperatures result in an increasing vapor pressure of the compounds. The influence of the atmosphere in the melter, particularly its water content, has been demonstrated with a basic glass consisting of 70% SiO_2, 15% B_2O_3, and 15% Na_2O at 1100°C (Fig. 2). Compared with a dry atmosphere, the weight loss increases by 400% after 1 h of melting if there is 50% water vapor in the atmosphere.[2] The investigations of this glass show that the weight loss depends on the square root of time spent in the melter. The volatility is obviously dependent on diffusion. In case of longer holdup in the melter this might result in inhomogeneity of the melt. Further investigations show that there is a linear dependence between the square root of the partial pressure of water and evaporation from alkali silicate glasses. Hold,[3] investigating compounds of Na_2O and SiO_2, found a direct dependence between partial pressure of water and volatility. Decreasing the particle size of the glass frit being fed resulted in increasing volatility, indicating the influence of adsorbed water. Dry CO_2 atmosphere increases the volatility by 250%, while there is no difference evident between melting in dry air and dry N_2 atmosphere. A similar effect of atmosphere on volatility can be expected for fission products as has been observed for the compounds of glasses.

EXPERIMENTAL SETUP FOR VOLATILITY MEASUREMENT

In order to determine the volatility of the fission products from the different phases in a more realistic way (not in high vacua and in different atmospheres), a new attachment is under development (Fig. 3). The layout of the equipment consists of a simultaneous thermoanalysis (TG and DTA) coupled with a mass spectrometer. Melting can be simulated exactly in the furnace of the balance. Physical and chemical transformations are detected by thermal gravimetry and by differential thermal analysis, respectively, while volatile species are identified with the

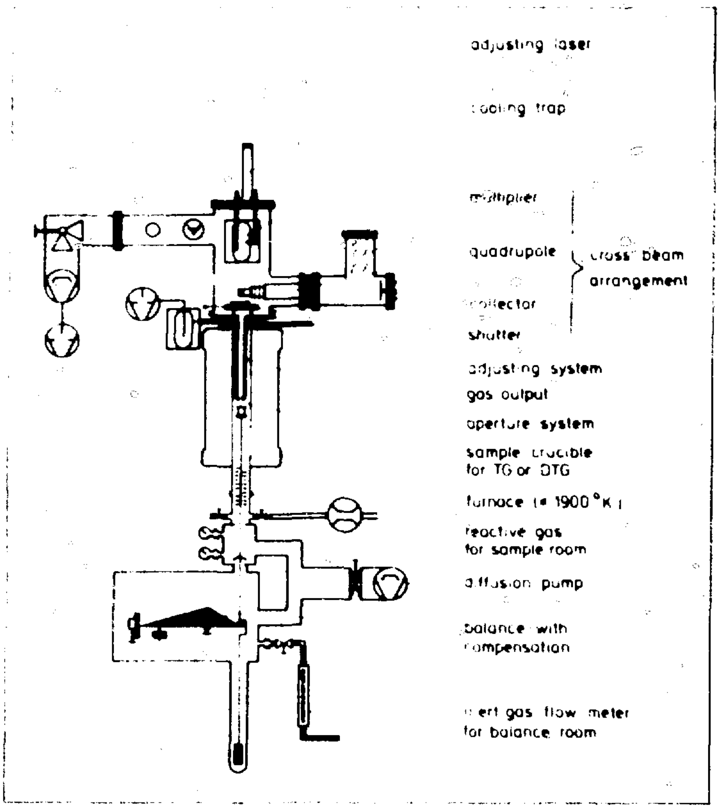
adjusting laser
cooling trap
multiplier
quadrupole
cross beam arrangement
collector
shutter
adjusting system
gas output
aperture system
sample crucible for TG or DTG
furnace (≈ 1900 °K)
reactive gas for sample room
diffusion pump
balance with compensation
inert gas flow meter for balance room

Fig. 3 High temperature coupling system for TG - DTA - MS apparatus.

mass spectrometer. The pressure range to be bridged extends from normal pressure in the sample container of the thermal balance to 10 [illegible] torr inside the mass spectrometer. As the metals or their gaseous components are condensable, the pressure reducing system has to be maintained at the temperature of the sample. Conventional components like capillary tubes are unsuitable due to the high temperature required. Platinum has to be excluded because of its catalytic effect at high temperature. A heated orifice system is under development. The pressure of one atmosphere in the sample room is reduced to high vacua in the mass spectrometer by differential pumping, so that the gaseous fission product molecules are directed by a molecular beam towards the electron impact ion source. It is intended to achieve detailed information on the volatility of the fission products during the solidification process with this equipment.

REFERENCES

1. J. L. Margrave, *Characterization of High Temperature Vapors*, John Wiley & Sons, Inc., London, New York, and Sydney, 1967.
2. K. P. Hanke and H. Scholze, *Glastechnische Berichte*, Vol. 50 (1977).
3. M. Hola, J. Matušek, and J. Hlaváč, *Silikaty*, Vol. 18 (1974).

A LABORATORY-SCALE GLASS MELTER FOR TESTING DEFENSE WASTE GLASS

D. GOMBERT II
Allied Chemical Corporation, Idaho Falls, Idaho

ABSTRACT

A one-liter Joule-heated glass melter was built to test the applicability of continuous melting to simulated high-level calcined defense waste. Inconel 690 electrodes and K-3 refractory brick were chosen for their corrosion resistance to fluoride glass. The melter maintained a full melt at 1100°C using 3 kW. After approximately two months of operation the melter was dismantled for metallurgical examination. The Inconel 690 electrodes were heavily corroded. A second melter is now in operation to verify the findings of the first melter run.

INTRODUCTION

The Idaho Chemical Processing Plant (ICPP) located at the Idaho National Engineering Laboratory (INEL) reprocesses defense-type nuclear fuel using a solvent extraction process.[1] The resulting high-level waste solution is calcined (dried) in a fluidized-bed process into a mixture of granules and powder known as calcine.[2] Zirconia calcine, which is about 50 wt.% CaF_2, was the type used in the glass melting work presented in this paper. Calcine is currently stored on site;[3] however, regulatory and environmental considerations may require an alternate form for disposal of high-level waste. One alternative being evaluated is a leach-resistant glass containing 25 to 40 wt.% calcine.[4] To test the applicability of continuous melting to the zirconia calcine, a laboratory-scale (1 liter) Joule-heated melter was built to vitrify calcine at 1100°C. The materials of construction, K-3 fused cast refractory and Inconel 690 electrodes, were chosen on the basis of 10-day static corrosion tests in a molten glass environment. These tests were designed to single out the materials most resistant to fluoride corrosion since this will be the most demanding requirement on the melter. The melter was operated at 1100°C for about two months, after which it was dismantled for materials examination. A second modified melter is now in operation to verify findings from the first melter.

CORROSION TESTS—MATERIALS SELECTION

The major concern with melter lifetime is high temperature fluoride attack on the refractory and electrode materials as the zirconia calcine is approximately 50 wt.% CaF_2. To test prospective melter fabrication materials, 10-day corrosion dip tests were done in a glass (No. 13) containing 33 wt.% simulated zirconia calcine, 34.5 wt.% SiO_2, 18.9 wt.% Na_2O, 8.6 wt.% B_2O_3, 1.4 wt.% Li_2O, 1.9 wt.% CaO, and 1.4 wt.% ZnO. Refractories were cut into samples measuring 2.5 x 2.5 x 7.6 cm, and electrode materials were cut into 0.64 x 2.5 x 7.6 cm samples. These samples were then immersed about halfway in the glass to provide corrosion information on the sample in the glass phase, in the gaseous phase above the glass, and at the phase interface. The melt temperature was maintained at about 1100°C. Twice each day, 20 grams of powdered batch materials were added to each sample to maintain a realistic environment both in the molten glass and in the gaseous phase in the furnace.

Candidate electrode material compositions and 10-day corrosion data are shown in Tables 1 and 2. As can be seen from the data, Inconel 601 and 690 were the most corrosion-resistant materials with weight losses lower than 5 wt.%. Metallurgical examination[4] of these two alloys showed that even though Inconel 601 experienced less weight loss and corrosive penetration than the 690, it is less

TABLE 1

Electrode Materials Composition in Wt.%

Element	Inconels 601	Inconels 617	Inconels 625	Inconels 690	Hastelloy C-4	Nitronic 50
Ni	60.3	54	61	60	58.3 to 65.3	11.5 to 13.5
Cr	23	22	21.5	30	14 to 18	10.5 to 23.5
Fe	14.1		2.5	9.5	3	52.4 to 61.3
Mo		9	9		14.0 to 17.0	1.5 to 3.0
Ta			3.65			
Al	1.35	1			1.0	4 to 6
Mn					2.0	0.1 to 0.3
Co		12.5				0.1 to 0.3
V						1.0
Si				0.03		
C					0.70	

TABLE 2

Electrode Corrosion Results

Material	Wt.% loss	Penetration, mm	
		Vapor phase	Glass phase
Inconel 601*	4.0	0.48	0.40
Inconel 617	18.0		
Inconel 625	54.0		
Inconel 690	4.3	0.70	0.45
Nitronic 50	34.0		
Hastelloy C-4	Destroyed		

*Showed extensive crystal growth.

desirable as an electrode material due to severe grain growth. Both the 601 and 690 showed similar attack in the gas phase, but in the glass phase the 601 showed substantially more grain growth. The major corrosion mode on both alloys was intergranular attack with varying amounts of internal precipitation.

Of the seven refractories tested, two (both high chrome types) showed no significant weight losses, rather a slight weight gain due to a thin glass coating. As can be seen in Tables 3 and 4, the five AZS (alumina–zirconia–silica) types (S-3, S-4, S-5, A, M), all high in Al_2O_3 and/or SiO_2, showed about 3 to 5 wt.% loss. The two high chrome types (K-3, E) both appear satisfactory. Therefore, on the basis of lower cost and higher electrical resistivity (to minimize current flow through the refractory) the K-3 was chosen over the E refractory.

MELTER FABRICATION AND OPERATION

The melter ceramics were bonded with a high chrome (17.59% Cr_2O_3) grout. The ceramic unit (0.2 x 0.3 x 0.46 m) was nested in silica insulation 10 cm thick contained in a 304L stainless steel box. Overall dimensions, feed system, tilting jack, and materials of construction are shown in Fig. 1. For start-up the feed chamber was filled with bits of glass and heated with a 600-watt resistance element until the glass became conductive enough for the electrodes, half submerged in the glass, to pass current (~600°C). Once the melt could be maintained with Joule heating alone, the resistance element was moved to the pour spout to keep the pour molten. A 316 stainless steel hood was then placed over the feed cavity to reduce heat losses and to contain off-gases to be collected for analysis.

The batch feed was augered through a downspout and fell directly into the melt. As the glass level rose, hydraulic pressure through the tunnel to the fining chamber raised the level there as well. The glass could be poured by tilting the melter with a hydraulic jack and allowing the melt to overflow through an Inconel 690 pour spout and into a 400-ml stainless steel beaker. Batch materials were added to the melt in large quantities (as much as 500-gram charges) with no foaming difficulties or loss of electrical conduction. At 1100°C the feed chamber used about 1.5 to 2.5 kW, while the fining chamber used about 0.8 to 1.2 kW. Samples of the glass poured by the melter were low viscosity, homogeneous, and opaque. The 400-ml cylindrical blocks were cut into pieces which showed very little porosity or color striation whether poured over a period of several hours or as little as 10 minutes.

RESULTS

After two months of operation the melter was shut down due to the deterioration of one of the feed chamber electrodes. The left electrode in the feed chamber had overheated and melted into the glass melt. It was found later as a solidified mass at the bottom of the chamber. The right-side electrodes from both the feed and fining chambers were examined and metallographic sections were taken above and below the glass level. The corrosive attack on the electrodes was much more severe than that indicated

TABLE 3

Refractory Compositions in Wt.%

Compound	Refractory type, wt.% A	K-3	E	M	S-3	S-4	S-5
Al_2O_3	98.70	60.40	4.7	94.50	50.13	49.69	47.32
Cr_2O_3		27.36	79.7				
Fe_2O_3	0.09	4.21	6.1	0.08	0.12	0.10	0.11
MgO		6.05	8.1	0.15			
Na_2O	0.03	0.31		3.90	1.10	1.10	0.84
ZrO_2					34.20	36.56	40.97
SiO_2	0.50	1.77	1.3	1.09	14.25	12.30	10.61
CaO				0.26			
B_2O_3	0.50				0.15	0.15	0.15
TiO_2				0.02	0.05	0.10	
Other	0.18		0.1				

TABLE 4

Refractory Corrosion Results

Refractory, wt.% loss						
K-3	E	S-5	S-3	S-4	A	M
0.0	0.0	3.4	3.7	4.5	4.9	5.1

by the 10-day tests. Both electrodes suffered precipitation throughout their cross sections. The attack also included spalling of corrosion product layers and much grain growth. Researchers at Savannah River Laboratories have also seen the same symptoms. In that case, an unbalanced SCR in the controlling electronics imposed a dc current which caused electrolysis to occur. The literature, our experiments, and data from outside sources indicate that there is probably no better metallic material than Inconel 690 available for use as an electrode. The use of graphite or molybdenum is not desirable since both materials would serve only as consumable electrodes which could be difficult to use in a remote process.

LABORATORY-SCALE MELTER II

A second laboratory-scale melter is now in operation to verify whether the findings in the first melter were technical difficulties in using this melting method for high-fluoride calcine or just operating errors. The second melter uses only one electrode circuit. The fining and feed chamber electrodes are connected electrically in parallel. This change eliminates the possibility of shorting to a ground electrode in the conductive glass melt. Also, the refractory pieces were cut more carefully to reduce the joint thickness between them and thereby lessen the possibility of glass leakage out of the chambers. During operation the current density on the electrodes will be maintained below 0.6 A/cm^2 since above this level rapid deterioration of the electrodes has been observed.

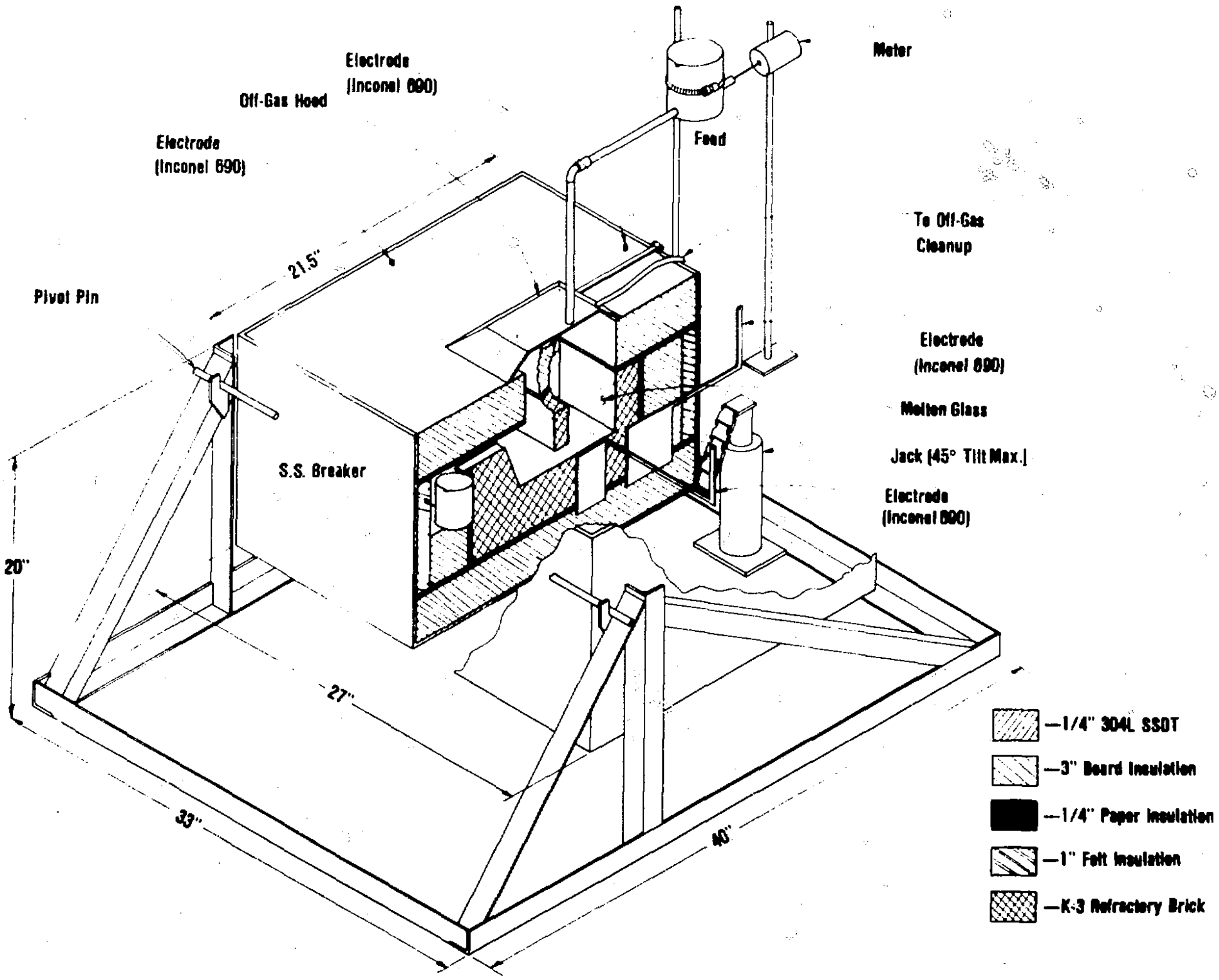
Electrode (Inconel 690)
Off-Gas Hood
Electrode (Inconel 690)
Meter
Feed
To Off-Gas Cleanup
Pivot Pin
21.5"
Electrode (Inconel 690)
Molten Glass
Jack (45° Tilt Max.)
S.S. Breaker
Electrode (Inconel 690)
20"
27"
33"
40"
—1/4" 304L SSOT
—3" Board Insulation
—1/4" Paper Insulation
—1" Felt Insulation
—K-3 Refractory Brick

Fig. 1 ICPP one-liter Joule-heated ceramic-lined glass melter.

The second melter is started in exactly the same way as the first melter. Glass No. 51 containing 21 wt.% simulated zirconia calcine, 52 wt.% SiO_2, 19 wt.% Na_2O, 6.3 wt.% B_2O_3, and 1.7 wt.% CuO was used as the initial melter charge. The experimental plan calls for melting glass containing 21 wt.% calcine for three weeks and then momentarily shutting down to replace one of the feed chamber electrodes. The used electrode can then be examined for corrosion. The following three-week period will be run with glass containing 27 wt.% calcine, and the last three-week period with glass containing 33 wt.% calcine. With an estimate of corrosion rate from each run, information will be gained on the rate of deterioration versus calcine loading in the glass. This data will provide an idea of what to expect using a continuous Joule-heated glass melter to melt zirconia-type calcine.

CONCLUSION

The first laboratory-scale melter was built based on short-term corrosion tests, literature, and private communications. After two months of operation, examination of the refractories and electrode materials indicated that while the K-3 ceramics fared very well, the Inconel 690 electrodes were severely corroded. To verify these findings, a new melter of similar design, with slight variations to correct problems noted with the first melter, was built. Tests are now being run to gain insight on how the deterioration rate of the electrodes is affected by calcine content and therefore fluoride concentration in the glass at 1100°C.

ACKNOWLEDGMENT

This work was done under the auspices of the United States Department of Energy contract DE-AM07-76IDO1540.

REFERENCES

1. C. M. Slansky, Radioactive Waste Management, *CHEMTECH*, p. 160, March 1964.
2. R. E. Commander et al., *Operation of the Waste Calcining Facility with Highly Radioactive Aqueous Waste, Report of the First Processing Campaign*, IDO-14662, Idaho Chemical Processing Plant, Idaho Falls, June 1966.
3. G. E. Lohse, *Safety Analysis Report for the ICPP High-Level Solids Radioactive Waste Storage Facility*, ICP-1005, Idaho Chemical Processing Plant, Idaho Falls, January 1972.
4. D. Gombert et al., *Vitrification of High-Level ICPP Calcined Wastes*, ICP-1177, Idaho Chemical Processing Plant, Idaho Falls, February 1979.

THE INFLUENCE OF HEAT TRANSFER ON THE POT VITRIFICATION PROCESS

J. B. MORRIS
Chemical Technology Division, AERE, Harwell, Oxon, United Kingdom

ABSTRACT

The experimental data on the working zone in pot vitrification show that the mean wall heat flux (2 W/cm^2) is independent of vessel size. A simple model of the heat transfer processes is developed in which natural convection through the glass-forming region is the controlling mechanism.

INTRODUCTION

When converting high-level waste into a monolithic block of glass cast in a stainless steel container, four processing steps must be accomplished:

1. Evaporation of water and nitric acid.
2. Calcination of solid nitrates to waste oxides.
3. Reaction between waste oxides and added chemicals to yield glass.
4. Casting of molten glass into the container.

The HARVEST vitrification route being developed in the U. K., which is a derivative of the earlier FINGAL process,[1] is unique in that all four steps are carried out as a single stage in a pot which eventually becomes the final container. The high-level waste is premixed with an aqueous solution/slurry of alkali nitrates, boric acid, and silica. The combined mixture is then fed into a vitrification pot mounted in a furnace at about 1000°C. The feed typically will have a concentration of 300 g/l and will consist of a mixture of one volume of high-level waste with 1⅔ volume of glass additive slurry.

Steps 1, 2, and 3 (evaporation, calcination, and glass formation) absorb thermal energy, and they take place in a working (or reaction) zone. Aqueous feed at room temperature enters the top of the working zone, and glass at about 1000°C appears at the bottom to occupy the base of the pot as step 4. Gases are liberated in the working zone (mainly steam and nitrous gases NO_x), and they emerge from the top at a temperature of 125°C or higher. The mean density of oxides in the working zone ρ_Z is less than the density of glass ρ_G, so the working zone occupies more space than the corresponding amount of glass. This is illustrated in Fig. 1 which shows the formation of a steady-state working zone. The size of the working zone must be kept under control in order to maintain an adequate freeboard in the top of the pot. The purpose of this paper is to review experimental data on the working zone and to discuss the importance of heat transfer in this context.

NATURE AND THERMAL REQUIREMENTS OF THE WORKING ZONE

Although the structure of the working zone is undoubtedly complex, it may be thought of as consisting of three subzones in which evaporation, calcination and glass formation take place as depicted in Fig. 2. Because of the many different chemical species present in high-level waste the actual boundaries between these subzones will necessarily be somewhat indistinct. Evaporation occurs in the central subzone which is at a uniform temperature of $T_1 = 125°C$; nucleate boiling ensures good heat transfer within this region. The second subzone surrounds this aqueous pool and is assumed to be a solid phase up to an isotherm T_2. Calcination occurs which for MAGNOX waste premixed with glass chemicals is complete at about 550°C (Ref. 2). The third subzone is a viscous fluid region through which gases are observed to flow. With the compositions currently

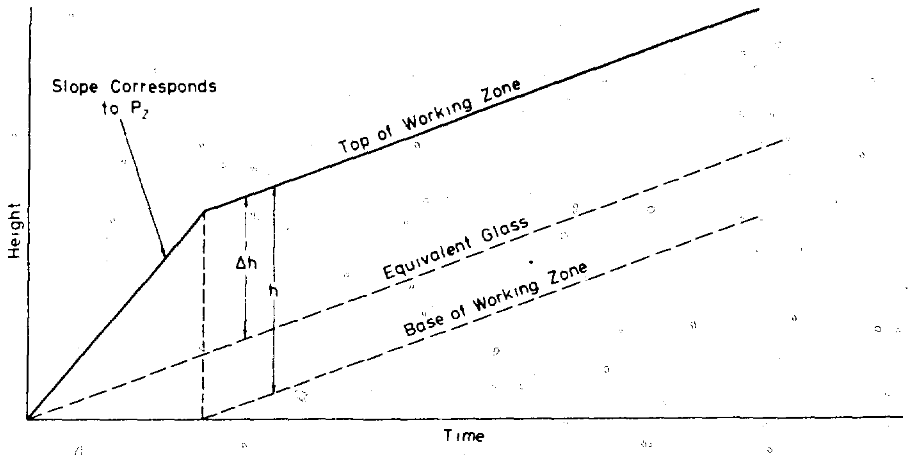

Fig. 1 Development of the working zone in pot vitrification.

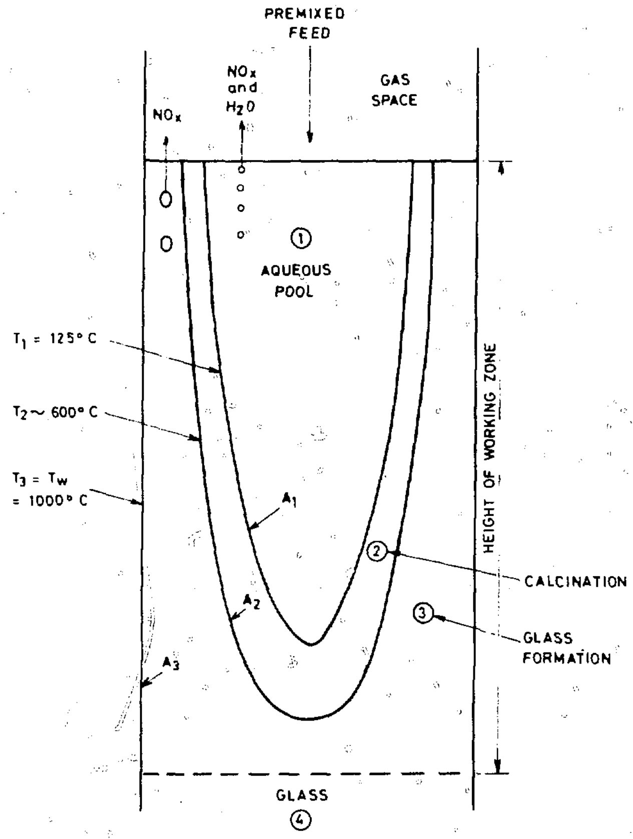

Fig. 2 Structure of the working zone.

being studied for HARVEST, glass formation is complete at 900 to 1000°C. Davis,[3] in an earlier study of the thermal aspects of the FINGAL process, showed that the structure of the working zone described above was confirmed in practice for vitrification in a 15 cm diameter pot. In the current inactive pilot plant program at Harwell using 45- and 60-cm diameter vessels, the presence of the three subzones can be seen at the exposed top surface.

Heat can be supplied to the working zone by three routes: (1) Radiation from the heated upper walls of the vessel to the top surface of the working zone, (2) Transfer from the walls of the pot in direct contact with the working zone, and (3) Transfer by convection through the molten glass beneath the working zone. According to Davis[3] the available evidence showed that route (1) contributed very little, probably because much of the aqueous pool is covered by a solid crust which serves as a thermal barrier. Heat transfer by route (2) will of course occur, and the extent to which route (3) contributes is considered later. The heat consumed by the working zone is shown in Table 1 computed in terms of the energy needed per unit

TABLE 1

Thermal Energy Requirements in HARVEST Vitrification per Unit Volume of Feed for a Concentration of 300 g (Oxides) per Liter

Subzone	Heat item	J/ml	% of total
Aqueous pool	Sensible heat 20 to 125°C	440	
	Latent heat of evaporation H_2O	1760	
	Decomposition of HNO_3 to NO_x	70	
	Total subzone 1 E_1 =	2270	65
Calcine	Decomposition of nitrates to NO_x (waste)	230	
	Decomposition of nitrates to NO_x (glass additives)	600	
	Sensible heat 125 to 700°C	250	
	Total subzone 2 E_2 =	1080	31
Glass formation	Sensible heat 700 to 1000°C	130	
	Total subzone 3 E_3 =	130	4
Total working zone	(1 + 2 + 3) E =	3480	100
Gas space	Sensible heat 125 to 1000°C	1950	

volume of feed (J/ml). The data are broken down into the requirements of the three subzones on the basis that all the H_2O and the excess nitric acid (0.6*M*) is evaporated in subzone 1, that all the solid nitrates (waste and alkali glass additives) are decomposed in subzone 2, and that no significant heat (other than sensible heat) is absorbed in glass formation in subzone 3 as suggested by Davis.[3] The calculations refer to a feed concentration of 300 g (oxides) per liter, but the total heat load E (J/ml) does not in fact vary much with feed concentration. An entry for sensible heat absorbed by the gas to 1000°C is also included in the table for comparison, but this will be ignored in computing the heat load on the working zone since most of any superheat will be added to the gases once they have left the working zone.

The thermal requirement $E = 3480$ J/ml is equivalent to 11,600 J per g of glass made. If the glass-making chemicals are added, not as a slurry but as anhydrous oxides (e.g., glass frit), the energy required is reduced by about 50% to only 5,200 J per g of glass made.

SIZE OF THE WORKING ZONE

In this section we review the experimental information on the size of the working zone from which an estimate of the available heat transfer area can be made.

The height of the working zone h is defined by:

$$h = \frac{\Delta h}{1 - \rho_Z/\rho_G} = \epsilon\, \Delta h \qquad (1)$$

where ρ_Z is the mean oxide density in the working zone, ρ_G is the glass density, and Δh is the observed excess height in the pot, i.e., the amount by which the total of depth material exceeds the equivalent height of glass. Before any glass has formed, ρ_Z can be deduced from the initial slope of the curve in Fig. 1, and under HARVEST conditions it is about 0.8 g/cm^3. ρ_G is 2.6 g/cm^3 and so ϵ is 1.44. Elliot and Grover[4] in their pilot plant studies in 10- to 30-cm diameter vessels called Δh the height of the working zone, but the definition of Eq. 1 is preferred since it equates h logically with the height of material not yet converted into glass.

Many of Elliot and Grover's experiments[4] were carried out at an optimum volumetric feed rate Q^* which correlated with vessel diameter D by the empirical equation:

$$Q^* = \delta D^2 \qquad (2)$$

(The optimum feed rate was the maximum which could be used without experiencing unstable conditions.) For a feed concentration of $C = 300$ g/l the parameter δ was equal to 4×10^{-3} cm/s. Examination of the results presented in Ref. 4 shows that at the optimum feed rate the excess height Δh^* is proportional to vessel diameter

$$\Delta H^* = \gamma D \qquad (3)$$

The empirical constant γ is 1.5.

It then follows from Eqs. 1, 2 and 3 that the corresponding heat transfer area A^* enclosing the working zone is given by

$$A^* = \pi D h^* = \pi \frac{\gamma\epsilon}{\delta} Q^* \qquad (4)$$

Since the volumetric feed rate determines the heat load on the working zone, Eq. 4 shows that the mean wall heat flux at the optimum feed rate is constant, independent of vessel diameter. This seems such a fundamental result that it suggests the same heat flux operates at other feed rates. Hence we generalize Eq. 4 thus

$$h = \frac{\gamma\epsilon}{\delta} \frac{Q}{D} \qquad (5)$$

At a feed concentration of 300 g/l the term $\gamma\epsilon/\delta$ has the value of 540 s/cm. Similarly the excess height Δh is given by

$$\Delta h = \frac{\gamma}{\delta} \frac{Q}{D} \qquad (6)$$

where the term γ/δ has the value 375 s/cm. Grover and Elliot[4] report an experiment in a 30-cm vessel in which the excess height Δh decreased by about 50% when the feed rate Q was reduced by the same amount, which is consistent with the generalization set out above.

From Eq. 5 the constant mean heat flux ϕ_W into the working zone through the vessel wall is given by

$$\phi_W = \frac{QE}{\pi D h} = \frac{1}{\pi} \frac{\delta}{\gamma\epsilon} E \qquad (7)$$

Substituting the relevant data for a feed concentration of 300 g/l gives $\phi_W = 2.0$ W/cm^2. It now remains to develop a heat transfer model which predicts this order of heat flux for any vessel diameter.

HEAT TRANSFER MODEL

An accurate model of the type of structure shown in Fig. 2 can be achieved only by numerical methods. However, since some of the physical parameters of the system are not precisely known (e.g., thermal conductivity and viscosity), this paper restricts itself to a simple analytical approach.

We cannot therefore expect such a model to agree exactly with the observed results, but if the agreement is *reasonably close*, we can feel confident that the basic principles are correct. More exact modelling can be performed as better data become available.

Returning to Fig. 2 it will be seen that heat is transmitted across the three subzones in series with each subzone also acting as a heat sink. The outer boundary of subzone 3 is the vessel wall at temperature T_3 and its area is

$$A_3 = \pi Dh \tag{9}$$

The outer boundary of subzone 2 is at temperature T_2. Its area A_2 is expected to be less than A_3. The work of Elliot and Grover[4] shows that the volume of the aqueous subzone 1 is approximately equal to a cone of height Δh and base D. Since the area A_2 encloses not only this aqueous phase but also the calcine phase, it is clear that A_2 cannot be smaller than about $A_3/2$ and may in fact be even closer to A_3. We therefore make the simplifying assumption that $A_2 = A_3$. We also assume that the thickness of the calcine subzone is small relative to its radius. Thus, in effect, we have reduced the heat transfer to a simple one-dimensional problem. Ignoring the cylindrical geometry in subzones 2 and 3 is not crucial, and since the boiling action ensures efficient heat transfer in subzone 1, its geometry is not relevant.

Thus significant heat transfer resistance is confined to subzones 3 and 2. For each subzone we set down its heat balance and the mechanism describing heat transfer as a function of temperature. The heat balances are:

$$\phi_3 = \frac{Q}{A}(E_1 + E_2 + E_3) \tag{10}$$

$$\phi_2 = \frac{Q}{A}(E_1 + E_2) \tag{11}$$

where ϕ_3 and ϕ_2 are the heat fluxes entering subzones 3 and 2, respectively.

Heat transfer in subzone 2 is by thermal conduction. This region is in motion since fresh material is entering through A_1 while calcined material leaves through A_2. However, for typical FINGAL conditions this velocity is negligible, and assuming that the heat load E_2 is absorbed uniformly throughout the region, the conduction equation is

$$\phi_2 - \frac{1}{2}\frac{Q}{A}E_2 = k_2\,\frac{T_2 - T_1}{L_2} \tag{12}$$

where L_2 and k_2 are the thickness and conductivity of the calcining subzone. Subzone 3 is a viscous fluid and so heat transfer is assumed to be by natural convection. Hence the mean flux through this region is controlled by convection.

$$(\phi_3 + \phi_2)/2 = \phi_c \tag{13}$$

where ϕ_c is the natural convection flux determined by the particular geometry, fluid properties, and temperatures of this subzone.

Eliminating ϕ_2 and ϕ_3 between the previous four equations leads to

$$\frac{Q}{A} = \frac{\phi_c}{E_1 + E_2 + E_3/2} \tag{14}$$

and

$$L_2 = \frac{k_2\,(T_2 - T_1)}{\phi_c}\,\frac{E_1 + E_2 + E_3/2}{E_1 + E_2/2} \tag{15}$$

Experimentally it is observed that $Q/A = \delta/\pi\gamma\epsilon = 5.9 \times 10^{-4}$ cm/s (Eq. 5), and so a test of the model is how close Eq. 14 predicts this value. Alternatively, virtually the same test is performed by comparing the calculated convective flux ϕ_c with the observed mean flux $\phi_w = 2.0$ W/cm^2 (Eq. 7).

TEST OF THE HEAT TRANSFER MODEL

Natural convection between solid surfaces and fluids is correlated by expressions of the type

$$\nu = B\,Ra^m \tag{16}$$

where $\nu = \phi x/k\theta$ and $Ra = \theta x^3 \rho^2 \beta g C/k\mu$.

Here ϕ = heat flux
x = length of surface
k = fluid thermal conductivity
θ = temperature difference
ρ = fluid density
β = fluid volume expansion coefficient
g = acceleration due to gravity
C = fluid specific heat
μ = fluid viscosity

For values of Ra lying between 10^4 and 10^9, the range appropriate in the present context, $B = 0.59$ and $m = 0.25$ for vertical surfaces, see Jakob.[5]

We have no experimental data for the physical properties of the fluxing mixture in subzone 3. The data appropriate to a typical HARVEST glass[6] are therefore used in the calculations. The chief uncertainty so introduced will be in viscosity μ which, although it appears only to the 0.25 power, is very sensitive to temperature. Gases (probably NO_x) rise through this subzone and so the effective viscosity may well be less than the corresponding glass value. Other properties may be modified for the same reason. The length x is taken arbitrarily as 100 cm, but ϕ is fairly insensitive to the actual value.

The convective heat transfer flux ϕ_c through subzone 3 is then calculated by treating the natural convection as two thermal resistances in series (hot surface A_3 to fluid, and fluid to cool surface A_2). The results are shown in Fig. 3 which shows ϕ_c as a function of T_3 for 3 values of T_2. For a typical wall temperature of T_3 = 1000°C the convective heat transfer flux is about 1.0 W/cm^2, the result being fairly insensitive to the temperature of the boundary of subzone 2. This is within a factor 2 of the observed flux $\phi_w = 2.0$ W/cm^2. In view of the simplifying assumptions

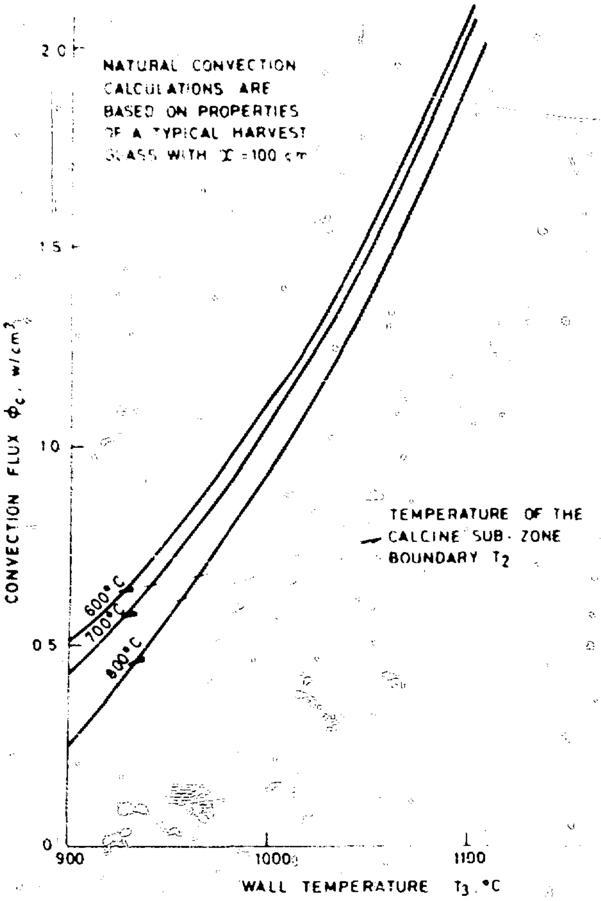

Fig. 3 Natural convection heat transfer between vertical surfaces in molten glass.

which had to be made, this agreement seems reasonable. If an allowance is made for the enhancement of convective circulation by the rising gas bubbles the agreement will be even closer. The source of this gas is thought to be alkali nitrates. These nitrates are the last to be thermally decomposed and since they melt before decomposition some could enter subzone 3 before decomposition is complete.

The model as summarized in Eqs. 14 and 15 satisfies the observed independence of wall heat flux ϕ_W on vessel diameter. It also shows that the size of the working zone (A) is controlled by heat transfer in the glass-forming subzone and not by processes in the calcination subzone. The latter result is a consequence of the implicit assumption that chemical rate processes do not influence the thickness L_2 of the subzone. For the intimately mixed feed used in FINGAL and HARVEST this assumption is probably [illegible] forming [illegible] thickness L [illegible] L [illegible] k [illegible] 0.004 W [illegible] K [illegible] approximately 40 [illegible] 10 [illegible] photographed [illegible]

The [illegible] L [illegible] much heat [illegible] convection from [illegible] FINGAL [illegible] tions, when [illegible] D [illegible] zone exposed to the [illegible] direct contact with the [illegible] wall [illegible] heat transfer is relatively unimportant.

CONCLUSIONS

A review of the experimental data [illegible] carried out under FINGAL conditions in vessels [illegible] from 10 to 40 cm in diameter has shown [illegible] the working (or reaction) zone varies [illegible] with the volumetric feed rate and inversely with the [illegible] diameter. It then follows that the average heat flux [illegible] into the working zone is constant [illegible] feed rate or vessel size and [illegible] W [illegible]. A simple model in which heat [illegible] transferred through (a) a glass-forming [illegible] (b) [illegible] subzone, and (c) an aqueous [illegible] zone predicts a wall heat flux of [illegible] W m^2. If an allowance is made for the enhanced convection caused by rising gas bubbles [illegible] glass-forming subzone, the quantitative agreement [illegible] proved. According to the model convective heat transfer through the glass-forming region is the controlling mechanism. Reductions in the height of the working zone can therefore be gained by improving the heat transfer in the glass-forming region.

REFERENCES

1. J. R. Grover, W. H. H[illegible], P. [illegible] and M. H. [illegible], The FINGAL Process, in [illegible] Symposium on the Solidification and Long-Term Storage of Highly Radioactive Wastes, USAEC CONF-660208, Richland, Washington, [illegible]
2. K. S. Chun and J. B. Morris, The Thermal Decomposition of HARVEST Feed Slurries and the Characterisation of the Product, AERE-R8921, Harwell, 1978.
3. W. Davis, Effects of Fission Product Heat on the Production Capacity of the FINGAL Process, AERE-R5268, Harwell, 1967.
4. M. N. Elliott and J. R. Grover, Scale Up of the Glass-Making Stage of the FINGAL Process, AERE-R4844, Harwell, 1965.
5. M. Jakob, *Heat Transfer*, John Wiley & Sons, New York, 1949.
6. A. R. Hall, unpublished work, AERE, Harwell, 1978.

IV. IMMOBILIZATION OF RADIOACTIVE WASTES—CERAMIC PROCESSING

RECENT DEVELOPMENTS IN LOW- AND INTERMEDIATE-LEVEL WASTE FIXATION BY CEMENT

[illegible] WITTE [illegible] F. KOSTER
[illegible] Kernforschungszentrum [illegible]
[illegible]

ABSTRACT

INTRODUCTION

PWR

BORON WASTE

A
PWR

H BO

[illegible] contains about 30,000 ppm boron [illegible] samples the boron content was [illegible] 000 and 45,000 ppm.

[illegible] components of radioactive waste [illegible] and borates, phosphoric acid and [illegible] phosphates, and tartaric acid and tartrates either [illegible] the setting of cement.[1-4] With respect [illegible] alkaline borates, this effect could be [illegible]. The effects of other constituents in power [illegible] could not be found thus far. In [illegible] the setting of cement, [illegible] reported elsewhere.[5]

[illegible] could be that in the presence of [illegible] calcium borate containing phases [illegible] the formation of compounds like tri-calcium [illegible] plays an important role in the compli[illegible] process of cement setting. The setting of boron [illegible] cement mixtures should, therefore, be [illegible] calcium. This can be achieved [illegible] addition of slaked lime, $Ca(OH)_2$, which [illegible] scale. The compressive strength [illegible] mixtures increases with increasing amounts of slaked lime added, until the stoichiometric amount of Ca [illegible] to $Ca(BO_2)_2$ has been reached (Fig. 1). Beyond [illegible] the compressive strength will decrease again, [illegible] because the cement will then contain unreacted lime of low strength. The compressive strength decreases [illegible] increased total boron content, as can be seen in Fig. 1 [illegible] 30,000 ppm and 45,000 ppm boron; but this influence [illegible] very significant. The leach resistance of samples [illegible] by the method described above compares well to the leach resistance of boron-free samples (Fig. 2).

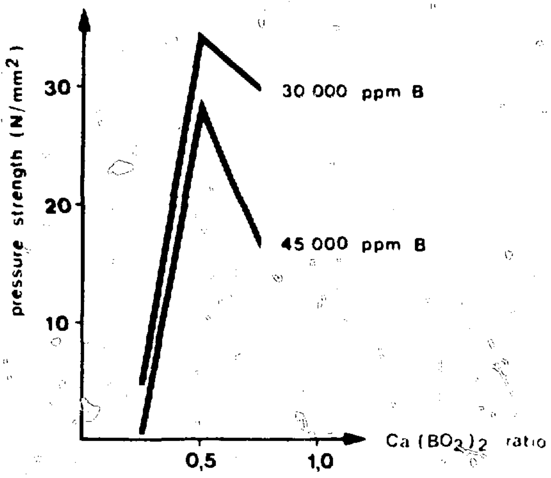

Fig. 1 Pressure strength of cement incorporated PWR sludge.

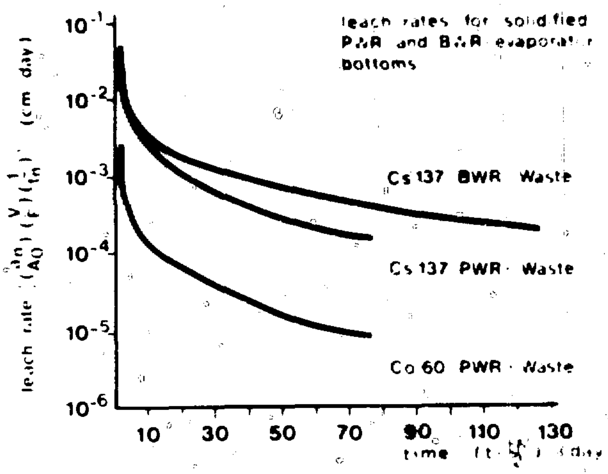

Fig. 2 Pressure strength of cement incorporated PWR sludge.

CEMENT CONTAINING MEDIUM ACTIVE SODIUM NITRATE WASTE

Purex-reprocessing of spent LWR nuclear fuel generates, among others, an intermediate-level-liquid-waste stream of about one m^3 per year and per ton of fuel reprocessed, which contains up to 450 g/liter of salt. Greater than 90% of this salt is sodium nitrate. In the German fuel reprocessing center, incorporation of these salts into cement is being considered.[6]

Research and development work at the Karlsruhe Research Center is aimed at the optimization of the final product with respect to parameters like behavior during mixing and setting, mechanical and chemical stability, and leach resistance.

For the interpretation of the results of leach tests shown in the following figures and tables, a leach coefficient D is used, which is defined by the expression

$$D = \frac{\pi m^2 V^2}{4F^2} \quad (\text{cm}^2\ \text{d}^{-1})$$

where D = leach coefficient (cm^2 d^{-1})

$m = (A_t/A_0)(1/\sqrt{t})\,(\text{d}^{-0.5})$

A_0 = sample activity at time zero

A_t = activity leached out of sample after leaching time t (days)

V = sample volume (cm^3)

F = sample surface (cm^2)

This leach coefficient is formally an equivalent to the diffusion constant of Fick's law. It can be correlated to the time dependent leach rate by

$$R = \rho\sqrt{D/\pi t} \quad (\text{g cm}^{-2}\ \text{d}^{-1})$$

where ρ is the specific gravity (g/cm^3).

Optimization of Cs and Sr Leachability by Additives

It is generally assumed that the cement leachability of Cs and other radionuclides can be reduced by adding minerals like vermiculite, bentonite, and zeolite. Whereas zeolite was excluded for reasons of economy (synthetic) and availability (natural), out of the above and other minerals a natural bentonite proved to be especially preferable in preliminary leach tests. Therefore this bentonite was selected for further studies.

Table I gives Cs and Sr leach coefficients with different cement samples containing different amounts of a special

TABLE I

Leach Coefficients (cm^2 d^{-1}) in 80 C Distilled Water of Cement Products Containing 10% by Weight of Simulated Waste Salts

Type of cement*		Without additive	With 10% NB†	With 10% NB + 6% BSH§
PZ 35F	Cs	6.4 E-2	8.1 E-4	9.3 E-4
	Sr	1.1 E-3	2.8 E-3	8.3 E-4
PZ 45F	Cs	1.0 E-1	1.3 E-5	1.3 E-5
	Sr	2.6 E-3	4.4 E-3	1.6 E-3
PZ 45F/HS	Cs	8.3 E-2	1.4 E-4	1.6 E-5
	Sr	2.1 E-3	3.4 E-3	8.0 E-4
EPZ 35F	Cs	5.7 E-2	1.3 E-4	2.5 E-6
	Sr	1.9 E-3	5.0 E-3	6.4 E-4
HOZ 45L/HS	Cs	4.5 E-2	2.0 E-6	2.9 E-7
	Sr	1.4 E-3	1.7 E-3	3.9 E-4
Pozzolanic cement	Cs	1.7 E-2	8.2 E-5	4.1 E-6
	Sr	7.7 E-4	1.3 E-3	2.8 E-4

*Abbreviations from DIN 1164: PZ = Portland cement; EPZ = "Eisenportland Zement" (contains up to 35% blast furnace slag); HOZ = "Hochofen Zement" (36% or more slag); 35,45 = minimum strength in N/mm^2; F = fast setting; S = slow setting; HS = high sulfate-resistance; PZ 35F is similar to Type-I Portland cement.

†NB = natural Ca-bentonite.

§BSH = barium silicate hydrate.

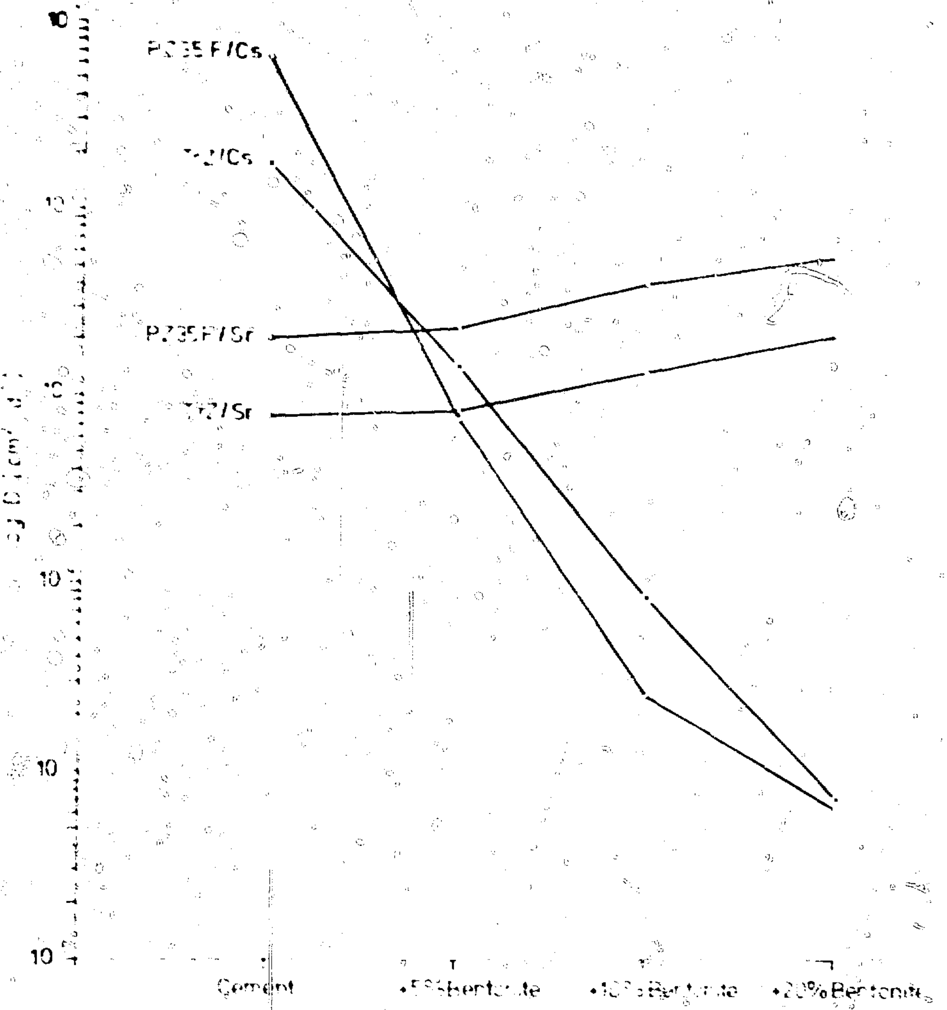

Fig. 3. [illegible]

natural bentonite. Figure 3 shows the influence of bentonite in graphical form. From the results the following statements can be made:

- Cs leach coefficients can be lowered up to four orders of magnitude, equivalent to a leach rate lower by two orders of magnitude, by adding bentonite. The Sr leach coefficient is scarcely affected. (High bentonite contents show even a slight negative effect.)
- The Sr leach coefficient can be lowered by a factor of 20 (leach rate by a factor five) by adding a cement hardening product (barium silicate hydrate type). This does not affect the Cs leach rate.
- A combination of both additives improves Cs and Sr leach resistance.
- Different types of cement do not differ from each other significantly if natural bentonite is present.

These statements have not been deduced only from the table but were checked with respect to their statistical significance by variance analysis. In a series of leach tests the influence of the leaching agent was checked (Table 2).

TABLE 2

Leach Coefficients (cm² d⁻¹) for Cs and Sr in Various Leachants Using the IAEA Method (20 °C)

		Distilled water	Tap water	NaCl solution	Salt brine
PZ 351					
without additive	Cs	4.1 1-4	2.4 1-4	[illegible] 1-4	7.3 1-5
	Sr	2.8 1-5	4.3 1-7	4.4 1-5	7.2 1-6
Wet 5% NB	Cs	6.9 1-5	2.6 1-5	9.9 1-5	1.3 1-5
	Sr	4.5 1-5	8.9 1-7	8.8 1-5	8.8 1-7
Wet 20% NB	Cs	2.7 1-7	1.9 1-8	7.2 1-7	2.1 1-8
	Sr	3.1 1-4	1.0 1-5	1.8 1-4	3.5 1-6
Pozzolanic cement					
without additive	Cs	3.1 1-4	4.4 1-5	2.2 1-4	1.6 1-5
	Sr	3.6 1-5	7.4 1-6	6.6 1-5	1.1 1-6

*PZ 351 is similar to Type I Portland cement.

Natural Ca-bentonite.

Saturated solution in equilibrium with NaCl, $MgSO_4 \cdot 6H_2O$, and $KCl \cdot MgCl_2 \cdot 6H_2O$ as solid phases. Its composition is (by weight) 34 $MgCl_2$, 2 $MgSO_4$, 6 KCl, 2 NaCl, 63 H_2O.

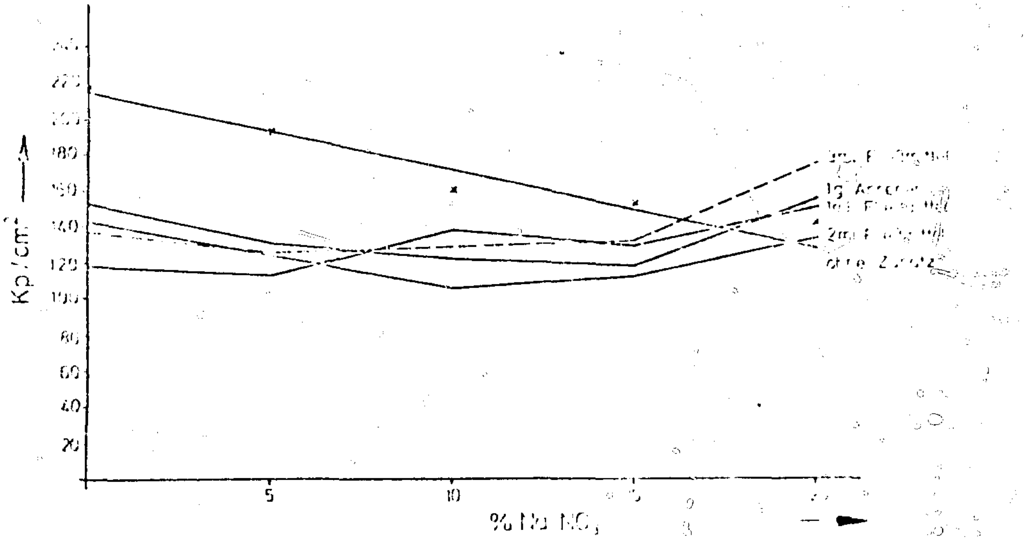

Fig. 4 Pressure strength as a function of NaNO$_3$ content.

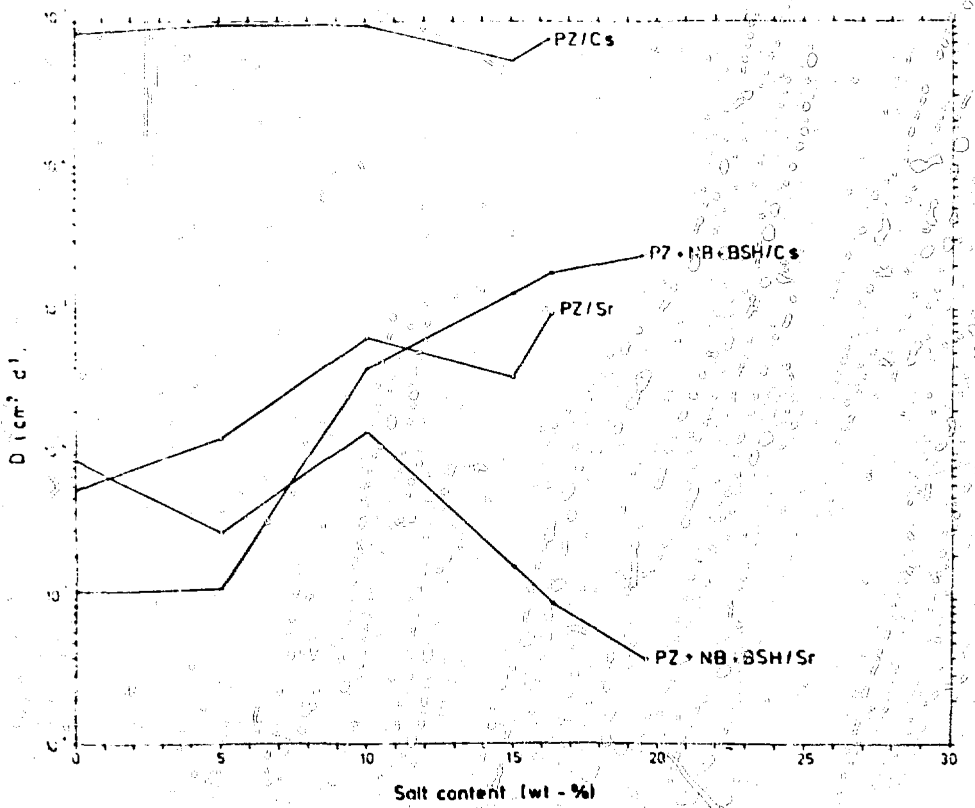

Fig. 5 Leach coefficient as a function of salt content.

Distilled water, tap water, NaCl solution, and salt brine were used as the leachants. Salt brine is assumed to contact the product as a consequence of the maximum credible accident when stored underground in salt formations.

With respect to the influence of the type of cement and of the bentonite addition, the previous statements could be confirmed. However, between distilled water and NaCl solution, on the one hand, and tap water and salt brine, on the other hand, there is a significant difference in leachability. The leach coefficient of the first group is, on the average, a factor of 25 higher than the second group. This may be due to the presence of metal ions like Ca and Mg which form nonsoluble silicates on the cement surface and thus reduce diffusion.

The Influence of Salt Content

In order to minimize the volume of solidified waste, the maximum amount of nitrate salt which can be incorporated into cement (with still acceptable product qualities) must be established. As yet, it is generally accepted that in order to produce cement of acceptable structural strength (i.e., about 50 Kp/cm^2) the concentration of sodium nitrate should not exceed 130 g per kg of cement.[4-7] Together with an acceptable water/cement ratio of <0.4, this would result in a salt content of <10 wt.% in the final product.

Sample tests containing up to 20 wt.% sodium nitrate show that strength and leach resistance with respect to Cs and Sr are fully within acceptable limits; the detailed results, however, cannot be fully explained as yet. Figure 4 shows results of tests on pressure strength. Whereas cement stone without additives shows a linear decrease from about 220 Kp/cm^2 (without $NaNO_3$) to about 140 Kp/cm^2 (20% $NaNO_3$), addition of different cement fluxes lower the pressure strength to 110 to 140 Kp/cm^2 between 0 and 15% $NaNO_3$ and may indicate even a slight increase at 20% $NaNO_3$. A significant influence of the type of cement flux could not be confirmed thus far.

Figure 5 shows the first results on leach tests. The advantageous effect of bentonite on the Cs leach coefficient and of the cement hardener on the Sr leach coefficient could be confirmed. In the case of Cs, however, the leach coefficient is independent of $NaNO_3$ content without additives, whereas with additives the leach coefficient increases by more than two orders of magnitude from 0 to 20 wt.% $NaNO_3$. The Sr leach coefficient, on the other hand, increases by about one order of magnitude without additives and decreases by more than one order of magnitude with additives. These results of $NaNO_3$ content influence were taken out of current research work and as yet cannot be fully explained. This work, however, is continuing.

REFERENCES

1. J. H. Leonard, and K. A. Gablin, Report 74-WA/NE-8, ASME Publication, November 1974.
2. *Zement-Kalk-Gips*, 14: 158 (1961).
3. *Zement-Kalk-Gips*, 25: 403 (1972).
4. W. F. Holcomb and S. M. Goldberg, Report ORP/TAP-76-4, 1976, Office of Radiation Programs of the U. S. Environmental Protection Agency.
5. H. W. Heacock and J. W. Riches, Report 74-WA/NE-9, ASME Publication, November 1974.
6. Report on the Planned Entsorgungszentrum (Nuclear Reprocessing and Disposal Center) in the Federal Republic of Germany for the Storage of Spent Fuel Elements, DWK, Hannover, September 1977.
7. R. H. Burns, *At. Energy Rev.*, 9(3) (1971).

FUETAP (FORMED UNDER ELEVATED TEMPERATURES AND PRESSURES) CONCRETES AS HOSTS FOR RADIOACTIVE WASTES

J. G. MOORE, G. C. ROGERS, J. H. PAEHLER, and H. E. DEVANEY
Chemical Technology Division, Oak Ridge National Laboratory, Oak Ridge, Tennessee

ABSTRACT

Cementitious solids formed at $\leq 250^\circ$C and ≤ 70.3 kg/cm^2 (1000 psi) offer excellent possibilities as hosts for radioactive wastes. Preliminary results are presented on the effect of mix composition, temperature, and pressure on the physical properties of the resulting solids. Initial leach results are encouraging in the assessment of the ability of these FUETAP concretes to isolate radionuclides from the environment.

INTRODUCTION

A generic investigation is in progress to determine the role of concretes in radioactive waste management. Current emphasis is on the concretes made by combining different cements with various admixtures to fix the radionuclides and allowing the mixtures to harden at $\leq 250^\circ$C and ≤ 70.3 kg/cm^2 (1000 psi).

Cementitious grouts are routinely used at Oak Ridge National Laboratory in the hydrofracture process for the fixation and permanent disposal of locally generated, intermediate-level waste solutions.[1-3] More recently, a process was developed for the fixation of ^{129}I as barium iodate in concrete.[4,5] Laboratory studies at the Savannah River Laboratories showed that the properties of concrete were adequate for the fixation of high-level radioactive wastes generated at the Savannah River Plant.[6] In addition, investigators at the Pennsylvania State University showed that concretes formed under high temperatures and very high pressures produced solids that showed promise for the immobilization and isolation of radioactive wastes.[7]

DISCUSSION

The purpose of the current investigation was to examine the potentialities of concretes formed under elevated but less stringent temperatures and pressures than the previous studies and, as in the case of the hydrofracture grouts, containing specific additives to fix the radionuclides. After scoping studies and a preliminary engineering evaluation[8] showed that the concept had promise, an experimental program plan was developed to determine the technological feasibility and acceptability of FUETAP concretes as hosts for radioactive wastes.[9] This report presents some results of the early studies associated with this investigation.

The initial FUETAP concretes used formulations based on previous experience with hydrofracture grouts. Specimens that were cured for 24 hr at elevated temperatures and pressures had a porosity of about 40% and compressive strengths ranging from 90 to about 400 kg/cm^2 (1300 to 5700 psi). The thermal conductivities ranged from 4×10^{-3} to 6×10^{-3} W/cm°K. The simulated waste sludge in all the tests had a composition based on an analysis of radioactive wastes stored at the Nuclear Fuel Services plant in New York (Table 1).

Concretes have been made with four different compositions (Table 2). The major variables examined in these formulations were the effects of the presence of nitrate and the ratio of fly ash to cement. Physical property measurements made on specimens prepared with type I portland cement in the various mixes are shown in Table 3. In these studies, the simulated sludge was mixed with the other dry components and added to water with or without sodium nitrate present. The wet mixes were immediately placed in an autoclave and brought to 250°C and 42.4 kg/cm^2 (600 psi) in 1.5 hr. They were cured at these conditions for 22.5 hr and then returned to ambient temperatures and pressure for the various measurements. The presence of

TABLE 1

Simulated Waste Sludge

Oxide	wt.%
Fe_2O_3	75.18
Al_2O_3	14.89
Cr_2O_3	4.94
NiO	4.78
SrO	0.14
$Ru(OH)_3$	0.03
CeO_2	0.04

TABLE 2

FUETAP Mix Compositions

	Composition, wt.%			
	Mix 1	Mix 2	Mix 3	Mix 4
Component				
Cement	37.54	38.94	23.24	27.55
Indian red clay	8.94	9.27	8.94	8.94
Fly ash	8.94	9.27	23.24	22.51
Simulated sludge	14.30	14.83	14.30	10.00
Quick-gel	0.41	0.42	0.41	0.40
$NaNO_3$	2.60	0	2.60	2.60
Water	27.27	27.27	27.27	28.00
Mix ratios				
Fly ash/cement	0.24	0.24	1.0	0.82
Water/fly ash + cement	0.59	0.59	0.59	0.56

TABLE 3

Effect of Mix Composition on FUETAP Concrete

Mix No.*	Compressive strength,†		Thermal conductivity, W/cm · K (x 10^3)	Porosity, %	Density, g/cm³
	kg/cm²	psi			
1	145	2060	4.4	47.6	1.56
2	134	1900	4.6	51.4	1.54
3	190	2700	4.9	39.4	1.75
4	299	4250	5.1	40.1	1.76

*All mixes were made with type I portland cement. Specimens were cured at 42.2 kg/cm² (600 psi) and 250°C, including the 1.5 hr required to reach curing conditions.

†Pressure required to crush a right-circular cylinder 4.8 cm diam by 10.2 cm.

nitrate had no apparent effect on these physical properties. The major changes were the result of varying the fly ash-to-cement ratio, with the maximum strength and conductivity obtained by a mix having a ratio of 0.82. Additional studies will be made in the future on the effects of the mix composition.

Several mixing and curing conditions were examined using mix 4 (Table 4). These specimens contained type I portland cement and were cured for 24 hr at 250°C and 42.2 kg/cm² (600 psi), except in those tests in which one of these conditions was the parameter in question. The only variable that caused an appreciable change was the heat-up time (i.e., the time required for the specimens to reach the desired curing conditions). Specimens that were taken to 250°C and 42.2 kg/cm² in 7 hr had about a 30% higher compressive strength than those that were taken to the curing temperature and pressure in 1.5 hr; however, there were no significant changes in any of the other physical properties.

The major effect that appears to be attributable to the presence of nitrate in the waste is the amount of water that may be removed by heating specimens to constant weight at 250°C (Table 5). Samples made with type I, type III or high-alumina cement, and containing 2.6 wt.% $NaNO_3$, appeared to have lost 3.5 to 5 times more water than similar specimens containing no nitrate. Because the water concentration in the final product will have a bearing on the amount of radiolytic or steam-generated gasification that could occur, additional studies will be made to determine the importance of this and other parameters in the removal of water from the concretes.

Leachability plays an important role in the evaluation of radioactive waste solid matrices in the unlikely event of an aqueous intrusion during storage or transportation. Dynamic and static leach studies are in progress using distilled water, local spring water, and simulated Sandia type B brine to determine the leachability of plutonium, cesium, and strontium from FUETAP concretes. The distilled water is used as a baseline for these studies, and the other two leachants represent aqueous media that might be encountered in real-life situations.

Sufficient data have not been collected in the initial leach tests to establish any definite leach mechanism; we have thus assumed that the leach rate is essentially diffusion controlled and have calculated the order of diffusivity based on models used in hydrofracture leach studies[2,3] (Table 6). The approximate order of diffusivity for cesium ranges from 10^{-15} cm²/s into distilled water or spring

TABLE 4

Influence of Various Parameters on FUETAP Concretes

Parameter	Range	Effect on physical properties
Curing time, hr	24–72	≥20% decrease in most properties
Heat-up time, hr	1.5–7	~30% increase in compressive strength
Curing temperature, °C	100–250	Insignificant
Curing pressure, kg/cm²	42–70	Insignificant
Cement type	III	Type I and Type III were equivalent; high alumina cement produced inferior solids

TABLE 5

Effect of Nitrate on the Removal of Water from FUETAP Concretes*

Cement type	Nitrate, wt.%	Compressive strength,† kg/cm²	psi	Water loss, wt.%‡
I	2.6	148	2060	46.9
	0	134	1900	12.1
II	2.6	142	2030	62.6
	0	152	2160	17.7
HAC§	2.6			72.2
	0	96	1360	14.6

*Mix 1 or 2, cured at 250°C and 42.2 kg/cm² (600 psi) for 24 hr (including the 1.5-hr heat-up time).

†Pressure required to crush a right-circular cylinder, 4.8 cm diam by 10.2 cm.

‡Loss on heating at 250°C until constant weights, total heating time 24 hr

§Lumnite, a high-alumina cement.

TABLE 6

Leachability of FUETAP Concrete*

Radionuclide	Approximate order of effective diffusivity, D_e, cm²/sec† Distilled water	Spring water	Sandia brine
[illegible]Cs	$10^{[illegible]}$	$10^{[illegible]}$	10^{-13}
[illegible]Sr	$10^{[illegible]}$	$10^{[illegible]}$	$10^{[illegible]}$
[illegible]Pu		$\leq 10^{-19}$	[illegible]

*Specimens prepared using mix 4 cured at 250°C and 42.2 kg/in² (600 psi)

†Sufficient data have not been collected to establish the leach mechanism. These estimated D_e values were calculated using models developed in the hydrofracture studies.[1]

‡After 1 month, data indicated corrosion was taking place; after 3 months, a total of 0.07% Pu had leached from specimen.

§Has not been measured.

water to 10^{-13} cm²/s into Sandia brine. Strontium is more leachable, with diffusivity values ranging from 10^{-11} to 10^{-10} cm²/s. There was essentially no plutonium leached into spring water in the three months the tests have been in progress indicating an order of diffusivity that is $\leq 10^{-19}$ cm²/s. The data suggest, however, that corrosion may be taking place in the distilled water test. About 0.07% of the plutonium has leached from the specimen in the 3-month period. More data must be collected before we can determine if corrosion is involved or if we are simply seeing a surface or subsurface effect during this early leach period.

A number of studies are currently in progress to further delineate the properties of FUETAP concretes (Table 7). Additional mix compositions and curing conditions are being investigated to determine their effect on such properties as porosity and thermal conductivity. At the same time, the effect these changes have on dewatering, leachability, and durability must be established.

The reaction rate of hydrogen and oxygen in the presence of FUETAP concrete was found to be ≥10 times the rate observed with ordinary cement pastes. The preliminary data suggest that, if the hydrogen and oxygen produced by radiolysis remain in close proximity to the FUETAP concrete, the recombination rate will exceed production even for very high alpha dose rates. Glove-box studies have been initiated to measure the overall effect of radiolysis occurring in FUETAP concretes containing alpha-emitting nuclides. The results of all these studies will be reported at a later date.

Studies are in progress to obtain data that can be used to estimate the durability or long term stability of these waste forms. In the initial tests, attempts were made to determine the reactivity of the solids to brine at elevated temperatures and pressures. The results showed the presence of calcium in the liquid phase after a specimen was immersed in 10 vol of brine for 4 days at 250°C and 175 kg/cm² (2500 psi). Additional data must be obtained to determine if the calcium lost was simply part of the lime produced during the hydration process or the dissolution of a small part of the calcium silicates.

TABLE 7

Studies in Progress on FUETAP Concrete

- Maximize properties of the host solid
  - Mix composition
  - Curing conditions
- Heat and radiolytic gas generation characteristics
  - Dewatering effect
  - Recombination rate of hydrogen and oxygen
- Effects of nonradioactive waste components
  - Nitrate
  - Hydroxide
- Fixation of specific nuclides
- Leachability of radionuclides
- Durability of host solid

In conclusion, the initial results on FUETAP concretes are most promising; however, additional work is required for a more nearly complete assessment of the potentialities of using such solids as radioactive waste hosts.

ACKNOWLEDGMENT

Research was sponsored by the Office of Nuclear Waste Management, Department of Energy, under contract W-7405-eng-26 with the Union Carbide Corporation.

REFERENCES

1. H. O. Weeren, Waste Disposal by Shale Fracturing at ORNL, *Nuclear Engineering Design*, 44: 291 (1977).
2. J. G. Moore, H. W. Godbee, A. H. Kibbey, and D. S. Joy, *Development of Cementitious Grouts for the Incorporation of*

Radioactive Wastes. Part 1: Leach Studies, ORNL-4962, Oak Ridge National Laboratory, April 1975.

3. J. G. Moore, *Development of Cementitious Grouts for the Incorporation of Radioactive Wastes. Part 2: Continuation of Cesium and Strontium Leach Studies*, ORNL-5142, Oak Ridge National Laboratory, September 1976.
4. W. E. Clark, The Isolation of Radioiodine with Portland Cement, Part I: Scoping Leach Studies, *Nuclear Technology*, 36: 215 (1977).
5. M. T. Morgan, J. G. Moore, H. E. Devaney, G. C. Rogers, C. Williams, and E. Newman, The Disposal of Iodine-129, in Proceedings of *Scientific Basis for Nuclear Waste Management*, Boston, G. J. McCarthy (Ed.), Plenum, NY, 1979.
6. J. A. Stone, *Evaluation of Concrete as a Matrix for Solidification of Savannah River Plant Waste*, DP-1448, Savannah River Laboratory, June 1977.
7. D. M. Roy and G. G. Gouda, High Level Radioactive Waste Incorporation into Special Cement, *Nuclear Technology*, 40: 214 (1978).
8. H. O. Weeren, W. Davis, Jr., and J. J. Perona, *A Preliminary Engineering and Economic Analysis of the Fixation of High-Level Wastes in Concrete*, ORNL/TM-6422 (in preparation).
9. J. G. Moore, E. Newman, and G. C. Rogers, *Radioactive Waste Fixation in FUETAP (Formed Under Elevated Temperature and Pressure) Concretes: Experimental Program and Initial Results*, ORNL/TM-6573, Oak Ridge National Laboratory, March 1979.

A LOW TEMPERATURE CERAMIC RADIOACTIVE WASTE FORM

D. M. ROY, B. E. SCHEETZ, M. W. GRUTZECK, A. K. SARKAR, and S. D. ATKINSON
Materials Research Laboratory, The Pennsylvania State University, University Park, Pennsylvania

ABSTRACT

Preliminary research on low temperature ceramic waste forms based upon modified calcium silicate and aluminate cements is described. Compositional and reaction variations, modified to achieve a strongly consolidated waste form which is resistant to significant change under the anticipated ambient, have been investigated. Extending previous studies in this laboratory, the recent work has utilized combinations of calcium aluminate cements and high early strength portland cements, different supercalcine waste formulations, and other additives. Both modified conventional cement composite consolidation methods and low-temperature hot pressing methods were used to incorporate the supercalcine into a consolidated form. Products after initial consolidation and after drastic accelerated leaching treatment (hydrothermal leaching) were characterized. Uranium and simulated transuranics were found to be highly resistant to leaching; strontium was relatively resistant in many cases; and cesium leaching was found to be compositionally dependent.

INTRODUCTION

Current plans to isolate nuclear waste center around deep geologic disposal. Central to this concept is the design of a stable radioactive waste form. This paper describes research on an alternative low-temperature ceramic waste form utilizing modified calcium silicate and calcium aluminate cements for which the solidification mechanism utilizes hydration bonding. Compositions and reaction variables have been investigated for normal cement formulations as well as for cements which have been compositionally adjusted in order to achieve a waste form which is adequately consolidated and would be predicted to be resistant to significant change under anticipated repository ambients.

Previous workers have shown that conventional cements are suitable for solidifying a variety of wastes.[1-3] Cement-based solidification furthermore provides relative ease of processing and low cost. At Oak Ridge National Laboratory a successful hydrofracturing technique has been employed for in-place solidification of intermediate level wastes in modified composition cementitious grouts for a number of years.[4,5]

In initial studies[6] rapid hardening portland cement and calcium aluminate cement-based materials were investigated, in combination with calcines of simulated Purex wastes PW-4b and PW-4c,[7a] which were treated at elevated pressures and temperatures in the range of 423 to 523°K (15 to 250°C). Very high strengths [up to 345 MPa (50,000 psi) compressive strengths] were achieved in the products. They were dense, impermeable[7a] and characteristically stable to an accelerated Soxhlet leaching test. Further, it is expected that related processing at elevated temperatures and lower pressures[7b] has much potential.

Recent studies have utilized formulations which include combinations of calcium aluminate cements and high early strength portland cements using different composition supercalcine[8] formulations, as follows: 20% supercalcine, 80% cement, with water added as required for solidification. They were typically consolidated by modified conventional technology involving hydration under normal ambient, utilizing special additives, as well as by hot pressing. The products were characterized and their properties investigated both after initial consolidation and after a series of drastic accelerated reaction conditions of hydrothermal leaching.

EXPERIMENTAL

Materials

The cements selected for this investigation were a commercially available ASTM Type III portland cement and a high alumina cement. Chemical analyses for these two cements are presented in Table 1. The compositions of the cements were adjusted in three different ways: (1) by adding silica in the form of solution as Ludox,* (2) by adding silica powder (made by dehydrating Ludox at 200°C for 3 hours), and (3) by adding Zeolon,† a synthetic zeolite.

TABLE 1

Chemical Analyses of Lone Star Type III and Secar 250

Oxide	Lone Star type III	Secar 250
SiO_2	21.11	0.2
Al_2O_3	5.04	72.0
Fe_2O_3	2.27	0.1
CaO	63.83	26.0
MgO	1.26	0.1
Na_2O	0.64 }	[illegible]
K_2O	0.73 }	
SO_3	3.96	

Two nonradioactive supercalcine[8] formulations, one a mixture of 77-2 and 77-3[9] and the other PSU-SPC-2 mixed with uranium, were used to determine the nature of the ability of the waste forms to isolate various radionuclides. The compositions of the supercalcines used are given in Tables 2 and 3.

Two series of cement mixtures were formulated. In the first series, commercial cements were mixed with simulated radioactive wastes; whereas in the second series, silica or Zeolon was added to the cements along with the radioactive wastes to adjust the CaO : SiO_2 ratio of the portland cement and the high alumina cement to that of tobermorite (CaO : SiO_2 ratio = 0.83 to 1.0) and anorthite (CaO : SiO_2 ratio = 0.5), respectively. Formulations of the adjusted cement mixtures are given in Table 4.

Sample Preparation Procedures

Two different sample preparation procedures were employed in this study. The first utilized the conventional cement paste mixing procedure. The additives were mixed with the cement and a minimum amount of additional water was added to give a working consistency. The pastes were transferred to a mold and compacted on a vibrating

TABLE 2

Composition of Supercalcine PSU-(SPC-2)+U Waste Form

Oxide	Oxide wt.%	Oxide	Oxide wt.%
La_2O_3	1.91	BaO	2.02
Pr_2O_3	1.85	Cs_2O	3.72
Nd_2O_3	6.00	Rb_2O	0.46
Sm_2O_3	1.45	Na_2O	0.15
Ce_2O_3	4.09	Al_2O_3	3.69
Y_2O_3	0.77	CaO	4.11
Gd_2O_3	13.72	SiO_2	15.82
P_2O_5	3.47	Fe_2O_3	3.90
ZrO_2	6.38	Cr_2O_3	0.45
MoO_3	6.68	NiO	0.18
SrO	2.73	U_3O_8	16.45

TABLE 3

Composition of 77-2 and 77-3 Waste Forms

Oxide	77-2 Oxide wt.%	77-3 Oxide wt.%	Oxide	77-2 Oxide wt.%	77-3 Oxide wt.%
La_2O_3	1.28	1.29	BaO	1.36	1.36
Nd_2O_3	6.07	6.09	Cr_2O_3	0.30	0.30
Gd_2O_3	9.39	9.43	Na_2O	5.99	6.02
Y_2O_3	0.52	0.52	Rb_2O	0.30	0.31
Ce_2O_3	2.74	2.76	NiO	0.12	0.12
ZrO_2	4.28	4.30	CdO	0.09	0.09
MoO_3	4.48	4.50	Ag_2O	0.08	0.08
Cs_2O	2.50	2.51	U_3O_8	10.12	10.17
Fe_2O_3	2.62	2.63	CaO	1.30	0.72
P_2O_5	5.49	8.34	Al_2O_3	16.30	16.36
SrO	0.92	0.92	SiO_2	23.76	21.20

---

*Ludox-ammonium-stabilized colloidal silica, E. I. du Pont de Nemours, Wilmington, Delaware.

†Zeolon-synthetic zeolite of the mordenite family, Norton Co., Worcester, Massachusetts.

TABLE 4

Adjusted Compositions of Cement Hosts

Sample	Lone Star type III, grams	Secar 250, grams	Silica,* grams	Ludox,† cc	Zeolon,‡ grams	Waste SPC 2+U, grams 200 mesh	Waste SPC 2+U, grams 60 +100, mesh	Deionized H_2O, cc	w/s**	Preliminary curing
A1	2.10		1.23			0.67		0.40	0.10	HP§
A2	2.10		1.13		0.11	0.67		0.40	0.10	HP
A3	2.51		1.48					0.40	0.10	HP
A4	2.51		1.35		0.13			0.40	0.10	HP
A5	26.32			29.44		8.36		25.07	0.78	60¶
A6	26.32			26.98	0.66	8.36		24.74	0.76	60
A7	31.51			35.33				25.00	0.84	60
A8	31.51			32.31	1.58			25.01	0.81	60
A9	2.10		1.23				0.67	0.40	0.10	HP
A10	26.32			29.44			8.36	22.98	0.74	60
B1		2.12	1.21			0.67		0.40	0.10	HP
B2		2.54	1.46					0.40	0.10	HP
B3		26.50		28.98		8.33		15.00	0.58	60
B4		31.79		34.77				15.00	0.63	60
B5		2.12	1.21				0.67	0.40	0.10	HP
B6		26.50		28.98			8.33	18.34	0.64	60

*Dehydrated at 200°C/2 hours and ground with agate mortar + pestle.
†Du Pont trademark for ammonia stabilized colloidal silica solution (0.5236 g/SiO_2 ml).
‡Zeolon, mordenite structure zeolite, Norton Co., Worcester, Massachusetts.
§HP = hot press 150°C, 50,000 psi, ½ hour.
¶60° = cured at 60°C.
**w/s = gm H_2O/gm solid in mix.

table for one minute and stored at 300°K (27°C) at greater than 90% relative humidity for 24 hours, after which the molds were removed and the samples coated with Protex-o-Cote* and stored at 333°K (60°C) to cure for 6 days.

The hot pressed samples were prepared as cylinders 12.7 mm in diameter by 12.7 mm high. The prepared cement mixtures were mixed with water (w/s = 0.1) and quickly transferred to the hardened steel hot press die, the inside of which was previously coated with stearic acid solution in acetone. The die was placed in the press and the paste pressed to the desired pressure (50,000 psi, 345 MPa) between two hardened steel plungers sliding through both ends of the die. The die was heated externally by a split furnace, while the temperature in the vicinity of the sample was monitored by a thermocouple placed in a groove in the top plunger. The pastes were pressed for 0.5 hr, measured from the time the temperature reached the final value of 423°K (150°C). Both pressure and temperature were kept constant during this period. The hot-pressed samples were then pushed out of the die by means of an extra long plunger, cooled in air, and stored in plastic vials for subsequent experiments. The details of the equipment and the experimental method are given elsewhere.[10,11]

Hydrothermal Treatment of Composite Waste Form

Approximately 35 milligrams of each of the processed waste forms and blank cement specimens were hydrothermally treated in a tenfold (wt.) excess of fluid to solid form. Two hydrothermal solutions were used in this study: one was deionized water and the other was NBT-6a-brine, the formulation for which was supplied by the U.S. Geological Survey (USGS). A gold ampule was sealed at one end; the waste and the water were carefully placed into the ampule, and the remaining end carefully sealed.

The experiments were performed in conventional 12.7 mm I.D. cold-seal pressure vessels[12] using water as the pressurizing medium. The temperatures of the experiments were nominally 473 and 573°K (200 and 300°C) with a nominal pressure of 31 MPa (300 bars).

Characterization

Both solution and solid phases from each of the hydrothermally treated specimens were characterized. The solutions above the charge were carefully decanted, and the solids were washed with deionized water. The solutions and the wash waters were diluted to 25 ml. All the elements reported, except cesium, rubidium and uranium, were analyzed with a computer-interfaced atomic emission spectrometer. Uranium was determined by a fluorometric method. Cesium and rubidium were analyzed with an atomic absorption spectrophotometer.

---

*A commercial low permeability plastic sealing material.

Qualitative elemental analysis for elements above neon was obtained by energy dispersive X-ray spectrometry on a scanning electron microscope. The microstructures of the waste forms and microcrystalline products were observed simultaneously by scanning electron microscopy. The bulk waste form was studied by grinding the samples and using X-ray diffraction to characterize the crystalline component phases in the waste form.

RESULTS

General Comparisons Based on Research in Progress

The experimental parameters being studied include:

1. Cement compositions
2. Initial processing conditions (a) normal processing at room temperature or elevated temperature and (b) hot pressing at 423 or 523 K [150 or 250°C]
3. Waste form added
4. Other additives
5. Accelerated hydrothermal "leaching" conditions with (a) deionized water or (b) bittern brine, as a function of (c) temperature, (d) pressure, and (e) time.

A significant number of experiments to complete the matrix of variables are in progress, and thus the overall results will not be presented in detail here.

Some comparisons between the results with composites of supercalcine ceramic within normally processed or hot pressed cement matrices [the latter prepared at 523°K and 345 MPa (50,000 psi)] were given previously.[13]

The hydrothermal reaction products, as revealed by scanning electron microscopic examination and X-ray diffraction, were predominantly the normal products of hydrothermal cement reactions, such as tobermorite[7b] (in addition to the unreacted supercalcine phases,[9] dominantly fluorite structure UO_2 solid solution phase). This was found to be true for both calcium aluminate and calcium silicate based cements. Characterization of the solids in the bittern brine reaction products indicates only the presence of cementitious phases, supercalcine phases, and simple and mixed halide salts.

The denser hot pressed samples were found to be, for a particular temperature, generally more resistant to radioactive waste element release to solution than were the less dense low temperature processed composites. Additionally, bittern brines generally (but not in every instance) were found to result in higher concentrations of leached species released to solution.

Effects of Experimental Parameters upon Hydrothermal Leaching

Tables 5 through 8 present the chemical analyses of solutions from cement-supercalcine composite samples treated hydrothermally for 6 or 7 days at 473°K and 300 bars (31 MPa), with deionized water having a 10 : 1 wt. ratio of water to solids. Table 5 illustrates the results of processing treatment [hot pressed (1 and 2) vs. normally cured (3 and 4)] of type III cement composites and shows the effect of composition (normal cements, 1 and 3; and compositionally adjusted samples, 2 and 4). The lowest values obtained for cesium release to solution (cesium being the most mobile species) were those in column 2, for the combination of hot pressed, compositionally adjusted samples; the next lowest was for column 4 (compositionally adjusted, normally cured specimens).

Table 6 gives comparable values for calcium aluminate cement composites. Similarly, values for cesium release were lower by an order of magnitude in the compositionally adjusted samples and were lower in the hot pressed compared with normally cured samples. Strontium was apparently well-fixed, as it was undetected in both compositionally adjusted samples.

Table 7 compares the effects of both the supercalcine grain size and processing conditions upon reaction characteristics, for type III cement composites. The densification effects due to hot pressing and the larger grain size of supercalcine (in the normally cured cement composite) both, apparently, causing lower surface areas to be exposed to solution, result in relatively lower cesium release.

Table 8 compares the results of similar experiments with calcium aluminate cement compositions. In this sequence are found the lowest cesium release values among the compositions investigated. The effect of compositional control is dominant in this sequence, irrespective of the processing condition or grain size of the supercalcine ceramic. This phenomenon is of particular interest, since at the same time substantial amounts of rubidium were removed in all instances. Of further interest are the observations that in all cases strontium was essentially not detected and all proved to be superior with respect to very low (or nondetectable) release of actinide simulators (neodymium and uranium).

DISCUSSION AND CONCLUSIONS

The results of preliminary experiments involving solidification of supercalcine ceramics in compositionally modified cement matrices and investigations of their behavior under drastic hydrothermal leaching conditions have been presented. The matrix solidification times were relatively short—one-half hour for hot pressing and 6 to 7 days for normal processing (28 days is the usual norm for ordinary cement solidification)—and yet the properties appear to be very favorable.

The products of normal solidification [at slightly elevated temperature (60°C) and atmospheric pressure] for only 6 to 7 days, as revealed by X-ray diffraction characterization and SEM studies of microstructures, were

TABLE 5

Comparison of Normal Portland Type III Cement vs Compositionally Adjusted Formulations Both of Which Were Hydrothermally Treated at 200 C in Deionized Water

	Hot pressed		60 C cured	
Elements analyzed	1 Normal cement, % in solution,* CCD-207-3‡	2 Adjusted, % in solution, CCD-206-3-A2	3 Normal cement, % in solution, CCD-207-3c	4 Adjusted, % in solution, CCD-206-3c-A5
Al	ND†	ND	0.4	ND
Ba	ND	0.6	0.4	1
Ca	§	354¶		[illegible]¶
Cr	0.4	3.6	ND	2.2
Cs	35.8	7.9	44.2	13.3
Fe	§	ND		ND
La	ND	ND	ND	ND
Mo	1.2	0.4	0.3	0.7
Na	§	862¶		465¶
Nd	ND	ND	ND	ND
Ni	1.9	ND	ND	ND
Rb	67.2	31.7	74	41.9
Sr	2.7	0.7	8.8	2.4
Si	1.3	2.1	1.1	7.0
U	0	0.03	0	0.1
Zr	ND	ND	ND	ND

*% of element leached from solid and now in solution.

‡CXX- = cement.

XCX- = supercalcine waste form.

XXD- = hydrothermal treatment in deionized water, B = [illegible]

-2XX- = 200°C hydrothermal treatment, 3 = 300 C.

-X07- = duration of hydrothermal treatment in days.

-3 = hot pressed Lone Star type III; -3C = 60 C cured Lone Star type III

-S = hot pressed Secar 250; -Sc = 60 C cured Secar 250

-AX, -BX = refer to Table 4 mixtures.

†ND, none detected.

§Not determined.

¶Assumes that all the element comes from waste; Na, Ca from cement.

expected cementitious phases (but modified to reflect the compositional adjustments) plus crystalline supercalcine phases which were dominated by a solid solution fluorite structure UO_2. The hot pressed samples revealed initially the presence of crystalline hydroxylated calcium silicate (or calcium aluminate) phases as well. After hydrothermal treatment with deionized water, relatively minor total phase change had taken place, but some recrystallization of the matrix phases was observed. Well crystallized tobermorite was a common product of the calcium silicate based matrix phase.

Analyses of solutions from hydrothermal leaching experiments showed that uranium and simulated transuranics (Nd, La) were highly resistant to even this drastic leaching environment, and strontium was also found to be relatively resistant. Considerable progress has been made even in these preliminary experiments in diminishing the amount of cesium released to solution. A rather surprising, though tentative, result was that under certain conditions the lower temperature product was equally favorable compared to the hot pressed product. Further, the amount of cesium leached hydrothermally at 473 K (200 C) from the cement supercalcine was low (2.5) compared to similar data for PNL 76-68 glass at 573 K (300 C) (4.3) (Ref. 14); however, it appears that the most favorable supercalcine composition by itself is less leachable [illegible]

The data presented for the low-temperature ceramic waste form, though preliminary, thus indicate the development of favorable physical and chemical properties, suggesting that a waste form using a cement-based binding mechanism may be utilized to produce a viable radioactive waste form for consolidating even intermediate to high-level wastes. Continued research is in progress to investigate a wider variety of chemistries and solidification conditions to optimize the products, to investigate effects of variables in the leach testing, and to provide a full assessment of the fixation potential for RW ions in a low-temperature cement-based ceramic waste form.

TABLE 6

Comparison of Normal Calcium Aluminate Cement Formulations vs. Compositionally Adjusted Formulations, Both of Which Were Hydrothermally Treated at 200°C in Deionized Water

Elements analyzed	Hot pressed 1 Normal cement, in solution,* CCD-207-S	 2 Adjusted, in solution, CCD-206-S-B5	60°C cured 3 Normal cement, in solution, CCD-207-Sc	 4 Adjusted, in solution, CCD-206-Sc-B3
Al	22.8	ND	16.2	5.4
Ba	ND	ND	5.9	ND
Ca	[illegible]	6.5	[illegible]	88.8
Cr	3.1	2.5	0.8	2.8
Cs	25.1	3.5	51.5	2.5
Fe	[illegible]	ND	[illegible]	ND
La	ND	ND	ND	ND
Mo	[illegible]	ND	[illegible]	0.2
Na	[illegible]	671	[illegible]	70
Nd	ND	ND	ND	ND
Ni	1.4	ND	4.6	ND
Rb	[illegible]	28.9	80.4	33.3
Sr	0.3	ND	7.6	ND
Si	[illegible]	0.5	1.1	7.5
U	0.001	0.02	0	0.2
Zr	ND	ND	ND	ND

*[illegible]

TABLE 7

Comparison of Hot Pressed vs. 60°C Cured Type III Cement Samples That Were Hydrothermally Treated at 200°C in Deionized Water

Elements analyzed	Hot pressed 1 CCD-206-3-A2* -200 mesh waste, in solution	 2 CCD-206-3-A9 -60 +100 mesh waste, in solution	60°C cured 3 CCD-206-3c-A5 -200 mesh waste, in solution	 4 CCD-206-3c-A10 -60 +100 mesh waste, in solution
Al	ND	ND	ND	0.8
B	[illegible]	0.2	1.7	1.8
Ca	[illegible]*	[illegible]	102*	335*
Cr	3.6	2.2	2.2	7.9
Cs	7.4	7.8	13.3	7.3
Fe	ND	ND	ND	5.9
La	ND	ND	ND	ND
Mo	0.4	0.1	0.7	0.5
Na	[illegible]*	[illegible]*	463*	643*
Nd	ND	ND	ND	ND
Ni	ND	ND	ND	ND
Rb	31.7	32.3	41.8	33.9
Sr	0.7	0.1	2.4	2.4
Si	2.1	ND	7.0	50.1
U	0.03	0.02	0.1	0.7
Zr	ND	ND	ND	ND

*[illegible] as for Table 5

TABLE 8

Comparison of Hot Pressed vs. 60°C Cured Calcium Aluminate Cements Hydrothermally Treated at 200°C in Deionized Water

	Hot pressed		60°C cured	
Elements analyzed	1 CCD-206-S-B1* −200 mesh waste, % in solution	2 CCD-206-S-B5 −60/+100 mesh waste, % in solution	3 CCD-206-Sc-B3 −200 mesh waste, % in solution	4 CCD-206-Sc-B6 −60/+100 mesh waste, % in solution
Al	ND	ND	5.4	0.2
Ba	ND	ND	ND	ND
Ca	1.7	6.5	88.8	18.4
Cr	2.3	2.5	2.8	2.5
Cs	3.5	3.5	2.5	3.3
Fe	ND	ND	ND	ND
La	ND	ND	ND	ND
Mo	ND	ND	0.2	ND
Na	588*	671*	70	743*
Nd	ND	ND	ND	ND
Ni	ND	ND	ND	ND
Rb	26.9	28.9	33.3	29.6
Sr	ND	ND	ND	ND
Si	2.3	0.5	7.5	2.9
U	0.02	0.02	0.2	0.02
Zr	ND	ND	ND	ND

*Abbreviations as for Table 5.

REFERENCES

1. *Alternatives for Long-Term Management of Defense High-Level Radioactive Waste*, ERDA 77-43, Idaho Chemical Processing Plant, Idaho Falls, Idaho, Technical Information Center, Oak Ridge, Tennessee, September 1977.
2. *Alternatives for Long-Term Management of Defense High-Level Radioactive Waste*, ERDA 77-42/1, Savannah River Plant, Aiken, South Carolina, Technical Information Center, Oak Ridge, Tennessee, May 1977.
3. J. A. Stone, *Evaluation of Concrete as a Matrix for Solidification of Savannah River Plant Waste*, Savannah River Laboratory Report DP-14488, June 1977.
4. H. O. Weeren, Waste Disposal by Shale Fracturing at ORNL, *Nuclear Engineering and Design*, 44: 291 (1977).
5. J. G. Moore and E. W. McDaniel, Fixation of Intermediate-Level Radioactive Waste in Hydrofracture Grout, *Ceramic Bulletin*, 57: 324 (1978).
6. D. M. Roy and G. R. Gouda, *Hot Pressed Cement in Radioactive Waste Management*, Report to Battelle Pacific Northwest Laboratories, BSA subcontract 841, August 1974.
7. (a) D. M. Roy and G. R. Gouda, High Level Radioactive Waste Incorporation into Special Cements, *Nuclear Technology*, 40: 214 (1978).
   (b) S. O. Oyefesobi and D. M. Roy, *Cement and Concrete Research*, 7: 95 (1977).
8. G. J. McCarthy, High-Level Waste Ceramics, *Transactions of the American Nuclear Society*, 23: 168 (1976).
9. J. L. McElroy, *Quarterly Progress Report*, PNL-2265-2, Pacific Northwest Laboratories, 1978.
10. G. R. Gouda, *Very High Strength in Cement Pastes Prepared by High Pressure Techniques Including Hot-Pressing*, M.S. Thesis, The Pennsylvania State University, 1972.
11. D. M. Roy, G. R. Gouda, and A. R. Bobrowsky, *Cement and Concrete Research*, 2: 349 (1972).
12. R. Roy and O. F. Tuttle, *Physics and Chemistry of the Earth*, 1: 138, Pergamon Press, London, 1956.
13. D. M. Roy, Cement Based Nuclear Waste Solidification Forms, in Proceedings of *High-Level Radioactive Solid Waste Forms*, Denver, NUREG/CP-0005, National Technical Information Service, Springfield, VA, 1979.
14. G. J. McCarthy, B. E. Scheetz, S. Komarneni, D. K. Smith, and W. B. White, Hydrothermal Stability of Simulated Radioactive Waste Glass, Preprint, to be published in *Solid State Chemistry: A Contemporary Overview*, Advances in Chemistry Series, American Chemical Society.
15. G. J. McCarthy, B. E. Scheetz, C. A. Smith, S. Komarneni, W. B. White, and D. M. Roy, Hydrothermal Treatment of Simulated High Level Nuclear Waste, *Ceram. Bull.*, 57: 358 (1978) (Abstract).
16. G. J. McCarthy, W. B. White, R. Roy, B. E. Scheetz, S. Komarneni, D. K. Smith, and D. M. Roy, Interactions Between Nuclear Waste and Surrounding Rock, *Nature*, 273: 216 (1978).

SOLIDIFICATION OF HLLW BY GLASS–CERAMIC PROCESS

N. OGUINO, S. MASUDA, and N. TSUNODA
Power Reactor and Nuclear Fuel Development Corporation, Tokai-mura, Ibaraki, Japan
I. YAMANAKA, M. NINOMIYA, I. SAKANE, S. NAKAMURA, and S. KAWAMURA
Nippon Electric Glass Co., Ltd., Otsu, Shiga, Japan

ABSTRACT

The compositions of glass–ceramics for the solidification of HLLW were studied, and the glass–ceramics in the diopside system was concluded to be the most suitable. Compared with the properties of HLW borosilicate glasses, those of diopside glass–ceramic were thought to be almost equal in leach rate and superior in thermal stability and mechanical strength. It was also found that the glass in this system can be crystallized simply by pouring it into a thermally insulated canister and then allowing it to cool to room temperature.

INTRODUCTION

For the solidification of HLLW the glass process has been extensively studied. It is pointed out, however, that glass is apt to phase separate or devitrify and result in the deterioration of leach resistance since the inside of the glass is maintained at higher temperature during a long period due to decay heat of the fission product. Glass–ceramic is a product obtained by heat treating glass and converting it into a thermodynamically stable state. It can be expected, therefore, that the above-mentioned weak points of HLW glass are removed in a HLW product made by the glass–ceramic process.

One objective of this study is to find out the most suitable glass–ceramic composition for the solidification of HLLW. The glass–ceramic systems studied were similar to those which were described as the candidates of HLW glass–ceramics.[1] Simulated oxides of HLLW from the reprocessing plant of PNC Japan were incorporated into the base glasses in the amount of 20 to 30 wt%. The maximum melting temperature of glasses was limited to 1300°C.

Another objective of this study is to develop the simple process for the crystallization of glass. The production of HLW glass–ceramic needs a heat treatment for crystallization, and considering the situation in hot operation, this process is desired to be as simple as possible. The studies were carried out to crystallize the glass cast in canister during the course of cooling without an independent process for crystallization.

COMPOSITIONS

The basic systems of glass–ceramics studied were
1. $CaO-MgO-Al_2O_3-SiO_2$ (D system)
2. $BaO-Al_2O_3-SiO_2$ (C system)
3. $CaO-TiO_2-Al_2O_3-SiO_2$ (P system)
4. $Li_2O-Al_2O_3-SiO_2$ (L system)

The simulated oxides of HLLW of PNC Japan were contained by 20 to 30 wt% in the base glasses of these systems. The composition of simulated HLW oxides in wt% are: 30.6 Na_2O, 9.05 ZrO_2, 8.96 MoO_3, 5.97 Fe_2O_3, 4.61 Cs_2O, 3.03 BaO, 1.85 SrO, 1.71 NiO, 1.30 MnO_2, 1.16 TeO_2, 1.12 Y_2O_3, 0.69 Rb_2O, 0.57 Cr_2O_3, 0.52 CoO, 3.92 La_2O_3, 5.11 CeO_2, 2.31 Pr_6O_{11}, 8.45 Nd_2O_3, 1.02 Sm_2O_3. Glasses were melted at 1300°C for 2 hr and cast into a mold and annealed. The homogeneous glass obtained was crystallized by heating at a rate of 300°C/hr from room temperature to 500°C and subsequently heated at a rate of

55°C/hr from 500°C to maximum (crystallization) temperatures and held for 4 to 8 hr at these temperatures.

For the fine-grained glass-ceramics obtained in each system, characteristics such as crystal phases, leach rate, thermal conductivity, thermal stability, etc. were evaluated. Crystal phases were identified by X-ray diffraction. In the measurement of leach rate, samples of 25 × 25 × 5 mm were immersed in 500 ml of distilled water at 100°C for 24 hr, and weight loss and the amounts of Cs_2O and SrO dissolved in water were measured. To evaluate the thermal stability, specimens were heated at 700°C for 1000 and 5000 hr, and the changes in crystal phases and leach rate were examined.

Glass - Ceramics Containing 20% HLW

In the D system, the compositions in the series $67.8(CaO + MgO + Al_2O_3 + SiO_2) + 9.5Fe_2O_3 + 2.7TiO_2 + 20HLW$ (wt %) with the CaO/MgO ratio of 3 : 1 to 1 : 1 were studied. In the C system, the compositions in the series $70(BaO + CaO + ZnO + Al_2O_3 + SiO_2) + 5TiO_2 + 5B_2O_3 + 20HLW$ (wt %) with the BaO/CaO/ZnO ratio of 10 : 5 : 2 were studied. In the P system, the compositions in the series $65(CaO + Al_2O_3 + SiO_2) + 10TiO_2 + 5B_2O_3 + 20HLW$ (wt %) were studied. In the E system, the compositions in the series $70(Li_2O + Al_2O_3 + SiO_2) + 6TiO_2 + 4ZnO + 20HLW$ (wt %) were studied. The glass-ceramics of the following compositions, D-62 (D system), C-27 (C system), P-50 (P system), and E-63 (E system) were excellent from the viewpoint of texture, deformation during heat treatment, and physical and chemical properties. Compositions, crystal phases, leach rate, and thermal stability are shown in Tables 1, 2, and 3, respectively. Thermal conductivity is shown in Fig. 1, and bending strength, thermal expansion coefficient, and thermal shock resistance are given in Table 4.

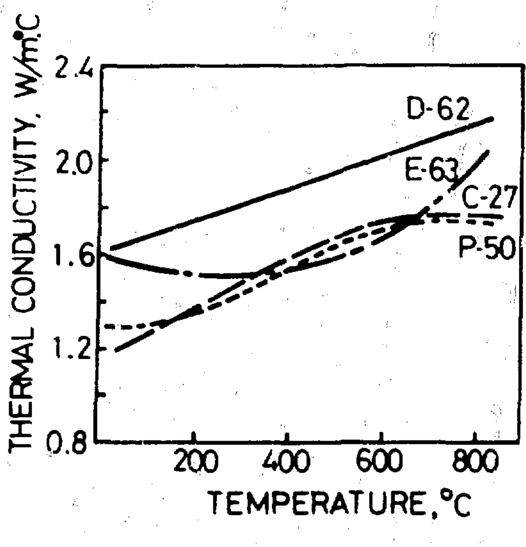

Fig. 1 Thermal conductivity of obtained glass - ceramics.

Glass - Ceramics Containing 30% HLW

In the D system, the compositions in the series $54.7(CaO + MgO + Al_2O_3 + SiO_2) + 8.7Fe_2O_3 + 3.2TiO_2 + 3.5B_2O_3 + 30HLW$ with the CaO/MgO ratio of 3 : 1 were studied. Without B_2O_3 addition it was difficult to obtain homogeneous glass because of marked phase separation (formation of Mo phase). Addition of more than 5% B_2O_3 reduced the crystallization tendency and increased the deformation during heat treatment. Therefore addition of B_2O_3 should be limited to below 5%. Glass-ceramic of D-210 composition was superior. Composition and crystal phases are shown in Table 1.

In the P system, the compositions in the series $56.5(CaO + Al_2O_3 + SiO_2) + 10TiO_2 + 3.5B_2O_3 + 30HLW$ (wt.%) were studied, and it is concluded that P-71 glass-ceramic was best. Chemical composition and crystal phases are shown in Table 1. In the C and E systems, homogeneous glass was not obtained because of marked phase separation.

Results

Results of the evaluation for glass-ceramics containing 20 to 30% HLW are summarized as follows.

1. The leach rate of D-62 was the lowest (Table 2), 3.6×10^{-5} g/cm² day in weight loss method, 5.3×10^{-5} in Cs_2O leach rate, and 7.0×10^{-5} in SrO leach rate. The deposition of $CaMoO_4$ phase was not harmful to leach resistance.

2. In thermal stability (Table 3), D-62, C-27, D-210 and P-71 were good showing almost no change in crystal phases and leach rate. In P-50, precipitation of $NaAlSiO_4$ (nepheline) and growth of sphene were observed, and the leach rate increased by a factor of 3. Growth of Li_2SiO_3 was observed in E-63, and the leach rate increased by a factor of 3.

3. In thermal conductivity D-62 was the highest over all temperatures (Fig. 1), which is most advantageous in removal of decay heat.

4. D-62 was highest in bending strength (1320 kg/cm²) and lowest in thermal expansion coefficient (Table 4). D-62 also had a high value of T_p and T_1 and good thermal shock resistance.

5. SEM shows that D-62 glass ceramic consists of fine-grained crystals of the size of 0.2 to 1.5 μ.

In conclusion, the D-62 glass - ceramic was considered to be the most suitable for the solidification of HLLW.

PROCESS FOR CRYSTALLIZATION

In the experiments described above, the glasses were crystallized by reheating from room temperature to crystallization temperatures as in the case of production of commercial glass - ceramics. However, it will be complicated to apply such a reheat treatment process to the crystallization of glass cast into canisters because of the very large

TABLE 1

Compositions and Crystal Phases of Glass Ceramic

	Sample No.					
	D-62, wt.%	C-27, wt.%	P-50, wt.%	F-63, wt.%	D-210, wt.%	P-71, wt.%
SiO_2	47.5	35.0	30.0	50.0	41.02	40.0
Al_2O_3	6.8	15.0	10.0	12.5	8.20	6.5
B_2O_3		5.0	5.0		3.50	3.5
Fe_2O_3	9.5				8.70	
TiO_2	2.7	5.0	10.0	6.0	3.20	10.0
CaO	6.8	4.0	25.0		4.10	10.0
MgO	6.8				1.37	
BaO		13.3				
ZnO		2.7		4.0		
Li_2O				7.5		
HLW	20.0	20.0	20.0	20.0	30.0	30.0
Total	100.0	100.0	100.0	100.0	100.0	100.0
Crystal phases	Fe_3O_4* $CaMoO_4$* $CaTiO_3$*	$CaMoO_4$ $CaTiO_3$	$CaSiO_3$ $CaMoO_4$ Sphene	Li_2SiO_3	$CaMoO_4$* Fe_3O_4* $CaTiO_3$*	$CaMoO_4$¶
Heat treatment	1100°C, 1 hr	850°C, 1 hr	900°C, 3 hr	800°C, 2 hr	900°C, 1 hr	900°C, 1 hr

*Diopside ($CaO \cdot MgO \cdot 2SiO_2$)
†hexa-Celsian ($BaO \cdot Al_2O_3 \cdot 2SiO_2$)
‡Perovskite ($CaTiO_3$)
§β-Spodumene ($Li_2O \cdot Al_2O_3 \cdot 4SiO_2$)
¶Sphene ($CaO \cdot TiO_2 \cdot SiO_2$)

TABLE 2

Leach Rate of Glass Ceramics

	Leach rate (g/cm² day)*		
Sample No.†	Weight loss	Cs_2O	SrO
D-62	3.6×10^{-5}	5.3×10^{-5}	7.0×10^{-5}
C-27	1.8×10^{-4}	1.1×10^{-4}	2.9×10^{-4}
P-50	5.6×10^{-4}	3.3×10^{-4}	9.0×10^{-4}
F-63	2.1×10^{-4}	1.9×10^{-4}	1.1×10^{-4}
D-210	6.5×10^{-5}	5.9×10^{-5}	7.4×10^{-5}
P-71	1.2×10^{-4}		

*Leach rate after immersion at 90°C for 24 hr in distilled water.
†Surface of 25 x 25 x 5-mm sample was polished by 1,000-mesh abrasive powder.

volume of glass. The most desirable is to crystallize the glass by slowly cooling after casting into a canister. It is a well-known fact that a crystalline body is obtained when a melt, which is instable and hard to form into glass, is cooled slowly. It has been proposed to make HLW products on this basis.[2] In general, however, it is difficult to obtain a fine crystalline body with good mechanical strength as the crystal tends to be coarse when it is cooled slowly. On the other hand, a melt of basalt can be converted into a fine crystalline body during cooling.[3] As the D system mentioned above is close to basalt in its composition, it is expected that a fine-grained crystalline body will be obtained during the cooling process.

The following is a description of experiments carried out for D-62 glass (Table 1). The DTA in cooling of a D-62 glass melt showed the exothermic peaks corresponding to the precipitation of diopside crystals at 900 to 1000°C, when the cooling rate was slower than 10°C/min.

The cooling conditions necessary to obtain a fine-grained crystalline body were studied. D-62 glasses were

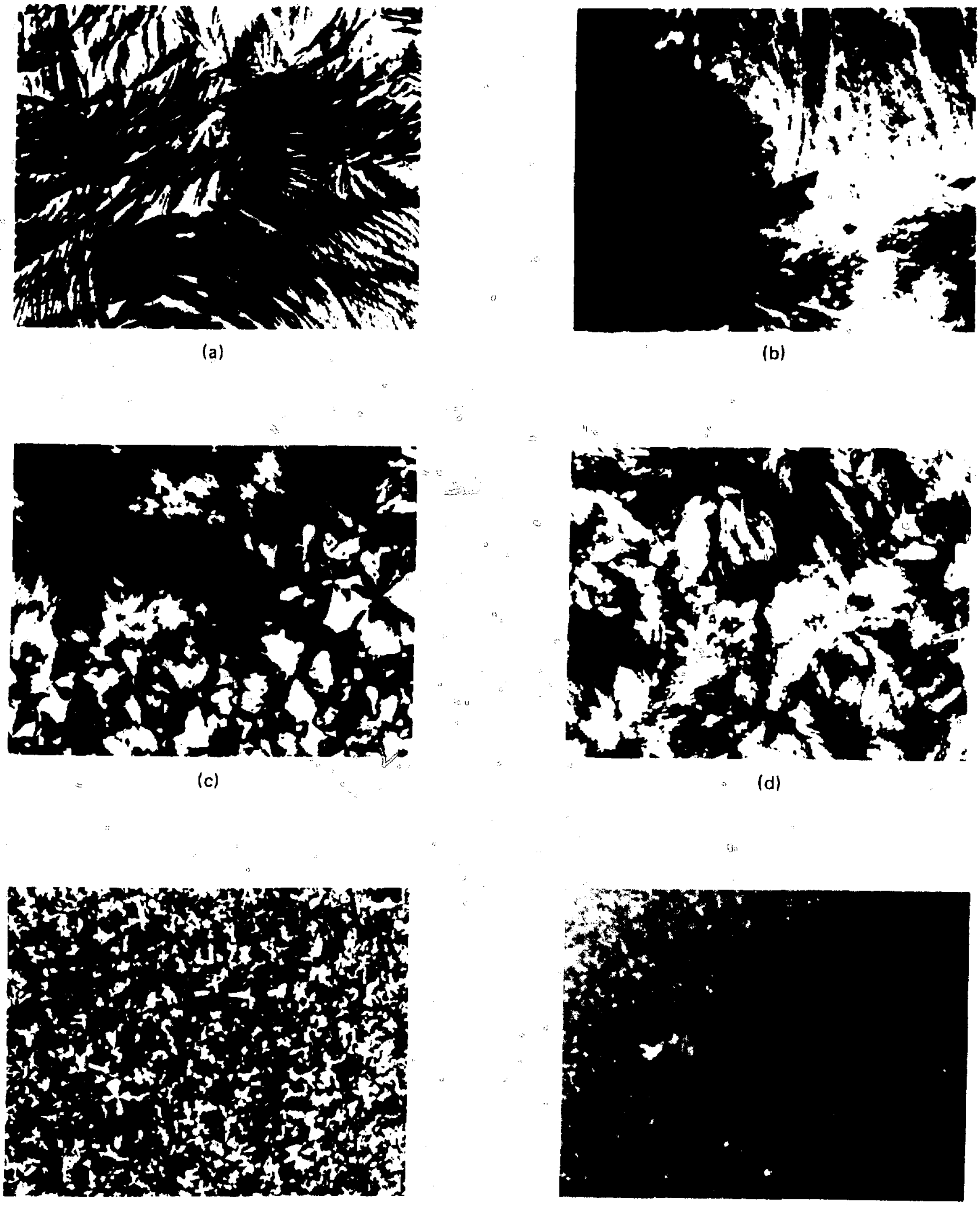

Fig. 2 The relation between the features observed by thin section microphotographs and heat treatment at various temperatures. (a) 1050, (b) 1000, (c) 950, (d) 900, (e) 850, (f) 800°C.

TABLE 3

Changes of Crystal Phases and Leach Rate of Glass Ceramics After Heating at 700°C for 1,000 and 3,000 hr

Sample No.	Description of X-ray trace	Leach rate, weight loss, g/cm² day		
		0 hr	1,000 hr	3,000 hr
D-62	No change	3.6×10^{-5}	3.6×10^{-5}	3.6×10^{-5}
C-27	No change	1.8×10^{-4}	1.9×10^{-4}	
P-50	Precipitate of $NaAlSiO_4$, appearance of sphene (111) peak	5.0×10^{-4}	8.5×10^{-4}	1.6×10^{-5}
F-63	Increase of intensity in Li_2SiO_3 (110) peak	2.1×10^{-4}	5.6×10^{-4}	
D-210	No change	6.5×10^{-6}	6.5×10^{-6}	6.6×10^{-6}
P-71	No change	1.2×10^{-4}	9.3×10^{-5}	

TABLE 4

Bending Strength, Thermal Expansion, and Thermal Shock Resistance of Glass Ceramics

Sample No.	Bending strength, kg/cm²	Thermal expansion, $\alpha \times 10^7$ (1/°C), 30 to 380°C	Tg,* °C	Tf,† °C	Thermal shock resistance, temperature difference, ΔT °C
D-62	1320	79	794	>1000	150
C-27	760	91	545	838	120
P-50	870	81	582	734	120
F-63	1270	78	502	734	150
D-210	1050	85	555	696	120
P-71	980	89	557	684	120

*Tg, dilatometric transformation point.
†Tf, dilatometric deformation point.

TABLE 5

Anneal Temperatures vs. Crystal Phases and Leach Rate

Temperature, °C	Crystal phases and XRD peak-height, arbitrary unit in parentheses	Leach rate, 10^{-5} g/cm²/day		
		Wt. loss	Cs_2O	Sr_2O
1050	Diopside, Fe_3O_4, $CaTiO_3$, $CaMoO_4$ (88) (8) (14)	5.65		
1000	Diopside, Fe_3O_4, $CaTiO_3$, $CaMoO_4$ (118) (8) (12)	4.50	5.85	12.1
950	Diopside, Fe_3O_4, $CaTiO_3$ (160) (8)			
900	Diopside, Fe_3O_4, $CaTiO_3$ (164) (12)	3.90	5.62	7.52
850	Diopside, Fe_3O_4, $CaTiO_3$ (154) (10)	4.20		
800	Diopside, Fe_3O_4, $CaTiO_3$ (128) (10)	4.32	6.82	9.05
750	Amorphous (glass)			
Quench	Quenched glass body (annealed)	~20		

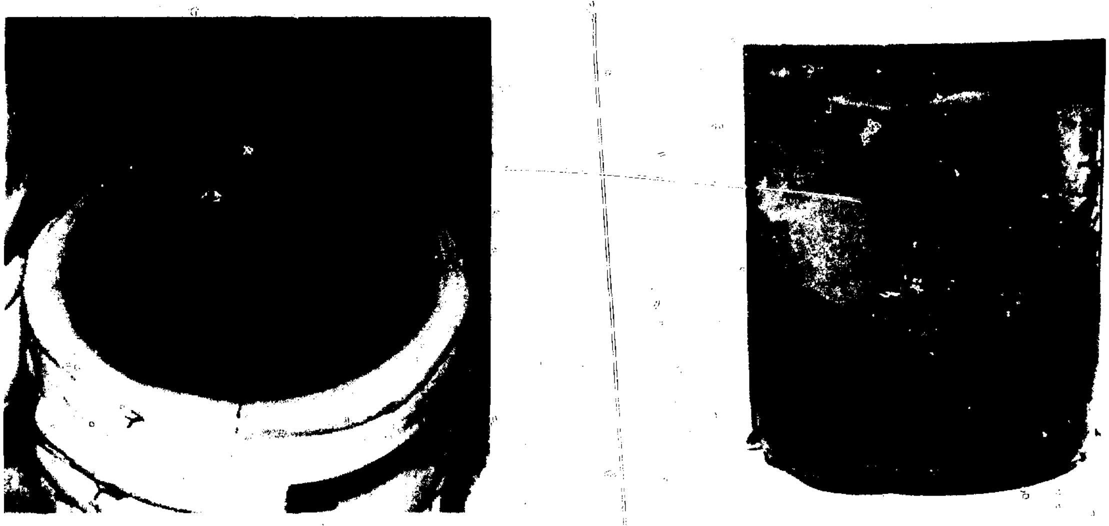

(a) (b)

Fig. 3 Cast and crystallization experiment. (a) Casting molten glass and gradually cooling for crystallization in the same canister. (b) Crystallized product (outside view).

melted at 1300°C for 1 hr in alumina crucibles, moved into the furnace at temperatures of 750 to 1050°C, maintained for 2 hr at these temperatures, and allowed to cool to room temperature. Thin section microphotographs are shown in Fig. 2, and crystal phases and leach rate data are shown in Table 5. It can be seen from Fig. 2 that fine-grained texture was obtained at 800 to 850°C. The leach resistances in Table 3 are almost similar to that obtained by reheat treatment (Table 2), and there was little change when the maintained temperature was varied.

Since the optimum temperature to obtain a fine-grained body was relatively low, it was thought that fine-grained glass-ceramics might be obtained by cooling the glass in a canister which is sufficiently thermally insulated.

The experiment was carried out using a cylinder made of stainless steel SUS304 with dimensions of 300 mm dia. × 350 mm long × 5 mm thick. The wall of the cylinder was insulated with asbestos cloth 30 mm thick. D-62 glass weighing 65 kg and melted at 1250°C was poured into the cylinder (Fig. 3a) and allowed to cool to room temperature after the insulated lid was put on. Cooling curves measured by the thermocouples inserted in the center and near the inside wall of the cylinder are shown in Fig. 4. The whole glass was converted into glass-ceramic (Fig. 3b), and the properties are given in Table 6. Although the texture became somewhat coarse because of a slower cooling rate than desired, the glass–ceramic had good properties. A little cavity appeared inside the glass–ceramic. This may be attributed to the volume contraction (~2%) during crystallization of the inner glass which crystallized after the circumference. No adhesion in the interface between the glass–ceramic and stainless steel was found, so defects caused by stress development (cracking, etc.) were not observed.

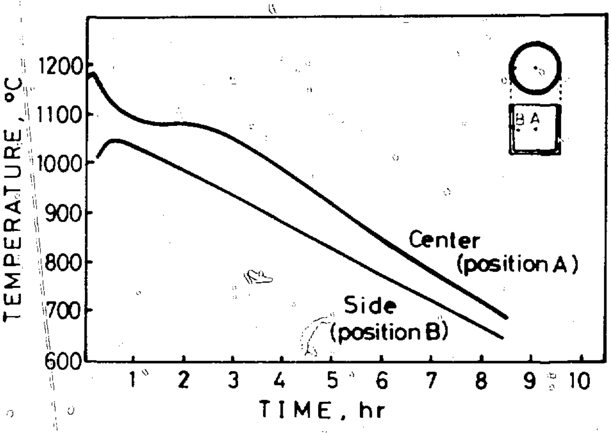

Fig. 4 Cooling curve of glass ceramics cast in thermally insulated canister, 300 mm in diameter, 150 mm high and 5 mm thick. A and B represent measured position.

TABLE 6

Properties of D-62 Glass–Ceramic Crystallized in Canister During Cooling

Crystal phases	Diopside, Fe_3O_4, $CaTiO_3$, $CaMoO_4$
Leach rate wt. loss	4.3×10^{-5} g/cm²/day
Cs_2O	5.6×10^{-5} g/cm²/day
SiO	7.5×10^{-5} g/cm²/day
Bending strength	1100 kg/cm²
Thermal expansion coeff.	81.8×10^{-7}/°C (30 to 380°C)
Softening temp.	>1100°C
Thermal conductivity	1.93 W/m/°C
Density	3.00 g/cm³
Thermal stability	No change after heating at 700°C for 3,000 hr

SUMMARY

The glass ceramic in the diopside system (D-62) was found to be suitable for the solidification of HLW. This glass ceramic was produced by slow cooling of the glass melt cast into a thermally insulated canister. By the process developed in this study a stable HLW glass ceramic can be produced by almost the same manner as in the HLW glass process.

REFERENCES

1. A. K. De et al., Development of Glass Ceramics for the *Incorporation of Fission Products*, *Bull. Am. Ceram. Soc.* 55, 500 (1975).
2. A. E. Ringwood, *Safe Disposal of High Level Nuclear Reactor Waste: A New Strategy*, Australian National University Press, Canberra, Australia, 1978.
3. Ten Voldán, The Melting and Crystallization of Basic Eruptive Rocks, *Advances in Glass Technology*, p. 382, Sixth ICG in Washington, D.C., U.S.A., Plenum Press, New York 1962.

COATING OF WASTE CONTAINING CERAMIC GRANULES

W. NEUMANN and O. KOFLER
Österreichische Studiengesellschaft für Atomenergie Ges.m.b.H., Institute of Metallurgy, Research Centre Seibersdorf, Vienna, Austria

ABSTRACT

Simulated high-level waste granules produced by fluidized-bed calcination were overcoated by chemical vapor deposition (CVD) with pyrocarbon and nickel in laboratory-scale experiments. Successful development enables pyrocarbon deposition at temperatures *of 600 to 800°K. The coated granules have excellent properties for* long-term waste storage.

INTRODUCTION

Research and development technicians in the field of high-level waste conditioning alternatives should not doubt the suitability of investigated and established techniques, e.g., vitrification, but should examine every possible method to store the waste "as stable as practical."

According to this motto the development work and investigations described below were initiated and carried out. With regard to the well established fluidized-bed calcination, which has already produced large quantities of calcined waste granules, this work concentrated on an additional alternative for conditioning these granules. Untreated granules are not sufficiently stable for long-term storage, particularly because of their solubility in water and low mechanical strength.

Coating these granules with a tight layer may improve the related properties. Some considerations[1] and experiments[2] in waste coating development have been performed previously. Nevertheless additional investigations and further development are justified. Previous experience in coating techniques, particularly in fluidized-bed chemical vapor deposition, was of great support.

PYROCARBON COATING

With regard to the well-known requirements for a protective layer, pyrocarbon was selected for the coating material. Pyrocarbon seemed to be one of the best possible *coatings.[3] It was used for coating of high-temperature* reactor fuel particles and stood up very well to the requirements. One must also consider that the properties required for high-temperature reactor fuel are not necessary for long-term storage of high-level waste. For example, high neutron dose rate or very high temperature resistance is not required.

One of the main advantages of pyrocarbon is its excellent resistance to leaching. Of course, there are some more advantageous properties of pyrocarbon.

- Fission product retention
- Temperature resistivity
- Low thermal expansion
- Good thermal conductivity
- High mechanical strength

Pyrocarbon properties are strongly dependent on coating conditions, i.e., deposition temperature, type of coating gas, etc., as well as the substrate on which it has to be deposited. The substrate was given by the fluidized-bed calcines because of the considerations mentioned below. A suitable coating process, which has to take into account the properties of calcined granules, was developed. It represents a further development of PyC deposition by CVD and is discussed later.

Fig. 1 [illegible]

Fig. 2 [illegible]

Substrate

In dealing with high level waste [illegible] one must keep in mind that [illegible] conditioning performance [illegible] costs. In order to use a simple [illegible] substrate the fluidized-bed calcine [illegible] Chemie pilot plant was used without further treatment before coating.

[illegible] APO₄ [illegible] them [illegible] can get by solidification [illegible] Mi[illegible] were mainly used. The [illegible] shape. In the first batch the [illegible] were irregular in shape with a mean diameter of [illegible] In the second batch, the granules were nearly spherical with a diameter of about 2 mm (Fig. 2). They were generated by solidification of simulated [illegible] level waste feed solution to which phosphoric acid was

TABLE 1

Maximum Processing Temperatures

	Salt cake	Spray calcine	Pot calcine	Calcine	Supercalcine	Phosphate glass	Borosilicate glass
T_{max}, K	310 to 720	970	695	670 to 1070	1170 to 1370	1170	1270 to 1670

	Sintered process	Glass-ceramic	Nepheline syenite	Hot isostatic press	Metal embedding Al matrix	Pyrocarbon coating
T_{max}, K	1235 to 1370	1270	1620	1620	900	600 to 800

added, therefore, their chemical composition was based on *aluminum phosphate*. The density of the granules was about 1.42 g cm^{-3}, which indicated a high porosity (~40% pores). Up to 1250 K the granules remained undamaged and did not even stick together.

Coating Performance

In waste coating, high-deposition temperatures are disadvantageous. Most coating processes, including pyrocarbon, are handicapped by the required high temperature. Although experiments to depress the deposition temperature of pyrocarbon below 1270 K were successful[5] by the use of acetylene as coating gas (gas composition 29% C_2H_2, 71% Ar; total gas flow 3500 cm^3/min), the temperature was still very high. Even at these temperatures particles tend to stick together, particularly if slight changes in chemical composition decrease the temperature resistivity. In any case, a calcined cake made of hot-waste-containing granules stuck and melted together should not occur in the fluidized-bed reaction tube.

Successful research and development work resulted in a further significant depression of the pyrocarbon deposition temperature. The use of a catalyzer, nickel tetracarbonyl, enables a coating temperature of about 800 K. Using this method, it is possible never to exceed a temperature limit of 823 K during the entire conditioning process. The reaction is

$$C_2H_2 \xrightarrow{Ni(CO)_4,\ cat.} 2C + H_2$$

The main advantages are

- Reduced fission product volatilization. It is negligible now.
- No problem with thermal resistivity of granules.
- Simplification of process performance as well as design and manufacturing of some equipment for the coating device, e.g., the heater. In general, solution of technical and experimental problems are easier at lower temperatures.

The temperature maximum required is compared with temperatures of other conditioning processes in Table 1 to illustrate the importance of the successful reduction.

Considering these recent results, pyrocarbon coatings should be considered a preferable waste conditioning alternative. Technical description and process performance data are given in Table 2.

TABLE 2

Data for the Coating Process and Device

Coating method: chemical vapor deposition in a fluidized bed
Fluidized bed: 2.5 cm diameter (graphite tube)
Dimensions: ~25 cm high
Heating element: electrical resistance heated graphite tube*

Coating parameters	Pyrocarbon coating	Nickel coating
Total gas stream	Pulsed	Pulsed
Coating gas	C_2H_2	$Ni(CO)_4$
Carrier gas	Ar	Ar
Catalyzer	$Ni(CO)_4$	
Temperature	600 to 800 K	470 K

*Could possibly be replaced by other heating elements for low-temperature deposition.

NICKEL COATING

Despite the advantages of carbon coatings, additional work was carried out to provide the granules with a pure nickel layer.[6] Based on the concept of depositing a protective coating by CVD at temperatures just a little above room temperature, one inevitably considers decomposition of metal carbonyls. The most suitable one is nickel carbonyl, which decomposes at very low temperatures.

Nickel deposition can be achieved at about 470 K, which is one-third the melting temperature of nickel. Nickel carbonyl is a colorless, flammable liquid (boiling point 316 K at 1 atm) of which the vapor is toxic, and it is about six times as dense as air. This required slight modifications to the coating device being used, especially to the gas supply system. The nickel carbonyl container had to be heated to achieve a sufficient vapor pressure. Nickel carbonyl was diluted in argon, which also acted as a carrier gas to prevent condensation in the line, which also had to

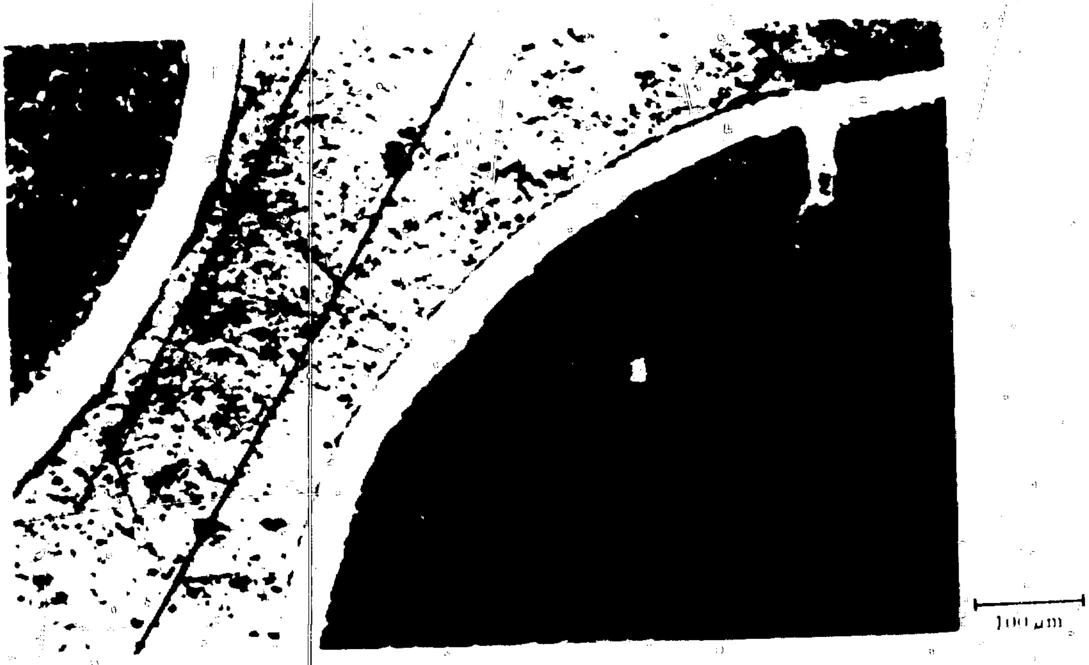

Fig. 3 Ceramographic section of Ni-coated granules

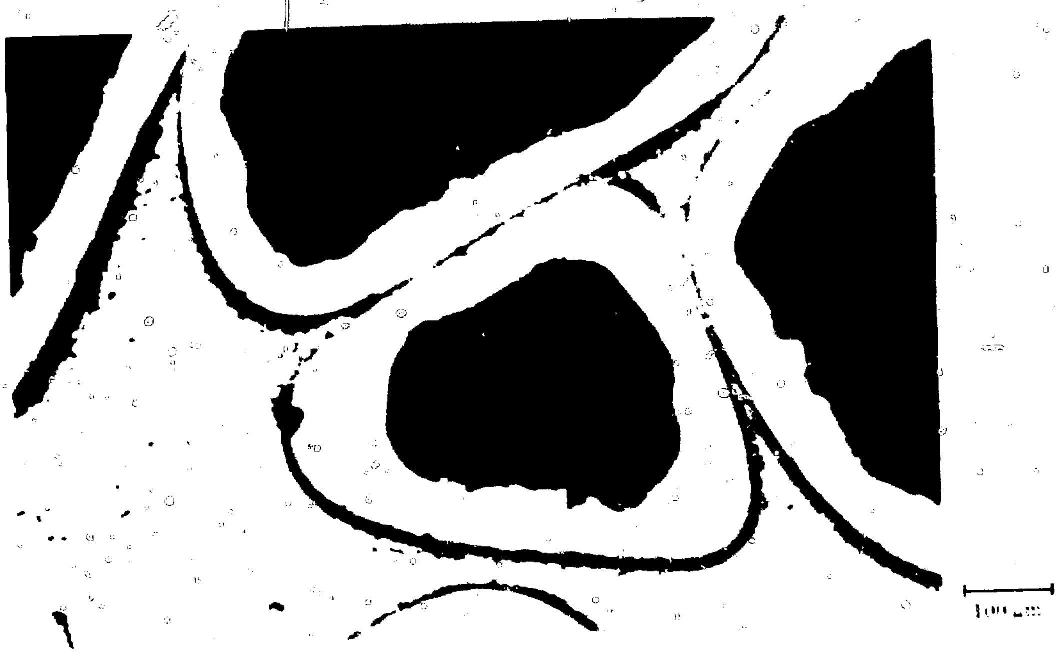

Fig. 4 Ceramographic section of Pd-coated granules

be heated. Because of the low coating temperature, only a little expansion of gas occurred in the reaction tube, which resulted in a remarkable reduction of fluidizing forces. A continuous gas stream did not yield sufficient movement of the granules. Pulsation of the inlet gas stream could solve this problem (Table 2).

PRODUCT CHARACTERIZATION

Micro-optical studies on ceramographic sections show adherent layers of PyC as well as of Ni. Pores and cracks on the outer surface of granules were coated and often even sealed. The average thickness of Ni layers is about 45 μm (Fig. 3) and of PyC layers, about 100 μm (Fig. 4). An average thickness is specified because the thickness data depend on the position of measurement. In a dimple in the irregular shaped granules the coating is thicker than on the top.

The following properties of uncoated granules could be significantly improved by coating:

- *Mechanical strength:* Single granules were tested by compressing them with a continuous deformation rate until fracture occurred. The maximum applicable load increased with PyC coating and Ni coating by about an order of magnitude.
- *Dust generation:* For every untreated granule of fluidized-bed calcines you can rub off a considerable amount of fines. This unavoidable effect causes undesired contamination. Coating with Ni and PyC prohibited the contamination by dust.
- *Temperature resistance:* Temperature causes damage to PyC at 1100 K in an oxidizing atmosphere. Ni-coated particles stick together at about 100 K, but the barrier effect is still guaranteed.
- *Thermal conductivity:* Thermal conductivity of every granule is low due to intergranular spaces and porosity. Although the high conductivity layers raise the thermal conductivity values of the whole particles, e.g., Ni by about three times and PyC by about two times, the absolute values are still low. The data obtained depend on the size and shape of the granules.
- *Suitability of metal embedding:* In order to achieve sufficient heat release and to prevent dispersion of the granules, coatings improve the particle-metal matrix contact because of the good wetting behavior of the layers. Therefore a better filling of small intergranular spaces can be achieved. In addition, the intragranular pores are sealed so that no leaching across the composite can occur.
- *Leach resistance:* Calcines are highly soluble in water. Leach tests in Soxhlet extractors on PyC-coated granules resulted in no detectable weight loss. Uncracked Ni-coated granules also show no weight loss if the specimen includes only a few damaged granules.
- *Porosity:* A drawback of waste calcines is their high porosity because a very large surface area is exposed to the leachant. Experiments showed that leaching water penetrates the whole particle. Coatings prohibit all penetration into the granules and prevent sucking by a capillary effect.

Major disadvantages of this approach are:

- *Conditioning of fines:* The fines generated by calcination cannot be conditioned by this method.
- *Technical performance:* Coating procedures in fluidized beds are more complex compared with other methods.
- *Necessity of additional conditioning steps:* Coated calcines require containment to avoid dispersion and to enable sufficient heat dissipation.

CONCLUSIONS

PyC and Ni coating is a feasible alternative to condition high-level waste containing granules. Low-temperature PyC coatings deposited on simulated HLW calcines in laboratory-scale experiments showed the advantages of this method. A conditioned product for long-term storage can be obtained by a process in which the temperature never exceeds 823 K.

Problems in coating technology due to this new field of application could be solved by some modifications on the rather well-known fluidized bed CVD. The process is not fully developed, but after further improvements in process technology it will represent a serious alternative to the management of waste fixation.

REFERENCES

1. M. De Bacer and M. S. T. Price, *Solidification and Disposal of Fission Product Waste*, O.E.C.D. High Temperature Reactor Project, 1973 Patent D.P.P.S.-213, Austrian Pat. Appl. No. A 9838/74.
2. J. M. Rusin et al., *Multibarrier Waste Forms, Part I: Development*, DOE-Report PNL-2668-1, Pacific Northwest Laboratory, 1978.
3. W. Neumann, *Coating of High Level Waste: Problems and Tasks* (in German), SGAE-Report No. 2674, Austrian Atomic Energy Research Ltd., Vienna, 1976.
4. E. Detilleux, H. Eschrich, and J. van Geel, *The Minerva Process: A Versatile Process for the Solidification of Liquid Radioactive Wastes from Nuclear Fuel Reprocessing*, ETR-294, Eurochemic, Mol, 1978.
5. O. Kofler and W. Neumann, *Conditioning of HLW Calcines, Part 1: Pyrocarbon Coating* (in German), SGAE-Report No. 2864, Austrian Atomic Energy Research Ltd., Vienna, 1977.
6. W. Neumann and O. Kofler, *Conditioning of HLW-Calcines, Part 2: Nickelcoating* (in German), SGAE-Report No. 2932, Austrian Atomic Energy Research Ltd., Vienna, 1978.

SOLIDIFICATION OF HLLW INTO SINTERED CERAMICS

KAZUO O-OKA,* TAKAO OHTA,* SIMIO MASUDA,† and NAOMI TSUNODA†
*Toshiba Corporation, Kawasaki, 210 Japan and †Power Reactor and Nuclear Fuel
Development Corporation, Tokai-mura, Ibaraki-ken, 319-11 Japan

ABSTRACT

Simulated HLLW from the PNC reprocessing plant at Tokai was solidified into sintered ceramics by normal sintering or hot-pressing with addition of some oxides. Among various ceramic products obtained so far, the most preferable was nepheline-type sintered solids formed with addition of SiO_2 and Al_2O_3 to the simulated waste calcine. The solid shows advantageous properties in leach rate and mechanical strength, which suggest that the ceramic product is a promising solid waste form. Other types of ceramic solids were prepared with additions of ZrO_2 or MnO_2, and some of them showed good characteristics.

INTRODUCTION

The most advantageous solid form of HLLW is a vitrified product which is currently accepted as the solid form of highly radioactive waste for long-term storage. It is desirable, however, to develop alternative solid waste forms with more stable properties than the vitrified form, since the diffusion of radionuclides should be minimized by all means.

One of the alternatives which may exhibit long-term stability is a ceramic form, such as "Supercalcine" or "Synroc," although the characteristics of those products are not yet well defined.

On the other hand, the solidification process of highly radioactive waste must be simple and convertible to continuous production. On that basis, the authors have made some preliminary investigations to produce solidified ceramics of HLLW from the PNC reprocessing plant at Tokai by normal sintering of the simulated waste calcine with the addition of several oxides. At the same time, some sintered ceramics were fabricated by hot-pressing as a reference for the comparison of properties.

DESIGN OF THE COMPOSITION OF CERAMIC PRODUCTS

The major constituents in the waste are, as oxides, Na_2O, MoO_3, ZrO_2, CeO_2, and lanthanide oxides represented as Nd_2O_3 among fission products. Simulated waste was prepared for the present experiments as a mixture of carbonates, nitrates, and oxides of all constituent elements except actinides. Particle size of each constituent was around 1 μm by grinding.

Prior to the sintering tests, the compositions of the ceramic solids were designed on mineralogical considerations. In order to immobilize each constituent, various refractory crystals containing constituents were first selected, and properties of those crystal phases were investigated.

Crystal phases of the major constituents such as Na_2O, MoO_3, and Nd_2O_3 were carefully checked from a mineralogical viewpoint. For example, melting temperature, thermal expansion, heat of formation, and lattice parameters of crystals relevant to the capability of incorporating ions were important with respect to the fixation of the nuclides.

A few candidate compositions were defined by combining the refractory crystals containing constituent elements. The representative composition designed is shown in Table 1. The main crystal of the composition is, as shown, nepheline, and other elements are immobilized as aluminates or aluminosilicates. The additives required to form those crystals can be calculated, therefore, as shown in the table. In the case of A, 146.51 g of additives are mixed with 98.1 g of the simulated waste giving 40 wt.% waste in the ceramic solid. Other candidates are zirconia and manganate ceramics with additions of ZrO_2 or MnO_2 and SrO to the simulated waste. The contents of the waste of the zirconia

TABLE I

First Candidate Composition of a Nepheline-Type Ceramic

Waste oxides			Additives, grams (wt.%)		
Constituents	Grams (wt.%)	Compounds	Al_2O_3	SiO_2	SrO
Na_2O	33.8	$Na_2O \cdot Al_2O_3 \cdot 2SiO_2$	56.14	65.54	
ZrO_2	9.9	ZrO_2			
		$ZrO_2 \cdot SiO_2$		(4.83)*	
Cs_2O	5.1	$Cs_2O \cdot Al_2O_3 \cdot 4SiO_2$	1.85	4.35	
Y_2O_3	1.3	$Y_2O_3 \cdot Al_2O_3$	0.59		
La_2O_3	3.0	$La_2O_3 \cdot Al_2O_3$	0.94		
Nd_2O_3	14.1	$Nd_2O_3 \cdot Al_2O_3$	4.27		
CeO_2	5.7	$CeO_2 \cdot Al_2O_3$	3.38		
NiO	1.9	$NiO \cdot Al_2O_3$	2.89		
Fe_2O	6.7	$Fe_2O_3 \cdot Al_2O_3$	4.36		
BaO	3.3	$BaO \cdot MoO_3$			
SrO	2.0	$SrO \cdot MoO_3$			
MoO_3	10.0	$SrO \cdot MoO_3 + BaO \cdot MoO_3$			2.2
Cr_2O_3	0.6	Dispersed			
Rb_2O	0.7				
Total	98.1		74.42	69.89 (74.72)*	2.2
		Total of additives			
		Composition A		146.51	
		Composition B		(151.34)*	

*Numbers in parentheses indicate additive and totals for composition B.

ceramics may rise to 60 wt.%. Chemicals with grain size of around 1 μm were used as additives.

SINTERING OF THE CERAMICS

The simulated waste and additives were weighed and mixed in a ball mill with and without binder. The mixtures were then put into a mold and preforms were fabricated for normal sintering. The preform size was 50 mm in diameter and 10 to 15 mm thick. Normal sintering was performed in an electric furnace at temperatures from 1000 to 1400°C. The waste content in the ceramics varied from 10 to 40 wt.% for nepheline type and from 30 to 60 wt.% for zirconate and manganate ceramics.

Dense ceramic solids were obtained by sintering at 1200 to 1300°C for 60 min in each material providing the content of the waste is properly adjusted. Ceramic solids were also fabricated by hot-pressing the compositions which yielded dense ceramics by normal sintering. Hot-pressing was performed at 1200 to 1300°C and at a pressure of 300 kg/cm^2 in an alumina mold.

Sintering tests of a few compositions gave the following results.

1. Dense nepheline-type ceramic solids were obtained from the composition of 30 to 40 wt.% waste oxides by normal sintering at a temperature around 1300°C for 60 to 90 min. Hot-pressing also gave dense nepheline ceramics at 1250 to 1300°C for 30 min.

2. Zirconate ceramics good in appearance were fabricated by normal sintering or hot-pressing when the waste content was around 40 to 50 wt.%. The operational data are similar to those for nepheline-type ceramics.

3. Manganate-type ceramics were fabricated similar to nepheline ceramics with a waste content around 50 wt.%.

4. Minor additives have considerable effects on the densification of ceramic solids. Addition of increased amounts of SrO to nepheline-type ceramics and addition of SiO_2 and SrO to zirconia and manganate types are effective in the densification of these ceramics.

5. Addition of a vinyl acetate binder to the mixture of chemicals is also effective in densification.

6. When the sintering temperature is high, e.g., 1400°C, some ceramics are half melted, and when the temperature is low, almost all are left as preforms.

Titanate-type ceramics were fabricated by sintering the simulated waste with additions of TiO_2, SrO, Al_2O_3, and in some cases SiO_2. Some looked well sintered.

CHARACTERIZATION OF CERAMIC SOLIDS

Characterization of the ceramic samples obtained in the sintering tests was carried out. Crystal phases of the ceramic samples were analyzed by X-ray diffraction. Figure 1 illustrates X-ray diffraction patterns of ceramic solids

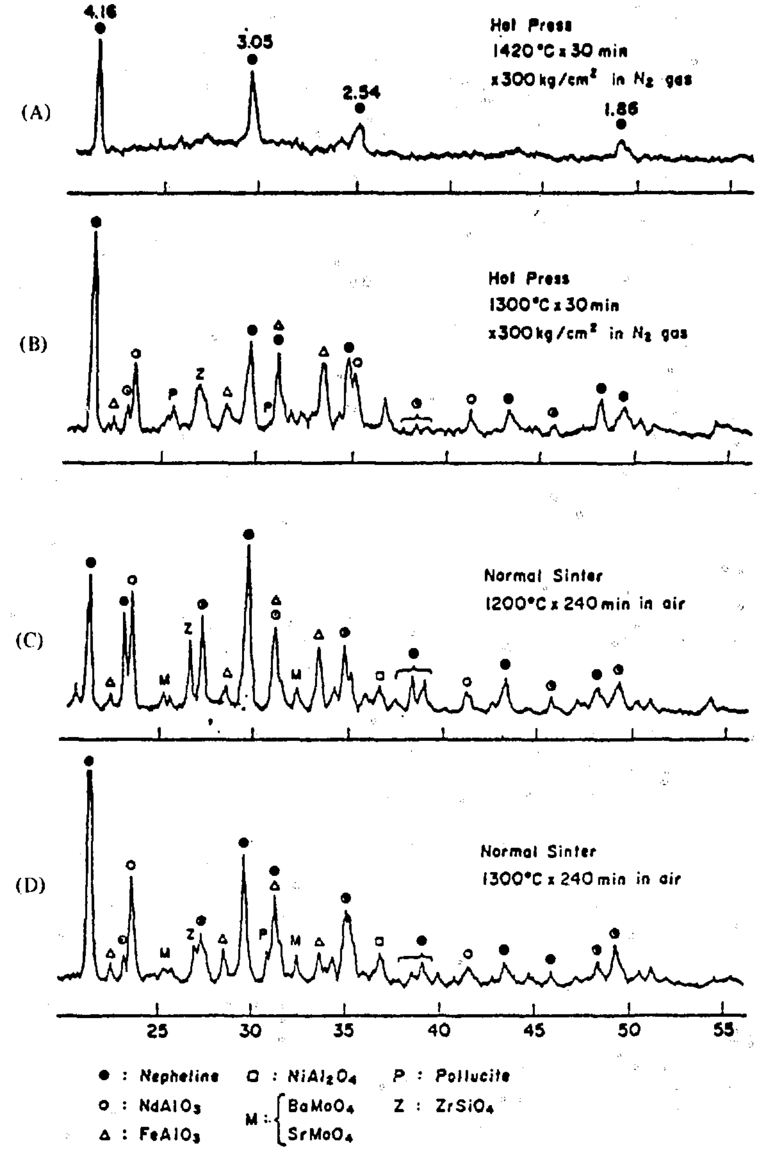

Fig. 1 X-ray diffraction patterns of solidified ceramics.

obtained from nepheline-type composition. The main crystal phase, nepheline, is clearly identified in diffraction peaks, and other expected crystals, such as Ba, $SrMoO_4$, $NdAlO_3$, $FeAlO_3$, $ZrSiO_4$, etc., are detected. Figure 2 illustrates the X-ray diffraction patterns of other types, such as zirconate, manganate and titanate compositions. ZrO_2 and fluorite crystals were detected in zirconate ceramics, but many unidentified peaks remain. Diffraction peaks observed in manganate and titanate ceramics were unidentified except for a few peaks of $SrO \cdot MnO_2$ in manganate and $SrO \cdot TiO_2$ and beta alumina in the titanate.

Bulk densities of ceramic samples were measured. Although theoretical densities of mixed ceramics are hard to calculate, they are tentatively estimated from those of composite crystals. Estimation shows that theoretical densities are 3.2 g/cm^3 for nepheline type when the waste content is 40 wt.%, 4.4 g/cm^3 for zirconate containing 50% waste, 3.9 g/cm^3 and 3.5 g/cm^3 for manganate and titanate, respectively, with 40% waste. Bulk densities of ceramics obtained by hot-pressing were more than 95% of the theoretical density (T.D.) when the temperature during processing is appropriate. Temperature range for proper hot-pressing for each type is from 1200 to 1300°C. Normal sintered ceramics, on the other hand, showed that their bulk densities are dependent not only on temperature and time for sintering but also on the composition of additives.

Dense nepheline ceramics (>90% T.D.) are obtained only when the sintering is performed at a temperature of 1300°C for 90 min or more on the composition containing excess SiO_2. Zirconate ceramics need a higher temperature and a longer time for densification than nepheline ceramics;

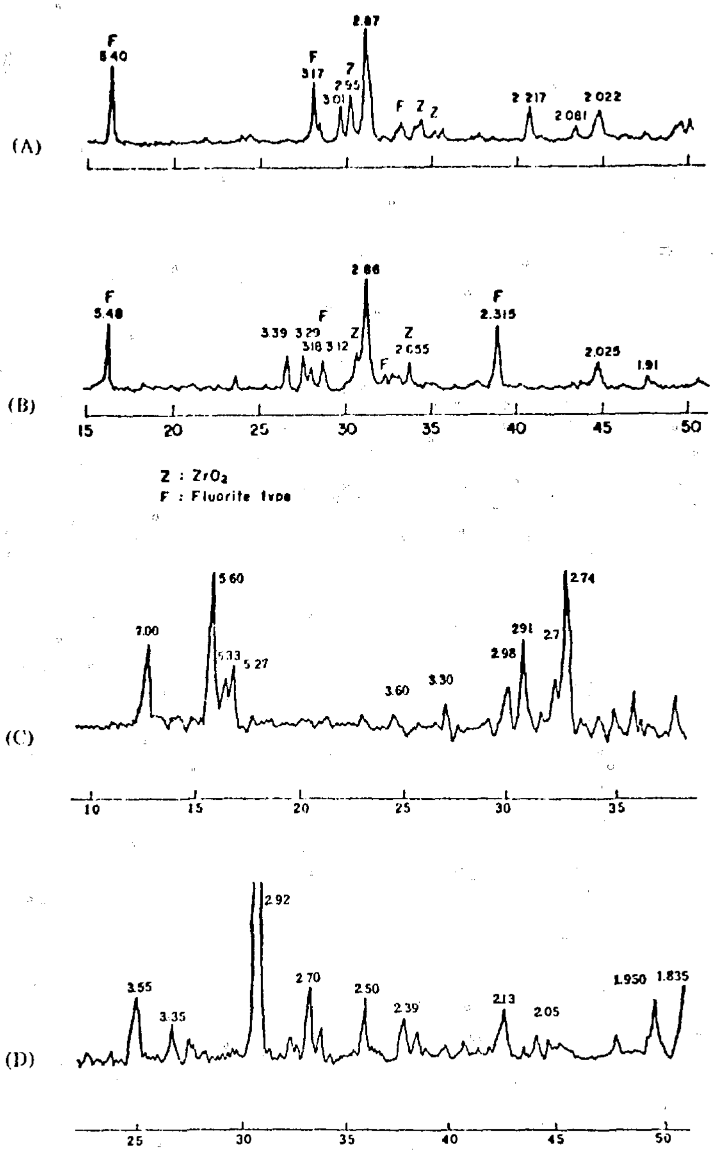

Fig. 2 X-ray diffraction patterns of ceramic solids. A and B, zirconate (normal sinter); C, manganate (normal sinter); D, titanate (normal sinter).

that is, a temperature of 1350°C or more and 200 min of time are needed. Bulk densities of manganate and titanate samples showed that densification was initiated at lower temperature, around 1100°C. Bulk density reaches 90% T.D. at that temperature. Figure 3 illustrates the change in bulk density of nepheline ceramics with sintering temperature.

Leach rates of dense samples were measured. Sample disks were cut and ground, and, after the measurement of surface area, sample pieces were immersed in boiling distilled water. The weight loss after 24 hr immersion gives the leach rate. Dense nepheline-type ceramics hot-pressed at 1250°C or more and some sintered at 1300°C showed leach rates of 5×10^{-5} to 5×10^{-6} g/cm^2 · day. Zirconate ceramics sintered at 1300°C had a leach rate of 5×10^{-4} g/cm^2 · day and those of manganate and titanate types were as low as 10^{-3} g/cm^2 · day, even for samples sintered at 1300°C.

Ceramic solids usually include pores, especially when they are made by a normal sintering process. Since the leach test was performed on bulk samples, open pores directly affect the leach rates. Thus the production of sintered ceramics should eliminate open pores by strict process control. Nepheline-type ceramics with appropriate additives and with 30 to 40 wt.% waste may constitute a solution to the ceramic solidification of HLLW.

Thermal expansion coefficients of the samples were measured. Nepheline types have coefficients of 90 to

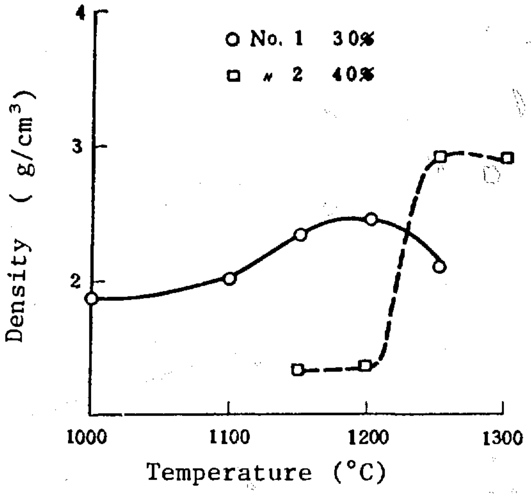

Fig. 3 Change of density with temperature during normal sintering of nepheline-type ceramics with 30 or 40 wt.% waste.

105 x 10^{-7}/°C for solids containing 30 to 40 wt.% waste. Zirconia types have higher values of 130 to 160 x 10^{-7}, manganate types have values of 110 to 150 x 10^{-7}, and titanate types have values of 80 to 120 x 10^{-7}. Thermal expansion coefficients of the solids increase with increasing amount of simulated waste because of the Na_2O content. Thermal expansion of ceramics can be estimated if they are theoretically dense by the additive law of the composite material.

Thermal conductivities of the ceramic products were measured. Dense ceramics of all types show values of 0.01 to 0.015 W/cm · °K. Thermal conductivities of natural rocks are around 0.02, and those of the solids obtained in the present tests are a little lower.

The mechanical strength of the ceramic solids was measured as bending strength on polished samples 5 x 5 x 30 mm. The values obtained for dense ceramics of each type are similar and are in the range of 100 to 200 kg/cm^2, which is close to values of sintered bricks of clay minerals.

PROCESS EVALUATION

The sintering process is generally simple and productive. When hot-pressing is necessary, however, production becomes intermittent and time-consuming. The authors considered this in fabricating the waste-containing ceramics by a simple sintering process. Although the answer is not quite clear yet, the results were encouraging, especially when the waste was sintered with Al_2O_3 and SiO_2 to form nepheline-type ceramics.

The other point to consider is the form of the waste. High-level waste from a reprocessing plant is in the liquid phase, so it is desirable to use HLLW as the starting material and put the additives in it, which will be our next experiment.

SUMMARY AND FURTHER DEVELOPMENT

Tests were performed to develop an alternative solidification process of HLLW from the PNC reprocessing plant. Since the properties of ceramics are expected to be appropriate as a solid form of radioactive waste, ceramic solids were made with simulated waste powder and additive chemicals by normal sintering and hot-pressing. Compositions of the waste-containing ceramics were designed from mineralogical considerations. Four types of compositions were tested: a nepheline type with additives of Al_2O_3 and SiO_2, a zirconia type with ZrO_2, and manganate and titanate types with MnO_2 and TiO_2. The contents of the simulated waste were varied from 20 to 60 wt.%. Sintering tests and characterization of the ceramic samples revealed the following.

- Dense ceramics were obtained by normal sintering at 1300°C and by hot-pressing at 1200 to 1300°C for nepheline and zirconate ceramics. Bulk densities of the solids were better than 90% T.D.
- Bulk densities of manganate and titanate ceramics reach 90% T.D. at a sintering temperature of 1100°C.
- Minor additives such as SrO or NiO have considerable effects on the densification and properties of the ceramic solids.
- X-ray diffraction analysis showed that the expected crystals were formed in nepheline-type solids either by normal sintering or by hot-pressing. X-ray diffraction peaks of other type solids are not well identified.
- Leach rates of nepheline-type solids are on the order of 10^{-5} to 10^{-6} g/cm^2 · day for samples sintered at 1300°C. No samples were fabricated which have leach rates of less than 10^{-4} g/cm^2 · day at 100°C.
- Thermal expansion coefficients, thermal conductivities, and bending strength were measured. Bending strength of the solids was as high as that of the fired clay bricks.

Further development is necessary in order to adopt ceramic solidification as an alternative for the solidification of HLLW. One of the main objectives is to improve the properties of the waste-containing ceramics, especially the chemical durability. The sintering operation and composition of the additives should be refined. For the simple solidification process, HLLW and liquid additives will be examined in the near future.

EMBEDDING METHODS OF SOLIDIFIED WASTE IN METAL MATRICES

W. NEUMANN
Österreichische Studiengesellschaft für Atomenergie Ges.m.b.H., Institute
of Metallurgy, Research Center Seibersdorf, Vienna, Austria

ABSTRACT

The embedding of simulated waste calcines by three different methods---vacuum-pressure casting, centrifugal casting, and metal stirred with the calcines—was investigated. The experimental performance is described and advantages and disadvantages noted. The feasibility of embedding fines by stirring in metal was shown. In addition, an estimation of the influence of porosity on the properties of composites was carried out.

INTRODUCTION

Solidification of high-level liquid waste is the main conditioning procedure for long-term storage. According to the safety requirements in this field, it is necessary to provide containment for the conditioned product. The containment should act as additional protection against damage of the solidified waste by mechanical impact, leaching, and temperature effects.

Vitrified waste cylinders are to be stored in stainless steel canisters in which the glass melt has been poured, as an example. Two additional functions of the container are necessary to store advanced waste products as well as calcined waste granules, i.e., avoiding dispersion and improvement of the release of radiation-induced heat. The latter cannot be provided by a canister alone.

These requirements are best fulfilled by embedding the granules or pellets in a metal matrix. Safety considerations in this field demand a product of very high quality. A careful selection of matrix material and development of suitable embedding methods must be carried out.

MATRIX MATERIAL

In the following tests an Al–12% Si alloy (G–AlSi 12; Al, 12.0 to 13.5% Si; 0.3 to 0.5% Mn, max. 0.4% Fe; max. 0.15% Ti; 0.1% Zn, <Mg, Cu) was used because of its excellent casting properties. Experiments with similar alloys have been conducted in the laboratories of Eurochemic[1] and INEL.[2] Comparative tests with lead (Pb, 2% Sb, <1% Sn) were performed by the use of only one embedding method, i.e., vacuum-pressure casting.

The matrix material has the properties required considering the following functions of the container:

- High corrosion resistance, particularly against water leaching
- High mechanical strength (tensile strength $\sigma_B = 18 \times 10^7$ N/m^2)
- High thermal conductivity ($\lambda = 145$ W/mK)
- Excellent resistance against radiation
- Compatibility with the solidified waste
- Fission product retention
- Temperature resistance (melting point 850°K)

In addition, economic considerations have to be taken into account. The selected matrix material is

- Easily available (commercial alloy G–AlSi 12)
- Cheap (~4.3 $/dm^3)

As far as easy handling and transport are concerned, the following properties exist for this alloy:

- Very good machinability
- Excellent casting properties
- Low specific weight ($\rho = 2.65$ g/cm^3)
- Hard to contaminate and easy to decontaminate

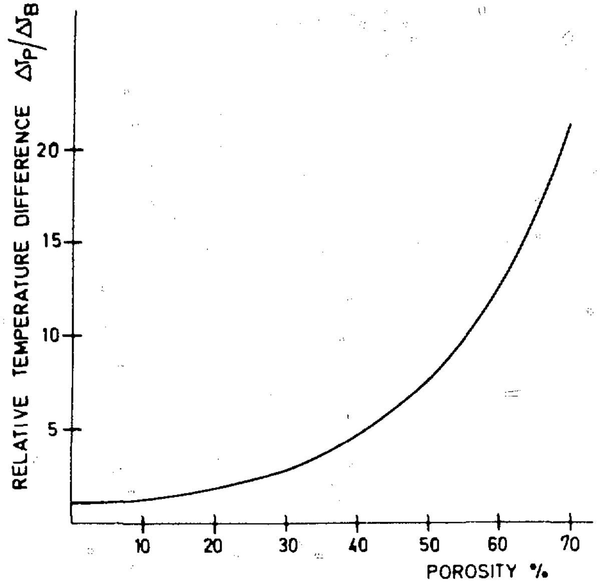

Fig. 1 Calculated difference between centerline and ambient temperature (ΔT_P of porous specimen/ΔT_B of bulk specimen) as a function of porosity.

PROCESS REQUIREMENTS

Running a process with high-level waste requires an embedding method which

- Should be as simple as possible to carry out with automated controls or by remote handling
- Generates little secondary waste by volatilization of radioactive components, dust generation, or contamination of parts of the equipment which must often be replaced
- Fills all the intergranular voids

Regarding the last point the influence of porosity should be noted. The thermal conductivity decreases significantly with increasing porosity. According to these results, the centerline temperature of a waste cylinder increases with increasing porosity (Fig. 1). The estimate of this increase is given by the ratio λ/λ_0 versus porosity, ζ, which was calculated by the use of the following equation

$$\frac{\lambda}{\lambda_0} = \frac{1 - \zeta}{1 + 11\zeta^2} \tag{1}$$

This equation was found to predict the behavior of porous materials, especially metals, and, considering the great difference in thermal conductivity of matrix material and of the ceramic granules, the equation characterizes the conductivity of composites also. Porosity in a composite additionally increases the centerline temperature; e.g., 10% porosity in a 50% metal–50% granule composite raises the temperature from 373 to 450°K.

High porosity is a particular drawback concerning *leach resistance*. The metal matrix acts as an additional barrier against access of a leaching medium. Porosity accelerates the leaching process since less intergranular barriers exist to retain the leaching medium.

The resistance against *mechanical deformation* strongly depends on porosity. Porous Al - Si test specimens showed no elastic deformation. That means small loads produce large plastic deformation by the collapse of the metal bridges between pores. Such deformation may decrease the leach resistance since the intergranular barrier could be destroyed.

EMBEDDING METHODS

Vacuum-Pressure Casting

It was found that the metal did not penetrate all intergranular voids if gravity forces only are used. These results are in close agreement with experiments of Lamb.[2] Even a pressure difference supplied by evacuation of the intergranular spaces could not fill all the voids. An additional driving force was necessary to push the metal melt between all the granules. Very good results could be obtained by increasing the pressure differential by a pneumatically driven piston.

The granules were filled in a crucible made of graphite or high-temperature resistant stainless steel. Solid metal was located above the granules in a crucible. After evacuation and heating by induction, the metal melted and began to fill the large voids first. At this moment the piston suddenly supplied a pressure on the metal surface and forced the melt between the granules. The piston was then removed to avoid subsequent undesired interaction with the metal melt. Cooling coils on the bottom of the crucible made possible a stepwise solidification from bottom to top avoiding shrinkage voids.

Advantages of the method are

- Simple procedure
- Easy to scale up
- Very low porosity of composite
- No shrinkage voids
- Very high granule content

Disadvantages are

- Vacuum required
- Possible contamination of piston surface

This method also allows casting of a protective zone around a nearly perfectly filled metal–granules composite.[3] The casting procedure remained unchanged, but the granules were filled in a cage made of stainless steel screen. Between the cage and the crucible wall a gap was provided to be filled with matrix material during casting. In this manner, a zone free of high-level waste containing granules could be achieved which acts as an additional protective barrier (Fig. 2).

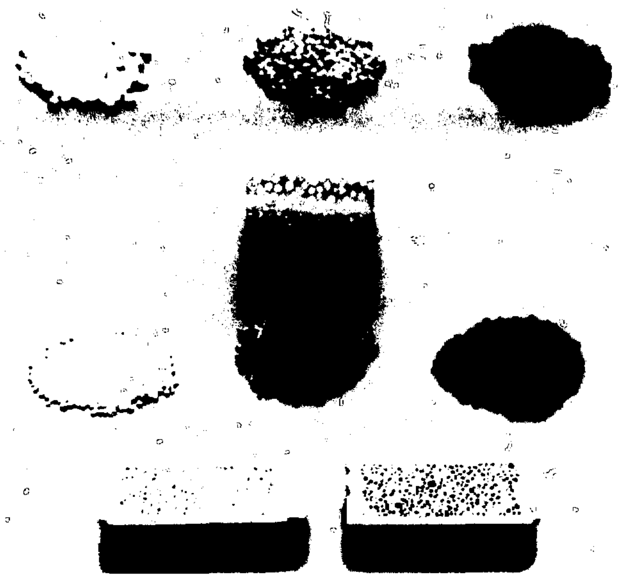

Fig. 2 Various composites with different granules embedded.

Advantages of the composite block with protective zone are

- No welding necessary
- No matrix container interface
- Improved leach resistance
- Improved mechanical strength

Disadvantages of this product are

- Contamination-free zone can be guaranteed only if a minimum granule size is defined
- Additional containment

Centrifugal Casting

The additional driving force described above could also be supplied by rotating the container. In a bench-scale apparatus one crucible was filled with preheated granules, another one with the metal. After metal melting both crucibles were tilted in a horizontal position and pushed in rotation around a perpendicular axis, so the metal was forced out of the melting crucible and into the mold with the granules. The gas in the intergranular voids was simultaneously pushed away if vacuum was not supplied. This method is usually carried out in practice by goldsmiths. An internally mounted grid prevented segregation due to centrifugal effects, which would occur because of the different specific gravities of porous granules ($\rho = 1.4\ \mathrm{g/cm^3}$) and metal ($\rho = 2.65\ \mathrm{g/cm^3}$). The grid can be replaced by a screen cage mentioned previously.

Annular waste cylinders could be produced by a similar centrifugal casting technique like casting of tubes.

Advantages of this method are

- Almost non-porous composite (Fig. 3)
- Very high granule content
- No vacuum necessary
- Possibility to cast various forms

Disadvantages are

- Maintenance of centrifuge
- Difficulties in scaling up
- Difficult handling

Thixo Casting

The experimental work with vacuum pressure casting represents a further development of this method. Studies with centrifugal casting apply a well-known technique to the problems under consideration. The following method is based on a newly developed embedding technique. The granules were stirred in the metal melt.

In all the casting techniques the great difference in density between metal and waste calcines causes segregation. Therefore an inhomogeneous distribution in the composite will occur unless a mechanical obstacle prohibits the driving up of the granules. But fines cannot be retained by a screen or other device. The problem to be solved using this method is the conditioning of calcined fines.

A chance to keep the calcines homogeneously dispersed in the metal seems to exist only if a high viscous, almost pasty metal melt (such as the state of metal used in thixocasting) delays the driving up until solidification occurs. The problem which remains is the initial dispersion of the calcines in the melted matrix. A possible solution seems to be stirring the fines together with the granules by a mechanical stirrer.

The feasibility of this method to achieve a homogeneous distribution was experimentally tested by stirring the fines together with the granules. Calcines (32% granules, 12% fines) were heated by induction together with the AlSi alloy. At a temperature of a few degrees above the melting point the mechanical stirrer mixed the components until all calcines were surrounded by metal. Then cooling started and solidification began immediately. The first results were encouraging, and further tests were performed with various types of stirrers to improve the dispersion. A stirrer like a feeding screw transported the fines in the melt

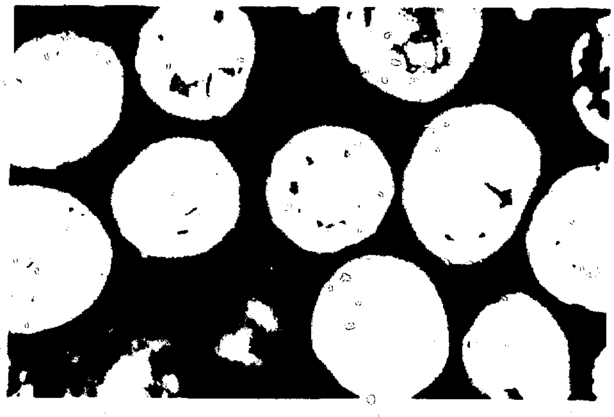

Fig. 3 Calcined granules in an AlSi matrix.

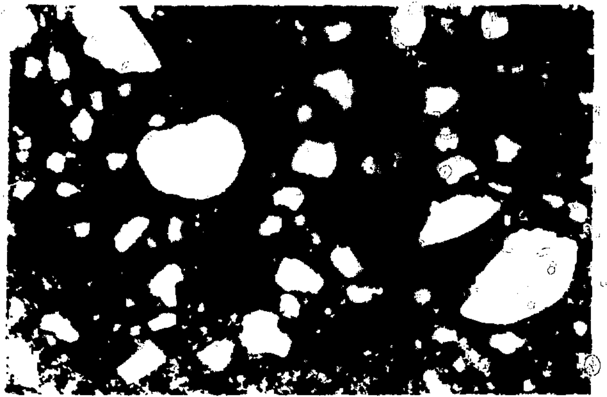

Fig. 4 Composite containing fragments as well as fines.

very well; nevertheless better results could be obtained with a stirrer which looked like a kneading hook.

Of course there are many problems left, so that extended test series are necessary to get the process ready for a "hot running."

Advantages of this method are

- Simple procedure
- No vacuum required
- Fines could be embedded (Fig. 4)
- Easy to scale-up

Disadvantages are

- Contamination of the stirrer
- Porous composite
- Restricted calcines content

REFERENCES

1. J. Van Geel, H. Eschrich, and F. Detilleux, Conditioning of Solid High Level Waste Products by Dispersion into Metal Matrixes, in *Radioactive Waste from the Nuclear Fuel Cycle,* AIChE Symposium, Vol. 72, Series 154, R. A. Tomlinson (Ed.), 1976.
2. K. M. Lamb, *Final Report, Development of a Metal Matrix for Incorporating High-Level Commercial Waste,* DOE Report ICP-1144, Idaho National Engineering Laboratory, 1978.
3. K. Brichta and W. Neumann, *Metal Embedding of Simulated HLW-Granules* (in German), SGAE-Report-2850, Austrian Atomic Energy Research Ltd., Vienna, 1977.

DEVELOPMENT OF CERMETS FOR HIGH-LEVEL RADIOACTIVE WASTE FIXATION

W. S. AARON, T. C. QUINBY, and E. H. KOBISK
Solid State Division, Oak Ridge National Laboratory, Oak Ridge, Tennessee

ABSTRACT

A method is currently under development for the solidification and fixation of commercial and defense high-level radioactive wastes in the form of ceramic particles encapsulated by metal, i.e., a cermet. The chemical and physical processing techniques which have been developed and the properties of the resulting cermet bodies are described in this paper. These cermets have the advantages of high thermal conductivity and low leach rates.

INTRODUCTION

A program has been initiated to develop and evaluate an alternate high-level radioactive waste fixation method which yields a cermet waste form. This method is based on technology previously developed for the preparation of special ceramic neutron dosimetry materials.[1] Only minor adaptations were required for the application of this process to the solidification and fixation of high-level wastes as cermets.[2] Both the processing method and the resulting product possess unique and advantageous features. Significant waste volume reductions together with high waste loadings and low process volatility losses of fission product radioisotopes have been realized in our experiments. The cermet form possesses high thermal conductivity, good leach resistance, durability, and high mechanical strength.

This cermet waste form fixes most of the radioactive elements in wastes as micron-size particles of crystalline ceramic oxides, aluminosilicates, or titanates, all uniformly dispersed in a metal matrix. The metal matrix is composed of hydrogen-reducible metals already present in the waste or added to formulate an alloy composition providing high thermal conductivity and resistance to corrosive environment such as those encountered in suggested geologic repositories. High mechanical strength and corrosion and leach resistance make this cermet a nearly ideal shipping form. The ceramic phases provide a first level of waste fixation, while the metal alloy phase of the cermet microencapsulates the ceramic particles and provides a second level of fixation.

CERMET PROCESSING

The basic process for this cermet formation has been reported;[3,4] however, significant process modifications have been made in recent months. A flow sheet for laboratory-scale, batch processing is shown in Fig. 1, where each operation is performed as an individual step. Shown in this flow sheet are the additive materials and subsequent products generated during processing. Developmental efforts now in progress should simplify the cermet preparative process so as to be amenable to continuous full-scale operations as illustrated in the abbreviated flow sheet, Fig. 2.

The first step in this process involves dissolution of the waste and of specific additives required for the formulation of the desired ceramic phases and the metal alloy matrix. Dissolution can be accomplished in nitric acid or, if the metal additives are in a soluble form, directly in molten urea. When dissolution is performed in nitric acid, the solution is concentrated by heating, and then urea is added. After the waste and additives are in solution in molten urea, the precipitation and calcination steps can be simultaneously performed by injection of the urea solution into a rotary calciner. The resulting calcine has been found to be somewhat agglomerated. Therefore, a spray calciner is now

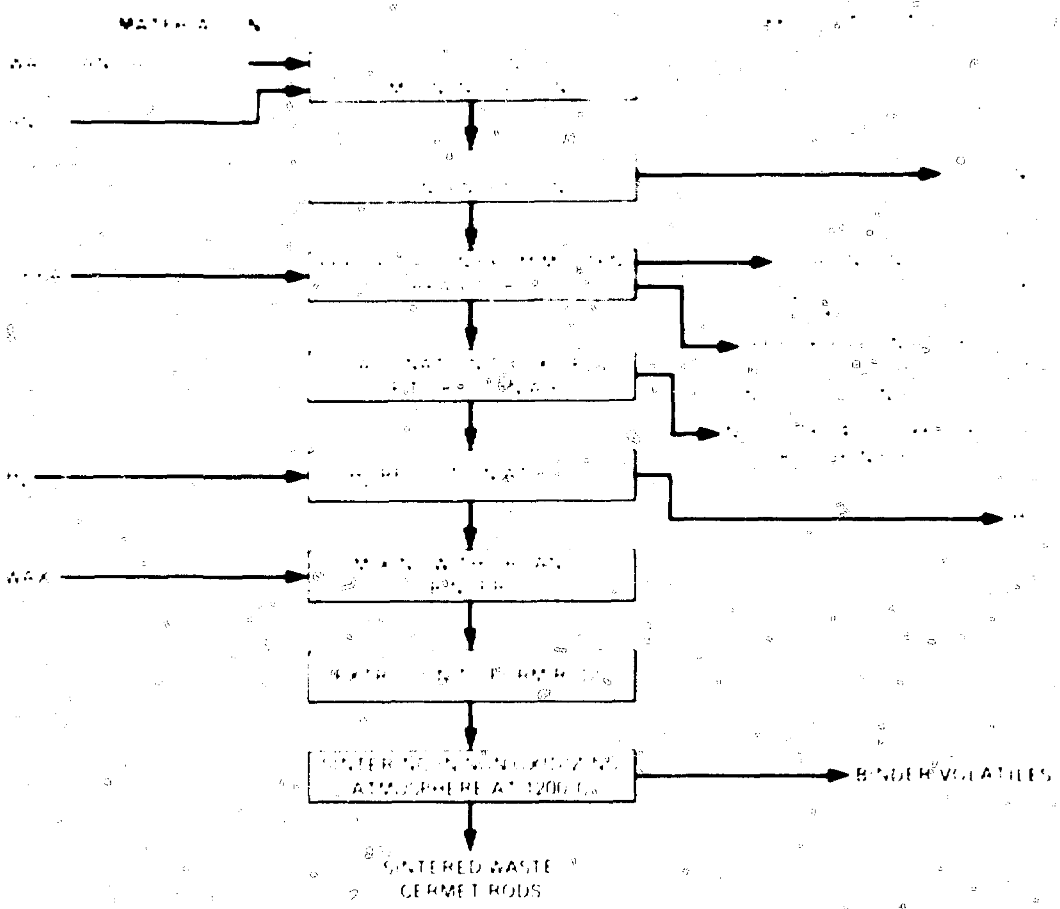
ATMOSPHERE AT 1200 C
BINDER VOLATILES
SINTERED WASTE
CERMET RODS

Fig. 1 Laboratory-scale operations used to produce cermet storage forms from high-level waste.

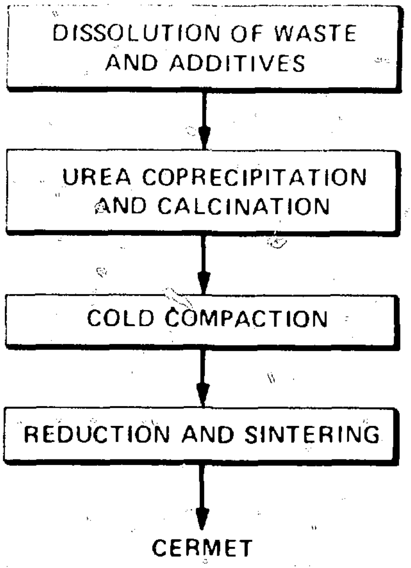
DISSOLUTION OF WASTE AND ADDITIVES
UREA COPRECIPITATION AND CALCINATION
COLD COMPACTION
REDUCTION AND SINTERING
CERMET

Fig. 2 Process improvements simplify preparation of cermet high-level waste forms.

being fabricated which should yield a calcine powder that can be readily densified.

Subsequent to calcination, the powder is compacted by extrusion or pressing into any of a variety of shapes. Water is now used as a binder because it has the advantage of being more easily removed from the compact during sintering than were the previously used organic binders. In the final processing step the reducible metal oxides, such as oxides of copper, nickel, iron, cobalt, etc., are reduced in a H_2 or CO atmosphere to metal and form an alloy which encapsulates the unreduced ceramic oxides. Thus, the final form has a metallic appearance, and this cermet is the storable form. Recent developments in our cermet sintering technology have very significantly reduced the required sintering times and temperatures.

Several aspects of this process, outlined by the flow sheets, merit further discussion. Throughout the chemical and physical processing steps, volatility losses of cesium, strontium, and particularly ruthenium are very low. In processing various simulated or actual wastes the maximum volatility losses encountered were 0.27% for cesium, 0.23%

[illegible] (SRP) [illegible] composition [illegible] described would require between 100 and [illegible] 10 tons of added nickel and between 40 and 700 tons of added copper. It can be seen that these amounts of metal additives required for the solidification of this large amount of waste into cermet are a reasonably small portion of the current and projected contaminated metal inventories.

CERMET CHARACTERIZATION AND EVALUATION

Cermet characterization and testing experiments are at various levels of completion. The largest effort has been performed on simulated waste cermets designed to represent Nuclear Fuel Services (NFS) acid Thorex waste, SRP sludge and acid wastes, and the projected Barnwell wastes. Simulated wastes containing key radiotracers, such as ^{137}Cs, ^{106}Ru, and ^{89}Sr, are being used to evaluate volatility losses during processing and the leachability of resultant cermets as a function of processing parameters. One experimental conversion of each of three high-level wastes, i.e., SRP sludge, SRP untreated acid, and NFS acid Thorex, has been performed in hot cells, and the resulting cermets are being evaluated.

Extensive observations on typical cermet samples by optical and SEM metallography have been made. The [illegible] NFS [illegible] SRP [illegible] 0.0 [illegible] W [illegible] were [illegible] respectively. The SRP waste had been out of the reactor approximately 8 months when it was processed to form a cermet. Using the latter "worst case" heat content, a cermet 0.152 m in diam × 3.048 m in length would have a calculated center-to-surface temperature difference of 29°C.

A variety of leach tests[8] have been performed on radiotracer-containing simulated wastes at ORNL and Pacific Northwest Laboratory (PNL). While the data obtained in these tests indicate low cermet leachability, the results are preliminary. Refined cermet leach testing techniques to generate quantitative leach data are being developed at ORNL. In the series of leach tests performed at PNL, all tests but one were complicated by galvanic coupling between the cermet samples and various metals within the different leach testing apparatus. The one meaningful experiment was a 3-day Soxhlet test which showed a cermet weight loss of 0.002%, corresponding to a calculated leach rate of 7×10^{-6} g cm^{-2}/d. Results based on ^{137}Cs analyses showed a total cesium release of 0.024%, while no ruthenium was detected as having leached in this test. This Soxhlet test was the only one for which data are available for comparison with a glass waste form. During identical Soxhlet testing of 78-68 glass at PNL, a rate of 2×10^{-4} g cm^{-2} d was determined using a weight loss method.[7] No value for cesium release during this test was

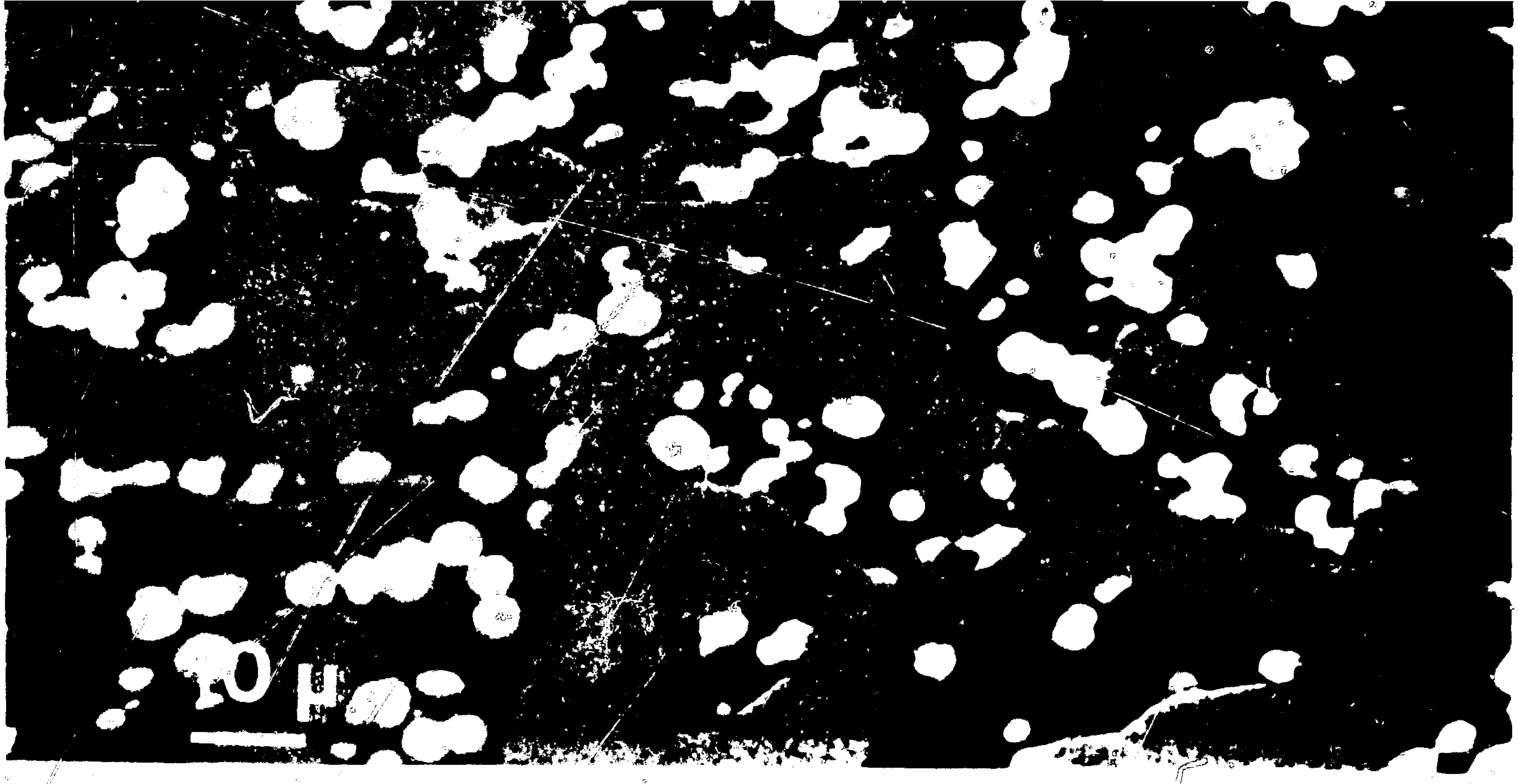

Fig. 3 SEM micrograph of a cermet formed [illegible]

ACKNOWLEDGMENTS

SUMMARY

[illegible] radioactive waste forms. Simulated waste [illegible] volatility [illegible] during processing and high waste loadings have been achieved in the formation of cermet from a variety of simulated and real high-level waste. The resulting cermet waste form possesses high thermal conductivity, mechanical strength, and a leach resistance and durability which appear to be comparable or better than the vitreous waste form. Continued refinement and development of the cermet processing techniques and in the evaluation and quantification of cermet properties are proceeding.

REFERENCES

[illegible]

D. B. Wa[illegible] Op[illegible] B[illegible] Operat[illegible] Dig[illegible] DOE/ORO [illegible] Ap[illegible] 1979.

6. *Alternatives for Long-Term Management of Defense High-Level Radioactive Waste*, ERDA 77-42/1, Vol. 1, Savannah River Plant, May 1977.

7. J. H. Westsik and R. P. Turcotte, *Hydrothermal Reactions of Nuclear Waste Solids, A Preliminary Study*, U. S. DOE Report PNL-2759, Pacific Northwest Laboratory, September 1978.

DENSIFICATION OF CALCINES AND DIRECT CONTAINMENT OF SPENT NUCLEAR FUEL IN CERAMICS BY HOT ISOSTATIC PRESSING

[illegible]

ABSTRACT

[illegible]

[illegible] In this paper [illegible] of the method will be discussed as well as some results from corrosion studies and the problems of obtaining relevant long-term corrosion data.

INTRODUCTION

Crystalline synthetic minerals have been suggested by several researchers as very suitable hosts for the immobilization and containment of radioactive waste, and McCarthy[1] gives a good overview. Minerals of high chemical stability often have very high melting points, consequently, fabrication of dense waste forms by conventional methods (e.g., sintering or melting) has obvious limitations regarding product quality and environmental factors in the processing plant. Good densification is important, as calcined powders of the desired mineral compositions containing the waste elements can have ten thousand to one million times more surface area per kg than a fully dense block of the same material and thus would have correspondingly higher total dissolution rates. The use of hot isostatic pressing (HIP) for consolidation and containment of nuclear waste into "rock-like solids" with the "immutability of the most stable minerals" has been suggested.[2] The relatively high pressure used in this pressing technique, as well as the three-dimensional application of pressure, makes it very

HOT ISOSTATIC PRESSING OF REPROCESSING WASTES

Hot isostatic pressing can be applied to produce dense blocks of a wide range of particulate wastes. Some examples are given in Fig. 1. Starting material could be different types of synthetic mineral assemblages.[3-6] It could also be fuel hulls in a suitable matrix (e.g., mullite), undissolved residues from the fuel dissolution tanks in a reprocessing plant, or ashes obtained by incineration of different organic radioactive materials. Each of these substances can be dried, optional mineral forming additions can be made, and the material can be filled into metal containers which are finally evacuated and welded tight. If the material has been dehydrated and denitrated at 900°C or higher, evacuation can be made cold or omitted. Alternatively, final evacuation is made at 750 to 800°C. A container with its content is then treated by HIP to a fully dense body with a minimum of active surface and in a form suitable for long-term storage. An important feature of the HIP process from an environmental point of view is that the metal container with the waste products can be hermetically sealed at a comparatively low temperature. The

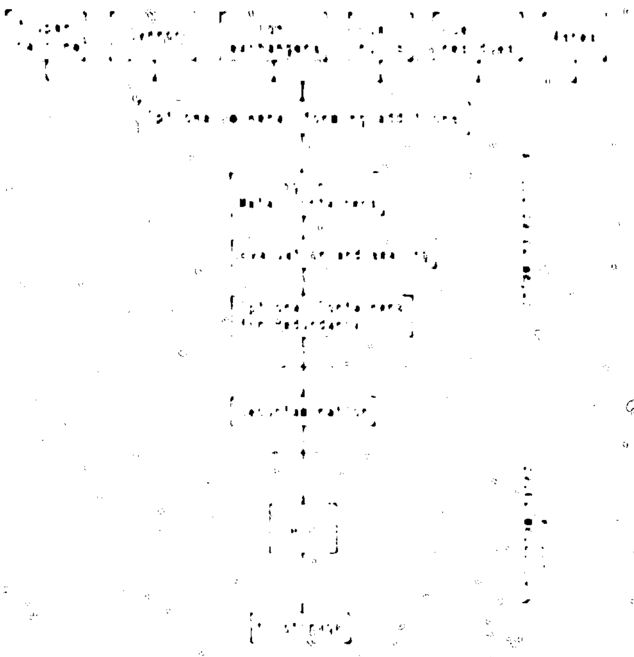

Fig. 1 [illegible]

heating up to the temperature for the final compaction is then done with the support of a high outside pressure in a gas tight container preventing any release of radioactive dust or fumes. This is a problem in conventional sintering or hot pressing and also in waste glass fabrication. Furthermore, the temperature needed for full densification can be kept low due to the action of the high pressure.

The only mechanism causing contamination of the hot isostatic pressing equipment is a leakage of the metal container, e.g., in a weld. The high pressure gas can then penetrate, and, when pressure is lowered, it can carry material out, contaminating the equipment. In order to bring the probability of this event down to an extremely low level, a number of independently sealed metal containers can be arranged one outside the other before the HIPing. This can be done without much sacrifice of space in the equipment, and the separate metal layers will, during the pressing process, bond together to one thicker metal envelope. Figure 2a shows a typical microstructure of simulated waste of type PW-4b treated to supercalcine (McCarthy[3]) and HIPed to full density (4.28 g/cm^3). It contains about 70% fission products. As the heat generation from such a product would be quite high, one possibility is to distribute the material in an array of axial holes in a metal cylinder, e.g., copper. After filling the holes with supercalcine powder a thick metal lid would be emplaced and an outer metal envelope hermetically sealed. During the HIP process the supercalcine would be fully densified and in intimate contact with the copper structure for good heat dissipation. A compact multibarrier waste form could be made in a single operation. Another possibility is to use a ceramic matrix to obtain microencapsulation of the supercalcine grains. Figure 2b shows a supercalcine in an aluminium silicate matrix. The fission product content is 21%.

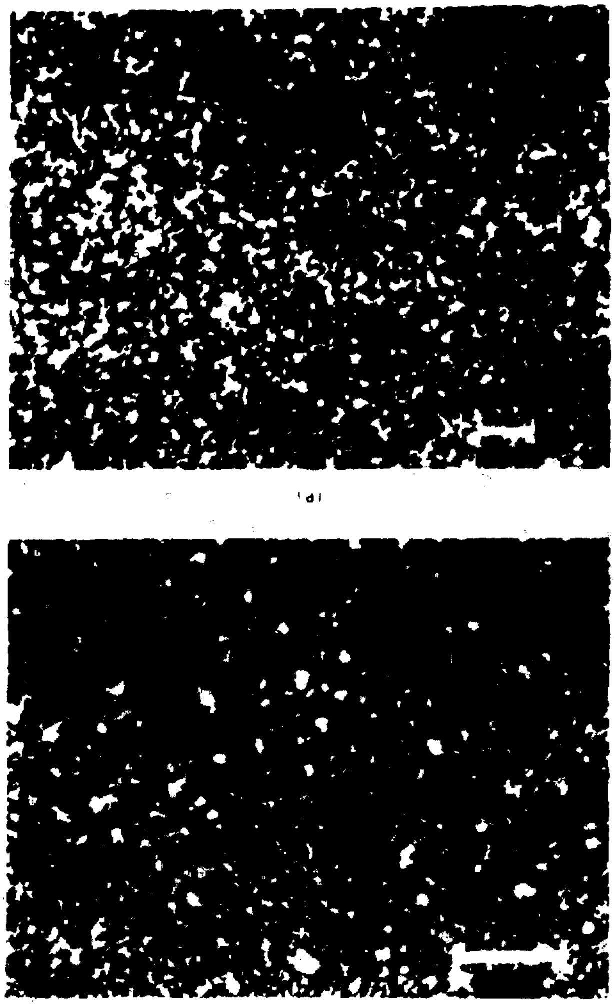

(a)

(b)

Fig. 2 Microstructure of supercalcine after hot isostatic pressing to full density. (a) without additions, (b) mixed in proportion 30/70 with mullite

Standard 72-hour Soxhlet leaching tests on crushed crystalline materials appear to give much higher leach rates than relevant for long-term corrosion. Results from investigations of this for aluminium oxide are discussed later in this paper. However, bearing this in mind a typical result might be of interest. Table 1 gives some values for a 30% supercalcine of a PW-4b 70% mullite mix HIPed to full density (3.53 g/cm^3). The fission product content was 21%. The material was crushed, and a fraction 250 μm to 350 μm was sieved out. The specific surface measured by BET was 1500 cm^2/g (which is much higher than for glass but supported by SEM studies of both materials). The higher leach rates obtained for the fission products than for the

TABLE I

[illegible]

[illegible] leach rates [illegible]

A [illegible] another [illegible] than the first [illegible] period [illegible] reported below [illegible] rates several orders of magnitude [illegible] in Table I are expected (at 100 C) [illegible] leach rates will [illegible] be obtained.

CANISTERS FOR SPENT NUCLEAR FUEL

In direct deposition of spent fuel rods the time until the waste elements have decayed to unharmful levels is very long. A canister with ability to isolate the content from the surrounding geologic media during these time periods gives, in addition to the *geologic barrier*, a redundancy that might be desirable or required. The principal design of such a container of a synthetic mineral is shown in Fig. 3. A mineral called corundum or sapphire, α-Al_2O_3, has been selected as the most suitable material because of its availability, good physical properties, and excellent chemical corrosion resistance.

With support from the Swedish utilities an intensive development program to demonstrate the feasibility of using such materials in canisters of the required size has been carried out.[7] A high-purity raw material (more than 99.8% Al_2O_3) was selected in order to be able to compare the properties of the synthetic material with the natural mineral. The feasibility study has shown that it is possible to make such canisters of fully dense material (more than 99.5% TD) using HIP (Fig. 4). The canister has an ID of 0.3 m and a 100-mm-thick wall. It can contain 150 BWR rods or about 400 kg uranium oxide. The total length of

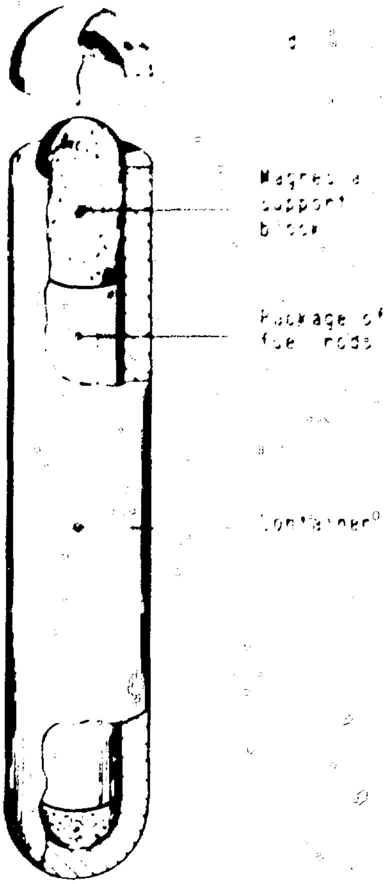

Fig. 3. [illegible]

the canister is about [illegible]. When the spent fuel has been placed inside the canister the lid is joined to the canister by a special high-pressure diffusion process using no additives. The surfaces are prepared for joining by diamond grinding, and a pressure of about 1000 atm at a temperature of 1350 C for 2 to 5 hours has been used for this bonding operation. Test bars cut out by a diamond saw across the joint of half-scale canisters show that the mechanical strength of the joint (373 ± 55 MN/m^2) is comparable to the strength of the lid (370 ± 45 MN/m^2) and the container wall (389 ± 22 MN/m^2). The tests were made in 3-point bending with 20 mm span on 3- × 3- × 48-mm test bars.

Attempts to determine the corrosion rate in groundwaters of typical composition in the Swedish bedrock (pH 7 to 9) have been carried out with a number of techniques in Sweden and abroad. An objective of these tests would be to compare the synthetic corundum material with the natural mineral. Data from the natural occurrences of corundum in alluvial materials, and particularly in laterites, show the long-term stability of alumina. Corundum hardly seems to weather at all even in heavily leached lateritic soils which it is known took of the order of 10 million years to form.[8]

Fig. 4 [illegible] being fitted to full scale, OD [illegible] m by [illegible] m long synthetic corundum canister

One difficulty in short-term corrosion studies apart from the very small effects that have to be measured is that, at 100°C or below, it may take years to take off the surface layers disturbed by sample preparation and obtain relevant steady-state corrosion rates. It is well-known that grinding or crushing processes can activate materials, e.g., by causing high dislocation densities or highly reactive points on crystals. The study of the low temperature solution of quartz by Morey et al.[9] illustrates this very clearly. For standard Soxhlet tests of HIPed α-Al_2O_3, the samples consisted of crushed material in the size range 250 to 350 μm. The surface area of typical samples was 400 cm^2/g as determined by standard BET measurements. With some samples an attempt was made to simulate aging by pretreating the crushed material in an autoclave at 140°C for 30 days in a sodium carbonate solution (10 mM CO_3^{2-}, pH 10.5 at 25°C). A stainless steel screen envelope containing approximately 1 gram of such a sample was used. The Soxhlet leaching was performed at ~100°C with the 10 ml cup drained every sixth minute. The tests were interrupted at regular intervals (minimum 3 days), and weight changes were measured. Figure 5 shows total corrosion and corro-

[illegible]

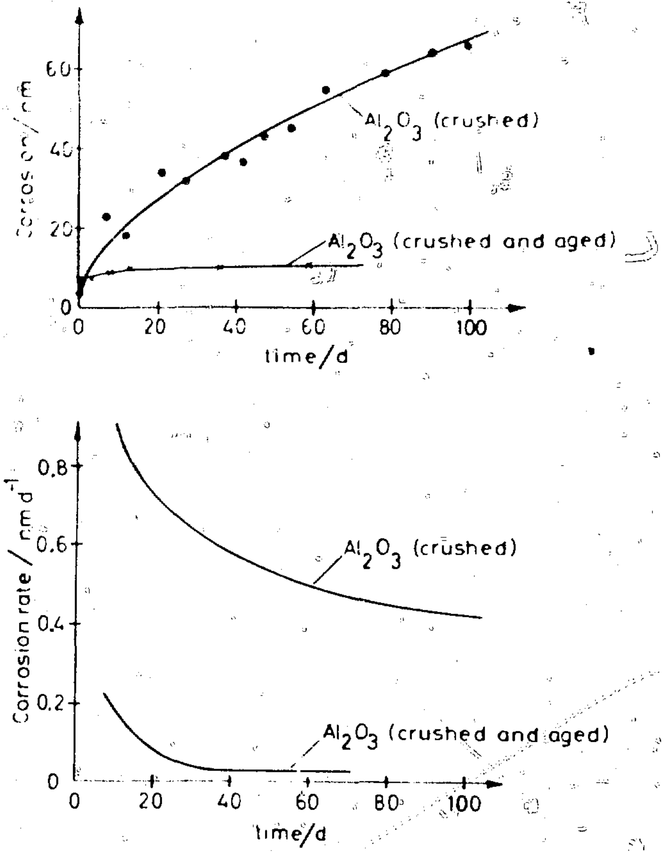

Fig. 5 Apparent corrosion and corrosion rate as function of time of hot isostatically-pressed α-Al_2O_3 (>99.8% Al_2O_3), density 3.974 g/cm^3, in Soxhlet leach testing (~100°C). Both as crushed and crushed and aged samples (by autoclaving in a carbonate solution) have been tested.

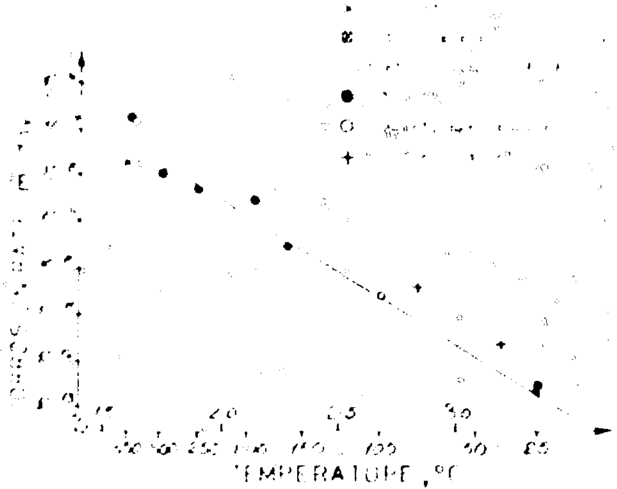

Fig. [illegible]

[illegible] with the synthetic material.

[illegible] that the synthetic material and the natural material behave in a similar way. From the results, which are not sensitive with respect to water chemistry, it follows that a 100-μm wall would require between 30 million year at 100°C and [illegible] billion year at 25°C for total corrosion. However, what would happen in groundwater is rather a transformation of the wall to another mineral. In a groundwater typical for a Swedish repository kaolinite, which is thermodynamically stable in this environment, would be formed. As this mineral is present with a very large exposed surface in the clay used as an overpack, dissolution rates in the groundwater of the kaolinite layer on the canister will be negligible.

REFERENCES

1. [illegible]
2. [illegible]
3. [illegible]
4. [illegible]
5. [illegible]
6. [illegible] B. F. K[illegible] [illegible] *Management of Radioactive* [illegible] IAEA [illegible]
7. *Handling and Final Storage of Unreprocessed Spent Nuclear Fuel*, [illegible] November 1978, available from Project KBS, Box 5864, S-102 48 Stockholm 5, Sweden.
8. B. J. K[illegible], W. S. Fyfe, and O. H. Leonardos, Jr., The Chemistry of Some Brazilian Soils: Element Mobility During Intense Weathering, *Chem. Geol.*, 1979 (in press).
9. G. W. Morey, R. O. Fournier, and J. J. Rowe, The Solubility of Quartz in Water in the Temperature Interval from 25°C to 300°C, *Geochim. et Cosmochim. Acta*, 26: 1029 (1962).
10. N. Ingri and L. O. Öhman, *Determination of the Corrosion Rates for Al_2O_3 in Carbonate Buffered, Chloride Containing Water at 80°C resp 40°C and pH 8.5* (in Swedish), Department of Inorganic Chemistry, University of Umeå, Sweden, January 1979.
11. D. J. Hydes and P. S. Liss, Fluorometric Method for the Determination of Low Concentrations of Dissolved Aluminium in Natural Waters, *Analyst*, 101: 922 (1976).
12. W. S. Fyfe, *Corrosion Rate of Al_2O_3* in Aqueous Solutions from 25 to 350°C, Geology Department, University of Western Ontario, Canada, November 1978, available from Project KBS, Box 5864, S-102 48, Stockholm 5, Sweden.
13. W. S. Fyfe and M. A. Hollander, Equilibrium Dehydration of Diaspore at Low Temperatures, *Am. J. Sci.*, 262: 709 (1964).

IMMOBILIZATION OF HIGH-LEVEL WASTES IN SYNROC TITANATE CERAMIC

A. E. RINGWOOD and S. E. KESSON
Australian National University, Canberra, Australia

ABSTRACT

The elements occurring in high-level nuclear reactor wastes can be safely immobilized by incorporating them within the crystal lattices of the constituent phases of a titanate ceramic, SYNROC. Close structural analogs of these phases ("hollandite," perovskite, and zirconolite) occur in nature and have survived for periods of 20 to 2000 million years in geological conditions far more extreme than would be encountered in any proposed radwaste repository. Moreover, ancient natural zirconolites, although metamict, appear to have successfully immobilized U and Th for periods exceeding 500 million years despite alpha-particle fluxes far more intense than those likely to be received by the titanate ceramic. Accelerated leaching tests in water and saline solutions show that SYNROC is unaffected after 24 hours at extreme conditions (up to 900°C and 5000 bars), whereas borosilicate glasses decompose within a few hours under much less severe hydrothermal conditions (e.g., 350°C and 1000 bars). The combination of these leaching results with the geological evidence for long-term stability indicates that SYNROC should be vastly superior to borosilicate glass in its capacity to safely immobilize high-level wastes.

A variant of the SYNROC process appears to be particularly well-suited for immobilization of U. S. military wastes. The modified ceramic waste form consists of the three major SYNROC phases (hollandite, perovskite, and zirconolite) plus a variety of refractory Fe–Al–Mn bearing titanates and spinels, which are thermodynamically compatible with the SYNROC phases. The SYNROC phases serve to immobilize fission products and actinides, while the additional refractory phases serve to immobilize the Fe–Al–Mn oxides, which constitute a very large proportion of the calcined sludges. These additional phases include pseudobrookite (Al_2TiO_5 $FeTi_2O_5$ ss), hercynite ($FeAl_2O_4$), ulvospinel (Fe_2TiO_4), ilmenite ($FeTiO_3$), and "BAIT" (essentially $BaAl_2Fe_8Ti_{13}O_{38}$). Waste-loadings about 4 times higher than those of glass could readily be achieved, offering considerable economic and safety benefits relative to glass technology.

INTRODUCTION

The safe immobilization of high-level wastes (HLW) resulting from reprocessing of spent nuclear fuel requires their isolation from the biosphere for periods of 10^5 to 10^6 years. It is widely assumed that this objective can be achieved by burial of the wastes in an appropriate geological repository. However, because repository integrity cannot be guaranteed with certainty over these very long periods, it is essential to provide an additional isolation barrier based on the stability of the waste form itself. We will demonstrate below that titanate ceramics produced by the SYNROC process constitute exceptionally inert and resistant waste forms and can serve as the primary barrier preventing the contamination of the biosphere.

INCORPORATION OF HLW IN CERAMIC MATERIALS

Borosilicate glasses containing up to 25% HLW are currently candidates for immobilization media; however, there is an increasing body of evidence to suggest that they are far from being optimum materials for this purpose. Borosilicate glasses readily devitrify and alter[1-3] in a period of days when subjected to modest hydrothermal conditions (water pressure of 300 to 1000 bars; temperatures 300 to 400°C). Alteration is accompanied by a deterioration of mechanical properties and an increase in the leachability of highly dangerous species such as cesium and actinides. Detailed studies show that glass-alteration mechanisms are complex and nonlinear, thereby making it difficult to predict the long-term stability of glass with respect to devitrification in a geological repository at lower temperatures (100 to 150°C).

Because ceramic waste forms consist of equilibrium assemblages of thermodynamically compatible phases, they are not prone to devitrification and its accompanying problems. Moreover, in certain cases, e.g., SYNROC, the long-term integrity of the waste form can be guaranteed with a high degree of confidence because the constituent phases are analogous to natural minerals which have survived a wide range of geological conditions for millions of years while retaining HLW elements in their crystal lattices.

INCORPORATION OF HLW IN SYNROC

Ringwood[4] outlined a process whereby HLW elements were immobilized as dilute solid solutions (i.e., as integral parts of the crystal lattices) in the constituent minerals of SYNROC ceramics and demonstrated that waste loadings of 10% were readily accommodated. When a mixture of oxides with the bulk composition shown in Table 1 is hot-pressed at 1200 to 1300°C and under mildly reducing conditions, it recrystallizes to form a unique titanate ceramic comprising three main phases: hollandite, perovskite, and zirconolite. The phase chemistry of SYNROC has been well characterized by detailed electron microprobe studies. Analyses of typical SYNROC phases are given in Table 1.

Our experiments have shown that almost the entire spectrum of HLW elements can be incorporated in the above three phases and in a few minor accessory phases.[3] This behavior is readily explained and understood in terms of the well-established principles of crystal chemistry. The structure of hollandite ($BaAl_2Ti_6O_{16}$) is similar to that of rutile, but there are also tunnels in one direction where very large cations, e.g., K^+, Ba^{2+}, Rb^+, Cs^+, and Pb^{2+}, may be accommodated. Moreover, many species in appropriate valence states, including Mg^{2+}, Co^{2+}, Ni^{2+}, Cu^{2+}, Fe^{2+}, Mn^{2+}, Cr^{3+}, Rh^{3+}, Te^{4+}, Mo^{4+}, Ru^{4+}, Sn^{4+}, and Zr^{4+}, are capable of replacing Ti and Al in the octahedrally coordinated lattice sites. Perovskite ($CaTiO_3$) is also capable of taking a wide range of elements into solid solution. The calcium site may contain Na^+, Sr^{2+}, Ba^{2+}, Cd^{2+}, REE^{3+} (rare earths), Y^{3+}, Cm^{3+}, Am^{3+}, and Pu^{3+}, while the titanium site may be occupied by Fe^{3+}, Al^{3+}, Cr^{3+}, Rh^{3+}, Pd^{4+}, U^{4+}, Sn^{4+}, Te^{4+}, Zr^{4+}, Mo^{4+}, and Nb^{5+}. Zirconolite ($CaZrTi_2O_7$) processes a structure related to that of pyrochlore, and a wide range of substitution is possible. The eight-fold sites may contain Na^+, K^+, Ca^{2+}, Sr^{2+}, Ba^{2+}, Pb^{2+}, Y^{3+}, REE^{3+}, Bi^{3+}, Zr^{4+}, U^{4+}, and Th^{4+}, while Ta^{5+}, Nb^{5+}, Fe^{3+}, and Mn^{3+} can substitute in the six-fold sites. Some ancient natural zirconolites have successfully trapped the equivalent of up to 100 bars helium in their crystal lattices for periods exceeding 500 million years. Phosphorus does not enter any of the three major phases of SYNROC but instead forms minor amounts of an orthophosphate phase, $(Ba,Ca)_3(PO_4)_2$. The SYNROC process operates under mildly reducing conditions, whereby ruthenium, rhodium, palladium, and tellurium are reduced to the metallic state (Te as NiTe). Detailed microprobe studies of the materials produced in our partition experiments have established that many fission products (including Cs, Rb, and Ba) are immobilized as dilute solid solutions within the hollandite phase, and that perovskite is the host for Sr. The actinides and REE are preferentially accommodated in zirconolite and, to a much lesser extent, in perovskite (see Table 2).

Structural analogs of the three major SYNROC phases occur in nature and are known to have survived unaltered for millions of years in conditions far more extreme than would be encountered in any radwaste repository. It is this fact which gives us a high degree of confidence in the long-term integrity of the SYNROC ceramic waste form.

TABLE 1

Model Bulk Composition of SYNROC Titanate Ceramic and Typical Chemical Compositions of Constituent Phases*

	SYNROC	Hollandite	Zirconolite	Perovskite
TiO_2	60.4	73.2	48.4	58.1
ZrO_2	9.9	0.3	32.0	0.5
Al_2O_3	11.0	12.6	3.3	0.3
CaO	13.9	0.3	16.1	41.1
BaO	4.2	12.3		
NiO	0.6	1.5		
Total	100.0	100.2	99.8	100.0

*Waste-loading is zero.

ACCELERATED LEACHING TESTS ON SYNROC AND OTHER WASTE FORMS

The relative stabilities of various waste forms were compared in our laboratory by means of accelerated hydrothermal leaching in H_2O and 10 wt.% NaCl solution at temperatures of 300 to 1000°C and pressures from 300 to 500 bars. Borosilicate glasses were found to disintegrate in less than 24 hours at 350°C and 1000 bars, and extensive losses of HLW elements were observed.[2,3] The phase pollucite ($CsAlSi_2O_6$), which is the host for Cs in both "supercalcine"[5] and the Sandia high-Ti ceramic,[6] likewise decomposes between 400 to 600°C in dilute saline solutions. On the other hand, the SYNROC titanate ceramic proved to be remarkably resistant to leaching, surviving unaltered in the extreme conditions of 900°C and 5000 bars. Electron probe microanalysis confirmed that the hazardous species Cs, Sr, and U were quantitatively retained by the hollandite, perovskite, and zirconolite phases, respectively. Moreover, no ion-exchange processes occurred in saline solutions. The remarkably inert nature of the

TABLE 2

Experimental Data Showing Host Phases for Principal HLW Elements in SYNROC

Major Phases

Hollandite ($BaAl_2Ti_6O_{16}$)	Zirconolite ($CaZrTi_2O_7$)	Perovskite ($CaTiO_3$)
[illegible]	[illegible]	[illegible]
[illegible]	[illegible]	[illegible]
[illegible]	[illegible]	[illegible]
[illegible]	[illegible]	[illegible]
[illegible]	[illegible]	

Accessory Phases

[illegible]

[illegible]

SYNROC [illegible] M[illegible] O[illegible] SYNROC [illegible] SO[illegible] W[illegible] SYNROC [illegible]

RADIATION DAMAGE

Experimental studies of this phenomenon [illegible] process. The zirconolite phase as the host for actinides will experience the most severe radiation damage. However, natural zirconolites 500 million years old containing up to 20 wt % $UO_2 + ThO_2$ have experienced alpha particle doses about 25 times those which SYNROC zirconolite would receive after 10^6 years. These natural minerals, while metamict, nevertheless appear to have quantitatively retained their U and Th. In some circumstances metamictization may be accompanied by volume expansion, which could ultimately give rise to microcracking in ceramics. However, it is anticipated that the ambient lithostatic pressures in a repository should tend to counteract this by promoting closure of cracks.

OPERATION OF THE SYNROC PROCESS

Because the recommended waste-loading in SYNROC is comparatively low (e.g., 10%), it is the inert additives and not the HLW calcine which determine the nature of the phase assemblage. This allows a great deal of flexibility in designing an optimum ceramic waste form. The waste-loading factor could nevertheless be increased to over 20% [illegible] flexibility. With compara[illegible] fluctuations in the [illegible] without modifica[illegible] favorable characteristics [illegible]. Detailed descriptions of the operation of the SYNROC process have been given by Ringwood and [illegible].

A [illegible] step toward producing SYNROC, it is [illegible] that the SYNROC additives be intimately and [illegible] mixed with the waste component as aqueous [illegible] to produce a starting material with a high degree of reactivity and homogeneity. After [illegible] the powder mixture would be admixed with a small amount of Ni powder and cold-pressed into a Ni canister. A final heating step under reducing conditions may be necessary at this stage for complete devolatilization. The canister would be closed with a Ni lid and then hot-pressed isostatically at 1200 to 1300°C, producing a dense, compact, mechanically strong material. During hot-pressing, mildly reducing conditions are maintained by the canister and admixed Ni powder. (Reducing conditions are essential for the successful immobilization of many radwaste species including Mo, Tc, and Cs.) Thus a single step accomplishes the synthesis of SYNROC ceramic, the incorporation of HLW elements into crystal lattices, and final encapsulation and sealing in a metal canister suitable for geological disposal. Moreover, volatile species such as Cs and Ru are quantitatively retained, minimizing radiological hazards. The simplicity of the hot pressing process makes it suitable for remote operation in hot cells[7] and suggests that the SYNROC process should be economically competitive with borosilicate glass manufacture.

APPLICATION OF THE SYNROC PROCESS TO U. S. MILITARY WASTES

The high-level wastes generated by the United States military reactor program have been handled differently [illegible] After [illegible] by the addition [illegible]

[illegible] Hanford and Savannah River [illegible] the waste [illegible] and other [illegible] bismuth [illegible] the essential [illegible] supernatant liquid [illegible] solution [illegible] as hydroxides [illegible]

The SYNROC [illegible] wastes. We [illegible] SYNROC [illegible] Al, Fe, Mn [illegible] titanate [illegible] hollandite [illegible] described in [illegible] stable and [illegible] amounts of Al, Fe, and Mn [illegible] chemically compatible with [illegible] would be produced. These titanate phases serve to immobilize the Al, Fe, Mn oxides which comprise the bulk of the calcined sludges. Because the SYNROC process is carried out under mildly reducing conditions, all Fe and Mn in these new phases would occur in the divalent state.

Therefore, we are effectively developing a ceramic material composed of normal SYNROC phases (which themselves immobilize 10 to 20 wt % fission products and actinides[1]) plus large amounts of inert spinel and titanate phases which immobilize Al, Fe, and Mn. These latter phases include pseudobrookite (Al_2TiO_5–Fe_2TiO_5 solid solution series), ilmenite ($FeTiO_3$), ulvöspinel ($FeTi_2O_4$), hercynite spinel ($FeAl_2O_4$), and a newly identified Ba-Al-Fe titanate (BAIT) with the approximate composition BaAl$_2$Fe$_2$Ti[illegible]O[illegible], which is related to the naturally occurring mineral davidite.[5] The optimum phase assemblages for this modified SYNROC ceramic were selected on the basis of our detailed experimental study[6] of the system BaO–Al_2O_3–FeO–TiO_2 under subsolidus conditions at 5 kbars and 1200 to 1400 °C.

The SYNROC process is able to accommodate the wide variations in sludge compositions which occur between individual tanks, although we would nonetheless advocate preliminary mixing so that typical "average bulk compositions" would be predominant. The optimum phase assemblage chosen for the SYNROC ceramic will depend on the relative proportions of Al_2O_3 and FeO in the sludges. By way of illustration, two typical cases are described below.

Sludge calcine containing Al_2O_3 > FeO wt %. Controlled amounts of BaO, CaO, ZrO_2, and TiO_2 would be thoroughly and intimately mixed with the washed sludges and the mixture calcined, preferably under reducing conditions. Hot-pressing under reducing conditions at 1200 to 1300 °C would produce a ceramic consisting of the phases hollandite [with FeO in solid solution as the $BaFe_2Ti_6O_{16}$ component], perovskite, zirconolite, pseudobrookite (Al_2TiO_5–$FeTi_2O_5$ ss), and hercynite-rich spinel ($FeAl_2O_4$).

Sludge calcine containing FeO > Al_2O_3 wt %. In this case there are three possible phase assemblages for the hot-pressed titanate ceramic: (1) one assemblage is perovskite, zirconolite, FeO-bearing hollandite, hercynite-rich spinel, pseudobrookite, and BAIT (optional); (2) alternatively, perovskite, zirconolite, BAIT, pseudobrookite, and ulvöspinel coexist with either ilmenite or hercynite-rich spinel; the crystallization of BAIT at the expense of hollandite may be suppressed to some degree by increasing the proportions of TiO_2 and BaO in the initial inert oxide additives; and (3) in rare cases where the sludge calcine contains FeO ≫ Al_2O_3, the assemblage perovskite, zirconolite, $BaFeTi_7O_{16}$-rich hollandite, ilmenite, and $FeTi_2O_5$-rich pseudobrookite is a viable alternative.

TECHNOLOGICAL CONSIDERATIONS

The modified SYNROC formulations for immobilizing military wastes would be produced by essentially the same procedure as discussed by Ringwood and co-workers[2-4] and previously in this paper. After washing and filtration, the sludges would be intimately mixed with pigment-grade TiO_2 and ZrO_2 and some suitable form of BaO, CaO, and Al_2O_3. The subsequent calcination step is best carried out under mildly reducing conditions. After cold-pressing and devolatilization, the desired titanate ceramic would be produced by isostatic hot-pressing in a suitable metal container. Alternatively, a lower-density ceramic might simply be produced by sintering in a reducing atmosphere without any container at all.

For military waste immobilization, the SYNROC process appears to offer major economic advantages over borosilicate glass. The costly and complex procedure of alkali-leaching Al_2O_3 from the sludges prior to glass manufacture is not required in the SYNROC process. Moreover, it may be possible to use inexpensive mild steel canisters in hot-pressing rather than Ni or stainless steel (the latter adds substantially to the cost of glass production).

Because the sludges contain only a small proportion (about 1 %) of fission products and actinides (excluding U), only small quantities of inert oxide additives are required for their immobilization. The bulk of the ceramic is made up of the Al-Fe-Mn oxides from the sludges. It follows that SYNROC ceramics could immobilize about 70% of calcined sludge, compared with about 25% in the case of glass. Actually, the waste-loading per unit volume is significantly higher because the density of SYNROC (~4.5 g/cc) is about 1.5 times that of glass. Thus SYNROC is capable of immobilizing about 4 times as much sludge per unit volume as does glass—a factor which offers considerable economic and safety benefits.

REFERENCES

1. G. J. McCarthy, W. B. White, R. Roy, B. E. Scheetz, S. Komarneni, D. K. Smith, and D. M. Roy, Interactions Between Nuclear Wastes and Surrounding Rock, *Nature*, 273: 216 (1978).
2. A. E. Ringwood, S. E. Kesson, N. G. Ware, W. Hibberson, and A. Major, Immobilization of High Level Nuclear Reactor Wastes in SYNROC, *Nature*, 278: 219 (1979).
3. A. E. Ringwood, S. E. Kesson, N. G. Ware, W. Hibberson, and A. Major, The SYNROC Process: A Geochemical Approach to Nuclear Waste Immobilization, *Geochem. J.* (in press).
4. A. E. Ringwood, *Safe Disposal of High Level Nuclear Reactor Wastes: A New Strategy*, Australian National University Press, Canberra, 1978.
5. G. J. McCarthy, High Level Waste Ceramics: Materials Considerations, Process Simulation and Product Characterization, *Nucl. Technol.*, 32: 92 (1977).
6. R. E. Schwoebel and J. K. Johnstone, The Sandia Solidification Process: A Brief Overview, in *Ceramic and Glass Radioactive Waste Forms*, Summary of Workshop, Germantown, Maryland, January 4–5, 1977, ERDA CONF-770102, 1977.
7. S. Larker, Hot Isostatic Pressing for Consolidation and Containment of Radioactive Waste, in Proceedings of *Scientific Basis for Nuclear Waste Management*, Boston, G. J. McCarthy (Ed.), Plenum, NY, 1979.
8. B. M. Gatehouse, I. E. Grey, and P. R. Kelly, The Crystal Structure of Davidite, *Am. Mineral.* (in press).

USE OF NATURAL ALUMINOSILICATES AND POROUS CERAMIC MATERIALS FOR THE INCLUSION OF RADIOACTIVE WASTES

E. N. LAZAREV, E. A. SHASHUKOV, YU. V. KUZNETSOV, and R. I. LYUBTSEV
V. G. Khlopin Radium Institute, Leningrad, USSR

ABSTRACT

Data on using the porous inorganic materials, such as diatomite and shamote, for the incorporation of radioactive wastes are presented. In laboratory-scale experiments on simulated liquid wastes it has been shown that the operations of solution absorption by porous materials, drying and calcination of salts in pores, and the subsequent conversion into glassy phosphate-silicate products seem to be promising from a technological point of view. This product is characterized by a sodium leaching rate of the order of 10^{-5} g/cm^2 · d and good resistance to crystallization. The content of various oxides in the wastes can attain 15 to 20 wt.%. The data on the dependence of plasticity and open porosity of the clay-like products on Na_2O, SrO, ZrO_2, and MnO_2 content are also given.

INTRODUCTION

For solving the problem of biosphere protection against long-lived radionuclides, one should take into account all the stages of waste management from processing to end disposal. The integral safety provided by a protection system is determined by safety parameters for each constituent part of this system (barriers). None of these barriers nor their features taken separately assure the reliability of radionuclide localization. So, a low leaching rate of radionuclides from a solid composite and a higher leaching rate from a different waste form bear no single valued indication in favor of the first composite without considering the protection system as a whole.

The recently outlined option for a necessary series of protection barriers in a radionuclide-containing solid composite[1] must envisage waste storage. In addition, this option should not only reflect the higher reliability of the protection system with increasing number of protection barriers but should also be complemented by notions about their correlation and compensation. The waste composition and thermal-physical characteristics of barriers should naturally be taken into consideration as well.

In Fig. 1 a possible approach to the quantitative evaluation of reliability for the complex protection system is shown. It is seen that the required reliability of the protection system, regardless of the evaluation method, could be guaranteed by protection barrier combinations. Stage curves within the barrier show the use of different materials and different conditions in the storage area.

On the basis of the presented concept for simplicity of technological operations and with decreasing cost of liquid MLW and HLW treatment, we study the incorporation of these wastes into clay-like and porous inorganic materials. The available published data[2-5] on the utilization of these materials and their properties are scarce in comparison with the information on glass. We report here some results of our investigations.

USE OF POROUS MATERIALS

Investigations on the use of porous materials were aimed at elimination of technical difficulties of calcination processes in fluidized-bed equipment or in spray drying, and the difficulties of one-stage processes, e.g., can melting, when liquid salt-rich waste was fed onto a small melt surface.[6] This is also connected with using cheap materials and facilitating the waste processing flowsheet as a whole. Our investigations have been conducted on diatomite and shamote, the characteristics of which are given in Table 1. The composition of simulated feed solutions is given in Table 2.

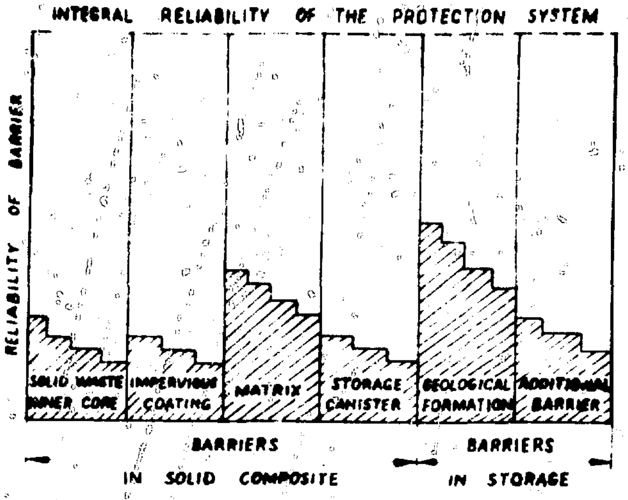

Fig. 1 Schematic of contributions of various barriers to the overall reliability for a waste protection system.

TABLE 1

Characteristics of Porous Materials Used in the Investigation

Porous materials	Composition, wt.%				Open porosity, %	Volume weight, g/cm³
	SiO_2	Al_2O_3	Fe_2O_3	CaO + MgO		
Diatomite	62	30	4	4	30	0.28
Shamote	56	35	5	4	34	0.38

TABLE 2

Composition of Simulated Wastes in Experiments on Porous Materials

Components	Concentration		
	Mole/liter	g/liter	Wt.% oxides
$NaNO_3$	1.95	166.0	50.3
$CsNO_3$	0.06	11.4	6.7
$Sr(NO_3)_2$	0.06	12.3	5.0
$La(NO_3)_3$	0.21	67.1	28.0
$Al(NO_3)_3$	0.16	34.9	7.0
$Fe(NO_3)_3$	0.02	5.3	1.5
$Zr(NO_3)_4$	0.01	3.4	1.5
HNO_3	3.00	189.0	

Absorption of waste solution and drying and denitration of salts in the pores, following conversion after phosphate addition, were studied. The work was performed on porous materials in the form of small cylindrical blocks. The blocks were placed in vessels of proper diameter, the feed solution was poured out to the upper level of the materials, and after exposure the solution was dry evaporated. Therefore, several operations of "absorption drying" were carried out, which makes it possible to introduce into the material more than 40 wt.% salts (as oxides). Then the salts were denitrated at 900°C. On evaporation, drying, and calcination, the material retained its mechanical structure, and no visible damage was observed. All the work was conducted under normal operating conditions. The content of residual nitrates was shown to be less than 1×10^{-4} mole g.

The study of distribution of oxides in the block volume revealed, in the case of diatomite, the change in their concentrations depending on the height (1.1 to 1.7 times) and depending on the diameter (1.2 to 1.5 times). On the addition of sodium metaphosphate at 1000°C to the "oxide-saturated" diatomite or shamote (4 weight parts per 1 weight part of porous oxide-containing material, i.e., ~2 mole per 1 mole, respectively), the material was dissolved completely; on cooling, a homogeneous glassy product was prepared. The complete dissolution occurred also on decreasing the weight ratio to 3 : 1 (molar ratio ~1.5 : 1). The same result can be obtained on the addition of orthophosphoric acid.

The sodium leaching rate from the final products for the first days was of the order of 10^{-5} g/cm² · d. In addition, the feed (diatomite and shamote), intermediate (oxide-containing diatomite and shamote), and final phosphate-silicate products were investigated by means of differential thermal analysis, IR-spectroscopy, and X-ray phase analysis. The feed calcine prepared from the solutions of the same composition in the absence of porous materials under the same conditions was investigated by all these methods.

X-ray phase analysis has shown transformations in calcine resulting in many crystalline compounds. Among the individual nontransformed oxides, iron oxide (Fe_2O_3) remained intact. The absence of nitrates and nitrites was confirmed.

During calcination the interaction of calcine components with carrier material was observed in pores. The sodium silicate phase (Na_2SiO_3) was particularly identified. The large interaction was established by IR-spectroscopy as well.

The final products at the molar ratios of charge to porous material (including oxides) equal to 2 : 1 and 1.5 : 1 are X-ray amorphous, which is indicative of glassy phosphate-silicate form. The resulting diatomite products were quite X-ray amorphous; in shamote a minor nonidentified crystalline phase was evident. The glassy product was also confirmed by IR-spectroscopy.

The results of differential thermal analysis of the diatomite and shamote products are presented in Figs. 2 and 3, respectively. The data obtained support deep transformations in the feed calcine and point to the interaction of calcine with porous materials. Furthermore, it is shown that the glassy phosphate-silicate products are highly resistant to crystallization. On DTA-curves, only slight endothermal effects, probably due to softening processes of the materials, were observed.

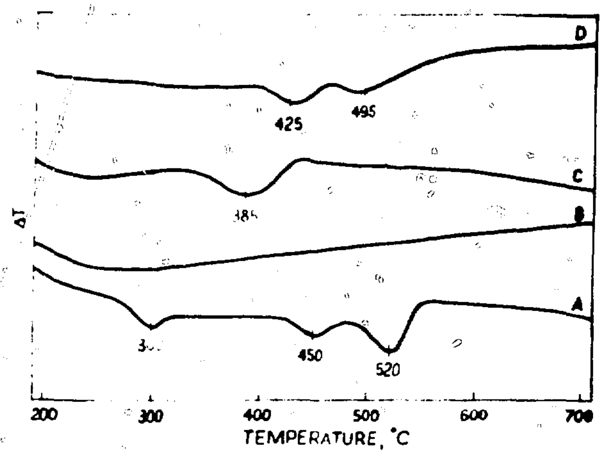

Fig. 2 DTA curves for diatomite at 10°C/min. A = calcine; B = diatomite; C = oxide-containing diatomite; D = phosphate-silicate product.

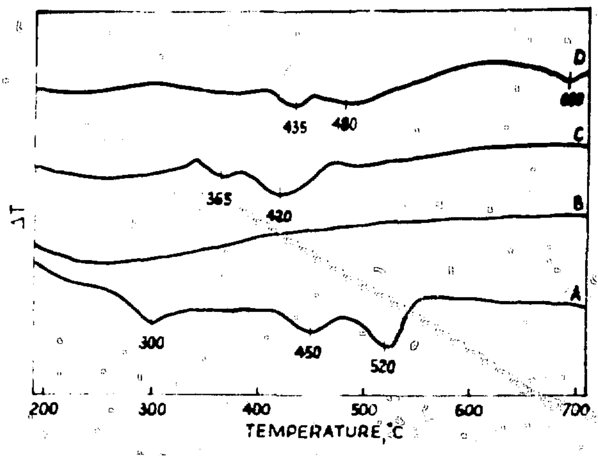

Fig. 3 DTA curves for shamote at 10°C/min. A = calcine; B = shamote; C = oxide-containing shamote; D = phosphate-silicate product.

USE OF CLAY-LIKE MATERIALS

In one of the communications we have already advanced some arguments in favor of using clay-like materials for incorporation of radioactive waste.[2] It should be added that these materials hold the greatest promise for including finely dispersed radioactive sludge, precipitates, spent inorganic sorbents, waste calcines, etc. In this report results are presented on the investigation of the incorporation of individual metal oxides into ceramics based on Cambrian clay in order to determine their influence on plastic properties of the mold mass and open porosity of sintered products. The investigations were conducted on Na_2O (in the form of NaOH), SrO, ZrO_2, and MnO_2.

Air-dried clay was crushed and mixed in a ball mill with some of these substances introduced in quantities of 10 to 50 wt.%; after mixing with water the plastic paste was prepared and cylindrical products were pressed at ~5 kg/cm^2. The products were dried and sintered at 900 to 1100°C.

An exception to these operations was NaOH. Plastic molding in the presence of this component was impossible even in the amount of 10 wt.%. Therefore, half-dried forming of pellets in press-forms was performed (at a moisture level of 5 to 10%). The products were sintered, depending on sodium content, within the range 750 to 850°C. The mixtures containing 50 wt.% SrO possessed no sufficient plastic properties. In the case of 10 to 30 wt.% SrO, the paste had good plasticity over the entire investigated range of ZrO_2 and MnO_2 additives.

The dependence of open porosity of sintered products on the content of individual components is shown in Table 3. It is seen in this table that in all cases the open porosity increases with increasing content of the substance introduced into clay. On incorporation of SrO and ZrO_2, close results were obtained; namely, low porosity (0.1 to 1.2%) at a content of 10 to 30 wt.% and a sharp increase in porosity (4.9 to 10.5%) at an oxide content of 50 wt.%. A similar dependence was found with MnO_2 incorporation, but the values of open porosity were higher—0.8 to 4.5% and 14 to 16%, respectively. This can be due to decomposition of dioxide and oxygen release on sintering. Higher open porosity occurred in the case of NaOH; it attains 2.1 to 7.3% with 20 to 30% content of NaOH.

TABLE 3

Dependence of Open Porosity of Ceramic Compositions on the Incorporated Components

Components	Content, wt.%	Open porosity, %
NaOH	10	1.2–1.9
	20	3.4–5.7
	30	2.1–7.3
SrO	10	1.0–1.2
	30	0.4–1.0
	50	5.1–10.5
MnO_2	10	0.8–3.0
	30	1.0–4.5
	50	14.0–16.0
ZrO_2	10	0.1–0.4
	30	0.1–0.8
	50	4.9–10.0

CONCLUSIONS

The use of porous inorganic materials, such as diatomite and shamote, compared with other techniques being developed for processing of radioactive waste, has shown that laboratory-scale experiments present some technical and technological advantages. First of all, the use of porous inorganic materials facilitates the calcination process of liquid wastes and the process operations under rather mild conditions. Moreover, the final phosphate-silicate glassy product is made of cheap, available materials. This product is at least competitive with phosphate glass since the sodium leaching rate is 10^{-5} g/cm^2 • d and is resistant to crystallization. The performed operations provide the incorporation of 15 to 20 wt.% waste oxides.

The use of natural clay-like materials for incorporation of various fine dispersed radionuclide containing substances also looks promising. The compositions based on these materials are prepared by means of plastic forming techniques and incorporate waste oxides up to 50 wt.%. However, more definite conclusions about the techniques being developed can be drawn only after the scaling-up operation and after verification of the results obtained on real wastes.

REFERENCES

1. J. M. Rusin, M. F. Browning, and G. J. McCarthy, Development of Multibarrier Nuclear Waste Forms, in Proceedings of *Scientific Basis for Nuclear Waste Management*, Boston, G. J. McCarthy (Ed.), Plenum, NY, 1979.
2. V. I. Zemlyanukhin, Yu. V. Kuznetsov, L. N. Lazarev, R. I. Lyubtsev, and E. A. Shashukov, Clay-Phosphate Ceramics and Vitromets: Alternatives to Monolithic High Level Waste Glass Products, in Proceedings of *Scientific Basis for Nuclear Waste Management*, Boston, G. J. McCarthy (Ed.), Plenum, NY, 1979.
3. W. J. Belter, Present and Future Programmes in the Treatment and Ultimate Disposal of High-Level Radioactive Wastes in the United States of America, in *Treatment and Storage of High-Level Radioactive Wastes*, pp. 3-22, IAEA, Vienna, 1963.
4. F. C. Arrance, Method for Disposing of Radioactive Waste and Resultant Product, U. S. Patent No. 3093593.
5. E. Podschus, A Process for Consolidating Radioactive Waste Solutions, Great Britain Patent No. 1435855.
6. *Techniques for the Solidification of High-Level Wastes*, IAEA, Technical reports series N 176, Vienna, 1977.

V. IMMOBILIZATION OF RADIOACTIVE WASTES—CERAMIC AND GLASS PROCESSING

VITRIFICATION OF ICPP HIGH-LEVEL ZIRCONIA CALCINE

J. R. BERRETH, D. GOMBERT II, and H. S. COLE
Allied Chemical Corporation, Idaho Falls, Idaho

ABSTRACT

High-level radioactive calcined defense waste (~50 wt.% CaF_2) is vitrified using a frit containing 66% SiO_2, 24% Na_2O, 8% B_2O_3, and 2% CuO. Effects of Na, B, Li, Zn, Cu, and P on viscosity and acid leach resistance were measured. The glass contains up to 9% fluoride. Glass properties were measured.

INTRODUCTION

Defense-type nuclear fuels are reprocessed at the Idaho Chemical Processing Plant (ICPP) to reclaim the unspent uranium.[1] The resultant high-level radioactive liquid wastes are *temporarily* stored before solidification by a fluidized-bed calcination process.[2] High-level wastes at the ICPP have been routinely calcined since 1963 and stored in near-surface engineered storage facilities.[3] Approximately 1700 m^3 of calcined waste has been produced. Composition of a zirconia type calcine, the most prevalent type produced, is shown in Table 1. Except for the fission products cesium and strontium, this calcine is quite resistant to leaching;[4] however, regulatory criteria may require that calcined waste be converted to less dispersible, more leach-resistant materials. An alternative being investigated at the ICPP is conversion of the calcine to a glass.[5] Zirconia calcine is quite refractory due to its alumina and zirconia content; also, it contains fluorides which are potentially corrosive at melting temperatures.

Glass formulations have been developed for several types of defense waste[6] and for use with commercial-type high-level wastes.[7-10] None of these glasses contain the high fluorides or zirconia content of the ICPP waste. To reduce processing and off-gas cleanup complexity during remote operation, our glass development work was limited to glasses with viscosity below 500 poise at 1050 to 1150°C. Two basic types of high-level waste vitrification processes have been investigated. One type is an in-can melting process[11] where melting temperatures are limited to ~1050°C. The other is the use of a melter such as the Joule-heated ceramic lined glass melter being developed for use in remotely operated facilities.[12] The glass developed at the ICPP is primarily for use in a ceramic melter process, although with slight modification it should also be suitable for in-can melting.

EXPERIMENTAL METHOD

Over 100 glasses were prepared at 1100°C using a wide range of glass-forming additives combined with 33 wt.% simulated calcine. Glasses were held at melting temperature for 3 hours before pouring into graphite molds for cooling. All of the glasses were of a borosilicate type. Based on a set frit composition, a matrix study was performed where all combinations of five minor frit components (Li_2O, P_2O_5, CuO, CaO, and ZnO) at a set percentage were varied to measure the effect of the components on melt viscosity and acid leach resistance. For the study, Na_2O and B_2O_3 were held constant in the frit at 24 and 14 wt.%, respectively, and the SiO_2 was varied with the minor components. In addition, the effects of varying Na_2O and B_2O_3 on melt viscosity and leach resistance were also measured.

Several leaching methods were evaluated on the experimental glasses. These included Soxhlet (boiling distilled water), simulated salt brine solutions, groundwaters, and buffered 1*M* acetic acid solution (pH 3.8) at 25°C. For leaching, 100 *ml* of solution was used with 4 g of glass. Glass samples were ground to a −16 to +32 mesh size range. Variation in leach resistance was most pronounced in the

TABLE 1

Composition, Wt.%, of Calcined ICPP Zirconia Waste

Al_2O_3	ZrO_2	CaF_2	CaO	NO_3^-	B_2O_3	Fission products and actinides	Miscellaneous
13–20	18–24	50–56	2–4	0.5–2	2.4	0.2–1	0.5–3

acetic acid solution. Buffered acetic acid leaching was used except where otherwise stated. Based on analysis of the melting and leaching data, seven glasses were chosen to study the effect of 25 to 40 wt.% calcine concentration on viscosity and leach resistance. The variation of calcine constituents, such as dolomite and alumina, and melt temperature (1050 to 1200°C) on melt viscosity and leach resistance was also measured. A frit composition was thereby selected which produced the best glass within the limits of the experimental tests.

Experimental glasses were analyzed for fluoride content using a potentiometric method which involves fusing a 5-g sample with NaOH, dissolving the fused mass in a sodium citrate–triethylamine–NaCl solution and analyzing the solution with a fluoride-specific ion electrode.[13]

EXPERIMENTAL RESULTS

The viscosity of experimental glass melts was determined on a relative scale ranging from 1 = ~50 to 100 poise to 5 = ~500 poise. Two major constituents in the experimental frits are soda and boron oxide. Melt viscosity decreased from just pourable (~500 poise) at 12 wt.% Na_2O to a readily pourable melt (50 to 100 poise at ~24 wt.% Na_2O) as shown in Table 2. As the B_2O_3 content increased from 8 to 18% in the frits containing up to 24 wt.% Na_2O the viscosity increased slightly, but at 28% Na_2O viscosity decreased with increasing B_2O_3. Leach resistance decreased slightly (less than a factor of 2) with increasing B_2O_3 content at 24% Na_2O content. Addition of just 2 wt.% P_2O_5 increased melt viscosity significantly; at 4% P_2O_5 the glass was too viscous to pour. The effect of P_2O_5 on leach resistance is not so pronounced; generally leach resistance is high when P_2O_5 is present up to 4%. Viscosity, with the addition of 2 to 4% Li_2O, either remained unchanged or decreased slightly, but Li_2O at 4 wt.% decreased leach resistance as much as a factor of 4. Leach resistance and viscosity decreased rapidly with the addition of up to 6 wt.% ZnO. Addition of CuO up to 4 wt.% appears to decrease viscosity and, at the same time, aid leach resistance.

At 33 wt.% calcine the effect of combining the minor frit constituents on glass viscosity and leach resistance was pronounced in several cases. Relative viscosities and acid leach resistances are shown in Table 3 for the possible combinations, at 0 or 2 wt.% of five minor additives, in the presence of 24 wt.% Na_2O and 14 wt.% B_2O_3. The best leach resistance is obtained using CuO and P_2O_5, either alone or together, or in combination with one or two other minor additives. Lithium, zinc, or calcium alone or in

TABLE 2

Representative Frit Compositions Tested Plus Viscosities and Leach Rates of Experimental Glasses Containing 33 Wt.% Zirconia Calcine

Frit No.	Frit composition, wt.% SiO_2	Na_2O	B_2O_3	P_2O_5	CuO	Li_2O	ZnO	Relative viscosity	Acid leach rate, wt.% lost/19 hr
37	70	12	14	2	2			5	0.6
34	68	16	14		2			5	0.7
64	64	20	14		2			5	0.7
50	60	24	14		2			2	0.3
58	56	28	14		2			2	0.6
66	56	24	18		2			3	0.2
67	52	28	18		2			1	1.8
51	66	24	8		2			2	0.1
63	58	24	14	2	2			4	0.1
68	56	24	14	4	2			5	1.0
57	58	24	14		2	2		2	0.5
60	56	24	14		2	4		2	2.0
61	58	24	14		2		2	3	0.2
70	56	24	14		2		4	2	0.5
108	54	24	14		2		6	1	10.0
41	68	16	14	2				5	0.5
35	66	16	14	2	2			4	0.4
42	64	16	14	2	4			3	0.3
73	62	16	14	2	6			5	0.7

TABLE 3

Effects of Minor Frit Constituents on Viscosity and Leach Rate for a Glass Containing 33 Wt.% Zirconia Calcine

Frit No.	Frit composition, wt.%* SiO_2	Li_2O	P_2O_5	CuO	CaO	ZnO	Relative viscosity	Acid leach rate, wt.% lost/19 hr
107	62						3	3.0
50	60			2			2	0.3
105	60		2				2	0.6
103	60					2	1	4.0
104	59				3		2	10.0
106	60	2					1	10.0
63	58		2	2			4	0.1
61	58			2		2	3	0.2
99	57		2		3		3	0.2
101	58	2	2				1	0.3
98	57			2	3		2	0.5
100	57				3	2	2	0.5
91	57	2			3		1	1.0
57	58	2		2			2	1.5
90	58	2				2	2	1.7
102	58		2			2	1	2.0
93	56	2	2			2	1	0.2
94	55		2	2	3		2	0.2
97	55		2		3	2	2	0.2
95	56	2	2	2			2	0.3
92	55	2	2		3		1	0.6
96	55			2	3	2	2	1.0
88	56		2	2		2	2	1.0
62	56	2		2		2	1	2.0
89	55	2		2	3		2	2.0
78	55	2			3	2	2	3.0
80	53	2	2		3	2	1	0.4
74	54	2	2	2		2	1	0.4
86	53		2	2	3	2	2	0.4
87	53	2	2	2	3		1	0.9
79	53	2		2	3	2	2	5.0
81	51	2	2	2	3	2	2	1.0

*Frit contains 24 wt.% N_2O and 14 wt.% B_2O_3.

combination with each other, or with other minor additives, generally produce a glass of decreased leach resistance. Combining P_2O_5 with one, two, or three minor additives will generally produce a highly leach-resistant glass. Glasses containing four or five minor additives, though, are not as leach resistant as are certain glasses produced with two or three additives.

Based on the above studies, seven glasses were selected for additional testing. Of the seven glasses (Nos. 50, 51, 66, 86, 94, 95, and 101) tested for ability to produce uniform melts at 1050, 1100, and 1200°C with calcine contents of 25, 33, and 40 wt.%, glass 51 consistently produced a low viscosity melt and leach-resistant glass, except at 1050°C and 40 wt.% calcine, where it was too viscous to pour. Up to 10% of the calcine in glass 51 can be replaced with dolomite (a calciner start-up material) and up to 15% of the calcine can be replaced with alumina (mixed waste) without significant increase in melt viscosity or leach rate.

If the fluoride present in the calcine were to volatilize during melting, corrosion of off-gas systems could be a problem. Results of fluoride retention in 50 to 100 g glass samples during melting are shown in Table 4. On these small samples, from 5 to 30% of the fluoride volatilized. On a larger scale, much less of the fluoride would be expected to volatilize, because of the much larger volume to surface area ratio and the cover of calcine that will be maintained over the melt. Also, severe corrosion of refractories in laboratory melting systems has not been noticed, which suggests control of corrosion in off-gas systems may not be too difficult.

When glass 51 (33 wt.% calcine) is melted at 1100°C, it retains about 60% of the CaF_2 in a crystalline form. At

TABLE 4

Effects of Melt Temperature and Calcine Loading on Glass 51 Fluoride Content

Calcine, wt.%	Fluoride content in glass	Melt temperature, °C		
		1050	1100	1200
25	Wt.% F⁻	4.9	4.9	4
	(% F⁻ lost)	(15)	(15)	(30)
33	Wt.% F⁻	6.9	6.2	8.7
	(% F⁻ lost)	(10)	(19)	(5.4)
40	Wt.% F⁻	8.2	8.7	6.7
	(% F⁻ lost)	(11)	(5.4)	(27)

TABLE 5

Soxhlet Leach Rates of Glass 51 Before and After Devitrification

Treatment condition		Acid leach rate, wt.% lost/19 hr	Soxhlet; distilled water, 11 days					
			Cs*		Sr*		Bulk	
Time, d	Temp., °C		Wt.% lost	g/cm² · d x 10^{-5}	Wt.% lost	g/cm² · d x 10^{-5}	Wt.% lost	g/cm² · d x 10^{-5}
		0.7	11.0	25.0	4.9	12.0	3.5	8.4
1	700	0.9	5.6	13.0	2.5	5.9	2.8	6.7
1	800	1.5	10.0	24.0	4.1	9.7	4.8	11.0
14	800	3.2	4.2	9.9	3.0	7.0	3.5	8.3
60	700	2.4			8.3	20.0	2.2	5.3
60	800				2.1	5.0	4.0	9.4

*Based on measured amounts in calcine.

25% calcine, the glass is completely amorphous. There is some indication that as the crystalline CaF_2 dissolves in the melt, leach resistance in acid decreases slightly (< a factor of 2). On holding glass 51 at 700 and 800°C for periods of 1 to 60 days, the crystalline CaF_2 content decreases about 35% and a hiortdahlite $[(Na,Ca,RE)_3Zr_{1-x}Si_2O_7)(F,OH,O)_2]$ structure appears. Acid leach rate (Table 5) increases from 0.7 wt.% lost to ~3 wt.% lost in 19 hours, but Soxhlet leach resistance remains essentially unchanged at ~8 x 10^{-5} g/cm² · d.

The leach resistance of glass 51 to various leachants is shown in Table 6. For this study, it was not possible to measure leach rates of less than 2.6 x 10^{-6} g/cm² · d. It is evident, though, that leach rates decrease rapidly after the first few hours of leaching. In acid the leach rate appears to approximately double with every 25°C rise in temperature.

CONCLUSIONS

Vitrification of zirconia calcine appears feasible at temperatures (~1100°C) which should be practical for remote operation. The glass is uniform without observable occlusions. Some fluoride volatility may occur, and an off-gas system similar to that presently used in the ICPP calcining process should be capable of scrubbing the fluoride.

Glass 51 has good ability to vitrify zirconia calcine and is not sensitive to expected variations in waste content or in waste composition. Devitrification of the glass does not result in loss of Soxhlet leach resistance. Leach resistance in a strong acetic acid solution (pH 3.8) can decrease, perhaps up to a factor of 10. Vitrification is one method which could be applied should regulatory criteria require an alternative for disposing of ICPP high-level waste. Vitrification is a relatively simple process which should be readily adaptable to remote operation.

TABLE 6

Leach Rates for Glass 51, 33 Wt.% Zirconia Calcine, in Different Leachants

Leachant	Temp., °C	Leach time, hr	Leach rate	
			g/cm² · d x 10^{-5}	Wt.% lost
Acid (HAc-Ac⁻ buffer, pH 3.8)	25	19	16 ± 2	0.5
	25	94	0.6 ± 0.3	0.09
	50	19	2.9 ± 4	0.9
	95	19	11.0 ± 20	3.5
Raw ICPP well water	25	19	2.1 ± 1	0.07
	25	94	*	*
Distilled water	25	19	3 ± 1	0.09
	25	94	*	*
Brackish WIPP groundwater	25	19	3 ± 1	0.08
	25	94	0.4 ± 0.3	0.07
Soxhlet (distilled water)	95	264	8 ± 2	4.5

*Below limit of detection (2.6 x 10^{-6}).

ACKNOWLEDGMENT

This work was performed under the auspices of the United States Department of Energy, contract DE-AM07-76 IDO1540.

REFERENCES

1. G. E. Offutt and H. S. Cole, *Run Report for the First Campaign of Co-processing Fuels at ICPP*, USAEC Report IN-1472, June 1972.
2. C. M. Slansky, Radioactive Waste Management, *Chemtech*, p. 160, March 1975.
3. B. R. Wheeler et al., Storage of Radioactive Solids in Underground Facilities: Current ICPP Practices and Future Concepts, in *Symposium on the Disposal of Radioactive Wastes into the Ground*, p. 421, International Atomic Energy Agency, Vienna, 1967.
4. M. W. Wilding and D. W. Rhodes, *Leachability of Zirconia Calcine Produced in the Idaho Waste Calcining Facility*, USAEC Report IN-1298, Allied Chemical Corp., June 1965.
5. D. Gombert II, H. S. Cole, and J. R. Berreth, *Vitrification of High-Level ICPP Calcined Wastes*, DOE Report ICP-1177, Allied Chemical Corporation, February 1979.
6. J. A. Kelley, *Evaluation of Glass as a Matrix for Solidification of Savannah River Plant Waste: Radioactive Studies*, USERDA Report DP-1397, E. I. du Pont de Nemours and Co., 1975.
7. J. E. Mendel, *The Storage and Disposal of Radioactive Waste as Glass in Canisters*, DOE Report PNL-2764, Pacific Northwest Laboratory, December 1978.
8. A. R. Hall et al., The Development and Radiation Stability of Glasses for Highly Radioactive Waste, in *Proceedings of Symposium on Management of Radioactive Waste from the Nuclear Fuel Cycle*, IAEA-SM-207/24, Vienna, March 1976.
9. R. Bonniaud, Vitrification in France of Fission Product Solutions, *Nucl. Tech.*, 34: 449 (August 1977).
10. W. Guber et al., Lab-Scale and Pilot-Plant Experiments on the Solidification of High-Level Wastes at the Karlsruhe Nuclear Research Centre, in *Proceedings of Symposium on Management of Radioactive Waste from the Nuclear Fuel Cycle*, IAEA-SM-297/49, Vienna, March 1976.
11. H. T. Blair, *Vitrification of Nuclear Waste Calcines by In-Can Melting*, USERDA Report BNWL-1061, Battelle Pacific Northwest Laboratories, May 1976.
12. C. C. Chapman and J. L. Beult, *A Continuous Glass Melter for Immobilization of Radioactive Waste*, DOE Report PNL-SA-6867, Pacific Northwest Laboratory, presented at 1978 Annual Amer. Nucl. Soc. Meeting, San Diego, California, June 1978.
13. D. R. Trammel, Analysis of Glassified Calciner Material for Fluoride, *Technical Division Quarterly Progress Report, January 1–March 31, 1978*, DOE Report ICP-1150, Allied Chemical Corporation, pp. 110-111, July 1978.

DEVELOPMENT AND CHARACTERIZATION OF THE GLASS-CERAMIC VCP 15 FOR IMMOBILIZATION OF HIGH-LEVEL-LIQUID RADIOACTIVE WASTE

W. GUBER,* M. HUSSAIN,† L. KAHL,* W. MÜLLER,* and J. SAIDL*
*Kernforschungszentrum Karlsruhe GmbH, Karlsruhe,
Federal Republic of Germany and †Pakistan Atomic Energy Commission

ABSTRACT

Complementary to the glass developments for HAW solidification, a glass-ceramic matrix was synthesized (VC 15) and the derived HAW-containing product (VCP 15) was investigated on both inactive and highly radioactive scales. In comparing the glass-ceramic matrix with the glass products, an improvement in thermal properties was found, but the leaching resistance was only slightly better. The main advantage of the glass-ceramic system is its higher thermodynamic equilibrium, which increases the long-term stability and safety of solidified HAW in final storage.

INTRODUCTION

The solidification of high-level-liquid waste generated from reprocessing of irradiated nuclear fuels in a borosilicate glass system is the most favored treatment method to make it suitable for final disposal. The safety in final storage and the available developed technology impose certain restrictions on the product properties. Work in different countries is being carried out to develop an optimum matrix which fulfills the necessary requirements.

Borosilicate glass products containing highly radioactive waste oxides are multicomponent systems with fission products, transuranium elements, corrosion products, and process chemicals which are incorporated in an undercooled metastable equilibrium state. The fraction of nonglassy substances in the HAW glass product is very small and consists of undissolved substances like oxides (CeO_2, ZrO_2) and noble metals (Ru, Rh, Pd) and the developed second phase (molybdate, titanate, tellurate), all of which can act as nuclei for crystallization.

If sufficiently undercooled, the glassy phase has a relatively high stability. The stability is defined by the relaxation time which is the period necessary for changes of structural configuration. The major influencing factor is the mobility of structural units dictated by the viscosity in the medium, provided that a crystallization process is possible only in a liquid state. The viscosity value at the transformation temperature of the glass (~500 °C) is about 10^{12} Pa • s and the change in the structural configuration may take place in a relaxation time of minutes, hours, or days. When viscosity increases to 10^{15} Pa • s, structural changes are, in practice, impossible in a definite time and the relaxation time is increased to greater than 1000 years. It has been calculated that configuration changes at a viscosity of 10^{24} Pa • s may occur after a period of 10^6 years,[1] i.e., when the temperature of final storage remains 200 °C, glass structure, even in the presence of crystal nuclei, does not change for a long period (perhaps over 10^4 years) and there is no risk of spontaneous crystallization. But an absolute safety guarantee does not prevail when the temperature increases by any means of accident.

A controlled crystallization caused by a two step annealing process (nucleation and crystallization) which leads to the development of a glass-ceramic structure improves safety. In this case a greater stabilization of the system has been established due to a greater thermodynamic equilibrium reached by heat treatment.

In 1971, the research and development discussed in this paper was started at the Kernforschungszentrum Karlsruhe, which led to the development of the glass-ceramic matrix VC 15 and to the investigation and description of the derived product VCP 15.[2-4]

THE COMPOSITION AND DEVELOPMENT OF GLASS-CERAMIC PRODUCTS

The [illegible] glass-ceramics is a [illegible] quite complicated. After several conventional [illegible] systems were investigated, a series of lower [illegible] (1200 C) glass-ceramics was developed to control the volatility of particular components. The chemical composition of a glass-ceramic matrix and selected glass-[illegible] given in Table 1.

The selection of a glass-ceramic matrix was done [illegible] to two categories of properties: production engineering and suitability for the final storage.

From the technological viewpoint the products would [illegible] these characteristics:

- Production using existing technology (melting temperature ≤ 1200 C with a melt viscosity ≤ 10 Pa · s)
- Low volatility of components during melting
- Electrical conductivity of the melt ≥ 3 × 10^2 S · m^{-1} (Siemens · $meter^{-1}$) at 1200 C for direct heating with electrodes immersed into the melt
- Low corrosion of the refractory lining in the melter

For the final storage, the following characteristics are desirable:

- Specific heat production ≤ 20 W/l product with resulting storage temperature ≤ 200 C (15 wt.% of HAW oxides)
- Leach resistance against different leachants (distilled water, brine, quartary brine) ≤ 1.0 × 10^{-8} kg · m^{-2} · s^{-1}
- Defined mechanical strength
- Defined physicochemical properties (recrystallization tendency, interaction with metal container, element transformation consequences, energy storage)

The glass-ceramic product VCP 15 contains TiO_2, K_2O, and Li_2O; all three are known as nucleation agents. In addition to its suppression of Cs volatility, TiO_2 acts as one of the main crystallization agents.

The fabrication of glass-ceramics is similar to vitrification technology in its melting procedure. HAW solution was denitrated and admixed to prefabricated pulverized VC 15 frit. After being dried and calcined, the mixture was melted 4 hours at 1200 C and then poured into a steel canister. The product was cooled to below the nucleation temperature. The cooling step was followed by a two step annealing process at the nucleation and crystallization temperatures. The temperatures mentioned were determined from the differential thermal analysis (DTA) diagram (Fig. 1) and by dilatometry. The nucleation and crystallization temperatures used were 430°C and 630°C, respectively. The partial crystallization of the product increased its density and caused volumetric contraction. Hence the block disengaged from the walls of the container and a gap around the block was formed. This complication was eliminated by adding a calculated quantity of low melting metal alloy (containing Pb, Sb, Bi, etc.) to the container after the first annealing step. The gap is thus filled and the surface of the block covered by a metal layer which represents an additional barrier against leaching of the product.

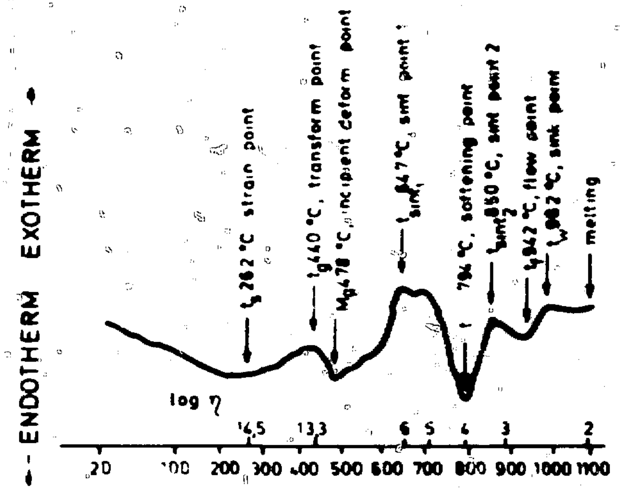

Fig. 1 DTA curve of VCP 15 glass-ceramics.

The glass-ceramic product VCP 15 has been characterized for a number of properties as were the glass products, GP 98, previously.[5] The changes in some of the properties caused by partial crystallization are as follows:

- Density from 2.8 kg · m^{-3} (for glass) to 3.0 kg · m^{-3} (for glass-ceramics)
- Thermal conductivity from 1.2 W · m^{-1} · K^{-1} (for glass) to 2.2 W · m^{-1} · K^{-1} (for glass-ceramic) (Fig. 2)
- Viscosity at 1150°C (Fig. 3)

The evaporation losses were determined by methods of thermogravimetry and radiometry. The volatility of the total mass or of a particular substance was characterized as the evaporation velocity.[5]

CRYSTALLIZATION BEHAVIOR AND PRODUCT STRUCTURE

The glass-ceramic has been prepared by a conventional glass melting process. The basic matrix VC 15 is a glassy substance prior to annealing. Its crystalline structure is developed after the annealing procedure, i.e., after the nucleation and recrystallization processes. The X-ray diffraction pattern of the product is very complex and shows, besides the weak lines typical for noble metals, CeO_2, and titanate, the lines for crystalline structures like perovskite, diopside, titanite, pollucite, etc.[6] Some of these minerals serve as a host phase for certain elements contained in the highly radioactive wastes (Sr, Cs, rare earth, actinides). The same minerals are found in the Australian SYNROC

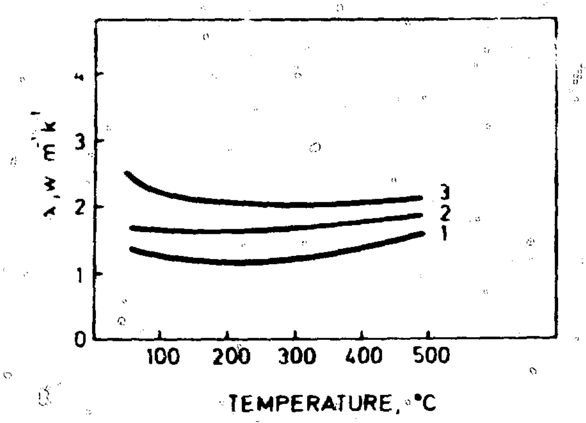

Fig. 2 Thermal conductivity as a function of temperature. (1) GP 98 glass product. (2) VC 15 basic glass-ceramics. (3) VCP 15 glass-ceramic product.

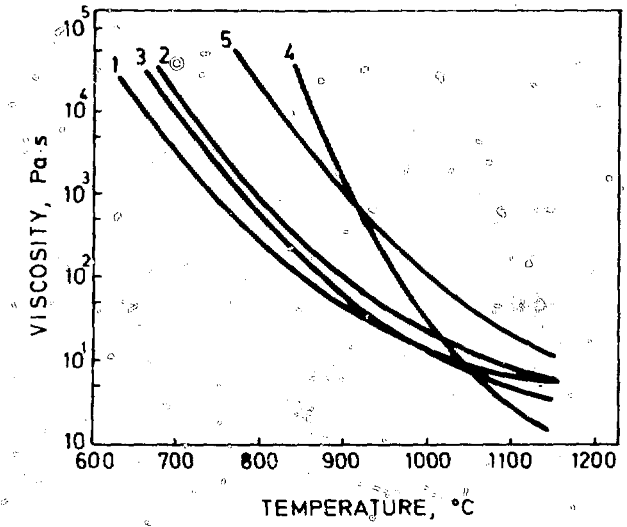

Fig. 3 Temperature dependence of viscosity of the melts. (1) VC 15. (2) VCP 15 (20 wt.% HAW oxide). (3) VCP 15 (20 wt.% HAW oxide, 5 wt.% Gd_2O_3). (4) VCP 15 (18.8 wt.% HAW oxide, 1.2 wt.% P_2O_5, 5 wt.% Gd_2O_3). (5) GP 98/12 (15 wt.% HAW oxide).

product[7] which contains, in comparison with VCP 15, a small quantity of a residual glassy phase. The SEM photographs of the fired and fractured surfaces of VC 15 and VCP 15 show a fine crystalline structure with crystal size below 100 μm.

The controlled crystallization influenced certain product properties, making them more suitable for the final storage. The values of density, thermal conductivity, and mechanical strength increased after recrystallization, whereas thermal expansion and specific heat decreased considerably. A summary of the main properties of HAW-containing glass-ceramic product VCP 15 is given in Table 1.

TABLE I

Composition and Physicochemical Properties of the Highly Radioactive Glass-Ceramic Product VCP 15

Composition of VC 15 Frit, wt.%			
SiO_2	50.0		
TiO_2	5.0		
Al_2O_3	10.0		
B_2O_3	5.0		
Na_2O	5.0		
K_2O	5.0		
Li_2O	10.0		
CaO	5.0		
MgO	5.0		
Composition of VCP 15 Product, wt.%			
VC 15 frit	85.0	or	81.0
HAW oxide	15.0		15.0
Gd_2O_3			4.0
Physicochemical Properties			
Density (kg · m^{-3})	2.9		3.0
Viscosity (Pa · s) at 1150°C	5.5		3.3
Temperature (°C) at 10 Pa · s	1086		1034
Thermal expansion (K^{-1} × 10^{-6}) at 100 to 400°C	12.5		11.2
Characteristic temperatures (°C)			
T_g, transformation point	440		507
M_g, deformation point	704		650
T_p, softening point	723		675
Thermal conductivity ($W \cdot m^{-1} \cdot K^{-1}$)			
At 400°C	2.10		2.00
At 167°C	2.20		2.03
Electrical conductivity ($S \cdot m^{-1}$) × 10^2 at 1150°C	1.1		1.4
Specific heat ($J \cdot kg^{-1} \cdot K^{-1}$) × 10^3	1.46		
Evaporation velocity from the melt at 1150°C ($m \cdot s^{-1}$) × 10^{-9}	1.9		2.1
Mechanical strength			
Impact test ($m^2 \cdot J^{-1}$) × 10^{-4}	6.3		6.4
Microhardness (kg · mm^{-2})	780		720
Energy storage after 2.3 × 10^{12} rads ($J \cdot kg^{-1}$)	1.08 × 10^5		
Na-diffusion coefficient at 1150°C ($cm^2 \cdot s^{-1}$)	1.5 × 10^6		
U(Pu)-diffusion coefficient at 500°C ($cm^2 \cdot s^{-1}$) (Ref. 6)	<2 × 10^{-17}		

HYDROLYTIC STABILITY OF THE PRODUCT

Hydrolytic stability of a solidified highly radioactive waste-containing product at high temperatures is an important property for final storage. Based on storage conditions, the leach rates in some media are of interest at normal and elevated (boiling) temperatures. Higher storage temperatures are caused by heat production from radioactive decay. Elevated pressure can be expected when stored in deep geologic formations, thus a combination of elevated temperature and pressure can exist.

The Soxhlet test was used as an internationally known quick method for leach testing. All tests were made according to ISO standard proposals (Table 2). Inactive leaching experiments showed mainly Si, Na, and B containing substances, i.e., the glass-phase components, were leached out from the glass and also from the glass-ceramic matrix. The removal of the glass phase from the product surface can be seen clearly on photomicrographs after the completion of a Soxhlet test. The selective leach rates of radioactive components from highly active specimens were several orders of magnitude lower than in the inactive experiments; hence these selective results should be used to estimate the radioactivity release by leaching as opposed to using the overall leach rates of inactive components. The lower leach rates of radioactive components from glass-ceramics in comparison with glass can be explained by the mineral host phases of the glass-ceramics previously mentioned which bind radioactive elements more firmly than in the glass.[9]

EXPERIMENTS WITH HIGHLY RADIOACTIVE SPECIMENS

The highly radioactive glass-ceramic specimens of VCP 15 were prepared as cylinders[6-8] (diameter 52 mm, volume ~350 cm^3) with the characteristics shown in Table 3. These specimens are being investigated according to a long-term investigation program. Besides the leach tests mentioned, a series of other measurements has been conducted which includes macroscopic (γ scanning) and microscopic (α, β, γ autoradiography) distribution of radioactivity, ceramographic investigations of the structure (optical and SEM), and storage experiments at normal and elevated temperatures in air and dry salt formations. Some specimens are three years old, and previous investigations have shown no considerable changes in their structure or in other properties. Leach tests of highly radioactive specimens showed considerable leach rates for a few nuclides such as ^{134}Cs, ^{137}Cs, ^{144}Ce, ^{125}Sb, ^{152,154}Eu, and ^{241}Am. Other actinides were not detectable. Noble metals Ru, Rh, and Pd were also not detectable in the leachant because of their elemental state in the specimen and resultant high degree of insolubility (caused by denitration of the HAW solution).

CONCLUSIONS

When the results of KfK borosilicate glass product (GP 98 12) (Ref. 5) and of glass-ceramic product (VCP 15) are compared, one can see that most of the properties of the glass-ceramics are better than those of the glass, especially thermal properties. The leach rates are also slightly better. The most important advantage of the glass-ceramics is their greater thermodynamic equilibrium and consequently improved product stability for long-term storage.

TABLE 2

Leach Rate Values for Highly Radioactive Glass-Ceramics VCP 15

Methods and substances	Leach rate (kg · m^{-2} · s^{-1})
Inactive Specimens	
Soxhlet test	
Distilled H_2O at 100°C (total)	7.9×10 [illegible]
SiO_2	8.4×10^{-10}
Na_2O	3.5×10^{-10}
B_2O_3	1.2×10^{-10}
Rock salt brine	
Room temperature (total)	1.2×10^{-10}
150°C (total)	2.9×10 [illegible]
Quinary brine	
Room temperature (total)	5.8×10^{-10}
145°C (total)	4.24×10 [illegible]
Highly Radioactive Specimens	
Distilled H_2O	
Room temperature	
Gravimetry (total)	6.5×10^{-10}
γ activity (total)	2.9×10^{-12}
α activity (total)	3.6×10^{-11}
^{134}Cs + ^{137}Cs/Ba	1.9×10^{-12}
^{144}Ce/Pr	2.3×10^{-12}
^{106}Ru/Rh	n.d.*
^{125}Sb	6.4×10^{-11}
^{152,154}Eu	2.5×10^{-11}
^{241}Am	4.1×10^{-12}

*Not determined.

TABLE 3

Characterization of the Highly Radioactive Glass-Ceramic Product VCP 15 Specimens

Fuel	Burn-up, MWd/t	Cooling time, Y	Fission product (f. p.) concentration, wt.%	Specific radioactivity, Ci/l α	β	Total
FBR	60,000	10.2	20	4	986	900
LWR	28,600	3.0	20 f. p. + 10 Gd_2O_3	52	4523	4575

REFERENCES

1. W. Hinz, *Silikate*, Vol. 1, No. 151, VEB-Verlag fur Bauwesen, Berlin, 1970.
2. W. Guber and J. Saidl, *Glass Ceramic As a Solidification Material for Highly Radioactive Waste*, p. 45, in ADB Annual Report 1972, KfK-2000 (KfK Kernforschungszentrum Karlsruhe GmbH), 1974.
3. W. Guber, L. Kahl, and J. Saidl, *Recent Experiments on Fixation of HAW in Karlsruhe*, Report KfK-2179 (KfK Kernforschungszentrum Karlsruhe GmbH), 1975.
4. W. Guber, J. Saidl, P. Darushy, and W. Hild, *Thermodynamically Stable Product for Permanent Storage and Disposal of HLW*, U. S. Patent 4,097,401, 1978.
5. W. Guber et al., Preparation and Characterization of an Improved

Borosilicate Glass Matrix for the Incorporation of HLW, in *Proceedings of Scientific Basis for Nuclear Waste Management*, Boston, G. J. McCarthy (Ed.), Plenum, NY, 1979, or Report KfK-2721 (KfK - Kernforschungszentrum Karlsruhe GmbH), 1979.

6. W. Guber et al., *Solidification of HLLW Radioactive Fission Product Solution*, p. 4[illegible], in ABRA Annual Report 1975, KfK 2[illegible] (KfK - Kernforschungszentrum Karlsruhe GmbH), 1976.

7. A. E. Ringwood, *Safe Disposal of High Level Nuclear Reactor Wastes: A New Strategy*, Australian National University Press, Canberra, Australia, and Norwalk, Connecticut, 1978.

8. W. Guber et al., *Solidification of HLLW Radioactive Fission Product Solution in a Borosilicate Matrix*, p. 17, in ABRA Annual Report 1976, KfK-2519 (KfK - Kernforschungszentrum Karlsruhe GmbH), 1977.

9. Hj. Matzke, Actinide Diffusion in Waste Glasses, *IAEA International Symposium on Thermodynamics of Nuclear Materials*, Paper IAEA-SM-236/5, Jülich, Federal Republic of Germany, January 29-February 2, 1979.

PHASE SEPARATION IN NUCLEAR WASTE GLASSES

M. TOMOZAWA,* G. M. SINGER,* Y. OKA,* and J. T. WARDEN†
*Materials Engineering Department and †Chemistry Department, Rensselaer Polytechnic Institute,
Troy, New York

ABSTRACT

An effective additive was found to suppress the liquid-in-liquid phase separation in a nuclear waste glass; namely, the addition of 0.3 wt.% carbon to the nuclear waste glass 77-107 eliminated the yellow liquid, making the resultant glass apparently homogeneous. Electron microscopy study showed, however, a heterogeneous microstructure even in apparently homogeneous glass specimens. The carbon addition appears to reduce the volume fraction of the second phase. In order to clarify the mechanism involved, the effect of oxidation state, especially Fe^{2+}/Fe^{3+} ratio, on the immiscibility temperature of a model system, Na_2O–SiO_2–B_2O_3 glass, with 0.5 mole % iron oxide was determined. The results can be explained in terms of ionic field strength of iron ions.

INTRODUCTION

When nuclear waste is incorporated into glasses, a water-soluble phase containing molybdenum often separates in the liquid state[1-3] causing a substantial decrease in chemical durability.

The composition and temperature range of liquid-in-liquid (glass-in-glass) phase separation are defined by the immiscibility boundary. When the immiscibility boundary is above the liquidus temperature, it is called stable immiscibility while immiscibility below the liquidus is called metastable immiscibility. A well-known example of metastable immiscibility is in the Na_2O–B_2O_3–SiO_2 system[4] which is used to produce high silica glass.[5]

Phase separation, observed in nuclear waste glass during melting, appears to be associated with stable immiscibility and is the obvious point of concern because it causes macroscopic inhomogeneity and consequent deterioration of chemical durability. In addition, the possibility of metastable immiscibility in nuclear waste glass should also be considered since this type of phase separation can take place when glass is held at a temperature near the glass transition temperature and can cause deterioration of chemical durability.[5]

The position of an immiscibility boundary is influenced by various factors. The field strength of cations[6-10] is recognized as an important parameter; the cation with the greater field strength has a greater tendency for phase separation.

Earlier it was reported[11-13] that the replacement of SiO_2 by silicon can suppress the phase separation tendency. However, silicon makes the glass melt extremely reactive with refractories (or canisters) and electrode materials in electric melting and is, therefore, not desirable.

The purposes of this investigation were to characterize the phase separation in nuclear waste glasses and to find an effective additive which could suppress the phase separation without causing detrimental phenomena such as high reactivity of the melt.

EXPERIMENTAL

The identification of liquid-in-liquid phase separation was made by visual inspection. Metastable immiscibility was observed with a single-stage replica electron microscope. For this purpose, the freshly fractured surface was etched with 5% HF solution for 5 sec at room temperature, and the replica was produced by shadowing with vapor-deposited platinum at approximately 45° and reinforcing with carbon. For transparent specimens the metastable immiscibility temperature was determined by observing the opalescence after heat treatment at various temperatures.

Nuclear waste glasses investigated were BNWL type 77-107, 76-68 and 72-260. Compositions of these glasses

TABLE 1

Composition of Nuclear Waste Glasses Investigated

77-107 – 2 parts of frit 77-268 + 1 part of waste PW-9
76-68 – 2 parts of frit 76-101 + 1 part of waste PW-8a-3
77-260 2 parts of frit 77-269 + 1 part of waste PW-7C

77-268		76-101		77-269	
	Wt.%		Wt.%		Wt.%
SiO_2	56.7	SiO_2	59.7	SiO_2	53.7
B_2O_3	19.4	B_2O_3	14.2	B_2O_3	13.4
Na_2O	3.0	Na_2O	11.2	Na_2O	11.9
K_2O	6.0	ZnO	7.45	K_2O	3.0
ZnO	7.5	CaO	3.0	CaO	1.5
CaO	3.0	TiO_2	4.45	TiO_2	9.0
TiO_2	4.5			Al_2O_3	3.0
				CuO	4.5

reported by BNWL are shown in Table 1. In addition, model glass composition $10Na_2O\ 50B_2O_3\ 40SiO_2$ (mole %) with 0.5 mole % iron oxide addition was studied to observe the relation between the immiscibility temperature and the oxidation state of glasses. The oxidation state of glass was modified by changing the melting temperature and was measured using both chemical analysis[14] and ESR.

RESULTS AND DISCUSSION

Liquid-in-Liquid Phase Separation in Nuclear Waste Glass

Of the three simulated nuclear waste glasses investigated, 77-107 exhibited the most serious visible phase separation problem and, therefore, an attempt was made to suppress this phase separation. Since the ionic field strength is the major factor in phase separation tendency, efforts to suppress phase separation have centered around lowering the field strength of cations present in the melt. As a result, it was found that a small addition of carbon is effective in eliminating liquid-in-liquid phase separation. Specifically, with 0.3 wt.% carbon added to 77-107, the yellow liquid separation disappeared completely.

The function of carbon here is to reduce the field strength of cations. Nuclear waste glass 77-107 contains various cations such as iron, titanium and molybdenum which can be reduced. An ESR study of Fe^{3+} was made to see the effect of carbon addition. At low temperature (12°K) the Fe^{3+} signal at $g = 4.2$ was much larger for 77-107 without carbon than for glass with carbon, indicating the reduction of Fe^{3+} to Fe^{2+} with carbon addition, as shown in Fig. 1. Compared with silicon, carbon is a milder reducing agent and is not expected to make the melt highly reactive with containers or electrodes in electric melting. In fact, carbon is used routinely in glass industries to manufacture amber glasses.

Earlier the use of carbon was mentioned to suppress phase separation,[11] but silicon was preferred since it is oxidized to SiO_2, one of the glass components. In view of the highly reactive nature of the silicon-containing melt and the widespread commercial use of carbon, it appears that carbon should be the preferred reducing agent to suppress the phase separation in nuclear waste glasses.

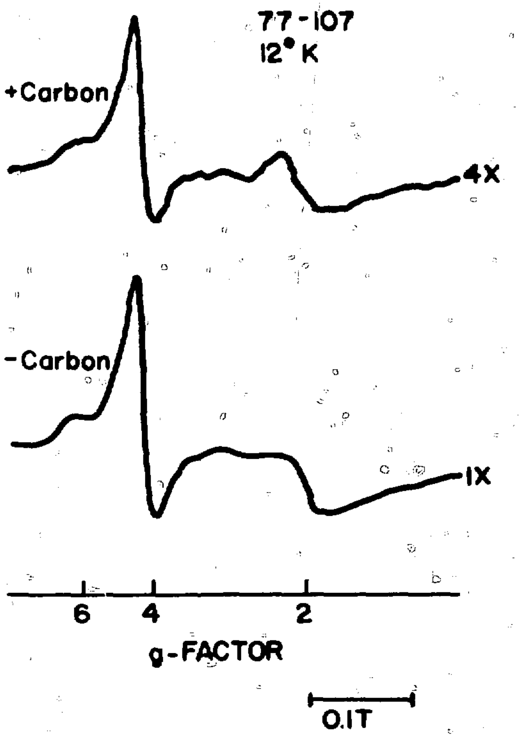

Fig. 1 ESR signal at 12°K from Fe^{3+} in 77-107 with and without carbon.

Glass-in-Glass Phase Separation in Nuclear Waste Glasses

Visibly homogeneous glasses can be heterogeneous in their microstructure, and this heterogeneous microstructure can strongly influence various properties of glasses including chemical durability.[6,15] The electron micrographs of fractured and etched surfaces of nuclear waste glasses are shown in Fig. 2. As can be seen in this figure, all specimens showed a heterogeneous microstructure. With the addition of carbon, the volume fraction of the second phase appears reduced. These specimens were quenched from the melt, thus it is not possible to obtain quantitative information from these micrographs. However, at least in some specimens, discrete second phase particles are protruding, indicating a silica-rich composition of these particles. With this type of microstructure, the matrix composition which controls the chemical durability of the specimen loses silica upon phase separation. Thus the chemical durability is expected to decrease with an increase in phase separation.

Effect of Oxidation State on Immiscibility Boundary

Carbon was found to be an effective suppressant of the liquid-in-liquid phase separation. A possible explanation is

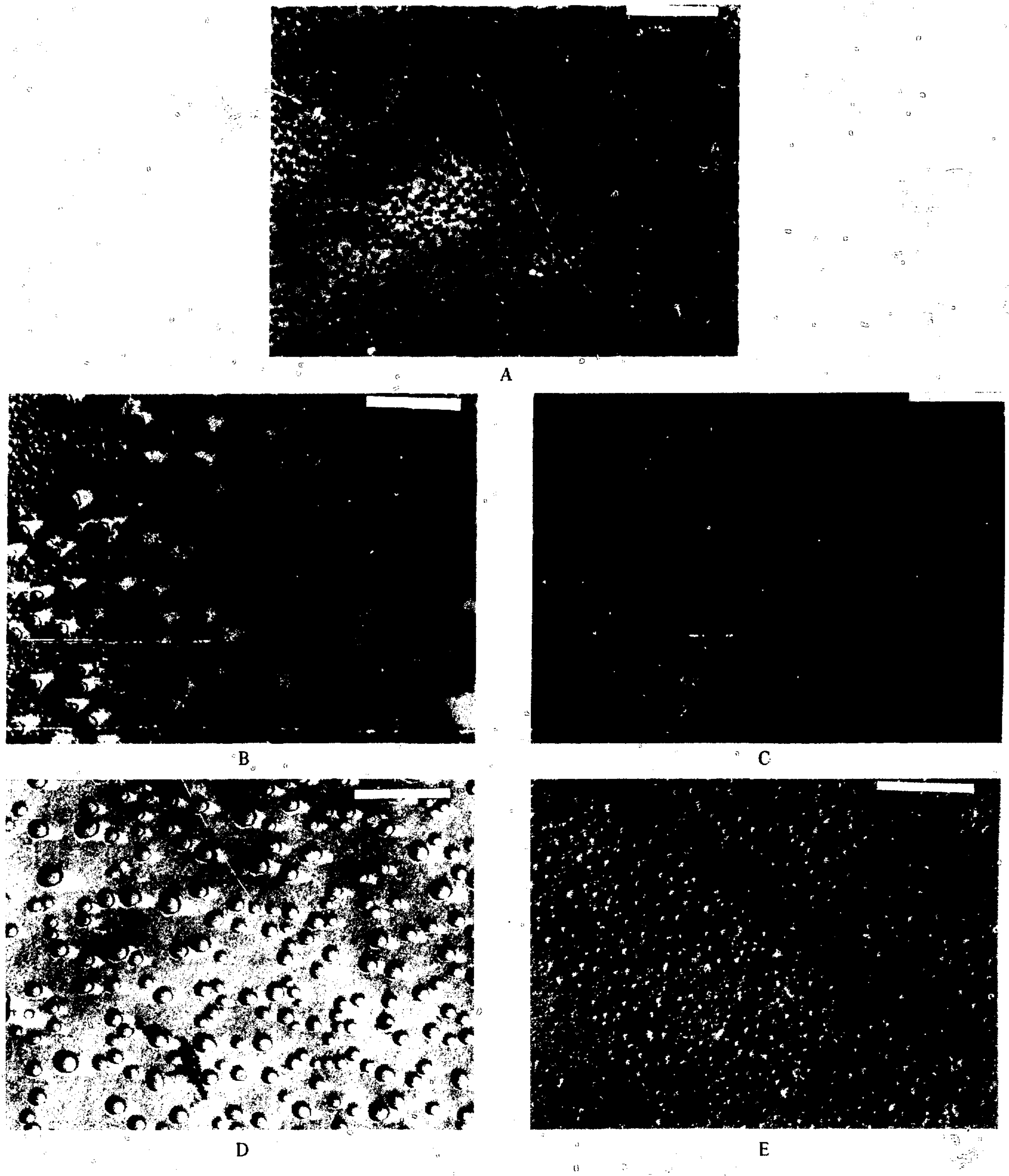

Fig. 2 Electron micrograph of nuclear waste glasses prepared at RPI, using frits and waste supplied by BNWL. (White marker is 5000 Å.)

A. 77-107 melted at 1050°C for 3 hr.

B. 77-107 melted at 1150°C for 3 hr.

C. 77-107 with 0.3 wt.% carbon melted at 1150°C for 3 hr.

D. 76-68 melted at 1050°C for 3 hr.

E. 77-260 melted at 1050°C for 3 hr.

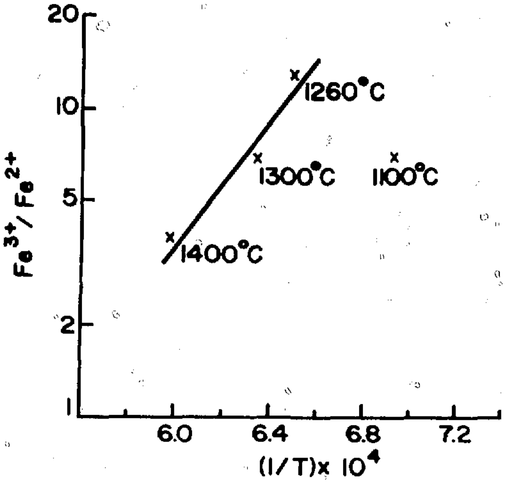

Fig. 3 Fe^{3+}/Fe^{2+} ratio and the melting temperature for $10Na_2O$-$50B_2O_3$-$40SiO_2$ mole % with 0.5 mole % iron oxide.

that carbon reduces the multivalent ions (such as iron ions), and the reduced field strength of the ion reduces the immiscibility tendency. To confirm this, a study was made on the effect of oxidation state, e.g., Fe^{2+}/Fe^{3+} ratio, on the immiscibility boundary of a model glass with composition $10Na_2O$ - $50B_2O_3$ - $40SiO_2$ (mole %). This glass can be melted at fairly low temperatures, ~1050°C, and has an immiscibility temperature of ~688°C. To this glass, 0.5 mole % iron oxide was added, and various Fe^{2+}/Fe^{3+} ratios were produced by changing the melting temperature under the same melt atmosphere. The immiscibility temperature was determined by heat treating specimens of 5 mm x 5 mm x 5 mm size at various temperatures for various lengths of time (20 min to several hours) and observing the appearance and disappearance of the opalescence.

At a constant oxygen partial pressure, i.e., air, the oxidation state expressed as Fe^{2+}/Fe^{3+} changes with the melting temperature in the following manner.[16]

$$\ln\left(\frac{Fe^{3+}}{Fe^{2+}}\right) = -\frac{A}{T} + B$$

where A and B are constants, and A is proportional to the standard enthalpy change ΔH° for oxidation reaction $Fe^{2+} \rightleftharpoons Fe^{3+}$ and is negative.

In the present study, melt temperatures of 1400, 1300, 1260 and 1100°C were chosen. The Fe^{2+}/Fe^{3+} ratios of the resulting glasses determined by chemical analysis are shown in Fig. 3. Data points for 1400, 1300, and 1260°C show a trend expected from the equation. The data at 1100°C, however, deviates from the straight line indicating that the melt had not reached equilibrium at this temperature in 20 hr. The corresponding immiscibility temperatures are plotted against the fractional ferrous content, as shown in Fig. 4. In this range of fractional ferrous quantity for this glass, the immiscibility temperature is uniquely determined by the oxidation state. The greater the amount of ferrous ion, the lower the immiscibility temperature, consistent with the observation on phase separation in nuclear waste glass. Thus it appears that the idea[8-10] of the ionic field strength being the dominant factor in shifting the immiscibility temperature is valid in the range of oxidation state shown here. This simple interpretation may not hold in general, however, since it is known that ferric iron ions (Fe^{3+}) can occupy both tetrahedral sites and octahedral sites, and ions in these two different sites are expected to have a different influence on the immiscibility temperature.

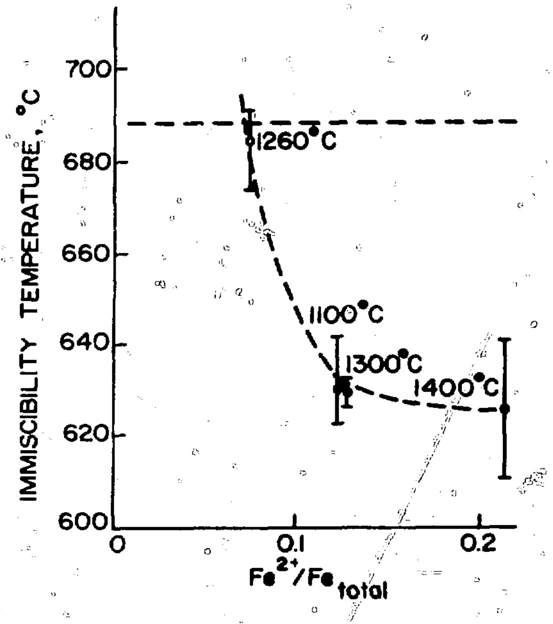

Fig. 4 Effect of oxidation state on the immiscibility temperature of $10Na_2O$-$50B_2O_3$-$40SiO_2$ mole % with 0.5 mole % iron oxide. Temperature near the data points indicates the melting temperature.

CONCLUSIONS

Addition of 0.3 wt.% carbon to nuclear waste glass 77-107 was found to be effective in eliminating the separation of a molybdenum-rich yellow phase. Electron microscope observations, however, showed a glass-in-glass phase separation in all of the nuclear waste glasses studied. Consistent with the effect of a reducing agent, i.e., carbon, on the phase separation of nuclear waste glass, an increasing fraction of ferrous ions reduced the metastable immiscibility temperature of a model glass system of $10Na_2O$-$50B_2O_3$-$40SiO_2$ (mole %) with 0.5 mole % iron oxide.

ACKNOWLEDGMENT

Financial support of the U.S. Department of Energy through Battelle, Pacific Northwest Laboratory under Contract No. EW-78-S-06-1088 is appreciated.

REFERENCES

1. J. E. Mendel and J. L. McElroy, *Evaluation of Solidified Waste Products*, DOE Report BNWL-1666, Pacific Northwest Laboratory, 1972.
2. J. B. Morris and B. E. Chidley, Preliminary Experience with the New Vitrification Inactive Pilot Plant, presented at *International Symposium on the Management of Radioactive Wastes from the Nuclear Fuel Cycle*, Vienna, Austria, March 22–26, 1976.
3. A. R. Hall, J. T. Dalton, B. Hudson and J. A. L. Marples, Development and Radiation Stability of Glasses for Highly Radioactive Wastes, presented at *International Symposium on the Management of Radioactive Wastes from the Nuclear Fuel Cycle*, Vienna, Austria, March 22–26, 1976.
4. W. Haller, D. H. Blackburn, F. E. Wagstaff, and R. J. Charles, Metastable Immiscibility Surface in the System $Na_2O-B_2O_3-SiO_2$, *J. Am. Ceram. Soc.*, 53(1): 34 (1970).
5. H. P. Hood and M. E. Nordberg, *Method of Treating Borosilicate Glasses*, U. S. Patent 2,215,039 (1940).
6. T. Takamori and M. Tomozawa, HCl Leaching Rate and Microstructure of Phase-Separated Borosilicate Glasses, *J. Am. Ceram. Soc.*, 61(11-12): 509 (1978).
7. B. E. Warren and A. G. Pincus, Atomic Consideration of Immiscibility in Glass Systems, *J. Am. Ceram. Soc.*, 23: 301 (1940).
8. A. Dietzel, Glass Structure and Glass Properties I, *Glastech. Ber.*, 22: 41 (1948).
9. E. M. Levin, Liquid Immiscibility in Oxide Systems, Chapter V in Phase Diagrams, *Materials Science and Technology*, Vol. III, Academic Press, Inc., New York, 1970.
10. M. Tomozawa, Effect of Oxide Nucleating Agents on Phase Separation of Simple Glass System, *Advances in Nucleation and Crystallization in Glasses*, Am. Ceram. Soc., Special Publication No. 5, p. 41, L. L. Hench and S. W. Freiman (Eds.), 1972.
11. J. L. McElroy, *Research and Development Activities, Waste Fixation Program, Quarterly Progress Report, October–December 1975*, BNWL-1994, Pacific Northwest Laboratory, 1976.
12. J. L. McElroy, *Quarterly Progress Report, Research and Development Activities, Waste Fixation Program, June–September 1975*, BNWL-1949, Pacific Northwest Laboratory, 1976.
13. C. C. Chapman, *Experience with a Joule Heated Ceramic Melter, While Converting Simulated High Level Waste to Glass*, BNWL-2071, Pacific Northwest Laboratory, 1976.
14. W. P. Close and J. F. Tillman, Chemical Analysis of Some Elements in Oxidation-Reduction Equilibria in Silicate Glasses, *Glass Technol.*, 10(5): 134 (1969).
15. M. Tomozawa and T. Takamori, Effect of Phase Separation on HF Etch Rate of Borosilicate Glasses, *J. Am. Ceram. Soc.*, 60(7-8): 301 (1977).
16. W. D. Johnston, Oxidation-Reduction Equilibria in Iron-Containing Glass, *J. Am. Ceram. Soc.*, 47(4): 198 (1961).

COMPATIBILITY OF ACTINIDES WITH HLW BOROSILICATE GLASS: SOLUBILITY AND PHASE FORMATION

C. T. WALKER* AND U. RIEGE†
*European Institute for Transuranium Elements, Karlsruhe, Federal Republic of Germany and
†Abteilung Behandlung radioaktiver Abfälle Kernforschungszentrum,
Karlsruhe, Federal Republic of Germany

ABSTRACT

Actinide oxides in the amounts expected in HLW glass are completely soluble in the glass. At 1400°K, the solubility of PuO_2 in borosilicate glass is about 4.5 wt.% and is unaffected by the addition of 20 wt.% HLW oxides. The presence of 10 wt.% Gd_2O_3 gives rise to a segregate phase of the type $Pu_{0.7}Ce_{0.2}Gd_{0.1}O_2$ and hence decreases the solubility of PuO_2 to 1.3 wt.%.

INTRODUCTION

In addition to fission product elements and the products of cladding corrosion, high-level waste (HLW) contains a number of different actinides. For a stable HLW glass product these actinides should be homogeneously dissolved in the glass. The formation of actinide-containing phases is undesirable because they may adversely affect the properties of the glass. For example, they may increase the rate at which actinides are leached from the glass; they may cause the glass matrix to crystallize during storage; or they may, as a result of helium production, decrease the mechanical strength of the glass. It is important, therefore, to establish the limits of solubility of the actinides in HLW glass.

EXPERIMENTAL

The solubility of actinide oxides (UO_2, NpO_2, PuO_2, AmO_2 and CmO_2) in two simulated (hence not radioactive) HLW borosilicate glasses was investigated by electron probe microanalysis. One glass contained 20 wt.% HLW oxides, the other 20 wt.% HLW oxides and 10 wt.% Gd_2O_3 (the neutron poison in the reprocessing plant). To determine whether the HLW constituents lower the solubility of the actinide oxides and enhance phase formation, the behavior of the actinide oxides in the base glass was first established. The compositions of the base glass and the two HLW glasses are given in Table 1.

HLW Borosilicate Glass Specimens

The investigation was performed on specimens of the base glass and the two HLW glasses that had been doped with known amounts of one of the actinide oxides. For example, a specimen of glass 98-20 doped with 10 wt.% PuO_2 and a specimen of glass 98-30 doped with 2 wt.% PuO_2 were used to determine the behavior of PuO_2 in HLW glass.

The doped glasses were prepared by mixing a known quantity of the actinide oxide powder with the powdered glass. The mixture was melted at 1400°K and held in the molten state for 2 hr to ensure a homogeneous product. The glass was slowly cooled to room temperature (10°K/min) and during cooling it was tempered for 1 hr at 900°K.

Electron Probe Microanalysis

A shielded Cameca MS46 electron probe microanalyser was employed at an acceleration voltage of 13 kV and beam currents of 20, 50, and 100 nA. The composition of the plutonium-containing phase in glass 98-30 doped with 2 wt.% PuO_2 was determined using the standard analytical procedure in which K values ($K = I/I_0$, where I is the

TABLE I

Composition of Simulated HLW Borosilicate Glasses

Constituent	Concentration, wt.% Glass 98-20, base glass* + 20 wt.% simulated HLW	Glass 98-30, base glass* + 20 wt.% simulated HLW + 10 wt.% Gd_2O_3
Glass components		
SiO_2	40.2	35.1
TiO_2	3.3	2.9
Al_2O_3	1.1	1.0
B_2O_3	10.8	9.5
CaO	2.2	2.0
Na_2O	21.9	19.1
Fission products†		
SrO	0.50	0.50
BaO	0.76	0.76
Cs_2O	1.36	1.36
Rb_2O	0.18	0.18
TeO_2	0.38	0.38
MoO_3	2.47	2.47
Ru	1.06	1.06
Rh	0.19	0.19
Pd	0.64	0.64
TcO_2‡	0.53	0.53
CdO	0.05	0.05
ZrO_2	2.36	2.36
Y_2O_3	0.28	0.28
La_2O_3	0.71	0.71
Ce_2O_3	1.60	1.60
Nd_2O_3§	2.90	2.90
Pr_2O_3	0.67	0.67
Cladding corrosion products		
Fe_2O_3	1.87	1.87
Cr_2O_3	0.53	0.53
NiO	0.29	0.29
Actinides		
UO_2	0.52	0.52
PuO_2	0.41	0.41
NpO_2	0.12	0.12
$(Am, Cm)O_2$	0.02	0.02
Gd neutron poison		
Gd_2O_3		10.0

*Composition (wt.%) : SiO_2 50.5, TiO_2 4.2, Al_2O_3 1.4, B_2O_3 13.6, CaO 2.8 and Na_2O 27.5.

†Concentrations correspond to those arising from a LWR-fuel irradiated to a burnup of 33000 MWdt^{-1} (Ref. 1).

‡MnO_2 substitute used.

§Nd_2O_3 content comprises (wt.%) : Nd_2O_3 2.23, Sm_2O_3 0.46, Gd_2O_3 0.06, Pm_2O_3 0.05 and Eu_2O_3 0.10.

characteristic X-ray line intensity from the specimen and I_0 is that from the pure standard) are obtained for each constituent and then corrected for the influence of atomic number, X-ray absorption and X-ray fluorescence using a standard ZAF program. In this work the program of Tong[2] was used.

The amounts of the actinide oxides dissolved in the borosilicate glasses were determined by direct measurement against a number of glass standards, each of which contained a known amount of one of the oxides under investigation. The usual analytical procedure could not be used because of problems associated with the analysis of oxygen, sodium, and boron. For these elements not only is it difficult to obtain reliable K values but, also, matrix corrections cannot be accurately calculated.

The glass standards contained only a small amount of either an actinide oxide or a fission product oxide. For example, the uranium glass standard contained 10 wt.% UO_2, the neptunium standard 4 wt.% NpO_2, the plutonium standard 2 wt.% PuO_2, and the cerium standard 5 wt.% Ce_2O_3. The amount of an oxide that could usefully be added to the borosilicate glass to produce a standard was restricted by its solubility; precision analysis required that the oxide was homogeneously dissolved in the glass and that no segregate phases were formed.

The low concentrations of the actinide oxides in the glass standards resulted in poor X-ray counting statistics that were a source of inaccuracy in the analyses. The errors resulting from the poor counting statistics, however, are judged to be small and in the worst case were probably of the order of the standard deviation that resulted from the point to point variations in the measured concentrations.

Borosilicate glass is an insulator and prior to electron probe microanalysis both the HLW glass specimens and the glass standards were coated with a conducting layer of aluminum about 15 nm thick.

RESULTS

Solubilities of Actinide Oxides

Figure 1 shows alpha-autoradiographs from two borosilicate glasses; one doped with 2 wt.% PuO_2, the other with 10 wt.% PuO_2. Inclusions containing plutonium were absent from the former glass, and the PuO_2 was homogeneously dissolved. The latter glass contained many PuO_2 inclusions; most of these were small ($<$ 100 μm in size), but a few were of the order of 200 to 300 μm in size.

The results of the solubility study are given in Table 2. The data consist of solubility values (with standard deviations) determined by EMPA in the presence of a segregate phase containing the actinide and solubility values that were inferred from the absence of the actinide in the segregate phases formed. The concentrations in Table 2 are the solubilities at the temperature of mixing (1400°K). Although the glass melt was cooled slowly, it is unlikely that room temperature equilibrium was obtained because the rate of diffusion of uranium and plutonium in borosilicate glass is slow.[3] For example, at 813°K (below the glass recrystallization temperature) the diffusion coefficient for ^{233}U is 4.1 x 10^{-17} cm^2/s.

Actinide oxides in the amounts expected in HLW glass are completely soluble in the glass (Tables 1 and 2). Indeed, there is a significant difference between the expected concentration of each actinide oxide and its solubility limit. For example, in glass 98-30 the solubility of UO_2 was at

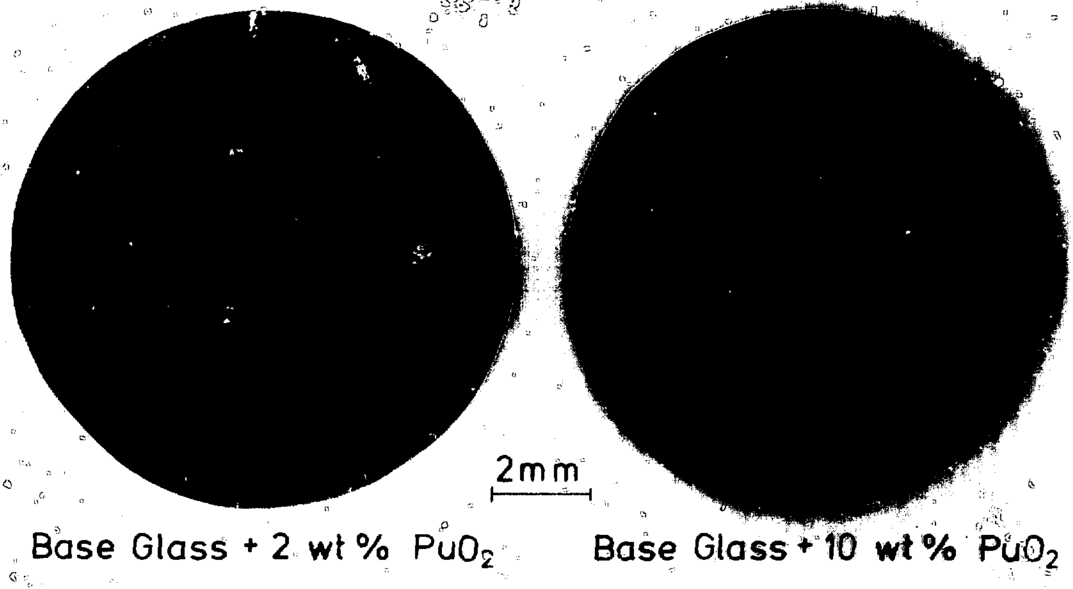

Fig. 1 Behavior of PuO_2 in borosilicate glass as revealed by alpha-autoradiography.

least 6 times greater than its expected concentration, the solubility of NpO_2 was 8 times greater than its expected concentration, and the solubility of PuO_2 was 100 times greater than its expected concentration. The solubilities of AmO_2 and CmO_2 were at least 50 times and 5 times greater than their expected concentrations, respectively.

The solubility of PuO_2 in borosilicate glass is about 4.5 wt.% (Table 2). This concentration was unaffected by the addition of 20 wt.% HLW oxides (glass 98-20). The presence of 10 wt.% Gd_2O_3 (glass 98-30), however, led to the formation of a segregate phase of the type $Pu_{0.7}Ce_{0.2}Gd_{0.1}O_2$ (Fig. 2 and Table 3) and consequently decreased the solubility of PuO_2 to 1.3 wt.%. The matrix of the glass contained 7.1 ± 0.4 wt.% gadolinium and 0.8 ± 0.1 wt.% cerium.

The solubility of fission product cerium is dependent on the plutonium content of the glass. In the presence of plutonium concentrations in excess of the solubility limit, oxide phases of the type $(Pu_xCe_{1-x})O_2$ precipitated, and less cerium was dissolved in the glass matrix.

TABLE 2

Solubilities of Actinide Oxides in Borosilicate Glass

Actinide oxide	Concentration, wt.%		
	Base glass	Glass 98-20	Glass 98-30
UO_2	>10.0	>5.4	>3.2, <5.4
NpO_2	>4.0	3.5 ± 0.3	3.2 ± 0.2
PuO_2	4.5 ± 0.3	4.4 ± 0.3	1.3 ± 0.4
AmO_2	>5.0	>5.0	>5.0
CmO_2	>0.09	>0.09	>0.09

TABLE 3

Composition of the Plutonium-Bearing Segregate Phases in 98-30 Borosilicate Glass Doped with 2 wt.% PuO_2

Element	Concentration, wt.%
Pu	67
Gd	8
Ce	12
Zr	<1
O*	12

*Determined by difference.

In addition to plutonium containing phases, HLW glass also contains many small (<5 μm in size) fission product inclusions (Fig. 2). Inclusions of molybdenum and the platinum group metals, ruthenium, rhodium, and palladium, were the most abundant. Figure 3 shows an accumulation of platinum metal inclusions at the bottom of a glass sedimentation column (80 mm high). Two types of inclusion are apparent. Spherical inclusions are an alloy of rhodium and palladium, whereas acicular inclusions are an alloy of ruthenium and rhodium. The finding of palladium in the acicular inclusions is an apparent one only and results from the superimposition of the Ru $L\beta_2$, the Rh $L\beta_1$ and the Pd $L\alpha_1$ X-ray lines.

CONCLUSIONS

1. The solubility of PuO_2 in borosilicate glass is about 4.5 wt.%. This concentration is unaffected by the presence

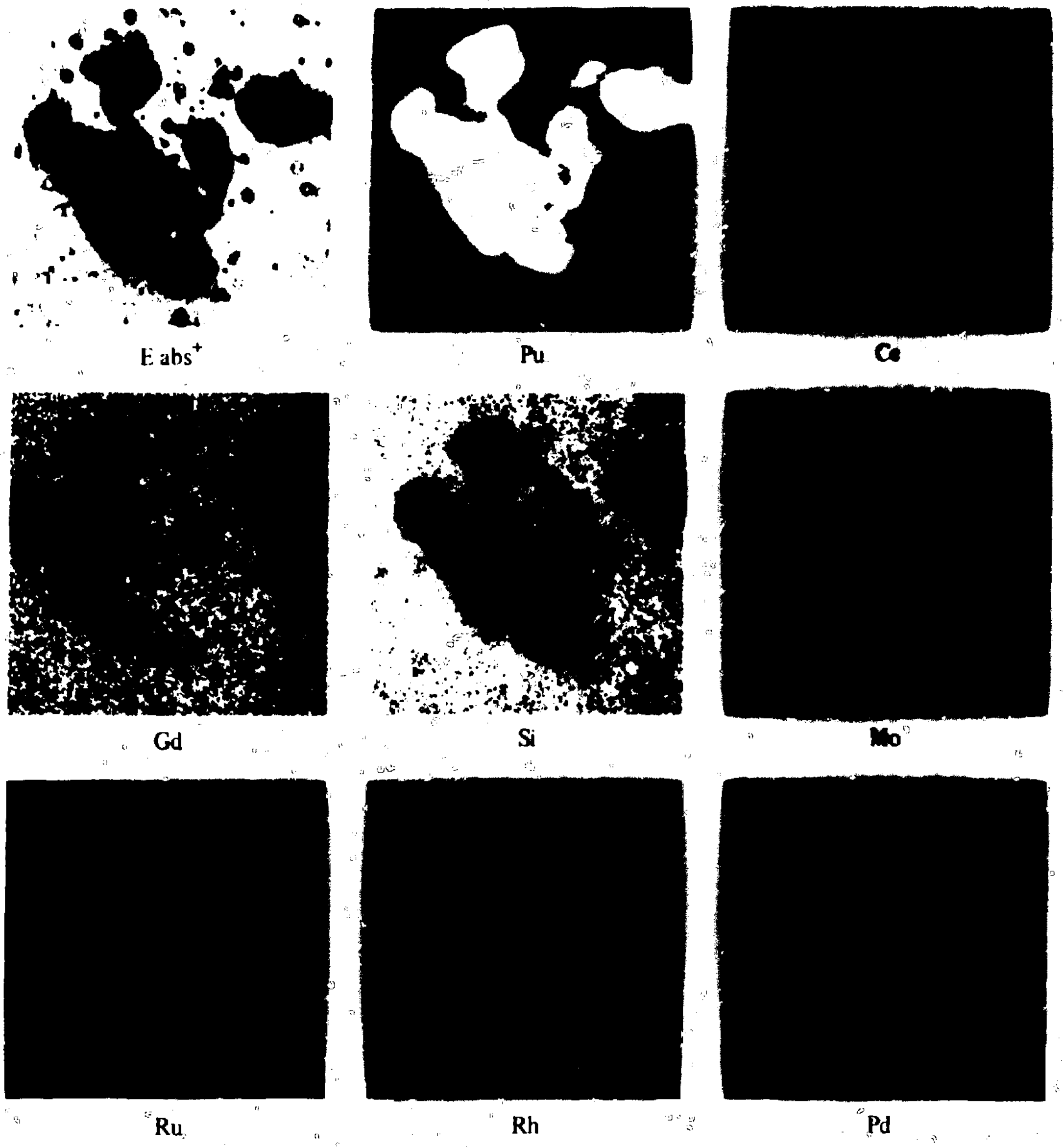

Fig. 2 Segregate phases in glass 98-30 doped with 2 wt.% PuO_2 as revealed by electron microprobe X-ray scanning.

of fission product elements in concentrations corresponding to a fuel burnup of 33 GWdt^{-1}

2. When the PuO_2 concentration in borosilicate glass exceeds the limit of solubility the following occurs:

(a) In the absence of fission product elements, PuO_2 inclusions form.

(b) In the presence of fission product elements, in concentrations corresponding to a fuel burnup of 33 GWdt^{-1}, a phase of the type $(Pu_xCe_{1-x})O_2$ precipitates.

3. In the presence of fission product elements in concentrations corresponding to a fuel burnup of 33 GWdt^{-1} and PuO_2 in excess of the solubility limit, up to 7 wt.% gadolinium is soluble in borosilicate glass. Excess gadolinium is incorporated in the $(Pu_xCe_{1-x})O_2$ type inclusions.

4. Gadolinium concentrations in excess of about 7.0 wt.% enhance the formation of phases of the type $(Pu_xCe_{1-x})O_2$ and, consequently, decrease the solubility of PuO_2.

5. The results of the solubility study support the view that borosilicate glass is a suitable medium for the incorporation of HLW. Indeed, in borosilicate glass it is possible to dissolve waste with much higher actinide concentrations than those expected in HLW.

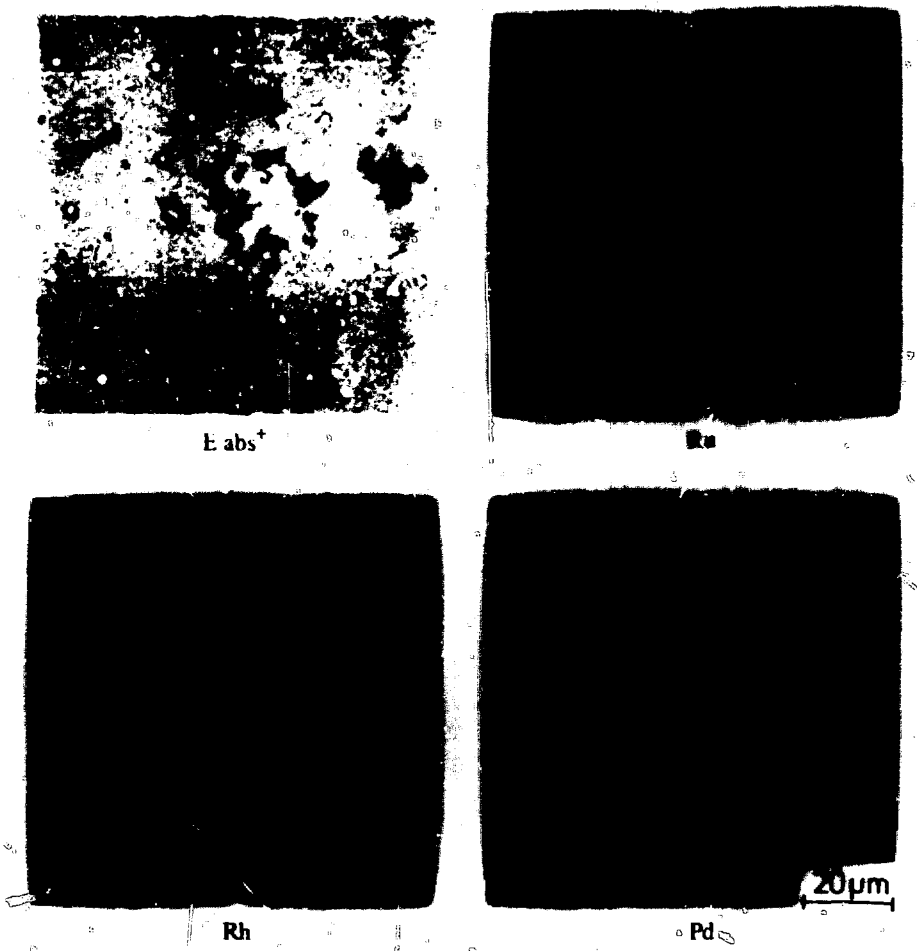

Fig. 3 Accumulation of noble metal inclusions at the base of a column of 98-20 glass doped with 5 wt.% UO_2 and 1 wt.% PuO_2. The glass had been held in the molten state for 25 hr.

REFERENCES

1. *Siting of Fuel Reprocessing Plants and Waste Management Facilities*, Report ORNL-4451, Oak Ridge National Laboratory, 1970.
2. M. Tong, Méthode de Correction en Microanalyse, *J. Micros. (Paris)*, 8: 276 (1969).
3. Hj. Matzke, Actinide Diffusion in Waste Glasses, in *Proceedings of International Symposium on Thermodynamics of Nuclear Materials*, Julich, Federal Republic of Germany, IAEA-SM-236/5 (1979).

AN INVESTIGATION OF CRYSTALLIZATION IN GLASSES CONTAINING FISSION PRODUCTS

G. MALOW
Hahn-Meitner-Institut für Kernforschung Berlin GmbH., Department of Nuclear
Chemistry and Reactor, Glienicker Strasse 100, D-1000 Berlin 39

ABSTRACT

Five potential solidification products for high-level waste (four borosilicate glasses and one celsian glass ceramic) have been *investigated in terms of crystallization. In all glasses and in the glass* ceramic, crystallization and recrystallization, respectively, were observed by heating above 773°K, however, at very different periods of time ($0.1d \leq t \leq 100d$). The noble metals precipitated into various phases. Crystal growth proceeded at the phase boundary glass-noble metal. In all products rare earth phases crystallized. Silicate phases rarely formed. The leach resistance (by the grain titration and Soxhlet tests) decreased after heat treatment in all cases. The changes were found to be within one order of magnitude for all products.

INTRODUCTION

Glasses are thermodynamically unstable and may spontaneously crystallize during long-term storage. In so doing, physical and chemical changes are brought about which may influence safety-related properties such as leach resistance. Therefore the extent of alteration and changes in leach resistance should be known. A joint program of the European Communities on characterization of waste forms was started in 1977. Five potential solidification products for high-level waste (four borosilicate glasses and one glass ceramic) are being investigated. The part of the program taken over by the Hahn-Meitner-Institut refers to effects of heat, i.e., crystallization, on the product properties. Some results will be reported in this paper.

The investigation is based on DTA, viscosity, SEM, and EPMA experiments and comprises the determination of "characteristic" temperatures of the products as well as the detection and identification of crystal phases. In order to characterize the chemical stability of heat-treated products on a relative basis, leach tests were carried out using a grain titration and Soxhlet method.

EXPERIMENTAL

The preparation and the heat treatment of the simulated inactive glasses F-SON 58.30.20, D-VG 98/3, UK-209, UK-189 and D-B 1-3 were done at AERE Harwell.[1]

Heat Treatment

The as-cast glasses were annealed at 773°K for 2 hr. The parent glass of the glass ceramic was heat-treated successively at 883°K for 3 hr and 1073°K for 10 hr to induce nucleation and allow crystallization.[2] Thereafter, the samples were held at temperatures of 773, 873, 973 and 1073°K for periods of 2 hr, 1 day, 10 days, and 100 days.

Leaching Methods

In the grain titration method, 2 g of glass powder with a grain size 0.315 to 0.500 mm was heated for one hour at 373°K in 50 ml of distilled water. Then 25 ml of the supernatant solution was titrated with 0.01 *N* HCl. The release of alkali from the glass powder is estimated by the acid consumption.[3]

A direct measurement of the leach rates from the weight loss of the glass samples was performed after leaching 1 g of glass powder with the grain fraction 0.200 to 0.315 mm, with 200 ml of distilled water in a platinum net for 72 hours at 372°K in a Soxhlet apparatus.

RESULTS AND DISCUSSION

Differential Thermal Analysis (DTA) and Viscosity Measurements

The glass F-SON showed medium exothermal peaks around 1025 and 1175°K, whereas a strong broad peak occurred at about 1245°K. The other three glasses, D-VG-98/3, UK-209 and UK-189, showed more or less weak exothermal peaks at about 925°K and in the range of 975 to 1015°K. At higher temperatures peaks appeared at about 1095°K with VG-98/3 and about 1175°K with the UK glasses. The parent glass D-B 1-3 showed the strongest DTA peaks of all tested samples. Exothermal peaks were observed at 995, 1065 and 1095°K. Transformation temperatures, T_g, were determined from the DTA curves. The measured viscosities of the glasses in a temperature range from 925 to 1500°K revealed values of 30 to 5×10^6 dPas. Viscosities at temperatures below 925°K have been obtained from extrapolated curves with an assumed viscosity of 10^{13} dPas at T_g. These values are listed in Table 1.

TABLE I

Properties of the Glass and Glass Ceramic

	F-SON 58.30.20	D-VG 98/3	UK-209	UK-189	D-B 1-3
Glass preparation temperature, T_M, °K	1425	1475	1275	1225	1475
100 dPas temperature, T_{100}, °K	1475	1325	1490	1370	1365
Transformation temperature, T_g, °K	823	793	773	773	823
Viscosity at 973°K, dPas	3×10^8	5×10^5	1.6×10^6	5×10^5	$\sim 10^8$
Viscosity at 1073°K, dPas	1.6×10^6	8×10^3	4×10^4	1×10^4	$\sim 3 \times 10^5$

Precipitation of Noble Metal Phases

The X-ray powder diffraction patterns of the as-cast glasses showed only a few weak traces for the glasses F-SON and D-VG-98/3. SEM and EPMA investigations revealed microscopic inhomogeneities for all glasses except D-B 1-3. Spots of strong enrichment of Ru, Pd, Rh and Te were detected. As an example Fig. 1a shows the SEM picture and Figs. 1b and d show X-ray mapping of Ru and Pd, respectively, of the glass F-SON annealed at 773°K for 100 days.

The solubility of the noble metals in the glasses is obviously extremely low, independent of the very different glass compositions. These constituents precipitated in the glasses in various phases (Figs. 1b and d) though their total concentrations are very low. X-ray mappings for Ru and Pd gave evidence of their very low concentrations in the glass matrix when compared with the precipitated quantity. Figure 1c revealed that the Ru phase might contain silicon. SEM micrographs at higher magnifications (≥8000x) showed, however, that this phase consisted of fine grains embedded in the glass matrix. The resolution of the EPMA was not high enough to decide whether the Si signal belonged to the Ru phase or the matrix. RuO_2 was detected after evaluating the X-ray diffraction patterns. Figure 1d shows an X-ray mapping for Pd. An identical picture was obtained for the Te distribution. A comparison with Fig. 1c indicates a silicon-free noble metal phase. The droplet-shaped precipitation is typical of this phase. X-ray diffraction analysis revealed that it might be Pd_3Te or PdTe.

Crystallization and Recrystallization

The heat treatment of the glasses caused an increase in the number and yield of crystalline phases. The number of crystal species and their yields varied considerably from glass to glass. For all glasses heat-treated above 773°K, crystallization effects became detectable but different annealing times were needed (Table 2). The shortest time was needed at the highest temperature, 1073°K, but this did not always lead to the highest crystal yields or the greatest structural change of the glass ceramic. Figure 2 shows SEM pictures of the most structurally changed samples. Figure 2a shows the glass F-SON heat-treated for 100 days at 1073°K, Fig. 2b a sample of D-VG-98/3 after 10 d at 1073°K, Fig. 2c UK-209 after 10 d at 973°K, Fig. 2d UK-189 after 100 d at 973°K. Figure 2e shows the untreated glass ceramic D-B 1-3, and Fig. 2f shows the product after a heat treatment of 100 d at 973°K.

All glasses contained waste constituents that can act as nucleating agents, especially the noble metals. Figures 1e

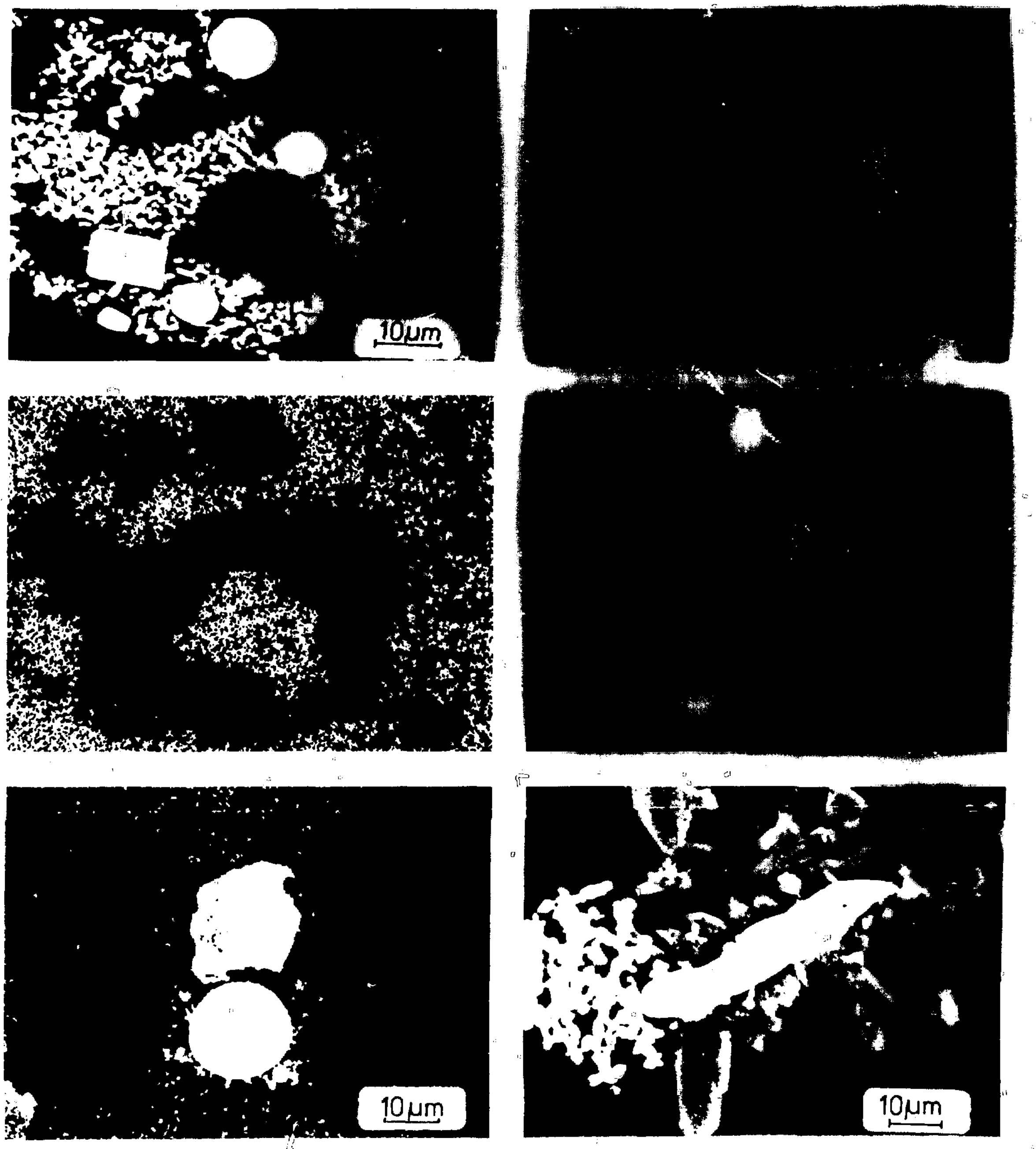

Fig. 1 (a) SEM micrograph of the glass F-SON 58.30.20.U2 heated 100 days at 773 °K. (b) X-ray mapping of ruthenium in Fig. 1a. (c) X-ray mapping of silicon in Fig. 1a. (d) X-ray mapping of palladium in Fig. 1a. (e) SEM micrograph of the glass F-SON 58.30.20.U2 heated 10 days at 973 °K. (f) SEM micrograph of the glass UK-209 heated 10 days at 973 °K.

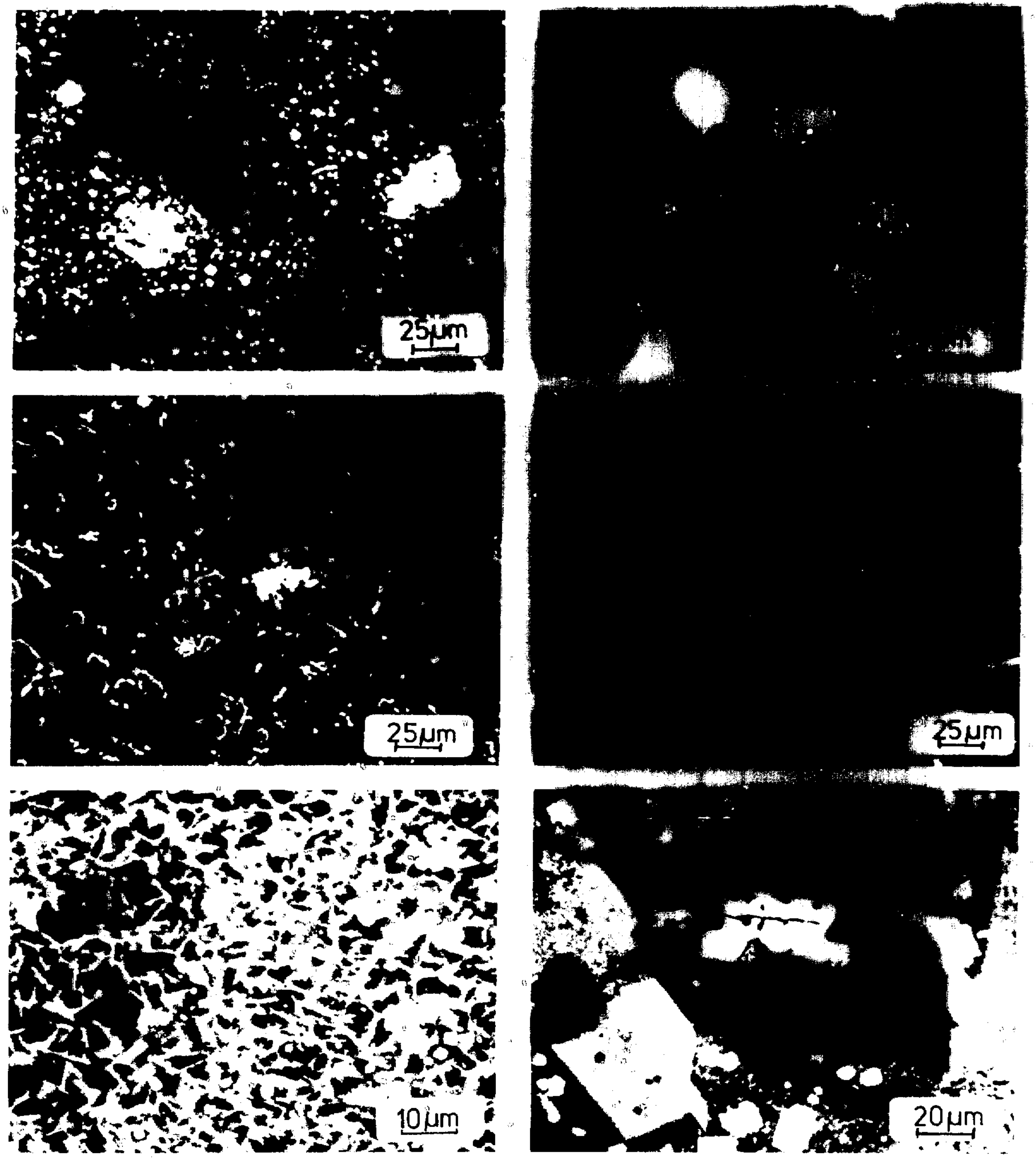

Fig. 2 (a) SEM micrograph of the glass F-SON 58.30.20.U2 heated 100 days at 1073°K. (b) SEM micrograph of the glass D-VG-98/3 heated 10 days at 1073°K. (c) SEM micrograph of the glass UK-209 heated 10 days at 973°K. (d) SEM micrograph of the glass UK-189 heated 100 days at 1073°K. (e) SEM micrograph of the glass ceramic D-B 1-3. (f) SEM micrograph of the glass ceramic D-B 1-3 heated 100 days at 973°K.

TABLE 2

Heat Treatment Conditions for Detectable Crystallization Effects of the Glasses and Structural Change of the Glass Ceramic

Temperature, °K	Time, days				
	F-SON 58.30.20	D-VG 98/3	UK-209	UK-189	D-B 1-3
773	100	>100	>100	100	>100
873	10	100	10	10	100
973	1	10	1	1	10
1073	0.1	0.1	0.1	0.1	1

and f show F-SON and UK-209 after heat-treating 10 days at 973°K; they clearly demonstrate the dominant role of the noble metal phase in the crystallization process. Crystal growth proceeded after starting at the glass noble metal phase boundary.

As seen in Fig. 2 the parent glass D-B 1-3 is most crystallized compared with the other glasses. The same result has been obtained after spontaneous crystallization at temperatures of about 1073°K without nucleation. Therefore it can be concluded that the tailored composition of the D-B 1-3 glass frit of the glass ceramic is more responsible for crystallization than the waste compositions.

The original fine structure of the glass ceramic (Fig. 2e) was lost after heat treatment as shown in Fig. 2f. Recrystallization was caused by the thermal instability and has led to developing more heat-resistant glass ceramics.[4]

The least thermally stable glass was F-SON exhibiting a relatively high crystallization yield as shown in Fig. 2a. D-VG-98/3 was least affected (Fig. 2b). The comparison of temperatures for maximum structural changes (Fig. 2) with the viscosities at 973 and 1073°K (Table 1) does not suggest a direct connection between the crystallization tendency and viscosity.

Crystal Phases

The evaluation of the X-ray diffraction patterns with the help of the ASTM powder diffraction file revealed that the crystalline phases compiled in Table 3 may be present in the products. In all products rare earth phases crystallized. Tetravalent cerium formed a cubic structure and trivalent neodymium and Ce, Pr, La formed hexagonal or cubic oxides, respectively. Moreover, other rare earth phases such as silicates, phosphates, and molybdates could be detected. A large quantity of rare earth titanate was contained in the glass ceramic.

The solubility of molybdenum in the glass melts is known to be limited. The small amount of homogeneously dissolved Mo in the glasses enhanced the precipitation of (Ba, Sr)-molybdate and Mo–nosean in the glasses F-SON, UK-209, and the glass ceramic D-B 1-3, respectively. Silicate phases rarely formed. In the glass VG-98/3 only tridymite could be detected by X-ray diffraction, whereas in F-SON (shown in Fig. 2a) the dark rod-shaped phase consisted only of silicon and perhaps oxygen, which suggested that it was also tridymite.

The relatively high magnesium content of the UK glasses led to the formation of Mg- and (Fe, Mg, Ni)-silicates and (Fe, Cr)-spinel. Originally the glass ceramic D-B 1-3 (Fig. 2e) mainly consisted of hexagonal-celsian–cymrite (white needles), rare earth titanate (white square-shaped crystals), and other species listed in Table 3. After heat treatment the fine crystalline structure got lost. The h-celsian cymrite phase transformed into the more stable monoclinic celsian, and additionally Mo–nosean was formed.

Leach Resistance

The results of the leaching experiments are listed in Table 4. The influence of heat treatment on leachability was different for the various glasses. The greatest effect has been detected for the glass F-SON and the lowest one for D-VG-98/3. The leach resistance was found to be either unchanged or deteriorated after heat treatment and decreased in the order of UK-209, D-B 1-3, UK-189, F-SON, and D-VG-98/3.

After up to 100 days at 773°K the leaching values did not change (Table 4); they represented the leach resistance of the various untreated products. None of the products achieved the leach resistance of commercial chemically highly resistant glasses. The UK-209 met the specifications for a chemically durable glass. Hydrolytic resistance of the glass ceramic D-B 1-3 and of the glasses UK-189 and F-SON is comparable with that of special technical glasses. The VG-98/3 exceeded the upper limit of the regulations and could not be classified. The thermal effect on the hydrolytic resistance was highest for F-SON glass resulting in an increase of about one order of magnitude (Table 4). The leachability of the other products also increased but did not exceed a factor of 5 (Table 4).

Although the glasses crystallized noticeably and the structure of the glass ceramic clearly changed at 1073°K, the hydrolytic resistance of all products but the F-SON glass did not change after heat treatment. As yet, the increase of the leachability could not be related to the crystallization yield of the glasses. The Soxhlet leach data revealed roughly the same sequence for the products. The weight loss appeared to be extremely high, the reason being that grains which became smaller in diameter during leaching than the mesh size fell through the platinum screen. A Soxhlet test as used at Harwell[5] avoided this effect. The leach rates of most of the products were also unaffected by any heat treatment. Nevertheless, the sequence of decreasing leach resistance in the products is the same as for the grain titration method.

CONCLUSIONS

1. The solubility of the noble metals in all glasses was exceeded. Nevertheless, at the glass melting temperatures at

TABLE 3

Possible Crystalline Phases in the Glasses Detected by X-Ray Diffraction Evaluation

Phases	F-SON 58.30.20	D-VG 98/3	UK-209	UK-189	D-B 1-3
Ruthenium dioxide, RuO_2	X	X	X	X	
Ruthenium				X	
Palladium telluride, Pd_3Te	X	X			
Palladium telluride, PdTe	X				
Palladium oxide, PdO	X			X	
Palladium, Pd		X		X	
Cadmium tellurate, $CdTeO_3$	X				
Rare earth tellurate, $(RE)_2Te_3O_9$	X	X			
Cerium dioxide, CeO_2	X	X	X	X	
Rare earth oxide, $(RE)_2O_3$	X		X		
Rare earth phosphate, $(RE)PO_4$	X		X	X	
Rare earth silicate				X	
Rare earth titanate, $(RE)_2Ti_2O_7$					X
Rare earth molybdate, $(RE)MoO_6$		X	X		
Rare earth borate, $(RE)BO_3$		X			
Barium strontium molybdate, $(Ba,Sr)MoO_4$	X		X		X
Molybdenum nosean, $Na_8AlMoO_4(SiO_4)_6$					X
Tridymite, SiO_2	X	X			
Magnesium silicate, $MgSiO_3$			X		
Magnesium iron nickel silicate, $(Mg,Fe,Ni)Si_2O_6$			X		
Celsian, $BaAl_2SiO_2O_8$					X
Pollucite, $(Cs,Na)AlSi_2O_6$					X
Iron chromium oxide, $FeCr_2O_4$				X	
Iron magnesium chromium oxide, $(Fe,Mg)(Cr,Fe)_2O_4$				X	

least Pd was soluble, since otherwise it could not precipitate as Pd–Te compounds.

2. The parent glass of the glass ceramic easily crystallized. In contrast, all the other glasses were quite stable when heat-treated; however, at higher temperatures they also crystallized. The high crystalline fraction in the glass ceramic was due to bulk crystallization. In crystallized glasses the glassy portion still remained high.

3. Some waste constituents crucially affected the crystallization process but did not lead to comparable results in the various glasses. Thus the composition of the glass frits was more responsible for crystallization than the waste.

4. Crystallization and recrystallization in the glasses and glass ceramics, respectively, is not expected to have drastic changes on the safety-relevant leachability under interim storage conditions.

ACKNOWLEDGMENT

The author thanks J. Borchardt for helpful X-ray diffraction indexing work and W. Lutze for fruitful discussions. This work was supported by the European Atomic Energy Community under contract 029-77-1 WASD.

TABLE 4

Leach Resistance of Heat Treated Glasses and Glass Ceramics

Heat treatment conditions		Hydrolytic resistance after grain titration method; consumption of 0.01 *N* HCl, ml/g				
Temperature, °K	Time, d	F-SON 58.30.20	D-VG 98/3	UK-209	UK-189	D-B I-3
773	0.1 to 100	1.49 ± 0.35	4.05 ± 0.40	0.17 ± 0.04	0.63 ± 0.14	0.28 ± 0.08
873	0.1 to 1	1.75 ± 0.13	3.36 ± 0.15	0.17 ± 0.02	0.79 ± 0.09	0.33 ± 0.08
	10	2.41 ± 0.10				
	100	3.06 ± 0.10	5.25 ± 0.13	0.66 ± 0.02		2.07 ± 0.04
973	0.1 to 1	2.49 ± 0.20	3.07 ± 0.23	0.21 ± 0.05	0.73 ± 0.07	0.43 ± 0.15
	10	8.36 ± 0.14				
	100	12.14 ± 0.11	4.73 ± 0.16	0.77 ± 0.02	2.24 ± 0.08	0.76 ± 0.04
1073	0.1	2.62 ± 0.11	3.57 ± 0.50	0.18 ± 0.01	0.56 ± 0.13	0.27 ± 0.05
	1	3.76 ± 0.13				
	10	12.85 ± 0.13				
	100	7.08 ± 0.27				
		Weight loss after Soxhlet leaching, %				
773	0.1 to 100	20 ± 7	12.3 ± 3.5	0.9 ± 0.3	4.8 ± 2.9	2.3 ± 0.6
873	0.1 to 10	19 ± 9	8.1 ± 2.4	1.1 ± 0.6	4.7 ± 2.2	2.0 ± 0.3
	100		20.0 ± 2.2	2.5 ± 0.7		8.7 ± 1.3
973	0.1 to 10	26 ± 10	7.3 ± 2.7	2.0 ± 0.6	5.9 ± 1.5	2.3 ± 0.5
	100					4.2 ± 1.0
1073	0.1 to 100	35 ± 9	15.0 ± 5.1	1.3 ± 0.5	4.1 ± 1.3	2.0 ± 0.7

REFERENCES

1. G. Malow, V. Beran, W. Lutze, J. A. C. Marples, J. T. Dalton, A. R. Hall, A. Hough, and K. A. Boult, *Testing and Evaluation of the Properties of Various Potential Materials for Immobilizing High Activity Waste,* First Annual Report EUR 6213EN, Commission of the European Communities, 1978.
2. A. K. Dé, B. Luckscheiter, W. Lutze, G. Malow, and E. Schiewer, Development of Glass Ceramics for the Incorporation of Fission Products, *Ceramic Bulletin,* 55: 500 (1976).
3. DIN 1211, *Technique to Test the Water Solubility of Glass Materials at 98°C and the Separation of Glasses into Hydrolytic Classes,* Deutsches Institut für Normung e.V., Berlin, 1976.
4. W. Lutze, J. Borchardt, and A. K. Dé, Characterization of Glass and Glass Ceramic Nuclear Waste Forms, in Proceedings of *Scientific Basis for Nuclear Waste Management,* Boston, G. J. McCarthy (Ed.), Plenum, NY, 1979.
Massachusetts, Nov. 28–Dec. 1, 1978.
5. K. A. Boult, J. T. Dalton, A. R. Hall, A. Hough, and J. A. C. Marples, Leaching of Radioactive Waste Storage Glasses, in Proceedings of *Ceramics in Nuclear Waste Management,* Cincinnati, CONF-790420, U. S. Department of Energy, Technical Information Center, Oak Ridge, 1979.

VISCOSITY AND ELECTRICAL CONDUCTIVITY OF GLASS MELTS AS A FUNCTION OF WASTE COMPOSITION

M. J. PLODINEC and J. R. WILEY
E. I. du Pont de Nemours and Company, Savannah River Laboratory, Aiken, South Carolina

ABSTRACT

Radioactive waste at the Savannah River Plant contains high concentrations of nonradioactive compounds of iron and aluminum. Simulated waste compositions containing varying ratios of iron to aluminum were added to glass melts to determine the effect on the melt properties. Waste containing high aluminum increased the melt viscosity, but waste containing high iron reduced the melt viscosity. Aluminum and iron both reduced the melt conductivity.

INTRODUCTION

Borosilicate glass is being evaluated for use as a matrix to immobilize Savannah River Plant (SRP) high-level radioactive waste sludges.[1-10] One process being studied is vitrification by spray calcination and Joule-heated electric melting (EM). The resistivity and viscosity of the glass melt are two of the most important properties for controlling the vitrification process.

The optimum range for melt viscosity is 10–50 poise. In this viscosity range, the glass is fluid enough to melt and homogenize and ensure adequate heat transfer; however, it is not fluid enough to allow excessive convection currents to occur. Excessive convection currents could cause corrosion–erosion of the melter materials (refractories and electrodes) and make control of the melter more difficult.

The optimum range for resistivity is between 1 and 10 ohm-cm. The glass in the optimum range is conductive enough to pass appreciable amounts of electric currents without requiring high voltages; however, it is not so conductive that excessive current densities are required at the electrodes to produce heat. Excessive current densities would reduce electrode life.

The effects of several simulated sludges (Table 1) on the viscosity and resistivity of melts containing the SRP reference frit, Frit 21 (Table 2), were determined. Sludge loadings and compositions spanned the expected range for SRP waste glass.

DEFINITIONS

The glasses that were studied obey the following equation for mass flow:

$$G = mS^n \qquad (1)$$

where G is shear stress, S is rate of shear, and m and n are functions of composition and temperature. When $n = 1$, the glass is Newtonian and $m = \eta$ (η = viscosity). When $n > 1$, the glass is pseudoplastic. If n or m depends on the amount of shearing, the glass is thixotropic.[11] The resistivity, ρ, of the glass is the product of the electrical resistance, R, and a cell constant, l, which depends on the measuring apparatus.

$$\rho\ (\text{ohm-cm}) = R\ (\text{ohm}) \times l\ (\text{cm}) \qquad (2)$$

EXPERIMENTAL PROCEDURES

Glass samples were prepared by heating mixtures of frit and sludge in an Al_2O_3 crucible for at least 3 hours at 1150–1200°C. Viscosities were determined using a rotating spindle viscometer.[12] Calibrations with both room temperature standards and a standard glass (NBS 710) were used. Resistances were measured with a high-temperature Pt electrode of the type developed at Battelle-Pacific Northwest Laboratory.[13] The electrode was calibrated with room

TABLE 1

Composition of Simulated Sludges

Sludge	Component, wt.%					
	Fe_2O_3	Al_2O_3	MnO_2	U_3O_8	CaO	NiO
High iron	61.4	5.6	4.1	14.2	4.2	10.5
Composite	31.6	46.4	10.3	6.1	3.3	2.3
High aluminum	6.0	86.3	4.9	1.5	0.4	0.9

TABLE 2

Composition of Reference Frit, Frit 21

Component	Wt.%	Mole%
SiO_2	52.5	52.5
Na_2O	18.5	17.9
B_2O_3	10.0	8.65
TiO_2	10.0	7.5
CaO	5.0	5.35
Li_2O	4.0	8.1

temperature KCl solutions to determine l° in Eq. 2. Measured resistances were corrected for the change in resistance of Pt with temperature.

The sludges used are listed in Table 1. The compositions are based on analyses of sludges from SRP waste tanks. High-iron and high-aluminum sludges represent extreme compositions for SRP sludges. Composite sludge is the weighted average of these analyses, reflecting the amount of sludge of each composition.

EFFECTS OF SLUDGE COMPOSITION AND CONTENT ON VISCOSITY

The viscosities of glass melts containing each of the sludges were measured over the temperature range 750–1200°C. At a constant temperature and sludge loading, the viscosity as a function of sludge composition increased in the order, high-iron sludge < composite sludge < high-aluminum sludge. The viscosity depended on the amount of both iron and aluminum contained in the sludge. Other sludge components had little effect on viscosity. Melts that contained more than 30 wt.% of sludges high in iron were non-Newtonian, pseudoplastic fluids. For melts within the expected composition range, this was not a problem.[14] Viscosities of Newtonian melts are shown in Fig. 1. The viscosity at 1150°C for these melts can be calculated from Eq. 3.

$$\log \eta = 1.2227 - \frac{0.613P_{Fe_2O_3}}{P_{SiO_2}} + \frac{1.728P_{Al_2O_3}}{P_{SiO_2}} \quad (3)$$

where P_X is the amount (wt.%) of component X in the final glass.

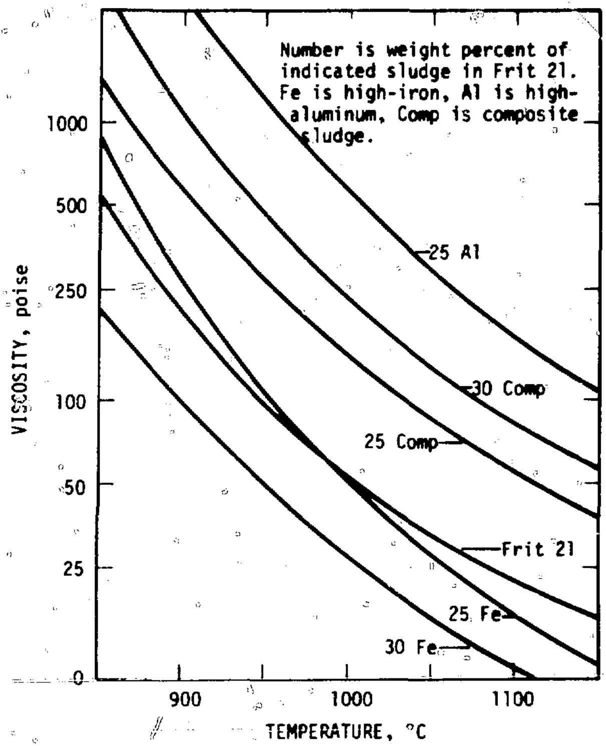

Fig. 1. Effect of waste composition on viscosity of SRP waste glasses.

EFFECTS OF SLUDGE COMPOSITION AND CONTENT ON RESISTIVITY

Resistivities of glass-sludge melts as a function of temperature are shown in Fig. 2. The resistivities of high-aluminum sludge melts were higher than those of melts made from other sludges. Resistivity increased with increasing sludge loading. Increasing the aluminum content increases melt viscosity. This reduces the mobility of charge-carrying ions (Na^+ and Li^+), thus increasing resistivity.[15] Increased sludge loading also reduces the alkali concentration in the melt.

Adding iron to glass melts affects electrical resistivity in the same way as adding aluminum, as long as the melt behaves as a Newtonian fluid. However, at higher sludge loadings or lower temperatures, this simple description fails to predict the complex behavior observed.[16]

ANOMALIES WITH HIGH-IRON SLUDGES

Melts containing ≥35 wt.% of sludges with large amounts of Fe_2O_3 were non-Newtonian, pseudoplastic fluids. Their resistivities were also not those expected from the simple viscosity-alkali concentration model. These melts were found to contain large numbers of ferrite-spinel (MFe_2O_4, M = Ni^{++}, Ca^{++}, etc.) crystals. Thus these melts are actually suspensions of these crystals in the glassy matrix. The rheological behavior of these melts is similar to

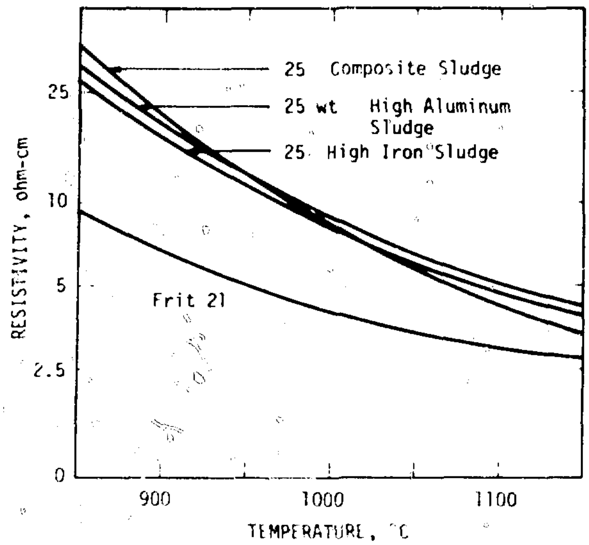

Fig. 2 Effect of waste composition on resistivity of SRP waste glasses.

that observed for suspensions of iron oxide in viscous media at room temperature.[17] The resistivity of these crystals varies with composition but is probably somewhat higher than that of Frit 21 alone at 1150°C and lower at temperatures in the 500–700°C range.[13]

If these crystals formed in a continuous melter, they could increase the apparent viscosity of the melt and eventually stop flow. For anticipated waste loadings in the glass (25–30 wt.% waste oxides), however, they are not expected to be a problem.

ACKNOWLEDGMENT

The information contained in this article was developed during work under Contract AT(07-2)-1 with the U. S. Department of Energy.

REFERENCES

1. R. H. Burns, Solidification of Low- and Intermediate-Level Waste, *At. Energy Rev.*, 9: 547 (1971).
2. R. M. Wallace, H. L. Hull, and R. F. Bradley, *Solid Forms for Savannah River Plant High-Level Waste*, USAEC Report DP-1335, E. I. du Pont de Nemours and Company, Savannah River Laboratory, Aiken, SC, 1973.
3. J. A. Stone, J. A. Kelley, and T. S. McMillan, *Sampling and Analyses of SRP High-Level Waste Sludges*, ERDA Report DP-1399, E. I. du Pont de Nemours and Company, Savannah River Laboratory, Aiken, SC, 1976.
4. R. S. Ondrejcin, *Chemical Compositions of Supernates Stored in SRP High-Level Waste Tanks*, USAEC Report DP-1347, E. I. du Pont de Nemours and Company, Savannah River Laboratory, Aiken, SC, 1974.
5. R. M. Wallace et al., Solid Forms for Savannah River Plant Radioactive Wastes, in *High Level Radioactive Waste Management*, p. 9, American Ceramic Society, 1976.
6. J. A. Stone, *Evaluation of Concrete as a Matrix for Solidification of Savannah River Plant Waste*, ERDA Report DP-1448, E. I. du Pont de Nemours and Company, Savannah River Laboratory, Aiken, SC, 1977.
7. J. A. Kelley, *Evaluation of Glass as a Matrix for Solidification of Savannah River Plant Waste. Nonradioactive and Tracer Studies*, ERDA Report DP-1382, E. I. du Pont de Nemours and Company, Savannah River Laboratory, Aiken, SC, 1975.
8. J. A. Kelley, *Evaluation of Glass as a Matrix for Solidification of Savannah River Plant Waste. Radioactive Studies*, ERDA Report DP-1397, E. I. du Pont de Nemours and Company, Savannah River Laboratory, Aiken, SC, 1975.
9. G. H. Thompson, *Evaluation of Mineralization Processes for SRP Wastes*, ERDA Report DP-1389, E. I. du Pont de Nemours and Company, Savannah River Laboratory, Aiken, SC, 1975.
10. J. A. Stone, *Separation of SRP Waste Sludge and Supernate*, ERDA Report DP-1441, E. I. du Pont de Nemours and Company, Savannah River Laboratory, Aiken, SC, 1976.
11. R. B. Bird, W. E. Stewart, and E. N. Lightfoot, *Transport Phenomena*, John Wiley & Sons, Inc., New York, p. 3, 1960.
12. R. L. Tiede, An Improved Method of Measuring Glass Viscosities, *J. Am. Ceram. Soc.*, 62: 537 (1959).
13. J. L. McElroy (Comp.), *Research and Development Activities, Waste Fixation Program, Quarterly Progress Report, April-June, 1974*, ERDA Report BNWL-1841, Battelle-Pacific Northwest Laboratory, Richland, WA, 1974.
14. M. J. Plodinec, *Viscosity of Glasses Containing Simulated Savannah River Plant Waste*, DOE Report DP-1057, E. I. du Pont de Nemours and Company, Savannah River Laboratory, Aiken, SC, 1978.
15. J. Stanek, *Electric Melting of Glass*, Elsevier North-Holland, New York, p. 16, 1977.
16. J. R. Wiley, *Electrical Resistivities of Glass Melts Containing Simulated SRP Waste Sludges*, DOE Report DP-1488, E. I. du Pont de Nemours and Company, Savannah River Laboratory, Aiken, SC, 1978.
17. C. M. McDowell and F. L. Usher, *Proc. R. Soc. (London), Ser. A*, 131(409): 564 (1931).
18. L. G. Van Uitert, Dc Resistivity in the Nickel and Nickel Zinc Ferrite System, *J. Chem. Phys.*, 23: 1883 (1955).

EFFECTS OF COMPOSITION ON WASTE GLASS PROPERTIES

G. B. MELLINGER and L. A. CHICK
Pacific Northwest Laboratory, Richland, WA

ABSTRACT

The electrical conductivity, viscosity, chemical durability, devitrification, and crystallinity of a defense waste glass were measured. Each oxide component in the glass was varied to determine its effect on these properties. A generic study is being developed which will determine the effects of 26 oxides on the above and additional properties of a wide field of possible waste glasses.

INTRODUCTION

A number of properties are important when evaluating potential waste glass compositions. Among these are the molten glass properties of viscosity, electrical conductivity, and residual crystals. Others, which are important in the final product, are chemical durability and resistance to devitrification. The behavior of each glass is dependent on its composition. In this study we determined the effect that each of the components in a particular waste glass composition had on all of the above properties.

The reference composition chosen for this work was a glass, being considered for solidification, of Savannah River defense waste. The oxide makeup of this glass and the variations tested are given in Table 1. Each component of the glass was varied individually. One component at a time was varied, and the amounts of the other components were maintained at the same ratios found in the base glass.

EXPERIMENTAL PROCEDURES

Glasses were prepared from batch chemicals (oxides, nitrates, carbonates). These were mixed using a mortar and pestle and were melted at 1050°C for two hours in air in platinum crucibles. Each batch produced 40 grams of glass.

Viscosity and electrical conductivity were measured in air at 1070°C. The viscosity apparatus was modified to allow electrical conductivity measurements to be made using the platinum spindle and crucible as electrodes. Conductivity measurements were made using alternating current at a frequency of 1000 Hz. The residual crystals present in each glass, after air quenching from the melting temperature, were determined from photomicrographs. The degree of crystallinity present was estimated visually, and a qualitative ranking of the glasses was made. Crystallinity was also measured using X-ray diffraction.

Chemical durability was tested in acid and base solutions at room temperature and in 99°C distilled water. Details of these tests have been reported.[1] In each case, percent weight loss of the sample as a result of the treatment was determined. Devitrification was evaluated from X-ray diffraction data of samples which had been cooled from the melting temperature at 6.25°C per hour.[2]

RESULTS

Table 1 summarizes the results obtained. The alkali metals (Na, Li, K) were found to have large effects on almost all properties measured. Their effects on a number of these properties are plotted in Fig. 1. The addition of alkali oxides results in the formation of alkali-oxygen bonds rather than silicon-oxygen bonds[3] and results in a weaker glass network. This allows the glass to flow more easily and results in a lowered viscosity. The relative weakness of the network also makes it more subject to chemical attack and leads to decreased chemical durability. The weaker or more open network may incorporate other atoms more easily. This may be the cause of the residual

TABLE 1

Summary of Composition Experiment*

Component	Base glass, wt.%	Variation, wt.%	Viscosity	Electrical conductivity	Crystallinity	Devitrification	99°C distilled water	Leachability† pH 4	Leachability† pH 9
Na_2O	13.9	5.0-15.0		++	-	0	++	++	0
Li_2O	3.0	0-6.0	-	++	--	0	++	++	0
K_2O	0	0-6.0	--	++	-	0	++	++	0
CaO	4.5	0-6.0	-	0	-	0	0	++	0
MgO	0	0-3.0	0	0	0	0	+	++	0
BaO	0	0-3.0	0	0	0		++	++	0
Al_2O_3‡	11.6	1.6-21.6	++		++	++	-	++	0
NiO‡	0.5	0-3.0	+	0	++	0	0	0	0
Fe_2O_3‡	7.9	0.4-15.4		0	++	+	0	+	0
TiO_2	7.5	0-10.0	-	0	0	+	--	-	0
B_2O_3	7.5	5.0-15.0				-	0	++	0
MnO_2‡	2.6	1.2-4.0	0	0	+	0		+	0
U_3O_8‡	1.5	0-4.0	0	--	-	0	-	0	0
ZnO	0	0-7.0	0	0	++	0	++	++	0
SiO_2	39.4								

*0 indicates negligible change with increase in this component; + and - indicate increases or decreases; ++ and indicate large increases and decreases, respectively, with component increase.

†+ in last two columns indicates an increase in leachability.

‡Components of waste.

crystallinity reduction present in the glass with alkali addition. The alkali ions are not strongly bound, and these charge carriers are consequently very mobile in the molten glass. This mobility produces the major effect that they have on electrical conductivity.

Oxides of the alkaline earths (Ca, Mg, Ba) were found to produce effects similar to those caused by the alkalis, although their influence was not as great. This is because these divalent ions are doubly bonded and are much less mobile in the glass.[3] The amounts of alkali and alkaline earths selected to use in a glass represent a compromise between the desirable lowering of viscosity and crystallinity in the melt and the undesirable increase of leachability.

Aluminum oxide had a number of adverse effects on the glass, including increasing viscosity and acid leachability. A high alumina content may constitute the limiting factor for the amount of waste that may be incorporated in a glass.

The oxides of aluminum, nickel, and iron had the most noticeable effects on crystallinity in the glasses, and crystal formation was more dependent on nickel than on iron concentration. This effect is shown in Fig. 2. The crystallinity in the glasses with the highest levels of these additions was 10 to 14%. The primary phase was nickel–ferrite spinel. The action of alumina in its formation is not well understood since only a small amount of aluminum was found in the crystals. The aluminum ions may occupy sites in the glass otherwise occupied by the iron. These displaced iron atoms might then precipitate in the crystalline form. Also, the aluminum addition may result in the formation of small precursor crystals which could act as nucleation sites for the spinel precipitates.

Alumina was found to be the largest contributor to devitrification, while nickel oxide had a negligible effect, as shown in Fig. 3. This indicates that the amount of crystallinity produced in the glass by nickel oxide addition is largely unaffected by heat treatment; it will come out of the glass rather quickly. The amounts of crystallinity induced by aluminum oxide addition, however, will be affected by heat treatment.

Titanium dioxide was the only component found to cause a large increase in pH-4 chemical durability, as seen in Fig. 4. It is of interest that it also caused a slight decrease in viscosity, since oxides that increase durability generally increase viscosity as well. Titania also contributed to devitrification. The amount may be somewhat hidden by the large amount of spinel also present. Small additions of titania to glasses may be used to enhance this acid durability.

Boron primarily affected viscosity and leachability. As with alkali metals, the amount of boron used in a glass composition is a compromise between an advantageous decrease in viscosity and an accompanying increase in leachability.

GENERIC STUDY

Studies of the above type are useful in determining the effect that a certain component has on a specific glass composition. They are also useful in determining the

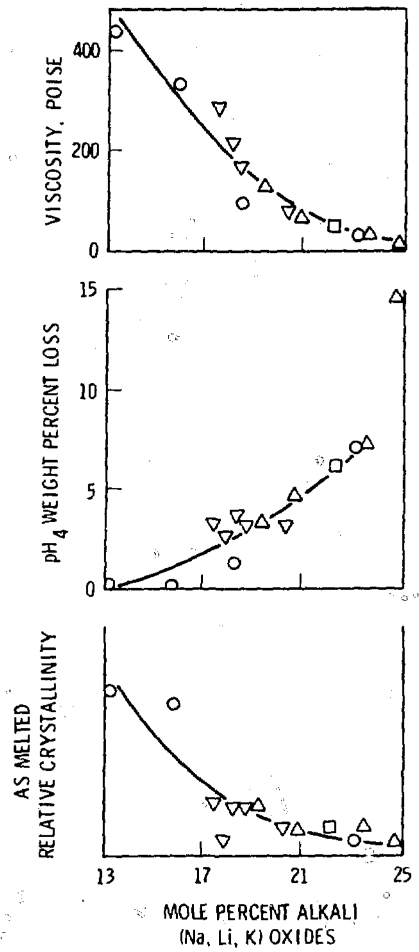

Fig. 1 Effect of alkali oxides on glass properties (○ = glasses when Na_2O was varied; △ = Li substituted for Na; ▽ = Li, Na, K substituted for each other).

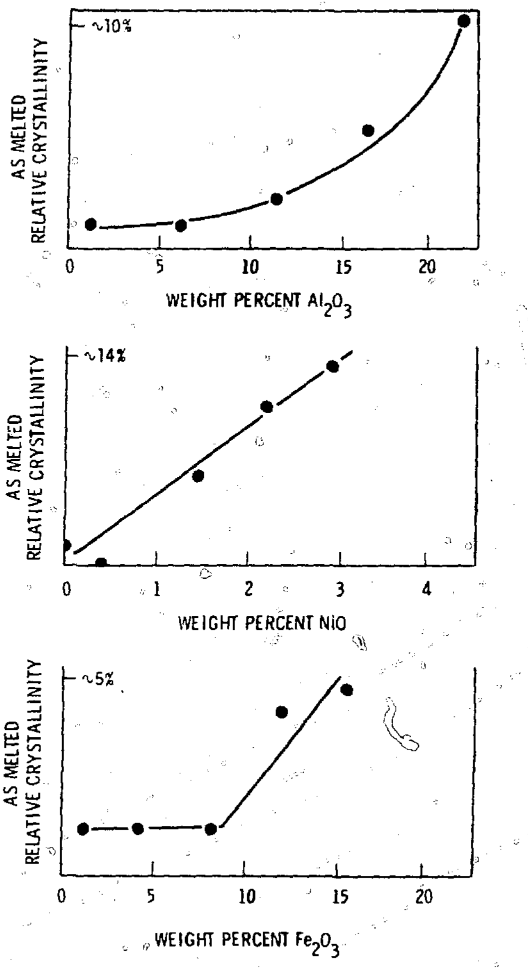

Fig. 2 Effect of Al_2O_3, NiO, and Fe_2O_3 on relative amount of crystallinity in as melted glasses.

approximate effects that a component may be expected to have on other glasses. However, they are not useful for predicting the properties of glasses—particularly those as complex as waste glasses. The properties of each composition must be experimentally determined.

A variety of nuclear wastes, including high-level, defense, and transuranic wastes, have been found to be amenable to vitrification. Each waste composition requires a different mix of glass additives in order to produce a product with optimum properties. There is a great deal of variation in the makeup of these glasses. Many compositions are tested for the immobilization of a new waste when a glass is being developed. It would be desirable to be able to predict the properties of a glass from its composition, as this would make appropriate composition selection easier. It would also help in determining what effect that changes in waste or glass-former makeup have on the glass.

A program to do this has been initiated at Pacific Northwest Laboratory. The properties of interest include those in the above study as well as volatility and radiation damage. Property data will be used to generate mathematical approximation models that will allow one to predict glass properties.

At least 55 different oxides may be found in waste glasses. To test all these variables would require an impossibly large number of experiments, but, by eliminating those elements that should not occur at concentrations >0.1 mole% and by combining into one variable some that are expected to have nearly identical effects, the list is reduced to 26 components. The elements and combinations comprising the experimental components are shown in Fig. 5.

To determine the feasibility of this experiment, a smaller version is being tested using 11 components. If modeling is successful and prediction is satisfactory, the full system will be examined. Because of the large number of possible compositions that can be made even with eleven components, the glasses to be examined are being chosen by a computer-aided statistical design.

Table 2 shows the eleven oxide components and their concentration ranges in mole%. Preliminary results on 25 melts in this system are encouraging. Partial quadratic

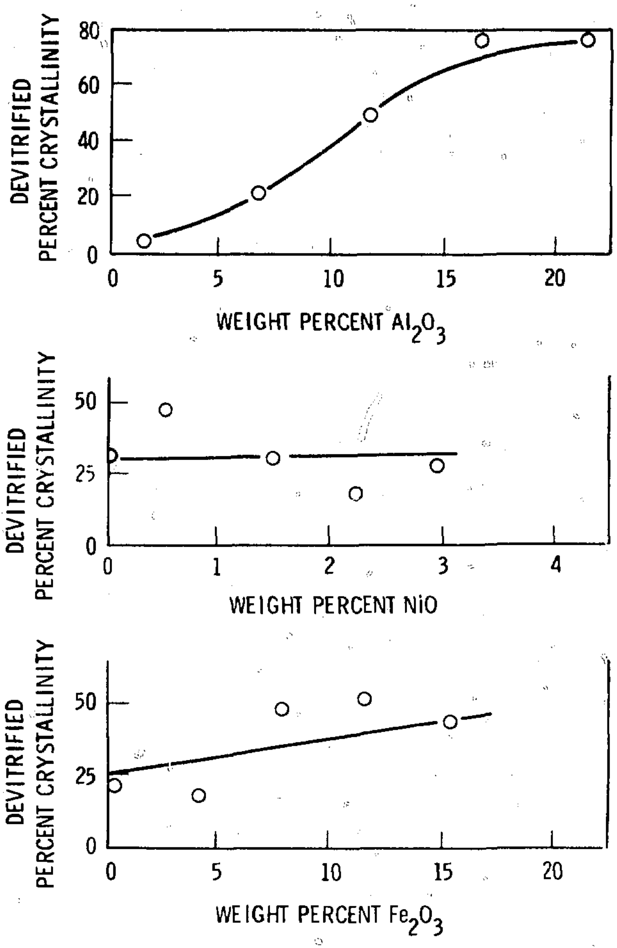

Fig. 3 Effect of Al_2O_3, NiO, and Fe_2O_3 on crystallinity in slow cooled (devitrified) glass.

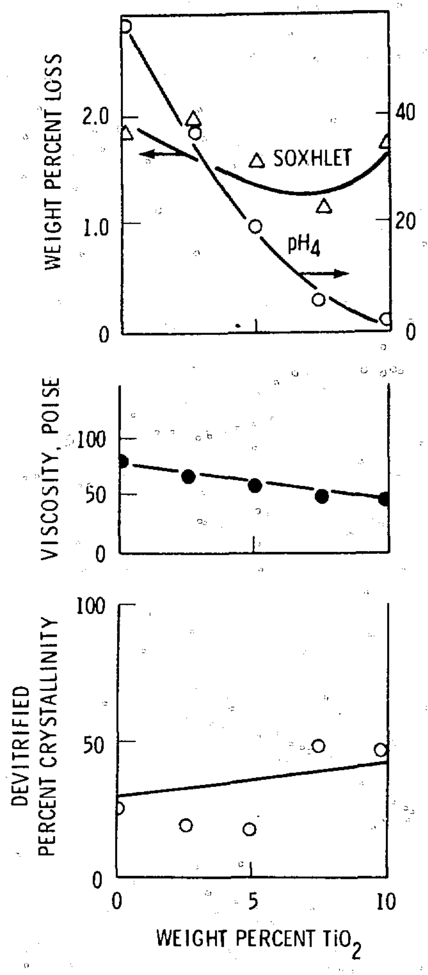

Fig. 4 Effect of TiO_2 on glass properties.

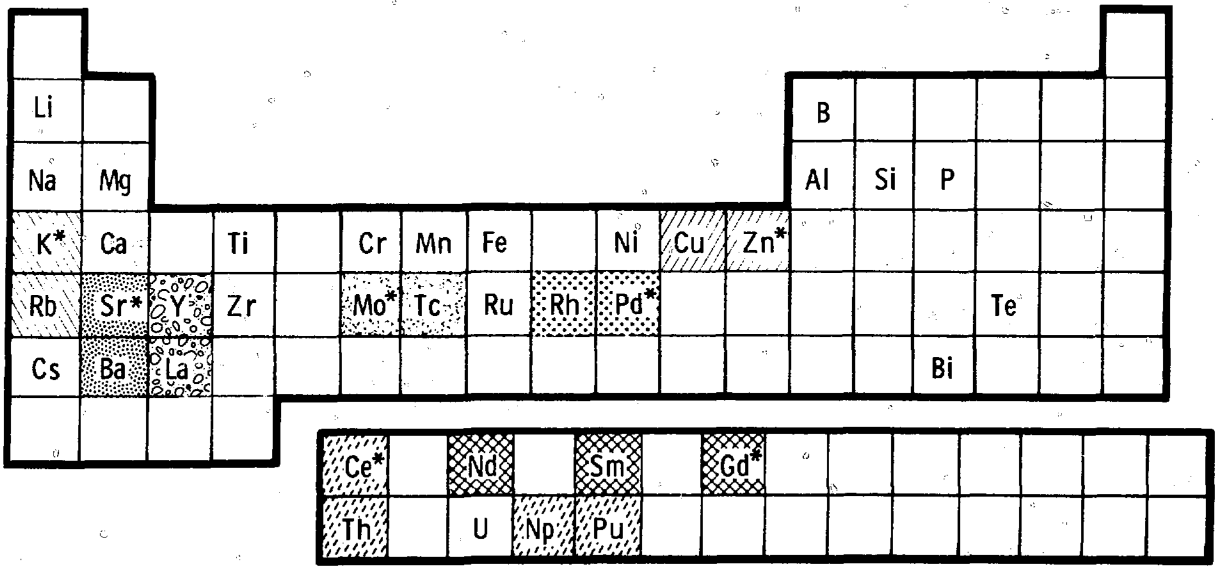
Li
Na
Mg
K*
Ca
Ti
Cr
Mn
Fe
Ni
Cu
Zn*
B
Al
Si
P
Rb
Sr*
Y
Zr
Mo*
Tc
Ru
Rh
Pd*
Te
Cs
Ba
La
Bi
Ce*
Nd
Sm
Gd*
Th
U
Np
Pu
*DENOTES REPRESENTATIVE OF GROUP

Fig. 5 Elements and combinations of elements to be examined in generic study.

TABLE 2

Eleven-Component Generic Waste Glass Properties Study

Component	Study values, mole%
Formers*	
SiO_2	42–58
B_2O_3	6–12
Al_2O_3	0–15
Modifiers†	
CaO	0–14
MgO	0–8
Na_2O	11–16
Intermediates‡	
ZnO	0–6
TiO_2	0–7
Cr_2O_3	0–3
Fe_2O_3	0–3
NiO	0–3

*Sum of formers must be between 55 and 75 mole%.

†Sum of modifiers must be between 14 and 34 mole%.

‡Sum of intermediates must be between 0 and 22 mole%.

models are fitting well for Soxhlet leaching, and for viscosity and electrical conductivity at 1250°C. Prediction accuracy is now being tested.

CONCLUSIONS

The properties of a glass are affected primarily by its composition. A waste component that has a large adverse effect upon the glass, such as alumina, will limit the concentration of waste which may be incorporated. Interactions between components such as aluminum, nickel, and iron may dictate that when a combination of these is present, lesser amounts of each may be put in a glass than would be possible if each were there separately. The selection of a glass composition for a waste will result from a compromise among optimizations of glass properties such as viscosity, chemical durability, and homogeneity.

ACKNOWLEDGMENT

This work was supported by the U. S. Department of Energy under Contract EY-76-C-06-1830.

REFERENCES

1. W. A. Ross, *Development of Glass Formulations Containing High Level Nuclear Wastes*, PNL-2481, Pacific Northwest Laboratory, Richland, WA, p. 7, February 1978.
2. R. P. Turcotte and J. W. Wald, *Devitrification Behavior in a Zinc Borosilicate Nuclear Waste Glass*, PNL-2247, Pacific Northwest Laboratory, Richland, WA, p. 3, March 1978.
3. F. V. Tooley, *The Handbook of Glass Manufacture*, Vol. II, Books for Industry Inc., New York, NY, 1974.

PHASE BOUNDARY EFFECTS IN METAL MATRIX EMBEDDED GLASSES

EDWIN SCHIEWER
Hahn-Meitner-Institut für Kernforschung Berlin GmbH, Department of Nuclear Chemistry and Reactor,
Berlin, Federal Republic of Germany

ABSTRACT

An investigation was performed to study reactions at the phase boundaries of glass-lead composites at temperatures up to the softening point of the glass. Some metal was oxidized at the boundary and penetrated into the glass. Solid-state diffusion was rate controlling. In the case of a phosphate glass, fission products were depleted in the boundary area. Molybdenum migrated into the lead, and cesium migrated into the glass core.

INTRODUCTION

An investigation was performed in the context of the PAMELA process for the solidification of HLLW. PAMELA is a pilot plant to produce borosilicate or phosphate glasses in the form of blocks or metal matrix composites.[1,2] The metal matrix composite was chosen here to study phase boundary effects between the glass and the continuous metallic phase, which was assumed to be lead. The solid waste forms tested were phosphate and borosilicate glass beads; their compositions are listed in Table 1. The phosphate glass was developed when the PAMELA process was first designed, whereas the borosilicate glass is a tailor-made product that might be converted into a glass ceramic. The properties of the borosilicate glass and of the glass ceramic were reported earlier.[3,4] Properties of the glasses are listed in Table 2 in regard to investigations on the metal–glass interface. Both glasses are very similar regarding their characteristic temperatures.

EXPERIMENTAL

The beads were produced from the melted glass which dripped from a platinum nozzle onto a corundum plate. The glass beads solidified upon cooling in a half-spherical shape with a diameter of 4 to 6 mm. Quartz ampules were then filled with the beads. Before adding the liquid lead (temperature 680°K), the neck of each ampule was narrowed so that the beads could not escape during filling with liquid metal. During the filling process the ampules were continuously flushed with nitrogen. The metal/glass product was then annealed in the ampule at temperatures between 573 and 873°K, the maximum annealing periods being one year at 573°K and eight days at 873°K. The annealed samples were then cut into smaller pieces to enable investigations of the metal/glass phase boundaries using scanning electron microscopy (SEM) and electron probe microanalysis (EPMA).

RESULTS

The phosphate glass contained ZrP_2O_7 crystals, whereas the borosilicate glass was found to be homogeneous. When annealing the samples below the transformation temperatures (T = 820°K to 850°K, Table 2), the glass beads remained essentially unaffected by the lead and were imperfectly wetted by the metal. In some cases, however, reaction zones became visible (3 μm wide after one year at an annealing temperature of 573°K) but were too narrow for EPMA.

Annealing in the range of transformation and softening caused reaction zones to form on the glass surface with well-defined boundaries between the lead and glass region. The glass structure changes above the transformation temperature[5] leading to a greater thermal expansion and a lowering in the surface tension,[5] which enables a better wetting of the glass beads.

TABLE 1

Composition of Glasses (wt.%)

	Borosilicate glass	Phosphate glass
	34.8 SiO_2	49.2 P_2O_5
	14.4 BaO	17.3 Fe_2O_3
	10.3 Al_2O_3	5.0 Al_2O_3
	5.3 CaO + MgO	
	4.9 ZnO	
	4.1 B_2O_3	
	3.6 ZrO_2 + TiO_2	
	2.1 Na_2O + Li_2O	
	0.5 As_2O_3	
Frit	80.0	71.5
	5.3 RE_2O_3 + CeO_2	9.9 RE_2O_3 + CeO_2
	4.0 Cs_2O + Rb_2O + Na_2O	5.4 MoO_3
	3.4 ZrO_2 + TiO_2	4.7 ZrO_2
	2.4 MoO_3	3.8 Cs_2O + Rb_2O
	1.9 Fe_2O_3 + Cr_2O_3	2.6 BaO + SrO
	1.2 BaO + SrO	1.3 Fe_2O_3 + Cr_2O_3
	0.6 Co_2O_3 + NiO	0.4 TeO_2
	0.5 U_3O_8	0.4 Co_2O_3 + NiO
	0.4 MnO_2	
	0.3 TeO_2	
Waste	20.0	28.5

TABLE 2

Properties of the Glasses

	Borosilicate glass	Phosphate glass
Temperature of producing glass beads $T_{60\,Pas}$, °K	1535	1465
Transformation temperature T_g, °K	850	820
Dilatometric softening point T_S, °K	910	855
Temperature of beginning crystallization (nucleation) T_N, °K	880	830
Crystalline phases	$BaAl_2Si_2O_8$ (celsiane) $RE_2Ti(Zr)_2O_7$ $BaMoO_4$ Ca–RE–silicate $CsAlSi_2O_6$ (pollucite)	$AlPO_4$ RE_2O_3 ZrP_2O_7

Figures 1(a) and 2(a) depict phase boundary areas for phosphate and borosilicate glasses after annealing at 873°K for periods of twelve and three hours, respectively. Their thicknesses are on the average 9 μm and 15 μm, respectively. At the innermost boundary [Fig. 1(a)] of the reaction zone of the phosphate glass, a second zone became apparent spreading homogeneously into the glass phase. This second zone contains crystals of ZrP_2O_7 (light) and $AlPO_4$ (dark). One can see from the EPMA that the second zone also contains lead [Fig. 1(b)]. From now on we shall refer to this zone as the diffusion zone. Figure 1(b–i) and Fig. 2(b–i) show the distributions of the major constituents (EPMA) in the area of the glass/metal phase boundary for both phosphate and borosilicate glasses.

The reaction zone of the phosphate glass essentially consists of the components lead, phosphorous and cerium [Fig. 1(b, c, and d)]. Lead and phosphorous are nearly homogeneously distributed, whereas cerium shows regions of enrichment. Zirconium and aluminum [Fig. 1(e and h)] were found to be enriched in spots, distributed over the area. Molybdenum [Fig. 1(f)] is concentrated at the boundary with the metal. Sometimes molybdenum-rich spots are found within the lead matrix. Iron and cesium [Fig. 1(g and i)] are depleted in the diffusion zone. The latter element is strongly enriched at the end of the lead diffusion zone. A more detailed analysis of Fig. 1(a) reveals that the reaction zone is not uniform. In the area directly adjacent to the lead, the ratio of the relative intensities of the EPMA X-ray signal is $I_{zone}/I_{lead} \approx 0.8$ for lead, whereas it is only ≈0.6 in the following zone. The width of the reaction zone becomes larger with higher temperatures and longer annealing periods. This is not true, however, for the diffusion zone. In Table 3 the widths of both zones in the phosphate glass are given at different temperatures and annealing periods. The width of the reaction zone increases with time, whereas the diffusion zone runs through a maximum of its width. The sum of both rises linearly with the square of the annealing time.

Figure 2(b and c) shows the X-ray mapping of lead and silicon, the major constituents in the reaction zone of the borosilicate glass. Cesium and calcium [Fig. 2(d and e)] are mainly found in the middle of the reaction zone, and barium, titanium, molybdenum and aluminum [Fig. 2(f, g, h, and i)] are on the outer boundary towards the lead. The ratio of the relative intensities of the characteristic X rays of lead is $I_{zone}/I_{lead} \approx 0.5$ throughout the reaction zone. A diffusion zone was not found.

DISCUSSION

Lead Oxidation

It can be assumed that under given experimental conditions the penetrating lead will be oxidized. This oxidation resulted from residual adsorbed oxygen on the glass surface, dissolved air from the glass, and oxidation by some glass constituents. The reaction of lead with MoO_3 leads to the formation of PbO and MoO_2.

The free enthalpy of the reaction is $\Delta H = -20.6$ kJ between 573 and 873°K (Ref. 6). From the molybdenum distribution [Figs. 1(f) and 2(h)] it was derived that lead was being oxidized by Mo^{6+}, because there is always a great deal of molybdenum at the metal boundary.

There are numerous indications that other glass constituents may oxidize the lead penetrating the reaction zone, e.g., Fe_2O_3 (Refs. 7 and 8), CeO_2 (Ref. 9), and TiO_2 (Ref. 10). U_3O_8 and TeO_2, which are usually present in

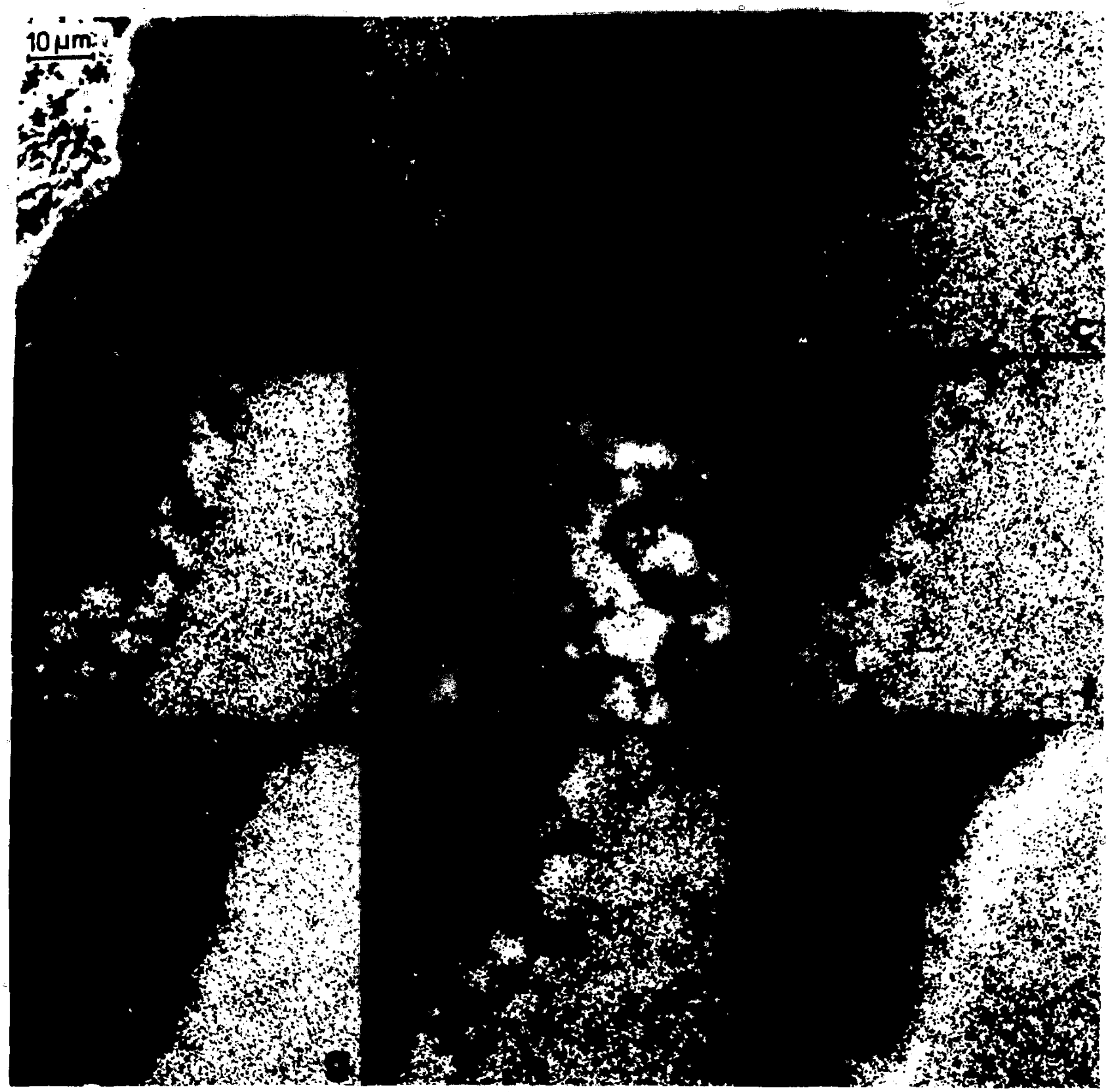

Fig. 1 (a) SEM micrograph of the phase boundary area of a phosphate glass - lead composite. Annealing temperature, 873°K; annealing time, 12 hr. (b) X-ray mapping of lead in Fig. 1(a). (c) X-ray mapping of phosphorous in Fig. 1(a). (d) X-ray mapping of cerium in Fig. 1(a). (e) X-ray mapping of zirconium in Fig. 1(a). (f) X-ray mapping of molybdenum in Fig. 1(a). (g) X-ray mapping of iron in Fig. 1(a). (h) X-ray mapping of aluminum in Fig. 1(a). (i) X-ray mapping of cesium in Fig. 1(a).

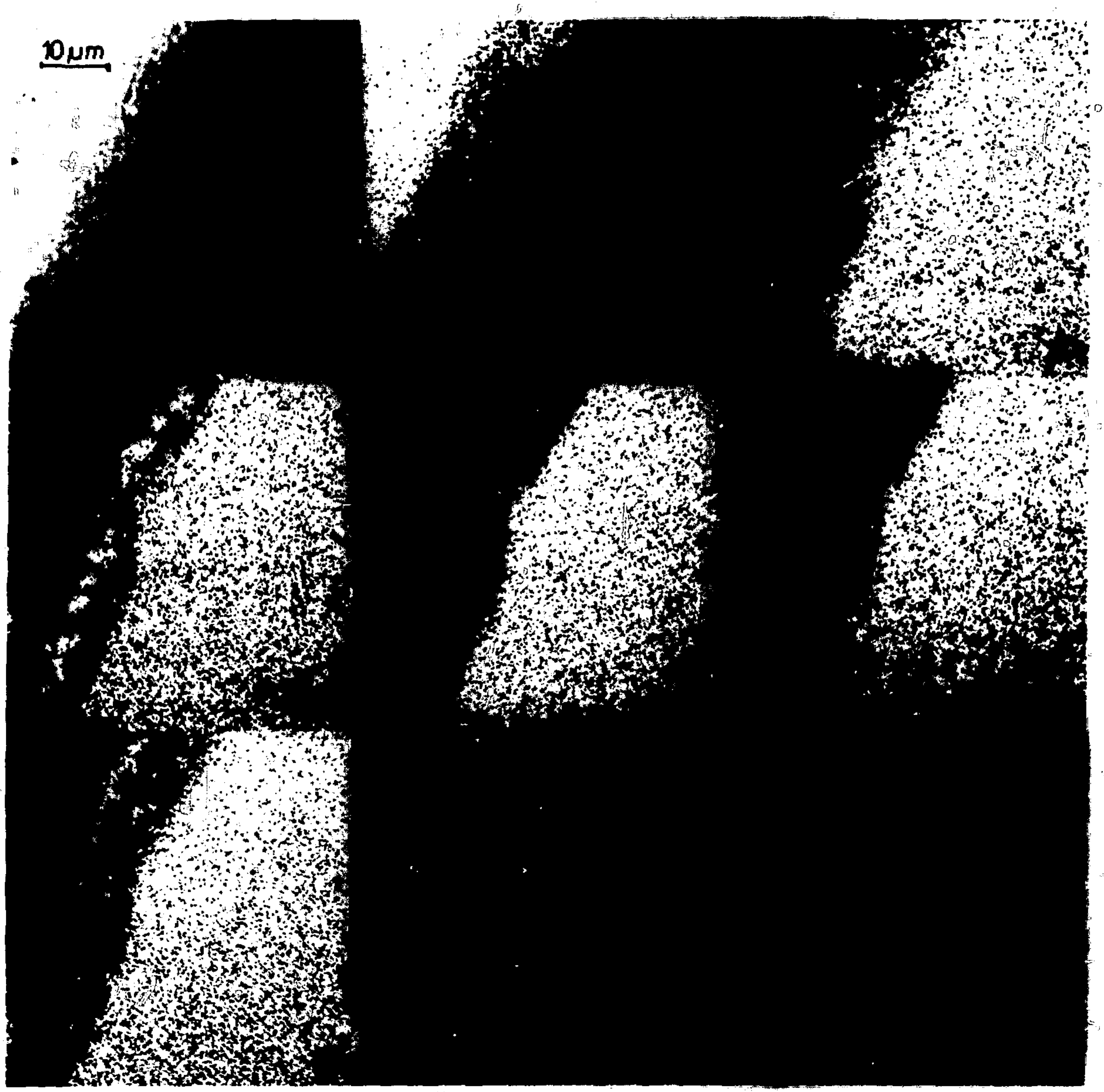

Fig. 2 (a) SEM micrograph of the phase boundary area of a borosilicate glass–lead composite. Annealing temperature, 873°K; annealing time, 3 hr. (b) X-ray mapping of lead in Fig. 2(a). (c) X-ray mapping of silicon in Fig. 2(a). (d) X-ray mapping of cesium in Fig. 2(a). (e) X-ray mapping of calcium in Fig. 2(a). (f) X-ray mapping of barium in Fig. 2(a). (g) X-ray mapping of titanium in Fig. 2(a). (h) X-ray mapping of molybdenum in Fig. 2(a). (i) X-ray mapping of aluminum in Fig. 2(a).

TABLE 3

Widths (μm) of Reaction and Diffusion Zones of Phosphate Glass

Annealing time, hr	Width of reaction zone		Width of diffusion zone		Width of both zones	
	At 823 K	At 873 K	At 823 K	At 873 K	At 823 K	At 873 K
12	4 ± 1	9 ± 2	4 ± 1	10 ± 3	8 ± 2	19 ± 5
48	7 ± 2	15 ± 5	14 ± 4	25 ± 5	21 ± 6	40 ± 10
192	30 ± 5	65 ± 10	5 ± 2	10 ± 5	35 ± 7	75 ± 15

rather low concentrations, may be reduced as well (U_3O_8 to UO_2, $\Delta H = -42.7$ kJ, and TeO_2 to Te, $\Delta H = -50.2$ kJ). Here Fe_2O_3 shall be dealt with in more detail because it is a major constituent of the phosphate glass. As is known for both borosilicate[7] and phosphate glasses,[8] the equilibrium constant of the Fe^{2+}–Fe^{3+} redox reaction is dependent on the acidity of the glass. At constant temperature and rising acidity, the equilibrium moves toward the Fe^{2+} side. In general, phosphate glasses are more acidic than borosilicate glasses.[5] Experiments carried out on molybdenum-free glasses resulted in reaction zones similar to those shown in Figs. 1(a) and 2(a). Hence, evidence is given for the reactivity of elements other than molybdenum.

Migration of Lead and Glass Constituents

The transport of lead via the phase boundary is expected to be of paramount importance for all phase boundary reactions reported throughout the study. This became evident from a comparison with nonembedded glass samples where nothing similar happened under the same annealing conditions. Few investigations have been reported in the literature on the transport phenomena at a lead/glass boundary.[6] In this work we were interested in the temperature range 573 to 873 K. No transport data were found for glass constituents. Only the penetration of lead was investigated,[11] and the diffusion coefficient was reported to be $D = 5.5 \times 10^{-13}$ cm^2 s^{-1} in a soda lime glass at 773 K. The question was left open as to whether lead migrates as such or in an oxidized state.

It was clear from the finding of the preceding chapter that the lead was oxidized under the applied experimental conditions. Numerous investigations on silicate glasses have been published dealing with the migration of oxidized lead, and it was reported that simultaneous migration of Pb^{2+} ions and O^{2-} ions[12,13] or transport of PbO molecules occurs.[14] Diffusion data derived from measurements on a lead silicate glass at temperatures above the transformation range[13] yielded $D_{823\,K} = 4 \times 10^{-12}$ and $D_{873\,K} = 4 \times 10^{-11}$ cm^2 s^{-1}. An estimation of a lead diffusion coefficient from the penetration depth yielded $D_{873\,K} = 1 \times 10^{-11}$ cm^2 s^{-1}, based on the equation $D = x^2/4t$ [$x = 15$ μm after 3 hr; see Fig. 2(a)] for the borosilicate glass. Values for the phosphate glass were derived from the sum of the reaction and diffusion zones and are $D_{823\,K} = 5 \times 10^{-12}$ and $D_{873\,K} = 2 \times 10^{-11}$ cm^2 s^{-1}. These values are in fair agreement with those measured in lead silicate glasses.[13] Hence, it may be assumed that the extent of the phase boundary area [Fig. 1(a and b)] is controlled by the diffusion of lead.

As to the migration of phosphate glass constituents, the following was concluded based on EPMA and high-temperature crystallization experiments.

1. In the reaction zone crystalline phases of $CePO_4$ as well as $4PbO \cdot P_2O_5$ or $3PbO \cdot P_2O_5$ could form. These compounds were found in lead phosphate glasses (70 to 90 mole% PbO) after Levin[15] at temperatures below 1100 K. The reaction zone of our phosphate glass has a high lead content.

2. Glass constituents not bound in crystal phases were found to have been driven out of the reaction zone. Different species were found on either side. Molybdenum migrated towards the lead matrix [Fig. 1(f)]. All the other constituents migrated in the opposite direction [see Fig. 1(g, h, and i)].

3. While lead diffuses from the reaction zone into the glass [Fig. 1(a and b)], constituents not bound in crystal phases migrate into the glass core. On the diffusion front of lead, an enrichment of these constituents is found, e.g., cesium [Fig. 1(h)]. This phenomenon is of practical importance because long-lived fission products such as cesium are depleted in the surface area and thereby protected from possible water attack. An in-depth study on this subject is in progress.

CONCLUSIONS

1. The glass/lead phase boundary of a metal matrix composite (HLSW form) is subject to chemical reactions above 820 K. The most important species is oxidized lead penetrating the glass phase.

2. The depth of the reaction zone is determined by the diffusion coefficient of Pb^{2+} in glass.

3. Fission products may leave the zone in both directions; for example, molybdenum migrates into the lead whereas cesium migrates into the glass core.

4. Crystallization in the reaction zone (borosilicate glass) prevents the constituents from escaping; that is, glass ceramics as the HLSW form should be less affected by the diffusing lead and might be preferred instead of glass.

ACKNOWLEDGMENT

The author thanks W. Lutze for discussions.

REFERENCES

1. W. Heimerl, Solidification of HLW Solutions with the PAMELA Process, in Proceedings of *Ceramics in Nuclear Waste Manage-*

ment, Cincinnati, CONF-790420, Technical Information Center, Oak Ridge, 1979.

2. J. van Geel, H. Eschrich, W. Heimerl, and P. Grziwa, Solidification of High-Level Liquid Waste to Phosphate-Glass Metal Matrix Blocks, in *International Symposium on the Management of Radioactive Wastes from the Nuclear Fuel Cycle*, March 22–26, 1976, Vienna, Austria.
3. A. K. De, B. Luckscheiter, W. Lutze, G. Malow, and E. Schiewer, Development of Glass Ceramics for the Incorporation of Fission Products, *Ceramic Bulletin*, 55: 500 (1976).
4. W. Lutze, J. Borchardt, and A. K. De, Characterization of Glass and Glass Ceramic Waste Forms, in Proceedings of *Scientific Basis for Nuclear Waste Management*, Boston, G. J. McCarthy (Ed.), Plenum, NY, 1979.
5. H. Scholze, *Glass*, 2nd ed., Springer-Verlag, Berlin–Heidelberg–New York, 1977.
6. R. C. Weast, *Handbook of Chemistry and Physics*, 57th ed., CRC Press, Cleveland, Ohio, 1977.
7. D. Ehrt, H. Reiß, and W. Vogel, Formation and Distribution of Fe_2O_3 Microphases in the Ground Glass System Na_2O–B_2O_3–SiO_2, *Silikattechnik*, 27: 304 (1976).
8. R. Majumdar and D. Lahiri, Equilibrium Studies of Fe in Alkali Phosphate Glasses, *J. Amer. Ceram. Soc.*, 58: 99 (1975).
9. O. H. El-Bayoumi and K. N. Subramanian, Crystallization of a Cerium Phosphate Glass, *J. Amer. Ceram. Soc.*, 60: 161 (1977).
10. C. P. Perry, F. K. Wilson, and D. L. Kinser, Thermodynamic Predictions of Reactions in Reduced Transition Metal Phosphate Melts, *J. Amer. Ceram. Soc.*, 58: 456 (1975).
11. J. Matoušek, Transport of Pb Ions at the Interface Between Silicate Glass and Molten Lead, *J. Amer. Ceram. Soc.*, 58: 521 (1975).
12. K. C. de Berg and I. Lauder, Oxygen Tracer Diffusion in Lead Silicate Glass Above the Transformation Temperature, *Phys. Chem. Glasses*, 19: 78 (1978).
13. R. Lindner, W. Hassenteufel, and Y. Ketera, Diffusion of Radioactive Lead in Lead Silicate Glass, *Z. Phys. Chem.*, 23: 408 (1960).
14. K. Hauffe, *Reaction in and on Solid Substances*, Springer-Verlag, Berlin, 1955.
15. E. M. Levin, C. R. Robbins, and H. F. McMurdie, *Phase Diagrams for Ceramists*, The American Ceramic Society, Columbus, Ohio, 1964.

A PELLETED WASTE FORM FOR HIGH-LEVEL ICPP WASTES

K. M. LAMB, S. J. PRIEBE, H. S. COLE, and B. D. TAKI
Allied Chemical Corporation, 550 Second Street, Idaho Falls, Idaho

ABSTRACT

Simulated zirconia-type calcined waste is pelletized on a 41-cm diameter disc pelletizer using 5% bentonite, 2% metakaolin, and 2% boric acid as a solid binder and 7*M* phosphoric plus 4*M* nitric acid as a liquid binder. After heat treatment at 800°C for 2 hours, the pellets are impact resistant and have a leach resistance of 10^{-4} g/cm^2 · day, based on Soxhlet leaching for 100 hours at 95°C with distilled water. An integrated pilot plant is being fabricated to verify the process.

INTRODUCTION

At the Idaho Chemical Processing Plant (ICPP) defense type nuclear fuels are reprocessed to recover uranium. The resulting high-level wastes are solidified by a fluidized-bed calcination process.[1] Currently there are ~1700 m^3 of calcined high-level wastes stored at the ICPP.[2] The composition of zirconia calcine stored at ICPP is shown in Table 1.

Pelletization is being considered as an alternative to calcination or vitrification prior to storing ICPP high-level wastes.[3] Fluidized-bed calcine, a mixture of bed particles and fines, has an angle of repose greater than 80°; therefore, the calcine has poor flow characteristics making it difficult to retrieve if recovery becomes necessary. Fluidized-bed calcine particles are porous and leachable for cesium and strontium, but quite leach resistant for other elements.[4] By pelletizing, a flowable and easily retrieved product is produced. Also, leachability and dispersibility are reduced. Pellets also have a relatively low preparation temperature and can be readily converted to another waste form such as a metal matrix.[5] Properties of the calcine, pellets, and glass are given in Table 2.

The development of a pelletized waste form included extensive pellet binder studies involving a total of 32 pelletizing experiments to evaluate different pellet forming binders. Using a 41-cm diameter disc pelletizer, the zirconia calcine was mixed with binders and then agglomerated into three 10 mm diameter spherical pellets. The pellet forming binders react with the calcine during pelletizing to form a cement-like material to improve green pellet strength and during heat treatment to impart leach resistance to the pellet.

DESCRIPTION OF PELLETIZING SYSTEM

A 41-cm diameter disc pelletizer with a throughput of 10 to 100 kg/hr was used for the developmental work. The pelletizer is operated by a 0.25 hp motor, and the pelletizer disc is the only moving part. Unlike most other agglomerating equipment, the disc pelletizer does not use high pressure to form pellets. A mixture of calcine and solid additives is fed onto the inclined rotating disc. Then a liquid binder is sprayed onto the mixture. As the disc turns, the solids, while rolling and tumbling, grow into pellets by a snowballing effect. The centrifugal action of the turning disc separates the pellets into three distinct and progressively larger sized streams: a seed stream, a growth stream, and a polishing stream. The polished pellets move to the edge of the disc and spill over to be collected. The polished product pellets are uniform in size and spherical in shape.

The size of the pellets is controlled by the speed and angle of the disc and the location of the solids feed and liquid spray. Increasing the disc speed or angle will decrease pellet size. The larger the size of the particles where the liquid is sprayed or where solids are fed, the larger the final pellet.

The solids are metered to the pelletizer at up to 60 kg/h using a screw feeder. The liquid binder is sprayed through a

TABLE 1

Composition of ICPP Zirconia Calcine

	Composition, wt.%
Al_2O_3	13–17
ZrO_2	21–27
CaF_2	50–56
CaO	2–4
NO_3	0.5–2
B_2O_3	3–4
Fission products	0.2–1.5

TABLE 2

Comparison of Alternative Waste Forms

Property	Waste form Calcine	 Pellet	 Glass
Density, g/cc	1.2 to 1.6	1.1 to 1.5	2.5 to 2.75
Waste content, g/cc	1.2 to 1.6	0.8	0.6 to 1.1
Preparation temperature, °C	500 to 550	800 to 850	1050 to 1200
Maximum stable temperature, °C	700	800 to 850	~300
Bulk leach resistance, $g/cm^2 \cdot d$ (100 hr Soxhlet)	$>10^{-3}$	10^{-4} to 10^{-5}	10^{-5} to 10^{-6}

hollow cone nozzle. A variable speed gear pump delivers the liquid to the nozzle at pressures up to 0.44 MPa and flows up to 30 l/hr.

PELLET BINDER STUDIES

Zirconia calcine can be pelletized on the disc pelletizer using only water as a binder, but it is a poor binder, producing flaky pellets of limited strength with leach resistance no greater than calcine. By using various combinations of solid and liquid binders, pellets can be made with much greater strength. The leach resistance of the pellets is also improved by the use of binders, because they can react with the soluble or leachable materials in the calcine to form insoluble compounds. These reactions normally take place during heat treatment at 800 to 850°C for two hours.

Liquid Binders

Four different liquid binders were studied: phosphoric acid (H_3PO_4), nitric acid (HNO_3), colloidal silica (SiO_2), and an alumina slurry. These binders were tested alone and in combination.

Phosphoric Acid. This acid has been shown to react with most of the metal oxides in the calcine to form stable and refractory compounds.[6] The two primary reasons for using H_3PO_4 as a liquid binder are (1) to form quick-setting aluminum (present in the calcine) phosphate cements which impart green and dried strength to the pellets and (2) to react with the calcine to form insoluble phosphate compounds during heat treatment to increase component leach resistance.

Nitric Acid. This acid is used in conjunction with H_3PO_4 as a liquid binder. Since the second ionizing proton of H_3PO_4 is not acidic ($pKa_2 = 7.21$), HNO_3 is added to increase the binder acidity to result in better reaction with the basic calcine and to decrease the liquid binder viscosity.

Liquid binder solutions with H_3PO_4 concentrations $\geqslant 9M$ are too viscous to spray in uniform patterns. This results in locally high amounts of liquid which forms large, odd-shaped particles instead of uniform pellets. Pellets made with liquid binders of less than $7M$ H_3PO_4 had poor leach resistance and were often odd shaped (Table 3).

Colloidal Silica. This was also tested as a liquid binder. Silica was added in an attempt to form pollucite type ($CsAlSi_2O_6$) compounds during sintering of the pellets. Pollucites, if formed, are leach resistant. If silica could replace some or all the H_3PO_4 used as a pellet binder, the pellets would also be more easily converted to glass if that were ever necessary.

Four pellet-forming runs were made using silica in the liquid binder. Two of the SiO_2 concentrations, 15 wt.% and 30 wt.%, did not wet the calcine particles or help them agglomerate. The basic (pH = 9.8) colloidal silica would not react with the basic metal oxides which make up the calcine. The colloidal silica could be mixed with $3M$ H_3PO_4 without gelling for at least 48 hours. As a liquid binder, the combined acid–silica solution was used to form uniform, although rough surfaced pellets. Since the properties, including leach resistance, of the silica-bound pellets were comparatively poor, the use of colloidal silica and SiO_2-H_3PO_4 solutions as liquid pellet binders was discontinued.

Aluminum Oxide. Fine α-Al_2O_3 slurried with phosphoric acid and aluminum phosphate solutions were tested as possible liquid binders. If during pelletizing the calcine particles could be coated with aluminum phosphate cement, the leach resistance and possibly the strength of the pellet would improve. Alpha-Al_2O_3 is practically insoluble in H_3PO_4. A slurry using 255 g/l of fine ($\leqslant .074$ mm) Al_2O_3 powder in a solution of $7M$ H_3PO_4 and $1M$ HNO_3 tended to plug the liquid binder spray nozzle. Because of the difficulties in spraying the slurried Al_2O_3 binder, another method of making an aluminum

TABLE 3

Effects of H_3PO_4 Concentration on Pellet Properties

H_3PO_4, *M*	Shape characteristics	Soxhlet leach rates, $g/(cm^2 \cdot d)$ Bulk	 Cesium
1	No pellets formed		
2	No pellets formed		
5	Rough, some odd shapes	1.4×10^{-3}	2.4×10^{-2}
7	Spherical, smooth	7.3×10^{-4}	6.8×10^{-3}
9	Oblong, rough	1.9×10^{-3}	2.3×10^{-1}

phosphate liquid binder was found. Powdered aluminum dissolved in H_3PO_4, although very viscous, was tried as a liquid binder. The leach resistance of pellets made using liquid aluminum phosphate and the slurried Al_2O_3 was low compared to pellets made with the same solids and just 7*M* H_3PO_4 and 2*M* HNO_3 as a liquid binder.

As a result of the liquid binder development experiments, a liquid binder solution of 7*M* H_3PO_4 and 4*M* HNO_3 was chosen as the binder to be used in future studies.

Solid Binders

Four different solids: bentonite, metakaolin, boric acid, and calcium hydroxide were tested as possible pellet binders. Various combinations of these binders were tested for their effect on pellet properties such as leach resistance, pellet shape, and both green and dried pellet strength. When adding solid binders, the object was to use enough binder to react with the desired calcine components, but not so much as to greatly increase the total volume of solids. Generally, solid binders were kept under 20% of the pellet weight. Solids containing 20% or more H_3BO_3 $Ca(OH)_2$ or metakaolin did not form pellets.

Bentonite. This was tested as a solid binder to increase cesium leach resistance. Cesium or strontium are taken into the bentonite structure by ion exchange.[7] When the pelleted calcine is heat-treated, bentonite reacts with the cesium to chemically fix it in the structure. The stoichiometric amount of bentonite needed in the pellet to bond all the cesium and strontium is ~1.0 wt.% of the calcine. Bentonite amounts above 5 wt.% tend to cause the green pellets to become sticky and adhere to each other and metal surfaces. The levels of bentonite used were 3 and 5 wt.%. Overall pellet leach resistance increased about a factor of 3 because of bentonite additions, whereas the cesium and strontium leach resistance increased by a factor of 4 to 5 (Table 4). For 100-hour Soxhlet leaches using distilled water at 95°C, cesium and strontium leach resistance was highest at bentonite concentrations of 5 wt.%.

TABLE 4

Effect of Bentonite on Pellet Leach Resistance

Bentonite content, wt.%	Soxhlet leach resistance, $g/(cm^2 \cdot d)$		
	Cesium	Strontium	Bulk
0	1.02×10^{-2}	3.15×10^{-4}	7.9×10^{-4}
3	4.53×10^{-3}	2.8×10^{-4}	9.9×10^{-4}
5	1.88×10^{-3}	8.0×10^{-5}	2.89×10^{-4}

Metakaolin (Calcine Kaolin). This clay can react with cesium much like bentonite. The calcined clay is used because it is generally more reactive than the hydrated clay.[8] Metakaolin begins reacting with cesium at temperatures as low as 500°C. In testing, as much as 20 wt.% metakaolin was added to the calcine. Testing indicated that more than 10 wt.% metakaolin made the calcine mixture very difficult to pelletize because metakaolin is not easily wetted resulting in poor agglomeration. Metakaolin in smaller quantities (5 wt.% or less) will fill voids between calcine particles and enhance pelletization. For appearance, strength, and cesium leach resistance, a few percent metakaolin is beneficial. The bulk leach resistance of pellets containing 2 and 5 wt.% metakaolin is similar, with the 2 wt.% pellets possibly having the better cesium leach resistance.

Boric Acid. This acid was tested as a solid binder over the range of 0 to 10 wt.% for many of the reasons H_3PO_4 was tested as a liquid binder. These are potentially improved pellet strength and leach resistance. Boric acid increases the pellet green strength by reacting with the basic oxides in the calcine. Boric acid will lower the sintering temperature of the pellet possibly decreasing pellet porosity during heat treatment. Boric acid, much like metakaolin, improves some physical properties of the pellets. However, more than 2 wt.% boric acid does not increase leach resistance.

Calcium Hydroxide. This was tested as a solid pellet binder in four runs. Calcium hydroxide or calcium oxide will react, similar to Al_2O_3, with H_3PO_4 and form stable cold setting cements.[9] By using $Ca(OH)_2$ in the solids mixture and a liquid binder containing H_3PO_4, the cement forming reaction was expected possibly to improve pellet strength and leach resistance. Concentrations as high as 20 wt.% $Ca(OH)_2$ were tested in pellets. Bulk leach rates were low, but pelletizing properties were poor. Lime, being a very strong base, reacts too vigorously with the H_3PO_4. The reaction heats the pellets and causes the evolution of steam. The steam causes the pellets to swell and to become porous and friable. Many of the pellets made with as low as 5 wt.% $Ca(OH)_2$ cracked during pelletizing or upon drying.

To make pellets with good leach resistance, good green and dried strength, good shape characteristics, and containing a high waste fraction, it was determined that 5 wt.% bentonite, 2 wt.% metakaolin, and 2 wt.% boric acid was a practical solid binder.

PILOT PLANT PROCESS FOR PELLETIZING ICPP CALCINED WASTE

A pelletizing pilot plant has been developed to pelletize the calcined waste. The pilot plant (Fig. 1) is intended to test, in an integrated continuous process, the techniques learned in laboratory experiments to produce hard, leach-resistant pellets from calcine.

In the pilot plant process, calcine and a premixed solid binder (56% bentonite, 22% boric acid, and 22% metakaolin) are fed to a 41-cm diameter rotating disc pelletizer from separate loss-in-weight feeders. These feeders give a very accurate and uniform feed rate based on weight of material. A screw mixer intimately combines the two feeds

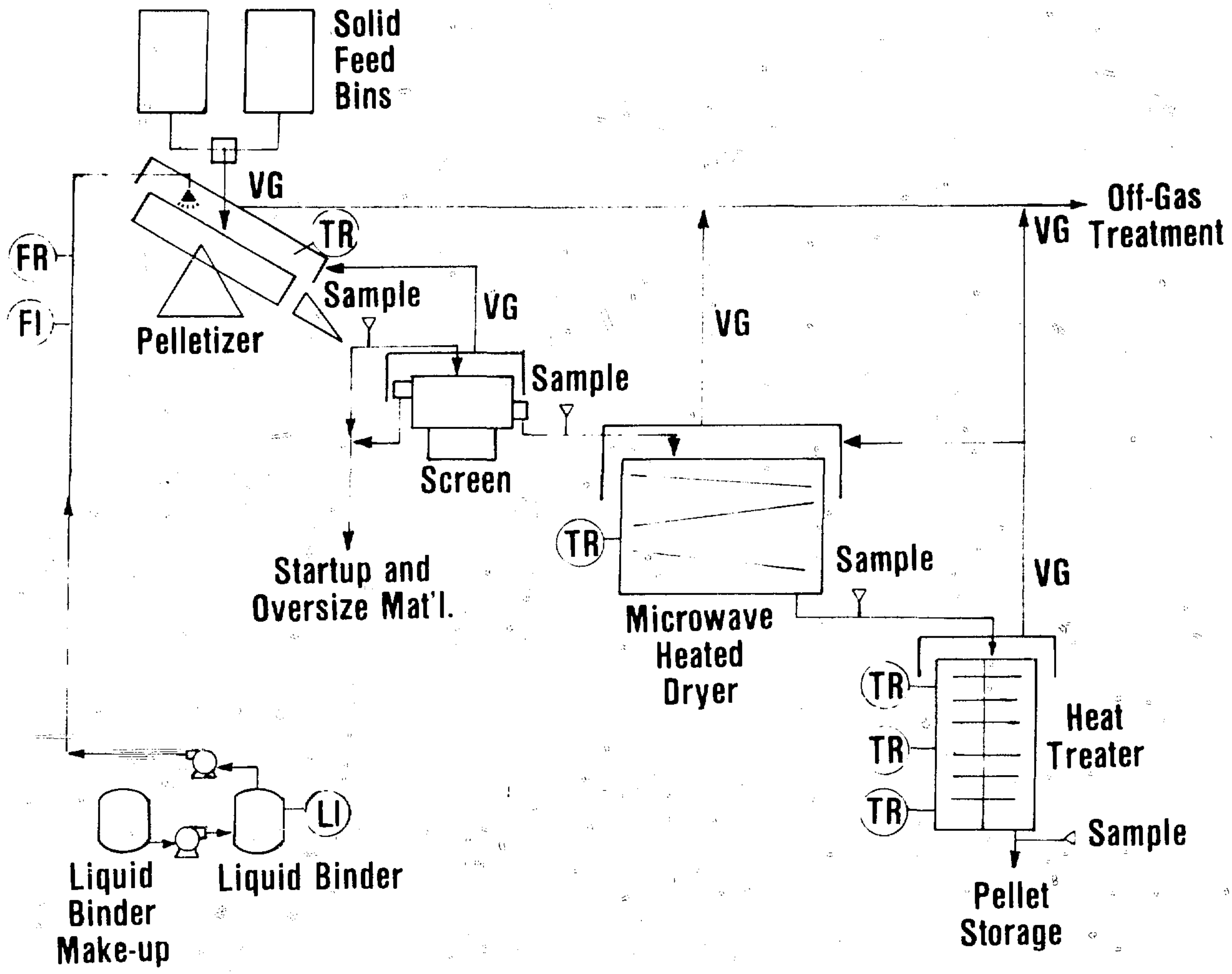

Fig. 1 Continuous pilot plant process for pelletizing simulated zirconia calcine.

(91% calcine, 9% binder) and conveys the mixture to the pelletizer. Liquid to solid ratio is ~1 : 2.2, and pellets of 3 to 6 mm in diameter are formed.

During initial start-up and following major changes in operating conditions, odd-sized particles can form on the pelletizer. A gyratory screen is used to remove all particles over 12 mm in diameter from the pellet stream. These pieces can then be broken and recycled. The pellets are dried at 150 to 200°C in a microwave heated dryer. Power is supplied by a 6 kW microwave generator.[10] Microwave energy was chosen because it has the advantage of drying a pellet uniformly throughout, in a short time (~15 min), and with relatively small equipment size. Drying pellets by conventional radiant energy in the same length of time dries the outer layer of the pellet first. As the interior heats and expands, the dry outer shell cracks, destroying the integrity of the pellet. Also, larger equipment is required.

After they are dried, the pellets are heat-treated at 800 to 850°C for two hours to promote a reaction between the calcine and additives. To maintain a continuous process and yet keep equipment size to a minimum, a heat treater was designed which consists of eight stacked trays rotating at about four revolutions per hour inside a kiln. The pellets revolve and drop from tray to tray through the unit by a set of paddles and slots in the trays. From the heat treater, the pellets are dropped into a canister for cooling and storage. The combined off-gas from the various process stages is cooled in a quench tower. Particulates and volatiles are then removed in a venturi scrubber and a filter system before the off-gas is vented to the atmosphere.

CONCLUSIONS

Pelletizing high-level ICPP zirconia calcine may be a practical alternative to vitrification or calcine storage. Pelletizing reduces the surface area of calcined waste by a factor of 1000 or more. This greatly reduces dispersibility and improves leach resistance. Reactions between solids and liquid pellet binders and calcine further increase leach resistance of the waste. Pellets have been made with bulk leach resistance nearly as great as the leach resistance of glass made from the same simulated calcine; however, the pellet leach resistance of cesium is approximately 10 times lower. The integrated pellet pilot plant will be used to verify a practical process. The pilot plant and development work will form the basis for determining the value of pellets as a waste form for ICPP waste.

ACKNOWLEDGMENT

This work was sponsored by the U. S. Department of Energy under contract DE-AM07-76IDO1540.

REFERENCES

1. R. E. Commander et al., *Operation of the Waste Calcining Facility with Highly Radioactive Aqueous Waste, Report of the First Processing Campaign*, AEC IDO-14662, June 1966.
2. *Alternatives for Long-Term Management of Defense High Level Radioactive Wastes, Idaho Chemical Processing Plant*, Idaho Falls, Idaho, USERDA 77-43, September 1977.
3. K. M. Lamb and H. S. Cole, *Development of a Pelleted Waste Form for High-Level ICPP Zirconium Wastes*, DOE ICP 1185, February 1979.
4. M. W. Wilding and D. W. Rhodes, *Leachability of Zirconia Calcine Produced in the Idaho Waste Calcining Facility*, AEC IN-1298, June 1969.
5. K. M. Lamb, *Final Report: Development of a Metal Matrix for Incorporating High-Level Commercial Waste*, DOE ICP 1144, March 1978.
6. W. D. Kingery, Fundamental Study of Phosphate Bonding in Refractories: 1, Literature Review, *Journal of the American Ceramic Society*, Vol. 33(8), August 1950.
7. J. Mukerji and P. B. Kayal, "Reaction of $CsNO_3$ and $RbNO_3$ with SiO_2 and Metakaolin, *Journal of the American Ceramic Society*, 57: 229 (1974).
8. *Use of Local Mineral in the Treatment of Radioactive Waste*, STI/DOC-10/136, International Atomic Energy, Vienna, June 1977.
9. W. D. Kingery, Fundamental Study of Phosphate Bonding in Refractories, *Journal of the American Ceramic Society*, Vol. 33(8), August 1950.
10. S. J. Priebe et al., *Application of Microwave Energy to Post Calcination Treatment of High Level Nuclear Wastes*, DOE ICP-1183, February 1979.

THE USE OF GLASS–CERAMIC MATERIALS FOR THE FIXATION OF RADIOACTIVE WASTES

A. A. MINAEV, S. N. OZIRANER, and N. P. PROKHOROVA
State Committee on Peaceful Use of Atomic Energy, Moscow, U.S.S.R.

ABSTRACT

This paper is concerned with the study of the crystallization of phosphate and silicate glasses. It was shown that temperature and time of storage influence considerably the crystallization of glasses and that crystallization very often increases their rates of leaching to a great extent. However, there are glasses in which crystallization does not result in leaching rate increase. It seems reasonable to use these materials for the fixation of radioactive wastes. The main reasons for the increase in the leaching rate during crystallization are the formation of porosity and soluble crystal phases.

INTRODUCTION

At present the vitrification method is considered to be the most reliable method throughout the world for the fixation of highly radioactive wastes. That is why a great deal of work is being done to study various glass systems, factors influencing crystallization, leaching rates, equipment problems, etc.

It is known that one of the basic requirements of the vitrification process which determines its economic characteristics is the quantity of radioactive wastes which can be introduced into the glass. Therefore, compositions are used which include the maximum quantity of radioactive wastes. However, glasses with a high content of radioactive wastes crystallize more readily during temperature treatment, which is not desirable because glass crystallization often leads to the deterioration of its properties. Crystallization mainly depends on temperature, which rises during storage as a result of radioactive isotope decay. Hence, to store wastes in vitrified blocks, it is necessary to maintain low temperatures to prevent crystallization. This makes vitrification processes and storage of the glass more difficult and expensive.

It is necessary to point out that the temperature of glass storage at which glass crystallization does not proceed is 100 to 150°C lower than the glass softening temperature and is 200 to 250°C lower than the melting temperature of crystal compounds of the same composition.

As a rule, the study of the thermal devitrification of glass is done during a short period of time (50 to 200 hours), while vitrified radioactive wastes are kept for hundreds of years. It is quite probable that during longer storage glasses will devitrify at lower temperatures than in the laboratory experiments.

In this paper an attempt is made to prove some inaccuracy in storage temperatures of the vitrified radioactive wastes when they are chosen on the basis of relatively short laboratory experiments. The possibility of using crystallized materials for the fixation of radioactive wastes is also shown.

EXPERIMENTAL

Since the composition of radioactive wastes destined for treatment may vary within a wide range, we studied both phosphate and silicate glasses with various oxide contents and with various ratios of sodium oxide to multivalent metal oxide. Phosphate glasses were melted at 900 to 1000°C, and silicate glasses at 1100 to 1150°C. The glasses were annealed at various temperatures for various periods of time. The presence of the crystal phases was determined by X-ray diffraction. Composition of the glasses and experimental results are shown in Table 1. The results in the table show that the time of annealing considerably influences the choice of the working storage temperature. The annealing of phosphate glasses at 400°C for as long as 500 hours causes no changes in the glasses.

TABLE 1

The Dependence of Crystallization on the Temperature and Time of Annealing

	Composition of samples, wt.%						Na : P	Annealing temperature and time, hr†												
								At 400°C				At 500°C			At 550°C			At 620°C		
No.	Na_2O	O.M.M.*	P_2O_5	SiO_2	B_2O_3	CaO	mol.	100	508	1084	1400	100	268	435	96	214	431	96	340	476
1	20	20		35	10	15											+		+	+
2	20	20		35	15	10													+	+
3	20	20		30	15	15											+		+	+
4	26	25	49				1.2			+	+	+	+	+						
5	24	30	46				1.2			+	+		+	+						
6	23	25	52				1.0				+		+	+						
7	21	30	49				1.0						+	+						

*Oxides include sodium oxide and oxides of multivalent metals (O.M.M.)

†—, absence of crystal phase; +, presence of crystal phase.

TABLE 2

The Influence of Crystallization on the Leaching Rate

	Composition of samples, wt.%			Na : P	Leaching rate, g/cm^2 · day x 10^{-6}		Composition of crystal phases formed during annealing
No.	Na_2O	O.M.M.*	P_2O_5	mol.	Before annealing	After annealing	
1	26.5	30.0	43.5	1.4	0.14	403.0	Na_3PO_4
2	28.8	24.0	47.2	1.4	0.6	170.0	Na_3PO_4
3	25.3	30.0	44.7	1.3	0.23	19.3	80% Na_2PO_4 + 20% $3Na_2O \cdot 2Al_2O_3 \cdot 3P_2O_5$
4	24.6	24.0	51.4	1.1	0.2	1.2	$3Na_2O \cdot 2Al_2O_3 \cdot 3P_2O_5$
5	21.3	30.0	48.7	1.0	0.27	0.2	$3Na_2O \cdot 2Al_2O_3 \cdot 3P_2O_5$
6	19.7	30.0	50.3	0.9	0.12	0.55	20% $AlPO_4$ + 80% $3Na_2O \cdot 2Al_2O_3 \cdot 3P_2O_5$

*Oxides include sodium oxide and oxides of multivalent metals (O.M.M.).

Increasing the time of annealing up to 1000 hours leads to crystallization of glasses with a molar ratio of sodium to phosphorus of 1.2. After 1400 hours, even glasses with a molar ratio of sodium to phosphorus of 1.0 become crystallized. The same is true of the silicate glasses. Annealing at 550°C for as long as 214 hours does not cause crystallization of the glasses under study. But an increase in the time of annealing at the same temperature results in the crystallization of some of the glasses under study. Silicate glasses are crystallized in shorter times of annealing at 620°C.

The data described above show that, in some cases, annealing even for as long as 500 to 700 hours does not guarantee the correct choice of the storage temperature from the point of view of glass crystallization. The data obtained show that an increase in the time of testing to more than 1000 hours may result in even further reduction of the storage temperature selected. Examples are glasses 5 and 6 (Table 1), which should be stored at below 400°C. This is about 300°C lower than for crystal substances of the same composition, whose melting temperatures were determined by differential thermal analysis and range from 650 to 700°C.

During crystallization, glasses of different compositions change their properties in different ways. Crystallization may have a strong effect on the leaching rate. There are glasses in which crystallization results in a thousandfold increase in their leaching rates. This makes such crystallized materials unfit for the fixation of highly radioactive wastes. However, there are also glasses whose crystallization does not increase their leaching rates or increases the leach rates only 5 to 10 times. These materials can be used for the fixation of wastes. Examples of such phosphate glasses are shown in Table 2. For glasses 1 through 3 with a molar ratio of sodium to phosphorus equal to 1.3 or 1.4, the leaching rate after annealing increases 100 to 1000 times, but for glasses 4 through 6 with a molar ratio of sodium to phosphorus equal to 1.1, 1.0, and 0.9, respectively, the leaching rate increases not more than 5 to 6 times, being equal to 1 x 10^{-6} g/cm^2 per day. From these data it follows that one may choose glasses whose crystallization does not increase the leaching rate. The increased thermo-

stability of such crystallized glasses means that they can be stored at higher temperatures than vitreous glasses.

To make a correct choice of such crystallizing glasses, it is important to know the reasons for the increase in the leaching rate. Our studies showed that the main reason for the increase in the leaching rate during crystallization of glasses is the formation of soluble crystalline compounds. Table 2 shows soluble and nonsoluble crystal phases formed during temperature annealing of phosphate glasses of various compositions. It was shown that when water-soluble sodium orthophosphate is one of the basic crystal phases the rate of leaching increases considerably (glasses 1 3), although, when the basic crystal phases are aluminum sodium orthophosphate or aluminum orthophosphate, the leaching rate changes insignificantly (glasses 4–6). Therefore it is important to know the phase diagram of the system under study.

Another reason for the increase in the leaching rate is the increase in the geometrical water-contact surface. However, it is not just a simple increase in the geometrical surface caused by roughness on the surface which results from crystallization. We experimentally showed that the formation of surface and volume porosity takes place during crystallization. This increases the water contact surface and consequently the leaching rate. Table 3 shows the way porosity influences the leaching rate. All samples with a low leaching rate are nonporous, while most of the samples with a high leaching rate are porous. There are some nonporous samples with a high leaching rate, but in these cases it is due to the presence of soluble crystal phases.

TABLE 3

Influence of Porosity of Crystallized Samples on Their Leaching Rate

	Composition of samples, wt.%					
No.	Na_2O	O.M.M.*	P_2O_5	Na : P mol.	Porosity	Leaching rate, $g/cm^2 \cdot day \times 10^{-6}$
1	21.6	29.0	49.4	1.0	+	40.0
2	25.0	34.0	41.0	1.4	–	5.0
3	26.1	34.0	49.9	1.2	–	5.5
4	28.8	24.0	47.2	1.4	+	133.0
5	30.0	20.9	49.1	1.4	+	2152.0
6	24.4	29.0	46.6	1.2	–	5.1
7	25.4	26.0	48.6	1.2	–	2.3
8	24.3	36.0	39.8	1.4	+	1835.0
9	28.0	26.0	46.0	1.4	+	533.0
10	27.0	34.0	39.0	1.6	–	1630.0
11	29.1	29.0	41.9	1.6	–	659.0
12	28.3	31.0	40.7	1.6	+	533.0

*Oxides include sodium oxide and oxides of multivalent metals (O.M.M.).

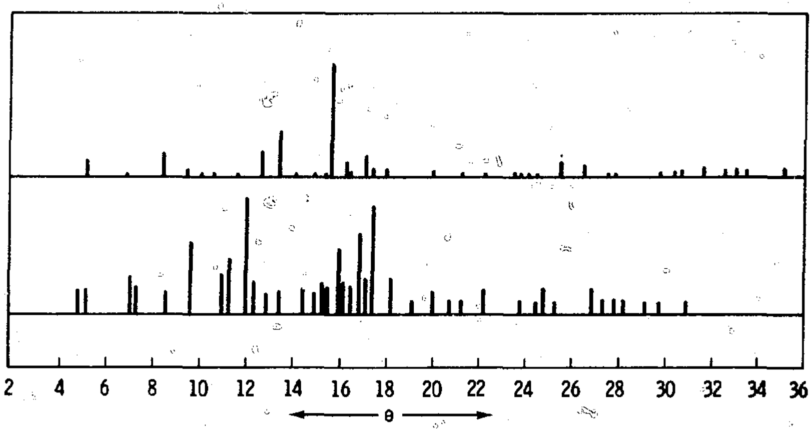

Fig. 1 X rayogramms of crystallized glasses with Fe(II) and Fe(III).

The formation and the properties of crystallized materials depend on the crystallization rate and the character of the crystal phases being formed. The presence of some elements in wastes has a strong influence on the crystallization rate and the character of the crystal phases. For example, the presence of iron in radioactive wastes accelerates the crystallization of phosphate melts. It is emphasized that not only the presence of iron but also its valency influence the crystallization rate. In Fig. 1 there are X-ray diffraction patterns of crystallized glasses of similar composition, differing only in iron valency. The glass sample with divalent iron was melted in argon to avoid oxidation of iron. From these data it can be seen that, during crystallization of glasses containing iron of different valency, different crystal phases are formed. We measured the crystallization behavior of these glasses at various melt cooling rates. Glasses containing divalent iron crystallize at cooling rates below 150 to 200°C per hour, while those containing trivalent iron crystallize at cooling rates below 20 to 30°C per hour only. Glasses containing no iron do not crystallize even at a cooling rate of 10 to 15°C per hour. Thus we may conclude that, first, the presence of iron in the melt influences the phosphate melt crystallization rate, and, second, the iron valency influences both the crystallization rate and the character of the crystal phases.

SUMMARY AND CONCLUSIONS

- The time and temperature dependence of the crystallization of some phosphate and silicate glasses which are used for the fixation of radioactive wastes was studied.
- The possibility of inaccuracy in the choice of the design storage temperature for solidified radioactive wastes in the glassy state was shown.
- The possibility of using crystallized glasses for the fixation of radioactive wastes was shown.
- It was shown that the main reasons for the increase in the leaching rate during waste glass crystallization are the formation of soluble crystalline compounds and the formation of porosity which increases the water contact surface.
- It was shown that the presence of some elements and their valencies influences the crystallization rate and the character of the crystal phases.

VI. LEACHING OF WASTE MATERIALS

RELATIVE LEACH BEHAVIOR OF WASTE GLASSES AND NATURALLY OCCURRING GLASSES

P. B. ADAMS
Corning Glass Works, Corning, New York

ABSTRACT

Simulated nuclear waste glasses of the sodium-borosilicate type with a low waste loading and of the zinc-borosilicate type with a high waste loading have been compared with obsidians. The results indicate that the waste glasses would corrode in "normal" natural environments at a rate of about 0.1 μm per year at 30°C and about 5 μm per year at 90°C, compared with obsidians which seem to corrode at, or less than, about 0.01 μm per year at 30°C and less than 1 μm per year at 90°C. Activation energies for reactions of the two waste glasses with pure water are about 20 kcal/g-mol.

INTRODUCTION

Obsidians have survived in the environment for long periods of time, many in excess of millions of years. Useful estimates of the long-term corrosion rates of nuclear waste glasses should result from a comparison with obsidians in the laboratory.

Naturally occurring obsidians are usually similar in composition to one another except for silica content. Typical silica concentrations are 75% (granite obsidian), 72% (rhyolite obsidian), 60% (trachyte and andesite obsidians), 56% (phonolite obsidian), and 50% (basalt obsidian).[1]

Silicate glass decomposition can, in general, be defined by two processes—alkali extraction which depends on the square root of time and silica dissolution which is linear with time. No ion will initially enter solution more rapidly than alkali, but eventually silica dissolution becomes the rate-controlling process. Thus, these two parameters have been of primary interest in this study.

EXPERIMENTAL

The compositions of the materials studied are shown in Table 1. They include a natural granite obsidian from the Nevada Long Valley Caldera, a synthetic andesite obsidian, a synthetic basalt obsidian, and two typical candidate nuclear waste glasses.

The synthetic obsidians and waste glasses were melted in platinum crucibles at 1300°C for 16 hours and annealed at 500°C. High purity batch materials were used for the synthetic obsidians. Waste glass Q was melted from 3.5% simulated waste calcine[2] PW 4b-4 plus batch materials. Waste glass R was melted from 67% frit glass 76-101 and 33% simulated waste calcine[2] PW 8a-2. The simulated waste calcine and frit glass 76-101 were provided by Pacific Northwest Laboratories.

Examination by optical and scanning electron microscopy showed a relatively large number of crystalline inclusions in the natural granite obsidian, a moderate number of inclusions in waste glass Q and a very few in glass R. None were seen in the synthetic obsidians.

Test specimens were prepared as grains or polished plates (1.25 cm square, 0.32 cm thick). "Standard tests" were made as follows:

(1) pH 4 "acid-base" test[2]: 42 to 60 mesh grains in 2.5% sodium acetate + 7.0% acetic acid, 19 hours, 25°C.*

(2) "Soxhlet" test[2]: 45 to 60 mesh grains in constantly renewed distilled water, 24 hours, 100°C.*

(3) Strong base test: plates in 5% NaOH, 6 hours, 95°C.*

---

*Result as weight loss.

TABLE 1

Composition* of Materials Studied

Constituent	Natural granite obsidian, %	Synthetic obsidian,‡ %		Nuclear waste glass,§ %	
		Andesite	Basalt	Q	R
SiO_2	74.6	60.1	49.7	38.1	40.1
		(60.0)	(50.0)	(39.4)	(40.6)
TiO_2		0.8	1.4		3.0
Al_2O_3	14.0	17.5	15.9	13.8	
Fe_2O_3†	2.0	6.6	11.9	5.2	11.3
MnO			0.3		
MgO		2.8	6.2	1.6	
CaO		5.1	9.1		2.0
Na_2O	3.8	3.7	3.2	17.3	13.0
		(3.6)	(3.2)	(16.5)	(12.5)
K_2O	5.3	2.1	1.5		
P_2O_5		0.3	0.5		0.5
ZrO_2				0.4	1.9
CeO_2				0.3	3.9
RuO_2				0.3	
B_2O_3				(17.1)	(9.4)
Cr_2O_3				0.9	0.5
La_2O_3				0.3	2.0
Cs_2O				0.3	0.5
NiO				0.6	0.6
MoO_3				0.5	2.5
F				1.9	
Other					¶

*Only constituents >0.2% shown.

†Includes Fe_2O_3 + FeO.

‡Analyzed values.

§Values computed from batch; those in parentheses represent analyzed results.

¶ZnO (5.0%), Nd_2O_3 (1.4%), TeO_2 (0.3%), Sm_2O_3 (0.3%), BaO (0.6%), SrO (0.4%), Pr_6O_{11} (0.4%).

(4) Weak base test: plates in 0.02*N* Na_2CO_3, 6 hours, 95°C.*

(5) Strong acid test: plates in 5% HCl, 24 hours, 95°C.*

(6) Water "powder" test[3]: 40 to 50 mesh grains in distilled water, 4 hours, 90°C.†

(7) Acid "powder" test[3]: 40 to 50 mesh grains in 0.02*N* H_2SO_4, 4 hours, 90°C.†

"Long-term" tests up to one year were also made at temperatures of 30, 60, and 90°C. Plate specimens were immersed in 30 ml of distilled water contained in polystyrene or glass tubes. These were placed in agitating (86 cycles per minute) constant temperature baths. In some cases the water was changed weekly; in other cases it was never changed. Blank samples were tested for all conditions. On conclusion of the test, the water was analyzed for sodium and silicon. Sodium was determined by conventional atomic absorption spectroscopy, silicon by DC plasma atomic emission spectroscopy after addition of hydrofluoric acid to the test solutions.

RESULTS AND DISCUSSION

Standard Tests

Table 2 shows results for standard tests on each material when ranked relative to the granite obsidian. (Note that the relative values do not indicate the ranking between tests.)

The alkali tests show increased solubility for the obsidians as silica content decreases; glass R is as resistant as granite obsidian. The strong acid test also shows increased solubility for the obsidians with decreasing silica; glasses Q and R are more soluble than any of the obsidians. The buffered weak acid (test 1), shows increased solubility for the obsidians with decreasing silica, but this does not seem to be the case in the unbuffered solution (test 7); glasses Q and R rank close to the andesite obsidian. Water tests for the obsidians show a dependence on silica content when the sample is bathed in pure water (test 2), but, if reaction products accumulate (test 6), all show the same solubility. (A 10 to 20 ppm SiO_2 in solution markedly depresses the silica reaction rate because of the very low activity of H_2SiO_3 present in solution[4] below pH 10.) Glasses Q and R are about ten times as soluble as andesite.

Long-Term Water Extraction Tests

Experiments were conducted up to one year using the granite and andesite obsidians and the two waste glasses. The resulting test solutions were classified into two groups: (1) those in which there was limited reaction product buildup (Lim RPB), including all tests in polyethylene

TABLE 2

Relative Values of Results for Standard Tests

Test type†	Relative results*				
	Obsidians			Glasses	
	Granite	Andesite	Basalt	Q	R
Alkali					
Strong (3)	1	2	2	10	1
Weak (4)	1	2	32	6	1
Acid					
Strong (5)	1	5	1025	5050	5000
pH 4 (1)	1	53	567	43	7
Powder (7)	1	1	3	32	8
Water					
Soxhlet (2)	1	4	25	62	37
Powder (6)	1	1	1	12	12

*Relative results between samples but not between tests.

†Number in parentheses refers to test description as numbered in text.

---

*Result as weight loss.

†Result as alkali extracted.

tubes that were changed weekly as well as those that were unchanged but had been on test for a short-reaction time and (2) those in which there was significant reaction product buildup (Sig RPB), including most samples tested in glass tubes (because glass tubes yielded silica up to 150 ppm) and solutions in polyethylene tubes that had derived substantial reaction products from the test specimen.

The sodium extraction data were calculated as "leach depth" (LD):

$$\text{LD, }\mu\text{m} = \frac{\text{Na}_2\text{O extracted, g}}{\text{sample area, cm}^2}\ \frac{1}{\text{density, g/cm}^3}$$

$$\frac{100\%}{\text{Na}_2\text{O in glass, \%}}\ 10^4 \quad \mu\text{m/cm} \qquad (1)$$

This term, LD, means that leaching (ion exchange) has occurred to at least this depth. Since the leach front is not a step function, the actual depth of reaction is slightly greater than calculated.

The data were then fit by least squares to the two-parameter expression

$$\text{LD} = A\sqrt{t}\,e^{\quad E/RT}$$

where A = scale parameter
t = time in weeks
E = activation energy parameter, kcal/g-mol
R = gas constant, kcal/g-mol °K
T = absolute temperature, °K

When the data are fit in this manner two assumptions are implicit: (1) the process is diffusion controlled over the entire test period time and (2) the activation energy is the only other factor influencing reaction rate. A typical computer plot is shown in Fig. 1. A good fit has not been obtained. Nonetheless, activation energies and slopes, or reaction rates recalculated as μm per year, have been computed and are shown in Table 3 for glasses Q and R.

Curves were also fit to the data by hand plotting as shown in Fig. 2 for the two waste glasses and for granite and andesite obsidians. A better fit has been obtained than was the case for the data forced to fit the mathematical expression. Two factors may account for this: (1) the reaction rate is probably approaching a constant value reflecting congruent glass dissolution and (2) more importantly, the buildup of reaction products is depressing the reaction rate, i.e., the boundary conditions are changing.

Slopes for reaction rates from the various curves at one week and 20 weeks are shown in Table 4, recalculated as μm per year. Comparison of one- and 20-week rates demonstrates that short-term data can lead to incorrect conclusions of long-term reduction rates. The rate at twenty weeks is more realistic but may still be higher than that which really occurs in nature (this could only be confirmed by still longer tests). Sig RPB rates at 20-weeks time are the most realistic of those presented here since they most nearly approximate natural conditions.

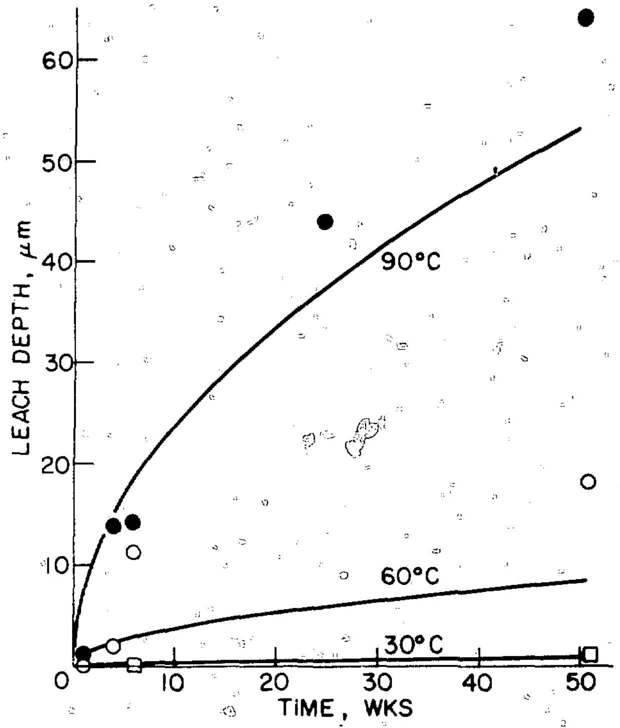

Fig. 1 Computer plot of glass R Lim RPB data [assuming that (a) the reaction is diffusion controlled and (b) the activation energy is constant with time and temperature].

TABLE 3

Computer Analysis of Data

Glass	Reaction extent*	Activation energy, kcal/g-mol	Reaction rate, μm/year 1 Week 30°C	 60°C	 90°C	 20 Weeks 30°C	 60°C	 90°C
Q	Lim RPB	16.1	1.0	12	86	0.2	2.5	19
	Sig RPB	12.2	0.7	4	19	0.2	0.9	4
R	Lim RPB	7.5	2.3	22	137	0.5	5	31
	Sig RPB	14.1	0.9	8	46	0.2	2	10

*Either limited (Lim) or significant (Sig) reaction product buildup (RPB).

Using points generated from the graphed data, the log of LD was plotted versus the inverse of temperature after the Arrhenius expression. Although this yields only three points (30, 60, and 90°C) for each data set, each point in fact represents a weighted average of several points, since it was taken from a curve drawn through several points. These are shown in Table 5. When there is no buildup in reaction products as a result of the increased temperature, the apparent activation energy does not change, e.g., glass Q at one week.

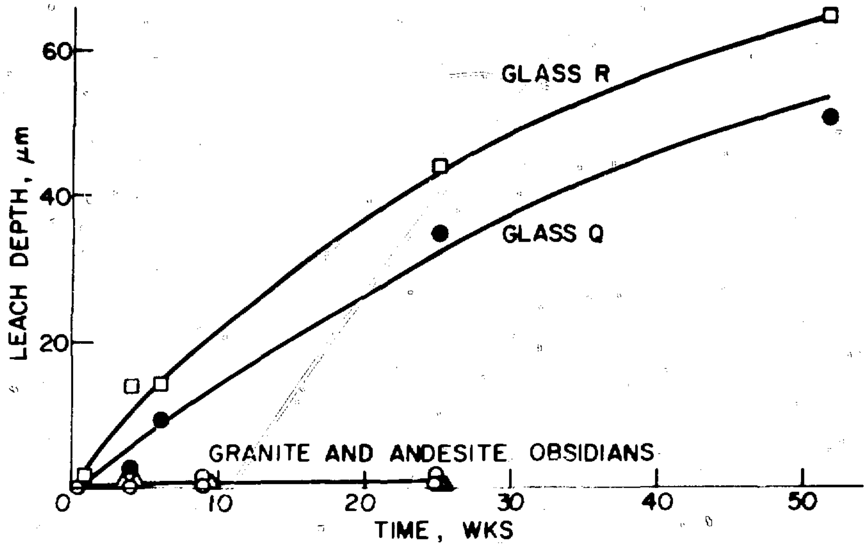

Fig. 2 Leach depth versus time at 90°C when there is Lim RPB in water.

TABLE 4

Sodium Reaction Rates (e.g., Slope of Curve) at 1 Week and 20 Weeks

Material	Reaction extent*	Reaction rate, μm/year 1 Week 30°C	60°C	90°C	20 Weeks 30°C	60°C	90°C
Obsidian							
Granite	Lim RPB	<0.1	<1	~1	<0.1	<1	<1
	Sig RPB	~0.01	<0.1	<1	~0.01	<0.1	<1
Andesite	Lim RPB	<0.1	<1	~1	<0.1	<1	~1
	Sig RPB	~0.01	<0.1	<1	~0.01	<0.1	<1
Glass							
Q	Lim RPB	1	12	80	0.2	7	65
	Sig RPB	1	3	10	0.04	1	3
R	Lim RPB	1	40	140	1	15	65
	Sig RPB	1	12	35	0.2	5	6

*Either limited (Lim) or significant (Sig) reaction product buildup (RPB).

TABLE 5

Activation Energies from Empirically Plotted Data

Glass	Reaction extent*	Activation energy, kcal/g-mol 1 Week 30–60°C	60–90°C	20 Weeks 30–60°C	60–90°C
Q	Lim RPB	15.4	15.4	18.7	16.2
	Sig RPB	10.6	10.6	11.5	10.3
R	Lim RPB	21.8	13.0	22.5	10.5
	Sig RPB	12.6	7.8	20.1	6.4

*Either limited (Lim) or significant (Sig) reaction product buildup (RPB).

The activation energy in pure water is about 18 kcal/g-mol for glass Q and about 22 kcal/g-mol for glass R. These values are consistent with those reported by Holland[5] for commercial glasses. If the activation energies are in fact different, the relative solubility of glasses Q and R will change with temperature.

Finally, using points generated from the lines of the graphed data, the log of LD was plotted versus the inverse of temperature after the Arrhenius expression. Figure 3 shows some results at 20 weeks for glasses Q and R. Where there is no buildup in reaction products all points fall on a straight line, as shown for glass Q. Where there is Sig RPB, the apparent activation energy changes. This is induced by different boundary conditions; that is, reaction products are present in one case but not in the other.

Silica measurements were made at 6, 25, and 51 weeks. They are less reliable than the sodium extraction data because of the low test sensitivity. However, assuming that the dissolution rate of silica is linear with time, the range of rates found is shown in Table 6. Those for glasses Q and R are in good agreement with the 20-week rates determined by sodium extraction. Those for the obsidians are higher than those found by sodium extraction; the sodium extraction rates are believed to be more reasonable.

CONCLUSIONS

The activation energies for two nuclear waste glasses when reacted with essentially pure water were found to be about 20 kcal/g-mol and were similar to those found for ordinary commercial glasses.[5] If, as the data show, the activation energy does not change from glass to glass, comparison at elevated temperatures cannot necessarily be used to predict relative corrosion rates at lower temperatures.

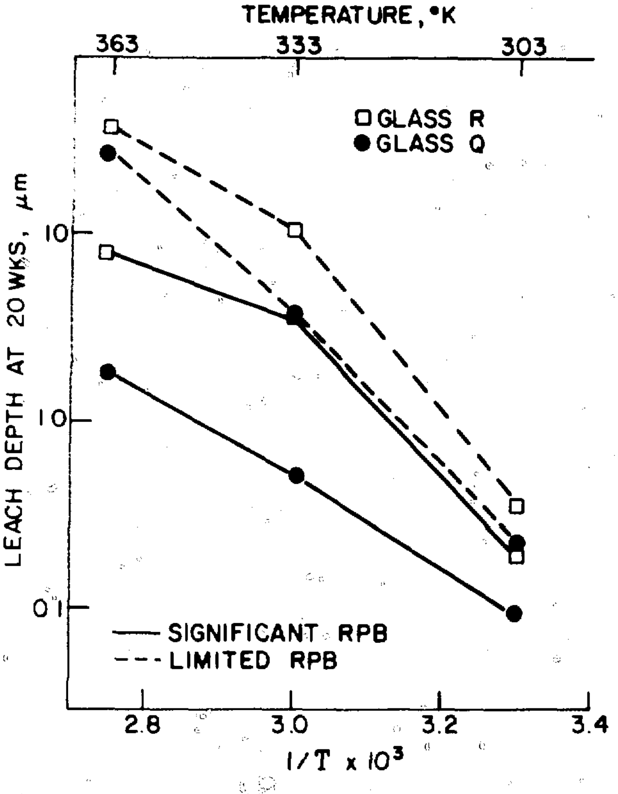

Fig. 3 Relevance of sodium data to the Arrhenius expression.

TABLE 6

Reaction Rate Ranges Based on SiO_2 *Dissolution Results*

Material	Reaction rate range, μm/year		
	30°C	60°C	90°C
Obsidian			
Granite	0.00 0.02	0.01 - 0.2	0.4 - 2
Andesite	0.00 0.06	0.4 - 4	0.4 - 9
Glass			
Q	0.02--0.2	0.6 – 6	1 - 25
R	0.02 - 1	2 – 16	1 - 40

The activation energy can also decrease dramatically to about 10 kcal/g-mol when the water becomes contaminated with reaction products from the glass or from other sources.

A simple mathematical expression which accounts for ion exchange and activation energy does not describe the data. Terms are needed that include the fact of a limiting rate due to congruent dissolution and of changing boundary conditions and different activation energy due to changing or changed solution chemistry.

Using standard water tests, the nuclear waste glasses rank 2 to 10 times more soluble than a basalt obsidian, 10 to 15 times more soluble than an andesite obsidian, and 10 to 60 times more soluble than a granite obsidian at temperatures between 90 and 100°C.

For the most likely case in nature of water containing dissolved silica and other ions, the rate of attack is best predicted using systems with significant reaction product buildup and using curve slopes or rates after a substantially long reaction time. From this work it is predicted that reaction rates would therefore be

	Microns per year		
	30°C	60°C	90°C
Obsidian			
Granite	~0.01	<0.1	<1
Andesite	~0.01	<0.1	<1
Basalt	~0.01	~0.1	<1
Glass			
Q	0.04	0.6	3
R	0.2	2	6

Finally, then, it is proper to ask how well these predicted rates agree with observed rates for natural obsidians. One approach is to approximate ion exchange rates from hydration rim measurements.[6] They show a rate of 0.003 μm/year for granite obsidian at 30°C and 0.01 μm/year for basalt obsidian compared to ~0.01 μm/year found for both in this work.

ACKNOWLEDGMENTS

This work was done under Pacific Northwest Laboratory Contract BSA 959, Prime Contract AT(45-1)-1830. Sample preparation and testing were done by Mrs. Laurie Corbett and Mr. J. K. O'Bryan. Sodium determinations were made by Mr. D. O. Robinson—silica determinations by Dr. R. A. Burdo.

REFERENCES

1. F. J. Turner and J. Verhoogen, *Aqueous and Metamorphic Petrology*, McGraw-Hill Book Co., New York, 1951.
2. W. Ross et al., Annual Report on the Characterization of High-Level Waste Glasses, PNL-2625, June 1978, Richland, Washington.
3. D. L. Rothermel and M. E. Nordberg, A Flame Photometric Estimation of the Durability of Glass, *Am. Ceram. Soc. Bull.*, 31: 324 (1952).
4. A. Paul and A. Youssefi, Alkaline Durability of Lime Silicate Glasses Containing CaO, FeO, and MnO, *J. Mater. Sci.*, 13: 97 (1978).
5. L. Holland, *The Properties of Glass Surfaces*, Chapman and Hall Ltd., London, 1964.
6. R. E. Taylor, *Advances in Obsidian Glass Studies*, Noyes Press, Park Ridge, N. J., 1976.

EVALUATION OF LONG-TERM LEACHING OF BOROSILICATE GLASS IN PURE WATER

F. LANZA and E. PARNISARI
Commission of the European Communities, Joint Research Centre, Ispra Establishment,
21020 Ispra, Italy

ABSTRACT

In order to confirm the validity of the model of the dissolving sphere, a series of tests of leaching of borosilicate glasses has been performed. The leaching rate is followed by measurements of weight loss and analysis of the surface composition. An accumulation at the surface of the less soluble cations is observed.

INTRODUCTION

The activity of the Joint Research Centre (JRC) in the field of highly radioactive waste is centered on the long-term risk evaluation connected to the presence of actinides. An evaluation of the long-term hazard of glass storage considers, as the most probable accident, the contact of the glass block with water and the subsequent leaching of radioactive material. Since a substantial amount of long-life actinides is present in the high activity wastes which are put in the glass blocks, the hazard evaluation must be performed, taking into account long-term glass leaching, to evaluate possible accumulation effects in the surrounding areas. From this perspective the leaching data needed for the risk evaluation are not those referred to short-term but rather to long-term conditions, which correspond to steady state.

Short-term tests show that the glass attack is not homogeneous and that some cations have a leaching rate which is higher than others. For instance, Na is leached more rapidly than Sr; however, after a certain leaching time, most of the values of the leaching rate tend to converge toward a common value.[1] This is quite understandable since, with the exception of monovalent cations, the mobility of ions in the glass is extremely low. We will then have initially an accumulation of the less leached ions at the surface. If we assume that the leaching depends not only on the glass composition but also on the surface gel composition, the leaching rate of the less leached ions will eventually increase.

It is reasonable to assume that in the long term the leaching rates tend toward a common value and that ultimately the glass undergoes homogeneous dissolution. Then the leaching rate of the different elements will coincide with the rate of weight loss. In the evaluation of the amount released in time for the calculation of the associated risk, the model of the dissolving sphere seems the most appropriate.[2]

During the leaching we will have a continuous evolution of the composition of the glass. Only when the surface layer composition does not change with time will we be able to say that a steady-state situation is reached. To verify this assumption it was decided to follow the weight loss for about one year, following also the composition of the surface layer to be able to determine if the proposed model is acceptable and if steady-state conditions have been obtained.

The tests have been conducted on a borosilicate glass containing simulated waste. The scope of the experiments was not to obtain precise data on a specific glass in well-defined conditions but rather to define the general mechanism of leaching over the long term. For this reason a glass composition has been chosen that can represent the glasses normally considered in Europe. Table 1 gives the glass composition.

TABLE 1

Glass Composition

Component	Wt.%	Component	Wt.%
SiO_2	48	Sm_2O_3	1.12
B_2O_3	15	CeO_2	0.76
Al_2O_3	5	SnO_2	0.03
Na_2O	18.49	ZrO	1.06
SrO	0.22	MoO_3	0.16
BaO	0.33	MnO_3	1.35
Y_2O_3	1.28	Fe_2O_3	3.25
La_2O_3	0.63	NiO	0.32
Pr_2O_3	0.31	CuO	0.04
Nd_2O_3	0.99	ZnO	0.03
		U_3O_8	1.38

EXPERIMENTAL

The leaching experiments were conducted in the apparatus shown in Fig. 1. The apparatus consists of a boiling pot, a condenser, and a thermostatized bucket in which the samples are located. Such an apparatus was preferred to the more common Soxhlet apparatus in order to avoid the uncontrolled flow of water around the sample when the bucket of the Soxhlet is emptied by the syphon action.

The boiling rate was regulated so that the flow rate through the bucket was 0.7 l/hr. Two working temperatures, 50 and 80°C, were used. One of the effects of leaching is to produce a layer of gel on the surface of the glass. In order to obtain an accurate weight loss measurement, it is necessary to dry the sample in a reproducible way. During this operation the gel is damaged, and some fissures appear in it. If the sample is reintroduced, such fissures will increase the leaching rate. As a matter of fact, a previous work[3] has shown that, when using a reintroduction system, the leaching rate was dependent on the number of reintroductions. At 80°C when the sample is extracted, dried, and reintroduced every week, the long-term leaching rate obtained is about double the leaching rate obtained by extracting the sample every three weeks. For this reason it was decided to avoid any reintroduction of the samples.

For each temperature, 20 samples were introduced in the extractor. A sample was extracted every three weeks, kept for three hours in a desiccator with silica gel, and weighed. The samples were prepared by casting a cylinder 10 mm in diameter in a graphite crucible and then cutting 10 mm-long pieces with a diamond saw. Two different surface conditions were then present. In order to see the effect of preferential leaching on the glass, some analyses of the composition of the surface layers were performed. The energy dispersion X-ray analysis (EDX) method in connection with an electron scanning microscope was used. The concentrations of Si, Na, Fe, Ni, Ce, and U were measured. Nonleached glass surface was used as a standard. For cerium and uranium analyses, in order to avoid overlapping of peaks in the X-ray analysis, an additional standard was prepared composed of a borosilicate glass containing a known amount of Ce and U. Three different zones were analyzed on each sample in order to detect possible inhomogeneities in the layers. The main problem in the interpretation of the analytical results is in the evaluation of the penetration of the electron beam.

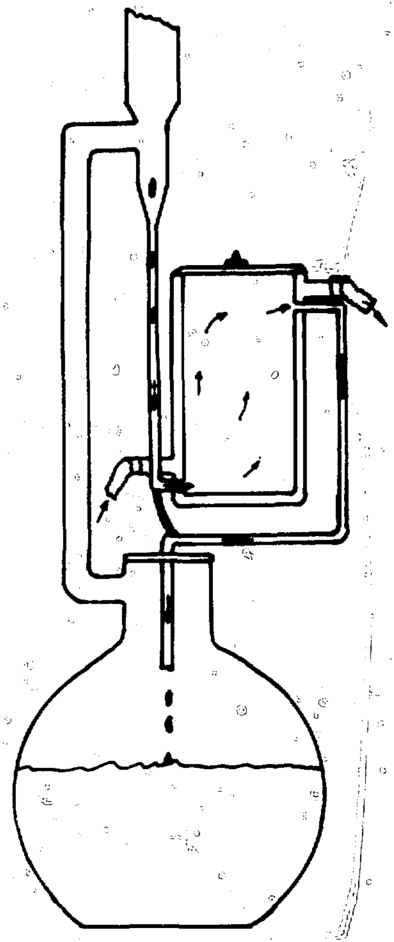

Fig. 1 Leaching apparatus with thermostatized bucket.

For the same acceleration voltage, the penetration depth is a function of the density of the layer and of the atomic number of its components. In the glass the penetration is 1 μm. Because the density of the gel layer can only be estimated, it is not possible to evaluate with precision the penetration depth. For surfaces with very low weight losses, the values obtained are an average of the layer composition and the bulk composition. For all these reasons the results obtained are to be considered semiquantitative.

RESULTS AND DISCUSSION

The total weight loss as a function of time is presented in Figs. 2 and 3. The test at 50°C was discontinued at 8000 hours due to an accident.

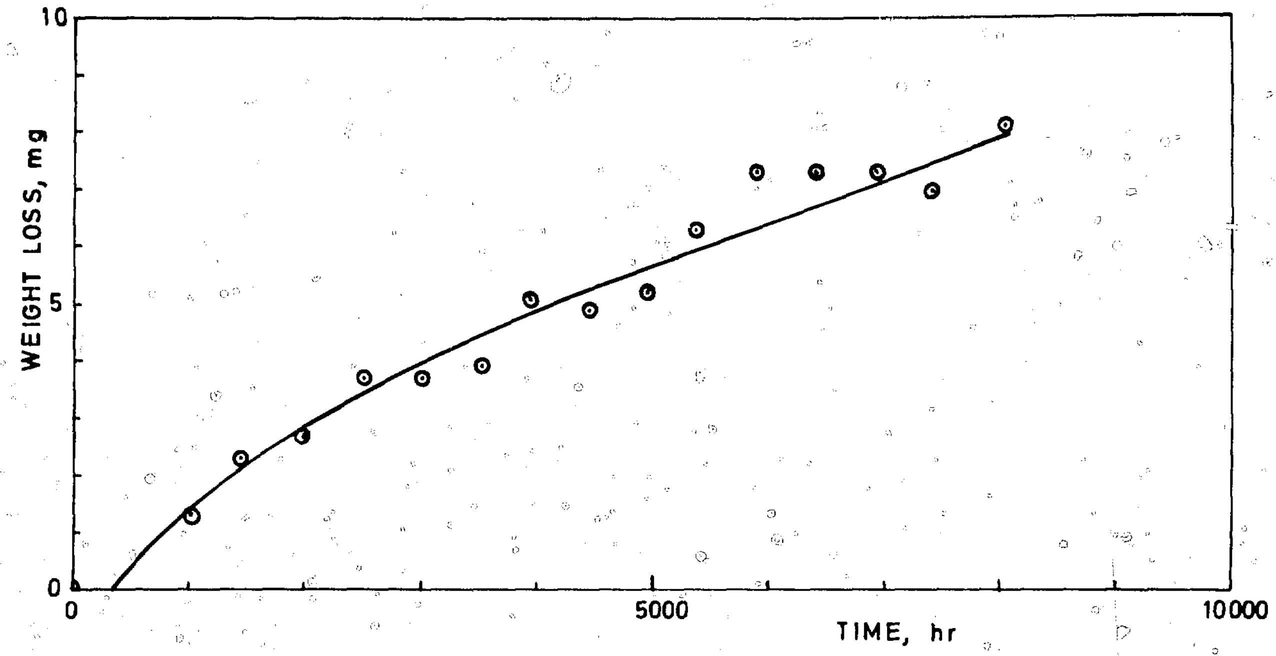

Fig. 2 Weight loss as a function of time (T = 50°C).

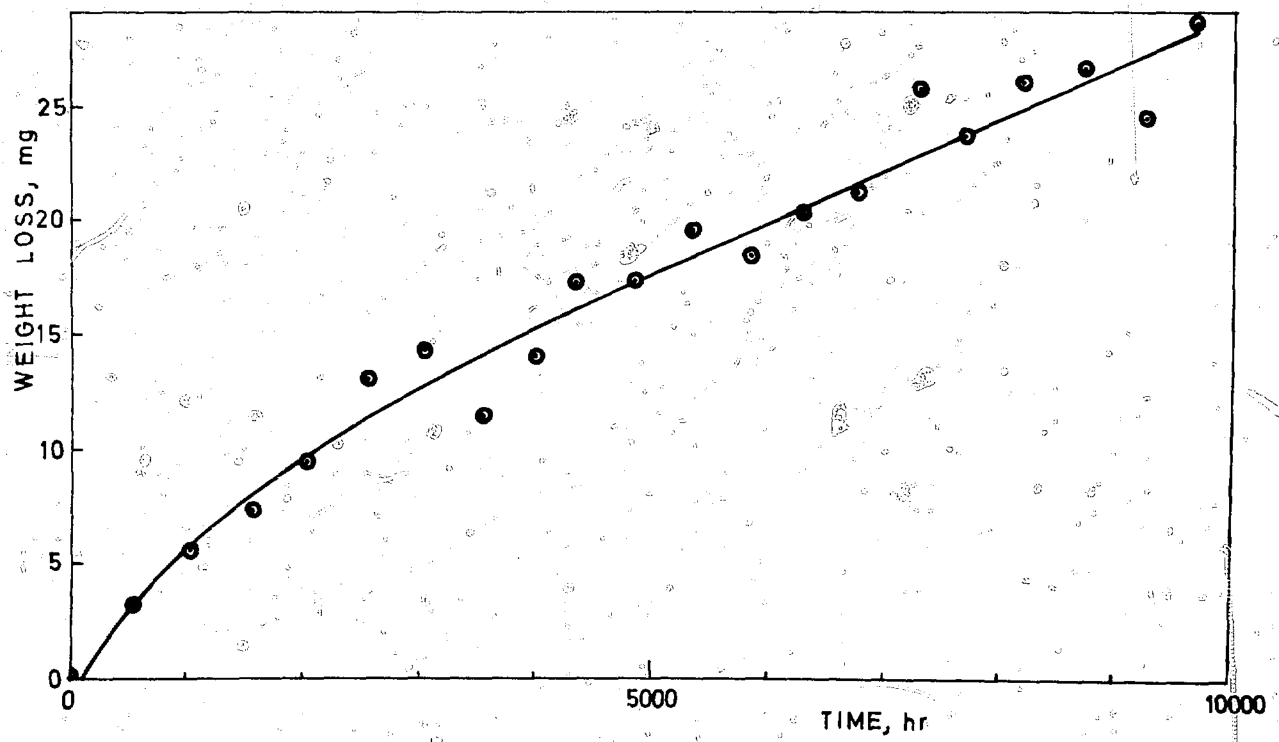

Fig. 3 Weight loss as a function of time (T = 80°C).

TABLE 2

Parameters of the Leaching Rate Formula

T, °C	a	b	t_0, hr	a^2/b^2, d
50	1.0×10^{-4}	5.7×10^{-7}	343	3×10^4
80	2.5×10^{-4}	3.6×10^{-6}	110	4.8×10^3

Looking at the diagrams, particularly those at 80°C, it is apparent that the points, initially, fit very well with the curve, but after a certain time the scatter increases. The curves were analyzed using the following formula:

$$\Delta Q/S = a\sqrt{t} + bt$$

The values of the parameters were obtained using a best fitting procedure. It was readily apparent that in both cases a large error was connected with the initial point. Rerunning the best fitting program without the initial point reduced the standard error appreciably. In this case, however, the theoretical curves do not pass through zero, but begin after a certain time as if an inhibition effect were present. The values of the coefficients and the equivalent inhibition time are given in Table 2. It seems likely that the inhibition effect depends on the difference existing between the lateral surface and the frontal surfaces of the cylindrical samples, a difference which disappears in time.

Heimerl et al.[4] pointed out that the time $t_x = a^2/b^2$ is the time at which the parabolic and the linear components give the same contribution to the weight loss. We can see from Table 2 that such values are very large, so, even after about one year, the main contribution to the weight loss comes from the parabolic component. As a consequence a small variation in the a coefficient causes a large variation in the b coefficient. The possibility of describing the plots by a simpler formula comprising only the parabolic component was examined; however, the best fitting of the experimental points gave rise to a standard error which was higher by a factor of 3. In this case as well, the curves did not pass from zero, but an inhibition time was apparent.

From the results of the analyses of Si, Na, Fe, Ni, Ce, and U, a plot showing the variation of the total amount of the cations as a function of time was obtained (Fig. 4). The first point, which is evident, is the general decrease in cation content of the superficial gel film. This is quite understandable if we take into consideration that the gel is strongly hydrated and also that H^+ can substitute for cations in the gel structure. The plots can be subdivided into three zones: first, one characterized by a rapid decrease followed by a second one in which large oscillations appear, and finally the third zone, stabilization. In tests at 50°C after 8000 hr the stabilization is not yet well defined.

In Table 3 are shown the values of concentration of the different elements, referred to the total amount of the analyzed cations, for three different leaching times. The surface composition changes drastically from a situation in which silicon is the predominant element to one in which iron is the major constituent. The different behavior of iron and silicon at the two temperatures can be easily understood by remembering that $Si(OH)_4$ solubility increases with temperature while $Fe(OH)_3$ solubility decreases. Other elements like Ce and Ni increase up to a relative maximum

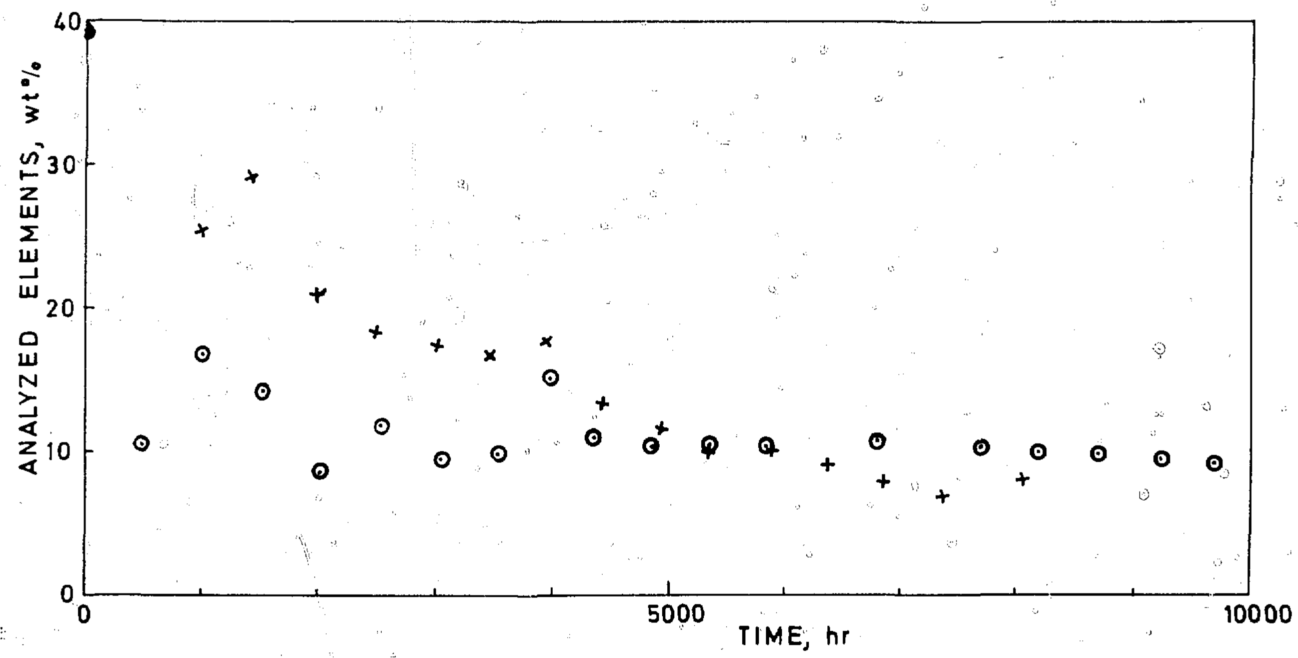

Fig. 4 Evolution of the total amount of the analyzed elements as a function of time (+ = 50°C, ⊙ = 80°C).

TABLE 3

Variations in Composition of the Surface Layer

t, hr	Si/Σ_i, %	Na/Σ_i, %	Fe/Σ_i, %	Ni/Σ_i, %	Ce/Σ_i, %	U/Σ_i, %	T, °C
0	57.0	31.5	6.2	0.6	1.7	2.9	50
3024	49.4	15.6	21.3	2.2	5.2	6.4	50
5871	37.0	18.5	30.5	2.1	4.28	7.3	50
8055	36.3	24.2	24.0	1.4	5.4	8.6	50
0	57.0	31.5	6.2	0.6	1.7	2.9	80
3040	13.7	10.3	59.4	2.7	5.3	8.5	80
5864	24.2	13.0	48.4	2.1	2.3	9.8	80
9263	15.9	13.2	57.6	1.3	1.8	10.3	80

and then tend to decrease slightly; however, uranium continues to increase. When the total value of analyzed cations is considered, it seems that after 9000 hr at 80°C a steady-state condition is reached. However, the data on single cations show that the variations in composition are continuing.

Also taking into account weight loss data, the leaching rate evolution can be subdivided into three zones:

- First, one in which differential leaching is prevalent due to solubility effects. The weight loss plot is regular; the relative concentration of the less soluble cation increases.
- Second, one in which the weight loss is also due to detachment of colloids from the gel layer. The composition of the layer shows large oscillation; the scattering of the weight losses increases.
- Third, one where the flaking continues but without affecting the composition of the gel due to its homogeneity. The composition of the main constituents is stable; however, the evolution of concentration of minor constituents continues. Probably ion exchange also plays a role in this stage.

CONCLUSIONS

The two parameters, parabolic and linear relations, describe with sufficient accuracy the weight loss evolution. However, it seems that leaching must continue much longer than one year to reach a time when the linear part is predominant. This is also confirmed by the surface analysis.

The analysis of the surface shows a complex evolution of the surface layer composition. Even after one year the uranium specific content continues to increase. This could account for specific leaching values lower than weight loss even after long periods.

REFERENCES

1. J. R. Grover, Glasses for Fixation of High Level Radioactive Wastes, in *Proceedings of the Symposium on Management of Radioactive Wastes*, OECD, Paris, 1972.
2. H. C. Clayborne and F. Gera, ORNL/TM 4639, Oak Ridge National Laboratory, 1974.
3. F. Lanza and E. Parnisari, *Evaluation of Long Term Leaching of Borosilicate Glasses*, EUR 5947 EN, 1978.
4. H. Heimerl et al., Studies on the Behaviour of Radioactive Waste Glasses, in *Proceedings of the Symposium on Management of Radioactive Wastes*, OECD, Paris, 1972.

DEVELOPMENT OF ALUMINOSILICATE AND BOROSILICATE GLASSES AS MATRICES FOR CANDU HIGH-LEVEL WASTE

G. G. STRATHDEE, N. S. McINTYRE, and P. TAYLOR
Atomic Energy of Canada Limited, Whiteshell Nuclear Research Establishment,
Pinawa, Manitoba, Canada

ABSTRACT

This paper covers the results of analyses of two radioactive nepheline syenite glass blocks recovered from in-ground leaching experiments at the Chalk River Nuclear Laboratories. Current research on borosilicate glasses for immobilization of high-level waste is also described.

INTRODUCTION

The pioneering development of work on a bench-scale process for solidification of high-level liquid waste glass in $(Na, K)_2O-CaO-Al_2O_3-SiO_2$ at the Chalk River Nuclear Laboratories (CRNL) was concluded in 1960. Until the current program was initiated in 1976 (Ref. 1), the only continuing commitment to high-level waste form research has been the monitoring of the second in-ground nepheline syenite glass block leach test at CRNL.[2] During the fall of 1978, two of the glass blocks, one each from the 1958 (Ref. 3) and 1960 in-situ experiments, were recovered for detailed analysis at the Whiteshell Nuclear Research Establishment. This paper compares results from our original and present research on the durability of high-level waste glasses.

IN-GROUND EXPERIMENTS AT THE CHALK RIVER NUCLEAR LABORATORIES

Twenty-five hemispheres of glass were buried in wet, sandy soil at 10°C in the waste management area at CRNL in each of the two in-situ leaching tests. The glass product was prepared by combining about 2 liters of high-level waste liquid with a mixture of 15 wt.% CaO and 85 wt.% nepheline syenite clay and firing at temperatures up to 1350°C in fireclay crucibles.[4] Laboratory studies at that time on both small cast samples and 2-kg hemispheres showed that steady-state leach rates measured at 20 to 25°C were less than 0.1 $\mu g/m^2$ sec (Refs. 3 and 4).

In the 1958 experiment, 25 of the 2-kg hemispheres from which the crucibles had been chiselled away, containing a total of 11 TBq of activity, were buried in a vertical array normal to the expected groundwater flow. Because the concentration of ^{90}Sr in water sampled from downstream wells was too low to detect, monitoring of that experiment was discontinued. The block recovered from that in-ground test has been analyzed by several techniques as discussed later.

The 1960 test was similar in principle to the previous one, except that the 25 blocks contained a total of 41 TBq of activity, were set in a more closely-packed vertical grid, and had slightly higher leach rates in standard laboratory tests. This experiment has been monitored intermittently since then by Merritt.[2] The 2-kg block retrieved from that emplacement has been analyzed radiochemically and by electron microscopy.

The recovery of each of these blocks was completed with minimum damage to the surface, since it was a major objective of the analyses to assess if there had been significant alteration of the glass–water interface. Initial visual inspection of each of the hemispheres in the WNRE hot cell suggested that little corrosion had occurred during the 20 and 18 years of exposure to flowing groundwater for the respective radioactive glass samples. The instrumental analyses supported that conclusion.

Analyses of the CRNL Glass Blocks

The first (1958) radioactive block was sampled for the exploratory analyses by chiselling the blocks in the hot cell to minimize damage to the exterior. This method yielded predictable cleavage of the glass in separate inactive trials. Chips taken from outer and inner surfaces were mounted for surface and alpha particle track analyses. Metallographically polished samples with surfaces normal to the leached interface were also prepared for optical and scanning electron microscopy. Significant results from the analytical campaign on the 1958 block were as follows:

- *Gamma Spectrometry* showed that ^{137}Cs distribution throughout the block was relatively uniform. The range was ±6% of the mean specific ^{137}Cs activity, which corresponded to a total of 155-GBq ^{137}Cs in the hemisphere.
- *Scanning Electron Microscopy (SEM)* on either cleaved or metallographically-polished chips did not reveal a significant surface alteration layer. The leach zone thickness was less than the 1 μm SEM limit of resolution. Energy-dispersive X-ray analysis (EDX) confirmed that no gradients normal to the outer surface were present in the concentrations of Na, K, Al or Si that may have been developed due to surface leaching. Some localized variation in Ca distribution was detected at both the outer surface and in the bulk and was attributed to inhomogeneity due to the original fabrication procedure rather than to aqueous corrosion at the glass groundwater interface.
- *X-Ray Photoelectron Spectroscopy (XPS)* showed that both Na/Si and Ca/Si ratios in the outer one- to two-nanometer layer of the weathered surfaces were *consistently lower than those measured in specimens* from the core of the block. The Al/Si and Ca/Si ratios were fairly uniform for all samples of bulk glass; therefore the direct observation of depletion of the exposed surface in Na and Ca was valid. The SEM technique did not resolve these reductions of Na and Ca concentrations at the surface. Strontium was detected on several outer surfaces, showing that the Sr had become more concentrated at the interface than in the interior of the block.
- *Alpha Particle-Track Autoradiography* was used to determine if major loss of alpha-emitting isotopes had occurred from the glass block surface. The resolution of 100 μm was inadequate to evaluate if concentration gradients existed due to leaching. No statistical difference was observed between track densities produced by α-decay of isotopes in samples from the block periphery or from the interior of the hemisphere.

The second (1960) block, which was retrieved from the in-situ test monitored by Merritt,[2] was analyzed radiochemically and by SEM-EDX. No significant change had occurred to the exposed glass surface and, except for the higher activity of ^{137}Cs in the 1960 block, little difference between the two recovered hemispheres was observed. This result was not surprising since the calculated thickness of the surface layer was only 36-nm, assuming complete ^{90}Sr leaching by groundwater to yield the quantity now on the soil. Of the analytical techniques employed, only the XPS data for the 1958 block give direct evidence for any cation depletion from the outer few atomic layers. We did not examine the 1960 block by XPS.

The surface chemical analyses of the CRNL glass blocks have confirmed the results of 18 to 20 years of in-ground leach test monitoring. Virtually no change has occurred to the glass surface exposed to flowing groundwater.

CURRENT HIGH-LEVEL WASTE IMMOBILIZATION PROGRAM IN CANADA

Borosilicate glasses are being developed as host matrices for high-level waste which might be separated from spent UO_2- or ThO_2-based CANDU* reactor fuel.[5,6] Because we intend to adapt existing high-level waste-processing technology to our needs, our initial effort has been directed at defining those physical and chemical variables which determine long-term durability of borosilicate glass containing simulated high-level waste. For the reasons stated in Ref. 6, the determination of the characteristics of dilute-waste glass products has been given priority. The following sections describe the scope of this work and some of our novel results.

Borosilicate Glass Compositions Investigated

Of these three categories of glass products: Waste–Na_2O–B_2O_3–SiO_2, Waste–Na_2O–CaO–B_2O_3–SiO_2, and Waste–Na_2O–ZnO–B_2O_3–SiO_2, the latter sodium borosilicate materials have been shown in screening tests to be superior. Standard leach-rate tests at 100°C have been used to compare the durabilities of these waste glasses. All initial work has been nonradioactive, and a few results are presented in Table 1 to illustrate the following points:

1. Leach rates (based on sodium loss) from polished sections increased with concentration of sodium in the product in every system, although the addition of up to 10 wt.% ZnO markedly improved the durability of the high-sodium content borosilicate glasses.

2. The leach rate of sodium from the Na_2O–B_2O_3–SiO_2 glasses exceeded the rate of loss of either Si or Al (a minor component of the waste mixture).

3. In the Na_2O–ZnO–B_2O_3–SiO_2 series, the rate of depletion of Na exceeded that of Zn, Si and Al. Separate surface analyses confirmed the concentration of Zn at the glass–aqueous solution interface.

4. Apparent congruent dissolution of the constituent elements Na, Ca, Al and Si occurred in the durability tests of the Na_2O–CaO–B_2O_3–SiO_2 products.

---

*CANada Deuterium Uranium.

TABLE 1

Simulated High-Level Waste Glass Compositions and Range of Leach Rates Observed During 60-Day Test at 100°C

Product No.	Product composition, wt.%: Waste*	Na_2O	ZnO	CaO	B_2O_3	SiO_2	IAEA leach rate (Na) at 5.2 Ms, 100°C, $\mu g/m^2 \cdot s$	Comparative leach rates†
1	6.8	10.0			18.4	64.7	0.7	Na > (Al,Si)
2	10.1	15.0			16.6	58.2	2.3	Na > (Al,Si)
3	13.5	20.0			14.7	51.7	250.0	Na > Si > Al
4	16.9	25.0			12.9	45.2	140.0‡	Na > Si > Al
5	6.8	10.0	10.0		16.2	56.9	1.0	Na > Zn, (Si, Al)
6	10.1	15.0	10.0		14.4	50.5	1.5	Na > Zn, (Si, Al)
7	13.5	20.0	10.0		12.5	44.4	1.7	Na > Zn, (Si, Al)
8	16.9	25.0	10.0		10.7	37.4	§	
9	6.8	10.0		10.0	16.2	56.9	15.0	Na > Ca > Si > Al
10	10.1	15.0		10.0	14.4	50.5	26.0	Na > Ca > Si > Al
11	13.5	20.0		10.0	12.5	44.0	48.0	Na > Ca > Si > Al
12	16.9	25.0		10.0	10.7	37.4	§	

*Composition of waste oxide mixture used in these experiments was (wt.%): FP oxides, 17.2, ThO_2, 60.0; Al_2O_3, 16.0; AlF_3, 6.1; Fe_2O_3, 0.54; Cr_2O_3, 0.13; NiO, 0.05.

†Concentrations of elements in brackets were below their detectable limit by AA.

‡The sample was depleted in sodium at this point.

§These glasses were not leached for the full test period because of poor sample durability.

The sodium zinc borosilicate glasses were selected for more detailed study of liquid liquid phase separation behavior, of hydrothermal reaction and alteration-zone product characterization. Surface analyses of constituent element depth profiles were completed, using scanning electron microscopy (SEM-EDX) and ion beam milling combined with X-ray photoelectron spectroscopy (XPS) or secondary ion mass spectroscopy (SIMS). The objective of these investigations was to assess the utility of these analytical techniques for providing information on the fine structure of surface films. We believe that it is necessary to validate predictive mathematical models of high-level waste glass leaching, by relating empirical observations of the loss of elements into water to the distribution of these species within the surface region of the host material.

Phase Separation in Na_2O–ZnO–B_2O_3–SiO_2 Glasses

The objective of this research has been to improve our understanding of the immiscibility behavior of this four-component system with respect to segregation into borate-rich and silicate-rich phases at elevated temperatures. The effects have been studied of progressive addition of Na_2O to a variety of ZnO–B_2O_3–SiO_2 compositions, including potential host matrices for high-level waste. Most samples were fused at 1300°C and then rapidly air-cooled to room temperature. The extent of phase separation was determined by SEM and replica-TEM examination of slightly HF-etched fracture surfaces of the glasses.

Addition of Na_2O to ZnO–B_2O_3–SiO_2 compositions suppresses the temperature at which phase separation occurs. Liquid separation occurs in the melt over a wide range of Na_2O-free compositions. About 2% Na_2O prevents phase separation in the melt at 1300°C, but extensive phase separation occurs rapidly on cooling. This becomes less extensive with increasing Na_2O content and is completely suppressed by about 8% Na_2O. About 10% Na_2O generally prevents phase separation, even on prolonged heating at 600°C, indicating that the subliquidus immiscibility surface is depressed below that temperature. Further work is under way to define the 600°C and 1300°C phase separation isotherms and is being extended to include waste-loaded glasses.

HYDROTHERMAL REACTIONS OF BOROSILICATE GLASSES

No crystalline products were recovered from hydrothermally-reacted Na_2O–B_2O_3–SiO_2 glasses even after 10 days at 200°C. Studies on the alteration of large specimens of sodium borosilicate glasses have confirmed that thick, silica-rich zones may develop which are depleted in Na and B. Surface preparation appears to influence the extent of hydrothermal reactions; for example, cleaved surfaces appear to be more durable than sawn or polished surfaces.

Hydrothermal alteration of powdered sodium zinc borosilicate glasses has been studied at temperatures up to 200°C. Surface crystallization can be readily detected after as little as 4 days exposure to water at 150°C. Glasses with a Zn : Si atom ratio of less than 1 : 2 yielded zincsilite, a zinc silicate which is structurally related to bentonite, as the major product. At higher Zn : Si ratios hemimorphite, $Zn_4Si_2O_7(OH)_2 \cdot H_2O$, was the major alteration product. Mixtures of these two phases were obtained at intermediate

Zn : Si ratios. No evidence was obtained for the participation of Na or B in these crystallization reactions.

The components of simulated high-level waste can affect the type of alteration products formed under hydrothermal reaction conditions. Glasses containing CaO, NiO, or Fe_2O_3 yielded hydrated calcium, nickel, and iron silicates, respectively. It appears desirable to formulate glasses which will yield hydrothermal alteration products with clay structures which possess ion-exchange capacity. The zincsilite and nickel and iron silicates fall into this category.

Analysis of the Surfaces of Simulated Waste Glasses After Leaching at 100°C

Two low-Na_2O glasses (numbers 1 and 5 in Table I) have been analyzed, using XPS and SIMS techniques, before and after leaching at 25 and 100°C for periods of time up to 60 days. The results support those observations noted above that some component elements are concentrated at the interface (e.g., Si, Zn) while others are depleted (e.g., Na, B) upon exposure of the glass waste products to water. The following conclusions are based on the results of the exploratory XPS and SIMS analyses:

1. Fractured surfaces were more representative of bulk sample composition than polished surfaces, which were found to be highly depleted in B, Th and Na within 2 nm of the surface prior to leaching.
2. In leaching tests at 25°C, the surface concentration of Na and B of glass #1 decreased significantly within the first 10 minutes, while initial loss of Th was followed by enrichment after 60 hours. Strontium was also concentrated at the glass–water interface.
3. At 100°C, Na and B were leached from the two-nanometer-thick surface region of glass #1 to below the detectable limit (of XPS) within 2 hours. Thorium became a major surface constituent with time, and strontium was also enriched relative to the bulk composition. The surface concentration of Zn remained high at the glass #5 interface.
4. The SIMS analysis greatly increased the sensitivity for analysis of many elements present in low concentration. Depth profiling by ion-beam milling of the surface to a depth of up to 0.1 μm yielded relative element/silicon ratios which were calculated as a function of time of sputtering. Enrichment of Mg, Ca, Sr, Zr, Ti, Ce and Fe was evident at the leached exterior of both glass #1 and glass #5. Similarly, depletion of K, Na and B was observed in each sample, although the alteration zone thickness of glass #5 was less than that for glass #1. These detailed analyses will be employed in the refinement of a model of waste glass durability.

Rock–Glass Leaching Experiment

To assess the qualitative and quantitative effects of exposing a simulated inactive waste glass to flowing water containing species dissolved from a typical granite, two rock–glass leaching tests were installed and operated, one for 370 days at 22°C and another for 100 days at 95°C. The 22°C experiment consisted of a cell of crushed dilute-waste borosilicate glass containing 4 wt.% ZnO (surface area 7.8 m^2) mounted in series between two similar columns of crushed White Lake granite (surface area 0.35 m^2). Air-saturated, deionized water was percolated upwards through the cells and sampled after each stage. Glass granules from each rock glass experiment were analyzed by SEM and compared with results for identical glass samples recovered from control tests without granite columns.

At 22°C, the glass downstream from the rock bed was characterized by a porous surface deposit with a morphology similar to that independently observed for both ZnO[7] and opal-CT lepispheres.[8] Due to surface roughness, our SEM-EDX analysis was unable to confirm quantitatively which species were present. However, it is probable that the slightly alkaline water from the rock bed not only increased the rate of glass corrosion, but also promoted ZnO precipitation. This solid phase has a minimum solubility at a pH of 9 (Ref. 9). The control glass surface appeared virtually unchanged at 22°C in deionized water.

At 95°C, the effect of the preceding granite bed had just a slight effect on the nature of the extensive surface deposit on the borosilicate glass, undoubtedly because the corrosion rate of the glass exceeded that of ion-exchange and dissolution reactions of the granite. The films were loosely adherent and could be removed by ultrasonic cleaning. The morphology of each deposit was similar and resembled that observed in the 22°C test.

In a separate experiment, an identical glass sample was prepared but was doped with 0.120 MBq of ^{137}Cs. Leach rates were measured for over 600 days at 22°C for both the rock–glass sample and the control sample. Leach rates were about 1 $\mu g/m^2 \cdot sec$ in each case. This suggests that the zinc-rich surface film does not provide significant resistance to loss of mobile cations such as cesium.

CONCLUSIONS

The surface analyses of two radioactive nepheline syenite glass blocks recovered from in-ground leaching tests at CRNL have confirmed that the alteration of the outer surface during 18 to 20 years of burial has been negligible. Under such mild storage conditions, the $(Na, K)_2O–CaO–Al_2O_3–SiO_2$ matrix is an excellent host matrix for high-level waste. The addition of ZnO to borosilicate glasses containing relatively small amounts of simulated high-level waste markedly improves the durability of these products in water at 100°C. The ZnO reduces leaching by formation of Zn-rich alteration-zone products, such as zincsilite and hemimorphite, or by deposition of ZnO in slightly alkaline conditions. Depth profiling of surface films has shown that ZnO alters the leaching behaviour of sodium borosilicate glasses. ZnO promotes subliquidus immiscibility in borosilicate glasses. A flow-through rock–glass leach test operated for more than a year at 22°C showed that species dissolved from a typical granite can significantly alter surface deposits formed on corroding glass. The properties of glass-corrosion films should be explicitly accounted for in waste-glass mathematical source-term models.

REFERENCES

1. J. Boulton (Ed.), *Management of Radioactive Fuel Wastes: The Canadian Disposal Program*, Atomic Energy of Canada Limited Report, AECL-6314 (1978).
2. W. F. Merritt, High-Level Waste Glass: Field Leach Test, *Nucl. Tech.*, 32: 88 (1977).
3. A. R. Bancroft and J. D. Gamble, *Initiation of a Field Burial Test of the Disposal of Fission Products Incorporated into Glass*, Atomic Energy of Canada Limited Report, AECL-718 (1958).
4. A. R. Bancroft, The Incorporation of Fission Products into Glass for Disposal, *Can. J. Chem. Eng.*, 38: 19 (1960).
5. A. J. Mooradian, *CANDU Fuel Cycles—Present and Future*, Atomic Energy of Canada Limited Report, AECL-5516 (1976).
6. D. J. Cameron and G. G. Strathdee, Materials Aspects of Nuclear Waste Disposal in Canada, in Proceedings of *Ceramics in Nuclear Waste Management*, Cincinnati, CONF-790420, U. S. Department of Energy, Technical Information Center, Oak Ridge, 1979.
7. J. Perkins, W. H. Luebke, K. J. Graham, and J. M. Todd, Anodic Corrosion of Zinc Alloys in Seawater, *J. Electrochem. Soc.*, 124: 819 (1977).
8. M. Kastner, J. B. Keene, and J. M. Gieskes, Diagenesis of Siliceous Oozes—I. Chemical Controls on the Rate of Opal-A to Opal-CT Transformation—An Experimental Study, *Geochim. Cosmochim. Acta*, 41: 1041 (1977).
9. W. Strumm and J. J. Morgan, *Aquatic Chemistry*, p. 173, Wiley-Interscience, New York, 1970.

THE LEACHING OF RADIOACTIVE WASTE STORAGE GLASSES

K. A. BOULT, J. T. DALTON, A. R. HALL, A. HOUGH, and J. A. C. MARPLES
A.E.R.E. Harwell, Didcot, Oxon, United Kingdom

ABSTRACT

Results are reported of leach tests under various conditions on glass compositions proposed for the vitrification of the highly radioactive waste from the reprocessing of Magnox fuel. Among the variables studied are waste composition, glass devitrification, the source and pH of the water, temperature, and radiation dose to the glass.

INTRODUCTION

Attack on the glass by water is the only likely method by which the radioisotopes contained therein can start their journey back to man's environment. It is therefore important to study the many variables that affect this rate of attack. The composition of the calcined waste from reprocessing Magnox fuel is shown in Table 1, expressed as wt.% oxides. The selected glasses have to be capable of dissolving about 25 wt.% of this waste and also have to be formed at less than 1050°C, the maximum operating temperature of the Harvest[1] process. The two glass compositions[2] that have been particularly studied are listed in Table 2.

EXPERIMENTAL TECHNIQUES

The techniques used have already been described.[3] Almost all the leach rates are obtained from the measured weight loss of polished glass coupons (20mm x 10mm x 1mm) exposed to water either in the familiar Soxhlet apparatus[3] or after heating in 2×10^{-5} m^3 of static water or after exposure to slowly flowing water (1×10^{-8} m^3/sec). In all cases the ratio of water volume to glass surface area is high compared to that likely in most disposal situations. Tests were continued for a time sufficient to achieve a measurable weight loss (i.e., a few mg). This varied from about a week at 100°C to many months at or below room temperature. For samples from the same batch of glass, the reproducibility[4] of the results was normally about ±15%, with the batch-to-batch variation being rather more.

RESULTS

Effect of Composition Changes

Most of our studies have been made on the ideal 209 and 189 compositions, but it was recognized that under production conditions variations from these could occur due to malfunctions of the feed pumps, leading to greater or lesser proportions of waste in the glass, or to settling out of sediments in the storage tanks, leading to changes in MgO and Al_2O_3 levels, or to changes in processing parameters leading to alterations in phosphate and sulphate concentrations. Glass samples were therefore made up based on 209 but with

a. Waste contents of 10, 25, 35 and 40 wt.%
b. Approximately half and approximately double the normal concentrations of MgO and Al_2O_3
c. 2 and 4 times the normal amount of sulphate
d. 1.5 times and one-quarter the normal amount of phosphate

The glasses with 40 wt.% waste had formation temperatures over 1200°C, and their preparation was discontinued. Thus 35 wt.% is about the limit of usefulness of this glass composition. The other samples were leach tested in a Soxhlet apparatus with the following results: (a) all compo-

TABLE 1

Composition of Magnox Waste*

Oxide	FPO_X	MgO	Al_2O_3	Fe_2O_3	Cr_2O_3	ZnO	NiO	U_3O_8
Wt.%	39.1	24.8	20.0	10.6	2.2	1.7	1.4	0.2

*Sulphate $(SO_4)^{2-}$, 0.4%; phosphate $(PO_4)^{3-}$, 1.2%.

TABLE 2

Composition of Glasses in Wt.% Oxides

Glass No.	SiO_2	B_2O_3	Na_2O	Li_2O	Waste	Formation temperature
189 (M5)	41.5	21.9	7.7	3.7	25.3	950°C
209 (M22)	50.9	11.1	8.3	4.0	25.7	1000°C

sitions tested, containing 35 wt.% waste or less, form glasses with leach rates no worse than 3 times that for the reference composition; (b) only the glasses with the doubled MgO contents have leach rates significantly worse than the reference value.

Effect of Crystallization

Glasses are only metastable and almost all glasses will start to crystallize if slow cooled or held at some elevated temperature. The crystals formed are usually less soluble than the parent glass but the residual glass matrix is often more soluble, and the devitrified glass can exhibit a higher leach rate. Among other heat treatments, samples of the two reference glasses have been annealed at 500, 600, 700 and 800°C for times of 2 hours, 1 day, 10 days, and 100 days. The longer of these times is not, of course, likely to be approached in practice. Most of these samples had partly crystallized as judged by their appearance, by microscopic study of a thin section, and by X-ray and electron microprobe examination.[4] The exact proportion of crystals is difficult to determine by any of these methods but is probably about 10% in the samples annealed for 100 days at 600°C (209) and 700°C (189). The leach rates of these samples are shown in Fig. 1, and it can be seen that no marked effect occurs on either glass. The results of other crystallizing anneals were similar. Thus, the small amount of crystallization that may occur in these glasses has no deleterious effect on the leach rate.

Effect of Time on Soxhlet Tests

Most of our Soxhlet tests are continued only for sufficient time to achieve a weight loss that can be measured with the necessary accuracy. In order to demonstrate that this does not give too high an answer, five samples of glass 209 were placed in a single Soxhlet apparatus and one removed at intervals for the leach rate to be measured. The results showed that the apparent leach rate decreased by only 20% between 1 and 11 weeks.

Effect of Temperature Using the Soxhlet Technique

Both compositions 189 and 209 were tested over a range of temperatures using the pressure controlled Soxhlet method. The results are shown in Arrhenius plots in Figs. 2 and 3.

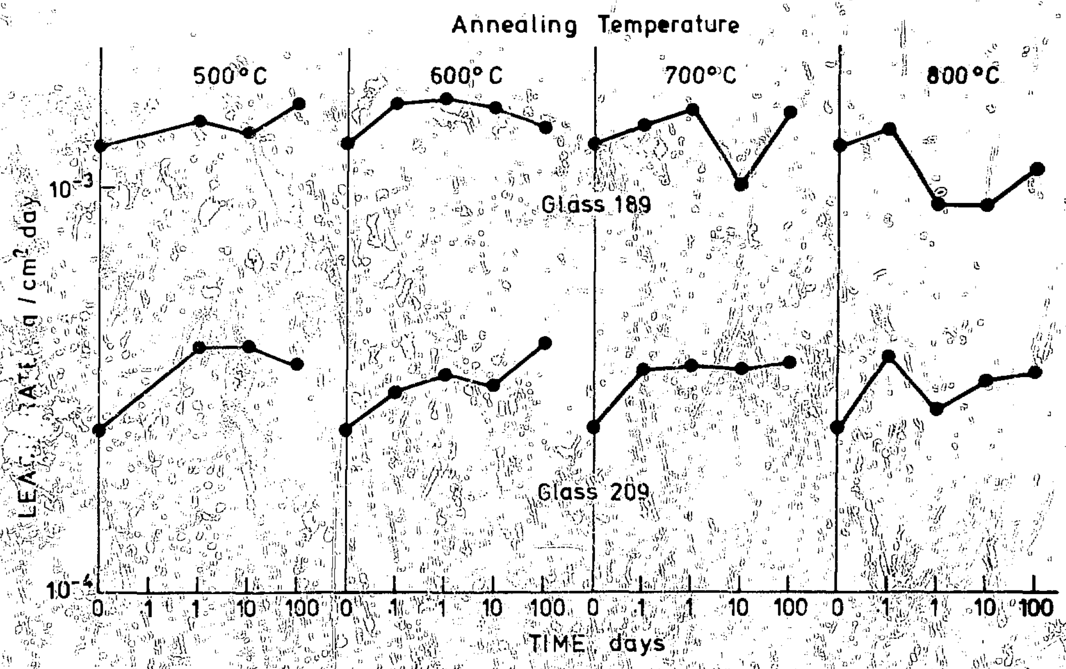

Fig. 1 The effect of crystallization on the Soxhlet leach rates of glasses 189 and 209.

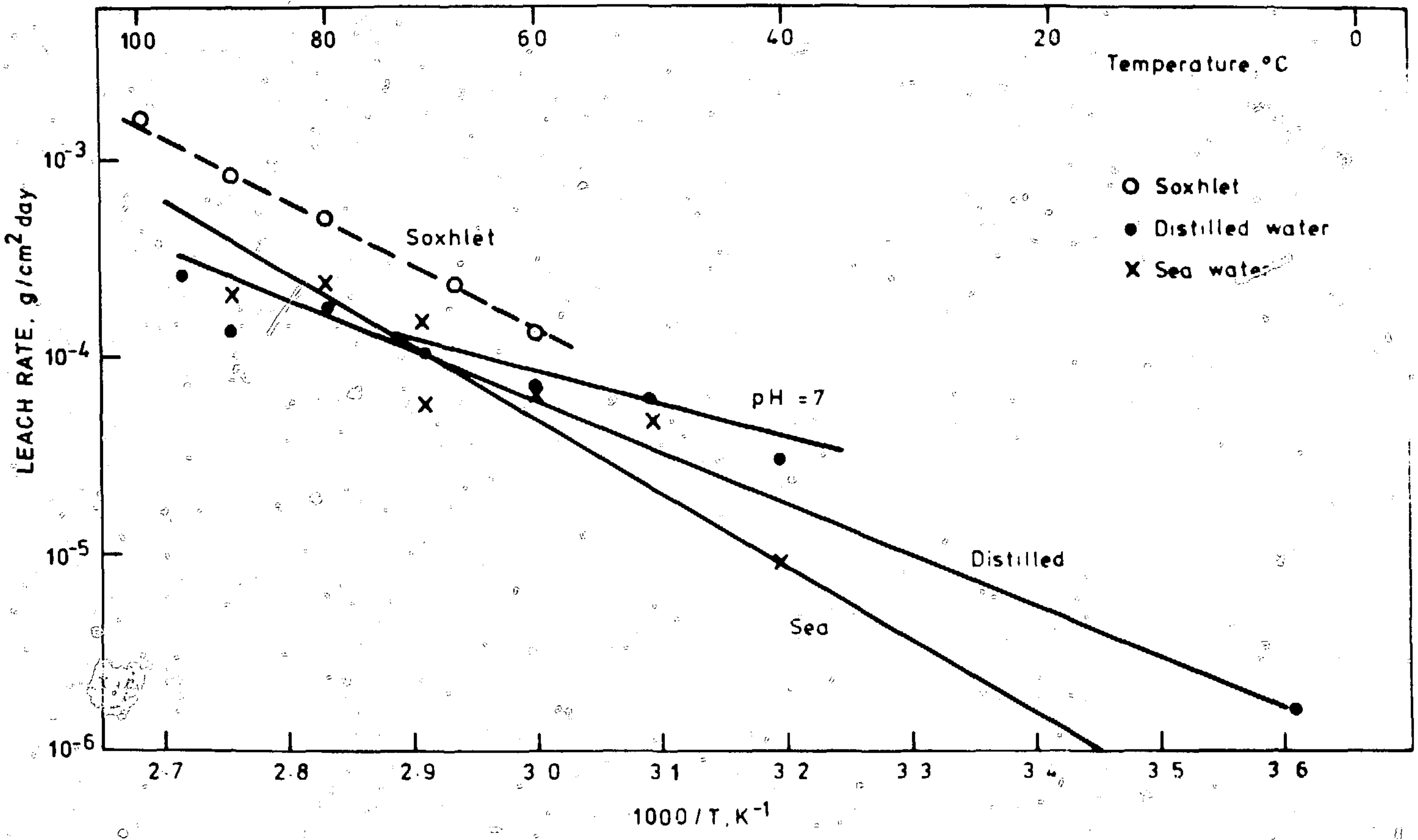

Fig. 2 Soxhlet and static water leach rates for glass 189. The Soxhlet results for temperatures below 100°C were obtained by boiling the water under reduced pressure. The leach rates in flowing water (pH = 7) are included for comparison (Fig. 4)

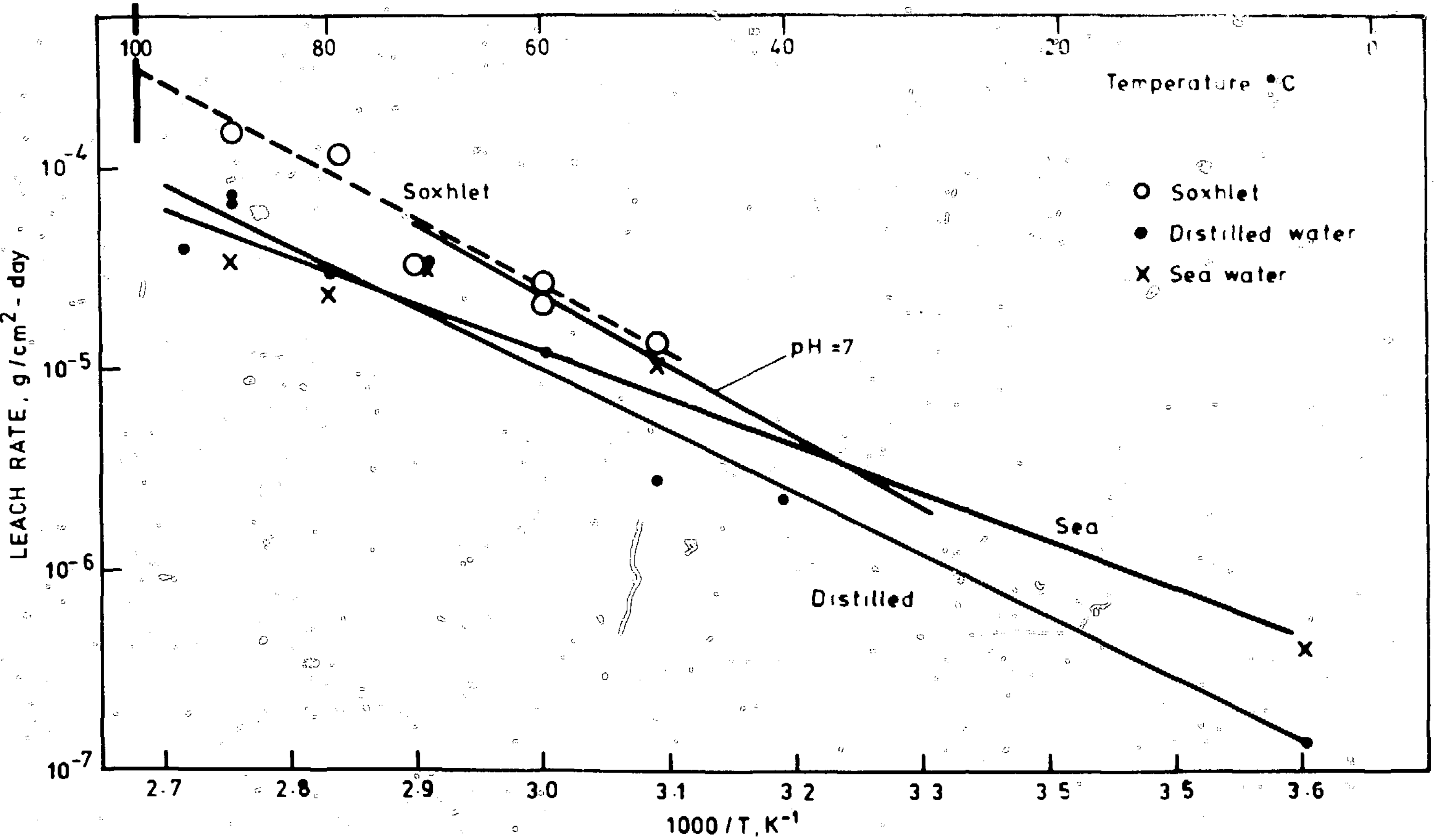

Fig. 3 Soxhlet and static water leach rates for glass 209. The vertical line at 100°C shows the spread of 11 different Soxhlet results

Effect of Different Waters

Soxhlet [illegible] method [illegible] water [illegible] water from the [illegible] water [illegible] A [illegible] distilled water and sea water are given in Fig. [illegible] and [illegible]. The results for the other water lie between [illegible] line.

As can be seen from Fig. [illegible] and [illegible], the difference in leach rates between distilled and sea water is little more than a factor of two at the higher temperature and about a factor of four at 40°C. Two Soxhlet tests at 90°C in water equilibrated with granite and with clay showed that while the granite water gave similar results to the water mentioned previously, the clay water which had a pH of 9.0 was more corrosive by about a factor of [illegible]. Also in Figs. 2 and 3 it is shown that the leach rate determined by the Soxhlet method is [illegible] times higher than that determined by the static method.

Effect of pH

The results of leach tests by the flowing method are shown in Fig. 4. It can be seen that the leach rates are [illegible] pH [illegible]

Effect of Specimen Irradiation

[illegible] particles [illegible] their energy by ionizing the atoms in their path. It is thought that [illegible] will have only a transitory effect and that almost all the atomic displacements in waste storage glasses will be caused by the α-decay of incorporated actinides. To test the radiation stability, samples of glass 189 were doped with [illegible] wt [illegible] Pu and stored to allow α-radiation damage to build up.

These samples were leach tested by the Soxhlet technique at yearly intervals after manufacture and the results are shown in Table 3. The 3-year sample doping time is equivalent to a storage time for the real waste of over 10[illegible] years unless the Magnox fuel is cooled for over [illegible]

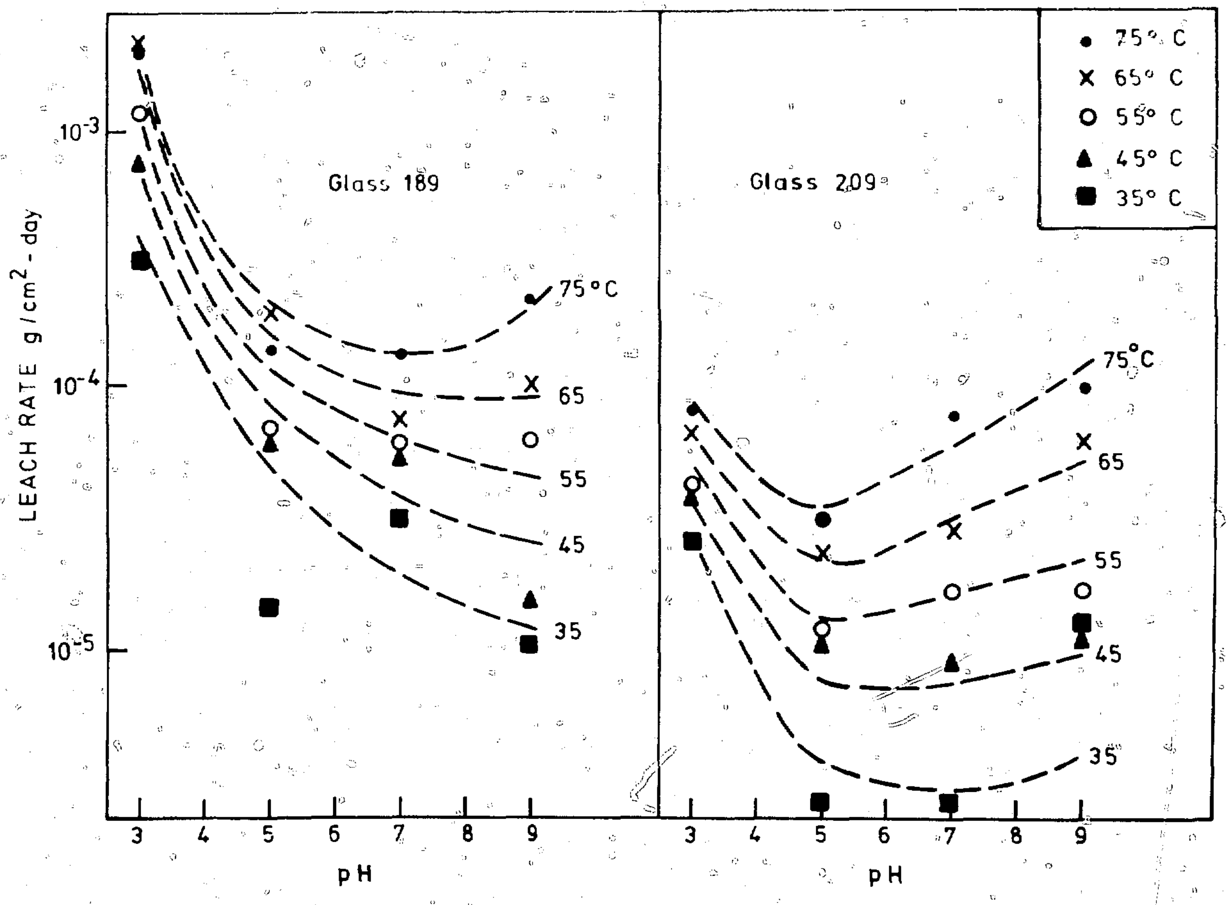

Fig. 4 The effect of pH on the leach rates of glasses 189 and 209 at different temperatures.

TABLE 3

Leach Rates of [illegible] PuO₂ Doped Samples After Storage

Holding temperature		Total dose over 3 years, disintegrations per g	Leach rates, g cm⁻² · day at 100°C		
First year, °C	Subsequent years, °C		After 1 year	After 2 years	After 3 years
[illegible]	[illegible]	[illegible]	[illegible]	[illegible] × 10	2.3 × 10
				2.4 × 10	
[illegible]	[illegible]	[illegible]	[illegible] × 10	[illegible] × 10	2.6 × 10
				2.2 × 10	

[illegible] Although the glasses were not [illegible] immediately after manufacture, the leach rates [illegible] after one year's storage at 50°C and 150°C are as [illegible] expected for the composition and were the same [illegible] PuO₂ doped control. The increase of about [illegible] for a second year was somewhat surprising [illegible] further deterioration occurred in the third year's storage.

Long Term Plutonium Leach Test

A platelet of glass 189 containing 5.5 wt % $^{239}PuO_2$ has been suspended in distilled water at room temperature and slowly turned by a synchronous motor. The water is changed every week (more frequently in the early stages), and the plutonium content of the leachate is determined by counting. The resulting leach rate has been approximately constant, after the first 20 days, up to 600 days. The equivalent bulk leach rate calculated from the plutonium leach rate is 1.5×10^{-6} g cm^{-2} · day. This is about half the leach rate determined by weight loss, i.e., the plutonium is leached from the glass at less than the average rate.

Formation of the Surface Layer

When glass is first exposed to leachant some elements are preferentially leached from the surface. These include sodium, lithium, and boron. This process leaves a porous surface layer on the glass composed of Fe_2O_3, the rare-earth oxides and, probably, the actinide oxides.[5]

Several specimens of glass 189 were leached in a Soxhlet apparatus at 100°C, and one was taken out every two or three days. The sample thickness was measured with a micrometer, both wet and after drying, and again after scraping off the porous layer. The layer thickness, both wet and dry, derived from these measurements shows a steady increase in layer thickness with time (Fig. 5). The density of the layer after drying, calculated from the weight and thickness, is quite low —about 0.4 ± 0.1 g/cm³, compared with a glass density of 2.63 g/cm³. A complication when considering the effect of the leach layer is that after 20 days for glass 189 when the layer is about 50 μm thick, it tends to break up and become detached.

CONSIDERATION OF THE LEACHING MECHANISM

The leaching of conventional high-silica glasses[illegible] proceeds by a two stage process. In water of low pH, H⁺ ions, probably as H_3O^+, diffuse into the surface of the glass, replacing the alkali cations, e.g., Na⁺, attached to the silica network. The latter then diffuse out of the glass into the leachate. A layer of hydrated silica, depleted in alkalis, thus forms on the surface of the glass, partly protecting the glass from further attack. In alkaline solutions, however, the silica network itself is attacked, and leaching of the glass is greatly accelerated.

The leaching of the waste storage glasses considered here differs from this mechanism in one important respect: the depleted surface layer is not protective, probably because its density is too low. As was shown above, the leach rate remains constant while the layer increases in thickness. This has the important consequence that the leach rate is not much increased in alkaline solutions — a decrease in the film thickness due to dissolution of the silica by alkali has little effect. In acidic solutions the leach rate is much increased, presumably because the cations in the glass are more rapidly attacked.

A further consequence of the instability and nonprotective nature of the depleted surface layer that forms at 100°C, in the presence of excess water, is that, after a short period during which equilibrium is established, the elements of the glass will be dispersed into the leachate in the same proportions as they occur in the glass. It may be that "leaching" is the wrong word to use for this attack since it is usually taken to imply selective removal of some elements. "Dissolution" might be more appropriate except that it is not certain that all the elements that have been removed from the glass are actually in solution rather than in suspension, e.g., as detached pieces of the surface layer. It should perhaps be noted that we have no direct evidence that these comments are also true at low temperatures since we have not yet been able to continue experiments for the few years necessary to establish equilibrium. On the other hand, however, there are no results that suggest that the leaching mechanism is different at low temperature.

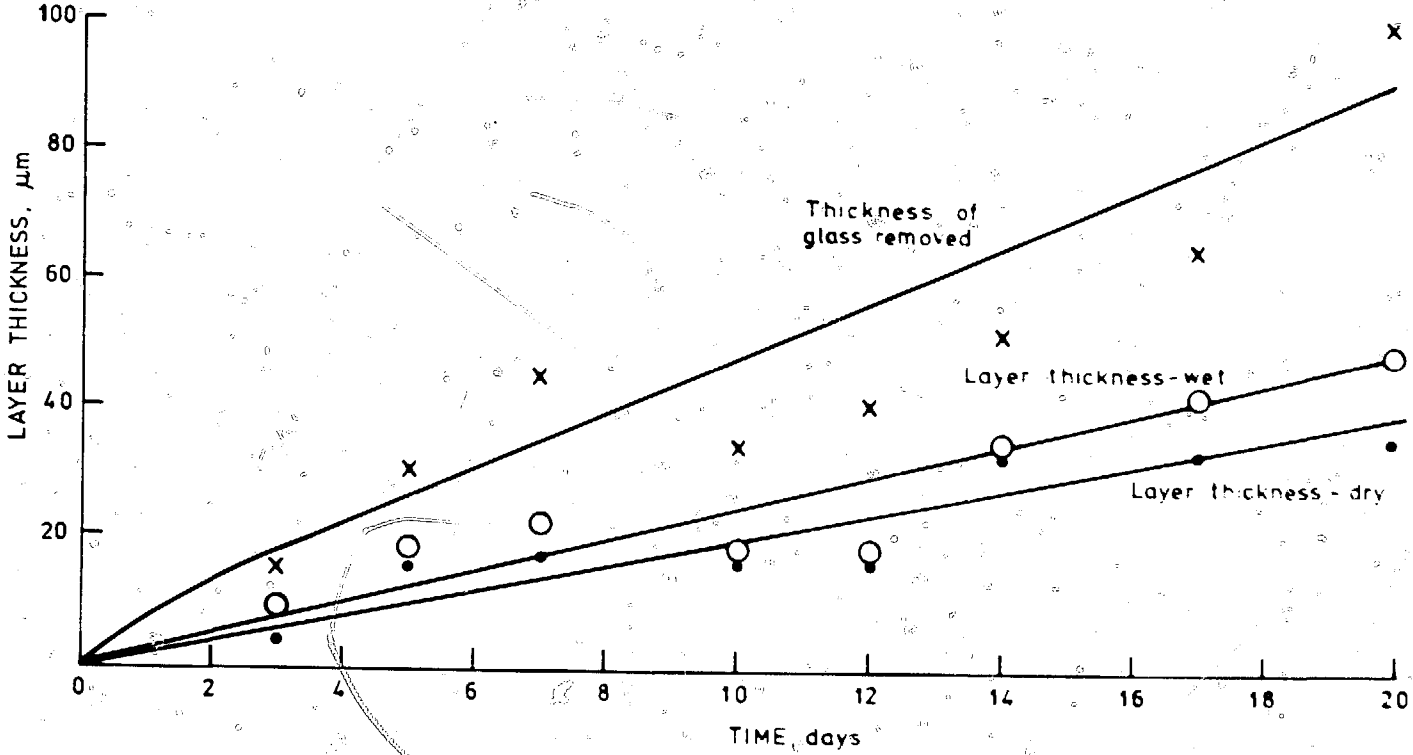

Fig. 5 The growth of the depleted surface layer on glass 180

ACKNOWLEDGMENT

Some of the results were obtained as part of a contract partly funded by the Commission of the European Communities.

REFERENCES

1. [illegible] M[illegible] and J. E. L[illegible], Performance Evaluation [illegible] with the [illegible] Vitrification Pilot Plant, in *Management of Radioactive Wastes from the Nuclear Fuel Cycle*, March 22-26, 1976, International Atomic Energy Agency, Vienna, 1976.
2. A. R. Hall, J. T. Dalton, B. Hudson, and J. A. C. Marples, Development and Radiation Stability of Glasses for Highly Radioactive Wastes, in *Management of Radioactive Wastes from the Nuclear Fuel Cycle*, March 22-26, 1976, International Atomic Energy Agency, Vienna, 1976.
3. K. A. Boult, J. T. Dalton, A. R. Hall, A. Hough, and J. A. C. Marples, Atomic Energy Research Establishment, Harwell, U. K., Report AERE-R [illegible] (1978).
4. G. Malow et al., Commission of the European Communities Report EUR 6215 (1978).
5. F. Lanza and E. Parnisari, Evaluation of Long-Term Leaching of Borosilicate Glass in Pure Water, in Proceedings of *Ceramics in Nuclear Waste Management*, Cincinnati, CONF-790420, U. S. Department of Energy Technical Information Center, Oak Ridge, 1979.
6. L. L. Hench, *J. Non-Crystalline Solids*, 25: 343 (1977).
7. A. Paul, *J. Mater. Sci.*, 12: 2246 (1977).

CORROSION BEHAVIOR OF ZINC BOROSILICATE SIMULATED NUCLEAR WASTE GLASS

D. E. CLARK, E. LUE YEN-BOWER, and L. L. HENCH
Department of Materials Science and Engineering, University of Florida
Gainesville, Florida

ABSTRACT

The corrosion behavior of a zinc borosilicate glass containing simulated nuclear wastes (SNWG) is evaluated in acidic, neutral, and basic solutions. Auger electron spectroscopy coupled with ion beam milling (AES-IM) and infrared reflection spectroscopy (IRRS) coupled with sequential polishing are used to determine the depth of the leached layers. Leaching rates based on solution analyses are calculated for several species including cesium and strontium. The leaching rates of some species from the glass are at least an order of magnitude greater in acidic than in neutral and basic solutions. Scanning electron microscopy in conjunction with energy dispersive X-ray spectroscopy (SEM-EDS) is used to monitor surface morphological changes that accompany glass corrosion.

INTRODUCTION

Two mechanisms of glass corrosion are well established in the literature: (1) ion exchange or selective leaching, and (2) network dissolution.[1-5] Ion exchange is a diffusion controlled process and is generally rate controlling when the solution in contact with the glass has a pH $\leqslant 9$ (Ref. 2). Network dissolution is a surface reaction involving the breaking of structural Si–O–Si bonds and is rate controlling when the pH $\geqslant 9$ (Ref. 2). The importance of solution pH and models used for predicting corrosion based on pH is discussed in detail in other papers.[6-8]

If the solubility product of any species in solution is exceeded, corrosion products may precipitate onto the glass surface. Under certain conditions, transformations within the surface such as dehydration, crystallization, and densification may also occur.[5] Both the mechanisms and kinetics of corrosion may be affected by these surface alterations.

In the early stage of corrosion the primary mode of attack is selective leaching of modifier ions from the glass, and the remaining SiO_2 is the major glass surface constituent. In a closed system the pH of the solution in contact with the glass surface increases due to an increase in OH^- ion concentration. The high OH^- ion concentration leads to the most damaging form of corrosion, namely, network dissolution.[5] When network dissolution is operative, all species in the glass dissolve simultaneously. The rate of network dissolution may be expressed by the kinetic equation

$$Q = kt \quad (1)$$

where Q = quantity of species in solution ($\mu g/cm^2$)
k = reaction rate constant
t = exposure time

During selective leaching, each species in the glass leaches at a different rate and these leach rates may be expressed with the following kinetic equation

$$Q = kt^{1/2} \quad (2)$$

where k is the reaction rate for specific species.

The objective of the present study was to characterize the corrosion behavior of the simulated nuclear waste glass 72-68(PW-4b-7(2.8)73.1)* exposed to a wide variety of environmental conditions. Several surface and solution

---

*Battelle, Pacific Northwest Laboratories; courtesy of Wayne Ross.

AUGER ELECTRON SPECTROSCOPY—ARGON ION MILLING

[illegible]

[illegible]

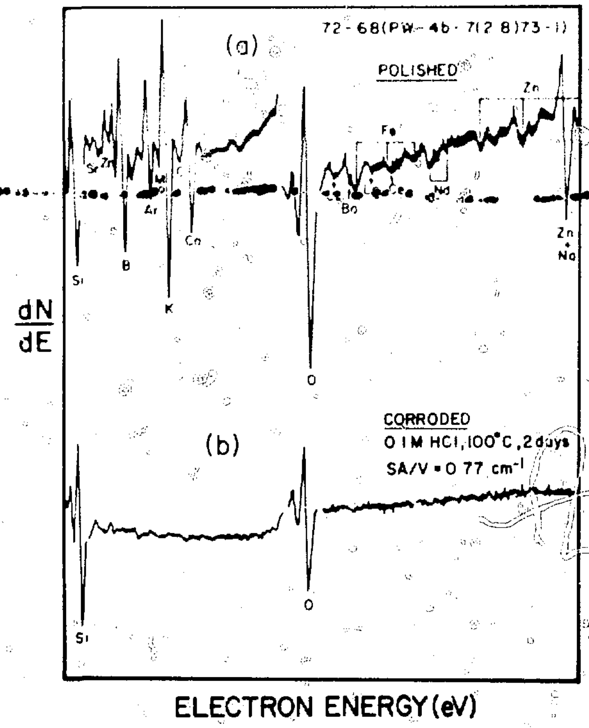

Fig. 1 Auger spectra for (a) polished surface of simulated nuclear waste glass and (b) surface after corroding in 0.1*M* HCl for 2 days.

[illegible] The depth of the leached layer [illegible] the OH⁻ attack on the Si–O–Si network.

Figure 3 illustrates the variations that occur in leached layer thickness and composition during autoclaving in distilled water with a static solution and a ratio of glass surface area (SA) to solution volume (V) of SA/V = 2.0 cm⁻¹. After 5 hr at 120°C the thickness of the leached layer is ~1000 Å based on the analysis of barium. The total depth of leaching was based on barium because it appears to be the most rapidly diffusing species. When selective leaching is the dominant mechanism of attack, all species leach at different rates, and a different depth profile is obtained for each element. After 14 hr at 120°C, the leached layer is ~500 Å for barium, indicating a changeover in corrosion mechanism from selective leaching to network dissolution between 5 hr and 14 hr. Although not shown, the thickness of the leached layer was still increasing after 400 hr on samples exposed to distilled water at 25°C at the same SA/V value. A concentration of heavy elements is also seen in the leached layer of specimens corroded under most conditions. However, data presented in a later section of this paper show the presence of cesium and strontium in solution after corrosion. Thus, even though the leached layer may have a tendency to retard leaching of the heavy elements, it does not completely prevent leaching of these elements.

INFRARED REFLECTION SPECTROSCOPY—SEQUENTIAL POLISHING

Bulk samples were examined by infrared reflection spectroscopy (IRRS) to observe the gross surface changes, if any, within a surface thickness of ~0.5 μm resulting from corrosion. There are several peaks of interest shown in the spectra in Fig. 4. On the uncorroded specimen, the peak at 1100 cm⁻¹ is attributed to the Si–O–Si stretching

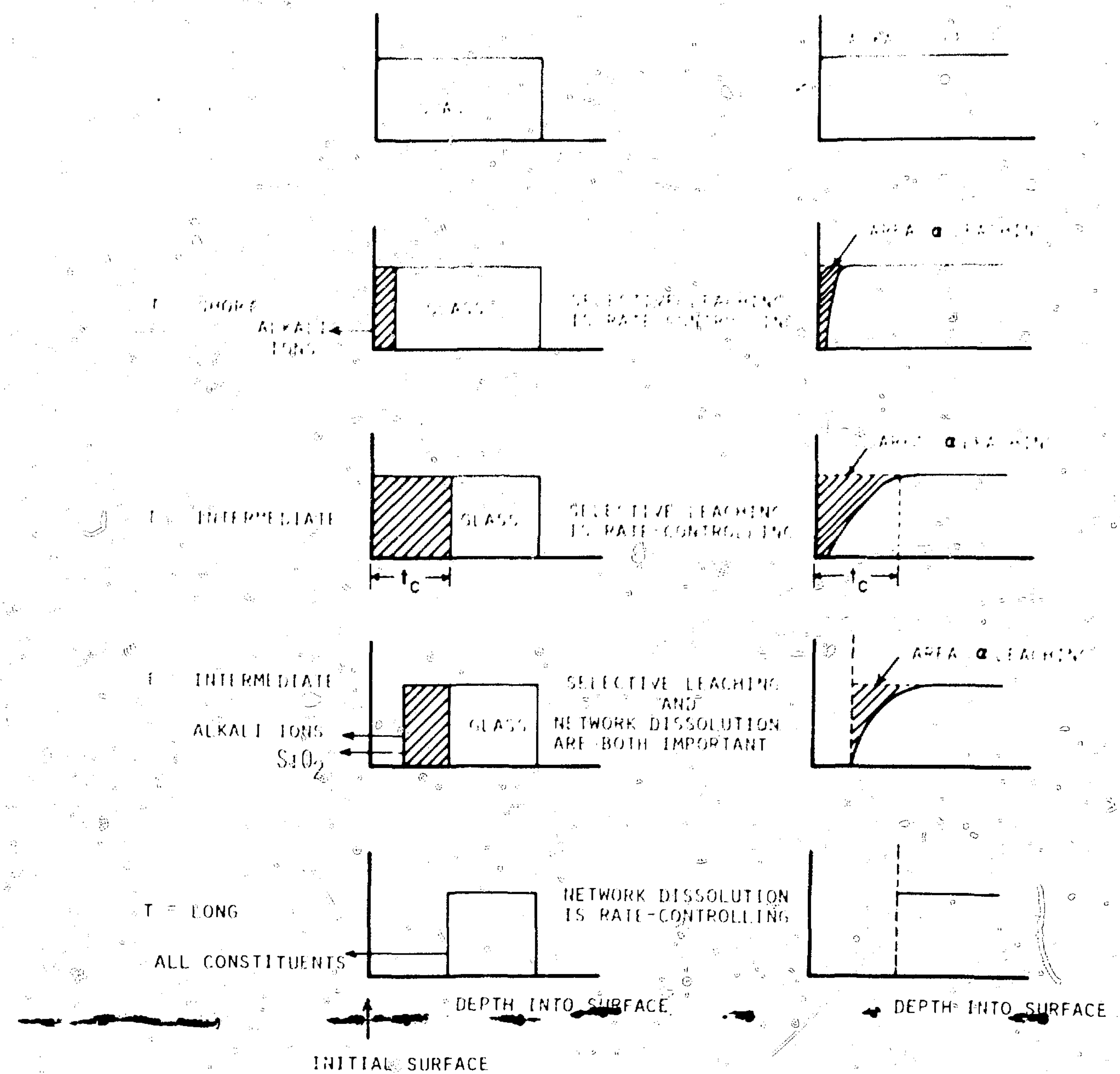
AREA α LEACHING
T = SHORT
ALKALI IONS
GLASS
SELECTIVE LEACHING IS RATE-CONTROLLING
AREA α LEACHING
T = INTERMEDIATE
GLASS
SELECTIVE LEACHING IS RATE-CONTROLLING
t_c
t_c
T = INTERMEDIATE
ALKALI IONS
SiO_2
GLASS
SELECTIVE LEACHING AND NETWORK DISSOLUTION ARE BOTH IMPORTANT
AREA α LEACHING
T = LONG
ALL CONSTITUENTS
NETWORK DISSOLUTION IS RATE-CONTROLLING
DEPTH INTO SURFACE
DEPTH INTO SURFACE
INITIAL SURFACE

Fig. 2 Schematic representation of glass corrosion mechanisms and associated depth compositional profiles.

vibration and the peak at approximately 940 cm^{-1} is due to the network modifiers such as Na_2O, K_2O, CaO and Cs_2O (Ref. 9). A spectrum of vitreous silica is shown in each graph for the purpose of comparison and instrument calibration.

Figure 4(a) shows that even in vigorously boiling water there is no measurable corroded layer after 10 hr, while the specimen corroded in 0.1*M* HCl under the same conditions [Fig. 4(b)] exhibited appreciable spectral changes. Spectral changes are associated with both leaching and network dissolution, and other investigations have demonstrated that the relative contribution to corrosion from each mechanism can be determined with IRRS.[5,9,10]

An IRRS sequential polishing technique was used to determine the depth of the corroded layer. The as-corroded bulk samples were first examined with the usual IRRS procedure. Subsequently, the specimens were weighed, abraded lightly with 600 grit SiC paper, reweighed, and again subjected to IRRS analysis. This procedure was repeated until no changes in the IRRS spectrum occurred with further abrasion. The thickness of the leached layer was calculated from the change in weight, sample surface area, and glass density. This procedure is outlined in detail elsewhere.[11]

Slight polishing of the specimen corroded for 10 hr in 0.1*M* HCl reveals a peak at 1060 cm^{-1} [polish #3 in

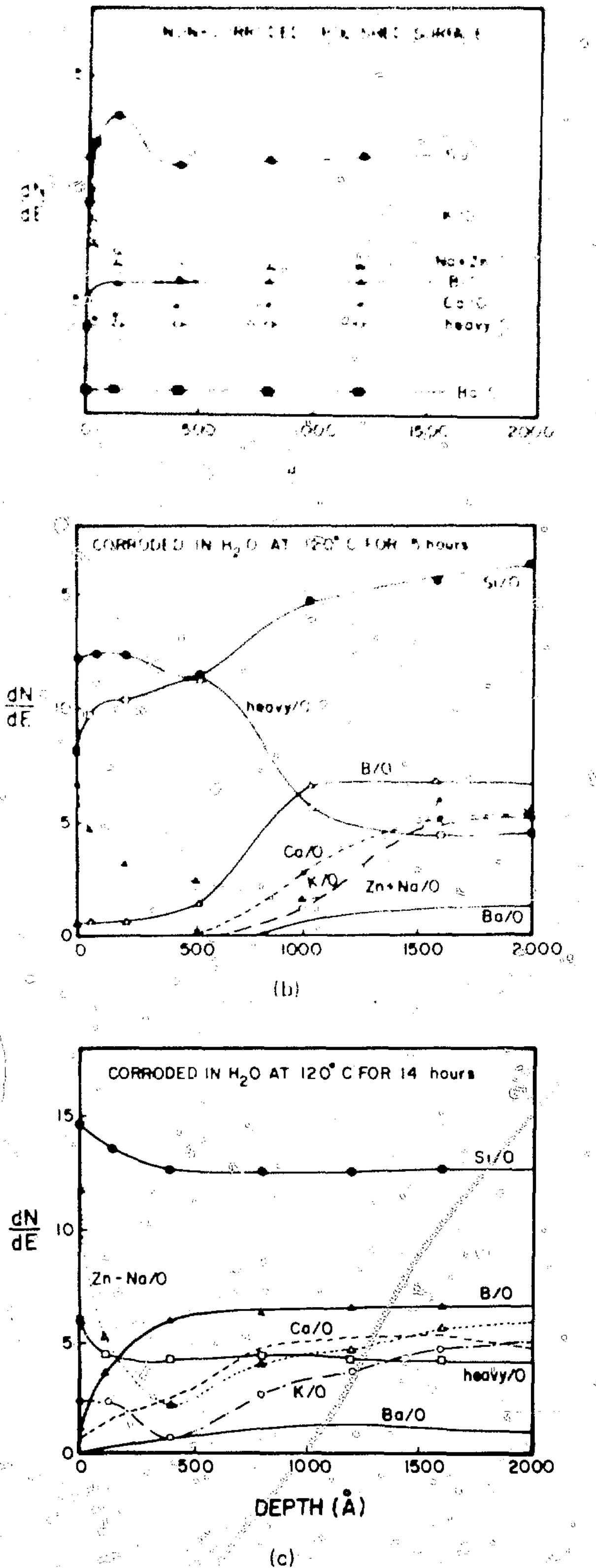

Fig. 3 Depth compositional profiles obtained with AES–IM for (a) a polished surface of simulated nuclear waste glass, (b) a surface corroded at 120°C for 5 hr in water, and (c) a surface corroded at 120°C for 14 hr in water.

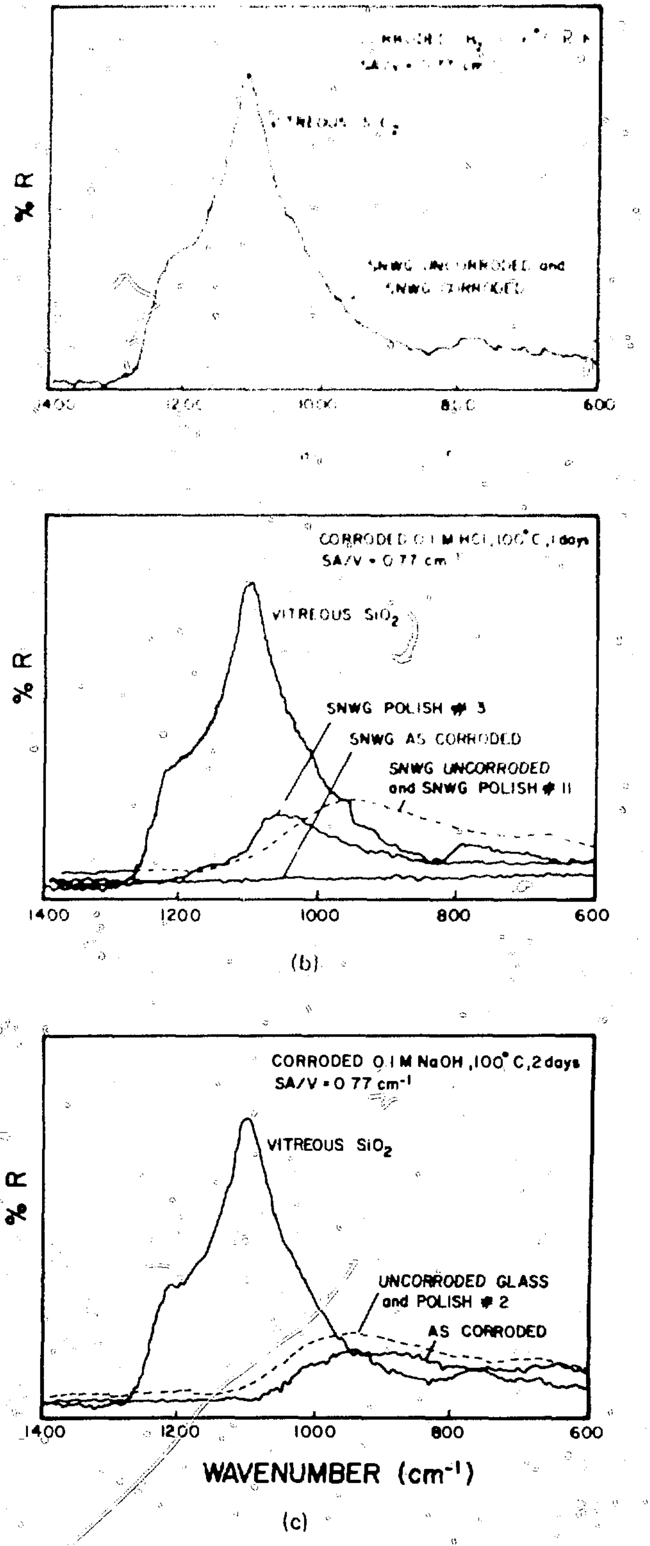

Fig. 4 Infrared reflection spectra for a simulated nuclear waste glass for (a) polished surface before and after corroding in water at 100°C for 10 hr; (b) a surface corroded in 0.1*M* HCl at 100°C for 1 day, including spectra after polishing the corroded surface; and (c) a surface corroded in 0.1*M* NaOH at 100°C for 2 days, including a spectrum after polishing the corroded surface.

[illegible] 0.1*M* HCl [illegible]

TABLE 1

Estimated Thickness of Leached Layer*

Environment, 100 C	Time	Thickness of leached layer (μm)*
H₂O	[illegible]	[illegible]
0.1*M* HCl	[illegible]	[illegible]
	[illegible]	[illegible]
	[illegible]	[illegible]
0.1*M* NaOH	[illegible]	[illegible]
	[illegible]	[illegible]

*SA/V [illegible]

Determined from IRRS [illegible] technique.

leached layer being dissolved at a more rapid rate than the bulk glass is leached. Similar spectra changes were observed during polishing for the 1 day and 2 day corroded specimens as for the 10-hr specimens. The density of the leached layer is probably somewhat less than the glass, thus the thicknesses of the leached layers are slightly greater than reported in this table.

Figure 4(c) presents IRRS spectra for the SNWG corroded in 0.1*M* NaOH. Minimal changes in the spectra are observed during corrosion and during polishing. These data suggest that less leaching occurs in the specimens exposed

SOLUTION ANALYSIS

[illegible] (SA/V) [illegible]

[illegible] SA/V [illegible]

The [illegible] rates shown in Table 2 were [illegible] kinetics. Equation 2 was used [illegible] rates are expressed in g/cm² d$^{1/2}$. Equation 1 was used to calculate the corrosion rate of the glass corroded in the 0.1*M* NaOH solution. The units for the corrosion rate in which the kinetics are linearly controlled are [illegible]. When the kinetics are diffusion controlled, the corrosion rate is different for each element but is constant with time for a particular element. This was observed for the acidic and neutral solutions. For instance, the leach rate in 0.1*M* HCl at 100 C is ~1 × 10^{-4} g/cm² d$^{1/2}$ for cesium and 1 × 10^{-3} g/cm² d$^{1/2}$ for zinc. When the kinetics are linearly controlled all species should leach out of the glass simultaneously. The leach rates expressed in g/cm²-d will be different for each element because their concentrations in the glass are different. However, the ratios of the concentra-

TABLE 2

Corrosion Rates of Elements from Nuclear Waste Glass 72-68(PW-4b(2.8)73-1)
(Corrosion Temperature of 100 C and SA/V = 0.77 cm^{-1})

Solution	Actual corrosion time	Ba	Ca	Cs	Na	Si	Sr	Zn
		g/cm² d$^{1/2}$						
H$_2$O	10 hr	NA*			6.5 x 10$^{-[illegible]}$	1.2 x 10^{-5}		8.1 x 10^{-7}
	2 days		4.9 x 10^{-7}	4.9 x 10^{-7}	6.9 x 10$^{-[illegible]}$	4.6 x 10^{-6}	2.8 x 10^{-7}	6.4 x 10^{-7}
	1 wk	2.4 x 10^{-6}	2.2 x 10^{-6}	1.1 x 10^{-7}	6.8 x 10^{-7}	1.4 x 10$^{-[illegible]}$	2.2 x 10^{-7}	9.8 x 10^{-7}
0.1*M* HCl	10 hr	NA	2.4 x 10^{-4}	2.4 x 10^{-4}	4.5 x 10^{-4}	1.5 x 10^{-4}	3.8 x 10^{-4}	2.7 x 10^{-3}
	1 day	NA	1.4 x 10^{-4}	5.2 x 10^{-5}	2.9 x 10^{-4}	8.8 x 10^{-5}	2.0 x 10^{-4}	1.9 x 10^{-3}
	2 days	NA	1.2 x 10^{-4}	1.3 x 10^{-4}	2.2 x 10^{-4}	6.9 x 10^{-5}	1.8 x 10^{-4}	1.3 x 10^{-3}
	4 days	NA	9.1 x 10^{-5}	9.1 x 10^{-5}	2.3 x 10^{-4}	3.0 x 10^{-5}	5.5 x 10^{-5}	8.4 x 10^{-4}
	4 days	8.8 x 10^{-5}	9.8 x 10^{-5}	9.8 x 10^{-5}	3.0 x 10^{-4}	2.3 x 10^{-5}	1.7 x 10^{-4}	1.2 x 10^{-3}
	1 wk	5.2 x 10^{-4}	2.8 x 10^{-5}	9.8 x 10^{-5}	1.7 x 10^{-4}	1.7 x 10^{-5}	9.0 x 10^{-5}	8.1 x 10^{-4}
0.1*M* HNO$_3$	1 wk	2.2 x 10^{-4}	6.5 x 10^{-5}	6.5 x 10^{-5}	1.9 x 10^{-4}	2.0 x 10^{-5}	9.4 x 10^{-5}	8.0 x 10^{-4}
		g/cm²-d						
0.1*M* NaOH	10 hr	NA		1.9 x 10^{-5}	NA	4.6 x 10^{-5}	6.0 x 10^{-6}	6.9 x 10^{-5}
	2 days	NA		7.2 x 10^{-6}	NA	7.9 x 10^{-6}	6.5 x 10^{-7}	1.3 x 10^{-5}
	1 wk	9.5 x 10^{-6}	2.4 x 10^{-7}	9.3 x 10^{-6}	NA	3.7 x 10^{-6}	2.7 x 10^{-7}	7.5 x 10^{-6}

*NA, not analyzed.

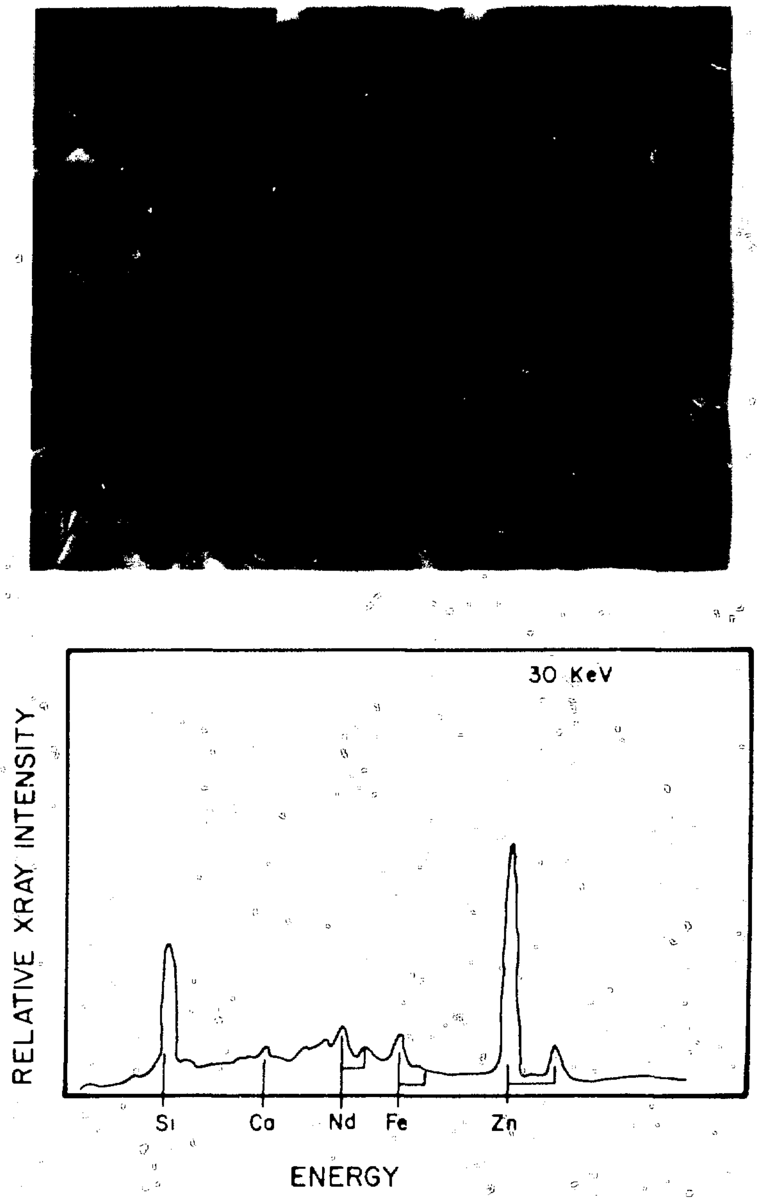

Fig. 5 SEM and X-ray spectrum of a simulated glass surface after autoclaving at 120°C for 120 hr.

tion of elements in solution should be the same as their ratios in the glass.

It is interesting to note that the corrosion rates are identical in 0.1*M* HCl and 0.1*M* HNO_3. This suggests minimal anionic effects and shows that a low pH medium is the more crucial factor.

Residues were observed in the acid solutions after removing the glass specimens. These residues appear to have a high concentration of SiO_2. Apparently, the extensive leaching that occurs in the acidic solutions results in unstable film formation on the glass surface that subsequently flakes off into solution. Recall that a decrease in film thickness was also observed between 10 hr and 1 day of corrosion using IRRS (Table 1).

A major problem that we have encountered is the heterogeneity of the glass specimens. Surface analysis data indicate that corrosion does not occur at equal rates over the surface of the glass. This problem complicates interpretation of the solution data, both the mechanisms and kinetics.

SCANNING ELECTRON MICROSCOPY–ENERGY DISPERSIVE X-RAY ANALYSIS

A scanning electron micrograph is shown in Fig. 5 for a specimen exposed to an autoclave environment maintained at 120°C for 120 hr. After exposure, numerous discrete crystals appear to be growing from the glass surface. The surface adjacent to the crystals is very porous, indicating extensive leaching. The X-ray spectra of the corroded surfaces are also shown in Fig. 5. The corroded surface is depleted of most elements in comparison to the abraded surface (not shown). Although not shown, the crystals completely cover the surface after 208 hr at 120°C and the X-ray spectrum for the surface indicates that the crystals are composed primarily of zinc and silicon.

SUMMARY

The process by which the SNWG glass corrodes appears to follow a simple two-mechanism model when the glass is exposed to neutral solutions maintained at <100°C. During the early stage of corrosion, ions are leached out of the surface of the glass leaving behind a stable silica-rich layer. The thickness of this layer increases with increasing exposure time as long as the selective leaching mechanism is rate controlling. Each chemical species leaches at a different rate from the surface as determined by both solution analysis and AES IM. If network dissolution ensues, all species go into solution in approximately the same proportion as they are present in the glass, and the thickness of the leached layer decreases.

When SNWG is corroded in an acid solution, extensive leaching occurs, and precipitates are observed in the corrosion cells after analysis. Even in acidic solutions a considerable quantity of silica is found in solution. The mechanism by which this silica dissolves into solution is different than that which occurs when network dissolution is rate controlling. In the acidic solution, extensive leaching of all ions with the exception of silicon occurs. Since the SNWG contains only 37.2 mole % SiO_2, this quantity is apparently not sufficient to form a stable structural network. Thus the unstable silica film (leached layer) physically falls off the surface of the glass during exposure. This could account for part of the precipitate found in the acid solutions.

The process of corrosion becomes more complicated when the glass is exposed to autoclave conditions. Both selective leaching and network dissolution still occur. In addition, crystals form on the surface of the glass. The formation of this crystal phase appears to be a complicated process, requiring an intermediate step whereby a zinc-rich gel forms over the silica-rich glass surface. Crystals grow from this gel and eventually cover the entire glass surface.

Although not confirmed, the presence of these crystals is thought to affect the kinetics of corrosion, i.e., the rate at which elements are removed from the glass.

ACKNOWLEDGMENTS

The authors thank Battelle, Pacific Northwest Laboratories for partial financial support and especially Wayne Ross for providing the glass samples. They also thank the Nuclear Regulatory Commission for partial financial support for this work under contract No. NRC-04-78-252.

REFERENCES

1. A. K. Lyle, Theoretical Aspects of Chemical Attack of Glasses by Water, *J. Amer. Ceram. Soc.*, 26: 201 (1943).
2. R. W. Douglas and T. M. El-Shamy, Reactions of Glasses with Aqueous Solutions, *J. Amer. Ceram. Soc.*, 50: 1 (1967).
3. D. E. Clark, M. F. Dilmore, E. C. Ethridge, and L. L. Hench, Aqueous Corrosion of Soda-Silica and Soda-Lime-Silica Glass, *J. Amer. Ceram. Soc.*, 59: 62 (1976).
4. D. M. Sanders and L. L. Hench, Mechanisms of Glass Corrosion, *J. Amer. Ceram. Soc.*, 56: 373 (1973).
5. D. E. Clark, C. G. Pantano, Jr., and L. L. Hench, *Glass Corrosion*, Glass Industry, New York, in press.
6. E. C. Ethridge, D. E. Clark, and L. L. Hench, Effects of Glass Surface Area-to-Solution Volume Ratio on Glass Corrosion, *J. Phys. and Chem. Glasses*, April 1979.
7. L. L. Hench, D. E. Clark, and E. Lue Yen-Bower, An Approach Towards Long Term Prediction of Stability of Nuclear Waste Forms, in Proceedings of *Ceramics in Nuclear Waste Management*, Cincinnati, CONF-790420, U. S. Department of Energy, Technical Information Center, Oak Ridge, 1979.
8. T. M. El-Shamy, J. Lewins, and R. W. Douglas, The Dependence of the pH of the Decomposition of Glasses by Aqueous Solutions, *Glass Tech.*, 13: 81 (1972).
9. D. M. Sanders, W. B. Person, and L. L. Hench, Quantitative Analysis of Glass Structure Using Infrared Reflection Spectra, *Appl. Spectroscopy*, 26: 530 (1972).
10. D. E. Clark, E. C. Ethridge, M. F. Dilmore, and L. L. Hench, Quantitative Analysis of Corroded Glass Using IRRS Frequency Shifts, *Glass Tech.*, 18: 121 (1977).
11. E. C. Ethridge, *Mechanisms and Kinetics of Binary Alkali Silicate Glass Corrosion*, Ph.D. Dissertation, University of Florida, 1977.

CHEMICAL DURABILITY OF NUCLEAR WASTE GLASSES

JOSEPH H. SIMMONS, AARON BARKATT, PEDRO B. MACEDO, PEHR E. PEHRSSON,
CATHERINE J. SIMMONS, ALISA BARKATT, DANH C. TRAN, HERBERT SUTTER, and MERVET SALEH
Vitreous State Laboratory, Catholic University of America, Washington, DC

ABSTRACT

Test methods are presented for the measurement of chemical durability of glass media proposed for nuclear waste fixation. The release rates of individual components are measured to determine matrix dissolution rates, possible transport of components through the matrix, and the corrosion mechanism. Measurement on a model glass, a borosilicate, and a high-silica glass fixation medium are reported. The extrapolation of short-term laboratory tests to long-time storage is discussed, and the essential parameters for accurate long-term predictions are determined and evaluated.

INTRODUCTION

One of the major problems in assessing the reliability of materials used for the fixation of radioactive wastes is the prediction of long-term dissolution rates from short-term laboratory tests. The presence in the wastes of radioisotopes with long half-lives (20,000 to 400,000 years) requires accurate predictions over time periods far beyond any experience with man-made materials. Therefore, the prediction of the long-term dissolution behavior of proposed fixation media must rely upon detailed laboratory tests on both man-made and old geological samples and upon the development of a comprehensive understanding of the processes which control material dissolution. As an additional complication, the radioactive waste isotopes include a wide range of elements which differ from each other in chemical behavior. For example, the alkali metals, the alkaline earths, the transition metals, and the rare earths and actinides are expected to exhibit different behavior during the dissolution process.

Below, we present results from leach tests conducted on simulated wastes fixated in borosilicate and high-silica glasses. During the leaching period, we monitored the dissolution rate of several waste components including alkali metals, alkaline earths, transition metals, rare earths, and an actinide, and we show how they differ and how the measurement of leach rates of some of these components can be misleading regarding long-term behavior. The problems of applying the results to the prediction of long-term dissolution behavior are discussed; models are presented for reliable long-term predictions, and the essential tests which must be conducted to allow the formation of these reliable predictions for long-term behavior are listed.

MECHANISMS OF CHEMICAL DISSOLUTION

Early work on silicate glasses containing alkali metal oxides and alkaline earth oxides[1-3] has shown that the attack of water on the glass starts as a diffusive process through which alkali cations are preferentially leached from the surface layers and replaced by protons leaving behind a porous high-silica layer. As the dealkalized layer becomes thicker, the rate of further diffusion of alkali out of the glass through this layer becomes progressively slower, until silica dissolution at the interface between the dealkalized layer and the solution begins to control the rate of the attack. At the long-time limit, a steady-state condition may be achieved, under which the rates of the two processes become equal and a leached layer of constant thickness and constant composition starts moving into the glass at a constant rate.

Differences in chemical durability among various silicate glasses reflect differences in the porous structure of the surface films and consequent differences in the rates of diffusion processes taking place in these films. Silicate long-term predictions of dissolution rates from short term laboratory tests and we will list the chemical measurements needed to obtain reliable extrapolations.

EXPERIMENTAL

Samples

Three samples were investigated in the present study. Sample 1 was a borosilicate glass supplied by Battelle Pacific Northwest Laboratories. The waste glass composition was designated as 76-68, containing 40.0% SiO_2 and 33.0% waste.[8] The composition of the simulated waste stream corresponded to PW-8a-2,[8] except that cesium was not simulated by potassium and was present at a higher concentration corresponding to PW-8a-1.

Sample 2 was a high-silica glass also loaded with PW-8a simulated wastes and formed by the Porous Glass Matrix Process (PGM) which consists of mixing the simulated waste compositions with high-silica porous glass powders, calcining the mixture, then drying and heating in a glass tube to form a solid glass rod. When the waste stream and the powders are mixed, the dissolved wastes are deposited within the pores of the powder while the solids are mixed with the powders. After sintering, the rod is composed of a core which consists of solidified glass powders fixating the dissolved waste components as an integral part of their structure with the powders sintered together to form a solid object and incorporating undissolved solid components of the wastes in their structure. The core is surrounded by a surface layer or cladding region which consists of the collapsed glass tube which is itself free of any waste components. This method yields a sample with a built-in high durability protective glass barrier.

Sample 3 was a specially-made low durability glass containing 1.6% thorium oxide. The compositions of the samples are shown in Table 1.

TABLE I*

Composition of Tested Glasses (Wt.%)†

Sample	Loading (total)	SiO_2	B_2O_3	Na	K	Cs	Ca	Sr	Zn	Fe	Ln (total)	Th
1	33.0	40.0	9.5	9.54	0.056	1.04	1.43	0.34	4.02	7.74	6.78	
2	15.3	79.3	5.3	1.60	0.672	0.17		0.16		3.67	3.22	
3	1.8	92.3		0.076	0.086							1.56

*Analyses were conducted using atomic absorption spectrometry and optical colorimetry.
†Samples 1 and 2 also contain the other components of the simulated wastes stream.

Measurements

All samples were tested as powders and were crushed in an agate mortar and sieved to collect the −42 to +60 mesh fraction (355 to 250 μm) using a set of brass sieves. Sample 2 was prepared with a Vycor tube envelope. Because of the excellent adhesion between the envelope and the glass core, they could not be separated mechanically, and some of the powder tested was Vycor. This was taken into account in the analysis of the data by calculating the weight fraction of the powder which did not exhibit any dissolution effects. We measured the leach rate as a function of time for Si, Na, Fe, Cs, Sr, Zn and total lanthanides for Samples 1 and 2 and Si, Na, and Th for Sample 3. The test temperature was 70 ± 1°C. We purposely selected powdered samples to expose a large surface area of the glass to chemical attack and obtain detectable concentrations of leached products. We chose a high temperature for the tests in order to accelerate the reaction kinetics. The soaking solution was deionized neutral water; its volume was 100 ml and the exposed surface area was approximately 400 cm^2.

RESULTS AND DISCUSSION

The amount of each component of the glasses from Samples 1 and 2 released to the bath by chemical dissolution is plotted in Figs. 1 and 2 as a function of time of exposure. The pH of the soaking solution did not change during the test. Since the samples exhibited high durability, there were no complications in the dissolution process due to the accumulation of dissolution products in the leaching solution.[11]

The matrix dissolution rate of both samples exhibits a decrease with time indicating that a protective layer is formed on the glass surface. The matrix dissolution rate appears to change as t^{-n}, with the exponent equal to one-half for the borosilicate glass and equal to one for the high-silica glass. This difference in rate indicates that the protective layer of the high-silica glass is more resistant to chemical attack. Indeed, toward the end of the 17-day testing period the rate of silica dissolution is 3.3×10^{-6} $g/cm^2 \cdot d$ for the borosilicate glass (Sample 1) and 3.0×10^{-7} $g/cm^2 \cdot d$ for the high-silica glass (Sample 2).

The leaching rate of sodium, cesium, and strontium during the testing period (17 days at 70°C) is higher by a factor of about 3 than the rate of silica dissolution. This shows that the mechanism of interaction between the

[illegible]

[illegible] state is achieved. Measurements showing leaching steady state would then use the lowest observed leach rate and overestimate the long-term dissolution rate, thus providing for a margin of safety.

However, there are three major problems with this approach. These are the slow attainment of steady-state conditions in materials of good chemical durability, the interaction of polyvalent ions with the dealkalized layer and the possible structural disintegration of the layer.

Attainment of Steady-State. Tests carried out on glasses proposed for radioactive fixation do not show the attain- [illegible] after a period of [illegible] the entire mechanism [illegible] cannot be verified.

Interaction of [illegible] with the Dealkalized [illegible]. [illegible] is far more [illegible] and polyva- [illegible] We have discovered [illegible] dealkalized [illegible] the glass [illegible] and can last [illegible] trapping [illegible] the laboratory [illegible] drastically as to [illegible] earths [illegible] when [illegible] dissolution [illegible] be expected from [illegible] leaching layer [illegible] increases with time [illegible] alkali [illegible] leached layer [illegible] may reach a [illegible] surface [illegible] leached layer may [illegible] glasses [illegible] absorption of water [illegible] subsequent [illegible] glass [illegible] possibility [illegible] steady state [illegible] the most pessimistic calculation [illegible] thickness of the surface layer [illegible] must be taken into account [illegible] may lead to [illegible] predictions of leach rates at levels which are higher by more than one order of magnitude than the actual rates measured at the end of the test. Detailed calculations concerning this effect are reported elsewhere.

The experimental work and discussion presented below will demonstrate the effect of layer formation and of surface absorption and ion exchange in the layer, on the mechanism of glass dissolution in a clean water medium. In conclusion, we will reiterate the problems which affect

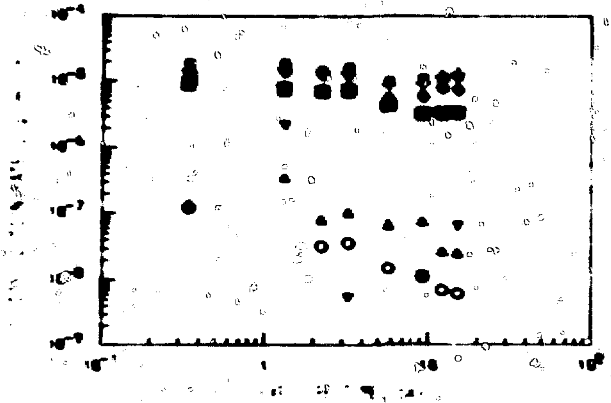

Fig. 1. Dissolution rates based on individual glass components for Sample 1, [illegible] silicate glass at 70 C. ■ SiO₂, [illegible] Na, [illegible] Cs, [illegible] Sr, [illegible] Zn, [illegible] Fe, ▲ total Ln.

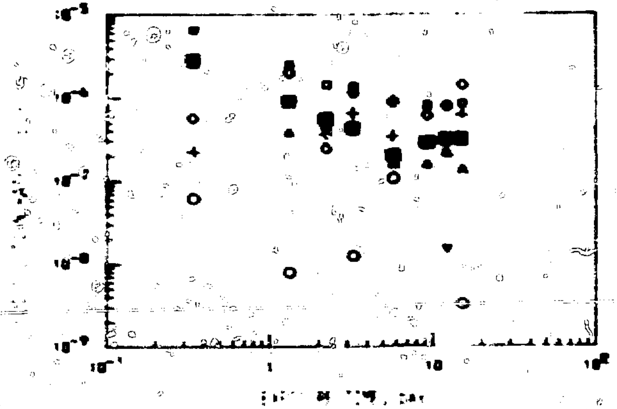

Fig. 2. Dissolution rates based on individual glass components for Sample 2, high-silica PGM glass at 70 C. ■ SiO₂, ○ Na, + Cs, [illegible] Sr, [illegible] Zn, [illegible] Fe, ▲ total Ln.

glasses and water is indeed dominated by the formation of a dealkalized surface layer. (Studies of other glass samples show that this effect becomes even more pronounced as the concentration of sodium in the original glass is lowered.) The results show that even after 17 days at 70 C the layer is still growing and steady-state conditions are not yet approached. Although the rates of leaching of silica appear to be levelling off (Figs. 1 and 2), the alkali ions and strontium are still preferentially leached away, and the mechanism of dissolution is still definitely incongruent.

The measurements also show that zinc, the lanthanide ions, and iron are leached away at relative rates (i.e., rates normalized for the concentration of each ion in the original glass) which are much slower than the matrix dissolution rate. This indicates that these cations undergo a considerable amount of readsorption in the growing surface layer. A more quantitative analysis of the dissolution process is based upon the calculation of the thickness of the dissolved layers corresponding to the leach rate of each of

TABLE 2

Equivalent Thickness of Leached and Dissolved Layers (nm) 17 Days at 70 C

Sample	SiO₂	Na	Cs	Sr	Zn	Ln*	Fe
[illegible]	[illegible]	[illegible]	[illegible]	[illegible]	[illegible]	[illegible]	[illegible]
[illegible]	[illegible]	[illegible]	[illegible]	[illegible]	[illegible]	[illegible]	[illegible]

*[illegible]

the components of the glass, obtained by integration over the entire test period. The results in Table 2 show that while the thickness of the dissolved matrix layer is only one third of the layer from which sodium, strontium and cesium have been dissolved (i.e., the dealkalized layer) the other multivalent cations leach out at a rate which is lower by as much as a factor of 200 (in the case of iron in Sample 1) than the rate of matrix dissolution. Table 2 also shows the progressively lower effectiveness of the readsorption process in the case of lanthanum (particularly in Sample 2) and zinc as compared with iron. It should be noted that the calculated thicknesses of the dissolved and leached layers at the end of the test are still small when compared with the average grain radius of 150 μm.

Since the rate of release of the lanthanides, zinc and iron is lower than congruent dissolution, it is expected that their concentration is increasing in the dealkalized layer. This process cannot go on indefinitely, and when steady state is reached and the dealkalized layer stops thickening, the leach rate of these ions will show an increase to a level comparable to the product of the matrix dissolution rate and their loading level.

Since at the end of the test period with Samples 1 and 2 the surface layer was still growing, it was attempted to test whether a renewed increase in leach rates of multivalent ions can be detected by using a thorium-containing sample with a much lower chemical durability in order to shorten the time scale of the experiment. The composition of this glass is listed in Table 1, the leaching rates of its components are plotted against time in Fig. 3, and equivalent layer thicknesses are given in Table 3.

According to the data in Fig. 3, the sodium leaching rate decreases as t⁻ᵅ, with α very close to one. According to Table 3, by the end of the third day of the test the thickness of the dealkalized layer reaches 120 μm, which constitutes a substantial fraction of the macroscopic radius of the sample, which is 3 mm. (Sample 3, unlike Samples 1 and 2, has not been crushed into powder.) The changes occurring at this point should be associated with completion of the rapid buildup of the surface layer rather than complete dealkalization of the glass. The rate of silica dissolution during Stage I, i.e., the first 3 days, has decreased slowly (α ≈ 0.5), while the initial rate of the thorium leaching has been close to that of SiO₂ during the second and third day, indicating readsorption in the growing surface layer.

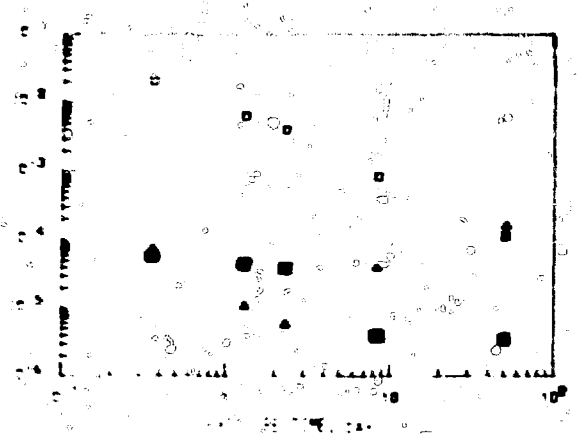

Fig. [illegible] ● SiO_2, [illegible] ▲ [illegible]

TABLE 3

Equivalent Thickness of Leached and Dissolved Layers (μm) Sample 3 (Th Glass), 70 C

Layer formed during	SiO_2	Na	Th
Stage I	[illegible]	[illegible]	[illegible]
Stage II	[illegible]	[illegible]	38.90

At the end of the third day (Stage II), the surface layer occupies a large part of the glass, and its further expansion is greatly slowed down. At this point the silica dissolution rate becomes much slower, as has been observed in alkali-rich silicate glass.[7] At the same time, thorium begins to leach away at a progressively increasing rate. After 50 days, more than 2% of the thorium initially present in the glass has already passed into the solution while the exposed silica skeleton remains almost intact. Since the leaching rates of SiO_2 and sodium continue to go down during Stage II, the renewed rise of the leaching rate of thorium cannot be attributed to a simple rupture of the surface layer. Thorium can be expected to resemble closely the chemical behavior of the other actinides, e.g., plutonium, in particular with respect to adsorption in the surface layer. The readsorption of various cations, based on the efficiency of their retention in the surface layer, is $Fe^{3+} > La^{3+} > Zn^{2+} > Sr^{2+}$. This result is supported by studies of Roman glass by Winter[12] which show that after prolonged corrosion and encrustation the content of silicon and aluminum in the dried crust is similar to that in the interior of the original glass, while sodium and potassium have completely disappeared from the crust. On the other hand, the crust becomes greatly enriched in divalent ions, according with the order $Mg^{2+} > Fe^{2+} > Ca^{2+}$. Both these series of results show an excellent agreement with the order of charge densities Z/r which are shown for the cations reviewed here in Table 4 together with the corresponding ionic radii.

This correlation, although based at present on a limited number of cations studied so far, indicates that cations with charge densities higher than 20 nm^{-1} can be expected to undergo certain amounts of readsorption and delayed leaching and that this effect is larger the higher the charge density. This indicates that the binding strength involved in the ion exchange and readsorption is controlled by the strength of the electrostatic interaction or polarization between the cation and the oxygen ion of the dealkalized $Si-O^-$ groups of the surface layer. Pure geometric considerations may also be important, as indicated by the fact that the loose structure of the dealkalized layer of the low-silica Sample 1 displays stronger readsorption of lanthanum and zinc than the more rigid surface layers of high-silica glasses such as Sample 2, where the size of the adsorption may be determined by the radius of the cavity vacated by the Na^+ ion, which has a radius of 0.097 nm. Finally, Pu^{4+} ($r = 0.093$ nm, $Z/r = 43.0$ nm^{-1}) can be expected to resemble Th^{4+} ($r = 0.102$ nm, $Z/r = 39.2$ nm^{-1}) and therefore to be subject to a *delayed* release into the bath rather than a permanently suppressed leaching process, as demonstrated above in the case of Th^{4+}. The surface layer resembles a chromatographic column in its delaying capacity and selectivity.

TABLE 4

Crystal Radii and Charge Densities of Cations

Cation	Mg^{2+}	Fe^{2+}	Ca^{2+}	Fe^{3+}	Ce^{4+}	Nd^{3+}	La^{3+}	Ce^{3+}	Zn^{2+}	Sr^{2+}
[illegible]	0.066	0.074	0.099	0.064	0.092	0.0995	0.1016	0.1034	0.074	0.112
[illegible]	30.3	27.0	20.2	46.9	43.5	30.2	29.5	29.0	27.0	17.9

CONCLUSIONS

The results presented here demonstrate the vital importance of understanding the formation processes and the chemistry of the dealkalized surface layer in order to make long-time predictions of the corrosion resistance of glasses loaded with radioactive waste elements. The results show that in high-silica glasses, the surface layer is less porous and the glasses have a much better chemical durability than low-silica glasses. The formation of the surface layer can occur over a prolonged time, particularly in high-silica glasses. However, it is important to attempt to carry out leaching tests for the longest possible periods relative to the time of surface layer formation. One reason for this requirement is the need to establish the stability of the layer against excessive stress and cracking. Another reason, based on this study, is the fact that as expansion slows down and the surface layer becomes saturated with respect to adsorbed multivalent cations, the observed leaching rates of such cations will drastically increase to catch up with the rate of matrix dissolution. Another requirement for the development of reliable test procedures is for such tests to include monitoring of the rates of dissolution of all the important elements of the glass structure. In particular, the leaching of alkali metal ions should be monitored as a guide to the evolution of the surface layer, and the silica matrix dissolution should be determined as a measure of the saturation of this layer and as a more realistic indicator of long-term removal of less mobile species.

REFERENCES

1. R. J. Charles, *J. Appl. Phys.* 29: 1549 (1958).
2. M. A. Rana and R. W. Douglas, *Phys. Chem. Glasses*, 2: 179 (1961).
3. L. Holland, *The Properties of Glass Surfaces*, Chapman and Hall, London, 1966.
4. L. L. Hench, *J. Non-Cryst. Solids*, 25: 343 (1977).
5. G. Johansson, B. Karlberg, and A. Wikby, *Talanta*, 22: 953 (1975).
6. T. M. M. El-Shamy, *Phys. Chem. Glasses*, 14: 1 (1973).
7. R. W. Douglas and T. M. M. El-Shamy, *J. Am. Ceram. Soc.*, 50: 1 (1967).
8. J. E. Mendel et al., *Annual Report on the Characteristics of High-Level Waste Glasses*, Battelle, Pacific Northwest Laboratories BNWL-2252 (1977).
9. D. Hubbard, E. M. Krumrine, and R. Stair, *Trans. Am. Geophys. Union*, 37: 767 (1956).
10. A. Barkatt, E. N. Boulos, R. P. DePaula, O. H. El-Bayoumi, N. Lagakos, P. B. Macedo, C. T. Moynihan, S. M. Rekhson, and J. H. Simmons, in Proceedings of *High-Level Radioactive Solid Waste Forms*, Denver, NUREG/CP-0005, National Technical Information Service, Springfield, VA, 1979.
11. T. M. M. El-Shamy and R. W. Douglas, *Glass Tech.*, 13: 77 (1972).
12. O. Winter, *7th International Congress on Glass, Part II*, 2, No. 229, Brussels, 1965.
13. *CRC Handbook of Chemistry and Physics*, R. C. Weast (Ed.), 58th ed., CRC Press, Cleveland, 1977.

CHEMICAL DURABILITY AND CHARACTERIZATION OF NUCLEAR WASTE FORMS IN A HYDROTHERMAL ENVIRONMENT

J. W. BRAITHWAITE and J. K. JOHNSTONE
Sandia Laboratories, Albuquerque, New Mexico

ABSTRACT

The chemical durability of a simulated copper borosilicate waste glass and titanate waste ceramic has been studied in hydrothermal environments which could possibly be encountered in a bedded salt or sub-seabed waste isolation repository. The major parameters investigated which affect matrix corrosion and cesium solubilization include solution saturation and equilibrium phenomena, solution composition (especially the Mg^{+2} ion concentration), pH, particle size, temperature, and time.

INTRODUCTION

The nuclear waste form and its encapsulating canister comprise the initial barrier to radionuclide dispersion in any waste repository. The high temperature durability of the waste form is important if the canister fails before the end of the period of high thermal output. If a canister can survive this thermal period, as current predictions indicate possible,[1] then the durability problem is reduced significantly because only slow low temperature leaching and corrosion processes will occur. However, if it is assumed that a canister is used which has a very short (less than 100-year) lifetime, then the chemical durability of the waste form in both high and low temperature isolation environments should be characterized.

Several deep geologic media are being investigated at Sandia Laboratories as potential repositories for high-level nuclear waste. These include bedded salt, sub-seabed sediments, and shale/tuff. For the first few hundred years of isolation, a unique hydrothermal environment may exist in either the bedded salt or sub-seabed waste repositories. The maximum interface temperature in either repository will be limited to 200 to 250°C and the lithostatic or hydrostatic pressure will be sufficient to prevent water vaporization. Brine intrusion into a bedded salt isolation site is not probable, but possible, whereas seawater will definitely saturate the sediments in a seabed repository. An in-depth description of possible early disposal environments for a bedded salt formation in southeast New Mexico and for the sub-seabed sediments in a mid-plate gyre region of the deep North Pacific was given in a previous paper.[1] A site-specific study has been undertaken to assess the durability of two candidate waste forms in the hydrothermal environments possible in both bedded salt (Waste Isolation Pilot Plant or WIPP) and the sub-seabed sediments. The results of the first phase of this study will be presented in this paper.

EXPERIMENTAL

The waste-form matrices which were evaluated included a copper borosilicate glass (76-199) obtained from the Battelle, Pacific Northwest Laboratory and a titanate ceramic which was fabricated and hot-pressed at Sandia. The glass was annealed and tested in both the unloaded and loaded state. The loading was accomplished by adding a simulated Barnwell chemical plant fission product oxide waste to the 76-199 frit before melting. Overall glass–waste composition was 30% waste oxides, 37% SiO_2, 9.8% B_2O_3, 8.4% Na_2O, 2.1% K_2O, 2.1% CaO, 6.3% TiO_2 1.1% Al_2O_3, and 3.1% CuO. The titanate waste ceramic was also fully loaded containing 25 wt.% of this simulated waste, 62.9% TiO_2, 2.1% Si, and 10% Zeolon 900.

Samples of these waste forms were exposed to simulated repository hydrothermal environments in autoclaves for periods of one week to three months. The majority of the experiments were conducted at 250°C and 16.5 MPa (2400 psi) in gold capsules (9.5 mm and 12.7 mm OD) containing small bulk waste form samples (3 mm cubes weighing 20 to 60 mg) and the desired solution (0.5 to 2 ml). A few experiments were also done in static 1-liter and stirred 1-gal stainless steel (deionized water tests only) and Hastelloy C-276 autoclaves when a large solution excess was desired.

Four leach solutions were used: (1) deionized (DI) water; (2) a high Mg^{+2} (35,000 ppm) saturated salt brine; (3) a saturated NaCl brine containing low Mg^{+2} (10 ppm); and (4) seawater. The seawater was considered to be a high Mg^{+2} (1,270 ppm) unsaturated salt brine. The first two brines are representative of possible solutions which may be encountered in WIPP environments. The composition, significance, and origin of these brines are given in Ref. 1. All four solutions had an initial pH near neutral. In addition to variable amounts of solutions, crushed bedded salt was added to some tests to better simulate actual emplacement conditions. It should be noted that one possible effect that is not being accounted for in these simulation experiments is that of radiation and radiolysis products of the brines. An effect on waste form durability could result because radiation will change the solution chemistry by increasing acidity and solution oxidizing potential.[1] This radiation effect was studied at 90°C; the results will be published at a later date.

Because of the complexity of the waste form solution interactions observed in this study and those recently documented,[2-4] it was felt that a combination of overall weight loss measurements, solution analyses, and product layer characterization were all needed to begin to assess waste form durability. Upon completion of each test, the waste form sample was dried and weighed to determine total weight loss. Typically, with the glass frit and glass waste samples, a distinct, friable, visually identifiable, alteration product or gel layer had formed on the reacting sample. This layer would often spall off after the sample was dried, or it could easily be removed mechanically. This removal was done, if possible, before the final weight was measured since the weight loss will be used as a measure of waste form alteration or matrix reaction.

The extent of loaded waste form leaching was defined as the quantity of Cs^+ and Sr^{+2} which was solubilized. The leach solutions were analyzed by atomic absorption spectroscopy for cesium in every case and for strontium, sodium, copper, and titanium on selected samples. The sodium, copper, and titanium analyses can be used as another gross indicator of matrix stability. Additionally, the final solution pH values of most solutions were measured.

Selected leached samples were mounted, cross sectioned, and examined both visually and by scanning electron microscope (SEM). Crystallinity and phase identification of the glass gel layers were attempted using standard X-ray diffraction techniques.

RESULTS AND DISCUSSION

Extraction of ions from the matrix could occur for a number of constituents at localized interior regions of a reacting particle where the solution chemistry is different from the bulk solution. Following diffusion of the ions outward, the formation of significant solid alteration products (precipitates, crystalline mineral assemblages, amorphous surface layers, etc.) or even sorption onto silica-gel layers could occur. The intrinsic leaching reaction would thus be masked, and the extent of detectable solubilization or apparent extent of leaching would be much lower than the actual release of the radionuclide from the original waste form matrix. These precipitation effects have been observed by other researchers who are studying the durability of a simulant zinc borosilicate waste glass at 300 to 350°C (Refs. 2 and 3). The formation of these secondary assemblages complicates the durability investigator's problems, but from a risk assessment point of view, their formation is desirable because the end result is a lack of significant solubilization of most radionuclides. The leach data given herein should not be used to calculate leach rate expressions because, as will be shown later, the time dependency is complex, and the necessary kinetic experimentation and modeling have not been completed.

The extent of matrix alteration (as measured by weight loss) along with cation solubilization results for the glass frit, the glass waste, and the titanate waste are given in Tables 1 to 3, respectively. Generally, the initial solution volume to sample surface area ratio used was from 2 cm to 5 cm. Significant deviations from both this ratio and the standard 3 mm cube sample size along with additional experimental observations are given in the "Comments" columns.

TABLE 1

Matrix Alteration and Cation Solubilization After Leaching 3 mm Borosilicate Glass Frit Cubes at 250°C and 17.9 MPa

Leachant	Time, days	Altered, %	Solubilized, %		Comments
			Na	Cu	
D.I. water	79	96	94	0.5	Final pH = 9.5 Solution to solid = 130 cm
D.I. water	7	23	20	L*	
NaCl brine	7	8		L	
NaCl brine	7	3			Solution to solid = 1 cm
Mg^{+2} brine	7	13		8	

*L denotes concentration less than detection limit.

Alteration Characteristics

The weight loss measurement used is a good indicator of matrix alteration because congruent matrix dissolution is

TABLE 2

Matrix Alteration and Cation Solubilization After Leaching 3 mm Copper Borosilicate Glass Waste Cubes at 250 C and 17.9 MPa

Leachant	Time, days	Final pH	Altered, %	Solubilized, % Cs	Sr	Cu	Comments
D.I. water	79	7.7	75	11.7	2.5	0.3	Solution to solid = 340 cm Na = 68 6 mm cylinders
D. I. water	14	9.2	5	1.1	1	1	
NaCl brine	14	7.5	12	3.9			200/270 mesh Solution to solid = 0.1 cm
NaCl brine	14	6.8	3	1.7			
NaCl brine	90	7.3	13	1.3			
Mg^{+2} brine	14	4.5	12	21.0			200/270 mesh Solution to solid = 0.1 cm
Mg^{+2} brine	14	4.5	10	5.0			
Mg^{+2} brine	90	3.9	50	4.5			
Seawater	7	4.3	15	17.0	4.8	0.7	
Seawater	90	5.0	49	8.4			
pH 1 H_2SO_4	14	1.8	12	6.3			
pH 1 saturated NaCl	14	1.9	3	1.7			
pH 12 NaOH	14	10.2	3	1.4			
pH 12 saturated NaCl	14	10.4	1	1.1			

not occurring. Therefore, accurate detection of changes in the matrix forming constituents, such as copper and titanium, is very difficult. A portion of this difficulty arises because of the previously mentioned formation of alteration and precipitation products. For example, copper could be detected only in the low pH Mg^{+2}-containing brines, and titanium was not detected in any of the titanate waste leach solutions. Nevertheless, observable weight changes occurred in almost every waste form sample leached.

Generally, the fraction of the glass frit, glass waste and titanate waste matrices which were altered or corroded during hydrothermal exposure increased as the solution salinity and/or sample surface area to solution volume ratio decreased. It is suggested from this result that reaction product saturation or equilibrium effects are important. Different dissolved products may be causing this effect in the various brine solutions for each waste form. For example, the alteration rate of glasses might be strongly influenced by the extent of saturation of sodium silicate or silicic acid in solution.

The retarding effect of increased solution salinity on alteration rates of the glass waste was observed at pH 1 and pH 12, but not in the near neutral brine solutions. This insensitivity might result because of the low alteration rates for the glass–waste in brine solutions compared with those of the glass frit. That is, the addition of waste simulant to the glass frit generally improved the alteration resistance of the frit. It was observed that thicker gel layers formed on equivalently altered glass–waste particles than on glass frit particles. A greater dissolution rate of the glass frit silica gel layer caused this difference in thickness. The difference in gel layer corrosion could be the result of the formation of a greater quantity of insoluble alteration products in the highly loaded glass waste. The thicker gel layer would be a more protective barrier by more effectively limiting the diffusion of both reactants and products to the reaction interface.

The retarding effect of lower solution volume to exposed sample surface area ratios on alteration rate was shown in the particle size data presented in Table 2. The alteration rate should be a function of the exposed surface area (particle size) since these reactions are heterogeneous. However, the alteration rate was not proportional to the exposed area by an order of magnitude probably because of the dominance of an equilibrium back reaction which occurred during alteration of the small 200/270 mesh particles.

The significant effect of magnesium content in the brines on alteration rate will be discussed in the next section. An increase in leaching time increased the extent of alteration of all waste forms in all cases, whereas the addition of excess salt to the saturated brine experiments had little effect on alteration rates.

Cation Leaching

The majority of the following discussions will center on cesium extraction. The leach rate of cesium is apparently the highest of the radionuclides, and most simple cesium compounds are soluble in solutions over very wide pH ranges. Generally, as can be seen from the data in Tables 2 and 3, cesium is indeed leached from the glass and ceramic samples and remains solubilized. The fraction of cesium extracted is less than the fraction of the waste form which is altered into a gel or product layer which is consistent

TABLE 3

Matrix Alteration and Cation Solubilization After Leaching 3 mm Titanate–Waste Ceramic Cubes at 250°C and 17.9 MPa

Leachant	Time, days	Final pH	Altered, %	Solubilized, %		Comments
				Cs	Sr	
D.I. water	90	10.3	10	4		
D.I. water	14	8.3	4	0.4	L	6 mm cylinder Solution to solid = 140 cm
NaCl brine	90	5.8	2	5		
Mg^{+2} brine	90	6.7	2	4		
Seawater	7		0	1	0	

with the observations which follow. The response of the polyvalent cations, like strontium or matrix constituents copper and titanium, is different and more complex than that for cesium. The leachabilities reported for cesium should even be labeled "apparent" because some cesium-containing minerals have been identified following the previously mentioned 300°C hydrothermal treatment of a loaded zinc borosilicate glass.[3] A number of the leach solutions will be analyzed using an emission spectrophotometer for dissolved silica, molybdenum, iron, uranium, boron, titanium, copper, strontium, cesium, and gadolinium in an effort to better quantify and broaden the understanding of the leaching mechanism.

The effects of a number of leach parameters on cation leachability are discussed in the following paragraphs.

Effect of pH and Leachant Composition. In general, the ability of a solution to extract cesium increased in the order: DI water ≃ NaCl brine < $MgCl_2$ brine < seawater. A saturation or equilibrium effect of reaction products, as was discussed previously in the alteration section, is also applicable to the leaching of cesium from the loaded wastes. That is, as the solutions become more and more saturated by increasing the extent of reaction or reducing the original solution to solid ratio, the rate of sodium, cesium, and strontium leaching decreases. Lower pH value solutions can promote higher cation solubilization if the solution is unsaturated. The solution saturation effect, however, is apparently greater than the low pH effect because low pH can be counterbalanced by solution saturation. For example, a pH = 1 solution produced a high alteration and cesium extraction, whereas a saturated NaCl, pH = 1 solution produced an alteration and cesium extraction comparable to the more neutral pH saturated salt solutions. Alterations and cation extractions are possibly higher in the Mg^{+2} containing brines because of two reasons: (1) a lower solution pH which results from the precipitation of $Mg(OH)_2$ or a Mg-oxysulfate phase at high temperatures, producing HCl (Refs. 1 and 5), and (2) magnesium appears to promote the glass alteration or devitrification reaction. Magnesium has been identified by emission spectrophotometer analysis to be a major component of reaction product layers formed in magnesium-containing brines. The seawater alterations and extractions are then highest because of a lower pH, solution unsaturation, and Mg^{+2} content. The role of Mg^{+2} in leaching is being studied in more detail presently. Little or no strontium was detected in the DI water or NaCl brines after leaching. The high Mg^{+2} brines (lower pH) contained strontium from the glass waste but little or none from the titanate–waste. The additions of crushed salt to saturated brines resulted in only minor changes in cation solubilization.

Effect of Particle Size. An increase in the rate of cesium extraction was detected when the glass–waste particle size was decreased from 3 mm cubes to 200/270 mesh powder (Table 2). However, this increase was orders of magnitude lower than that which should have resulted if the rate were inversely proportional to either the particle size (linear kinetics) or the square of particle size (parabolic or diffusion kinetics). This insensitivity resulted because the leach data was not collected before important kinetic parameters, such as pH, degree of solution saturation, and particle agglomeration could change significantly. In order to alleviate this problem, two well agitated experiments were performed in large excess of DI water using two different sized glass–waste particles. Solution samples were withdrawn at various times and the following *initial* cesium leach data resulted: 4.0%/day for 3 mm particles and 0.4%/day for 6 mm particles. As can be seen, a definite size effect exists. However, these initial leach rates again do not vary linearly or with the square of particle size. Thus, further insight into the rate controlling steps has not been provided.

Effect of Time. In an excess of DI water, the fraction of cesium extracted from the glass–waste increases with increasing time. The rate, however, decreases with increasing time. For example, a leach rate of 1.7%/day after one day decreases to 0.7%/day after 9 days and to 0.3%/day after 42 days when leaching 3 mm cubes at 250°C in DI water. This decrease in rate is consistent with diffusion controlled parabolic kinetics under the constant solution chemistry and surface area conditions of the above tests. Photomicrographs and electron microprobe mapping of elemental distributions of cross-sectioned samples of leached frit and glass–waste reveal a classical unreacted shrinking core alteration-leaching mechanism. Diffusion of a reactant or product through the gel layer would then control the rate. The shrinking reaction interface will produce a decrease in area when the total fraction altered exceeds 30%, and a deviation from the above simple parabolic kinetics will result.

This same diffusion controlled solubilization mechanism, however, is not applicable when the leaching is not done in an excess of solution. Under these low solution-surface area conditions, the amount of cesium in solution remains constant or decreases after a short period of time.

This observation was also made by McCarthy et al.[3] and was attributed to the steady-state precipitation of a cesium-containing phase after the concentration reached a saturation level. To check the validity of this proposal under our study conditions, a number of long-term, sampled leach experiments are in progress.

Effect of Temperature. A series of stirred experiments were conducted in an excess of DI water at 150, 200, and 250°C in order to find the temperature coefficient or activation energy for initial cesium release. The resulting data were too scattered to calculate an accurate coefficient, but the trends indicate that a very low activation energy (2 to 5 Kcal/mole) will result, which is also consistent with a solution diffusion controlled process and agrees well with that reported by the Battelle researchers of 4.4 Kcal/mole (Ref. 2).

Product Characterization

As discussed in the previous section, a shrinking unreacted core was evident when electron microprobe elemental maps and photomicrographs of corroded glass frit and glass waste cross-sectioned samples were observed. A very definite reaction zone at the inner surface was apparent along with another zone of reaction on the outer surface. Additionally, significant gel layer cracking occurred in the glass samples exposed to the DI water leachant which appeared to fill in with a different reaction product. An interpretation of these results will be possible only after the electron microprobe quantitative analysis results are complete.

The original glass frit and glass–waste were amorphous to X-ray diffraction analysis. The gel layers on selected glass samples were removed and also subjected to X-ray diffraction analysis. Significant devitrification of the glasses had occurred, but no crystalline phases including those identified by others[2,3] ($NaFeSi_2O_6$, weeksite, or hydroxyapatite) were found in this study. Also, the crystallization which occurred on the interior surfaces of the gold tubing in the studies by McCarthy et al.[3] was absent on our gold containers. Both of these discrepancies probably resulted because of the lower temperature used in this study (250 versus 300 and 350°C).

CONCLUSIONS

1. The leaching and devitrification of a simulated copper borosilicate waste glass with possible hydrothermal repository environments appear to be rapid enough that these conditions should be avoided if the waste form is to be an effective barrier to release.

2. The titanate–waste ceramic showed better resistance to attack than the glass–waste. However, further extensive study is needed before its suitability for withstanding hydrothermal environments could be guaranteed.

3. The ability of a solution to alter the glass–waste matrix and extract cesium increased in the order deionized water ≃ NaCl brine < $MgCl^2$ brine < seawater.

4. Solution saturation and equilibrium phenomena appear to be important matrix alteration and cesium solubilization parameters. Actual repository conditions of low flow velocities and low solution to solid ratios would, therefore, be helpful in improving waste form durability.

5. Lower pH values lead to increased cation solubilization.

6. The composition of the brine leachants is of major importance with the Mg^{+2} ion probably playing the key role.

ACKNOWLEDGMENT

This work was supported by the U. S. Department of Energy under contract DE-AC04-76DP00789.

REFERENCES

1. J. W. Braithwaite and M. A. Molecke, High Level Waste Canister Corrosion Studies Pertinent to Geologic Isolation, *Nucl. Waste Management and Tech.*, Vol. 1(1), (1979).
2. J. H. Westsik and R. P. Turcotte, *Hydrothermal Reactions of Nuclear Waste Solids, A Preliminary Study*, DOE Report PNL-2759, Pacific Northwest Laboratory, 1978.
3. G. J. McCarthy et al., *Reaction of Water with a Simulated High-Level Nuclear Waste Glass at 300°C, 300 Bars*, DOE Report SA-35, Rockwell Hanford Operations, 1978.
4. J. G. Moore, H. W. Godbee, and A. H. Kibbey, Leach Behavior of Hydrofracture Grout Incorporating Radioactive Wastes, *Nucl. Technol.*, 32: 48 (1977).
5. J. L. Bischoff and W. E. Seyfried, Hydrothermal Chemistry of Seawater from 25° to 350°C, *Amer. J. Sci.*, 278: 836 (1978).

HYDROTHERMAL STABILITY OF SPENT FUEL AND HIGH-LEVEL WASTE CERAMICS IN THE GEOLOGIC REPOSITORY ENVIRONMENT

GREGORY J. McCARTHY, WILLIAM B. WHITE,* SRIDHAR KOMARNENI, BARRY E. SCHEETZ,
W. PHELPS FREEBORN and DEANE K. SMITH*
Materials Research Laboratory and *Department of Geosciences, The Pennsylvania
State University, University Park, PA

ABSTRACT

The stability trends for four simulated waste forms (spent fuel, a reference glass, a supercalcine ceramic and a coated ceramic) under hydrothermal conditions (100 to 300°C; 400°C for the coated ceramic; 300 bars) with solutions alone and in contact with basalt and shale are summarized.

INTRODUCTION

Terminal storage in underground rock formations is presently considered the most feasible method of isolating high-level nuclear power plant wastes from the biosphere. One of the many factors that will need to be considered in geologic repository design is the effect of the heat produced by radionuclide decay. Heat would have certain effects on the physical properties of the repository rock and, if combined with the encroachment of water pressurized by the rock overburden, would promote substantial chemical reactions within the immediate repository.[1,2] This combination of hot and pressurized water would give hydrothermal conditions.

The occurrence of hydrothermal conditions could have various ramifications for nuclear waste isolation. If containment of the wastes is maintained throughout the thermal period, then the solutions would only alter the nearby rock, overpack, etc. However, if the hydrothermal solutions contact the waste due to breach of containment, alteration of the waste and interaction with the repository environment could take place.

Both the rate and the products of these interactions are, of course, strongly temperature dependent, so increases in the volume of the waste and/or the repository can be adopted to reduce temperatures. But, as the authors have pointed out,[1,2] this may not be necessary if the alteration–interaction products are themselves suitable "source terms."

In this paper we summarize the stability trends noted over the past 2½ years of waste–rock interactions research for three potential waste forms in the presence of hydrothermal solutions alone and of solutions in contact with repository rock. The experiments are closed systems. Closed system experiments are ideal for exploring the reactivity of solid–liquid systems and establishing the direction of thermodynamic equilibrium. The experiments simulate the case where superheated water is admitted through a breached canister and reacts with the waste in a region where the chemistry of the waste initially dominates the course of the reactions. In time, the surrounding rock dominates the chemistry, so a second type of experiment includes suitable amounts of repository rock in the sealed system.

EXPERIMENTAL

The experimental procedures are described in detail elsewhere.[2-5] Run conditions included temperatures from 100 to 300°C at 300 bars pressure. Spent fuel and two ceramic waste forms, a reference glass (PNL-76-68) and a supercalcine ceramic (SPC-4), were treated under these conditions with deionized water, an artificial Hanford groundwater and a bittern brine. The waste forms were all nonradioactive simulations. The bittern brine was a Ca–Mg–K–Na–Cl solution provided by the United States

Geological Survey. Details of the compositions of waste forms and solutions are found in Refs. 2–6.

A fourth waste form was included in several experiments. This was a multibarrier product consisting of supercalcine ceramic (SPC-2) disc pellets coated first with pyrolytic carbon and then with Al_2O_3 (Refs. 7 and 8). The durability of this coated ceramic was tested at 300 and 400°C.

The stability trends based on the research detailed in Refs. 2 to 6 and 9 to 12 are summarized in Tables 1 and 2. The results pertain to the temperatures given. In Table 1 it is seen that the bittern brine attacks spent fuel and glass at 200°C and supercalcine ceramic at 300°C with the effect that major amounts of numerous hazardous elements (or their analogs, e.g., Ln for Am, Cm) are released into solution.[2,6] The results indicate that for any of these waste forms, hydrothermal conditions should be avoided by lower thermal loadings of the waste and/or the repository or that these forms should be protected from contact with hydrothermal brines throughout the thermal period.

TABLE 1

Hydrothermal Reactivity Trends in Bittern Brine

Waste form	Alteration of solid	Elements in solution
Spent fuel, 200°C		Major* Cs, Sr, Ln,† Ba, Rb, U Minor* Mo
Reference glass (PNL-76-68), 200°C	Not crystallized Solid intact	Major Cs, Sr, Ln, B, Rb, Ba, Zn Minor U, Mo, Si, Ni Trace* Fe
Current crystalline ceramic (SPC-4), 300°C	Several minerals altered New phases formed Some are stable	Major Cs, Sr, Ln, Rb, Ba, Ni Minor Cr, Si Trace Fe
Coated ceramic, 400°C	Some recrystallization of Al_2O_3 outer coating	No detectable Cs or Rb

*Major indicates >10% of the amount originally in the solid; minor, 0.5 to 9.0%; and trace, <0.5%.

†Ln is lanthanides (La, Ce, Pr, Nd, Sm, Gd, Y).

In experiments lasting up to a month at 300 and 400°C, the coated ceramic showed no releases as evidenced by optical examination of the pellet and analyses of the contacting brines for two of the most easily extracted elements, cesium and rubidium.[11]

Table 2 summarizes the stability trends for the four waste forms in solutions typical of silicate rocks and in contact with basalts and shales. In these closed system experiments, the major phase in spent fuel, uraninite (UO_2), remained largely unaltered, but substantial amounts of the fission products cesium, rubidium, and sodium could be extracted by contacting solutions.[9] Trace levels of uranium were also taken into solution. When the solutions were also in contact with basalt or shale the extracted elements were "fixed" in solids by reaction to form the mineral-like phases pollucite and powellite.[1,2,10] Also, no detectable uranium was found in solution, so it appears that the low Eh (reducing) properties of basalt and other rocks would be a geochemical advantage in isolation of spent fuel and the other waste forms.[9]

The alteration of the reference glass in deionized water and a typical silicate groundwater at 300°C has already been reported in detail.[1–5] Yet, in the presence of low Eh

TABLE 2

Hydrothermal Reactivity Trends in Deionized Water and Silicate Groundwaters

Waste forms	Alteration of solid	Elements in solution	Waste-rock interaction effects
Spent fuel, 200°C	Uraninite (UO_2) Unaltered	Major* Cs, Rb, Mo Trace* U	Cs, Rb, Mo fixed by interactions UO_2 stable in low Eh solutions
Reference glass (PNL-76-68), 300°C	Complete	Major Na, B, Mo, Cr Minor* Cs, Si, Ni, Rb, Ca Trace U, Ln, Sr, Ba	Most elements in solution fixed by interactions New mineral-like phases
Current crystalline ceramic (SPC-4), 300°C	None†	Minor Na, Rb, Mo, Si Trace Cs, Sr, Ba, Ca	Released elements fixed by interactions Solid-solid interactions
Coated ceramic, 400°C	None	No detectable Cs or Rb	None

*Major indicates >10% of the amount originally in the solid; minor, 0.5 to 9.0%; and trace, <0.5%.

†Crystallinity of synthetic minerals enhanced; NCS phase crystallized.

[illegible] in contact with silicate rocks, waste–rock interactions could convert the glass–rock composite into a suite of stable mineral-like phases. Results to date with basalt and shale suggest that cesium and strontium are removed from the solution resulting from the interaction of water and glass by precipitation as phases related to the minerals pollucite and feldspar. For these two elements, the interaction products are less soluble than the original waste glass. Thus, it may not be necessary to lower waste loadings in glass to avoid the possibility of hydrothermal alteration, because the interaction products may not represent any loss of immobilization. However, considerably more experimental work is needed to establish [illegible]

Research in progress indicates a marked reduction of alteration crystallization rates in deionized water at 200°C (Ref. [illegible]). The seven major synthetic mineral phases in the supercalcine ceramic were not significantly reacted after 300°C deionized water treatments lasting up to six months. X-ray characterization indicated some enhancement in crystallinity and cation exchange among the phases. Similarly, an intimate mixture of the ceramic and basalt given the same treatments did not show any interaction discernable by X-ray diffraction.[9] Noncrystalline phases (constituting perhaps 5 to 10 vol.%) in the ceramic were crystallized by the hydrothermal solutions.[2]

Small amounts of a number of the elements in the ceramic were extracted by the hydrothermal solutions.[2] Using the same reasoning just discussed for glass, many of these elements could be fixed by interactions with the silicate repository wall rocks. Experiments to explore this question are not yet complete.

CONCLUSIONS

The experimental results indicate that with either the glass or the ceramic, the end result of hydrothermal conditions in the repository could be quite similar when viewed on the scale of the immediate repository. The glass could interact strongly with the silicate rocks to form mineral-like substances. The supercalcine ceramic could interact only slightly. In both cases, the resulting solutions could contain little of the radionuclides of concern.

The apparent stability of certain synthetic mineral phases in the ceramic holds considerable promise for the development of second generation waste forms tailored for long-term stability (i.e., very low releases) under even severe repository environments. Meanwhile it appears that coated ceramics could fulfill any systems requirements for an especially durable waste form.[11]

ACKNOWLEDGMENT

This research is supported by the U. S. Department of Energy through the Office of Nuclear Waste Isolation and Rockwell Hanford Operations.

REFERENCES

1. G. J. McCarthy et al., Interactions Between Nuclear Waste and Surrounding Rock, *Nature* 273, 216 (1978).
2. G. J. McCarthy, S. Komarneni, B. E. Scheetz, and W. B. White, Hydrothermal Reactivity of Simulated Nuclear Waste Forms and Water Catalyzed Waste-Rock Interactions, in Proceedings of *Scientific Basis for Nuclear Waste Management*, Boston, G. J. McCarthy (Ed.), Plenum, NY, 1979.
3. G. J. McCarthy and B. E. Scheetz, *Annual Progress Report, High Level Waste Basalt Interaction, February–September 1977*, DOE Report RHO-BWI-C-2[illegible], The Pennsylvania State University, May 1978.
4. G. J. McCarthy et al., *Simulated High Level Waste Basalt Interaction Experiments, Second Interim Progress Report*, DOE Report RHO-BWI-C-10, The Pennsylvania State University, Jan. 1978.
5. G. J. McCarthy, B. E. Scheetz, S. Komarneni, and D. K. Smith, *Reaction of Water with Simulated High Level Nuclear Waste Glass at 300°C, 300 Bars*, DOE Report RHO-BWI-C-[illegible], The Pennsylvania State University, October 1978.
6. W. B. White et al., *Reaction and Devitrification of a Borosilicate Nuclear Waste Storage Glass with Magnesium-Rich Brine*, DOE Report ONWI Sub. 78 E512-[illegible], The Pennsylvania State University, in press, 1979.
7. J. M. Rusin, M. F. Browning, and G. J. McCarthy, Development of Multibarrier Nuclear Waste Forms, in Proceedings of *Scientific Basis for Nuclear Waste Management*, Boston, G. J. McCarthy (Ed.), Plenum, NY, 1979.
8. J. M. Rusin, R. O. Lokken, and J. W. Wald, Characterization and Evaluation of Multibarrier Nuclear Waste Forms, in Proceedings of *Ceramics in Nuclear Waste Management*, Cincinnati, CONF-790420, U. S. Department of Energy, Technical Information Center, Oak Ridge, 1979.
9. B. E. Scheetz et al., *Simulated High Level Waste Basalt Interaction Experiments, Annual Progress Report*, DOE Report RHO-BWI-C-33, The Pennsylvania State University, November 1978.
10. S. Komarneni, B. E. Scheetz, and G. J. McCarthy, *Hydrothermal Interactions of Cesium and Strontium Phases from Spent Unreprocessed Fuel with Basalt Phases and Basalts*, DOE Report RHO-BWI-C-48, The Pennsylvania State University, January 1979.
11. G. W. McCarthy, Crystalline and Coated High-Level Waste Forms, in Proceedings of *High-Level Radioactive Waste Forms*, Denver, NUREG/CP-0005, National Technical Information Service, Springfield, VA, 1979.

DEVITRIFICATION AND LEACHING EFFECTS IN HLW GLASS—COMPARISON OF SIMULATED AND FULLY RADIOACTIVE WASTE GLASS

J. W. WALD and J. H. WESTSIK, JR.
Pacific Northwest Laboratory, Richland, Washington

ABSTRACT

[illegible]

INTRODUCTION

A [illegible] high-level radioactive wastes [illegible] 20 years [illegible] (HLW) [illegible]. This study describes work that was performed to assess the phase behavior and chemical durability of four waste glass compositions that were formed using actual high-level waste and to compare their [illegible] simulated nonradioactive glasses formed under identical conditions of time and temperature.

The four glasses examined in this study represent a range of compositional variations that are assumed to occur as a result of four different types of potential reprocessing techniques applied to high-level power reactor wastes. The principal differences between the four waste streams and the glass types developed to handle these particular waste types are summarized in Table I. While all four are borosilicate glasses, their exact compositions have been optimized for each waste type. The waste streams encountered differ from one another as a result of reprocessing variations, especially chemical additions.

The scope of this work involves the examination and characterization of waste glass products formed with fully radioactive, high-level nuclear waste. Of particular interest are the effects of high radiation field on the physical and microstructural properties of this waste type. Comparisons to nonradioactive glasses were made to answer the question as to whether a simulated waste glass product can typify a fully radioactive waste glass product.

The study of phase behavior through microstructural analysis was performed using these analytical methods: optical microscopy, X-ray diffraction, X-ray fluorescence, scanning electron microscopy (SEM), and electron microprobe analysis (EMP). The analysis of highly radioactive glass samples, although not altogether routine, was accomplished by conventional methods through the use of a shielded electron microprobe and remote metallographic equipment. Standard samples employed in the analysis related the radioactive samples to the nonradioactive counterparts. Detailed examination techniques of the nonradioactive samples have been described fully elsewhere[1] and will not be discussed here at any length.

EXPERIMENTAL

Full-Level Glass Preparation

The four high-level nuclear waste glass compositions examined in this study were prepared from a single batch of high-level power reactor fuel processed by the Purex method. Total burnup was approximately 28,000 MWD/MTM with a three-year hold time prior to reprocessing. The high-level waste was calcined to a powder prior to incorporation in the glass.

In order to account for the variations expected as a result of differences in the reprocessing techniques for the waste types studied, it was necessary to make nonradioactive chemical additions to three of the four glass

TABLE 1

Main Elemental Characteristics of Waste Glasses 72-68, 76-68, 77-107, and 77-260

Nomenclature	Principal characteristics
72-68	Clean waste (Zr [illegible]), high Zn glass [illegible]
76-68	High Fe, Na waste
77-107	High Na waste, high B glass [illegible]
77-260	High Gd, Na waste, glass [illegible] Ti, Cu

compositions. Table 1 highlights the basic differences between the four glasses studied which have waste loadings of approximately 30%. All nonradioactive chemical ingredients were added to the respective glass frits prior to entry into the hot cell. Glass frit calcine mixtures were mechanically blended before melting. Glasses 72-68, 76-68, and 77-260 were melted at 1050°C for 3 hr in 304L stainless steel crucibles, whereas glass 77-107 was melted at 1150°C for 3 hr in stainless steel prior to water quench. Each glass batch was broken out of its stainless steel crucible and crushed to a coarse particle size, divided into two smaller batches, placed into Al_2O_3 crucibles, and reannealed. The reannealing process consisted of heating all melts from 25°C to 1050°C at 250°C/hr, holding for [illegible] hrs, removing one batch of each composition for an air quench to 25°C, and crystallizing the remaining samples by cooling at [illegible]°C/hr to 25°C. Individual specimens were removed from each of the as-prepared and intentionally devitrified melts by core drilling approximately 0.25-in. diameter plugs.

Full-Level Glass Examination

The full-level glass samples were prepared for optical and microprobe examination using standard metallographic techniques. Nonradioactive glass samples of similar composition were prepared along with the full-level glasses to serve as standards for the analytical examination.

Cored samples of both as-prepared and devitrified HLW glass were leach tested in accordance with a long-term leach procedure based on the IAEA technique outlined by Hespe.[2] The technique involves the use of uniform size cylinders that are leached in deionized water at 25°C with weekly changes of leach solution. Elemental analysis of the leachate solutions was performed by radiochemical analysis techniques.

Simulated Waste Glass Preparation and Examination

Four simulated waste glass compositions were prepared concurrently with the full-level glass samples described above in order to relate their properties on a one-to-one basis. All simulated glasses contained nonradioactive compounds, with the exception of depleted uranium, and were prepared in identical fashion to those glasses prepared in the hot cell. With all operational parameters standardized, it was [illegible] the [illegible] properties [illegible]

A [illegible] PW-4 [illegible] and [illegible] simulated glasses [illegible] X-ray diffraction, optical [illegible] SEM [illegible] glasses.

Static leach tests were [illegible] on the [illegible] active glasses using the IAEA procedure described in the previous section as well as [illegible] polished surface [illegible] The latter leach test allowed [illegible] postleach glass surfaces as well as [illegible] leachate solutions over the [illegible] Coupled Plasma (ICP) technique.

RESULTS AND DISCUSSION

Devitrification Effects

X-ray diffraction analyses of the [illegible] glasses studied indicated the presence of crystalline phases in both the as-prepared and the intentionally devitrified [illegible]. The as-prepared glasses typically contain melt [illegible] such as RuO_2 or $NiFe_2O_4$, while the intentionally devitrified glasses contain crystallization products as well. Table 2 details the phases identified in the glasses studied. The compositions indicated reflect major constituents. Several minor contributors to true phase compositions are often observed.[1]

TABLE 2

Principal Crystalline Phases Observed in Devitrified Waste Glasses 72-68, 76-68, 77-107, and 77-260

72-68	76-68	77-107	77-260
RuO_2	RuO_2	RuO_2	RuO_2
$NiFe_2O_4$	$NiFe_2O_4$	$NiFe_2O_4$	$NiFe_2O_4$
Pd	Pd	Pd	Pd
CeO_2	CeO_2*	CeO_2*	CeO_2*
Zn_2SiO_4*		$CaMoO_4$*	$Gd_2Ti_2O_7$*
$SrMoO_4$*			$Ca_2Gd_8(SiO_4, PO_4)_6O_2$*

*Devitrification phase

Total crystallinity was measured by X-ray diffraction (using Al_2O_3-glass standard mixtures) and was found to vary significantly from glass to glass as well as from the as-prepared condition to the devitrified condition. Table 3 lists crystallinity measurements made on the four glasses studied.

TABLE 3

Total Crystallinity Measured by X-Ray Diffraction for Glasses 72-68, 76-68, 77-107, and 77-260

Glass	As-prepared, wt %	Slow-cooled devitrified, wt %
[illegible]	[illegible]	[illegible]
[illegible]	[illegible]	[illegible]
[illegible]	[illegible]	[illegible]
[illegible]	[illegible]	[illegible]

[illegible] HLW [illegible] simulated glasses [illegible]

[illegible] depletion of elemental species in the glass [illegible]. An example of this analysis for glass 72-68 is listed in Table 4. From analyses of this type elements [illegible]

TABLE 4

Glass Phase Analysis by Electron Microprobe for Full Level and Simulated Glass 72-68 (Percentage of Element Present)

	Si	K	Ca	Zn	Sr	Ru	Cs	Ce	U
Simulated									
As-prepared	12.1	0.2	1.4	17.6	0.4	0	1.6	3.0	12.3
Devitrified	12.9	0.08	1.5	11.3	0.5	0	1.5	2.9	9.8
Radioactive									
As-prepared	13.0	0.2	1.5	18.3	0.5	0	0.9	2.5	15.3
Devitrified	13.5	0.1	1.8	13.4	0.6	0	1.1	2.0	11.6

for the formation of crystalline phases can be inferred without specific X-ray diffraction analysis, and depletion of glass-forming elements can be related to possible decreased durability in a leaching environment.

It is clear from this analysis that the simulated and full-level glass compositions behave similarly. The absence of ruthenium from the glass phase (as RuO_2) is always observed in nonradioactive studies. Decreased levels of zinc and uranium are indicative of the formation of Zn_2SiO_4 and $Ca(UO_2)O_2$ in this glass composition. Microprobe [illegible] similar results, however [illegible] were not conclusive because [illegible] crystalline dispersions and [illegible] probe.

Leach Effects

The [illegible] leach tests indicate that [illegible] difference between the leach rates of [illegible] radioactive glass formulations. [illegible] glass leach rates of the four glasses based on their releases of cesium. These are average leach rates over an eleven-week period and are calculated using the equation

TABLE 5

Leach Rates of Waste Glasses Based on Cs, Sr, and Eu* (IAEA, 25°C)

	Cesium		Strontium, simulated	Europium, radioactive
	Simulated	Radioactive		
[illegible]	[illegible]	[illegible]	[illegible]	[illegible]
[illegible]	[illegible]	[illegible]	[illegible]	[illegible]
[illegible]	[illegible]	[illegible]	[illegible]	[illegible]
[illegible]	[illegible]	[illegible]	[illegible]	[illegible]
[illegible]	[illegible]	[illegible]	[illegible]	[illegible]
[illegible]	[illegible]	[illegible]	[illegible]	[illegible]
[illegible]	[illegible]	[illegible]	[illegible]	[illegible]
[illegible]	[illegible]	[illegible]	[illegible]	[illegible]

*[illegible]

$$\text{Leach rate } (g/(cm^2 \cdot d)) = \frac{A \times W}{A_0 \times SA \times t}$$

where A is the amount of the element or isotope released in the interval t, A_0 is the initial quantity in the glass, and W and SA are the weight and geometric surface area, respectively, of the glass samples. The release rates of ^{137}Cs from the fully radioactive glasses are the same as the release rates of elemental cesium from the simulated formulations of the same glasses. This comparison holds for both the as-prepared and the devitrified samples and strongly suggests that gamma radiolysis effects are not important in the leaching process.

Table 5 also shows that devitrification causes very small changes in leach rates for these glasses based on cesium, strontium, and europium. Previous studies on 72-68 and 76-68 glasses revealed that devitrification does increase the leach rates of these two glasses.[3,4] However, the devitrification in the earlier work was more extensive because it was

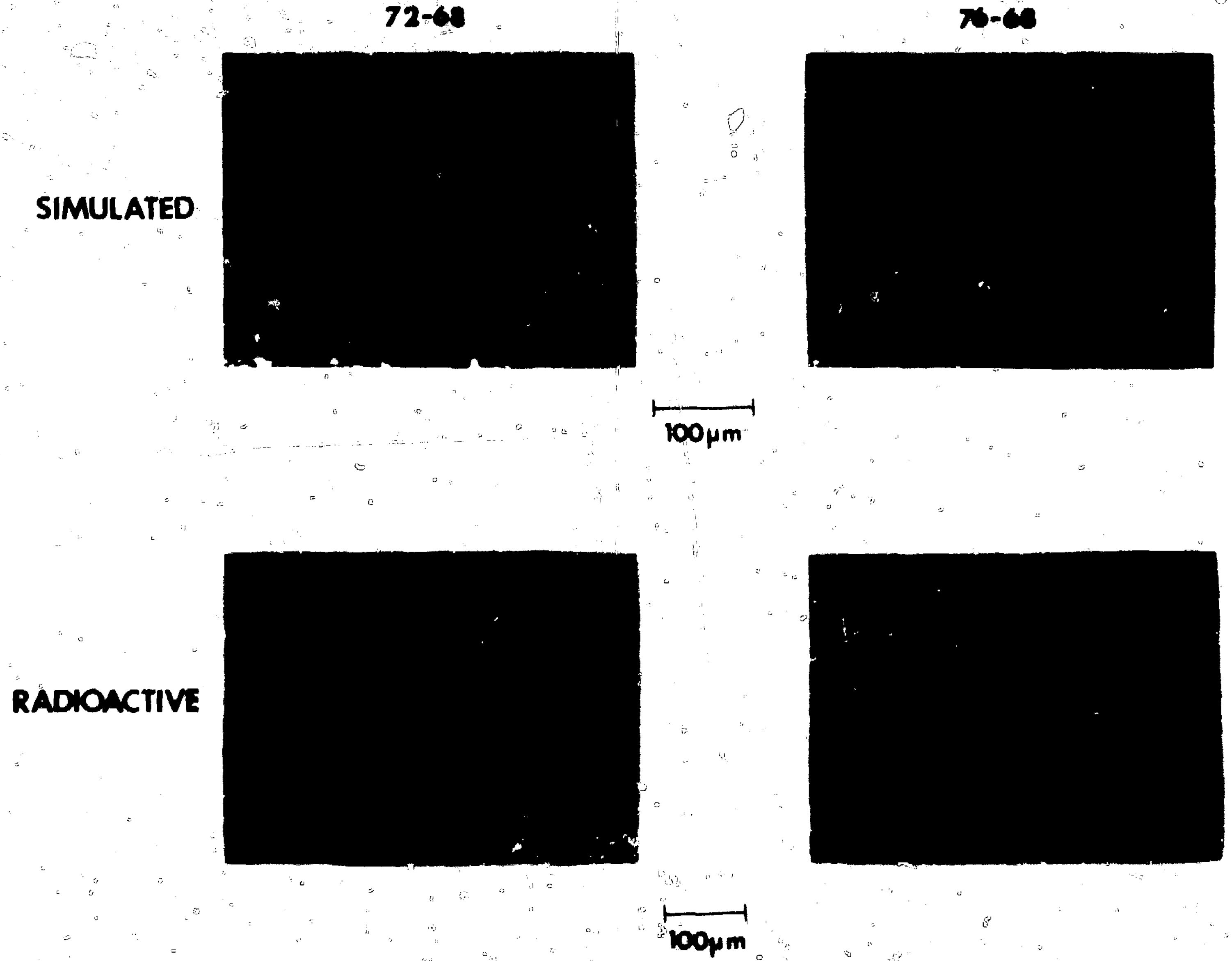
72-68
76-68
SIMULATED
RADIOACTIVE
100µm
100µm

Fig. 1 Microstructural characteristics of simulated and radioactive glasses 72-68 and 76-68 intentionally devitrified by slow cooling (6°C/hr) from the melt temperature.

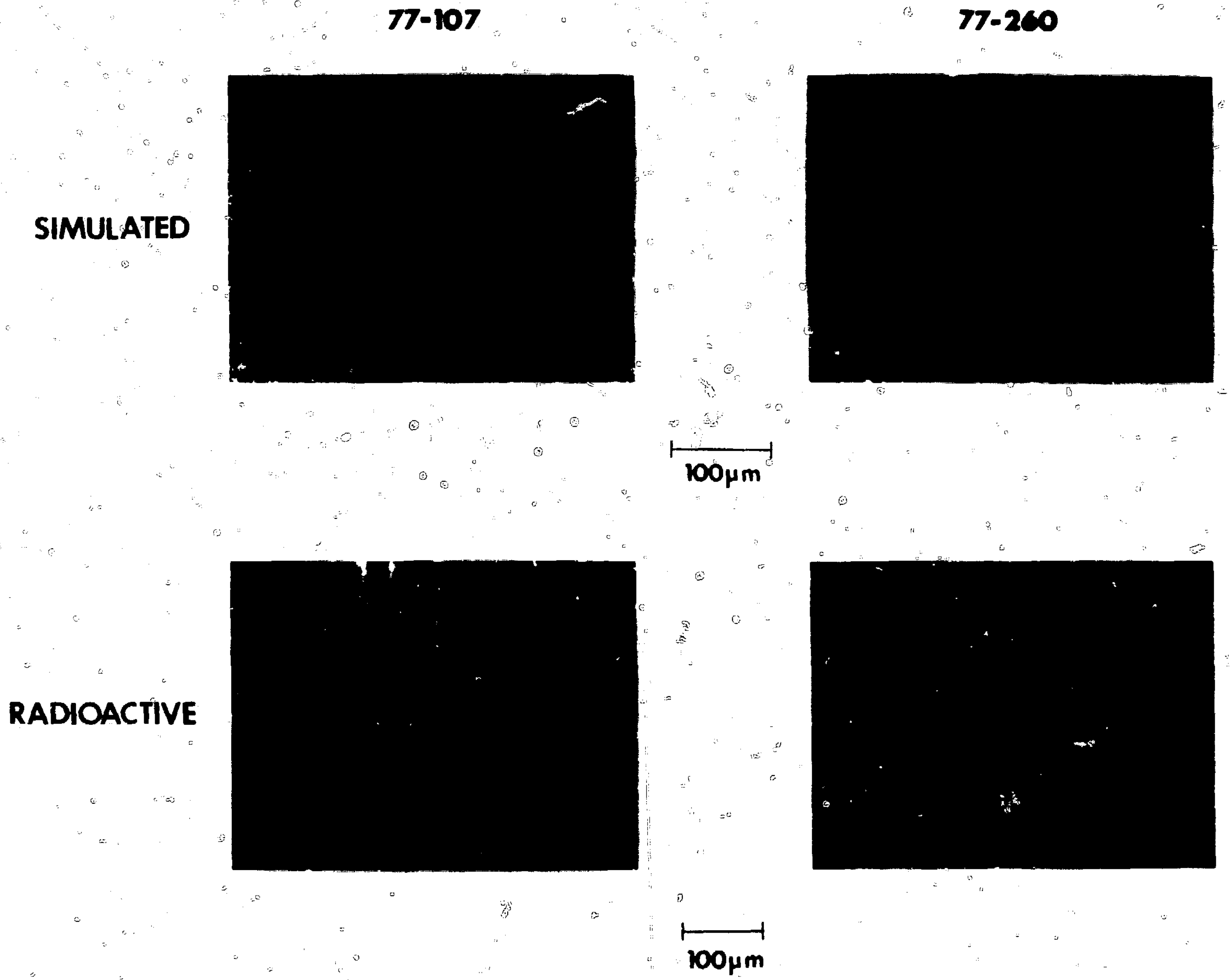
77-107
77-260
SIMULATED
RADIOACTIVE
100μm
100μm

Fig. 2 Microstructural characteristics of simulated and radioactive glasses 77-107 and 77-260 intentionally devitrified by slow-cooling (6°C/hr) from the melt temperature.

TABLE 6

Relative Releases of Elements from Nonradioactive Glasses* (1 Week, 75°C)

	Si	B	Zn	Na	Ca	Ba	Sr	Mo	U
72-68									
As prepared	0.2	0.2	0.2	1	0.3	0.2	0.2	0.1	0.01
Devitrified	0.2	0.2	0.2	0.7	0.4	0.2	0.1	0.1	0.01
76-68									
As prepared	0.03	0.03	0.5	0.2	0.1	0.03	0.02	0	0.01
Devitrified	0.02	0.02	0.07	0.07	0.2	0.02	0.01	0	0
77-107									
As prepared	0.2	0.2	0.5	0.6	0.3	0.1	0.2	0.1	0.01
Devitrified	0.06	0.6	0.5	0.3	0.2	0.3	0.03	0	0
77-260									
As prepared	0.02	0.01	NP†	0.1	0.1	0.03	0.03	0	<0.01
Devitrified	0.01	0.01	NP	0.1	0.1	0.01	0	0	0

*These relative releases are fractions of the element found in solution normalized to the fraction of sodium released from the as-prepared sample of 72-68 glass.

†NP, not present.

induced by longer treatment (e.g., two months) at higher temperatures. Thus the devitrified samples used in the present study should not necessarily show the same leach rate trends as more highly devitrified samples. The parameter which does appear to affect the leach rates is the total glass composition, i.e., 72-68 versus 77-107. In general, 72-68 is the least effective in fixing the wastes, while 77-260 is the most effective.

In order to further compare the four glasses, polished sections (nonradioactive) were exposed to 75°C deionized water for one week ($SA/V_{H_2O} = 0.01$). Each sample was examined optically before and after the test, and the solution was chemically analyzed (ICP). In general, the test confirms trends seen in the long-term 25°C tests. The analytical data in Table 6 suggest that glasses 76-68 and 77-260 are comparable and about one order of magnitude more durable than glasses 72-68 and 77-107. There is an interesting microstructural corollary in that glasses 76-68 and 77-260 show little change optically whereas glasses 72-68 and 77-107 had cracked "mud flat" surfaces following the leach test. There was evidence in all four glasses for preferential leaching of glass in regions where RuO_2 crystals concentrated.

Several points can be made considering the data in Table 6 with regard to leaching mechanisms. First, no reaction close to congruent dissolution is occurring since release rates for sodium are 5 to 10 times the rate for silicon and ~100 times the rate for uranium. It is also notable that the network formers (silicon and boron) are equally extracted, even though phase separation is expected at the 100 Å scale in borosilicate systems. (In high temperature autoclave tests,[5] there is evidence for highly preferential extraction of boron; this is under further study.) Finally, although devitrification clearly affects the leaching mechanism in visual observation, the changes in elemental release rate are remarkably small. Since the devitrified samples are 60 to 80% vitreous, many elements contained in crystalline phases are also present in comparable concentrations in the glass phase. It is, nevertheless, clear from this work and other studies[6,7] that well-formulated glasses do not show major property changes as a result of devitrification.

CONCLUSIONS

Devitrification and leaching analyses of four waste glasses have been investigated to compare nonradioactive compositions to compositions made using fully radioactive waste calcine. The following points summarize the major findings of this study:

- Melt insolubles and crystallization products are found to the same extent in both radioactive and nonradioactive glasses of similar composition. A high radiation field appears to have no effect on the crystallization behavior.
- The results of long-term IAEA static leach tests indicate no significant difference between the average leach rates of the fully radioactive and nonradioactive glass formulations.
- Glass composition is more important than the extent of devitrification in determining leach rates.
- In both short-time tests at 75°C or longer leach tests at 25°C elemental analyses suggest that congruent dissolution does not occur.

ACKNOWLEDGMENT

This work was supported by the U. S. Department of Energy under Contract EY-76-C-06-1830.

REFERENCES

1. R. P. Turcotte and J. W. Wald, *Devitrification Behavior in a Zinc Borosilicate Nuclear Waste Glass*, PNL-2247, Pacific Northwest Laboratory, 1978.
2. E. D. Hespe, Leach Testing of Immobilized Radioactive Waste Solids, A Proposal for a Standard Method, *Atomic Energy Rev.*, 9(1), 1971.
3. W. A. Ross et al., *Annual Report on the Characterization of High-Level Waste Glasses*, PNL-2625, Pacific Northwest Laboratory, 1978.
4. J. E. Mendel et al., *Annual Report on the Characterization of High-Level Waste Glasses*, PNL-2625, Pacific Northwest Laboratory, 1978.
5. J. H. Westsik, Jr., and R. P. Turcotte, *Hydrothermal Reactions of Nuclear Waste Solids—A Preliminary Study*, PNL-2759, Pacific Northwest Laboratory, 1978.
6. S. E. Mendel, *The Storage and Disposal of Radioactive Waste as Glass in Canisters*, PNL-2764, Pacific Northwest Laboratory, 1978.
7. W. J. Weber et al., Radiation Damage in Vitreous and Devitrified Simulated Waste Glass, in Proceedings of *Ceramics in Nuclear Waste Management*, Cincinnati, CONF-790420, U. S. Department of Energy, Technical Information Center, Oak Ridge, 1979.

LONG-TERM LEACH RATES OF GLASSES CONTAINING ACTUAL WASTE

J. R. WILEY and J. H. LeROY
E. I. du Pont de Nemours and Company, Savannah River Laboratory, Aiken, South Carolina

ABSTRACT

Leach rates of borosilicate glasses that contained actual Savannah River Plant waste were measured. Leaching was done by water and by buffer solutions of pH 4, 7, and 9. Leach rates were then determined from the amount of ^{137}Cs, ^{90}Sr, and plutonium released into the leach solutions. The cumulative fractions leached were fit to a mathematical model that included leaching by diffusion and glass dissolution.

INTRODUCTION AND SUMMARY

Methods to solidify Savannah River Plant (SRP) defense waste are being developed at Savannah River Laboratory (SRL). Borosilicate glass is being evaluated as a solidification matrix because it has good mechanical properties, resists leaching by water, and can accommodate a wide range of waste compositions.

Initial long-term leach tests at SRL used distilled water at room temperature as the leachant.[1,2] Those tests provided basic data to demonstrate the feasibility of glass as a solidification matrix and to compare glass with other candidate matrices. The tests showed that there were no large (systematically greater than 10X) changes in glass leaching as a function of SRP waste composition.

This paper presents results of a recent series of tests, conducted according to a draft procedure[3] of the International Standards Organization (ISO), that measured leaching with buffer solutions of pH 4, 7, and 9 as well as distilled water. The 4 to 9 pH range spans that of most groundwaters. Leach tests were made at room temperature for 200 days. Results showed that the pH 4 (acetate) buffer was the most aggressive leachant, followed in turn by the pH 9 (carbonate) buffer and the pH 7 (phosphate) buffer. Leaching in distilled water was slower than in any buffered solution. Initial leach rates were typically 10^{-6} g/cm^2 d and decreased to 10^{-8} to 10^{-9} g/cm^2 d by the end of 200 days. There were no large differences in release rate of the three radionuclides monitored in the tests: ^{90}Sr, ^{137}Cs, and plutonium. Plots of cumulative leaching versus time (t) showed that leach rates were primarily controlled by diffusion during the first 100 days and controlled primarily by dissolution thereafter.

BACKGROUND

Two nuclear fuel reprocessing facilities have operated at SRP since the early 1950's to produce nuclear materials for national defense programs. Acidic wastes that contain fission products, traces of actinides, and larger quantities of nonradioactive chemicals, are produced by fuel dissolution and subsequent separation processes. The waste is made alkaline with NaOH so it can be stored in carbon steel tanks. Adding the NaOH causes oxides and hydroxides of fission products, waste actinides, and metals (principally iron, aluminum, and manganese) to precipitate and form a sludge on the bottom of the waste tanks. The insoluble sludge confines most of the hazardous radionuclides and makes up about 10% of the waste volume.

Current plans for long-term waste management at SRP are to remove waste from the storage tanks and use ion exchange to separate ^{137}Cs and remaining traces of ^{90}Sr and plutonium from the salt solution.[4] These separated radionuclides would be mixed with the highly radioactive sludge, which would then be solidified in a high-integrity matrix.

TABLE 1

Representative Compositions of SRP Sludge

Element	Amount in sludge, wt.% High Fe	High Al	Range
Fe	32.8	3.1	3.1–32.8
Al	2.3	33.5	1.5–33.5
Mn	2.0	2.3	1.7–10.8
U	9.2	0.9	0–15.4
Ca	2.3	0.2	0.2–2.9
Ni	6.3	0.5	0.3–6.3

Because of the variety of separation processes that have been used at SRP during the past 25 years, the waste sludges span a wide range of chemical compositions (Table 1). This heterogeneity requires that candidate matrices be able to accommodate a wide variety of waste compositions without appreciably changing the integrity of the final form. The large amount of nonradioactive chemicals dilute the radionuclides, however, so that the heat produced by SRP waste is only about 0.1 watt/liter.

PROCEDURE

Because previous tests showed that borosilicate glass was compatible with all sludges sampled to date (representing about 80% of the high-heat waste at SRP) and because leaching was nearly independent of sludge type, only two sludges were used in the tests of pH effects on leaching. Sludges chosen were a relatively high aluminum sludge from Tank 16 and a relatively high iron sludge from Tank 13 (Table 2). Washed, dried, powdered sludge from these tanks was mixed with glass-forming frit (35 wt.% sludge to 65 wt.% frit, Table 3). The mixtures were melted at 1150°C for 3 hours, poured into a graphite crucible, and annealed 1 hr at 500°C. Resulting buttons were about 1.5 cm tall, 2 cm in diameter, and weighed about 12 grams.

TABLE 2

Principal Elements in Two Actual SRP Sludges

Element	Amount in sludge, wt.% Tank 13	Tank 16
Fe	25.6	13.9
Al	8.7	16.6
Mn	7.9	2.6
U	4.2	4.5
Ca	1.8	2.9
Ni	0.5	0.3

Leachants with pH 4, 7, and 9 were made, respectively, from 0.05*M* solutions of acetic acid, phosphoric acid, and sodium bicarbonate. Sodium hydroxide solution was added to adjust the pH of each solution. During leaching, each button rests on a stainless steel screen welded 2.5 cm above the bottom of a 5 cm diameter stainless steel vessel. Each vessel holds 200 ml of leachant. Leachant is pumped in and out of each vessel by a multichannel peristaltic pump.

TABLE 3

Composition of Glass-Forming Frit

Component	Amount, wt.%
SiO_2	52.5
Na_2O	18.5
Li_2O	4.0
B_2O_3	10.0
TiO_2	10.0
CaO	5.0

Leaching was done according to the draft ISO procedure. Temperature was maintained at 22 to 23°C. The ratio of leachant volume to glass surface area for the buttons ranged from 10 to 14 cm. Leachant was changed daily during the first week, weekly for the next 3 weeks, and biweekly thereafter. Leaching has continued nearly a year, and data have been analyzed through 200 days. Methods of

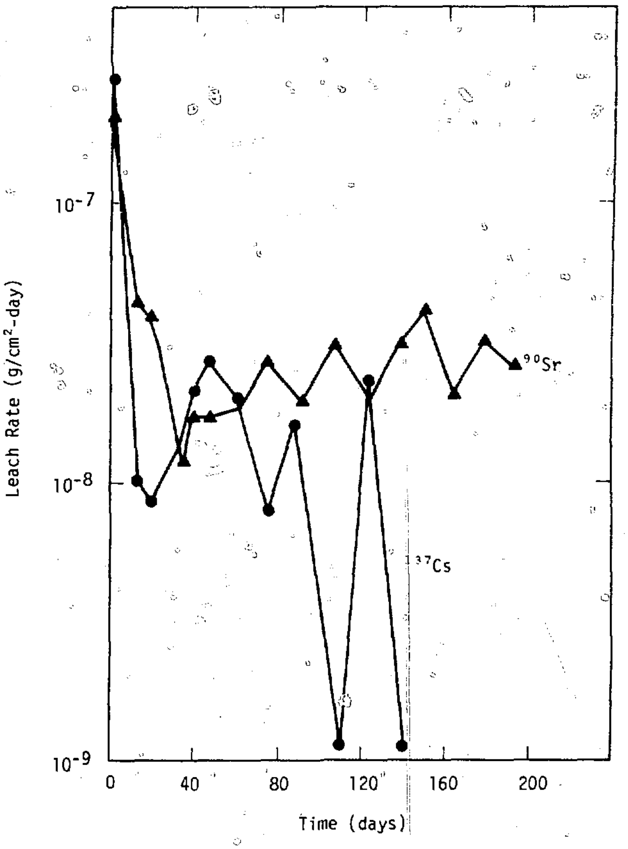

Fig. 1 Leach rates in water (frit 21 to 35 wt.% TK 13 sludge).

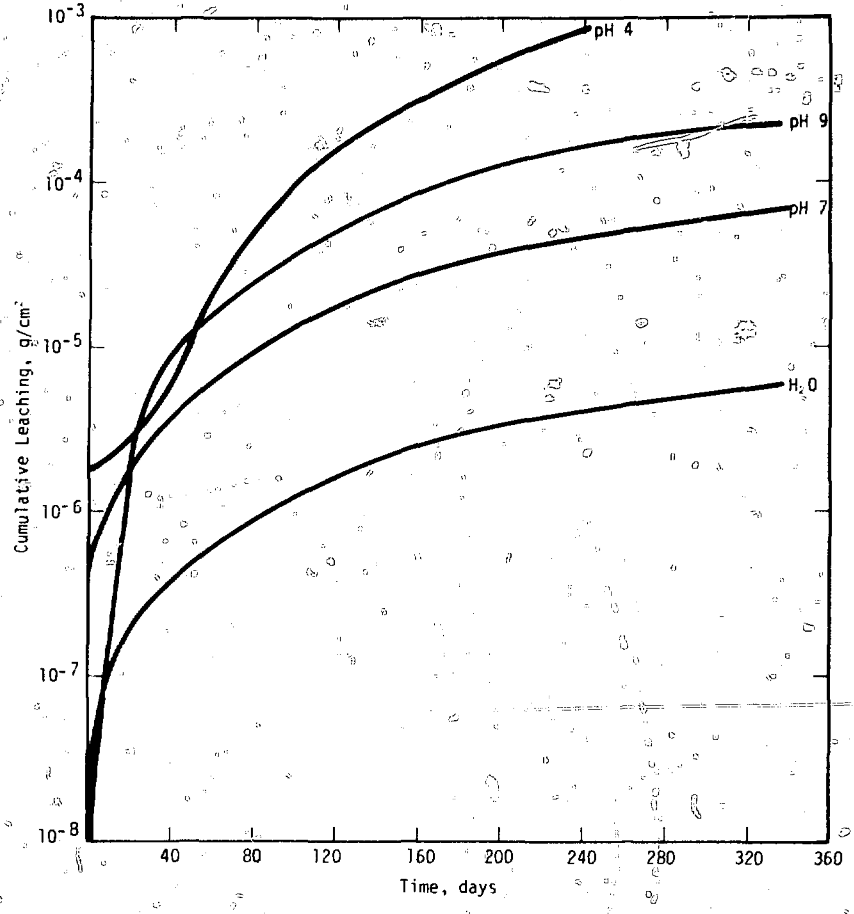

Fig. 2 Cumulative leaching based on ^{137}Cs analysis (frit 21 to 35 wt.% TK 13 sludge).

measuring ^{90}Sr, ^{137}Cs, and plutonium in the leachant have been described previously.[2]

DISCUSSION

A typical plot of leach rate versus t is shown in Fig. 1. The relatively high initial rate decreases rapidly during the first few weeks and then becomes nearly constant after 100 days. The fluctuations in leach rate are typical of those seen by other investigators.

Interpreting leach data is facilitiated by integrating the leach rate data to give a curve of cumulative leaching versus t (Figs. 2–4). For leaching based on ^{137}Cs and ^{90}Sr analyses (Figs. 2 and 3) the curves show clearly the relative aggressiveness of the four leachants: pH 4 > pH 9 > pH 7 > water. Except for the pH 4 curve, the curves for leaching based on plutonium analyses (Fig. 4) show the same trend. In all three figures, the pH 4 curves have a different shape from the other curves. In Figs. 2 and 3, pH 4 leaching appears to accelerate after about the first month.

The pH 4 (acetate) buffer differs from the phosphate and carbonate buffers in that acetate forms stable complexes with most of the sludge components. This complex formation could enhance the rate of attack by the acetate buffer. Thus, the aggressiveness of the pH 4 buffer may be more than just a pH effect. Accelerated (90°C) tests at Battelle, Pacific Northwest Laboratory have also shown that the acetate system is an unusually aggressive leachant.[5]

Several mathematical models have been used to describe leaching by both the diffusion of ions through the solid matrix and by dissolution of the matrix.[2,6] These models predict that initially leaching will be diffusion controlled (characterized by a linear plot of cumulative leaching versus $t^{1/2}$) and that after longer times leaching will be dissolution controlled (characterized by a linear plot of cumulative leaching versus t).

Figures 2, 3, and 4 show that cumulative leaching is nearly linear after 100 days, indicating that leaching has almost reached the point of being completely dissolution controlled. When plotted against $t^{1/2}$, cumulative leaching is consistent with a diffusion controlled rate from about two weeks through 100 days (Fig. 5). Leaching during the first two weeks typically decreases too rapidly to be satisfactorily fit by diffusion–dissolution models.

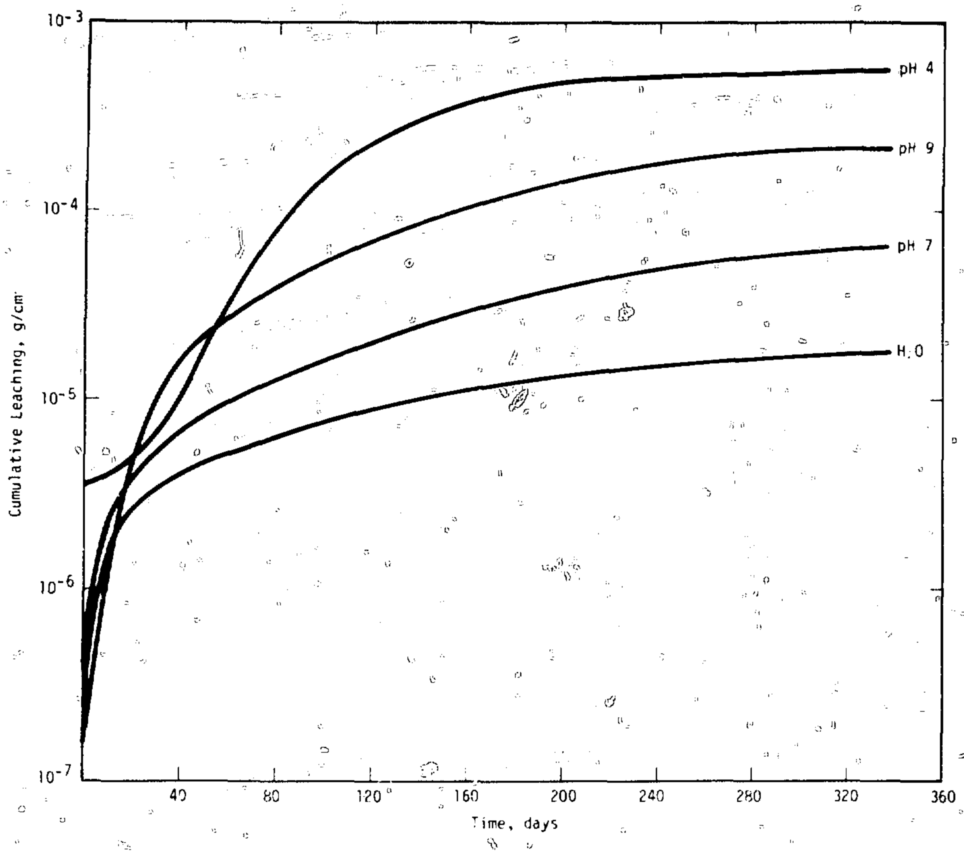

Fig. 3 Cumulative leaching based on ^{90}Sr analysis (frit 21 to 35 wt.% TK 13 sludge).

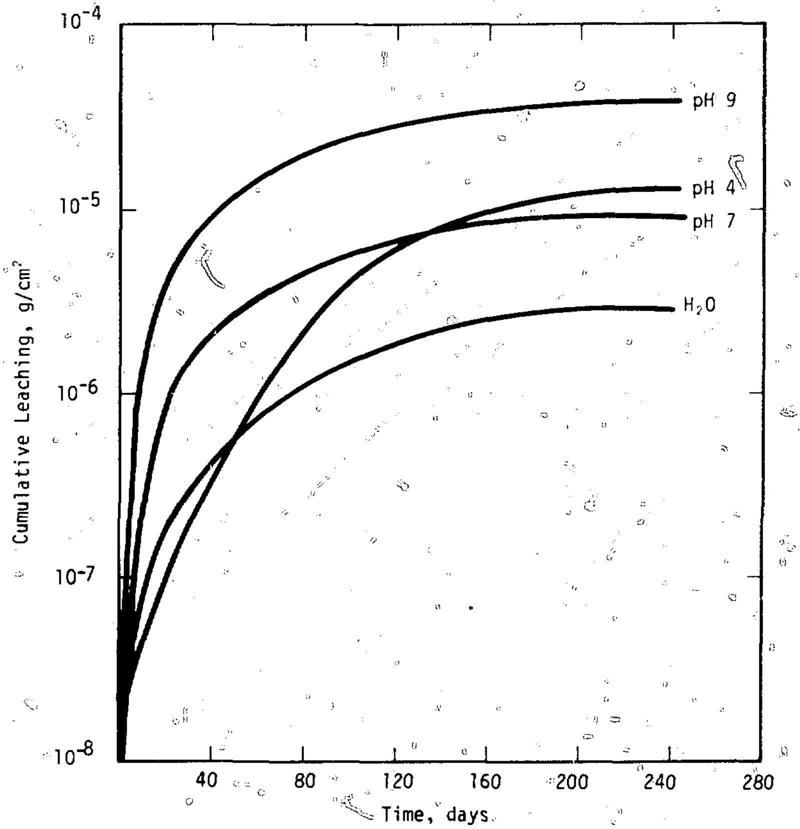

Fig. 4 Cumulative leaching based on Pu analysis (frit 21 to 35 wt.% TK 13 sludge).

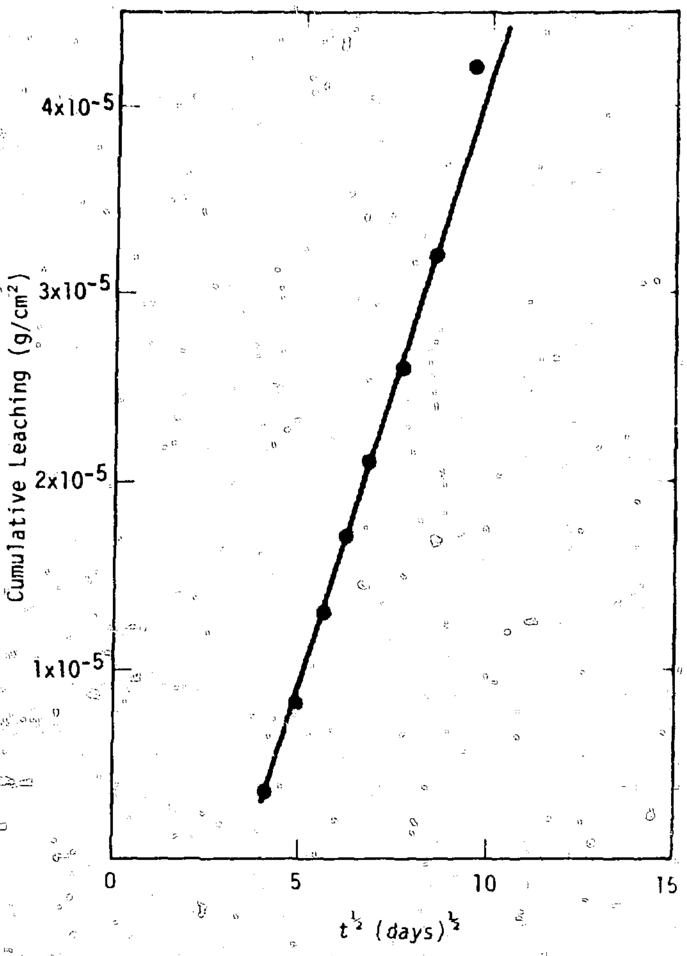

Fig. 5 Diffusion controlled leaching (frit 21 to 35 wt.% TK-13 sludge, ^{90}Sr analysis, leachant pH = 9).

SRL PROGRAM

The present tests of pH effects on glass leaching will be continued for at least another year to measure dissolution-controlled leaching. Surfaces of nonradioactive glass samples will be analyzed by X-ray photoelectron spectroscopy to define chemical changes at the glass surface during leaching. A set of repository-specific tests will also be started. These will include leaching in brine solutions at temperatures that can realistically be expected for SRP defense waste.

ACKNOWLEDGMENT

The information contained in this article was developed during the course of work under contract AT(07-2)-1 with the U. S. Department of Energy.

REFERENCES

1. J. A. Kelley, *Evaluation of Glass as a Matrix for Solidification of Savannah River Plant Waste: Radioactive Studies*, DP-1397, E. I. du Pont de Nemours and Co., Savannah River Laboratory, 1975.
2. J. R. Wiley, Leach Rates of High Activity Waste from Borosilicate Glass, *Nucl. Tech.*, March 1979.
3. Draft ISO Standard: Long-Term Leach Testing of Radioactive Waste Solidification Products, ISO/TC 85 SC 5 WG 5 N 22.
4. J. R. Wiley, Decontamination of Alkaline Radioactive Waste by Ion Exchange, *Ind. Eng. Chem., Process Des. Dev.*, 17: 67 (1978).
5. W. A. Ross et al., *Annual Report on the Characterization of High-Level Waste Glasses*, PNL-2625, Pacific Northwest Laboratory, 1978.
6. J. W. Godbee and D. S. Joy, *Assessment of the Loss of Radioactive Isotopes from Waste Solids to the Environment, Part I: Background and Theory*, ORNL-TM-4333, Oak Ridge National Laboratory, 1974.

VII. PROPERTIES OF NUCLEAR WASTE FORMS

SIMULATIONS OF RADIATION DAMAGE IN GLASSES

M. ANTONINI, F. LANZA, and A. MANARA
Commission of the European Communities Joint Research Centre, Ispra Establishment, Ispra, Italy

ABSTRACT

[illegible]

INTRODUCTION

One of the proposals for storing the waste materials from spent fuel reprocessing plants in a stable form is that of incorporating them in glass. Borosilicate glasses have a low leaching coefficient[1] and high resistance to beta and gamma radiation.[2] If this type of glass is to be used for final storage, its resistance to radiation damage will have to be considerable. The waste material also contains a certain amount of alpha-emitting nuclides, some of which have extremely long half-lives. The risk associated with any waste storage system will consequently continue to be significant for a very long time. The total amount of radiation, particularly alpha radiation, will increase accordingly. The radiation could influence the risk associated with storage of radioactive waste by either changing the leaching coefficient, by increasing the specific surface due to cracks of the glass body, or even by pulverization. The cracking of the glass cannot be easily foreseen due to the difficulty of measuring possible internal stresses which could be generated by the radiation. As it is not possible to reliably extrapolate from low irradiation doses, it is necessary to test samples at the required integrated dose. In this context stored energy, which is probably the most significant and measurable effect of radiation damage, becomes of great importance. It is usual to consider the phenomenon of stored energy in light of possible temperature excursions of damaged solids. The values that have been found for borosilicate glasses[3,4] indicate that this effect will be negligible in practice. From a general point of view, stored energy can in fact be a very important index of the accumulation of defects and their possible saturation. It is for this reason that we have concentrated our studies on the stored energy.

The total amount of radiation which waste glasses must sustain safely is difficult to define. It depends not only on the strategy used in waste management but also on an evaluation of the time needed to decrease the associated risk to negligible levels.[3,5] As a first approximation, it can be said that the glass must sustain a total damage corresponding to 0.5 dpa (displacements per atom) (about 500,000 years). It must be noted, however, that the waste management strategies increasingly consider glass as the conditioning medium for all the alpha-contaminated waste streams. It seems likely, therefore, that this value will have to be revised and a higher number of dpa taken into consideration.

In order to rapidly reach a high level of damage, two different types of simulation have been tested. The first one makes use of the fission of uranium to produce the damage. The chosen glass is doped with uranium and irradiated. The dpa obtained is limited by the need to avoid too high a temperature inside the glass. The second one consists of bombarding the glass with an external beam of highly energetic heavy ions. The sample must be very thin but the method has the advantages of reducing the time required to reach heavy damage (~1 dpa) to the order of a few hours and of avoiding the necessity of adding additional components.

DEFINITION OF THE DAMAGE UNIT

One of the most important points in the simulation of radiation damage is the definition of a method of dose evaluation. Such a method is required in order that a comparison of the relative effects and importance of different types of radiation can be made.

In the first evaluation of radiation damage to glasses incorporating waste under beta gamma radiation, the concept of total adsorbed energy was assumed. This concept is reasonable if it is applied only to types of radiation which dissipate their energy by a single mechanism, namely ionization. As a matter of fact, only very strong beta rays (>1 MeV) cause significant atomic displacement. Such a concept cannot be accepted for other types of radiation such as alpha particles and the associated emitter recoil having a mixed type of dissipation ionization and displacement of atoms.

One possible method of dose evaluation is the calculation of the specific number of events. This solution is perfectly acceptable if the material is subjected to only one type of radiation, for example, in the study of neutron irradiation on the properties of glasses.[5] In the case where alpha radiation is predominant, this solution might be acceptable.[4] However, this method does not take into account the different energy with which alpha particles are emitted from the various nuclides. Previous experiences[1,2] with borosilicate glasses have shown, however, that beta gamma radiation, which dissipates energy mainly by ionization, does not have a significant effect on stored energy. It therefore seems worthwhile to examine the possibility of using the other principal mechanism of energy dissipation, i.e., atom displacement, as a unit of dose.

The displacement of atoms in crystalline materials is considered to be the most important mechanism by which a fast particle produces lattice defects. In glasses having noncrystalline structures and various types of bonds, the concept of the displaced atom assumes particular significance. It is, in fact, difficult to speak of vacancies or interstitials in glasses in the same way as in crystalline media. Nevertheless, the existence of short-range order may justify, at least to a first approximation, an evaluation of the damage using criteria analogous to those used for crystals.

Table 1 summarizes the results of the calculation of displaced atoms due to different types of radiation.[7] It should be noted that this evaluation is based on a displacement energy of 25 eV. This value may be questionable, and some theoretical and experimental studies on simple glasses such as fused silica are being undertaken in order to help clarify this problem. However, it can be seen that, although a better approximation would lead to changes in the absolute values given in Table 1, their relative values will remain unchanged (with the exception of beta rays).

Finally, it should be remembered that neglecting the energy dissipated by ionization is acceptable only as a first approximation. It is not unlikely, for instance, that such an energy plays a role in the radiation annealing phenomenon.

TABLE 1

Number of Displaced Atoms by Different Types of Radiation

Type of radiation	Our evaluation	Evaluation from Ref. 3	Comments
α	130	140	
α recoil	2000	1500	1 - 6 MeV
n (fast)	200		
Fission		^{137}Cs 29,600	In Al_2O_3
fragment	25,000	^{97}Zr 15,000	(Ref. 10)
Ni^{6+} (46.5 MeV)	8000		

DESIGN OF EXPERIMENTS

Experiments were conducted on a type of borosilicate glass prepared in our laboratory,[8] which can be considered representative of the glasses commonly taken into consideration in Europe. Into the glass matrix has been incorporated 20% of simulated waste oxide. Table 2 gives the composition of the glasses.

TABLE 2

Glass Composition

Component	Wt.%	Component	Wt.%
SiO_2	48	CeO_2	0.76
B_2O_3	15	SnO_2	0.03
Al_2O_3	5	ZrO_2	1.06
Na_2O	18.49	MoO_3	0.16
SrO	0.22	MnO_2	1.35
BaO	0.33	Fe_2O_3	3.25
Y_2O_3	1.28	NiO	0.32
La_2O_3	0.63	CuO	0.04
Pr_2O_3	0.31	ZnO	0.03
Nd_2O_3	0.99	U_3O_8	1.38
Sm_2O_3	1.12		

In order to provide the correct amount of fission in the sample, part or all of the natural UO_2 has been substituted with enriched UO_2 using two levels of enrichment, 11% and 90% of ^{235}U. The homogeneity of uranium in the glass has been verified using a nitrocellulose tracking film. The sample was put in contact with the film for 24 hr and then treated with concentrated NaOH. Microscopic observation did not show traces of agglomeration.

Due to the very high thermal absorption of ^{10}B, irradiation in a neutron spectrum as existing normally in an experimental reactor does not give acceptable results. The thermal neutrons are absorbed preferentially near the surface so that the number of fissions at the center of the sample are lower by an order of magnitude compared to those arriving at the surface of the sample. There is, thus, the risk of examining effects due to the differential radiation rather than to the radiation itself. This effect can be overcome either by irradiating thin sheets or by shielding the glass samples from thermal neutrons with a Cd shield. In the present work the second technique was chosen. The glass was irradiated in the form of cylinders 10 mm in height and 10 mm in diameter.

Calculations were made to evaluate the effect of a Cd sheet 1 mm thick around the pellets, subdividing the glass pellets in six concentric zones. The results show that the fission density at the center is 91.5% of that at the surface. This is considered acceptable. Of course this homogeneity is accompanied by a lower fission density since the contribution of thermal neutrons practically disappears and only epithermal and fast fission are involved.

The irradiation experiment, which was called **BONI** (*Borosilicate Glass Neutron Irradiation*), was based on two irradiations each of three capsules. Each capsule containing glass samples was enclosed in cadmium canning 1 mm thick. The capsules were made of aluminum and were provided with two grooves for the insertion of thermocouples. The irradiations were performed in the pool-side facility of the HFR reactor at Petten, the Netherlands. The first irradiation lasted 44 days while the second lasted 10 days. The details of the irradiation are given in Ref. [7]. Thermal *calculations show that a temperature of 68°C was obtained* during irradiation at the center of the most charged sample. Table 3 gives the ^{235}U content, the total amount of *fission/cm^3, and the dpa for each capsule.*

External irradiation has been performed on borosilicate glasses of the same composition at the V.E.C. (Harwell, England) using a collimated beam of 46.5 MeV Ni^{6+} ions. Moreover, borosilicate glasses of composition 189E, already examined by Hall et al.[3] using Pu recoils, have also been irradiated. Sample dimensions are 5 x 5 x 1 mm for the BONI type slabs or 5 mm diameter by 0.5 mm thick for 189E disks. The thickness is limited by the small penetration (11 μm) of heavy ions to enhance the signal to background ratio during calorimetric tests. Dose measurements were made by recording the charge accumulation on the insulated sample holder. Secondary emission of electrons was eliminated by providing a counter potential of 100 volts. The sample holder was water cooled during irradiation. Some samples were coated with a 300 Å silver layer to provide a ground path preventing charge accumulation and breakdown and to avoid large temperature gradients across the samples. However, not all of the samples were coated. This circumstance allowed us to examine the effects of the thin silver films during heavy ion bombardment. During irradiation the target was tilted step by step at various angular positions to give a uniform distribution of radiation damage over the entire range of Ni ions. Depth distributions of energy deposition were calculated using a computer program described by M. D. Matthews.[4] In Fig. 1 a typical depth distribution of simulated atomic displacements is illustrated. Some oscillations are observable around the mean value. Dose rates are in the range 4 to 12 x 10^{11} Ni^{6+} cm^{-2} · sec corresponding to 4.5 x 10^{-5} and 1.35 x 10^{-4} dpa per sec, respectively. This rate is about 10^3 times faster than that achieved in fission fragment damage and about 10^4 times faster than that obtainable with Pu recoil. An upper limit for the irradiation temperature is estimated at ~150°C. Further considerations about the real temperature during irradiation will be made in the next section.

TABLE 3

BONI Irradiation

Capsule	^{235}U content, wt.%	Fission/cm^3	dpa	Eq. α density, α/cm^3
BONI I				
1	1.76	4 x 10^{17}	0.36	9.4 x 10^{18}
2	1.11	1.34 x 10^{17}	0.12	3.15 x 10^{18}
3	0.11	3 x 10^{16}	0.027	7.1 x 10^{17}
Blank	0.008	1.1 x 10^{15}	0.001	2.6 x 10^{16}
BONI II				
1	1.76	1.48 x 10^{17}	0.133	3.5 x 10^{18}
2	1.11	5.8 x 10^{16}	0.052	1.4 x 10^{18}
3	0.11	9.8 x 10^{15}	0.0088	2.3 x 10^{17}
Blank	0.008	2.4 x 10^{14}	0.0002	5.6 x 10^{15}

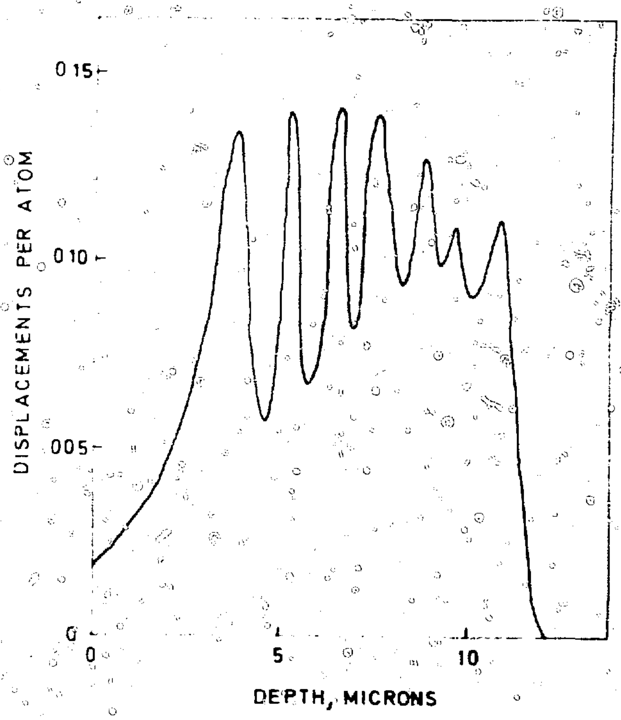

Fig. 1 Depth distribution of displaced atoms due to target tilting.

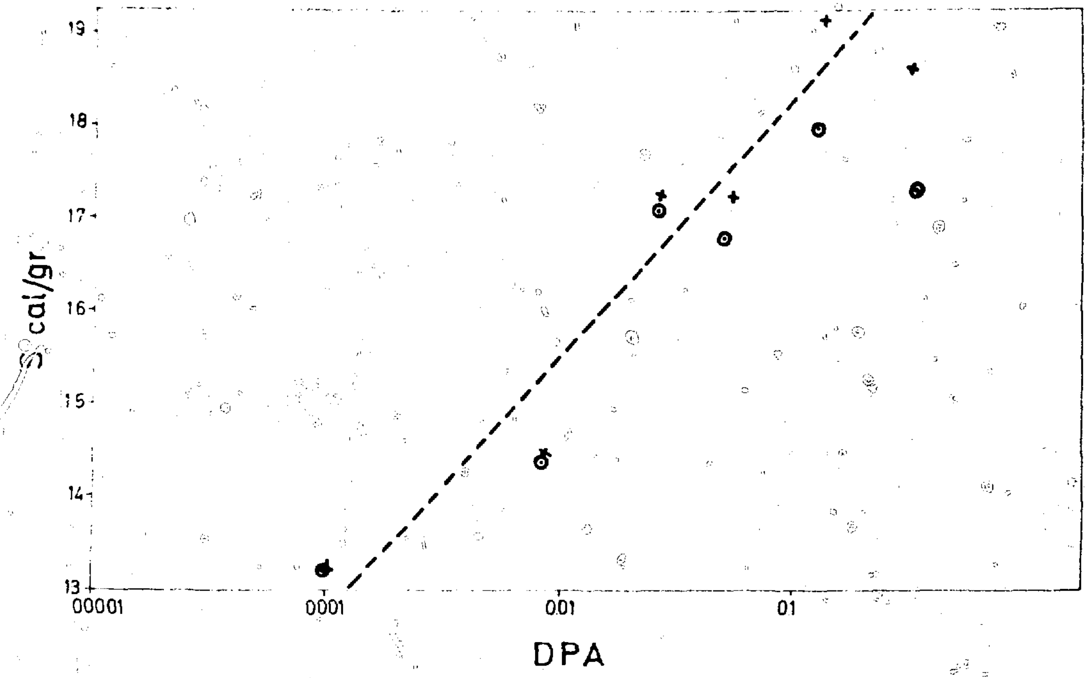

Fig. 2 Stored energy in BONI glass as a function of displacements per atom (dpa). x = data corrected for temperature effect from data in Ref. 6.

RESULTS AND DISCUSSIONS

The stored energy measurements were performed using a Dupont DSC 910 scanning microcalorimeter. The rate of energy release at a heating rate of 10°C/min was recorded between about 50°C and 550°C. The energy release was calculated from the difference between the first and second runs on the sample after irradiation. A third run was made to make sure that all the energy was released during the first run. In this case the second and the third runs appeared superimposed. The results obtained on samples loaded with uranium and irradiated are shown in Fig. 2. We can see that in the field explored the dependence on dose is very weak as shown in the semilogarithmic plot.

An uncertainty exists regarding irradiation temperatures. The gamma radiation contributes to the glass heating 0.6 W/g while for the most charged capsule (BONI I-1, BONI II-1) the fission heat contributes 1.24 W/g. As a consequence, thermal calculations show that the central temperature for the BONI I-1 capsule is 72°C, while for the BONI I-3 capsule it is 50°C. A temperature correction will then give a slight increase in the values of stored energy at the higher doses. Due to this uncertainty it is not possible to state whether there is a logarithmic dependence on dose or a total saturation effect. An experiment at higher doses with better temperature control is under way and will help clarify this point.

The results of stored energy measurements performed on samples irradiated with heavy ions are reported in Table 4. When taking into account the rather different types of irradiations and in particular the much higher dose rates obtained with heavy ions with respect to fission fragments, the values of stored energies for the glass samples of the BONI type are in good agreement.

It is thus possible to consider with some confidence the results which can be achieved by this external irradiation technique. When comparing the results for BONI samples irradiated under the same conditions at 0.1 and 1 dpa, respectively (Table 4), a saturation effect seems more likely. However, the total amount of energy stored at saturation has a strong dependence on the temperature of irradiation. This can be deduced from the comparison between samples irradiated with and without a silver coating. For example, silver coated glass 189E gives a value about 1.5 times higher than 189EII, uncoated, although it has received only one tenth of the dose. It can be argued that the metal coating keeps the irradiated surface at

TABLE 4

Heavy Ion Irradiation

Sample	dpa	dpa/sec	Cal/g
Glass			
BONI*	0.1	1.35×10^{-4}	40
BONI	0.1	1.35×10^{-4}	35
BONI	1	1.35×10^{-4}	30
189E*	0.1	1.35×10^{-4}	65
189E	1	1.35×10^{-4}	40

*Coated with a 100 Å silver film.

approximately the temperature of the sample holders (i.e., the temperature of the cooling water) while the uncoated surface is at a higher temperature due to the large energy deposition of heavy ions in a relatively small insulating sample thickness. Other possible effects due to the coating, such as the diffusion of silver atoms into the glass during bombardment, are still being considered. Preliminary results of back scattering analysis seem to show the presence of silver atoms only at the glass surface.

A strong dependency of stored energy upon the temperature of irradiation has been reported by Mendel et al.[4] and Hall et al.[3] The interpretation of this phenomenon requires more systematic measurements of glasses irradiated at various controlled temperatures as well as a theoretical study of the annealing mechanisms. Both of these activities are now being developed. If we compare the stored energy values obtained with the two different simulation methods with those obtained by loading the glass with alpha emitters,[3,6,9] the following points can be underlined. The use of displacements per atom as a unit of dose seems appropriate for the study of radiation damage of glasses. The results obtained using a simulation with fission are somewhat lower than those obtained with alpha emitters. It is difficult to decide whether this is due to imperfect control of the temperature or if it is a secondary effect of radiation annealing caused by the large amount of ionization energy dissipated by fission fragments.

The tests performed using the accelerator have a very high dose rate. Nevertheless the stored energy increases at most by only a factor of 2 to 3. We thus conclude that the dose rate does not have a very high influence on stored energy.

REFERENCES

1. M. N. Eliot, J. R. Grover, and W. H. Hardwick, Fixation of Radioactive Waste in Glass, in *Proceedings of the Symposium on Treatment and Storage of High Level Radioactive Wastes,* Vienna, IAEA, 1963.
2. R. Bonniaud, F. Laude, and G. Sombret, Experiences Collected in France. Vitrification of Concentrated Solutions of Fission Products, in *Proceedings of the Symposium on Management of Radioactive Wastes from Fuel Reprocessing,* Paris, OECD, 1972.
3. A. R. Hall, J. T. Dalton, B. Hudson, and J. A. C. Marples, Development and Radiation Stability of Glasses for Highly Radioactive Wastes, in *Proceedings of the Symposium on Management of Radioactive Wastes,* Vienna, IAEA, 1976.
4. J. E. Mendel et al., *Annual Report on the Characteristics of High Level Waste Glass,* BNWL-2252, Pacific Northwest Laboratories, 1977.
5. K. Scheffler, U. Riege, W. Hild, and A. T. Jakubick, *On the Problem of Safe Disposal of Alpha Containing Waste from Reprocessing and Fuel Fabrication Long-Term Behavior of Highly Active Radioactive Glasses,* KFK-2170, 1975.
6. W. Primak, J. H. Fuchs, and P. Day, *J. Am. Ceram. Soc.,* 38: 135 (1955).
7. F. Lanza, A. Manara, F. Van Rutten, *Simulation Possibilities of Radiation Effects in Glasses Used for Conditioning High Activity Waste,* EUR 5560e, Joint Research Center, 1976.
8. F. Lanza, Simulation of Alpha-Damage in Glasses by Means of Uranium Fission Induced by Epithermal Neutrons, in *Proceedings of the First HFR Users Meeting,* CEC, Petten, 1977.
9. M. D. Matthews, AERE R 7805, Harwell, August 1974.
10. K. Scheffler and U. Riege, *Investigations on the Long Term Radiation Stability of Borosilicate Glasses Against Alpha-Emitters,* KFK 2422, 1977.

RADIATION EFFECTS IN VITREOUS AND DEVITRIFIED SIMULATED WASTE GLASS

W. J. WEBER, R. P. TURCOTTE, L. R. BUNNELL,
F. P. ROBERTS, and J. H. WESTSIK, Jr.
Pacific Northwest Laboratory, Richland, Washington

ABSTRACT

The long-term radiation stability of vitreous and partially devitrified forms of high-level waste glass was investigated in accelerated experiments by ^{244}Cm doping. The effects of radiation on microstructure, phase behavior, density, impact strength, stored energy, and leachability are reported to a cumulative radiation dose of 5×10^{18} α decays/cm^3. This dose produces saturation of radiation effects in most properties.

INTRODUCTION

Glass is recognized as the most highly developed solid form for the storage of high-level nuclear wastes.[1] All high-level waste (HLW) solids will be subjected to gamma, beta, neutron, and alpha self-radiation. The major potential for detrimental long-term effects is from the spontaneous alpha decay of the long-lived actinide elements.[2,3] In an alpha-decay event, a high-energy alpha particle (~5.5 MeV) and recoil nucleus (~0.1 MeV) are produced. Nearly all the energy of the recoil nucleus is lost through elastic collisions, thereby causing atomic displacements. In the case of the alpha particle, most of the energy is lost in ionization, but enough energy is lost in elastic collisions to account for some displacements (<20% of total). Both these displacements and the stable helium atoms which result from the capture of two electrons by the alpha particles, and which must be structurally accommodated, may affect the long-term integrity and stability of waste solids.

The present study considers the radiation effects from the alpha decay of ^{244}Cm on vitreous and partially devitrified forms of HLW glass. The effects of radiation on density, phase behavior, microstructure, stored energy, leachability, and impact strength are investigated to a cumulative dose of 5×10^{18} α decays/cm^3, which is equivalent to ~10^3 years storage for high-level wastes from the reprocessing of commercial spent fuel[4] (3.3% enriched UO$_2$ fuel) and over 10^6 years for some defense wastes.[5]

EXPERIMENTAL METHOD

The simulated HLW glass examined is a borosilicate glass, designated 77-260 (Ref. 6). This glass is characterized by a waste composition high in gadolinum and sodium and a glass frit high in titanium and copper. The glass was doped with 2 wt.% ^{244}Cm (added as an oxide powder) which has a half-life of 18.1 years. One vitreous and two partially devitrified forms of this glass composition were prepared for experimentation. Each of the three sample types were melted at 1100°C for 2 hours in an air atmosphere. The vitreous sample was air quenched and annealed at 530°C for 1 hour before furnace cooling. One glass was partially devitrified by slow cooling at 6°C/hr from 1050°C to produce large crystals (~25 to 100 μm in size). A fine dispersion of small crystals (<5 μm in size) was introduced in the third glass by annealing at 700°C for one week.

Density measurements were made on 3-gram specimens by the buoyancy technique to an accuracy of about ±0.001 g/cm^3. Conventional optical and scanning electron microscopy (SEM), energy dispersive X-ray spectroscopy (EDXS), and quantitative X-ray diffraction (XRD) methods were used. Alpha-autoradiography was undertaken using cellulose nitrate and NaOH etching.[7] Impact tests were conducted at the beginning and conclusion of this study by impacting cylindrical specimens (1.3 cm diameter, 1.3 cm height) at 160 ft lbs and subjecting the remains to sieve analysis. Stored energy release was measured by differential scanning calorimetry (DSC), as previously described in detail.[2] Leach rates were measured using dynamic Soxhlet and acid-base (pH4 and pH9) leach tests.[8] The leach tests were carried out at three different dose levels on cylindrical wafers (1.3 cm diameter, 0.25 cm thickness).

RESULTS AND DISCUSSION

The typical microstructures observed in each of the three sample types are shown in Fig. 1 (a, b, and c). The vitreous sample (Fig. 1a) is found to contain about 2 wt.% crystals, mostly insoluble RuO_2 and palladium. Both partially devitrified samples are about 30 wt.% crystalline. The slow-cooled sample (6°C/hr) shown in Fig. 1b contains mostly large crystals, 25 to 100 μm in size. The other sample (Fig. 1c), devitrified at 700°C for one week, contains a high density of uniformly dispersed crystals less than 5 μm in size. The two major devitrification products identified in both partially devitrified samples were $Ca_3Gd_7(SiO_4)_5(PO_4)O_2$, with a hexagonal (apatite) crystal structure, and a gadolinium titanate phase (indeterminable stoichiometry) with a cubic crystal structure.

As expected from the similarity of actinide and rare-earth oxide chemistry, curium also appears in these crystalline phases. Estimates of the curium concentration levels were made both by energy dispersive X-ray spectroscopy (EDXS) on the SEM and by alpha-autoradiography. The autoradiographic technique, which is more accurate, could be used only for the slow-cooled (6°C/hr) sample containing large crystals. A typical alpha-autoradiograph and corresponding optical micrograph are shown in Figs. 1d and 1e, respectively. Table 1 gives the estimated concentration factors, normalized to the glass matrix, in each case.

Table 1

^{244}Cm Concentration in Devitrified 77-260 Waste Glass

Component phase	Relative concentration		
	Alpha-autoradiography, 6°C/hr	SEM-EDXS data	
		6°C/hr	700°C, 1 week
$Ca_3Gd_7(SiO_4)_5(PO_4)O_2$	6	~4	~2.5
Gd-titanate	4	~4	~2.5
Residual glass	1	1	1

X-ray diffraction analysis of the vitreous sample revealed no changes in structure as a result of self-radiation. The diffracted X-ray intensity ratio, I/I_0, of a principal reflection in each of the two major crystalline phases in the partially devitrified samples is shown in Fig. 2 as a function of accumulated dose. The gadolinium titanate phase is essentially stable with respect to radiation effects; however, the apatite structure, $Ca_3Gd_7(SiO_4)_5(PO_4)O_2$, has transformed from a crystalline to an X-ray amorphous (metamict) state. Similar behavior of an apatite structure has been observed in supercalcine.[9] The stability of the gadolinium titanate is somewhat surprising, since in another study of a glass-ceramic waste form, a rare-earth titanate (also cubic structure, but different composition) was observed to become X-ray amorphous at doses comparable to those reached in this study. Obviously, the role of structure type and composition in radiation-induced amorphization needs to be further explored. The rate of amorphization of $Ca_3Gd_7(SiO_4)_5(PO_4)O_2$ appears to be greatest in the slow-cooled (6°C/hr) sample. This is likely due to the higher ^{244}Cm concentration in the crystals of this sample, as suggested by the SEM-EDXS results of Table 1. Accurate lattice constant measurements were not possible. Data indicate that a may increase by as much as 3% in the apatite structure; the change in c_0 is small. No measurable lattice constant change was observed in the gadolinium titanate.

The initial densities of the samples increased with the degree of devitrification. The initial density of the slow-cooled (6°C/hr) sample was 3.201 g/cm^3, the initial density of the 700°C annealed sample was 3.189 g/cm^3, and the initial density of the vitreous sample was 3.153 g/cm^3. The changes in densities as a function of accumulated alpha decay are shown in Fig. 2. The density change in the vitreous sample is among the smallest measured in any glass,[6] <±0.1%. The density change in the 700°C, one-week-annealed sample saturated at −0.45%, while a saturation value of about −1.0% was reached in the slow-cooled sample. The decrease in density for both partially devitrified samples is partly the result of the volume change associated with the $Ca_3Gd_7(SiO_4)_5(PO_4)O_2$ phase and partly due to the behavior of the residual glass.

The results of the stored energy measurements are also shown in Fig. 2. The stored energy does not exceed 30 cal/g for any of the samples and is similar in behavior to other waste glasses previously studied.[2,6,8] The vitreous sample exhibits a significantly higher energy release than either of the two partially devitrified samples. This behavior is partly due to the reduced fractional volume of glass in the partially devitrified samples; assuming that the stored energy in the residual glass phase has saturated (a reasonable assumption, even though the ^{244}Cm concentration in the glass is lower), then the contribution of the residual glass phase to the stored energy release is reduced proportionately to its fractional volume. The other reason for the lower energy release in the devitrified samples is that the maximum temperature limit under test conditions is 600°C, which is sufficient to anneal damage in the glass phase but is not high enough for full recovery of damage in the crystalline phases. As a result only a fraction of the stored energy in the crystalline phases contributes to the observed stored energy release values.

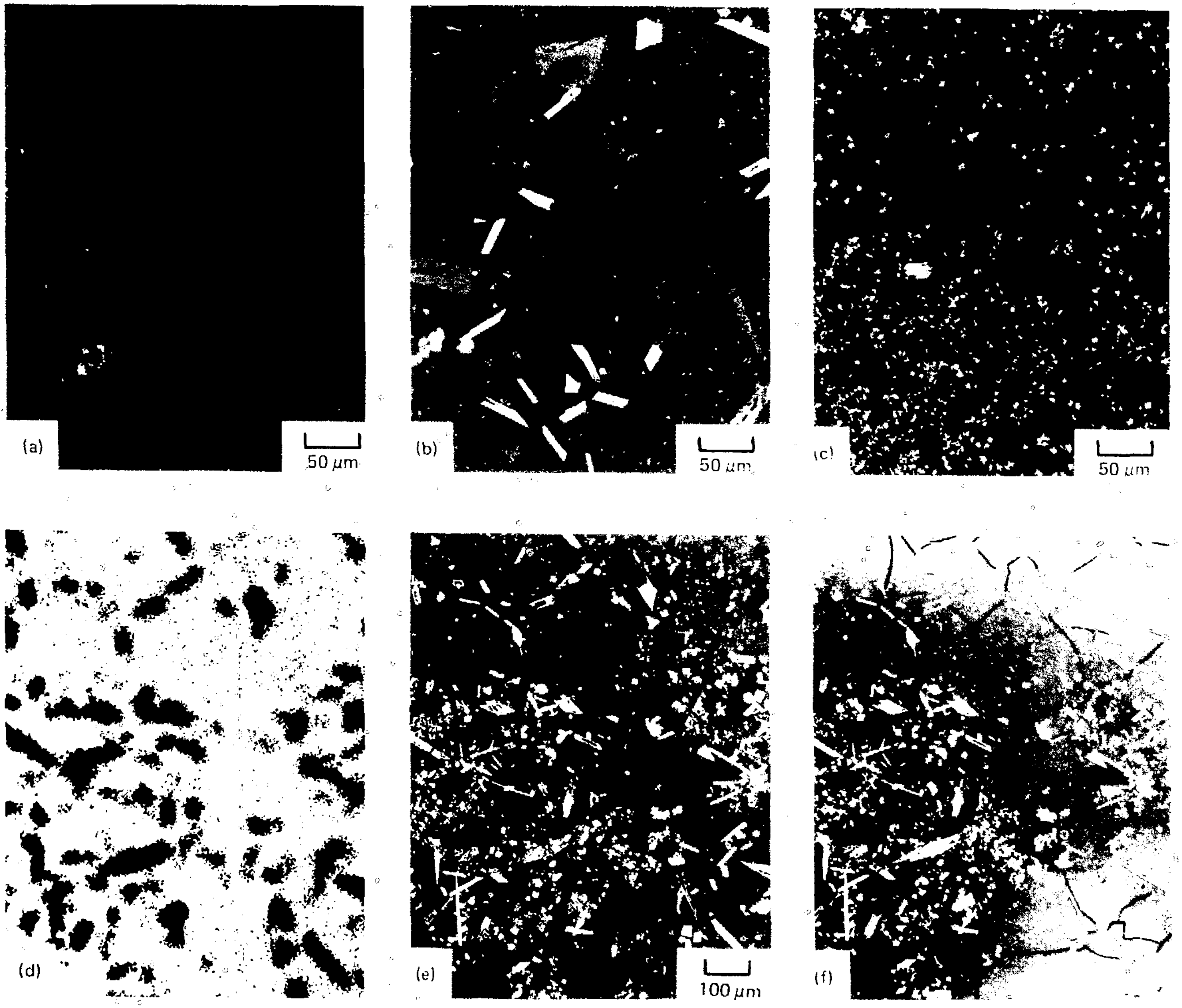

Fig. 1 Initial microstructures in the three waste glass forms investigated and alpha-autoradiograph with corresponding optical images before and after microfracturing. (a) As-prepared, vitreous sample; (b) Partially devitrified sample cooled at 6°C/hr; (c) Partially devitrified sample annealed at 700°C for one week; (d) Alpha-autoradiograph of region shown in (e) and (f); (e) Slow-cooled sample (6°C/hr) exhibiting no microcracks after 2×10^{16} α decays/cm^3; (f) Microcracks developed in same area after 8×10^{17} α decays/cm^3.

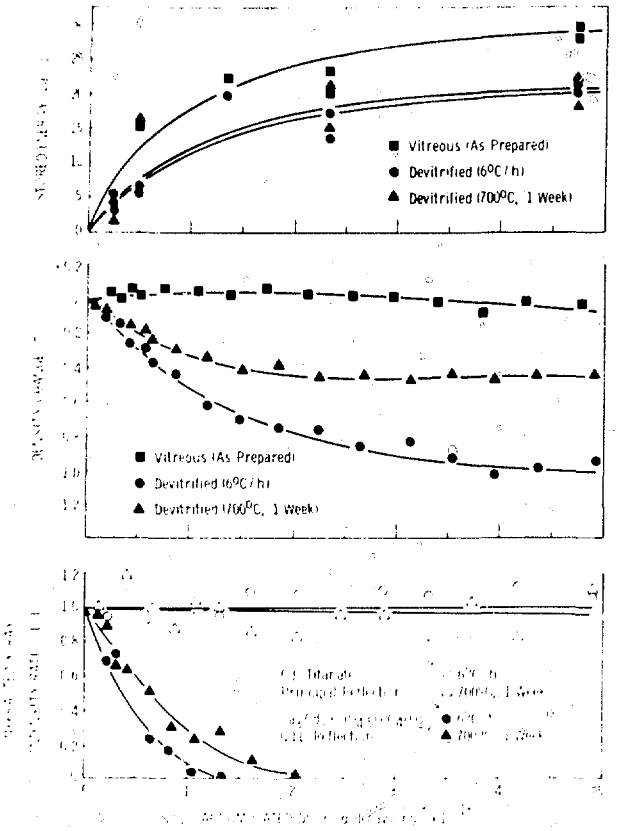

Fig. 2 Changes in diffracted X-ray intensity ratio (I/I_0), density, and stored energy as a function of accumulated dose in ^{244}Cm doped 77-260 simulated waste glass.

One of the major objectives of this study was to verify an expectation that devitrified glasses would microfracture under radiation-induced swelling of ingrown crystalline phases. Based on previous studies, we also believed that crystallite size would be an important factor. In fact, the observed behavior clearly matched expected changes. The vitreous sample is not physically affected by self-radiation even though it contains fine crystalline inclusions (mostly RuO_2 and palladium). Under anhydrous conditions, the partially devitrified sample containing small crystals (700°C, one week) is also not affected; this behavior is similar to that observed in fine-grained nuclear waste glass ceramics. In the slow-cooled sample containing large crystals, microcracks developed under anhydrous conditions in the dose range from 2×10^{16} to 8×10^{17} α decays/cm^3, as shown in the identical area micrographs in Figs. 1e and 1f. The cause of the cracking is the volume change associated with the amorphization of the apatite phase, $Ca_3Gd_7(SiO_4)_5(PO_4)O_2$, which is complete at about the same dose level where microcracking saturates.

In order to examine an expected strength reduction in the presence of water, samples with an accumulated dose of 4.5×10^{18} α decays/cm^3 were immersed in room temperature water for three weeks and reexamined. The vitreous sample remained unchanged, the 700°C annealed sample (small crystals, uncracked) developed a few cracks, and the extent of the microcracking did not significantly change in the slow-cooled (large crystals) sample. Since glass-crystal thermal expansion differences could be a factor, identically prepared, but undoped, samples were also exposed to water. No effects were observed in any of the undoped samples, confirming that the observed microfracturing is a result of radiation-induced stresses.

The impact test results are shown in Fig. 3. The data indicate that the samples have marginally better impact performance than soda-lime-silica glass. There is a trend in the low-dose samples toward the expected results, i.e., that the devitrified samples appear tougher than the vitreous sample. Since the normal data spread is about ±5%, the *stacking order may be fortuitous. The data also suggest that* the self-radiation did not negatively affect the impact performance. This is somewhat surprising in view of the internal stresses and microfracturing associated with the amorphization of the apatite phase. The impact test, which has been routinely used to examine different glass compositions, was designed with the idea that the crystallites might be surrounded by large tensile stress fields that result from differential thermal expansion or from radiation-induced volume changes. These stresses are released during

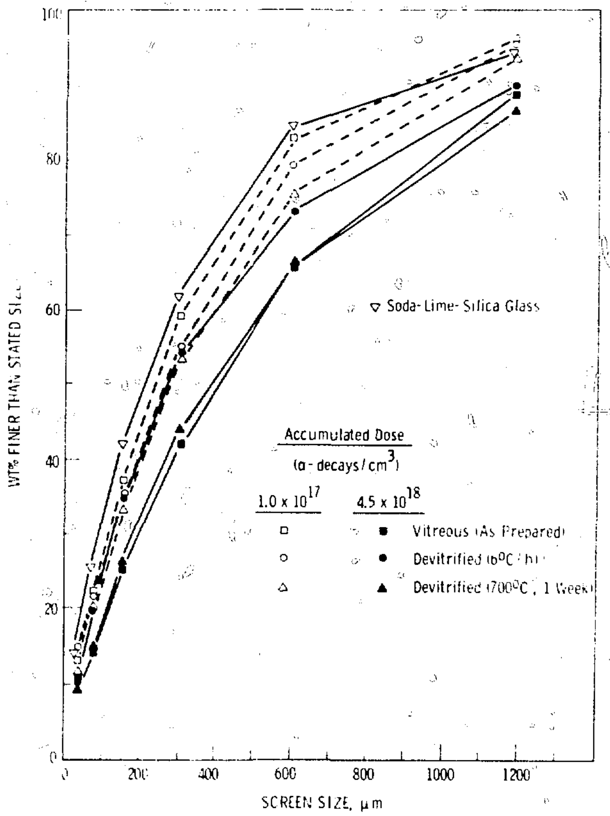

Fig. 3 Particle sizes produced by 160 ft lb impact on ^{244}Cm doped 77-260 simulated waste glass at two different dose levels. Results are compared to undoped soda lime silica glass.

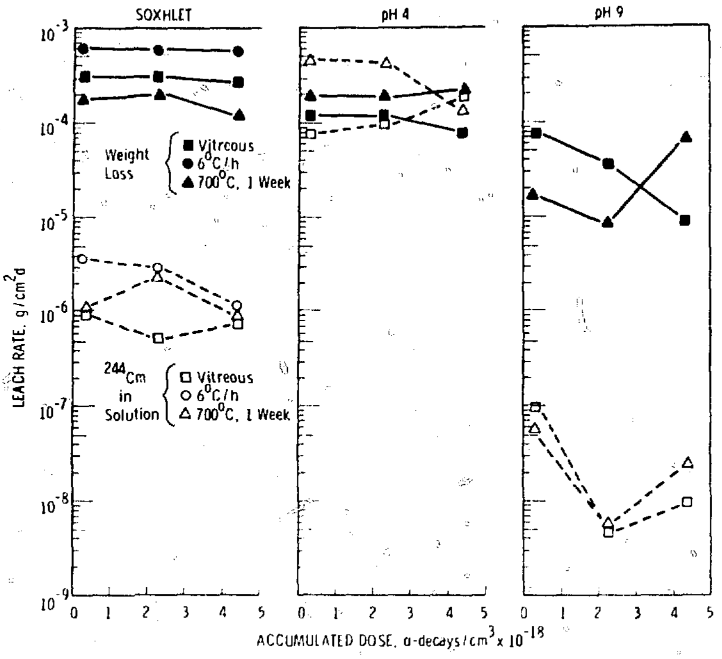

Fig. 4 Leach rates as a function of accumulated dose in ^{244}Cm doped 77-260 simulated waste glass.

the fracture process with an expectation that the particle size distribution should be changed depending on stress level. In spite of observed microfracturing, the particle size distribution in impact appears to be relatively constant.

The leach test results are shown in Fig. 4. The leach rates, expressed in grams of glass per cm^2 of the geometric surface area per day, are calculated using both weight loss and ^{244}Cm concentration in solution. It is clear that leach rates are not significantly affected by self-radiation. Although this noneffect has been previously reported for waste glasses,[8,10] this is the first experimental evidence that amorphization of crystalline phases may not cause major changes in leach rates. Since ~20 to 45% of the curium present was concentrated in the apatite phase, we conclude that amorphization of the apatite phase increases leach rates by less than a factor of ten. (The change could be approximately zero.) Obviously, this question must be further explored, particularly in studies of nuclear waste ceramics.

Another important observation is that leach rates based on weight loss are, in general, higher than those based on ^{244}Cm solution analysis. This suggests that the ^{244}Cm is retained to a high degree by both the glass and devitrification products and that the more soluble elements (alkali, boron) are the major species leached. There has been no attempt to correct the data of Fig. 4 for the increased area due to microfracturing (geometric area was used). Hence, as with the impact behavior, it appears that microfracturing has no measurable effect on the net material leached. Further studies of the importance of microcracking are in progress.

CONCLUSIONS

The results of this study allow several major conclusions:

- Physical–structural changes in the devitrified glasses are larger than in the vitreous form. Nevertheless, effective radiation-induced changes in density, leachability, impact behavior, and stored energy are small in all cases.
- In this study, the gadolinium titanate phase with a cubic structure is stable to self-radiation. The apatite structure, $Ca_3Gd_7(SiO_4)_5(PO_4)O_2$, is unstable and transforms to an X-ray amorphous state. There is a relatively large radiation-induced increase in crystal volume, causing microfracturing of the glass matrix. The cracking is minimal if the crystals are small (≲5 μm).
- For the glass composition studied, self-radiation does not significantly affect chemical durability or impact performance. Neither the observed crystalline phase amorphization nor the microfracturing causes large changes in the net material leached or the impact particle size distribution.

ACKNOWLEDGMENT

This work was supported by the U. S. Department of Energy under contract EY-76-C-06-1830. The contributions to this study by G. D. Maupin, J. E. Gose, D. H. Parks, and E. H. Shade are gratefully acknowledged.

REFERENCES

1. J. E. Mendel, *The Storage and Disposal of Radioactive Waste as Glass in Canisters*, DOE Report PNL-2764, Pacific Northwest Laboratory, 1978.
2. F. P. Roberts, G. H. Jenks, and C. D. Bopp, *Radiation Effects in Solidified High-Level Waste—Part 1, Stored Energy*, DOE Report BNWL-1944, Pacific Northwest Laboratory, 1976.
3. R. P. Turcotte, *Radiation Effects in Solidified High-Level Wastes—Part 2, Helium Behavior*, DOE Report BNWL-2051, Pacific Northwest Laboratory, 1976.
4. R. P. Turcotte and F. P. Roberts, Phase Behavior and Radiation Effects in High-Level Waste Glass, in *Ceramic and Glass Radioactive Waste Forms*, DOE Workshop, CONF-770102, Germantown, MD, January 4–5, 1977.
5. N. E. Bibler and J. A. Kelley, *Effect of Internal Alpha Radiation on Borosilicate Glass Containing Savannah River Plant Waste*, DOE Report DP-1482, Savannah River Laboratory, 1978.
6. W. A. Ross et al., *Annual Report on the Characterization of High-Level Waste Glass*, DOE Report PNL-2625, Pacific Northwest Laboratory, 1978.
7. R. L. Fleischer, P. B. Price, and R. M. Walker, *Nuclear Tracks in Solids*, University of California Press, 1975.
8. J. E. Mendel et al., *Annual Report on the Characterization of High-Level Waste Glasses*, DOE Report BNWL-2252, Pacific Northwest Laboratory, 1977.
9. J. L. McElroy, *Quarterly Progress Report, Research and Development Activities, Waste Fixation Program*, DOE Report PNL-2265-2, Pacific Northwest Laboratory, 1978.
10. K. Scheffler and U. Riege, *Investigations on the Long-Term Radiation Stability of Borosilicate Glasses Against Alpha-Emitters*, KFK-2422, Kernforschungszentrum, Karlsruhe, Germany, 1977.

EFFECTS OF IRRADIATION ON STRUCTURAL PROPERTIES OF CRYSTALLINE CERAMICS

F. W. CLINARD, Jr., and G. F. HURLEY
University of California, Los Alamos Scientific Laboratory, Los Alamos, NM

ABSTRACT

Stability of crystalline ceramic nuclear waste may be degraded by self-irradiation damage. Changes in density, strength, thermal conductivity, and lattice structure are of concern. In this paper, structural damage of ceramics under various radiation conditions is discussed and related to possible effects in nuclear waste.

INTRODUCTION

Crystalline ceramic forms of nuclear waste must exhibit stability over extremely long storage times. Self-irradiation is a major potential source of structural degradation which can reduce waste stability. The principal source of radiation damage in nuclear waste is spontaneous decay of alpha-active isotopes of actinide metals such as plutonium, americium, neptunium, and curium.[1] Damage effects are similar regardless of the isotope considered; alpha decay produces a recoil ion which is born with an energy of ~100 keV and loses this energy primarily by collisional processes. The ~5 MeV alpha particle loses most of its energy through electronic excitation and therefore causes less collisional damage than does the recoil ion. However, the helium gas deposited in the lattice is itself a source of degradation. Beta-emitting isotopes in nuclear waste are not a major source of displacement damage, but transmutation products resulting from beta decay can alter material behavior by inducing compositional changes.

Little information is available on alpha decay-induced damage in ceramics or on the detailed characteristics of ceramic nuclear waste. This paper considers the broad question of radiation-induced structural changes in ceramics and relates these changes to possible effects in ceramic waste.

IRRADIATION-INDUCED STRUCTURAL CHANGES

Swelling

One or more phases in multiphase ceramic waste may swell under irradiation, with consequent fracture of the swelling phase and perhaps of the waste mass itself. The resulting increase in surface area will lead to accelerated dissolution if leaching agents are present. In addition, fracture will decrease thermal conduction, thus increasing waste temperature and thermal stresses which may cause further degradation.

Ceramic waste will be damaged to a level of roughly one displacement per atom (dpa)* in ~10^2 to 10^5 yr if alpha decay events are uniformly distributed,[2] with higher localized damage levels anticipated if actinide isotopes are concentrated in certain phases. At 1 to 10 dpa, swelling of most ceramics falls within the range zero to a few percent, as shown by the neutron irradiation data of Table 1. Uniform swelling is not necessarily detrimental. However, differential or constrained swelling beyond that which can be accommodated elastically (on the order of 0.3 vol %) or plastically may lead to fracture. Some noncubic ceramics such as Al_2O_3 swell anisotropically and are therefore more likely to suffer structural deterioration (e.g., by grain boundary separation) than are those that swell isotropically.

Swelling of ceramics can occur by two mechanisms: an accumulation of point defects which dilate the lattice and the creation of new lattice sites. Lattice dilational swelling

---

*Dpa values for ceramics are rough estimates, since displacement energies are unknown in almost all cases.

TABLE 1

Changes Induced in Ceramics by Neutron Irradiation to ~1 to 10 dpa

Ceramic	Irradiation temp., °K	Fluence, n/m²*	Swelling, vol %	Reduction in thermal conductivity, %†	Aggregated defects resolved	Ref.
Al_2O_3	1015	2.8×10^{25}	1.9	53	Voids and dislocation tangles	3
$Y_3Al_5O_{12}$ ‡	1015	2.8×10^{25}	0.0	62	Clusters	3, 4
SiC	825	2.7×10^{25}	1.2	87		5, 6
ZrO_2–6% Y_2O_3	650	3.5×10^{25}	0.2		Dislocation loops	7
	875	3.2×10^{25}	1.6		Pores and tangles	7
	1025	2.8×10^{25}	0.0		Clusters	7
$MgAl_2O_4$ ‡	1015	2.8×10^{25}	0.0	8	None	3
Si_3N_4	1015	2.8×10^{25}	0.3	53	None	3, 4
BeO–5 SiC	1015	2.8×10^{25}	3.3	~60		3

*$E_n > 0.1$ MeV except >0.18 MeV for SiC.
†Derived from thermal diffusivity data, except for SiC.
‡Single crystal.

is greatest at low temperatures where point defects can remain isolated, and this growth often correlates with lattice expansion measured by X-ray diffraction. Creation of new lattice sites typically involves such phenomena as condensation of vacancies into voids and conversion of interstitials to lattice atoms (e.g., by precipitation into interstitial loops). These defect aggregates are usually large enough to be observed by transmission electron microscopy (TEM). Figure 1 shows an example of aggregates, in this case voids and dislocation tangles, in Al_2O_3. Aggregated defects seen in other ceramics are listed in Table 1. The mechanism and magnitude of swelling vary with temperature and the ceramic under consideration; the 3% vol change for SiC at 300°K appears to be due to lattice dilation,[5] whereas that observed in Al_2O_3 at elevated temperatures roughly coincides with measured void volume.[8] Ceramics which swell by the formation of new lattice sites tend to show a swelling peak as a function of temperature, but location of the peak is not typically at the same fraction of the absolute melting point as that observed for most metals (0.4 to 0.6 T_m). The swelling peak for $ZrO_2-6\% Y_2O_3$ (Table 1) occurs at ~0.29 T_m, whereas other ceramics show peaks at temperatures ranging from 0.21 to 0.53 T_m (Ref. 9).

Insoluble gases can enhance swelling at elevated temperatures by stabilizing voids against re-solution. Since an alpha-decay-induced damage level of 1 dpa is accompanied by formation of a large amount (~1000 appm) of helium,[2] gas effects may play a major role in determining swelling behavior of nuclear waste.

Strength

Stresses on ceramic waste may arise from macroscopically or microscopically constrained swelling, thermal stresses, dead weight, or stresses from geological effects. Good fracture strength is important in preventing mechanical failure and concomitant pulverization from any of these sources. Strength of brittle ceramics is determined by the stress required to extend a flaw, according to the relationship $\sigma_f c^{1/2} = K_c$. Here σ_f is the fracture stress, c is flaw size, and K_c is the fracture toughness. Thus irradiation damage can affect strength if flaw size or fracture toughness is altered.

Change in Fracture Toughness. Since fracture toughness is proportional to the product (Young's modulus × fracture surface energy), increases or decreases in strength could be brought about by a change in either of these terms. Fracture toughness of sapphire is increased by high-temperature irradiation which produces microvoids.[10] Here the voids are viewed as impeding the crack front, thereby effectively producing an increase in energy for crack propagation. Factors which might reduce fracture toughness would include any reduction in crack blunting processes or a reduction of modulus. Changes in the latter are not usually large, while changes due to the former would likely be limited to a reduction in that portion of the fracture energy attributable to plastic blunting processes.

Change in Crack Size. A number of damage effects could result in changes in crack size. Anisotropic swelling such as that seen in Al_2O_3 results in intergranular separation and concomitant loss of strength.[11] Differential swelling, which occurs in SiC bodies containing free Si, results in loss of strength due to production of cracks.[12] Another mechanism for flaw size change is in-situ high-temperature deformation leading to surface roughening. This process has been observed to operate in the absence of radiation effects[13] and may be worsened by radiation-induced creep such as that seen in UO_2 (Ref. 14). However, the opposite effect could occur if enhanced creep or diffusion results in blunting of cracks.

Not all ceramics are brittle, and most become ductile at sufficiently high temperatures. Fracture strength of ductile ceramics is related to the flow stress, because plastic deformation initiates flaws or causes preexisting flaws to

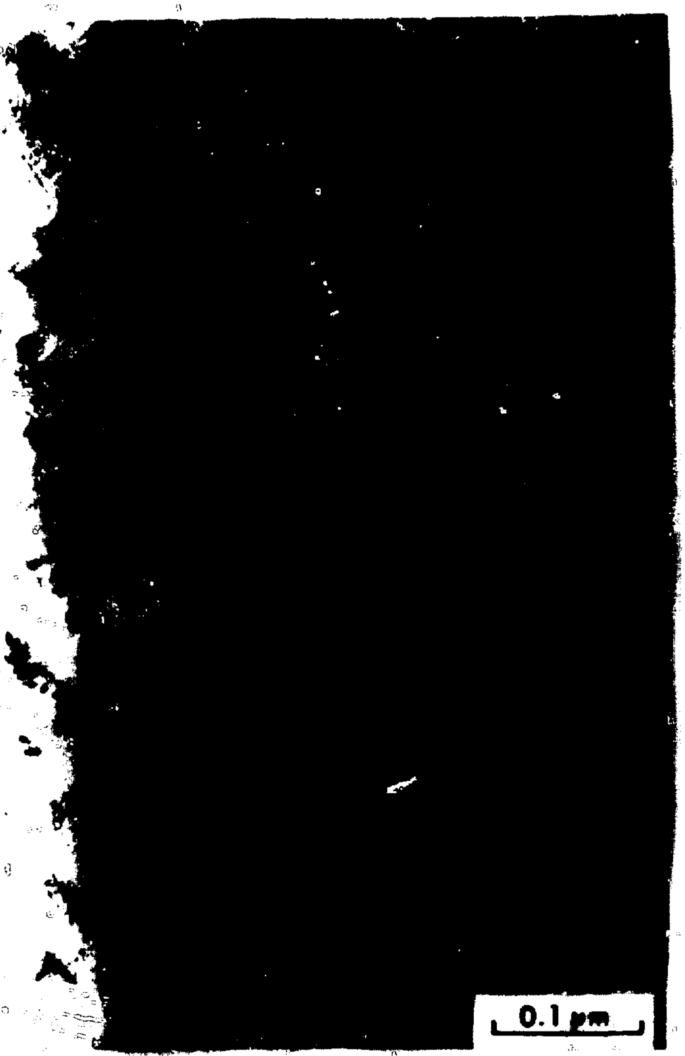

Fig. 1. Voids (aligned along the c axis) and dislocation tangles in Al_2O_3 after irradiation to 4.3×10^{25} n/m^2 at 875°K.

grow; either can become the fracture-initiating defect. Thus fracture occurs at a low stress compared with that expected from preexisting flaws. Magnesium oxide is an important example of this type of behavior; the effect of irradiation is to harden the material and hence raise the fracture stress.[15]

Grain boundary phenomena are of particular concern when considering effects of irradiation on strength. It has been observed in elevated-temperature tests of $^{238}PuO_2$ that helium from alpha decay forms an extensive network of gas bubbles along grain boundaries:[16] this could lead to a significant loss of strength. Denudation of aggregated damage near grain boundaries which act as sinks for defects might result in reduced swelling in these zones and consequent high internal stresses, even in cubic materials. Finally, the nature of both intergranular and intragranular fracture can affect the morphology of new surfaces formed and thus alter subsequent leaching behavior.

It should be noted that some phenomena affecting strength (e.g., slow crack growth and atomistic processes) were not addressed in this section, nor will those described necessarily affect strength of ceramics at 1 to 10 dpa.* The question of strength changes under irradiation is complex, and, as is the case for all structural properties relevant to nuclear waste, must ultimately be answered by experimentation.

Thermal Conductivity

A reduction in thermal conductivity will result in higher operating temperatures and thermal stresses, either of which can degrade waste structure. One source of reduced thermal conductivity is cracking of the waste mass, as mentioned above. Another is the presence of radiation-induced lattice defects which scatter the phonons by which heat is conducted. The magnitude of the latter effect is shown for a number of ceramics in Table 1. It is apparent that large changes are to be expected near room temperature. When this property is measured at elevated temperature, the fractional degradation is lessened due to a reduction in conductivity of the starting material as a result of increased phonon phonon scattering. For example, in neutron-irradiated single-crystal Al_2O_3 the reduction is 45% at RT but only 15% at 723 K (Ref. 17). Thus at higher operating temperatures degradation is expected to be lessened but can remain significant.

---

*Price[5] found that the strength of cubic SiC is little changed by irradiation to this dose level.

A tendency toward saturation of the reduction is typically observed. SiC exhibits saturation below 10^{25} n/m^2 (~1 dpa),[18] while fourteen other ceramics approach or have reached this condition at ~2 x 10^{26} n/m^2 (~20 dpa).[16] Higher irradiation temperatures, where defects are more likely to be observed in the form of large aggregates, are typically characterized by a lesser reduction in thermal conductivity.[16] This is consistent with calculations which show that smaller defects are more effective at scattering phonons.[19]

Results in Table 1 show that the nature of defects in different ceramics can vary greatly with fixed irradiation conditions. The slight reduction in thermal conductivity observed for $MgAl_2O_4$ (indicating a probable low point defect content) and the absence of aggregated defects suggest that defect recombination and annihilation occur relatively easily in this material. Such behavior would be desirable in ceramic nuclear waste and, if not an intrinsic property, could perhaps be engineered into the material. For example, a finely dispersed second phase could be added to refine grain size and supply interphase boundaries, both of which will increase surface area available for defect trapping and annihilation. This approach has been used to inhibit void formation in stainless steel.[20] Not just thermal conductivity but all physical properties of importance to nuclear waste stability are subject to improvement by reengineering of materials, if known principles of radiation damage control are applied.

Lattice Structure

Radiation-induced disordering of crystalline ceramics can cause a gradual transition to an amorphous or glassy structure. (This effect is termed metamictization when induced in minerals by radioactive decay.) Major changes in important structural properties such as density, strength, and thermal conductivity may result. In addition, the higher free energy of the glassy structure is likely to increase leaching rates. Amorphization can take place over a wide range of damage levels, depending on the material; irradiation with heavy ions results in transformation at ~0.1 to 100 dpa,[21] while a similar damage dose is required for metamictization of minerals.[22] Since nuclear waste will be damaged to ~1 to 10 dpa, amorphization must be considered a possibility.

The following factors seem to favor amorphization

- Low ionic bonding character
- Open lattice structure
- High water content

Naguib and Kelly[23] surveyed the heavy-ion irradiation behavior of 56 nonmetals and found that those with ionicity ≤ 0.47 show a strong tendency to amorphize. It was suggested that such considerations as the absence of an electrostatic term in the disorder energy of covalently bonded materials may be responsible. Taylor and Ewing[24] compared the structure of the thorite phase of $ThSiO_4$ (which is often found in the metamict state) with that of the always-crystalline huttonite phase of the same material. They found that the principal difference is the presence of a network of large interconnected void spaces in the lattice of thorite. It has been postulated that an open lattice structure can relatively easily accommodate lattice disorder and that this might increase the likelihood of metamictization. Also, thorite is characterized by a high water content which may enter the lattice through interconnected void spaces.[24] Since the presence of water has been found to accelerate amorphization of electron-bombarded silicates,[25] this may be an important factor in establishing the likelihood of amorphization.

SUMMARY

At the damage level anticipated for ceramic nuclear waste (~1 to 10 dpa), some ceramics undergo major structural changes while others are little affected. The following material characteristics seem to enhance irradiation stability of one or another material.

- Cubic crystal structure
- High helium permeability
- Large internal surface area
- High fracture toughness
- High ionic bonding character
- Dense atomic packing
- Low propensity for absorption of water

These are phenomenological observations, gained by observing the effect of a particular characteristic on irradiation behavior of one ceramic or a class of ceramics; thus contradictions are inevitable. For example, dense atomic packing may suppress amorphization but could enhance lattice dilational swelling. Nevertheless, in cases where irradiation stability of a ceramic nuclear waste form is found to be inadequate, it should be possible to apply knowledge of the role of these factors to development of more stable waste forms.

ACKNOWLEDGMENT

This work was performed under the auspices of the U. S. Department of Energy.

REFERENCES

1. G. H. Jenks and C. D. Bopp, *Energy Storage in High Level Radioactive Waste and Simulation and Measurement of Stored Energy with Synthetic Wastes*, Oak Ridge National Laboratory Report ORNL-TM-3781 (1973).
2. F. W. Clinard, Jr., Radiation Damage in Ceramics, in *Proceedings of the ERDA Workshop on Glass and Ceramic Radioactive Waste Forms*, U. S. Energy Research and Development Administration Report CONF-770102, p. 147 (1977).
3. G. F. Hurley and J. M. Bunch, Swelling and Thermal Diffusivity Changes in Neutron-Irradiated Ceramics, submitted to *J. Am. Ceram. Soc.*
4. F. W. Clinard, Jr., and L. W. Hobbs, talk presented at the Annual Meeting of the American Ceramic Society, Detroit, Michigan, May 1978.
5. R. J. Price, Effects of Fast Neutron Irradiation on Pyrolytic Silicon Carbide, *J. Nucl. Mater.* 33: 17 (1969).
6. R. J. Price, Thermal Conductivity of Neutron-Irradiated Pyrolytic β-Silicon Carbide, *J. Nucl. Mater.*, 46: 268 (1973).
7. F. W. Clinard, Jr., D. E. Rohr, and W. A. Ranken, Neutron Irradiation Damage in Stabilized ZrO_2, *J. Am. Ceram. Soc.*, 60: 287 (1977).
8. F. W. Clinard, Jr., J. M. Bunch, and W. A. Ranken, Neutron Irradiation Damage in Al_2O_3 and Y_2O_3, in *Proceedings of the International Conference on Radiation Effects and Tritium Technology for Fusion Reactors*, U. S. Energy Research and Development Administration Report CONF-750989, Vol. II, p. 498 (1976).
9. L. W. Hobbs, Application of Transmission Electron Microscopy to Engineering Practice in Ceramics: Radiation Damage, *J. Am. Ceram. Soc.*, in press.
10. G. F. Hurley, Los Alamos Scientific Laboratory, Department of Energy (Office of Fusion Energy) Special Purpose Materials Annual Progress Report for 1978, USDOE report, in press.
11. R. S. Wilks, J. A. Desport, and J. A. G. Smith, The Irradiation-Induced Macroscopic Growth of α-Al_2O_3 Single Crystals, *J. Nucl. Mater.*, 24: 80 (1967).
12. R. B. Matthews, Irradiation Damage in Reaction-Bonded Silicon Carbide, *J. Nucl. Mater.*, 51: 203 (1974).
13. N. J. Tighe, The Structure of Slow Crack Interfaces in Silicon Nitride, *J. Mater. Sci.*, 13: 1455 (1978).
14. A. A. Solomon, Radiation-Induced Creep of UO_2, *J. Am. Ceram. Soc.*, 56: 164 (1973).
15. R. A. Sambell and R. Bradley, The Strength of Irradiated Magnesium Oxide, *Philos. Mag.*, 9: 161 (1964).
16. B. A. Mueller, D. D. Rohr, and R. N. R. Mulford, *Helium Release and Microstructural Changes in* $^{238}PuO_2$, Los Alamos Scientific Laboratory Report LA-5524 (1974).
17. G. F. Hurley, Los Alamos Scientific Laboratory Controlled Thermonuclear Research Program Progress Report for 1977, Report LA-7474-PR, in press.
18. R. P. Thorne, V. C. Howard, and B. Hope, Radiation-Induced Changes in Porous Cubic Silicon Carbide, *Proc. Brit. Ceram. Soc.*, 7: 449 (1967).
19. P. G. Klemens, G. F. Hurley, and F. W. Clinard, Jr., Reduction in Thermal Conductivity of Ceramics Due to Radiation Damage, in *Proceedings of the Second Topical Meeting on the Technology of Controlled Nuclear Fusion*, U. S. Energy Research and Development Administration Report CONF-760935-P3, p. 957 (1977).
20. B. N. Singh, Inhibited Void Formation in Dispersion-Hardened Austenitic Stainless Steel During High-Energy Electron Irradiation, *J. Nucl. Mater.*, 46: 99 (1973).
21. H. M. Naguib and R. Kelly, The Effect of Ion Bombardment on the Structure of Bi_2O_3, MoO_3, TeO_2, and V_2O_5, *Radiat. Effects*, 25: 79 (1975).
22. B. Lustman, Irradiation Effects in Uranium Dioxide, in *Uranium Dioxide: Properties and Nuclear Applications*, J. Belle (Ed.), USAEC, p. 431 (1961).
23. H. M. Naguib and R. Kelly, Criteria for Bombardment-Induced Structural Changes in Non-Metallic Solids, *Radiat. Effects*, 25: 1 (1975).
24. M. Taylor and R. C. Ewing, The Crystal Structures of the $ThSiO_4$ Polymorphs: Huttonite and Thorite, *Acta Crystallogr.*, B34: 1074 (1978).
25. L. W. Hobbs, Case Western Reserve University, private communication, 1979.

THE METAMICT STATE RADIATION DAMAGE IN CRYSTALLINE MATERIALS

RICHARD F. HAAKER and RODNEY C. EWING
Department of Geology, University of New Mexico, Albuquerque,
New Mexico

ABSTRACT

Metamict minerals provide an excellent basis for the evaluation of long-term radiation damage effects, particularly such changes in physical and chemical properties as microfracturing, hydrothermal alteration, and solubility. This paper summarizes pertinent literature on *metamictization and proposes experiments that are critical to the* elucidation of structural controls on radiation damage in crystalline phases.

INTRODUCTION

Metamict minerals are a class of radioactive materials which were initially crystalline but are now amorphous to X-ray diffraction. Although the exact mechanism for the apparent loss of crystallinity is not understood, it is certain that structural damage from alpha particles and recoil nuclei are critical to the process. Since these minerals have been severely affected by radiation damage, as well as exposed to weathering and alteration processes over geologic periods of time, they may serve as useful analogues to crystalline waste forms which are subject to similar processes. The purpose of this paper is to provide background information on the process of metamictization and to summarize experiments which are designed to elucidate the structural controls on radiation damage. To illustrate the changes in physical and chemical properties accompanying progressive radiation damage, zircon [tetragonal $(Zr,U)SiO_4$], a widely studied metamict mineral, will be discussed in detail.

THE METAMICTIZATION PROCESS

Minerals containing as little as 0.5 wt.% UO_2 or ThO_2 may become metamict. Accompanying the metamict transition are decreased density, refractive index, and birefringence; and increased hydration, alteration and microfracturing.[1] As the crystal structure becomes increasingly disrupted, X-ray diffraction maxima broaden, shift to lower values of 2θ, and ultimately become indistinguishable from background. The X-ray diffraction pattern of a metamict mineral is similar to that of a glass.

Zircon: A Case Study

Because of its wide use in uranium/lead age dating, zircon is one of the most thoroughly studied metamict minerals. Many of the early studies on radiation damage effects in zircon were undertaken to investigate the possibility of using radiation damage as a means of estimating age.[2,3] Radiation damage proved unsatisfactory as an age-dating technique. Nonetheless, data accumulated during these investigations offer a clear picture of the process of metamictization in zircon.

Holland and Gottfried[3] measured the physical properties of zircon as a function of degree of metamictization. The zircons were of gem quality and completely unaltered. They were dated and total alpha dosages were calculated from measurements of their present alpha activity, lead content and thorium/uranium ratios.

Densities were determined by the flotation method and plotted as a function of total alpha particle dosage. Specimens with total alpha dosages in excess of approximately 10^{15} α/mg had reduced densities. For dosages above

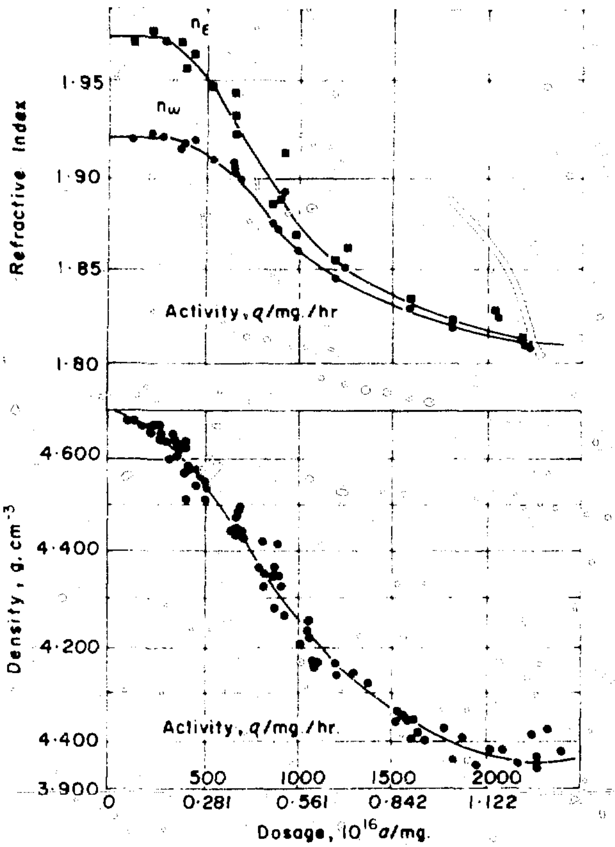

Fig. 1 Refractive indices and density of Ceylon zircons as a function of total alpha dosage.[1]

2×10^{15}, the density decreases rapidly from 4.65 g/cm^3 to a saturation density of 3.96 g/cm^3 for specimens with alpha dosages of approximately 11×10^{15} α/mg (Fig. 1).

X-ray powder diffraction was used to monitor changes in unit cell dimensions as a function of total alpha dosage. It was determined that expansion rates of unit cell parameters are quite anisotropic. c increases about twice as rapidly as a, for dosages below approximately 2.3×10^{15} α/mg. At higher dosages the situation is reversed, a increases faster than c, so that unit cell parameter changes for saturated material represent an approximately isotropic expansion. At low dosages, peak shapes remain approximately unchanged, but at alpha dosages above 2×10^{15} α/mg, line broadening becomes progressively more severe (Fig. 2). For specimens with dosages of 5 to 7×10^{15} α/mg, all but the most intense diffraction maxima are indistinguishable from background. Metamict zircons which have a density of approximately 4.0 g/cm^3 (i.e., a dosage of 10^{16} α/mg) display an essentially featureless X-ray diffraction pattern.

Refractive indices, N_w and N_e, were measured for the same set of zircons and plotted as a function of radiation dosage (Fig. 1). At dosages above 1.5×10^{15} α/mg, refractive indices and birefringence decrease rapidly. Completely metamict specimens with dosages in excess of approximately 11×10^{15} are optically isotropic.

The structure of the metamict state, whether glassy or crystalline, has been the subject of considerable debate. It is certain that metamict minerals cannot be composed of crystallites exceeding approximately 0.01 μm, as this is the lower limit of crystallite sizes which will diffract X rays. That metamict minerals do not diffract X rays and can store amounts of energy which are comparable to their heats of fusion (e.g., 89.1 cal/gm for gadolinite[4]) has supported the contention that metamict minerals are glassy.

Transmission electron microscopy is better suited to the study of the metamict state since electron diffraction patterns can be obtained on samples having a mean crystalline size of less than 0.01 μm. Bursill and McLaren[5] have applied TEM to the study of metamict zircon (dosage ~10^{16} α/mg). When flakes of metamict zircon were examined by TEM, diffraction patterns revealed that they were composed of slightly misoriented zircon crystallites approximately 0.01 μm in diameter (Fig. 3). In this instance, it appears that metamict zircons are nonvitreous. It is striking that the electron diffraction patterns of Bursill and McLaren are essentially those of a simple crystal.

Chemical changes in zircon as a function of degree of metamictization are poorly understood and poorly documented. That lead is not retained well by metamict zircon is obvious since metamict zircons give discordant U/Pb radiometric ages. However, it should be noted that (1) the majority of all published U/Pb ages are discordant[6] and (2) the question of lead retentivity is not particularly relevant to radioactive waste disposal, as production of radiogenic lead will be negligible during the time scale of concern (10^6 years).

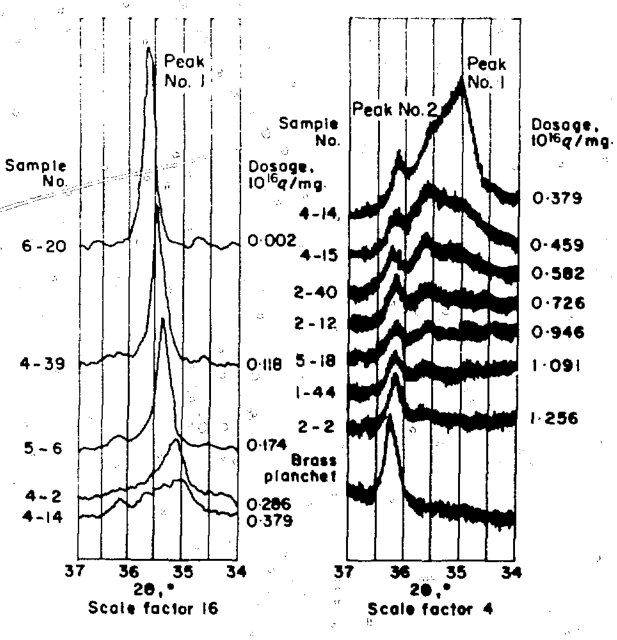

Fig. 2 Shape of the (112) diffraction maxima of zircon as a function of total alpha dosage.[3]

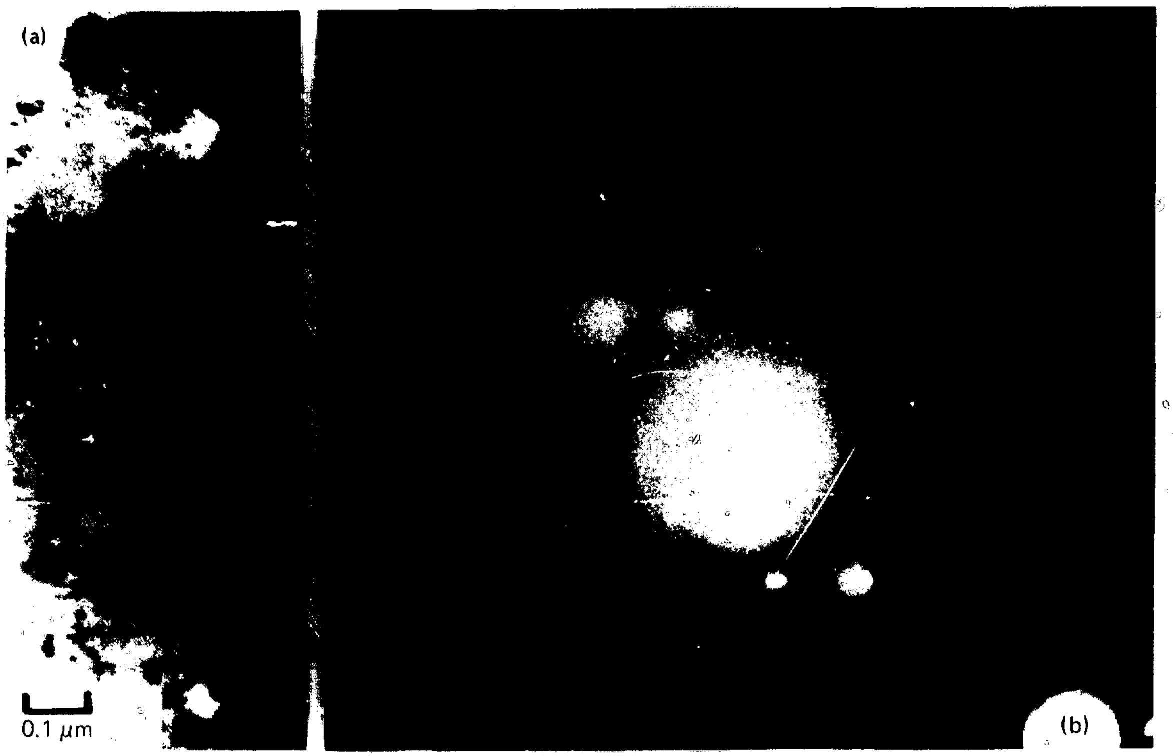

Fig. 3 TEM image and electron diffraction pattern[5] of a flake of metamict zircon (dosage ~10^{16} α/mg).

Loss of uranium from metamict zircon is not well documented. A study of the hydrothermal stability of lead and uranium in a single metamict zircon suggests that uranium loss is insignificant under the following conditions: 500°C, 1000 bars, 2 molal NaCl solution.[7] This is consistent with the observation that metamorphism increases the U content of nonmetamict zircon.[8] It should, however, be noted that the mobility and solubility of uranium varies enormously as a function of Eh, pH, total carbonate concentration, and temperature. Only minor loss of uranium would be expected under the experimental conditions of Pidgeon et al.[7] More significant leaching of uranium may be observed in an oxidizing, acidic, or basic environment with significant carbonate concentrations and a temperature of 100°C or less.

Another aspect of alteration of metamict zircon is loss of silica. Annealing metamict zircons at temperatures of 1000°C often results in a material whose powder pattern may be indexed as $ZrSiO_4 + ZrO_2$ or ZrO_2, suggesting loss of silica from the crystal structure. A study of the compositions of 69 zircon and thorite specimens indicates these minerals are frequently five- to ten-mole % deficient in SiO_2 (Ref. 9). Many of the published analyses used in that study may be of questionable quality. More extreme loss of SiO_2 from metamict zircon resulting in replacement of zircon by ZrO_2 has been observed by Bylinskaya and Perets.[10]

The distribution of uranium within zircon crystals is often inhomogeneous. As a result, single zircon crystals are sometimes zoned with alternating uranium-rich metamict, altered layers, and fresh unaltered layers with low uranium concentrations.[11] Since zoned zircons are inhomogeneous, it is difficult to estimate how compositions have been affected by preferential leaching of metamict zones. It is apparent that the metamict zircon is more altered than adjacent layers of nonmetamict zircon.

STRUCTURAL CONTROLS ON RADIATION DAMAGE

Some structures are markedly more susceptible to radiation damage than others. To illustrate how great the differences in susceptibility may be, it is useful to compare the alpha decay rates of a typical metamict zircon with $^{238}PuO_2$, a compound with the uraninite fluorite structure which suffers only minor radiation damage effects (Table 1).

TABLE 1

A Comparison of Zircon and $^{238}PuO_2$

	Zircon	$^{238}PuO_2$
Actinide content	1% UO_2	
Alpha decay rate (α/mg · day)	8.5×10^4	4.9×10^{13}
Ratio of decay rates	1.0	5.8×10^8
Radiation effect	Becomes metamict	Becomes 2% less dense[12]

Several structural generalizations concerning the structure of metamict minerals may be made. Metamict minerals tend to have (1) complex compositions, (2) channels or interstitial voids which may accommodate displaced atoms or water, and (3) uranium or thorium present though not necessarily essential to their structures.

Monazite, monoclinic $CePO_4$, is a natural host for actinide elements and normally has a high stability toward radiation damage. It is a common phase in supercalcine formulations. In contrast to zircon which contains less than 4 wt.% $(U,Th)O_2$ and is commonly metamict, monazite containing 20 wt.% $(U,Th)O_2$ is seldom reported in the metamict state. If, like the uraninite structure, monazite is shown to be stable to the high alpha disintegration rates expected from the presence of 0.5 to 1 wt.% plutonium + curium + americium, it would appear to be an excellent candidate for isolating actinide elements. Although natural monazite may contain 20 wt.% $(U,Th)O_2$ and remain nonmetamict, this does not necessarily imply that monazite as a waste phase containing 0.5 to 1 wt.% plutonium + curium + americium will be immune to metamictization. Furthermore, rare occurrences (perhaps based on incorrect identifications) of metamict monazite[13] and isostructural huttonite[14] ($ThSiO_4$) suggest that particular compositions of this phase may be subject to metamictization. Before monazite, or any crystalline phase, is accepted as a waste form, it must be verified that anticipated compositions are stable and that the phase is not subject to adverse effects resulting from radiation damage. Experiments to determine the suitability of monazite (and additional crystalline phases) as actinide hosts are being planned at Battelle, PNL.

EXPERIMENTAL

Since typical HLW contains 0.1- to 0.2-mole % americium + curium + plutonium whose half-lives are negligible in comparison with the 10^9 to 10^{10} year half-lives of natural uranium and thorium, substantial radiation damage effects in actinide host phases are a distinct possibility.[15] Monazite-like and zircon-like phases are possible hosts for actinide elements in ceramic-crystalline waste forms. Experiments to determine their structural stabilities to radiation damage are necessary.

Phases of interest include the two pairs of isomorphous minerals huttonite–monazite and thorite ($ThSiO_4$)–zircon. These phases will be synthesized with small amounts of plutonium or curium substituting for cerium, thorium, and zirconium. Radiation damage in these phases will be monitored by X-ray diffraction methods in conjunction with determination of changes in physical properties. Solubility and leachability of these phases will also be determined as a function of degree of metamictization.

CONCLUSIONS

Radiation damage effects in actinide-containing phases may not be deleterious to the waste form. Metamictization is undesirable only if it results in (1) excessive increases in volume, (2) extensive microfracturing, or (3) increased leach rates. Since uranium- and thorium-containing minerals do not contain plutonium, curium, or americium, they must be considered imperfect analogues to waste phases. The effects of high-alpha particle fluxes and recoil nuclei on monazite-like phases are not known; only when the crucial experimental data on radiation damage effects is available can informed conclusions be made.

Radiation damage simulation experiments should, for orthosilicate and orthophosphate structures, lead to an understanding of the interrelationships among the degree of metamictization, alpha particle dosage, alpha activity and structure dependent self-annealing processes. The understanding of the process of metamictization and empirical data on the solubility and leachability of synthetic "metamict minerals" will provide information on the suitability of orthosilicates and orthophosphates as actinide hosts. These radiation damage experiments will also determine if there is an upper limit to the amounts of plutonium + americium + curium which may be isolated in monazite-like phases without unacceptable radiation damage effects.

ACKNOWLEDGMENT

This work was supported by Battelle, PNL under contract EY-76-C-06-1830.

REFERENCES

1. R. C. Ewing and R. F. Haaker, The Metamict State: Radiation Damage in Crystalline Phases, in Proceedings of *High-Level Radioactive Solid Waste Forms,* Denver, NUREG/CP-0005, National Technical Information Service, Springfield, VA, 1979.
2. P. M. Hurley and H. W. Fairbairn, Radiation Damage in Zircon: A Possible Age Method, *Bull. Geol. Soc. Am.*, 64: 659 (1953).
3. H. D. Holland and D. Gottfried, The Effect of Nuclear Radiation on the Structure of Zircon, *Acta Crystallogr.*, 8: 291 (1955).
4. A. Pabst, The Metamict State, *Am. Mineral.*, 37: 143 (1952).
5. L. A. Bursill and A. C. McLaren, Transmission Electron Microscope Study of Natural Radiation Damage in Zircon, *Phys. Status Solidi,* 13: 331 (1966).
6. D. York and R. M. Farquhar, *The Earth's Age and Geochronology,* Pergamon Press, New York, 1972.
7. R. T. Pidgeon, J. R. O'Neil, and L. T. Silver, Uranium and Lead Isotopic Stability in a Metamict Zircon Under Experimental Hydrothermal Conditions, *Science,* 154: 1538 (1966).
8. T. E. Krogh and G. L. Davis, Additions of Uranium to Zircons and Migrations of Strontium and Rubidium During Regional Metamorphism in the Greenville Province in Ontario (Abstract), *EOS (American Geophysical Union Transactions),* 54: 494 (1974).
9. F. A. Mumpton and R. Roy, Hydrothermal Stability Studies of the Zircon–Thorite Group, *Geochem. Cosmochim. Acta,* 21: 217 (1961).
10. L. V. Bylinskaya and N. A. Perets, Formation of Baddeleyite After Metamict Cyrtolite, *Miner. Paragenezisy Miner. Metsomaticheskikh Metamorf. Gorn. Porod.*, 1975, P. M.

Tatarinov (Ed.), Leningrad Otd: Leningrad USSR (*Chem. Abstr.*, 84: 108518 (1976)).

11. F. S. Larsens, C. L. Waring, and Joseph Berman, Zoned Zircon from Oklahoma, *Am. Mineral.*, 38: 1118 (1953).
12. R. P. Turcotte and T. D. Chikalla, Concentrated Defects in PuO_2 in *Defects and Transport in Oxides*, Martin S. Seltzer and Robert I. Jaffee (Eds.), Plenum Press, New York, 1974.
13. M. D. Kharkhanavala and J. Shankar, X-Ray Study of Natural Monazite, *Proc. Indian Acad. Sci.*, 60A: 67 (1954).
14. A. V. Kosterin and V. N. Zuev, Hydrothermal Huttonite, *Zap. Vses. Mineral. O-va.*, 91: 99 (1962).
15. G. J. McCarthy, High Level Waste Ceramic Materials Considerations, Process Simulation, and Product Characterization, *Nucl. Technol.*, 32: 94 (1977).

RADIATION DAMAGE STUDIES ON SYNTHETIC NaCl CRYSTALS AND NATURAL ROCK SALT FOR WASTE DISPOSAL APPLICATIONS

R. W. KLAFFKY,† K. J. SWYLER,* and P. W. LEVY*
*Brookhaven National Laboratory, Upton, New York, and †Los Alamos Scientific Laboratory, Los Alamos, New Mexico

ABSTRACT

Radiation damage studies are being made on synthetic NaCl and natural rock salt crystals from various localities, including potential repository sites. Measurements are being made with equipment for recording the radiation-induced F-center and colloid particle absorption bands during irradiation with 1.5 MeV electrons at various temperatures. A technique has been developed to resolve the overlapping F-center and colloid bands. The resulting spectra and curves of absorption versus dose provide information on colloid particle size and concentration and activation energies for processes occurring during colloid formation; additional data suggest that both strain and radiation-induced dislocations contribute to the colloid formation process.

INTRODUCTION

As part of the program to dispose of radioactive waste in underground repositories, radiation damage studies are being made on natural rock salt. The radiation levels from the waste are expected to produce considerable radiation damage in the salt.[1-4] Radiation damage considerations will enter into repository site selection, engineering, and risk assessment. It is expected that radiation damage effects will be particularly important in assessing any physical and chemical interactions that might occur between the encapsulated waste and the surrounding rock. For example, the chemical reactions between canisters, under either wet or dry conditions, and normal rock salt could differ appreciably from chemical reactions with irradiated rock salt containing colloid sodium particles and an equivalent amount of chlorine in undetermined form. Furthermore, these interactions will take place in a gamma-ray radiation field as long as the canister integrity is maintained, but alpha-particle and beta-ray irradiation will be involved if the canister opens and mixing occurs. Since the surrounding rock will be continuously irradiated, it is prudent to make measurements under conditions where it is possible to study effects occurring during irradiation which might not be detected if measurements are made only after irradiation. Such studies can be conveniently made with the unique equipment at Brookhaven National Laboratory for making optical measurements on samples while they are irradiated with electrons.

Until recently a large part of the information on radiation damage to rock salt was obtained with synthetic crystals.[1-3] This work showed that irradiation at temperatures expected in rock adjacent to canisters would produce F-centers (electrons trapped on chlorine atom vacancies), colloidal sodium metal particles, interstitial dislocation loops, and, presumably, chlorine atom clusters. The F-centers and colloid particles can be conveniently studied by optical absorption techniques since they produce absorption bands at ~2.6 eV (472 nm) and 2.1 eV (585 nm), respectively. Appreciable information on radiation effects in both natural and synthetic NaCl, particularly on stored energy effects, is contained in a publication by Jenks and Bopp.[3]

A thorough characterization of radiation damage in both synthetic NaCl crystals and natural rock salt from various localities, including localities under consideration as repository sites, was initiated recently. The apparatus for making optical absorption measurements during electron irradiation is used to record absorption spectra as often as every 40 sec on samples contained in a temperature-controlled chamber during and after irradiation with 1.5 MeV electrons.[4] Measurements are made at different temperatures and dose rates, on "unstrained" samples, and on samples plastically deformed prior to irradiation. At temperatures where colloid formation is observed, the F-center absorption grows to a saturation level and at this point the colloid formation rate increases from a very low to a rapidly increasing value. The F-center saturation level varies strongly with temperature and dose-rate but is only slightly dependent on plastic deformation or the geological origin of the natural samples. The dose required for F-center saturation and rapid colloid growth decreases with increasing deformation. The colloid formation rate is strongly temperature dependent; it is low at 125°C, increases to a maximum at roughly 175°C, and is negligible at 300°C.

The radiation-induced F-center and colloid absorption bands strongly overlap. To obtain reliable growth kinetics the bands must be resolved well enough to obtain precise absorption versus dose curves. A technique for making this resolution is described below. This leads to a number of useful results. The average colloid particle concentration and radius are obtained by fitting the classical Mie theory expression for colloid particle extinction coefficients to the resolved colloid band.[5] Accurate F-center saturation levels are obtained from which one may determine activation energies that can be compared to those in the Jain–Lidiard treatment for radiation-induced colloid growth.[6] Finally, it has been shown that cycles of irradiation, annealing, and reirradiation produce a reduction in the dose required for the onset of rapid colloid growth similar to that produced by plastic deformation. This observation suggests that radiation- and strain-induced dislocations play equivalent roles in colloid formation.

COLLOID ABSORPTION BAND ANALYSIS

The numerical procedure for resolving recorded spectra into separate F-center and colloid absorption bands proceeds in two steps. First, the shape of the F-band—and the combined F- and M-bands if the latter is present—is determined from spectra recorded as the F-center band is approaching saturation and rapid colloid band growth is commencing. The spectrum chosen is subtracted from spectra recorded at later times. If this choice is satisfactory, the resulting spectra contain only the colloid absorption introduced by additional irradiation. However, if the resulting spectra contain detectable F-band contributions, another trial spectrum is chosen and the procedure repeated. At doses where this subtraction can be made, the resolved colloid band and the chosen F-band (shape) are fitted to the measured spectra by a procedure which adjusts the F- and colloid-band intensities until a least squares best fit is obtained. Figure 1 shows the separate F-band and colloid band obtained for a synthetic NaCl crystal subjected to a 250 Mrad dose at 153°C. The solid line through the data points (upper curve) is the sum of the two components.

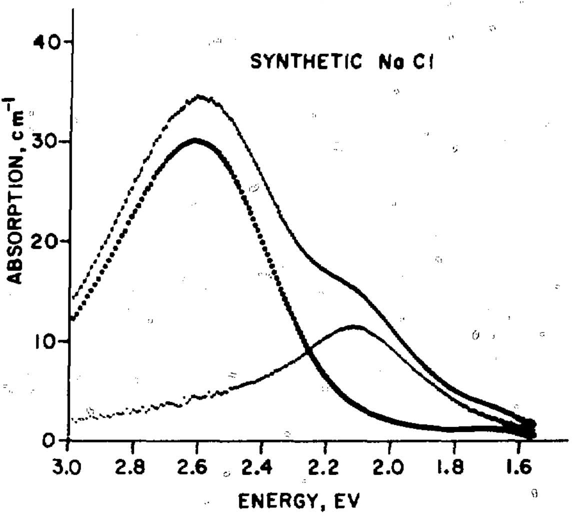

Fig. 1 Typical radiation-induced absorption spectrum for synthetic NaCl resolved into F-center (2.6 eV) and Na metal colloid (2.1 eV) bands using the resolution procedure described in the text.

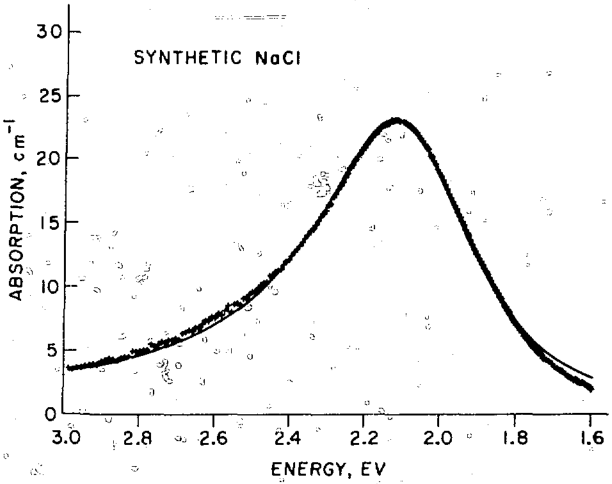

Fig. 2 Measured sodium metal colloid absorption band (+ + + +) and a best-fit theoretical extinction curve (———) computed from Mie theory modified for small particles. The numerical values obtained from the theoretical curve are: average colloid radius = 1.44 nm; plasma frequency = 7.96×10^{15} Hz; number of colloid particles/cm^3 = 7.2×10^{14}; and the colloid volume fraction = 9.0×10^{-6}.

The resolved colloid bands, such as those shown in Fig. 2, have been analyzed to obtain data on the average particle diameter and colloid particle concentration. The Kreibig and Fragstein[7] modification of the Mie[5] theory for small particles (< 10 nm radius) was used with an appropriately adjusted plasma frequency. An adequate fit was obtained using only the electric dipole term in the extinction coefficient expansion. Figure 2 shows the fit obtained for the resolved colloid band shown in Fig. 1. The Fig. 2 analysis yields 1.44 nm for the average colloid particle radius and 7.2×10^{14} cm^{-3} for the colloid particle concentration. In future studies this analysis will be used to determine the average colloid particle radius and concentration during irradiation at different temperatures.

TEMPERATURE DEPENDENCE ON THE F-CENTER SATURATION LEVEL

The resolution procedure described above provides curves of F-center concentration versus dose which increase monotonically to a well-defined plateau or saturation level (Fig. 3). At a given temperature the colloid formation is low until the F-centers reach saturation and increases at a much greater rate at higher doses.

In the Jain–Lidiard theory of radiation-induced colloid formation, the F-center saturation level plays an important role.[6] The theory assumes that the F-center diffusion is controlled by a single thermally activated process during irradiation at a given dose rate. Also, the temperature dependence of the F-center saturation level is determined by the F-center diffusion process. In this case an Arrhenius plot of log saturation level versus 1/T should contain a single linear component. The theory also predicts that the activation energy would be one-half the thermal diffusion energy, and, since Jain and Lidiard used 0.8 eV, the value obtained from the Arrhenius plot should be 0.4 eV.

An Arrhenius plot obtained from measured F-center saturation levels is shown in Fig. 4. The saturation levels were obtained from growth curves made by resolving recorded spectra into F-center and colloid bands. The data have *not* been corrected for temperature dependent changes in F-center bandwidth, but this would introduce very small changes. Clearly, there are two linear regions in Fig. 4. This could occur if there were two thermally activated processes controlling the F-center saturation levels. The activation energies are approximately 0.2 eV for the low temperature region and approximately 0.9 eV for the high temperature one. Neither of these values is close to the 0.4 eV expected by Jain and Lidiard. The low temperature region corresponds to the temperature range where colloid formation is most rapid, i.e., the 150–185°C region. These observations, together with previous dose rate and annealing measurements, indicate that a number of processes may be involved in F-center and colloid formation. For example, the low temperature process may involve a transient radiation-induced species as an ionized F-center while the high temperature process may represent the annealing of radiation-induced F-centers. Finally, the existence of these two processes must be reconciled with the occurrence of the maximum in the colloid formation rate observed in the 150–185°C region.

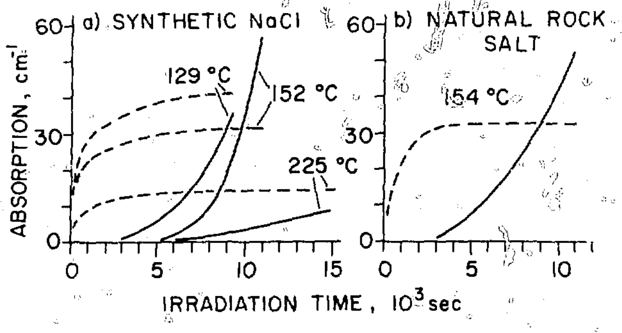

Fig. 3 Growth of F-center (– – – –) and colloid (———) absorption bands during irradiation with 1.5 MeV electrons at 120 Mrads/hr in (a) synthetic NaCl and (b) natural rock salt (from Ref. 4).

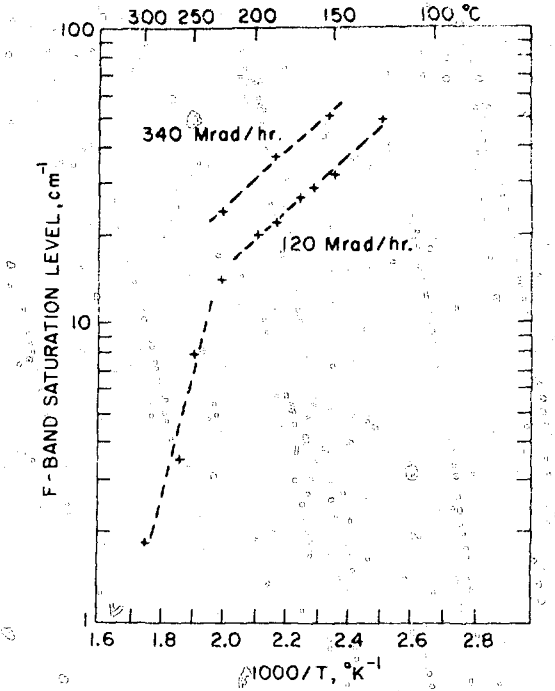

Fig. 4 F-center saturation levels versus reciprocal temperature for synthetic NaCl crystals irradiated with 1.5 MeV electrons at 120 and 340 Mrads/hr. The high and low temperature regions correspond to activation energies of 0.9 and 0.2 eV, respectively.

DISLOCATION-RELATED EFFECTS IN NATURAL AND SYNTHETIC ROCK SALT

As described above, in both natural and synthetic salt crystals and at temperatures where colloid formation is observed, the dose required to achieve F-center saturation roughly corresponds to the dose at which the colloid formation rate increases from a low to a relatively high value. The magnitude of this *induction period dose* is decreased by plastically deforming the samples prior to irradiation. A remarkably similar reduction is effected by a cycle of irradiation, annealing and then reirradiation to establish the modified induction period. These observations suggest that an increase in dislocation density decreases the induction period dose. To test this hypothesis, yield point measurements were made on synthetic NaCl samples

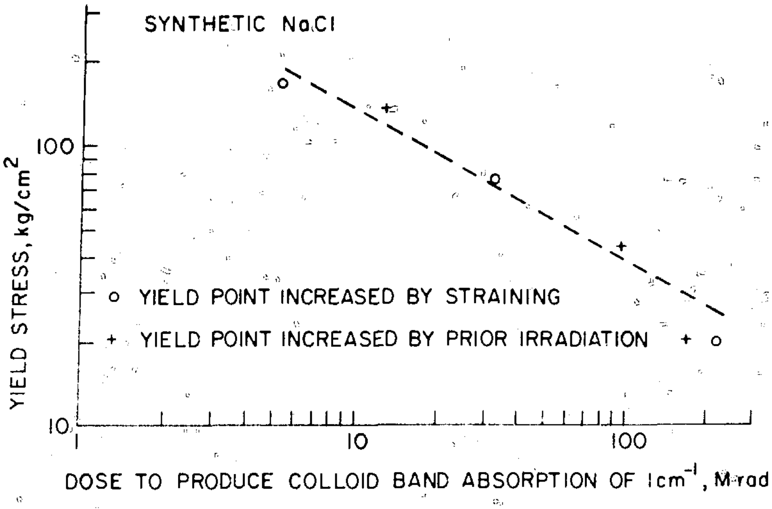

Fig. 5 Yield stress versus dose required to produce rapid colloid growth. This curve demonstrates that strain- and radiation-induced dislocations play equivalent roles in the colloid formation process.

subjected to irradiation and annealing cycles. From these data, Fig. 5 was made which provides a measure of the presumed dislocations introduced by irradiation. Several results are illustrated by Fig. 5. First, the points obtained from both sequences lie close to the same line. Second, if the yield point is a valid measure of dislocation density, this plot implies that strain-induced and radiation-induced dislocations play equivalent roles in the radiation-induced colloid formation process.

The induction period dose required to produce rapid colloid growth has been studied in a variety of natural rock salt crystals irradiated at 150°C. Yield point measurements were made on corresponding samples to determine if the induction period doses were related to the dislocation density. A number of results are summarized in Table 1. First, the saturation levels are nearly the same for all samples. Second, the induction period doses for natural samples are significantly lower than for synthetic crystals. Third, the yield stresses for natural samples are clearly higher than those for the synthetic samples. However, the induction period doses for AEC 8 and Alt Aussee samples are not proportional to yield stress as one might expect.

Part of the differences in induction period and yield point data for natural samples can be attributed to the dislocation density present when the measurements are started. This is consistent with current information indicating that most bedded salt has been plastically deformed. Some of the differences between natural and synthetic salt and samples from different locations can probably be attributed to other factors. For example, the colloid formation kinetics in natural salt differs from that in synthetic NaCl in some respects. Also, impurities may be important—the Alt Aussee salt contains a relatively high level of bromine. Additional studies on impurity and dislocation related properties are under way.

TABLE 1

F-Center Saturation Level, Induction Period Dose, and Yield Stress in Natural and Synthetic NaCl Samples Irradiated at 1.2 x 10^8 rads/hr and 150°C

Sample	Synthetic NaCl	Natural rock salt	
		AEC 8	Alt Aussee
F-center saturation level, cm^{-1}	30.0	32.5	28.9
Induction period dose, Mrads	170–240	74	28.0
Yield stress, kg/cm^2	20–22	32	34.0

ACKNOWLEDGMENT

Research was supported by the DOE Office of Nuclear Waste Isolation at Battelle Memorial Institute and by the DOE Division of Basic Energy Sciences. The manuscript was written under Contract EY-76-C-02-0016 with the U. S. Department of Energy. Accordingly, the U. S. Government retains a nonexclusive, royalty-free license to publish or reproduce the published form of this contribution or allow others to do so for U. S. Government purposes.

REFERENCES

1. L. W. Hobbs and A. E. Hughes, *Radiation Damage in Diatomic Materials at High Doses*, AERE Report R8092, Harwell, United Kingdom, 1975.
2. L. W. Hobbs, Point Defect Stabilization in Ionic Crystals at High Defect Concentrations, *J. Phys. (Paris), Colloq.*, 37: C7-3 (1976).
3. G. H. Jenks and C. D. Bopp, *Storage and Release of Radiation Energy in Salt in Radioactive Waste Repositories*, ORNL Report 5058, Oak Ridge National Laboratory, 1977.

4. K. J. Swyler, R. W. Klaffky, and P. W. Levy, Radiation Damage Studies on Natural and Synthetic Rock Salt for Waste Disposal Applications, in Proceedings of *Scientific Basis for Nuclear Waste Management*, Boston, G. J. McCarthy (Ed.), Plenum, NY, 1979.
5. M. A. Smithard and M. Q. Tran, The Optical Absorption Produced by Small Sodium Metal Particles in Sodium Chloride, *Helv. Phys. Acta*, 46: 869 (1974).
6. U. Jain and A. B. Lidiard, The Growth of Colloidal Centres in Irradiated Alkali Halides, *Philos. Mag.*, 35: 245 (1977).
7. V. Kreibig and C. V. Fragstein, The Limitation of Electron Mean Free Path in Small Silver Particles, *Z. Phys.*, 224: 307 (1969).

CRYSTAL CHEMISTRY OF THE SYNTHETIC MINERALS IN CURRENT SUPERCALCINE-CERAMICS

GREGORY J. McCARTHY, JOHN G. PEPIN, DIANE E. PFOERTSCH, and DAVID R. CLARKE*
Materials Research Laboratory, The Pennsylvania State University, University Park, PA, and
*Rockwell Science Center, Thousand Oaks, CA

ABSTRACT

Crystal chemistry of the synthetic mineral phase assemblages in current supercalcine-ceramics has been investigated. X-ray diffraction and a variety of electron optical tools (SEM, STEM, electron microprobe) have been used to characterize the crystal structure types and solid solution substitutions.

INTRODUCTION

The "supercalcine concept" states that the complex mixture of elements that is high-level nuclear waste can be modified with chemical additives and thereby tailor-made into an assemblage of high-integrity mineral-like crystalline phases.[1-8]

Research on ceramic waste forms began at the Pennsylvania State University (PSU) in 1973 in cooperation with Pacific Northwest Laboratories (PNL). It continued earlier research into idealized rare earth (RE) and actinide (An) ceramics based on the billion-year-old sedimentary resistate minerals as models.[9] The high-level waste management policy at the time was retrievable surface storage (the "RSSF") for about 100 years, pending a decision on permanent disposal. The design specifications on ceramic waste forms included low leachability, low waste volatilization during processing, and compatibility of all phases at temperatures as high as 800°C. Waste loading was to be as high as reasonably possible and at least comparable to the reference high-level waste (HLW) product, glass. The first step in processing this ceramic was to be calcination using the well-developed spray or fluidized-bed technologies. The precursor powder to this ceramic would physically resemble ordinary calcine but would have superior properties, hence the name "supercalcine." After a crystallization-sintering step, the products would become "consolidated supercalcines" or "supercalcine-ceramics."

During the early stages of research many mineralogies (i.e., crystalline phase formation models) were explored. These included titanates, zirconates, niobates, phosphates, aluminates, silicates, and aluminosilicates.[1,10] Both dry mixing of calcine plus additives and liquid-phase mixing of high-level liquid waste (HLLW) plus liquid additives prior to calcining were explored.[11] The latter procedure was found to be far more satisfactory for producing homogeneous and reactive mixtures that required minimal thermal treatment for crystallization and consolidation. Consolidation by routine sintering as well as hot-pressing were utilized.[5,12] The requirement for a cesium host phase that was simultaneously refractory, leach resistant, and capable of containing substantial Cs led to a suite of mineralogies based on pollucite ($CsAlSi_2O_6$) as this host phase.[13] Starting in 1975, these mineralogies have been utilized in cold engineering-scale demonstrations of crystalline ceramics at PNL.[8,13]

In this paper we describe the details of the crystal chemistry of the synthetic minerals of the low-sodium Purex-process supercalcine-ceramics developed over the last four years. (Related mineralogies for Thorex process and high-sodium Purex-process supercalcine-ceramics have been developed at PSU but have not yet been applied in engineering-scale tests at PNL.)

EXPERIMENTAL PROCEDURES

Preparation

Detailed discussions of the preparation of bench-scale simulated supercalcines and of engineering-scale spray supercalcines are found in Refs. 2, 5, 10, 11, 13, and 17. Seven specimens are discussed in the present paper. Two are press and fire pellets of spray supercalcines supplied by PNL (SPC-2, SPC-4), two are disc pellets of these supercalcines fabricated at PNL, and two are press and fire pellets of the two supercalcines to which the appropriate amount of uranium had been added. Uranium is a major constituent of the Purex-process PW-7-based wastes, but it has not been possible for PNL to include this radioactive element in the spray supercalcine runs. The U was later incorporated in the spray supercalcines at PSU according to the following procedure:

(1) Fire "as received" SPC-2 or SPC-4 for 5 hr at 800°C to remove most water and nitrates.

(2) Add an appropriate amount of 1*M* $UO_2(NO_3)_2$ solution and enough deionized water to make a uniform slurry.

(3) Dry the slurry rapidly at 120°C and calcine the resulting powder at 600°C for 2 hrs.

These specimens are designated as SPC-2+U and SPC-4+U. The last specimen, called PSU-SPC-2+U, was a press and fire pellet of a batch of SPC-2+U that had been prepared at PSU by a boil-down procedure followed by calcining at 600°C for 2 hr.

The same press and fire procedure was used for each of the specimens prepared at PSU: 0.75 in. (1.91 cm) pressed at 12,500 psi (86.2 MPa); pellets placed on a platinum boat and fired in air at 1200°C for 2 hr. All of the supercalcines had been given a 900°C/2 hr prefiring to remove the remaining H_2O and NO_x (typically 5 to 10% by weight) and to simulate the heat treatment schedule used for the disc pellets at PNL. The oxide compositions and waste loading of the five supercalcines are given in Table 1.

X-Ray Diffraction and Microchemistry

Each specimen was thoroughly characterized by X-ray diffraction (XRD). Diffractograms were obtained on a Siemens diffractometer using CuKα radiation, a diffracted beam monochrometer, a scintillation detector, and solid state electronics at scan rates of 2° and ½°/minute. The data were corrected by the use of an NBS Si SRM-640 standard (a_0 = 5.43088 Å). Unit cell parameters from least-squares refinements were obtained using unambiguously indexed reflections of the phases of interest. Elemental chemistry (for elements heavier than Ne) of individual supercalcine-ceramic phases was obtained by energy dispersive X-ray spectrometry (EDXS) on a variety of electron-optical instruments. A JEOL 50 A scanning electron microscope (SEM) and an ETEC Autoprobe electron microprobe (EM) were applicable to those phases having grain sizes greater than ~10 μm. Two scanning transmission electron microscopes, one at PSU (Philips EM 300) and one at the Rockwell Science Center (Philips EM 400) have been used for phases having smaller grain sizes.

TABLE 1

Compositions of Supercalcine-Ceramics, wt.%

Oxide	SPC-2	SPC-2+U	PSU-SPC-2+U	SPC-4	SPC-4+U
Waste					
U_3O_8		16.5	16.5		16.8
CeO_2	16.3	13.7	4.1	6.8	5.6
RE_2O_3*	19.0	15.9	25.7	30.2	25.2
ZrO_2	7.6	6.4	6.4	7.8	6.5
MoO_3	8.0	6.7	6.7	8.2	6.8
P_2O_5	4.2	3.5	3.5	4.3	3.5
BaO	2.4	2.0	2.0	2.5	2.1
SrO	1.6	1.4	1.4	1.7	1.4
Cs_2O	4.5	3.7	3.7	4.6	3.8
Rb_2O	0.5	0.4	0.5	0.6	0.5
Na_2O	0.2	0.1	0.1	0.2	0.2
RuO_2	0.5	0.4		0.5	0.4
Fe_2O_3	4.7	3.9	3.9	4.8	4.0
Cr_2O_3	0.5	0.4	0.4	0.5	0.5
NiO	0.2	0.2	0.2	0.2	0.2
CdO	0.2	0.1		0.2	0.1
Ag_2O				0.1	0.1
Additives					
CaO	4.9	4.1	4.1	2.1	1.7
SrO	1.2	1.0	1.2	2.6	2.1
Al_2O_3	4.4	3.7	3.7	4.5	3.8
SiO_2	19.1	15.9	15.9	17.6	14.7
Waste loading	70.5%	75.3%	75.1%	73.2%	77.7%

*RE = La, Pr, Nd, Sm, Eu, Gd, Y (plus RE as a stand-in for Am + Cm).

RESULTS AND DISCUSSION

Synthetic Mineral Synthesis

The first step in development of supercalcine-ceramics, and a crucial step in their characterization, is the synthesis of each synthetic mineral phase by the same procedures (calcination, press and fire, hot pressing, etc.) used for the full scale preparation. Nominal stoichiometries of each of the phases in every mineralogy developed to date has been synthesized. Its solid solution behavior for elements in the wastes and for additives are always investigated. For examples, see Ref. 14 for Na, Ca, Sr, Ba, rare earth (RE = trivalent La, Pr, Nd, Sm, Eu, Gd, Y), Ce, and PO_4 behavior in the apatite structure solid solution (A_{SS}) phase; see Ref. 7 for Ca, RE, Ce, U, Th, and Si behavior in the monazite (M_{SS}) phase. In some cases a full isothermal phase diagram is determined as in the scheelite structure solid solution (S_{SS}) and fluorite structure solid solution (F_{SS}) phases.[15,16] Being able to synthesize a phase whose diffractogram matches the corresponding reflections in the complex supercalcine-ceramic is a key step in phase identification. Mechanical mixtures of these phases closely match the full supercalcine-ceramic diffractogram. The phases are also used in quantitative XRD phase analysis of the various products.

Compatibility Studies

Once it has been found that a particular phase can be synthesized, it is next necessary to determine its compatibility with other supercalcine phases under relevant conditions. More than 300 separate studies of the type described in Refs. 2, 5, 11, and 17 have been used to establish the compatibility of synthetic minerals in current supercalcine-ceramics under the following conditions: 2- to 4-hr crystallization-consolidation firings at 1000 to 1200°C; indefinitely (i.e., for months to years) at 800°C (the maximum RSSF centerline temperature). While compatibility studies have focused on these two sets of conditions, it should be recognized that compatibility relations may not be the same at higher firing temperatures.

X-Ray Phase Analysis

A typical X-ray diffractogram of a supercalcine-ceramic is shown in Fig. 1. Individual reflections have been marked and deconvoluted for seven crystalline phases. The phase identification code and nominal compositions are given in Table 2. One phase shown in Fig. 1 is not listed in this table. In most supercalcine-ceramics there is also a zirconia-rich phase, sometimes isostructural with the tetragonal phase of ZrO_2 and sometimes having the cubic fluorite structure that has been designated T_{SS}. Two other phases in the phase formation model were expected to be present below the detection level of the X-ray powder methods. The presence of the ferrimagnetic $(Fe,Ni)(Fe,Cr)_2O_4$ phase in crystallized SPC-2 was confirmed by the action of a hand magnet on the powder. The presence of a Ru phase, presumably RuO_2, was ascertained indirectly by Ru volatilization tests and compatibility studies.

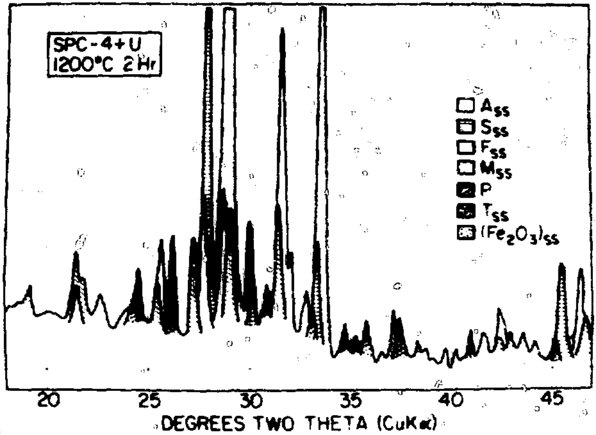

Fig. 1 A portion of the X-ray diffractogram of SPC-4+U.

In addition to the numerous reflections from crystalline phases, note the gradual rise in background at lower 2θ angles. Most of this rise is due to instrumental behavior (as determined with the silicon standard mount) and scattering from the glass mount, but a contribution also comes from one or more of the X-ray amorphous phases present in an engineering-scale supercalcine-ceramic. In industrial applications, the composition of the HLLW feed is expected to vary from the average by a substantial amount. Thus, to make supercalcine formulations adaptable for such conditions, excess additives are deliberately included in each formulation. For example, to insure that excesses of Cs and Mo in HLLW will be incorporated into refractory phases, excess Ca, Al, and Si were incorporated into the SPC-2 and

TABLE 2

Crystal Chemistry of Major Supercalcine-Ceramic Phases*

Nominal composition	Structure type	Code	EDXS† chemistry
$(Ca,Sr)_2RE_8(SiO_4)_6O_2$ ‡	Apatite	A_{SS}	major: Si,Ca,RE(Gd,Nd > La > Ce > Pr > Y) minor: Sr,Zr,[Al]
$REPO_4$	Monazite	M_{SS}	major: P,RE(Nd,Gd > La > Pr)
$(U,Ce,Zr,RE)O_{2\pm x}$	Fluorite	F_{SS}	major: U,Zr,RE(Gd > Ce > Y,Sm)
$(Cs,Rb,Na)AlSi_2O_6$	Pollucite	P	major: Cs,Al,Si minor: [Ca],[Fe]
$(Ca,Sr,Ba)MoO_4$	Scheelite	S_{SS}	major: Mo,Ca,Sr,[Ba]
$(Fe,Cr)_2O_3$	Corundum	$(Fe_2O_3)_{SS}$	major: Fe minor: Cr
$(Ni,Fe)(Fe,Cr)_2O_4$	Spinel	SP_{SS}	major: Fe minor: Ni,[Cr]
RuO_2	Rutile	RuO_2	major: Ru

*Brackets around an element indicate that it was not observed in the particular phase in every supercalcine-ceramic.

†Energy dispersive X-ray spectrometry.

‡RE = rare earths La, Ce, Pr, Nd, Sm, Gd, Y.

SPC-4 formulations. Most or all of this excess material remains amorphous during the short crystallization-consolidation firing and contributes its incoherent scattering to the diffractogram background.

As shown in Table 1, except for U, the only significant differences among the various supercalcine-ceramic compositions are in the RE's, the alkaline earths (Ca and Sr), and Si. These differences are more easily related to crystal chemistry when compositions are expressed as millimoles in the original formulation.

MILLIMOLAR CONCENTRATIONS

	SPC-2	SPC-4	PSU-SPC-2+U
Rare earths			
Ce	161	51	51
Nd	61	133	73
Gd	7	153	155
Others	127	21	78
Alkaline earths			
Ca	150	62	150
Sr	47	68	54
Silicon (Si)	539	489	539

The wide variation in RE concentrations between SPC-2 and SPC-4 resulted from use at PNL of a less expensive, but not representative, commercial mixture of RE's in SPC-2. In SPC-4, compositions were closer to the correct fission product RE ratios of PW-7, and in PSU-SPC-2+U the exact ratios were used. Refined cell parameter data for five of the major synthetic minerals in these supercalcine-ceramics are listed in Table 3. Many crystal chemical insights result from examination of the data in Tables 2 and 3, combined with knowledge of the waste chemistry, as is discussed below.

Apatite. The cell volumes of the SPC-2 A_{ss} phases are larger than for SPC-4 because of the greater proportion of large RE's (La, Ce^{3+}) used in the SPC-2 feed. When U is added to the PNL-SPC-2 batch, the A_{ss} phase drops to a minor contributor whose reflections are too weak to be used in a refinement. This occurs because the $UO_{2+x}F_{ss}$ phase stabilizes CeO_2 in the Ce^{4+} oxidation state rather than as Ce^{3+} in A_{ss}. In PSU-SPC-2+U, where the RE distributions are correct, the A_{ss} phase gave moderately intense reflections that could be used in a unit cell refinement. The $Ce^{3+} \rightleftharpoons Ce^{4+}$ redox reaction is temperature dependent. The SPC-2 disc pellets fired only to 1110°C by PNL have a less intense A_{ss} phase and a smaller A_{ss} cell because most of the Ce crystallizes in the CeO_2-rich F_{ss} phase. In the 1200°C firing, more of the Ce^{4+} is reduced to Ce^{3+} which reacts with available Ca and Si to form A_{ss}. The A_{ss} cell is larger because of the large ionic radius of Ce^{3+}. This mechanism is confirmed by crystallization of SPC-2 in nitrogen rather than air. Diffractograms of the product (see Fig. 4 of Ref. 6) indicate that nearly all of the CeO_2 is reduced. Understanding the crystal chemistry of any A_{ss} phases formed in crystalline ceramics or devitrified glasses is important because A_{ss} is a potential host for the α-emitting actinides (An). These elements usually cause A_{ss} to become metamict.[18] Because it may influence An solid solution behavior, care should be taken to select the correct RE/Ce ratio in simulated wastes, and CeO_2 should not be considered as a crystal chemical stand-in for UO_2.

Scheelite. SPC-4 based formulations have more Sr and less Ca additives than SPC-2 formulations. The ionic radius of Sr^{2+} is larger, and thus the SPC-4 unit cells are larger. Note that within the error of the measurements, the unit cell sizes are virtually identical for each group of formulations. This indicates that the phases are relatively pure alkaline earth molybdates and do not incorporate, and are not otherwise affected by, the differences in RE, Ce, and U concentrations. The EDXS studies of S_{ss} crystals confirmed this.

Monazite. The RE elements in supercalcine-ceramics are partitioned into either three or four phases (A_{ss}, F_{ss}, M_{ss}, and T_{ss}). We have found that the larger RE's (La, Pr) crystallize preferentially in the M_{ss} phase. This is clearly reflected in the cell sizes. The SPC-2 formulations prepared at PNL with higher proportions of La and Ce have the larger cell parameters while PSU-SPC-2+U and the SPC-4's with high concentrations of the small Gd^{3+} ion have smaller cells.

Fluorite. The cell parameter data of the F_{ss} phases correlate to the concentrations of U, Ce, Zr, and RE. In the absence of U, the F_{ss} phase is a CeO_2–ZrO_2–RE_2O_3 solid solution. Note that, with the higher firing temperature of the SPC-2 prepared at PSU compared to SPC-2 disc pellets, more Ce is reduced and incorporated into A_{ss}, which leads to a larger cell parameter for the former. Between SPC-2 and SPC-4, the former had the anomalously high Ce concentration which would be expected to bring the cell parameter closer to the 5.41-Å of pure CeO_2. Also, SPC-4 had the required high concentration of smaller Gd^{3+} ions. The F_{ss} phase preferentially incorporates the smaller RE^{3+} ions and this somehow also leads to incorporation of larger ZrO_2 concentrations. The combination of these substitutions gave the remarkably low 5.19-Å cell parameter. Part of the reason for the availability of so much RE was the lower concentrations of Ca and Si in SPC-4 which were apparently inadequate for full crystallization of RE^{3+} in A_{ss}. When U is added, the cell parameter tends toward the 5.44 to 5.47 Å range of UO_{2+x}. In the presence of UO_{2+x}, Ce remains oxidized and is concentrated in the F_{ss} phase as was noted earlier in the discussion of A_{ss}.

Pollucite. The Cs, Rb, and Na concentrations were the same in every batch, so the similarity of cell parameter in every case but one is expected. The SPC-2 pellets were unique in being prepared at a lower temperature. It is possible that at this temperature the small Na^+ crystallizes in the pollucite phase and gives the small unit cell; while at the higher temperature, Na forms in the noncrystalline intergranular phase.

TABLE 3

Unit Cell Parameters* for Supercalcine-Ceramic Phases

	Solid solution structure type				
	Apatite (A_{SS}), hexagonal $P6_3/m$	Scheelite (S_{SS}), tetragonal $I4_1/a$	Monazite (M_{SS}), monoclinic $P2_1/n$	Fluorite (F_{SS}), cubic Fm3m	Pollucite (P), cubic Ia3d
SPC-2 PNL spray calcine; pelletized and fired at 1200°C in air for 2 hr at PSU	a_0 = 9.558(4) c_0 = 7.032(16) v = 556.4	a_0 = 5.31(2) c_0 = 11.83(3) v = 333	a_0 = 6.820(8) b_0 = 7.050(8) c_0 = 6.499(8) β = 103.53(10) v = 303.8	a_0 = 5.342(3) v = 152.4	a_0 = 13.640(4) v = 2537
SPC-2 disc pellets Prepared at PNL; crystallization-consolidation at 1110°C for 8 hr	a_0 = 9.520(6) c_0 = 7.004(7) v = 549.7	a_0 = 5.32(2) c_0 = 11.83(3) v = 334	a_0 = 6.800(8) b_0 = 7.026(8) c_0 = 6.475(8) β = 103.72(10) v = 300.5	a_0 = 5.355(4) v = 153.9	a_0 = 13.611(9) v = 2522
SPC-2+U Prepared at PSU from PNL spray calcine + U nitrate; fired at 1200°C for 2 hr	Too few reflections for refinement	a_0 = 5.314(8) c_0 = 11.824(10) v = 333.7	a_0 = 6.809(8) b_0 = 7.061(8) c_0 = 6.497(8) β = 103.64(10) v = 303.6	a_0 = 5.384(3) v = 156.1	a_0 = 13.649(9) v = 2543
PSU-SPC-2+U Complete batch prepared at PSU by boil-down procedure; fired at 1200°C for 2 hr	a_0 = 9.480(4) c_0 = 6.957(8) v = 541.5	a_0 = 5.300(8) c_0 = 11.851(8) v = 332.9	a_0 = 6.750(8) b_0 = 6.998(8) c_0 = 6.433(8) β = 103.98(10) v = 294.9	a_0 = 5.339(3) v = 152.2	a_0 = 13.639(4) v = 2537
SPC-4 PNL spray calcine; pelletized and fired at 1200°C for 2 hr at PSU	a_0 = 9.505(4) c_0 = 6.978(3) v = 545.9	a_0 = 5.382(4) c_0 = 11.971(6) v = 346.8	a_0 = 6.749(4) b_0 = 6.968(4) c_0 = 6.413(4) β = 103.50(10) v = 293.3	a_0 = 5.192(3) v = 140.0	a_0 = 13.646(4) v = 2541
SPC-4 disc pellets Prepared at PNL; crystallization-consolidation at 1230°C for 4–8 hr	a_0 = 9.497(4) c_0 = 6.976(4) v = 544.9	a_0 = 5.378(4) c_0 = 11.999(8) v = 347.1	a_0 = 6.749(4) b_0 = 6.971(4) c_0 = 6.432(4) β = 103.96(10) v = 293.7	a_0 = 5.190(3) v = 139.8	a_0 = 13.643(4) v = 2539
SPC-4+U Prepared at PSU from PNL spray calcine + U nitrate; fired at 1200°C for 2 hr	a_0 = 9.505(4) c_0 = 6.975(4) v = 545.7	a_0 = 5.378(4) c_0 = 11.931(8) v = 345.1	a_0 = 6.761(6) b_0 = 6.950(8) c_0 = 6.439(8) β = 103.72(10) v = 293.9	a_0 = 5.347(3) v = 152.9	a_0 = 13.648(6) v = 2542

*a_0, b_0, c_0 in Å; β in degrees; v in Å^3.

Tetragonal ZrO_2. In SPC-2 and SPC-2+U pellets, a phase rich in ZrO_2 occurs. It appears to be isostructural with the tetragonal high temperature polymorph of ZrO_2 ($P4_2/nmc$) and has cell parameters as follows:

	SPC-2	SPC-2 disc pellets	SPC-2+U
a_0	3.639(3)	3.622(6)	3.621(3)
c_0	5.236(9)	5.220(7)	5.229(4)
v	69.3	68.5	68.6

This phase was not observed by XRD in PSU-SPC-2+U, but it was identified by STEM. In addition to Zr there were minor U, RE, and Ce. Inclusion of these ions stabilized the tetragonal polymorph. In the other specimens most of the Zr was incorporated in the cubic F_{ss} phase.

Microchemistry

Determinations of the microchemistry of individual phases in supercalcine-ceramics are still under way. Most of the phases have grain sizes below ~10 μm so the EDXS characterization has been confined principally to STEM instruments. The bulk of the results to date has been obtained on SPC-4, a hot-pressed SPC-2, and PSU-SPC-2+U specimens. Table 2 gives the EDXS chemistry for eight of the synthetic minerals in the specimens. Two other phases were also noted in PSU-SPC-2+U by STEM. A minor crystalline phase with Al > Si > Fe may be a Fe-substituted mullite forming from the excess Al + Si additives. There is also a minor glassy intergranular phase whose chemistry has not yet been determined.

CONCLUSIONS

While the basic mineralogies were designed to be the same, the exact formulations of SPC-2 and SPC-4 based ceramics differed. Investigating the effects of these differences has led to increased understanding of the crystal chemistry in these ceramics. New mineralogies for apatite-free and high-sodium supercalcine-ceramics have been developed and need now to be tested on the engineering scale. Finally, it has been shown that solidification of reprocessing wastes into crystalline ceramics having tailored crystal chemistries is feasible, and considerable innovation can be looked forward to in this area in the near future.

ACKNOWLEDGMENTS

This research has been supported by the U. S. Department of Energy and its predecessors through Battelle, Pacific Northwest Laboratory. Early research on synthetic minerals was supported by the U. S. National Scientific Foundation.

REFERENCES

1. G. J. McCarthy, Atomic Level Isolation, in *Quarterly Progress Reports, Waste Fixation Program*, J. L. McElroy (Ed.), DOE Report BNWL-1826, Pacific Northwest Laboratory, p. 43, January–March 1974.
2. G. J. McCarthy and M. T. Davidson, Ceramic Nuclear Waste Forms. I. Crystal Chemistry and Phase Formation, *Am. Ceram. Soc. Bull.*, 54: 782 (1975).
3. J. E. Mendel et al., High-Level Radioactive Waste Management Research and Development Program at Battelle Pacific, M. H. Campbell (Ed.), American Chemical Society, Washington, DC, *Adv. Chem. Ser.*, 153: 106 (1976).
4. R. Roy, Rational Molecular Engineering of Ceramic Materials, *J. Am. Ceram. Soc.*, 60: 350 (1977).
5. G. J. McCarthy, High Level Waste Ceramics: Materials Considerations, Process Simulation and Product Characterization, *Nucl. Technol.*, 32: 92 (1977).
6. J. M. Rusin et al., *Multibarrier Waste Forms, Part I: Development*, DOE Report PNL-2668-1, Pacific Northwest Laboratory, pp. 7-28, 1978.
7. G. J. McCarthy, W. B. White, and D. E. Pfoertsch, Synthesis of Nuclear Waste Monazites, Ideal Actinide Hosts for Geologic Disposal, *Mater. Res. Bull.*, 13: 1239 (1978).
8. J. M. Rusin, M. F. Browning, and G. J. McCarthy, Development of Multibarrier Nuclear Waste Forms, *Scientific Basis for Nuclear Waste Management*, G. J. McCarthy (Ed.), pp. 169-180, Plenum Press, NY, 1979.
9. G. J. McCarthy, *Solid State Chemical Aspects of Radioactive Waste Disposal*, Final Report, NSF Contract GK-27781, The Pennsylvania State University, 1973.
10. G. J. McCarthy, Supercalcine Development, in *Quarterly Progress Reports, Waste Fixation Program*, J. L. McElroy (Ed.), DOE Reports BNWL-1841, -1871, -1893, -1908, Pacific Northwest Laboratory, July 1974–June 1975.
11. G. J. McCarthy, *Advanced Waste Forms Research and Development, Annual Report*, DOE Report COO-2510-5, The Pennsylvania State University, 1975.
12. G. J. McCarthy and M. T. Davidson, Ceramic Nuclear Waste Forms: II. A Ceramic-Waste Composite Prepared by Hot Pressing, *Bull. Am. Ceram. Soc.*, 55: 190 (1976).
13. G. J. McCarthy, Supercalcine Development, in *Quarterly Progress Reports, Waste Fixation Program*, J. L. McElroy (Ed.), DOE Reports BNWL-1932, -1949, -1994, Pacific Northwest Laboratory, April–December 1975.
14. G. J. McCarthy, Crystal Chemistry of the Rare Earths in Solidified High Level Nuclear Wastes, in *Proc. 12th Rare Earth Res. Conf.*, Vail, CO, C. E. Lundin (Ed.), pp. 665-676, July 1976.
15. G. J. McCarthy, R. G. Johnston, and D. E. Pfoertsch, Thermal Stability of Supercalcine: II. The Scheelite, Sodalite and Pollucite Solid-Solution Phases, *Bull. Am. Ceram. Soc.*, 57: 358 (1978).
16. J. G. Pepin and G. J. McCarthy, Phase Relations in the System U–Th–Ce–RE–Zr–O: I. Literature, *Bull. Am. Ceram. Soc.*, 57: 358 (1978).
17. G. J. McCarthy, *Advanced Waste Forms Research and Development, Comprehensive Progress Report*, DOE Report COO-2510-12, The Pennsylvania State University, pp. 13-16 (1977).
18. W. J. Weber et al., Radiation Damage in Vitreous and Devitrified Simulated Waste Glass, in Proceedings of *Ceramics in Nuclear Waste Management*, Cincinnati, CONF-790420, U. S. Department of Energy, Technical Information Center, Oak Ridge, 1979.

POROUS GLASS MATRIX METHOD FOR ENCAPSULATING HIGH-LEVEL NUCLEAR WASTES

P. B. MACEDO, D. C. TRAN, J. H. SIMMONS, M. SALEH, A. BARKATT, C. J. SIMMONS,
N. LAGAKOS, and E. DEWITT
Vitreous State Laboratory, Catholic University of America, Washington, D. C.

ABSTRACT

A novel process which uses solidified porous high-silica glass powder to fixate radioactive high level wastes is described. The process yields cylinders consisting of a core of high-silica glass containing the waste elements in its structure and a protective layer also of high-silica glass completely free of waste elements. The process can be applied to waste streams containing 0 to 100% solids. The core region exhibits a higher coefficient of thermal expansion and a lower glass transition temperature than the outer protective layer. This leads to mechanical strengthening of the glass and good resistance to stress corrosion by the development of a high residual compressive stress on the surface of the sample. Both the core and the protective layer exhibit extremely high chemical durability and offer an effective fixation of the radioactive waste elements, including ^{239}Pu and ^{99}Tc which have long half-lives, for calculated periods of more than 1 million years, when temperatures are not allowed to rise above 100°C.

INTRODUCTION

Contamination of groundwater, if it comes in contact with disposed nuclear waste, can occur by leaching action on the fixation medium. While the importance of high chemical durability in achieving safe disposal criteria is well *recognized, little attention has been given to the minimization* of exposed surface. The dissolution of waste products from fixation materials and dissemination into the surroundings is a function of both the chemical durability of the material and its surface-to-volume ratio. An increase in exposed surface-to-volume ratio by a factor of ten can be obtained through breakage or powdering of the fixation medium. The resulting increase in material dissemination to the surrounding bath is equivalent to an increase in dissolution rate by the same factor.

Glasses break by brittle fracture which occurs through the catastrophic growth of surface flaws when exposed to a high tensile stress. Breakage may be avoided by several mechanisms. First, the stresses in the glass may be reduced. These develop during cooling and are due to the contraction of the glass. If different portions of the glass cool at different rates, then large stresses will develop. This problem may be minimized by reducing cooling rates and by designing glass fixation materials with low coefficients of thermal expansion. Some stresses in the glass occur by external events, such as impact or static stresses during storage. Breakage occurs when the tensile stress at a crack tip is large enough to propagate it. Failure may occur immediately (catastrophic crack propagation) or after a long period of slow crack growth (delayed failure). The second mechanism which may be used to prevent breakage operates by preventing the stresses at the glass surface, where the cracks are present, from becoming high tensile stresses. This is accomplished by designing materials which, upon cooling, develop a large residual *compressive* stress on the surface.[1] Since the net stress at the crack tip is the sum of all stresses present, this large residual compressive stress avoids breakage and delayed failure as long as the applied tensile stresses are smaller in magnitude. This mechanism is the major mode of strengthening glass and is used in glass tempering processes.

In this paper, we describe how both low coefficient of expansion and strengthening by residual surface stresses may be obtained in a glass fixation medium for high-level nuclear wastes. This process can be applied to the high-silica glasses which have exhibited superior chemical durability at temperatures below 100°C in aqueous solutions.

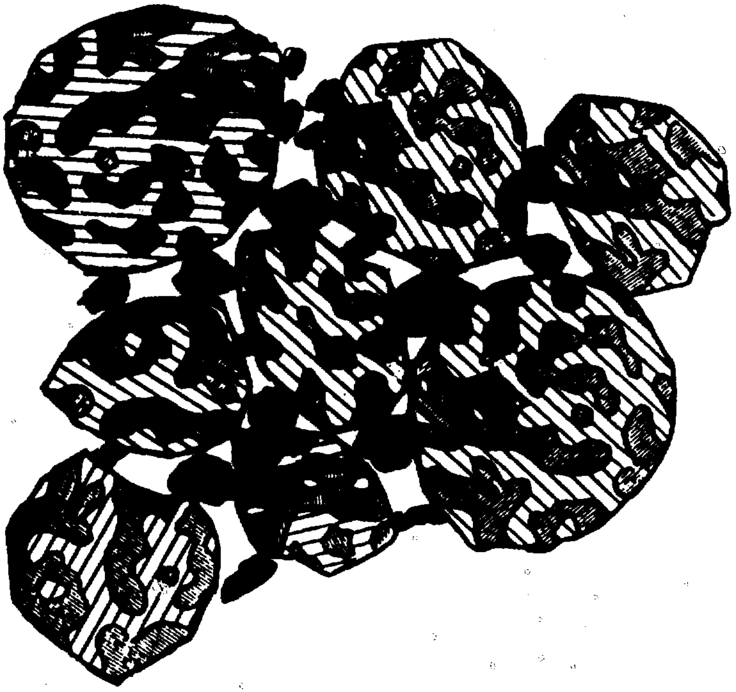
PORE SIZE: 0.01 TO 0.02 MICRONS
GRAIN SIZE: 10 TO 300 MICRONS

Fig. 1 Schematic representation of porous glass matrix process. The large grains represent the porous glass powder, ▭, with dissolved waste, ▨, in the pores. The waste solids, ■, are located interstitially between the grains.

THE POROUS GLASS MATRIX PROCESS

The high residual surface compression necessary for strengthening is obtained by developing a layered material with a core and a surface or cladding region. If the core region has a higher coefficient of thermal expansion and a lower glass transition temperature than the cladding region, the composite, during cooling after fabrication, will exhibit a high compressive stress in the surface or cladding region. If the cladding material is made up of a high-silica glass, then it will also exhibit a low coefficient of thermal expansion, a very high chemical durability, and a high resistance to devitrification.

A fabrication process achieving these objectives was developed. The process consists of mixing the high-level liquid wastes and solid precipitates with a dry porous high-silica glass crushed into powder. The pores within each grain vary between 0.01 and 0.02 μ and the grains themselves vary from 10 to 300 μ in diameter.

When the porous powder is mixed with a waste stream, the liquid penetrates into the pores of the powder and deposits any dissolved wastes present in the liquid, while the solid precipitates are deposited between the grains of the powder (Fig. 1). Drying and heating allow the pores to collapse, thus trapping the dissolved wastes in the glass matrix of each powder grain. The mixture is then heated inside a high-silica glass tube with a sealed end. After the powder sinters and traps the intergranular solids, the tube itself collapses on the high-silica glass and waste mixture. The collapsing temperature depends upon the specific composition of the high-silica glass tube; it ranges from 900° to 1300°C. (The latter temperature is due to the present use of commercial Vycor tubes and can be readily lowered by use of modified Phasil tubes.[2]) A solid glass material thus obtained consists of a core, which contains the waste element oxides fixed in a solid high-silica glass matrix, and an outer cladding layer composed of a high-silica glass totally free of waste components. The core has a silica content of >80 mole %, thus satisfying very high chemical durability criteria. In addition the core has a higher coefficient of thermal expansion than the cladding layer. Therefore during cooling, high residual compressive stresses are developed at the surface of the object, and good strengthening may be achieved. The cladding layer also provides multibarrier protection to chemical attack and exhibits a very high chemical durability. This high-level waste solidification process, termed "Porous Glass Matrix" (PGM) process, offers good physical and chemical stability

TABLE 1

West Valley PW-8a Waste Composition

Oxide	Reported, wt.%	Simulated, wt.%	Oxide	Reported, wt.%	Simulated, wt.%
Na_2O	16.62	16.62	TeO_2	0.86	
Fe_2O_3	34.29	34.29	Cs_2O	1.14	1.14
Cr_2O_3	1.36	1.36	BaO	1.85	1.85
NiO	1.74	1.74	Y_2O_3	0.05	0.05
P_2O_5	1.58	1.58	La_2O_3	6.05	6.05
Rb_2O	0.21	0.21	CeO_2	12.09	12.09
SrO	1.25	1.25	Pr_6O_{11}	1.06	1.06
ZrO_2	5.84	5.84	Nd_2O_3	3.62	3.62
MoO_3	7.54	7.54	Sm_2O_3	0.64	0.64
Rh_2O_3	0.36	0.36	Eu_2O_3	0.17	0.17
Ag_2O	0.104	0.104	Gd_2O_3	0.43	0.43
CdO	0.15	0.15			

TABLE 2

United Kingdom UKM-22 Waste Composition

Oxide	Reported, wt.%	Simulated, wt.%	Oxide	Reported, wt.%	Simulated, wt.%
Al_2O_3	19.89	19.89	ZrO_2	5.57	5.57
Rb_2O	0.43	0.43	PO_4	0.93	0.93
Cs_2O	3.00	3.00	Cr_2O_3	2.18	2.18
MgO	24.68	24.68	MoO_3	6.89	6.89
SrO	1.25	1.25	Fe_2O_3	10.63	10.63
BaO	1.48	1.48	RuO_2	2.65	2.65
Y_2O_3	0.66	0.66	NiO_2	1.40	1.40
La_2O_3	1.71	1.71	PdO	1.71	1.71
Pr_6O_{11}	1.67		ZnO	1.71	1.71
Nd_2O_3	7.08	7.08	U_3O_8	0.23	Replaced by CeO_2
CeO_2	3.85	3.85	SO_4	0.39	0.39

for radwaste fixation and can handle both military and commercial reprocessed wastes containing from 0 to 100% solids and be readily adapted to equipment used for the borosilicate glass process.[3]

LONG-TERM CHEMICAL DURABILITY

The chemical durability of high-silica fixation media prepared via the PGM process for the encapsulation of simulated military and commercial radwastes, such as the West Valley PW-8a waste[3] (Table 1), the United Kingdom UKM-22 waste[4] (Table 2), and the Savannah River Plant waste[5] (Table 3), was tested and compared against the chemical durability of waste glass prepared via the borosilicate process.[3] The chemical durability test was conducted by immersing powdered glass samples in distilled water at 45 and 70°C for a variety of times up to 10 days. The rate of silica release into the distilled water at 45 and 70°C was measured and is representative of the release rate of most waste elements in the glass.[6] The rate of release at 20 and 100°C was obtained by extrapolation of the measured rates. The rates are summarized in Table 4. The high-silica PGM glass exhibits a lower dissolution rate than the borosilicate glass.

In order to determine the expected behavior of fixation materials in terms of their ability to prevent dissolution of waste materials by an aqueous environment, a calculation was conducted to evaluate the amount of each radioactive isotope released into the surrounding bath as a function of storage time. The amount Mi of radioisotope, i, released into the surrounding medium due to a dissolution of the glass was calculated as a function of storage time, t, and initial concentration in the waste, Mo_i, by the following expression:

$$\frac{Mi}{Mo_i} = \alpha_i\, e^{-t/\tau_i}\left(\frac{2Dt}{\rho r_0} - \frac{D^2t^2}{\rho^2 r_0^2}\right)$$

$$+\ \alpha_j\left(\frac{2Dt}{\rho r_0} - \frac{D^2t^2}{\rho^2 r_0^2}\right)\left(\frac{\tau_j}{\tau_i - \tau_j}\right)\left(e^{-t/\tau_j} - e^{-t/\tau_i}\right)$$

TABLE 3

Savannah River Plant Waste Composition

Salts in feeds 5 and 6	Reported, wt.%	Simulated, wt.%	Oxides in feeds 5 and 6	Reported, wt.%	Simulated, wt.%
$NaNO_3$	2.28	2.28	Na_2O	2.98	2.98
$NaNO_2$	0.20	0.20	Fe_2O_3	36.87	36.87
$NaAlO_2$	0.20	0.20	Al_2O_3	7.48	7.48
NaOH	1.02	1.02	MnO_2	10.41	10.41
Na_2CO_3	0.08	0.08	U_3O_8	3.45	*
Na_2SO_4	1.06	1.06	CaO	2.75	2.75
$Na_2C_2O_4$	0.0013	0.0013	NiO	4.57	4.57
NaCl	1.91	1.91	SiO_2	3.34	3.34
NaF	0.19	0.19			
$NaHHgO_2$	0.0007				
Starch	0.00003	0.0003			
Na EDTA	5.62	5.62			
$NaBO_2$	0.00001	0.00001			
C	2.58	2.58			
Hg	1.27				
HgI_2	4.00				
Zeolite	7.73	7.73			

*U_3O_8 is replaced by 2.12 wt.% CeO_2 in simulation tests.

TABLE 4

Dissolution of Glass Matrixes at Various Temperatures

	PGM glass	Borosilicate glass	T(°C)
Concentration of radwaste	20%	13-30%	
Matrix dissolution rate, $g/cm^2/day$	2.9×10^{-10}	7.9×10^{-8}	13
	6.75×10^{-10}	1.3×10^{-7}	20
	9.4×10^{-8}	2.7×10^{-6}	70
	9.7×10^{-7}	1.11×10^{-5}	100

where the isotope i is the decay product of the isotope j; D is the matrix dissolution rate; ρ is the glass density; r_0 is the radius of the waste glass rod; τ_i and τ_j are the mean lifetimes of isotopes i and j, respectively; and α is the ratio of the concentration of each isotope in the dissolved glass to the concentration of each isotope loaded in the glass. Generally, α is unity, unless the glass contains several regions with different waste element concentrations such as in a multibarrier protection system. Then α becomes the ratio of the concentration of wastes in the outer barrier which is dissolved to the concentration in the bulk. The values of the constants used in the calculations were $r_0 = 1$ cm and $\rho = 2.5$ g/cm^3 for both fixation media. Calculations were conducted for a borosilicate glass of composition 76-68 with waste composition PW-8a-2 ($\alpha = 1$) and for the high-silica PGM glass with (a) complete exposure of the core region ($\alpha = 1$, no protective barrier) and (b) a protective barrier which exposes the core over 0.2% of the total area corresponding to inadvertent breakage ($\alpha = 0.002$). Other values of constants assumed are given in the figure captions. The calculations are conducted for two specific long-lived isotopes, namely ^{99}Tc and ^{239}Pu, which have half-lives of 212,000 and 24,400 years, respectively. Plutonium-239 is a decay product of ^{243}Am with a half-life of 7,400 years. These calculations also involve various types of thermal conditions during storage which include one scenario with storage at 100°C for the initial 100 years and at 20°C thereafter.

For a storage condition of 100°C for the first 100 years and 20°C thereafter, the accumulated ^{239}Pu and ^{99}Tc released are shown in Figs. 2 and 3, respectively, for the borosilicate glass, for the PGM, high-silica core, and for the latter with a protective glass layer and a surface exposure of 0.2% due to expected breakage. These results show clearly the effect of the differences in chemical durability between the high-silica and the borosilicate glass (see Figs. 2 and 3, curve 1) for radwaste fixation. The further reduction in release rate afforded by the protective barrier with a 0.2% surface exposure is seen in the comparison of curve 3 with curve 2.

SUMMARY AND CONCLUSIONS

In conclusion, high-silica nuclear waste disposal glasses were prepared by the PGM process for the fixation of commercial and military reprocessed wastes. They consist of a core matrix containing the waste elements as an integral part of a high-silica glass structure, surrounded by a cladding region of lower thermal expansion coefficient and higher glass transition temperature which is totally free of waste elements and which exhibits a high surface compression (30,000 to 70,000 psi) during the cooling step of the process giving rise to a high strength material.

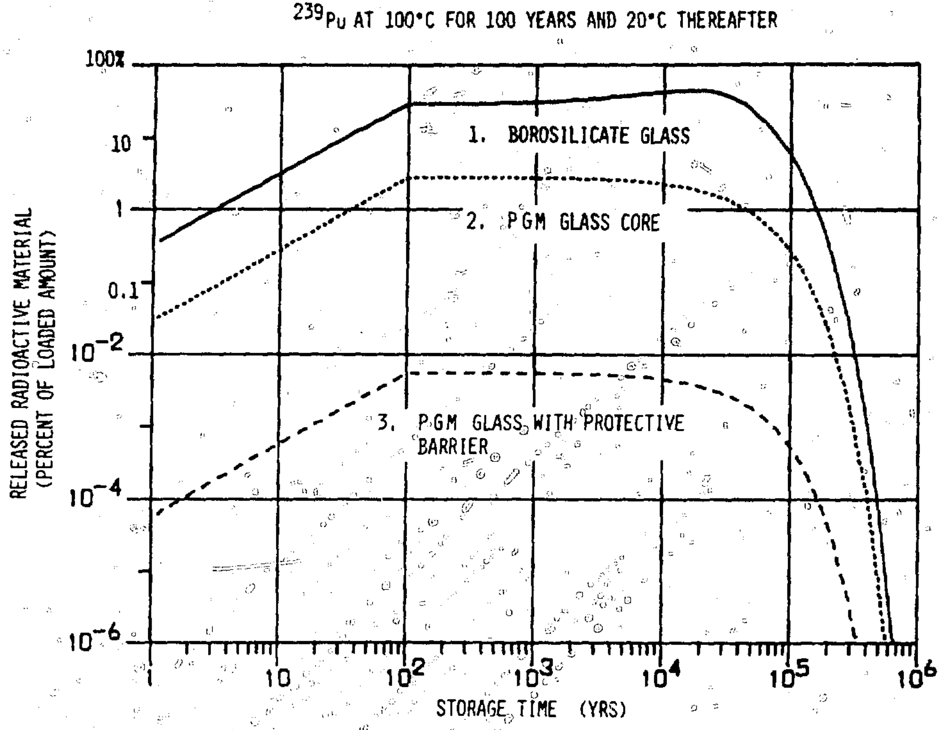

Fig. 2 Calculation of accumulated dissolved ^{239}Pu as percentage of amount loaded, based on measured rates of dissolution of the matrix for (1) borosilicate glass, (2) high-silica glass core, and (3) the latter with a nonloaded protective glass barrier which exposes 0.2% of the core due to expected breakage.

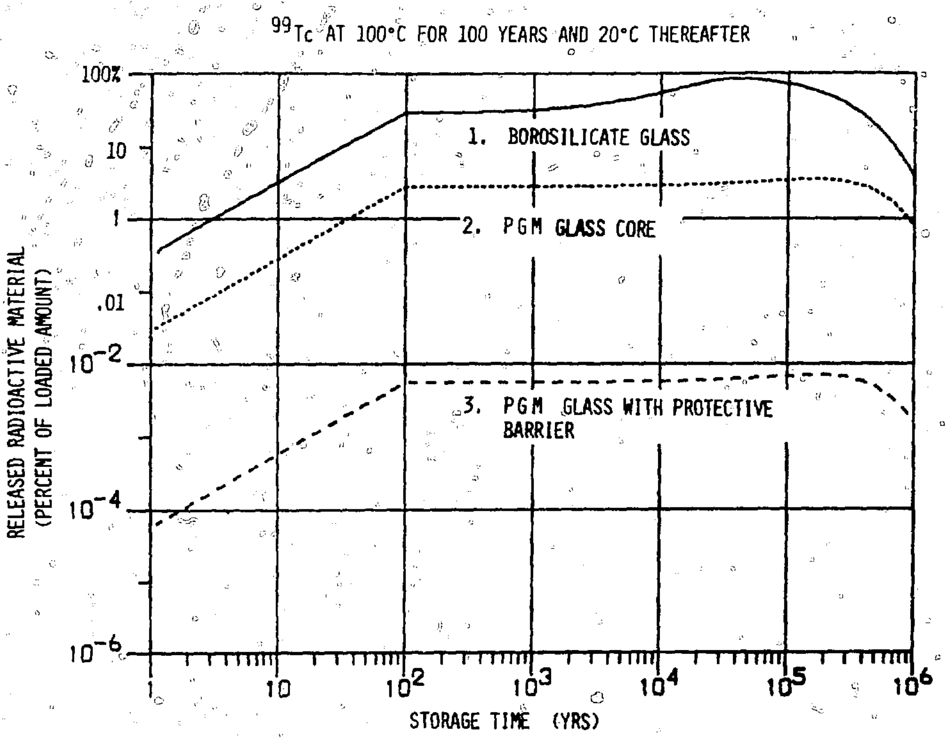

Fig. 3 Calculation of accumulated dissolved ^{99}Tc as percentage of amount loaded, based on measured rates of dissolution of the matrix for (1) borosilicate glass, (2) high-silica glass core, and (3) high-silica glass core with a nonloaded protective glass barrier which exposes 0.2% of the core due to expected breakage.

In addition to its high mechanical stability, the PGM glasses exhibit a very high chemical durability in their core and their cladding region. If the cladding layer is 1 mm thick, it will take over a million years to dissolve at room temperature. This provides an excellent multibarrier protection to the waste fixation medium. Calculations of the release of ^{239}Pu and ^{99}Tc to the environment show that the high-silica PGM glasses are able to provide effective fixation of the most pernicious elements present in the waste stream despite their extremely long half-lives. This effective fixation is afforded with or without multibarrier protection, although a protective barrier is desirable for the increased margin of safety.

ACKNOWLEDGMENT

The sponsor of this research was the National Patent Development Corporation, New York City, NY.

REFERENCES

1. R. K. Mohr et al., Strengthening of Optical Fibers by Molecular Stuffing, to be published.
2. P. B. Macedo et al., Porous Glass Process for Encapsulating Radioactive Commercial and Military Wastes in High-Silica Glasses, to be published.
3. J. E. Mendel et al., *Annual Report on the Characteristics of High Level Wastes*, BNWL-2252, Pacific Northwest Laboratory, 1977.
4. J. A. C. Marples, personal communication, Harwell, England, 1978.
5. Preliminary Technical Data Summary (No. 2) for the Defense Waste Processing Facility, Savannah River Laboratory, issued in March 1979.
6. J. H. Simmons et al., Chemical Durability of Nuclear Waste Glasses, in Proceedings of *Ceramics in Nuclear Waste Management*, Cincinnati, CONF-790420, U. S. Department of Energy, Technical Information Center, Oak Ridge, 1979.

THE EFFECT OF IMPACT ENERGY ON SOLID-WASTE COMPOSITES OF BRITTLE AND DUCTILE MATERIALS

W. J. MECHAM, L. J. JARDINE, and M. J. STEINDLER
Argonne National Laboratory, Argonne, Illinois

ABSTRACT

[illegible]

INTRODUCTION

R[illegible] the impact [illegible] resistance to fracturing [illegible] properties of most [illegible] forms. These properties will likely determine whether a given waste form can satisfy waste [illegible] being formulated by the EPA, NRC, and DOE for wastes from the nuclear fuel cycle. A method is [illegible] analysis of the resistance to fracture (measured in terms of dispersibility) by mechanical impacts that could occur prior to final geologic isolation for two generic solid waste forms: (1) a glass monolith and (2) a composite body consisting of ceramic pellets or glass beads embedded in a continuous metallic phase. This latter form is also referred to as a metal matrix or a metal-encapsulated waste form. Reviews have been made of the general status of the metal-matrix technology[1] and of current ceramic pellets based on a lead matrix.[2]

[illegible]

HIGHLIGHTS OF LITERATURE REVIEW OF IMPACT TESTS RELEVANT TO WASTE FORMS

Approach Used in Literature Review

Two [illegible] by Battelle Pacific Northwest Laboratory [illegible] Savannah River Laboratory [illegible] the impact analysis [illegible] waste forms provided the initial citations for the literature search, including the major work on spent-fuel shipping casks. However, information from the specialized technical literature on the practical aspects of brittle fracture caused by impacts is very limited and was supplemented by relevant topics treated in the more generalized reference literature, specifically: deformation of materials,[7] properties of ceramics,[8] glass,[9] lead,[10] and of the particulate state of matter,[11] fracture mechanics of ceramics,[12] engineering studies of mineral crushing,[13] and design factors for waste forms.[14]

A Summary of Impact Tests Made with Full-Scale Components

Studies of the impact behavior of large shipping casks for transportation of radioactive materials have been summarized as a designer's handbook.[5] This summary included both recommended design principles and engineering properties for shielded casks made of lead and steel and the results of impact tests. The deformations of these ductile materials were correlated with the input kinetic energy of impact for a practical range of impact velocities and other conditions. Impact deformation was measured by the displacement volume ΔV (m^3) of the configuration change resulting from plastic flow of the steel and lead. The total volume V_0 of each material remained constant, but a fractional volumetric deformation was measured by $\Delta V/V_0$. Plastic flow was found to take place when local stresses exceeded the dynamic flow stress, σ_D (Pascals, Pa), which was a threshold stress for plastic deformation, a characteristic property of each of the materials. The fundamental relationship of impact deformation to impact energy was expressed by the energy balance equating the input mechanical energy of impact, W_I, to the energy absorbed in deformation, W_D, by the product of the dynamic flow stress σ_D and displacement volume ΔV.

$$W_I = W_D = \sigma_D \Delta V \tag{1}$$

While Eq. 1 is shown for only one component, it also was shown to apply to lead/steel composites for which the total impact energy is equal to the sum of the deformation energies of the two components. Reference values of σ_D for lead and for mild steel were 6.0×10^7 Pa and 3.5×10^8 Pa, respectively.[5] Since the lead has the lower threshold stress for deformation, it would absorb impact energy preferentially to steel; however, the application of stress to the outside of the cask required that the steel shell (which was outside the lead) be deformed as a precondition for the deformation of the lead. The application of this method to impact analysis was successful (for purposes of engineering accuracy) in a number of scale-model studies.[5] The lead and steel apparently showed no significant strain-rate sensitivity, which is a fact important for both (a) the establishment of principles of scale modeling and (b) the application of impact energy in tests without regard to impact velocity. Recent studies at a number of research sites have established this engineering approach to impact analysis to various materials and designs of shipping casks.[15] A full-scale demonstration of acceptable impact resistance of typical large shipping casks at speeds up to 80 mph was made at Sandia Laboratories.[6] These demonstrations were designed on the basis of calculational models and of impact tests of reduced-scale models embodying the above principles of impact deformation of ductile materials.[6]

Preliminary impact testing of ½-scale (and smaller) models of canistered glass monoliths simulating high-level waste was performed at Battelle Pacific Northwest Laboratory (PNL), in support of the analysis of risk in high-level waste-management operations.[3] A literature review made as part of this study disclosed that there were conflicting theories of brittle fracture and an absence of data on impact breakup of glass monoliths. Also, the literature on brittle fracture did not establish the validity of scaling laws for interpretation of small-scale model tests and lacked definitive information on brittle/ductile composites.[3]

Impact tests of reduced-scale (½ and ⅙) models were carried out[3] on simulated glass-filled stainless steel canisters at impact velocities of up to 80 mph (35.2 m/s) and at temperatures of about 20 to 425°C. Both reference waste glass compositions and devitrified versions were used.[3] The maximum impact velocity was equivalent to about 620 J/kg of canister mass. Photographs made of the model canister striking a concrete pad at an impact velocity of 13.2 m/s indicated that the duration of impact was about 2 milliseconds. At this velocity, the impact showed rebound heights indicating the fraction of impact energy going into total deformation (object and barrier) was about 88%. Microphotographs of glass fragments smaller than 5 μm showed a shape factor of about 12; this is to be compared with a factor of 6 for cubes and spheres.[3]

In these tests, the impacted monoliths in stainless steel canisters were examined for cracks in the stainless steel canister, particle-size distributions of glass fragments, and total surface areas of fragments. The results were stated to be pioneering efforts providing (at best) order-of-magnitude estimates of effects for realistic cases. The principal quantitative results were the measurements of the total surface area of glass fragments and the mass fraction of particles of respirable size (i.e., smaller than 10 μm). At the highest impact velocity (35.2 m/s), the fragmentation generated a 40-fold increase of the original glass surface area. The mass fraction of glass particles of respirable size was found to range from 10^{-8} in the control specimens (zero impact velocity) to 10^{-4} for 35.2 m/s impact velocity. The report[3] concluded that the limited program did not establish the scaling laws for brittle fracture of glass monoliths and that the strain-rate dependence of the glass behavior was still unknown.

An Evaluation of Engineering-Scale Tests

The strategies of engineering design used in the work leading to successful full-scale demonstration of impact resistance of shipping casks made of steel and lead could probably be used successfully for composites of brittle and ductile materials. However, the literature on this subject lacks a widely accepted theory and does not define the practical effectiveness of engineering-design methodology. This is particularly true for impact fracture of brittle materials, where further work is needed to establish a useful relation of impact deformation to impact energy, as has been done for ductile materials. For example, the principal results obtained in the realistic model studies at PNL were plotted as a function of impact velocity,[3] and the empirical data showed decided curvature, making interpolation and extrapolation seem difficult. However, the same results if replotted as a function of impact energy are nearly linear, suggesting that energy correlations for brittle materials may be more useful, as was the case for ductile materials.

Laboratory-Scale Tests of the Impact Fracture of Brittle Materials

A preliminary laboratory-scale investigation of impact resistance of glass and concrete waste forms was made[4] at the Savannah River Laboratory (SRL). Reference waste solid compositions (one for glass and five for concrete) were prepared in the form of 10-g cylinders (1.3 cm diameter and 2.5 cm long). The glass specimens were borosilicate glass, specially formulated for SRL wastes, and had a density of 3.0 g/cm^3 and compressive strength in the range of 4.5×10^{11} to 6.9×10^{11} Pa in static load tests.[16]

The small glass specimens were placed in a device for conducting impact tests which consisted essentially of a "hammer" and an "anvil," each made of hardened tool steel. A 2-kg weight falling distances of up to 80 cm provided a maximum single-drop impact energy of 15.7 J, which was applied to the flat end of the specimen. The impact resulted in fragmentation outward from the unconfined sides of the cylindrical specimen. Repeated impacts were used to obtain cumulative energies up to 94 J on the 10-g specimens. Particle-size distributions were determined by sieving techniques with five screens, sized in the range of 2.0 to 0.125 mm. With some samples, the material passing the smallest sieve was also analyzed by a Coulter counter. Geometrical surface areas were calculated (assuming cubical symmetry) from the size fractions. For impact energies in the range of 2.0 to 7.8 J/g, the ratio of energy input to surface area of resulting fragments was nearly constant $(1.06 \pm 0.11) \times 10^3$ J/m^2. For the glass specimens, no particles were detected[4] of a size smaller than 8 μm.

Specimens of concrete (without additives) showed about the same total surface area of fragmentation per unit of energy as the glass specimens showed. However, concrete with additives (40% waste sludge) averaged about 2.5 times higher surface area for the same energy input. The concrete[4] also had a significantly higher proportion of particles of respirable size (i.e., smaller than 10 μm).

Impact tests of small, uncanistered glass specimens have been also conducted at PNL in an approach similar to that at SRL. Small (3 g) specimens of reference glasses and ceramics were impacted at energy inputs of 9 to 130 J/g (Ref. 15). In some cases, particle sizes were measured by screening, but the total surface areas were not reported. In other cases, the total surface area was measured by the Brunauer Emmett Teller (BET) method (which is based on gas adsorption), but no particle size determinations were made.[17] The specific impact energies of these tests were higher by more than an order of magnitude than in the SRL tests or in the PNL engineering-scale tests cited above. It was observed in these impact tests of small uncanistered glass specimens that the overall impact proceeds in stages, even for a single impact by a falling weight. The first (primary) impact results in an explosive fragmentation of the original body, and the downward movement of the impact ram then crushes the primary fragments in successive stages.[17]

Evaluation of Laboratory-Scale Tests

The above tests in which glass specimens of a certain size were fragmented by multiple impacts were found to give a nearly constant ratio of input energy to fracture surface area, 1.06×10^3 J/m^2, over a range of energy inputs. This fact suggests that the effects of impacts may be determined by γ_0, the surface-energy property of the material, which has been theoretically defined but is difficult to measure in practical terms. It is also known that surface energy and hardness of solids are related, and both increase with increasing intermolecular forces.[8] However, in actual mechanisms of fracture, the mechanical energy input required to produce brittle fracture is much larger than can be accounted for by the equilibrium surface energy γ_0 of the material.

The dissipation of input mechanical energy in the single-impact fracture of brittle material has been measured by a calorimetric method.[13] The BET gas adsorption method was used to measure the increase of surface area of glass and quartz specimens impacted by a dual-pendulum device. The specimens were impacted inside a calorimeter so that the heat generated could be subtracted from the impact mechanical energy to obtain the true surface energy, which was found to be less than 5.0 J/m^2 and probably about 1.0 J/m^2. The input surface-energy requirement was about 77 J/m^2 in these tests.[13]

PRELIMINARY FORMULATION OF CALCULATIONAL MODELS OF IMPACT FRACTURE OF BRITTLE MATERIALS IN CERAMIC–METAL COMPOSITES

Introduction

The conversion of impact energy into measurable deformations of materials can be outlined as follows: (1) A massive body falling freely in the earth's gravity acquires velocity and kinetic energy. (2) If this moving body makes contact with an essentially unyielding surface, a deceleration occurs in which the velocity decreases as the deceleration force on the outside surface of the body (at the zone of contact) results in a linear (inward) deformation of the body. (3) This deformation is initially elastic, and the elastic deformation energy is stored throughout the volume of the body as the product of the compressive stress in the material and the volumetric deformation. (4) In the continuing deformation process, the elastic stress increases to a maximum when the velocity of the body has fallen to zero and all the kinetic energy has been converted into elastic energy. (5) For impact velocities well below the speed of sound, the conversion of kinetic energy to elastic energy is independent of velocity and of the time rate of elastic deformation. (6) If stresses in some region of the body exceed the elastic limits, the material can deform by plastic flow (if ductile) or by fracture (if brittle). (7) In such cases, the stored elastic energy is consumed in the inelastic geometric deformation and in heat from frictional effects. (8) The partitioning of inelastic deformation energy among different materials in a composite body depends on the different threshold stresses for inelastic deformation, the configuration of the body, and the conditions for the extent of deformation, including the limitations of energy available. (9) Inelastic deformation of brittle materials by impacts takes the form of fracture into fragments, i.e., transformed into particulate solids, which can consume energy by contact friction under compression. (10) The characterization of particulate matter requires the specification of both the total surface area formed and the mass fractions of particles according to the range of size of particles in the fraction. (11) Particulate solids resulting from comminution processes generally exhibit a size distribution characterized by a mean size and a standard deviation, such as that described[11] mathematically by the lognormal probability function.

Energy and Stress in Brittle Fracture

The deformation of ductile material in mechanical impacts is well established for a wide range of materials and of impact conditions of practical interest. When the impact force results in a compressive stress in the material above the value of the dynamic flow stress (σ_D), a property of the material, the material deforms inelastically (irreversibly) by plastic flow, as a local change in volumetric configuration measured as displacement volume ΔV. The deformation behavior of the ductile material is such that essentially all energy absorbed inelastically in the material results in plastic flow; that is, for impact energy absorbed inelastically, $W_D = \sigma_D \Delta V$, as given in Eq. 1 above. It is understood that σ_D is a composite property of the body which is a function of the fundamental elastic modulus, Poisson's ratio, and the tensile yield stress and, in practice, is independent of the configuration of the body and the conditions of impact for materials that do not show sensitivity to rate of strain. Equation 1 has been found approximately valid for practical materials, shapes, sizes, and velocities of impact.[5]

The impact deformation of brittle material differs from that of ductile material in the different ratios of heat produced from the required mechanical energy input for a given amount of deformation. In brittle fracture, only about 1% of the impact energy is consumed by the surface energy; the balance forms heat. In impact deformation of ductile material, the heat effect is much less. For fracture (i.e., surface area is increased by a factor of 10 or more), the brittle body is fragmented into many small pieces and the energy is consumed in frictional contact of these pieces in compressive impacts as well as in breaking atomic bonds in the formation of new surfaces. If γ_0 is the equilibrium surface energy, W_I is the impact energy absorbed, and ΔS_I is the total surface area formed in the fracture, then

$$\Delta S_I = \frac{yW_I}{\gamma_0} \tag{2}$$

where y is the fractional efficiency with which W_I is converted to γ_0 and y must be defined for the size, configuration, and impact conditions. This is done by the conceptual fracture processes described below.

From a general conceptualization of the type of compressive fracture of brittle material that occurs in an impact, a threshold compressive stress σ_C for fracture can be estimated as σ_T/μ, where σ_T is the tensile fracture stress and μ is Poisson's ratio. Both μ and σ_T are basic elastic properties of the material.[7,8] The estimated compressive stress calculated in this way is consistent with reported properties of glass.[8,16] For a practical case of extensive fracture, the body must receive the above threshold compressive stress $\sigma_C = \sigma_T/\mu$. From this stress the elastic work W_C stored at the value of compressive stress sufficient to cause fracture can be calculated as a one-dimensional approximation as

$$W_C = \frac{V_0 \sigma_T^2}{2E\mu^2} \tag{3}$$

where V_0 is the original volume of the brittle body and E (Young's modulus) is an elastic property of the material.

From conceptualization of the tensile fracture of a brittle body under short-term static loads, the ratio of surface area to energy can be found in terms of the new surface, $2S_0$ (S_0 is the cross-sectional area), produced in a single cross-sectional fracture and the stored elastic tensile energy W_T required as input energy to raise the tensile stress to the elastic limit, i.e., to the tensile fracture stress σ_T. This elastic energy may be calculated as

$$W_T = \frac{V_0 \sigma_T^2}{2E} \tag{4}$$

From Eq. 4, the energy/surface area ratio can be stated in terms of the general case, where the surface area formed is ΔS_I as

$$\frac{\Delta S_F}{S_0} = \left(\frac{4E}{\sigma_F^2}\right)\left(\frac{W_F}{V_0}\right) \tag{5}$$

where W_F is the input energy absorbed by both fracture and friction and S_0 is the original cross-sectional area of the material through which the tensile stress was applied. Although this conceptual model is based on pure tensile fracture, the ratio $W_F/\Delta S_F$ derivable from Eq. 5 is believed to apply generally and to be valid as an approximation to the more practical compressive fracture model of Eq. 3; that is, the efficiency of the conversion of elastic energy of tensile fracture in Eq. 5 is at least as high as the compressive fracture in Eq. 3. The energy efficiency y of equation 2 can then be compared to the ratio $W_F/\Delta S_F$ in Eq. 5. Since surface energy γ_0 is defined as a property of the material only, we see that energy efficiency y is a function of the material and of the surface to volume ratio S_0/V_0. The extent to which y depends on geometrical configuration of the body and on the conditions of impact must be verified experimentally. The above model implies fracture is a function only of W_F/V_0 and of S_0/V_0.

The surface-energy relations for brittle fracture can be summarized from Eqs. 2 and 5 as

$$W_F = \left(\frac{\gamma_0}{y}\right)\Delta S_F = \left(\frac{V_0\sigma_F^2}{4S_0E}\right)\Delta S_F \tag{6}$$

which has a form analogous to Eq. 1 for ductile materials. Calculations by Eq. 6 are in approximate agreement with limited data.[4,13]

Models for Brittle Fracture in Ceramic–Metal Composite Bodies

The energy and threshold stress for deformation of ductile material is given in Eq. 1. The energy and threshold stress required for fracture of brittle material is given by $\sigma_F\ \mu$. The total energy W_I available from the impact for deformation and fracture of a composite is

$$W_I = W_D + W_F \tag{7}$$

Impact resistance of a reference design of a metal-matrix waste package can be measured by the increase in surface area ΔS_F, which is considered to constitute an increased potential for entering the human environment by aqueous leaching. This increase in surface area is related to energy as in Eq. 6. The energy available for generation of this surface area is a residual energy of the energy remaining from the original impact energy W_I after the absorption of energy by the deformation W_D of the stainless steel canister wall *and* of that portion of the total lead that lies between the surface of the brittle body and the external source of impact force. The actual extent of fracture will depend on the input energy of impact and on competitive processes for dissipating the energy.

A summary composite model relating fracture surface area to impact energy can be obtained from Eqs. 1, 6, and 7:

$$\Delta S_F = (W_I - \sigma_D\Delta V)\left(\frac{4E}{\sigma_F^2}\right)\left(\frac{S_0}{V_0}\right)$$

$$= (W_I - \sigma_D\Delta V)\left(\frac{y}{\gamma_0}\right) \tag{8}$$

Equation 8 shows two equations in a total of 10 variables, most of which are properties of materials measurable independently of impact conditions. The above model is "calibrated" for a waste form when the remaining two degrees of freedom are established experimentally.

The above conceptual and calculational models provide a basis for design, development, and testing of ceramic–metal composite waste forms.

REFERENCES

1. L. J. Jardine and M. J. Steindler, *A Review of Metal Matrix Encapsulation of Solidified Radioactive High-Level Waste,* DOE Report ANL-78-19, Argonne National Laboratory, 1978.
2. L. J. Jardine and M. J. Steindler, A Perspective of Metal Encapsulation of Waste, in Proceedings of *Scientific Basis for Nuclear Waste Management,* Boston, G. J. McCarthy (Ed.), Plenum, NY, 1979.
3. T. H. Smith and W. A. Ross, *Impact Testing of Vitreous Simulated High-Level Waste in Canisters,* DOE Report BNWL-1903, Battelle, Pacific Northwest Laboratory, 1975.
4. R. M. Wallace and J. A. Kelley, *An Impact Test for Solid Waste Forms,* DOE Report DP-1400, Savannah River Laboratory, 1976.
5. L. B. Shappert et al., *A Guide for the Design, Fabrication and Operation of Shipping Casks for Nuclear Applications,* DOE Report ORNL-NSIC-68, Oak Ridge National Laboratory, 1970.
6. H. R. Yoshimura, *Crash Testing of Spent-Nuclear Fuel Shipping Systems,* in *Proceedings of the Symposium on Waste Management,* Tucson, Arizona, March 6–8, 1978, DOE Report SAND-78-0451C, Sandia Laboratory, 1978.
7. F. A. McClintock and A. S. Argon, *Mechanical Behavior of Materials,* Addison-Wesley Publishing Co., Inc., Reading, Mass., 1966.
8. W. D. Kingery, *Introduction to Ceramics,* John Wiley & Sons, Inc., New York, 1960.
9. J. R. Hutchins and R. V. Harrington, Glass, in *Kirk-Othmer Encyclopedia of Chemical Technology,* 2nd ed., John Wiley & Sons, Inc., New York, 1966.
10. Wilhelm Hofmann, *Lead and Lead Alloys,* Springer-Verlag, New York, 1970.
11. G. Herdan et al., *Small Particle Statistics,* Academic Press, Inc., London, 1960.
12. R. C. Bradt et al., *Fracture Mechanics of Ceramics,* Vols. 1 and 2, Plenum Press, New York, 1973.
13. R. A. Zeleny and F. J. Piret, Dissipation of Energy in Single-Particle Crushing, *Ind. Eng. Chem., Proc. Des. Dev.,* 1: 37-41 (1962).
14. W. J. Mecham, W. B. Seefeldt, and M. J. Steindler, *An Analysis of Factors Influencing the Reliability of Retrievable Storage Canisters for Containment of Solid High-Level Radioactive*

Waste, DOE Report ANL-76-82, Argonne National Laboratory, 1976.

15. Proceedings of a Seminar on Transport Packaging for Radioactive Materials, organized by the International Atomic Energy Agency and held in Vienna, August 23–27, 1976.
16. J. A. Kelley, *Evaluation of Glass as a Matrix for Solidification of Savannah River Plant Waste*, DOE Report DP-1382, Savannah River Laboratory 1975.
17. J. L. McElroy, *Quarterly Progress Report, Research and Development Activities, Waste Fixation Program January through March 1977*, DOE Report PNL-2265, Battelle, Pacific Northwest Laboratory, 1977.

STRESS ANALYSIS OF GLASS–CANISTER INTERACTION: A STUDY OF RESIDUAL STRESSES AND FRACTURING

F. A. SIMONEN and J. R. FRILEY
Pacific Northwest Laboratory, Richland, Washington

ABSTRACT

Residual stresses and cracking in canisters filled with vitrified nuclear waste are simulated using finite element computer calculations. Cooling rates, internal heat generation, and thermal expansion coefficients significantly affect stress levels. Glass behavior within the softening temperature range is taken to follow the instant freezing concept of Bartenev.

INTRODUCTION

In the vitrification of calcined radioactive wastes it has long been recognized that thermal and residual stresses are set up in both the glass and canister during cooling of the molten glass. Such stresses have been manifested as cracking of the glass and as tensile residual stresses in the walls of the canisters. The causes and consequences of cracking of high-level waste glass in large canisters are discussed elsewhere.[1]

This paper describes computer simulations of the solidification and cooling process which predict time histories of stress in the glass canister system. Existing finite element computer programs were adapted to perform these simulations, and a collection of case studies was performed. The results permit interpretation of canister residual stress measurements and glass fracturing observations which are available from engineering development trials of the vitrification process. The objective of the analyses is to relate stress levels and cracking to processing variables (i.e., cooling rates, thermal treatments, canister size, etc.). In addition, the results indicate the extent to which experimental observations of cracking in nonradioactive glass can be applied to the radioactive situation.

Two analytical models are described. The first model is one-dimensional and focuses on the factors that govern residual stresses in the canister as well as the contained glass. The second analytical model is two-dimensional in scope and is applied to the prediction of crack patterns within the glass.

ONE-DIMENSIONAL ANALYSIS OF RESIDUAL STRESSES

Temperature and stress states in a typical longitudinal slice of glass canister system were considered. Results of steady-state and transient thermal analyses, based on the ANSYS[2] finite element computer program, supplied temperature data to a companion finite element stress analysis program. The hardening behavior of the glass during cooling was treated by the instant freezing concept of Bartenev.[3] More complex rheological models of glass behavior in the softening range have been applied, in which the effect of temperature on stress relaxation is represented by a contraction of the time scale.[4] An equivalent time, ζ, is defined as:

$$\zeta = t\,\Phi(T)$$

For commercial soda–lime glass, the shift function, Φ, can be represented as

$$\log_{10}\{\Phi\} = 0.03861\,(T - 538)$$

where T is the temperature in °C. Numerical studies, however, indicated that such phenomena have little effect on stresses in the glass canister system.

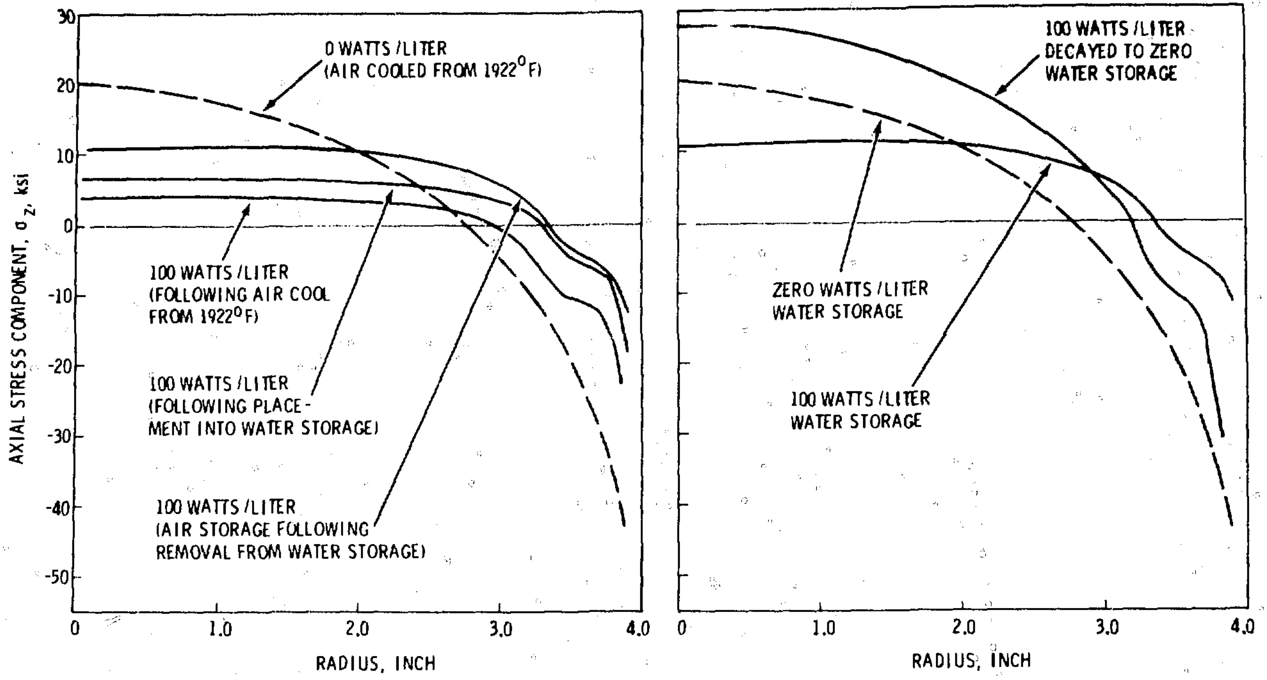

(a) EFFECT OF HEAT CONTENT ON GLASS STRESS

(b) CHANGE IN GLASS STRESS AS HEAT CONTENT OF GLASS DECREASES DURING PERIOD OF STORAGE

Fig. 1 Effect of heat content and cooling conditions on glass stress.

Stresses associated with various cooling conditions for an eight-inch diameter canister of glass produced by the in-can melting process have been predicted. A significant variable in these calculations was the rate of internal heat generation due to radioactive decay. The heat rate was varied from 0 to 100 watts/liter. Thermal and mechanical properties were for a typical borosilicate glass and a 304L stainless steel canister as given in Table I. The solidification temperature for the instant freezing concept was taken as 1067°F, based on the softening behavior of the selected glass composition.

TABLE I

Thermal and Mechanical Properties

	E	ν	α
Canister and fins (304L SS)	28×10^6 psi	0.3	9.6×10^{-6} °F^{-1}
Glass	11×10^6 psi	0.3	5×10^{-6} °F^{-1}

Predictions of tensile residual stresses in the walls of canisters (levels at or near the canister material yield strength) are consistent with stress measurements on experimental canisters. Such stresses are due primarily to the higher thermal expansion coefficient of the canister material relative to the glass.

Figure 1 shows predicted stress levels in the glass for various cooling conditions. Also, differences between non-heating glass and a high heat content glass of 100 watts/liter are shown. In all cases, filling was by the in-can melting process. The predictions showed a profound effect of internal heat generation on both glass and canister stresses. The presence of internal heat within the glass results in a predicted reduction of residual stress in the glass and a predicted reduction or even elimination of the tensile residual stress in the wall of the canister. Steady-state thermal gradients in the glass due to internal heat generation result in compressive stresses at the center of the glass and tensile stresses at the outer surface. This stress pattern partially cancels the residual stresses of internal tension and external compression that develop during cooling of the glass from processing temperatures.

For cooling rates typical of proposed vitrification processes, glass stresses can attain theoretical levels approaching 30,000 psi. Since such stresses are well in excess of typical glass strengths, the analyses clearly indicate that cracking of the glass will occur, as has been observed in process development trials.

Changing the thermal environment by placement in water storage increases glass tensile stresses in response to a reduction of tensile residual stress in the canister wall due to rapid cooling of the hot canister. The loss of tensile stress in the canister wall implies a loss in the radial compressive loading on the outer surface of the glass and hence a reduction in the associated compressive contribution to the total stress state in the glass.

As shown in Fig. 1, the glass stress increases as the heat generation rate in the glass decreases in response to

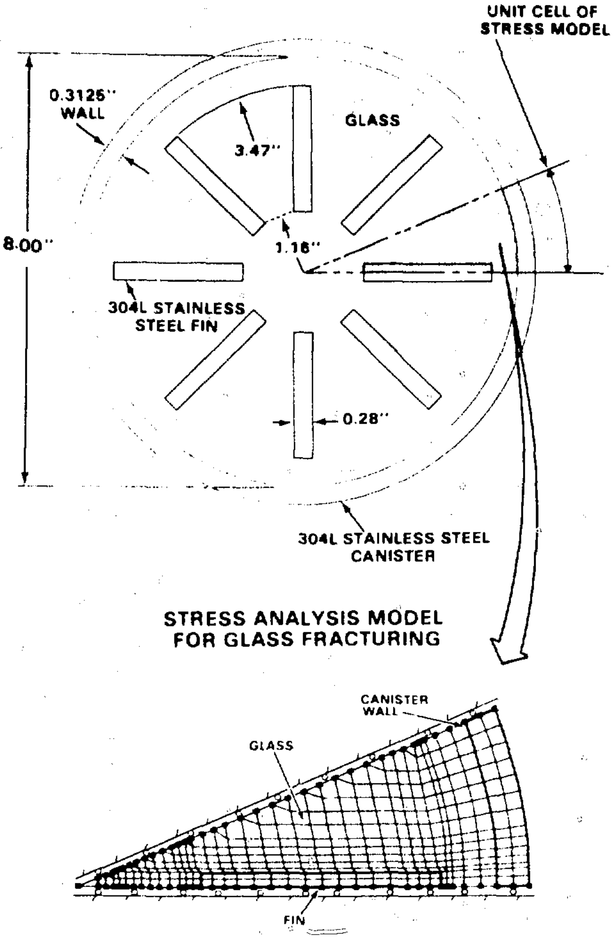
UNIT CELL OF STRESS MODEL
0.3125" WALL
GLASS
3.47"
8.00"
1.16"
304L STAINLESS STEEL FIN
0.28"
304L STAINLESS STEEL CANISTER
STRESS ANALYSIS MODEL FOR GLASS FRACTURING
CANISTER WALL
GLASS
FIN

Fig. 2 Glass-filled 8-inch diameter canister with eight internal fins.

radioactive decay. The analyses suggest that radioactive glass with high heat rates will be less extensively cracked initially but may over long time periods continue to crack in response to a decaying heating rate.

TWO-DIMENSIONAL ANALYSIS OF GLASS FRACTURING

The cross section of the eight-inch diameter canister (Fig. 2) with eight internal fins for enhancement of heat transfer was modeled. The glass had no internal heat generation and was taken to be cooled from melting temperatures (say 1°C/hr). Stresses were due solely to the fact that the coefficient of thermal expansion of the steel fins and outer wall was greater than that of the glass. As a result, additional cooling after the glass solidified had the following effects:

- The outer shell tended to compress the glass cylinder.
- The radial fin tended to shrink away from the surrounding glass.

The thermal expansion effects were studied by use of finite element modeling. The finite element program used in this analysis was a modified version of the code described by Wilson.[5] A sixteenth symmetry model of the canister cross section was used to formulate the mesh configuration shown in Fig. 2. Boundary conditions were imposed to restrain circumferential motion at the radial boundaries of the mesh.

The finite element solution was performed so as to allow glass cracking due to tensile stresses. Cracking was simulated by treating the glass as an orthotropic material with zero elastic modulus normal to the crack face in the manner described, for example, by Glenn.[6] The loading was a 1000°F temperature decrease, with the glass–canister–fin assembly taken to be stress free at the so-called instant freezing temperature. The glass material was then allowed to crack in regions where tensile stresses exceeded some initial threshold. Using the orthotropic properties for the cracked glass in these regions, the analysis was repeated using a diminishing glass strength with each iteration.

Figure 3 shows a graphical interpretation of the predicted cracking process. Final crack patterns are shown for assumed glass strengths from 0 to 10,000 psi. The cracking initiates at the ends of the fins and subsequently extends around each fin. Figure 4 shows a cross sectional canister of the same dimensions as the finite element model, and a similarity of the cracking patterns around the fins can be seen. The sectioned canister also shows extensive cracking near the outside surface of the glass. This mode of cracking is the subject of present investigations. Cracking near the outside surface is thought to be due to thermal expansion mismatch between the canister and the glass in the axial direction. Thermal gradients during cooling may also be a factor.

DISCUSSION

Analytical models of cracking have proven useful in interpreting observations, in estimating the effects of internal heat generation, and in identifying means to minimize the extent of cracking. However, quantitative predictions of cracking (e.g., net increase in surface area and particle size) are currently not possible. The consequences of cracking of high-level waste glass is discussed in a previous publication,[1] where it is concluded that the amount of cracking in high-level waste glass can be controlled to meet expected waste form criteria. In most situations the amount of cracking typically observed in simulated waste glass should have no significant effect on the safety of surface operations. Cracking will, however, result in increased surface area and increased leaching rates in the disposal environment. However, recent data[7] suggest that the quantity of leached material in the disposal environment will not increase in proportion to surface area and that other factors are more critical in accelerating leach rates.

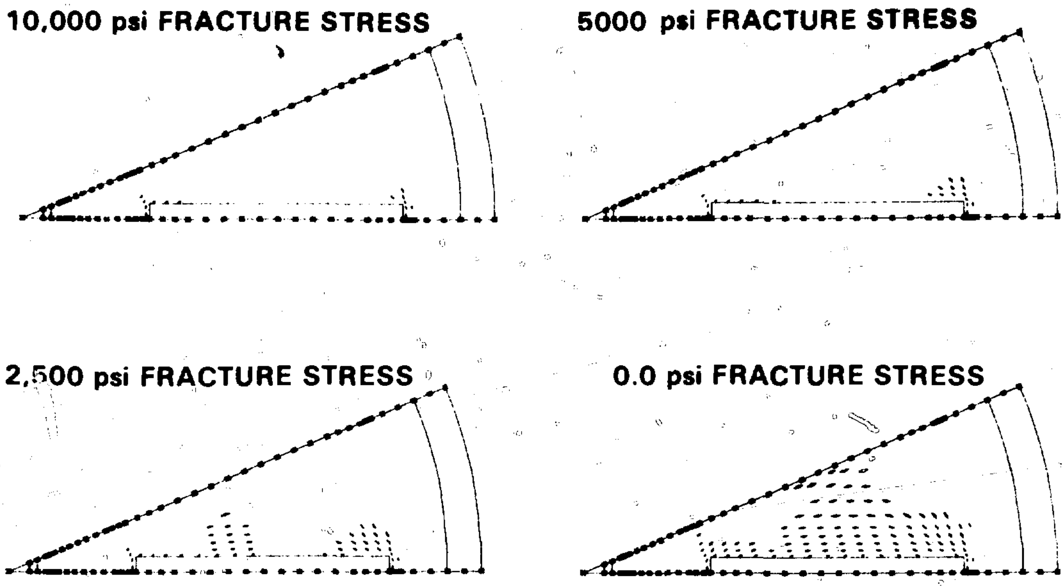
10,000 psi FRACTURE STRESS
5000 psi FRACTURE STRESS
2,500 psi FRACTURE STRESS
0.0 psi FRACTURE STRESS

Fig. 3 Predicted cracking patterns in glass-filled canister - 8-inch diameter canister with eight internal fins.

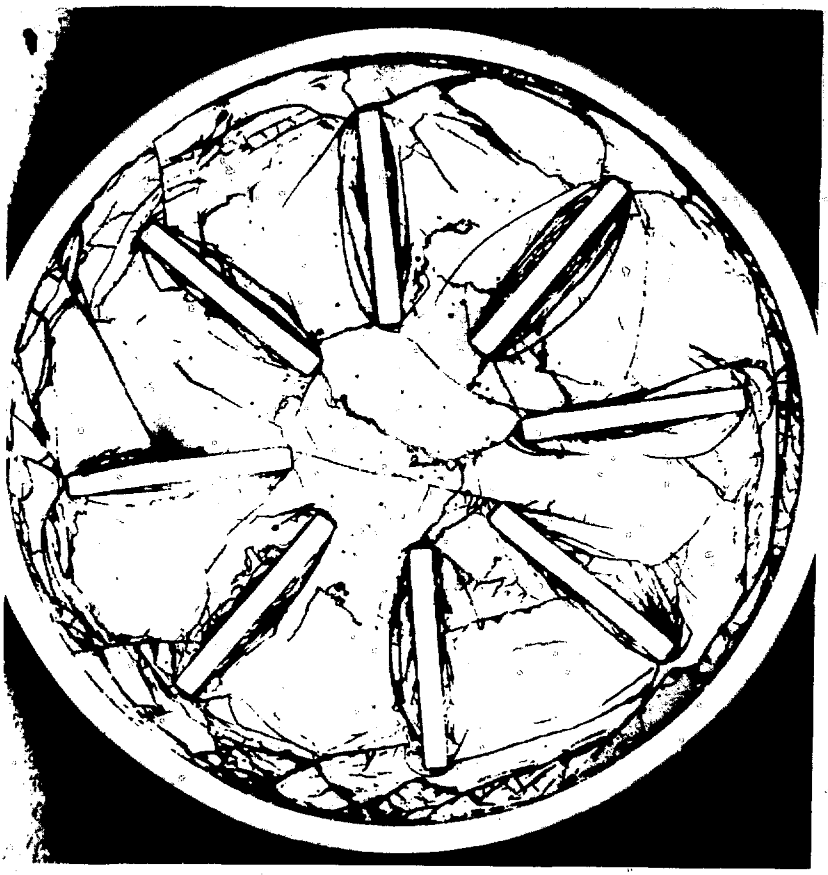

Fig. 4 Glass cracking pattern as seen in sectioned 8-inch diameter canister.

ACKNOWLEDGMENT

This paper is based on work performed for the U. S. Department of Energy under contract EY-76-C-06-1830.

REFERENCES

1. S. C. Slate, L. R. Bunnell, W. A. Ross, F. A. Simonen, and J. H. Westsik, Jr., Stress and Cracking in High-Level Waste Glass, in Proceedings of *High-Level Radioactive Solid Waste Forms*, Denver, NUREG/CP-0005, National Technical Information Service, Springfield, VA, 1979.
2. G. J. DeSalvo and J. A. Swanson, *ANSYS Engineering Analysis User's Manual*, Swanson Analysis Systems, Elizabeth, PA, March 1975.
3. G. H. Bartenev, Tempering of Glass, *Zh. Tekk. Fiz.*, 19(12): 1423-1433 (1949).
4. E. H. Lee, T. G. Rogers, and T. C. Woo, Residual Stresses in a Glass Plate Cooled Symmetrically from Both Surfaces, *J. Am. Ceram. Soc.*, 48(9): 480, September 1965.
5. E. L. Wilson and R. M. Jones, *Finite Element Stress Analysis of Axisymmetric Solids with Orthotropic Temperature Dependent Materials Properties*, Air Force Report No. BSD-TR-67-333, September 1967.
6. L. A. Glenn, The Fracture of a Glass Half-Space by Projectile Impact, *J. Mech. Phys. Solids*, 24: 96 (1976).
7. W. A. Ross et al., *Annual Report on the Characterization of High-Level Waste Glasses*, PNL-2625, Battelle, Pacific Northwest Laboratories, Richland, WA, June 1978.

VIII. IMMOBILIZATION OF SPECIAL RADIOACTIVE WASTES

UTILIZATION OF BOROSILICATE GLASS FOR TRANSURANIC WASTE IMMOBILIZATION

J. A. LEDFORD and P. M. WILLIAMS
Rockwell International, Golden, Colorado

ABSTRACT

Incinerated transuranic waste and other low-level residues have been successfully vitrified by mixing with boric acid and sodium carbonate and heating to 1050°C in a bench-scale continuous melter. The resulting borosilicate glass demonstrates excellent mechanical durability and chemical stability.

INTRODUCTION

A process has been developed to immobilize various types of transuranic residues resulting from typical operations at nuclear materials facilities. Residues are combined with a minimum of chemical additives in an externally heated metal vessel to produce a borosilicate glass. The glass is formed into small buttons which exhibit highly desirable physical, mechanical, and chemical characteristics.

DISCUSSION

Waste Characterization

Transuranic (TRU) waste, as generated at typical nuclear materials facilities, exhibits an extreme range of physical characteristics. In order to successfully process a majority of these materials, a two-phase development effort was undertaken at the Rocky Flats Plant. The first phase, volume and weight reduction, is accomplished primarily through incineration. Ash from the incinerator is combined with other suitable waste streams and necessary additives for further volume reduction and immobilization in the second phase. This two-phase approach results in an overall TRU waste immobilization system which is capable of processing a great diversity of materials.

Incineration is accomplished through a fluidized-bed incinerator (FBI) developed as a part of the program.[1] A listing of typical materials processed through the incinerator is given in Table 1, and the chemical composition of the resulting ash appears in part of Table 2. Two constituents of the input to the incinerator produce ashes which differ significantly in composition from the ash produced by combustion of "ordinary" materials such as paper, plastics, booties, and coveralls. The ash from high efficiency particulate air (HEPA) filters and tributyl phosphate is therefore reported separately in Table 2. The effectiveness of the first phase of the process is indicated by the considerable volume (97%) and weight (88%) reductions realized. However, as the residue of the FBI is partially soluble and highly dispersible (83 wt.% of particulates $< 200\,\mu$), it is apparent that immobilization, the second phase of the program, is desirable. Other wastes considered for introduction into the process at this point include inorganic ion exchange resin and diatomite filter aid. Typical chemical compositions of these materials are given in Table 2.

Process Development

Investigation of a number of possible waste forms and consideration of the composition of the waste to be immobilized resulted in the selection of the vitrified form for further development. Examination of the waste composition (Table 2) indicates that very nearly all the essential ingredients for forming a glass are present in the wastes. Only addition of small amounts of B_2O_3 (as H_3BO_3) and Na_2O (as Na_2CO_3) is necessary to produce glass with the desired properties. As a result, large waste-to-additive ratios can be obtained producing a waste form that is highly

TABLE 1

Typical Materials Processed Through the Fluidized Bed Incinerator

PVC plastics
Paper
Shoe covers
Organic ion exchange resin
Polyethylene
Waste chemicals
Rubber
Wood
HEPA filters
Leather
Reverse osmosis membranes
Naphtha
Methylene chloride
Trichloroethylene
Hydrazine
Oil
Methyl cellulose
Tributyl phosphate

TABLE 2

Chemical Composition of Simulated Waste Streams by Wt.%

Chemical compound	Ordinary waste ash, %	Tributyl phosphate ash, %	HEPA filter ash, %	Diatomite filter aid, %	Inorganic ion exchange resin, %
NaCl	5.0				
Na_2CO_3	30.0	17.2			
Cr_2O_3	10.0	3.0	1.2		
Al_2O_3	35.0	10.4	11.9	2.4	24.9
SiO_2	12.0		39.6	87.2	58.5
Na_2SO_4	5.0		1.2		
C	3.0	0.5	3.8		
Na_3PO_4		68.9	3.6		
MgO			33.9		
Fe_2O_3			2.6	1.4	
CaO			2.2	0.5	13.7
Na_2O				3.6	
H_2O				4.9	2.9
	100.0	100.0	100.0	100.0	100.0

weight and volume efficient. Glass also exhibits inherent characteristics such as nonflammability, high structural strength, and chemical stability, that indicate its applicability as a final waste form for long-term storage.

Early development criteria demanded that the process demonstrate maximum possible simplicity and component longevity since it will have to operate with limited access due to the containment requirements for radioactive material processing or may have to operate remotely. Therefore, an externally heated reactor vessel in an electric furnace was chosen because this type of equipment is both simple and well proven. The vessel, however, did present some challenges.

As molten glass is highly corrosive, reactor material investigations were limited to those materials known to be extremely corrosion resistant as well as capable of withstanding temperatures of approximately 1000°C. Certain metals appeared to satisfy these criteria. Laboratory tests in which coupons of test materials were submerged in molten glass for 500 hours indicated that Inconel 600 and 690 alloys were likely candidates. A vessel was subsequently fabricated from a length of Inconel 600 pipe and placed into operation. After 40 hours of operation, sufficient deterioration had occurred to prevent its further use. Another vessel fabricated from a length of Inconel 690 pipe operated continuously for more than four months. Destructive examination at the end of that period revealed no evidence of serious corrosion or other deterioration.

Another of the development criteria demanded that the output of the process be uniform and easily handled. Various sizes of molds of graphite and steel were investigated, as were marble forming machines. All were rejected, however, because of mechanical complexity. Early work in preparing specimens of glass for tests involved pouring glass from crucibles onto a metal plate to form small buttons. This technique is the basis for the forming method which was finally adopted and is presently in use.

Production Process

A bench-scale vitrification facility, processing simulated nonradioactive wastes, has been in operation for several years at the Rocky Flats Plant. Consisting primarily of feeding, melting, and forming stages, the process complies fully with the criterion of simplicity. Blended wastes and additives are introduced into the hopper of the screw feeder (Fig. 1) to be conveyed, as required, to the reactor. The feeder is a commercially available unit which employs a straight-thread, noncompressing screw. It is supplied with a

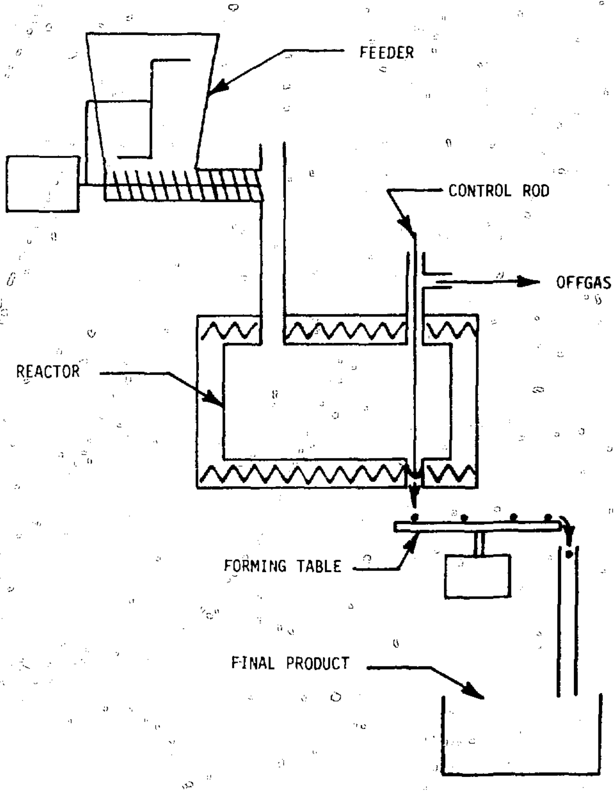

Fig. 1 Vitrification schematic.

[illegible] hopper and is driven by a variable speed motor to allow changing demands of the reactor to be met. The reactor vessel is wholly contained in a furnace heated by 14 silicon carbide glowbars 2.5 cm in diameter. The interior of the furnace, which is approximately a one-meter cube on the exterior, measures approximately 61 cm long, 38 cm deep, and 50 cm wide. Power is provided by a 240-volt, three-phase variable supply capable of delivering 8 kilowatts to each of three independently controlled zones. A temperature controller integral with the power supply maintains an overall temperature of approximately 1050°C. The furnace is a standard commercially available item and as such requires no significant on-site design or construction effort. The relatively large heated chamber of the furnace allows a departure in design from the vessels constructed of lengths of pipe. Fabricated primarily of Inconel 690 plate 0.63 cm thick, the redesigned vessel is approximately square in cross section (the corners have been rounded to facilitate construction) measuring 23 cm wide, 23 cm deep, and 50 cm long. Molten glass occupies approximately one third of the reactor's gross volume of 24 liters.

Penetrating the top near one end is an Inconel 600 pipe, with an inside diameter of 5.25 cm, which serves as the feed port or inlet to the vessel. Another Inconel 600 pipe, 2.66 cm inside diameter, penetrates the top near the other end and serves as control rod guide and off-gas outlet. Directly below this pipe is the glass outlet, an Inconel 600 pipe cap, which measures 2.66 cm inside diameter, with a 0.64 cm diameter hole through the bottom. The glass flow control rod, a length of 1.9 cm diameter Inconel 690 threaded at one end and machined to a point at the other, is installed through a threaded portion of the off-gas outlet in such a way that rotation of the rod causes it to move vertically. The conical end of the rod can thus be withdrawn from the hole in the glass outlet, in which it normally rests, and glass flow can be initiated and regulated. Since the glass outlet is totally within the heated chamber of the furnace, a hole has been provided through the refractory and furnace bottom directly below the outlet to allow the glass to drop onto the forming table. The feed port and control rod guide/off-gas outlet are of a sufficient length to extend through the refractory and furnace top so as to be accessible from outside.

In actual operation, the control rod is positioned to allow glass to accumulate at the outlet until the weight of the collected material overcomes surface tension and a drop of glass falls. In the absence of other variables, the volume of material in each drop is relatively constant. The drops are allowed to free fall onto the surface of a rotating metal disc where they form small, roughly hemispherical buttons which, due to the constant volume of material, are virtually identical to one another. Some experimentation was necessary before an acceptable material for the disc was found. Initial efforts using common materials such as aluminum and stainless steel were unsuccessful as the heat transmitted to the disc from the rapid cooling buttons caused severe warping. Inconel alloys are the only materials which have to date proven satisfactory. After residing on the forming table for a period sufficient to allow adequate cooling, the buttons encounter a stationary plow which removes them from the disc. After further cooling, they are accumulated for future transportation and storage.

Product Characteristics

The product of the process is a button of glass with a flat bottom and domed top, round in plan, measuring approximately 10 mm in diameter and 6 mm in height. Each button is dark green to black in color, opaque, weighs about 0.75 gm, and occupies a volume of 0.3 cc. Packing density of the product is 1.5 gm/cc. The product, in bulk, is easily conveyed by a number of means and can be introduced into containers of various sizes and configuration. Thus, the final shipping container can be chosen to facilitate handling with small capacity equipment. A standard thirty-gallon drum filled with buttons would weigh less than 180 kg.

Statistically significant sampling of the output of the process is facilitated by the product form. As the buttons are virtually identical to one another, randomly chosen samples can be considered with confidence to represent accurately the characteristics of the process output. Any number of tests of product quality, including destructive evaluation and determinations of product composition, can be performed with no adverse effect on the product actually destined for storage. A series of such destructive and nondestructive tests have been developed to measure the performance of the product. The tests evaluate such properties as impact resistance, compressive strength, resistance to damage from extreme temperature change, abrasion resistance, and leach resistance. They are applied periodically to a randomly chosen sample of the output of the process as a part of the quality assurance program, as well as to indicate the effects on the output of intentional changes in input composition and process operation. Buttons currently produced are capable of withstanding a free fall of more than 9 m onto a concrete surface and the impact of a 2.5 cm diameter steel rod weighing 1.35 kg falling through a distance of one meter. These results, together with the results of tests to determine resistance to heat and leaching, allow the buttons to qualify for the designation of special form material as determined by the United States Department of Transportation.[2]

Resistance to leaching has been evaluated through two methods. Buttons submerged in a brine solution in a static test for more than a year have experienced no statistically significant changes in weight. Dynamic tests, using Soxhlet extraction apparatus and deionized water, have produced leach rates on the order of 10^{-4} gm/cm² · day. Comparison with leach rates of 10^{-5} gm/cm² · day, as determined by the same procedure for commercially prepared borosilicate glass, indicates a high level of performance, especially for a glass prepared primarily from wastes. Other tests involving elevated temperatures and pressures are contem-

[illegible]

FUTURE WORK

A [illegible] to verify the applicability of the process [illegible]. While the reactor [illegible] installed at the time of construction will be an externally heated metal [illegible], the facility is capable of accepting another type of reactor currently being developed. A Joule-heated ceramic-lined glass reactor has been operated successfully, and development of an improved version of that unit is in progress. It is expected that higher temperature operation, improved [illegible], and reduced off-gas generation will be some of the advantages of this type of reactor.

CONCLUSIONS

The externally heated metal vitrification reactor described has been in operation for more than two years but [illegible] Glass [illegible] while accepting [illegible] the [illegible] compatible with the process. [illegible] including [illegible] agents.

REFERENCES

1. D. L. Ziegler and A. L. Johnson, "Fluidized Bed Incineration of Transuranic Contaminated Waste," *Proceedings of the NEA/IAEA Technical Seminar on Treatment, Conditioning and Storage of Solid Alpha-Bearing Waste and Cladding Hulls*, Paris, 197[illegible].
2. *Code of Federal Regulations*, Title 49, Transportation, CFR 398, December 31, 1976.

CRYSTALLOCHEMICAL STABILIZATION OF RADWASTE ELEMENTS IN PORTLAND CEMENT CLINKER

C. M. JANTZEN and F. P. GLASSER
Department of Chemistry, University of Aberdeen, Old Aberdeen, Scotland

ABSTRACT

Most of the elements present in a model PW 4b radwaste have been successfully incorporated during clinkering into the calcium silicate and ferrite phases comprising Portland cement. The bulk composition of a model waste has been systematically altered by the addition of other nonradioactive components to produce an inherently cementitious material. This has the advantage that (1) the radwaste ions are substituted directly into the crystal structure of the anhydrous cement phases, (2) the unhydrated cement continues to behave as a ceramic, (3) during hydration the radwaste ions can be more readily incorporated into the hydration products, and (4) the hydration products should represent a close approach to thermodynamic stability during storage in geological environments, e.g., low pressures and temperatures between 0°C and ~180°C.

INTRODUCTION

The development of radwaste storage systems requires a sophisticated approach to contend with the many nuclear, chemical, and engineering problems which arise as well as the very long time scale (~10^4 to 10^5 years) envisaged for containment. The longer the life expectation of the containment system the progressively more difficult it becomes to ensure that the containment system will retain its integrity under adverse geological conditions. The long-term survival of glasses in uncontrolled natural environments is, in our view, questionable.

WHY CONSIDER CEMENT CLINKER FOR RADWASTE STABILIZATION?

The reasons for considering a cement clinker system can be summarized as follows:

1. Portland cement clinkers are a ceramic material and possess many of the desirable attributes of ceramics.

2. The properties and phase compositions of the relevant cement-forming systems are well understood.

3. Many of the mineral phases present in cements are chemically inert across a broad spectrum of geological conditions.

4. When reaction with the environment particularly with water occurs, the products of reaction are naturally cementitious, insoluble in groundwater, and immobile.

THE NATURE OF PORTLAND CEMENT

Anhydrous cement clinkers are essentially ceramics. Cement clinker is similar to many ceramics in that the clinker is composed of oxide and silicate phases, the phase composition of the raw material is completely altered during the firing, and the final stages of sintering are achieved in the presence of a reactive liquid phase. A typical Portland cement has the composition shown in Table 1. For present purposes this is only a "base" composition which will be modified by inclusion of radwaste constituents. Ordinary Portland cement consists almost entirely of four principal phases. These are solid solutions but have the idealized compositions Ca_3SiO_5,* Ca_2SiO_4, $Ca_3Al_2O_6$, and $Ca_4Al_2Fe_2O_{10}$. When cement hydrates, the products of hydration consist mainly of a poorly crystalline gel. Because this gel is the main cementing agent in constructional concrete, much is known about its cementitious properties and its durability in a wide range

---

*3C[illegible]
2C[illegible] [illegible] C_4AF

[illegible] cements. [illegible] concretes made at some time in the [illegible] naturally occurring deposits [illegible]. The time span of these observations extends over [illegible] × 10 years for modern cements [illegible] for Roman cements [illegible] extends over 2 × 10 years. More [illegible] geological occurrences of [illegible] for example at Larne, Northern Ireland [illegible] the stability of [illegible], and [illegible] polymorph of C S [illegible] can be extended over 2 × 10 years. The C S [illegible] originally formed by igneous intrusions some [illegible] years ago, are only partially hydrated. The spatial [illegible] and textures in this deposit suggest that these [illegible] are very insoluble and remain relatively immobile under a wide range of environmental conditions, including [illegible] at depth as well as near-surface weathering.

PREVIOUS WORK

Although much work has been done on setting aqueous solutions of radwaste ions with cement, virtually no work has been done on incorporating radwastes at the clinker stage. We have recently described the use of clinkers as a ceramic[1] using model waste formulations suggested by McCarthy and Davidson.[2] The waste may be incorporated as either dry powder or liquid form. The alkaline earths, Sr, Ba, the lanthanons, and Y are soluble at ~10% total level in C_2S and C_3S, while these elements plus Ce and Zr are appreciably soluble in the ferrite phase. Loadings in excess of the solubility limits of clinker phases were shown to produce a lanthanon apatite when silica is present. The apatite behaved as an inert "ceramic" phase while the C_2S solid solutions reacted slowly with water to give a slightly hydrated cement which exhibited low leach rates for both Nd and Sr. Therefore, radwaste-doped cementitious phases with or without the presence of inert ceramic-type phases, i.e., Ln-apatite, appear to afford scope for the development of promising containment systems.

MOLYBDENUM AND CESIUM SUBSTITUTIONS

Experimental

Mixtures for sintering experiments were made using commercially-available reagent grades of $CaCO_3$,* Al_2O_3,* Fe_2O_3,* and crushed optical-grade quartz† as well as various reagent grade carbonates, oxides, and kaolin. Dried reagents were weighed out in 1- to 20-g batches, wet blended in agate mortars, redried, placed in Pt crucibles, and fired in electrically heated muffles in air. It was necessary to grind and resinter batches several times until complete reaction was obtained.

TABLE 1

Chemical Composition of Portland Cement

Oxide	wt.%
CaO	[illegible]
[illegible]	[illegible]
[illegible]	[illegible]
SiO_2	21 24
$Na_2O + K_2O$	[illegible] 4
SO_3	[illegible]
MgO	[illegible]

For molybdenum substitutions, $CaMoO_4$ was formed from $CaCO_3$ and MoO_3 by sintering overnight at 750 °C. This enabled entrapment of the molybdenum in a ceramic phase, stable up to 1445 ± 5 °C (Ref. 3), prior to being mixed and resintered into cementitious silicate, aluminate, or ferrite phases. A similar method was employed for coupled substitution of cesium and molybdenum by starting with Cs_2MoO_4 made from $CsCO_3$ and MoO_3 heated overnight at 650 °C.

Lastly, cesium substitution into combined C_2S–C_4AF mixtures was attempted by first forming $CsAlSiO_4$ (pollucite), following the technique of Gallagher, McCarthy, and Smith.[4]

The phase compositions were determined by powder X-ray diffraction using a Hägg-Guinier focusing camera and $CuK_{\alpha 1}$ radiation. The amount of molybdenum retained and its distribution between the phases present were determined by CORA, a Kratos transmission electron microanalyzer, while bulk cesium was determined by atomic absorption.

Types of Substitutions

The molybdenum and cesium substitutions were of three types:

1. Single element substitution of molybdenum into C_2S and C_3S lattices for Si^{4+}, into C_3A for Al^{3+}, and into C_4AF for Fe^{3+}
2. Multiple element substitution of molybdenum and cesium into C_3S (molybdenum to replace Si^{4+} and $2Cs^+$ to replace Ca^{2+})
3. Single-element substitution of Cs^+ into two-phase mixtures of C_2S and C_4AF

The ratio of Mo/Cs in a type 1 substitution was kept at ~2 by addition of both Cs_2MoO_4 and $CaMoO_4$, this being the ratio found in a PW-4b radwaste. The amount of Cs^+ substituted into the C_2S–C_4AF mixtures (type 3) was also predetermined by the approximate Cs/Fe ratio found in a PW-4b radwaste.

---

*"AnalaR," a trademark of British Drug House, Poole, Dorset, England.

†Thermal Syndicate, Ltd., Wallsend, Newcastle, England.

TABLE 2

Molybdenum Substitutions*

Composition	Temperature (°C)	Time (hr)	Phases present†
[illegible]			
[illegible]	[illegible]	[illegible]	[illegible]
[illegible]	[illegible]	[illegible]	[illegible]
[illegible]	[illegible]	[illegible]	[illegible]
[illegible]			
[illegible]	[illegible]	[illegible]	[illegible]
[illegible]	[illegible]	[illegible]	[illegible]
[illegible]	[illegible]	[illegible]	[illegible]
[illegible]	[illegible]	[illegible]	[illegible]
[illegible]	[illegible]	[illegible]	[illegible]
[illegible]	[illegible]	[illegible]	[illegible]
C_3A			
[illegible]	[illegible]	[illegible]	[illegible]
[illegible]	[illegible]	[illegible]	[illegible]
C_4AF			
90Ca$_4$Al$_2$Fe$_2$O$_{10}$ 10Ca$_4$Al$_2$FeMo[illegible]O[illegible]	[illegible]	[illegible]	C_4AF + [illegible]
90Ca$_4$Al$_2$Fe$_2$O$_{10}$ 10Ca$_4$Al$_2$FeMo[illegible]O[illegible]	[illegible]	[illegible]	C_4AF
85Ca$_4$Al$_2$Fe$_2$O$_{10}$ 15Ca$_4$Al$_2$FeMo[illegible]O[illegible]	1300	144	C_4AF + $CaMoO_4$
85Ca$_4$Al$_2$Fe$_2$O$_{10}$ 15Ca$_4$Al$_2$FeMo[illegible]O[illegible]	1380	24	C_4AF + $CaMoO_4$
80Ca$_4$Al$_2$Fe$_2$O$_{10}$ 20Ca$_4$Al$_2$FeMo[illegible]O[illegible]	1300	144	C_4AF + $CaMoO_4$
80Ca$_4$Al$_2$Fe$_2$O$_{10}$ 20Ca$_4$Al$_2$FeMo[illegible]O[illegible]	1380	24	C_4AF + $CaMoO_4$

*All molybdenum substitutions started with $CaMoO_4$ made by sintering $CaCO_3$ and MoO_3 at 750°C overnight. Excess $CaCO_3$ was added accordingly.

‡Ca_2SiO_4 was used instead of component $CaCO_3$ and SiO_2.

†tr = trace; R = Rhombohedral; T_1 = Triclinic.

Results

Type I. Molybdenum substitutions into the calcium silicates were attempted at 1300°C, about 150°C lower than the melting point (1445 ± 5°C) of $CaMoO_4$. Although 5.8 wt.% MoO_3 was added to the C_2S preparation as the theoretical end member $Ca_2MoO_{4.5}$ and 4.7 wt.% MoO_3 to the C_3S preparation as the theoretical end member $Ca_3MoO_{5.5}$, i.e., assuming molybdenum to be pentavalent, the CORA analyses revealed that no significant amount of molybdenum was present in the C_2S or C_3S phases (Table 2). Moreover, the CORA analyses revealed that the reaction was incomplete for the C_3S substitution. Particles of C_3S, C_2S, and Ca_3MoO_6 were identified in the doped C_3S preparation by CORA analysis although present in such small amounts that they were undetected by X-ray diffraction. However, when the samples were resintered for 24 to 45 hours at a somewhat higher temperature (~1380°C), the CORA analyses revealed that 4.5 wt.% MoO_3 out of the 5.8 wt.% MoO_3 added was retained in the C_2S phase while the X-ray diffraction analysis revealed the presence of $CaMoO_4$. Thus most of the Mo was in solid solution in C_2S and the remainder present as $CaMoO_4$. Starting with prepared C_2S instead of the component oxides did not change the resulting products (Table 2). The CORA analyses of the molybdenum doped C_3S ranged from 1.9 to 4.9 wt.% MoO_3 with an average of ~3.6 wt.% out of the 4.7 wt.% MoO_3 added. However, the corresponding X-ray diffraction analysis did not indicate the presence of a second molybdenum phase suggesting that at 1380°C, C_3S accepts most, if not all, the molybdenum corresponding to a 10% doping of the $Ca_3MoO_{5.5}$ end member. Higher dopings, i.e., 15 and 20% $Ca_3MoO_{5.5}$, retained two calcium molybdate phases, Ca_3MoO_6 and $CaMoO_4$, even after brief firings at 1380°C (Table 2).

The calcium aluminate, C_3A, did not accept molybdenum doping but formed a stable aluminum molybdate phase, and, therefore, further experiments with CA* and $C_{12}A_7$† were not attempted. The calcium aluminoferrite phase, C_4AF, did not crystallochemically accept

---

*CA = CaO · Al_2O_3.

†$C_{12}A_7$ = 12CaO · $7Al_2O_3$.

TABLE 3

Cesium Substitutions

Composition	Temperature, °C	Time, hr	Phase present
[illegible]	[illegible]	144	[illegible]
[illegible]	[illegible]	24	[illegible]
[illegible]	[illegible]	[illegible]	$C_4AF + \beta$-$C_2S + \gamma$-C_2S
[illegible]	[illegible]	24	$C_4AF + C_2S$
[illegible]	[illegible]	[illegible]	$C_4AF + \beta$-$C_2S + \gamma$-C_2S
[illegible]	[illegible]	24	$C_4AF + C_2S$

[illegible] PW-4b [illegible]

[illegible] 144 [illegible] PW-4b [illegible] Starting with $CsAlSiO_4$ (pollucite) [illegible]

[illegible]

[illegible]

molybdenum at 1300°C but formed MoO_2 as a second phase. CORA analyses confirmed that molybdenum was not present in the ferrite. However, an additional firing at 1380°C for 18 hr produced a single ferrite phase at 10 mole % doping of the theoretical end member $Ca_4Al_2FeMo_{0.[illegible]}O_{10}$ (Table 2). CORA analyses of this product revealed that 2.0% of the 2.1% MoO_3 added was retained. Therefore, C_3S and C_4AF are the most promising clinker phases for crystallochemical retention of molybdenum, although firing temperatures close to 1380°C are required to promote reaction in single-phase preparations.

Type 2. Coupled substitution of Mo^{5+} for Si^{4+} and $2Cs^{+}$ for Ca^{2+} were tried for C_3S rather than C_2S in view of the retention of molybdenum by C_3S in type 1 substitutions. Ten mole percent of a hypothetical $Cs_2Ca_5Mo_4O_{18}$ end member were added as Cs_2MoO_4, $CaMoO_4$, and CaO (Table 3). Firing at 1300°C for 144 hours produced C_3S plus CaO and $CaMoO_4$. An additional firing overnight, close to the temperature of stability of $CaMoO_4$, yielded only R-C_3S* and a trace of CaO. Encouragingly, atomic absorption revealed that ~1.0% of the 1.9% added was retained after firing first at 1300°C for 144 hours and subsequently for 24 hours at 1380°C. Further experiments of this nature are currently in progress.

Type 3. Experiments to crystallochemically substitute $2Cs^{+}$ for Ca^{2+} in C_4AF and C_2S were based upon the hypothetical end member compositions $Ca_{3.5}Cs_{1.0}Al_2Fe_2O_{10}$ and Cs_4SiO_4. Since pollucite, $CsAlSiO_4$, was used as the starting "cesium-ceramic" phase, it was not expected that substitutions leading to substituted, single phase C_4AF or C_2S could be made. Therefore, the remaining bulk chemistry was adjusted on the trial assumption that 50–50 mixtures of undoped C_2S with doped C_4AF or doped C_2S with undoped C_4AF might be formed. Firings at 1300°C produced the expected mixtures of C_4AF together with β- and γ-C_2S (Table 3). These samples contained 1.75 to 2.5% Cs_2O, respectively, and 50% of the Cs_2O remained after firing at this temperature for 120 hours. Additional heat treatment at 1380°C for 24 hours caused partial melting, and the sample became contaminated with pieces of Pt foil, thereby making it difficult to obtain an accurate analysis for Cs_2O.

Summary

In the present work cementitious phases have been found to be good crystallochemical hosts for both molybdenum and cesium. Volatilization may be reduced by using stable precursor molybdenum or cesium compounds or generating these in situ by an appropriate thermal ramp. In summary, results of this study and a previous paper[1] demonstrate that β-C_2S is, in general, a slightly better host for Ln^{3+} elements, either singly or in combination, than C_3S. This is summarized in Fig. 1 which has been recast to weight percent. Likewise, Sr, Ba, and Nd dopings could be higher in C_4AF were it not that the Sr:Ba:Nd ratios were adjusted to the Fe:Zr:Ce ratios appropriate to a PW-4b radwaste.

Molybdenum substitutes both for Si^{4+} in C_2S and C_3S as well as for Fe^{3+} in C_4AF. Clearly from Fig. 1, Mo^{5+} is more soluble in C_3S than C_2S. Therefore, β-C_2S is a good crystallochemical host for Ln^{3+} ions while C_3S is more favorable for Mo^{5+} and/or Cs^{+}, and the calcium aluminoferrite, C_4AF, appears to be a good crystal host for many common radwaste ions.

---

*R = Rhombohedral.

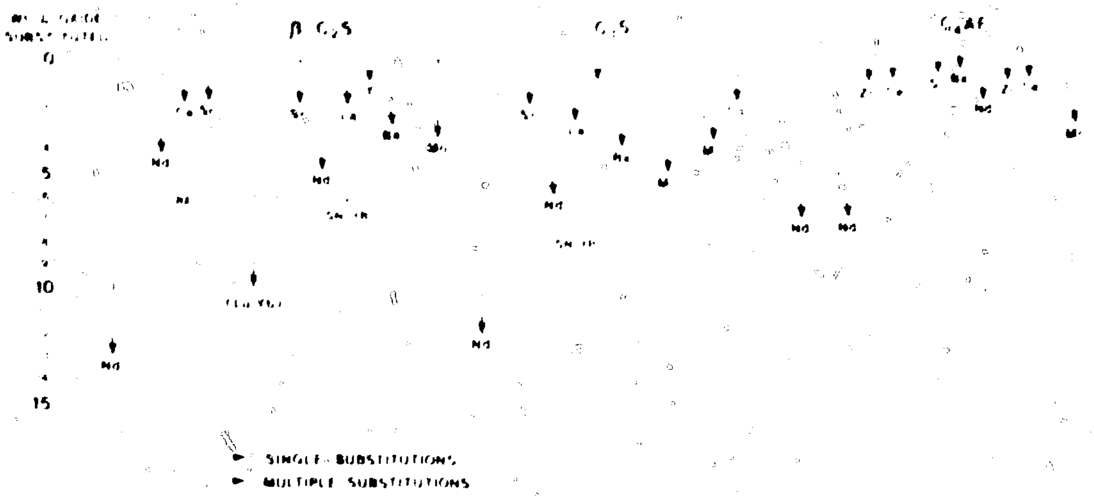

Fig. 1 Schematic [illegible] C_2S, C_3S and C_4AF [illegible] substitutions are given in Ref. 1 [illegible]

PHASE RELATIONS IN C_2S-FERRITE RADWASTE SYSTEMS

Previously the solid-solution crystallochemical relations and the partition of elements between coexisting apatite and Ca_2SiO_4 solid solutions had been explored.[1] The apatites were found typically to be enriched in lanthanons although they can be a host for a variety of ions (Sr, Ba, Etc.) in solid solution. However, the presence of excess Ca and Al with lanthanons yielded Ca-Ln aluminates, Ln aluminate or a lanthanon melilite, typically $CaNdAl_3O_7$ (Ref. 1). Likewise, large dopings of radwaste ions into C_4AF also produced Ca-Ln aluminates and the lanthanon melilite.[1] Therefore, the compatibility of doped C_2S-apatite with doped and undoped C_4AF were examined. A new phase appearing, whose X-ray diffraction pattern is similar to a mineralogic phase found in blast-furnace slags called ceraltite,* was given the approximate formula (Ca, Ce, La, Nd, Pr) (Ti, Al, Fe)O_3 by Rudneva and Malysheva[5] and Lapin, Kurtseva, and Knyazeva.[6] Since only Ca, Nd, Al, and Fe were present in our model system we retained the use of the name ceraltite but redetermined its approximate formula by analysis of selected grains in the multiphase preparations with CORA.† Studies of this phase show that it has a range of compositions, close to $2CaO \cdot Ln_2O_3 \cdot 2[(Fe_2O_3)_{1-x}(Al_2O_3)_x]$, where Ln is typically Nd and the value of x ranges between 0.0 and 0.33. The phase undoubtedly has substantial range of single-phase homogeneity although Fe^{3+} and Al^{3+} are partially, but not completely, interchangeable. Solid solutions apparently extend from the Fe^{3+} end member to a molar Fe/Al ratio ~2.0. Beyond this ratio, a second Al_2O_3-rich phase, usually $CaNdAl_3O_7$, is also obtained.

Ceraltite is unreactive towards water and behaves as a ceramic. Although it has been classified by its discoverers[5,6] as a perovskite of the ABO_3 type, it is not clear if this classification is correct. The $CaO-Nd_2O_3-Al_2O_3-Fe_2O_3$ system already contains several perovskites, i.e., $NdFeO_3$ and $NdAlO_3$, and distorted perovskites, $Ca_2Fe_2O_5$ and its aluminous solid solutions, as well as pseudoperovskites, such as $Ca_3Al_2O_6$. It will be appreciated that the presence of so many perovskite-like phases complicates the interpretation of the phases present by X-ray powder diffraction methods.

The phase relations of ceraltite with other phases can best be depicted in a series of figures, together with Table 4. Figure 2 shows the tetrahedra $CaO-SiO_2-Nd_2O_3-R_2O_3$. Both Al_2O_3 and Fe_2O_3 have been projected to the R_2O_3 corner. The join C_2S-Nd apatite shows clearly; it is the assemblage designated F in Table 4. This join is marked by extensive mutual solid solution. The positions of other assemblages, A, B, and E, are shown. These enable us to define the coexistence of C_2S solid solutions with Nd apatite, ceraltite and ferrite (C_2F-C_2A solid solutions). Melilite, $CaNdAl_3O_7$, does not occur in these assemblages, which are comparatively rich in Nd_2O_3.

It is also convenient to represent these phase relations in nongeometric form. Permissible combinations found in the course of experimental study are shown in Fig. 3 and indeed the sequence of cementitious plus inert phases found with increasing wt.% Nd_2O_3 in doped and undoped C_2S-ferrite mixtures is (1) C_2S-ferrite (0.5 to 1.5% Nd_2O_3) → (2) C_2S-ferrite-ceraltite (1.5 to 9.5% Nd_2O_3) → (3) and (4) C_2S-ceraltite (5.0 to 12.0% Nd_2O_3) →

---

*Ceraltite is the earlier name for celanite.[7]

†Twenty-seven sinters were prepared for the compositions indicated by the CORA analyses, and the phase purity of the sinters was determined from powder diffraction photographs. In this way it was possible to converge on the composition given.

TABLE 4

Compatibility of C_2S + *Ln* Apatite with C_4AF*

Composition, Ca_2SiO_4 $Nd_4Si_3O_{12}$	Starting phases	Nd-doped C_4AF 75%	Nd-doped C_4AF 50%	Nd-doped C_4AF 25%	Undoped C_4AF 75%	Undoped C_4AF 50%	Undoped C_4AF 25%
[illegible]	γ C_3S	B	B	B	A	A	A
[illegible]	[illegible] C_2S	B	B	C‡	A	A	B
10	[illegible] C_2S + [illegible] C_3S	B	B	C‡	A	B	n.d.
20	[illegible] C_2S + Ap	B	B	C‡	A	B	C
[illegible]	[illegible] C_2S + Ap	B	B	C‡	A	B	C
40	[illegible] C_2S + Ap	B	B	D‡	A	B	D
55	[illegible] C_2S + Ap	B	B[illegible]	E‡	B	B	E
65	[illegible] C_2S + Ap	B	D[illegible]	E‡	B	B	E
75	[illegible] C_2S + Ap	B	D[illegible]	E‡	B	C	F

* Assemblages: A = γC_2S + C_4AF
B = γC_2S + C_4AF + ceraltite
C = γC_2S + ceraltite
D = α′C_2S + γC_2S + ceraltite
E = α′C_2S + γC_2S + ceraltite + apatite
F = α′C_2S + apatite

[illegible] days [illegible] at 1500°C unless indicated.
‡ Analyzed after 4 days and 30 days at 1300°C.
[illegible] days at 1500°C.
[illegible] days at 1500°C and 1350°C.

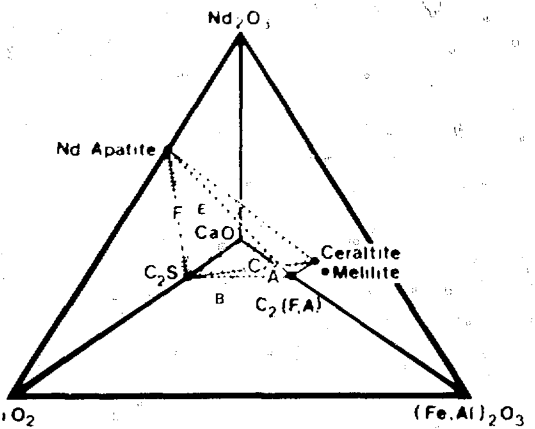

Fig. 2 Schematic phase diagram showing compatible phases in the CaO-rich regions of the system CaO–Nd_2O_3–SiO_2–$(Fe,Al)_2O_3$. (Fe and Al oxide components have been projected to the same apex. Lettered features refer to assemblages given in Table 4.)

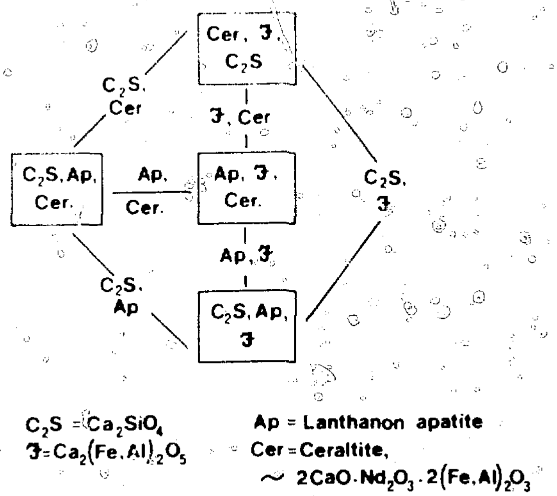

Fig. 3 Scheme showing compatible phase assemblages in the systems of the type CaO–Ln_2O_3–SiO_2–Fe_2O_3–Al_2O_3.

(5) C_2S-ceraltite-apatite (~12 to 16% Nd_2O_3) → (6) C_2S-apatite (~16 to 23% Nd_2O_3).

The projection of Fe and Al oxides at the same point brings some disadvantages. It is easier to see the phase relations in the system without SiO_2 in Fig. 4, where the range of C_3A solid solutions is shown by a solid segment extending towards "C_3F" and $NdAlO_3$. The spatial orientation of this plane is suggested by dashed lines. $NdAlO_3$ and $NdFeO_3$, shown by a crosshatched line, are presumed to form complete solid solutions. The extent of Ca substitution in these is not known. The composition of melilite, which appears to accommodate little Fe, lies near the base. C_2F forms solid solutions extending towards C_2A and these include some Nd. The extent of ferrite solid solutions is shown by a wedge-shaped region. Finally, the ceraltite composition is shown in its appropriate position on the plane C_2F–$NdFeO_3$–$NdAlO_3$ and the two-phase region of ceraltite and ferrite solid solutions indicated by a series of tie lines. This figure is useful in demonstrating the different behavior of Fe and Al relative to Nd during crystallochemical substitution in both cementitious and inert ceramic phases.

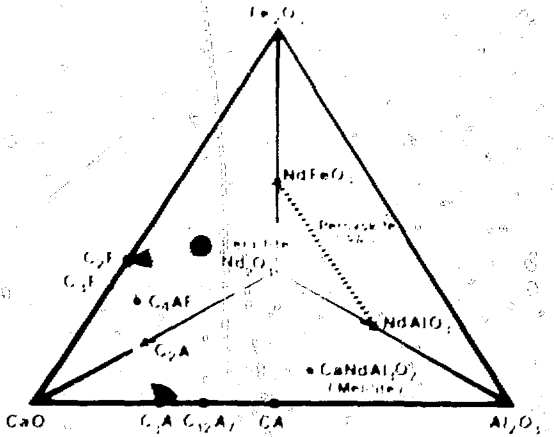

Fig. 4 Phase diagram [illegible] phase relations [illegible] of the type CaO–Al₂O₃–Fe₂O₃–SiO₂ (Phase relations were determined for [illegible] Nd³⁺ [illegible]. Known region [illegible] solid solution [illegible] are represented by [illegible] hatched line [illegible] represented by shading. The lines connecting [illegible] compositions [illegible] the coexistence of these phases.)

CEMENT CLINKER FOR RADWASTE STORAGE

This paper, together with results given previously,[1] enables a preliminary assessment of the process to be made. Most of the components present in a model PW-4b radwaste can be accommodated in a clinker consisting of β-Ca_2SiO_4 and "ferrite" phases. Reaction is achieved by static sintering of the appropriate batch composition, typically for 12 to 24 hr at 1300°C. No dust is produced. It is realistic to expect clinker loadings to reach 8 to 10 wt.% radwaste. At higher loadings, other phases form which are unreactive towards water. The presence of some β-Ca_2SiO_4 produces an inherently cementitious material, and its tough, gel-like hydration products are resistant to leaching.[1]

[illegible] wide range of environmental [illegible].

ACKNOWLEDGMENTS

Thanks are extended to Dr. Eric Lachowski for the CORA analyses, and to Mr. Alan Griggs for his assistance. This work is being supported by the Science Research Council (U.K.).

REFERENCES

1. C. M. Jantzen and F. P. Glasser, Stabilization of Nuclear Waste Constituents in Portland Cement, *Am. Ceram. Soc. Bull.*, in press (197[illegible]).
2. G. J. McCarthy and M. T. Davidson, Ceramic Nuclear Waste Forms: I, Crystal Chemistry and Phase Formation, *Am. Ceram. Soc. Bull.*, 54, 782 (1975).
3. I. M. [illegible] and V. M. Zhukovskii, The Equilibrium Diagram of the CaO–MoO_3 System, *Russ. J. Inorg. Chem.*, 18, 1182 (1973).
4. S. A. Gallagher, G. J. McCarthy, and D. K. Smith, Preparation and X-Ray Characterization of $CsAlSiO_4$, *Mater. Res. Bull.*, 12 1183 (1977).
5. A. V. Rudneva and T. Ya. Malysheva, New Slag Minerals Cephitosyl and Coelanite, *Dokl. Acad. Sci. U.S.S.R.*, 136 183 (1961).
6. V. V. Lapin, N. N. Kurtseva, and D. N. Knyazeva, A New Aluminiferous Rare-Earth Mineral with a Perovskite Structure from Slags, *Comp. Rend. Acad. Sci. U.S.S.R.*, 134, 1025 (1960).
7. M. H. Hey, Twenty Second List of New Mineral Names, *Min. Mag.*, 32 941 (1961).

IODIDE AND IODATE SODALITES FOR THE LONG-TERM STORAGE OF IODINE-129

DENIS M. STRACHAN and HARRY BABAD
Rockwell Hanford Operations, Richland, Washington

ABSTRACT

[illegible]

INTRODUCTION

Because of its long half-life ($t_{\frac{1}{2}} = 1.7 \times 10^7$ years), the high water solubility of most of its compounds, and its affinity for the thyroid gland, ^{129}I is a biohazard. Research to date has been to identify materials for the removal of this isotope from the off-gas streams of reprocessing plants and the use of these materials for its long-term storage. Typical scrubbing processes use silver- or lead-exchanged zeolites or mordenites[1] (AgX or PbX), hyperazeotropic nitric acid[2] (Iodox Process), and silver-loaded silica.[3] A solution of mercury nitrate also may be used to remove iodine from the off-gases. Silver nitrate-coated Berl saddles are used at the Rockwell Hanford Operations (Rockwell) Purex Plant to sorb iodine from the off-gas. For long-term storage, Yarbro et al.[2] proposed to convert the HI_3O_8 from the Iodox Process to $Ba(IO_3)_2$ to then be mixed with concrete for storage. Mailen and Horner[4] proposed to precipitate PdI_2 by judicious adjustment of oxidation states in the fuels dissolver solution. The PdI_2 so precipitated would, however, remain with the bulk of the waste and would not be selectively removed. Thus the radioiodine could be volatilized when such sludges are sent to a vitrification plant or some other high-temperature waste immobilization process. While I-Pb-X, albeit PbI_2, I-Ag-X (AgI) and $Ba(IO_3)_2$ are very insoluble, these compounds perhaps are not forms for long term storage.

In the work described here, sodalite $[Na_8(AlSiO_4)_6 \cdot Cl_2]$, a naturally occurring mineral, is proposed as a suitable material for long-term storage of radioiodines in a geologic repository. Sodalite, found in the nephelite-syenite, igneous, and other rocks, is sometimes formed as an alteration product of nephelite ($NaAlSiO_4$). Tomisaka and Eugster[5] studied the sodalites $[Na_8(AlSiO_4)_6X_2$, where X = Cl, Br, I, and OH] and found that iodide sodalite has a cubic unit cell of dimension $A_0 = 0.9014$ nm. They also *suggested that, while the naturally occurring mineral* has a cubic cell belonging to the space group I43m, the synthetic sodalites may have a polymorph with a primitive cell belonging to the space group P43m. They prepared their iodide sodalite from synthetic nepheline and NaI in sealed, inert metal capsules and crucibles and at pressures from 0.1 to 200 MPa. Chloride sodalite decomposed at temperatures greater than 1503°K. Barrer and Cole[6] reported that iodide sodalite may be heated to about 1120°K without destruction of the crystalline lattice.

Barrer et al.[7] reported on the preparation of chlorate sodalite $[Na_6(AlSiO_4)_6 \cdot 1.83NaClO_3 \cdot 0.68H_2O]$. This compound was stable up to about 920°K. Above this temperature, it decomposed to chloride sodalite by evolution of oxygen. A three-step reaction mechanism was proposed:

1. $2NaClO_3 \rightarrow NaClO_2 + NaClO_4$
2. $NaClO_2 \rightarrow NaCl + O_2$
3. $NaClO_4 \rightarrow NaClO_2 + O_2$

Neither the bromate nor the iodate analog was reported.

The sodalite aluminosilicate lattice consists of truncated octahedra which provide large "cages" in which to place ions or atoms. These large [illegible] entrance and exit of small atoms or ions such as Ar and Cl. However, large ions such as I [illegible] be trapped [illegible] made in a cage. Such properties suggest that [illegible] sodalite, may be suitable for the long-term storage of ^{129}I. Sodalite should be comparable with [illegible] basalts or shale. The large zeolite cages [illegible] also provide for storage of the radioactive product ^{129}Xe. After decay has taken place, the charge on the remaining sodium ion would be distributed over a number of other sodium atoms as shown by Barrer and Cole.[8] After sufficient time, a black, air-stable sodalite phase[5] might result. This phase upon exposure to water at 36[illegible]°K would eventually leach the free sodium leaving the sodalite lattice unchanged.[8] These considerations led us to study sodalite for the storage of ^{129}I.

EXPERIMENTAL

Two methods of preparation of the sodalite were used.

1. Clay Preparation. Kaolin clay (KCS Kaolin, Georgia Kaolin Co.) was mixed with 19M NaOH and solid NaI, $NaIO_3$, or KIO_3 in stoichiometric amounts in a polyethylene bottle. Sufficient water was added to make a thick paste and the mixture allowed to stand overnight at room temperature. The mixture was then dried at 380°K to a free-flowing powder.

2. Aluminosilicate Gel. Barrer and White[9] used gels of alumina and silica suspended in aqueous alkali and excess NaCl to prepare sodalite. In our work, homogeneous gels were prepared by dissolving $NaAlO_2$ and NaI, $NaIO_3$, or KIO_3 in a minimum amount of deionized water. Colloidal silica (Ludox AS-40) was added and the resulting solution heated while stirring until the mass gelled. The ratio of Ludox to $NaAlO_2$ was 1.83 : 1 by weight or 0.73 : 1 as $SiO_2 : NaAlO_2$. These gels were then dried overnight in an oven at 346°K. Sodium aluminate was chosen as the starting material since other salts of aluminum contain either anions which would compete for the same sites as iodine or nitrates that cause the release of I_2 gas upon heating. Similarly, use of organoaluminum compounds would result in reducing conditions when the organic fragments were burned during heating.

Consolidation

Both iodide and iodate sodalites were cold-pressed and fired at temperatures up to 1270°K without visible loss of iodine. Although no quantitative measurements of iodine loss were made, subliming I_2 would have been easily visible even in small quantities.

Both iodide and iodate sodalites were vacuum hot-pressed in 38.1 mm graphite dies. Consolidation of the sodalites occurred at 13.8 MPa and a die surface temperature of 1470°K. No method was available for measuring the temperature at the sample, but it is estimated that the [illegible]

Chemical Analysis

[illegible] HI. The resulting HI solution was treated with 1M HNO_3 and the iodine was extracted with [illegible] and then re-extracted into 0.02 M $NaHSO_3$. The iodine content was determined by X-ray fluorescence. Alternately, the iodine was determined in the toluene extract [illegible] UV spectrophotometer at [illegible]0 nm. Both X-ray and spectrophotometric techniques were used to determine the iodine in water leachates of the sodalite samples.

Leach Rate Measurements

Both Paige and Soxhlet leach tests were done according to well-established methods[10] on crushed and sieved samples.

RESULTS AND DISCUSSION

Crystal Structure

Results from powder X-ray diffraction scans of two hot-pressed samples are shown in Table 1. These data indicate that, at the high temperatures used to prepare these samples, iodate sodalite decomposes by loss of oxygen to form iodide sodalite.

Although the actual destruction mechanism for iodate sodalite was not investigated, it would not be surprising to find a mechanism similar to the decomposition of chlorate sodalite.[7] Only diffraction peaks for the sodalite phases are shown in Table 1. Table 2, however, lists the other peaks found in the diffraction scans of sodalites prepared either by cold-pressing and firing or by hot-pressing which did not match those reported by Tomisaka and Eugester.[5] The intensity of these lines seems to vary depending on processing conditions. Attempts to fit these lines to other phases such as nepheline, carnegieite, NaI, $NaIO_3$, albeit crystobalite, etc., failed. Tomisaka and Eugester[5] mentioned a similar phenomenon and have ascribed it to polymorphism in these sodalites. Both the observed and literature powder diffraction peaks in Table 1 were indexed assuming a unit cell belonging to the space group I43m, which requires that the sum of the Miller indices for each peak must be an even number (h + k + l = 2n).

In Table 2, the extra lines from the powder diffraction patterns were indexed according to the primitive cell P43m (h + k + l = 2n + 1). For the primitive cell, there is no restriction on the values of h, k, and l. There is excellent agreement (Table 2) between the calculated d spacings for the polymorph with A_0 = 0.9014 nm and the observed values. It appears, therefore, that the sodalites prepared in this study are polymorphs, possibly high-temperature

TABLE 1

Results from Powder X Ray Diffraction Scans of Sodalites*

Reflection			Iodide sodalite				Iodate sodalite	
			Tomisaka		This work		(this work)	
h	k	l	d, nm	I/I	d, nm	I/I	d, nm	I/I
1	1	0	0.6[illegible]	[illegible]	0.641	[illegible]		
2	0	0	0.45[illegible]	1[illegible]	0.452	22	0.452	9
2	1	1	0.36[illegible]	100	0.369	100	0.369	100
3	1	0	0.285[illegible]	2	0.288	2	0.289	3
2	2	2	0.260[illegible]	12	0.2608	10	0.260	10
3	2	1	0.2409[illegible]	53	0.2411	53	0.241	30
4	0	0	0.225[illegible]	10	0.2256	8	0.225	4
3 4	3 1	0 1	0.2125[illegible]	56	0.2126	32	0.213	33
4	2	0	0.201[illegible]	[illegible]	0.2016	4	0.202	4
4	2	2	0.18[illegible]	4	0.1841	3	0.185	3
4 5	3 1	1 0	0.1[illegible]66	4	0.1768	3		
5	2	1	0.164[illegible]	8	0.1646	8	0.164	5
4	4	0	0.15[illegible]4	[illegible]	0.159[illegible]	8	0.159	[illegible]
6 4	0 4	0 2	0.15[illegible]28	8	0.1504	6	0.150	6
6 5	1 3	1 2	0.14624	12	0.1464	12	0.146	
5	4	1	0.1[illegible]		0.1391	2		
6	2	2	0.13589		0.1359	3		
6	3	1	0.13290	0	0.1328	4		
4	4	4	0.13011		0.1302	3		
7	2	1	0.12266		0.1226	5		

*Sodalite lines only.

Calculated.

TABLE 2

Extra Diffraction Peaks for Iodide Sodalite

Observed peaks		Polymorph indexing			
d, nm	I/I	d, nm*	h	k	l
0.5009	4				
0.4084	23	0.4031	2	1	0
0.3191	6	0.3187	2	2	0
0.2670	5	0.2718	3	1	1
0.2499	2	0.2500	3	2	0
0.2354	5				
0.1923	5	0.1922	3	3	2
0.1665	2	0.1674	5	2	0
0.1620	2				

*Calculated on A_0 = 0.9014 nm.

forms. Annealing of samples at lower temperatures to verify this possibility has not yet been done. Only very weak diffraction peaks remain unindexed.

Chemical Analyses and Densities

Analyses of the solids for iodine indicate that theoretical amounts (22 mass %) of iodine can be incorporated.

TABLE 3

Iodine Contents and Densities of Hot Pressed Sodalites

Sample	Method of preparation	Iodine content,	Density, of theoretical
1	CBS NaI	12.[illegible] 20.4	96.[illegible] 91.5
2	CaI NaI	9.9	
3	CBS KIO_3	22.0 17.[illegible]	93.5 99.3

Table 3 shows the results of the iodine analyses. Two sample pellets were prepared for samples 1 and 3. Sample 3 gave the powder X ray diffraction pattern with the strongest polymorph lines. The fact that there is good agreement between calculated and observed diffraction maxima and that the sample has the maximum amount of iodine further supports the assignment of the polymorph structure of these samples.

Bulk densities of the hot pressed pellets were about 70%. However, densities of small pieces of the pellet (Table 3) were greater than 90% of theoretical density (2.613 Mg m^{-3}). Microcracking caused the bulk densities to be lower.

Leach Rates

It has been noted that the Soxhlet leach test is a good test of sample consolidation.[11] Table 4 lists the leach rates

TABLE 4

Leach Rate Data for Sodalites

Sample	Paige test, kg/(m² · d)*	Soxhlet test	
		Fraction I lost, %	Mass lost, %
1	4×10^{-4}	10	8.4
1a	1.5×10^{-4}	35.4	29.1
3	4.7×10^{-4}	42.4	34.7

*To convert from kg/(m² · d) to g/(cm² · d), divide by 10.

for the sodalite samples. Sample 1 was very well consolidated, and the Soxhlet leach rate was correspondingly low. Sample 1a was not uniform and did not appear to be fully consolidated at the pellet center. Sample 3 was initially an iodate sodalite. The release of O_2 during fabrication, while not destroying the unit cell structure, seemed to have an effect on the sintering of the crystal grains. Both Soxhlet and Paige leachates were analyzed for iodine. These data indicate that the iodine is very well immobilized in the sodalite lattice. In the case of sample 1, the relative amount of iodine lost during the Soxhlet test nearly equals the relative mass loss indicating that the iodine was leached at the same rate as the rest of the aluminosilicate lattice. There was insufficient amount of sample 2 from which to obtain a valid leach rate.

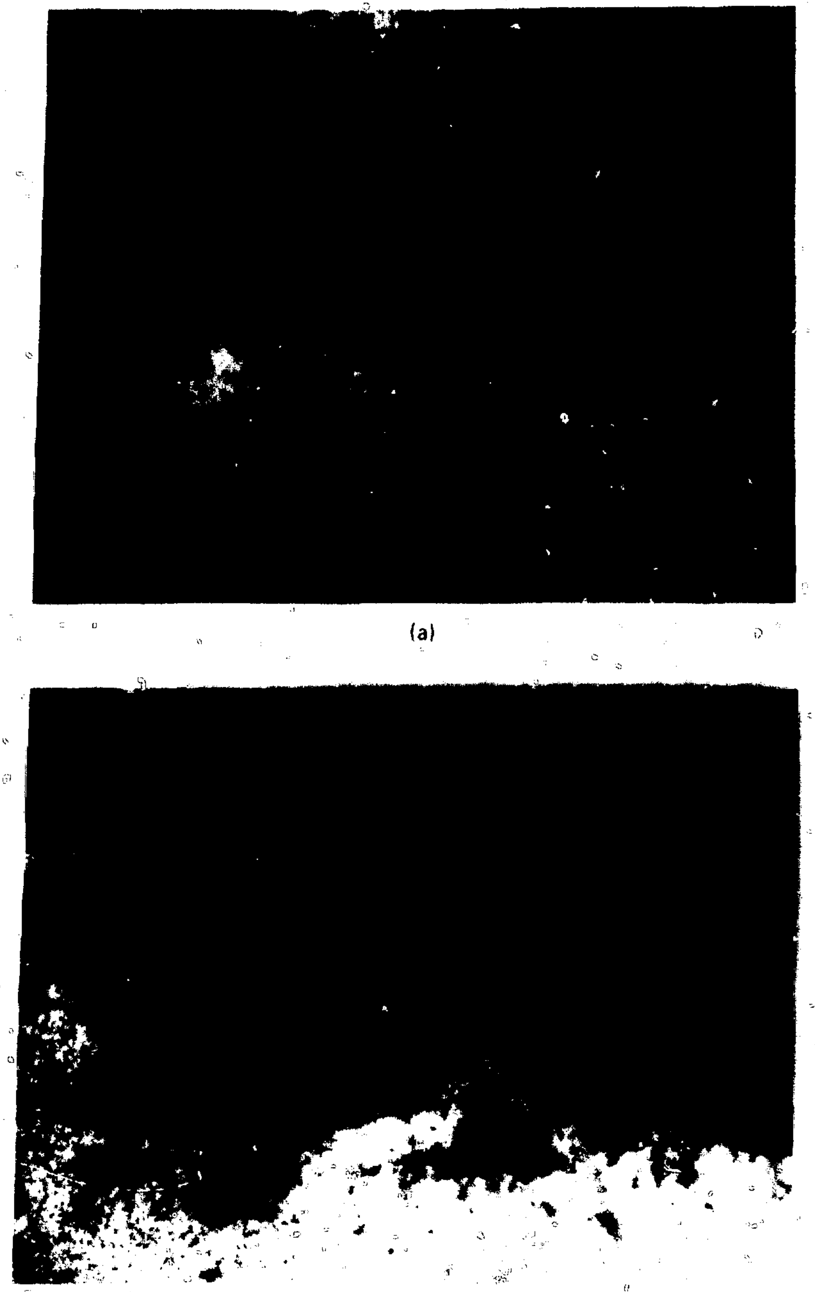
(a)

(b)

Fig. 1 Photomicrographs of the typical microstructures of Iodine Sodalite samples (1a, crossed Nicols, 1250 x) (1b, crossed Nicols, 250 x).

Microstructure

Figure 1(a) shows the microstructure of a typical hot-pressed iodide sodalite in the thin section under crossed Nicols. These samples are typically very fine grained. The grains are indistinguishable even after a brief etching with HF.

Inhomogeneous consolidation of sample 1a is evident from the photomicrograph [Figure 1(b)]. The portion of the sample shown at the bottom of Figure 1(b) was more porous and defied polishing. Microcracking mentioned earlier is clearly visible.

CONCLUSIONS

Initial studies indicate that the polymorph referred to by Tomisaka and Eugester^5 may be a high-temperature phase with a positive [illegible] PI [illegible] Leaching studies [illegible] bilized in a lattice [illegible] stability. [illegible] iodide [illegible] converts iodide [illegible] large [illegible] produced by [illegible] that iodide [illegible] the long-term [illegible] effort to [illegible] define the [illegible]

ACKNOWLEDGMENTS

Support [illegible] well Research [illegible] studies [illegible] contract [illegible]

REFERENCES

[illegible]

[illegible] *Proceedings* [illegible] 1974.

[illegible]

[illegible] *Nuclear Technology* [illegible]

[illegible]

[illegible] 1976 [illegible]

[illegible]

[illegible]

PROCESSES FOR IMMOBILIZATION OF HIGH-LEVEL SOLID WASTES BY GLASS AND CERAMIC MATRICES

K. H. LIN, W. L. CLARK, and W. B. HOWERTON
Chemical Technology Division, Oak Ridge National Laboratory,
Oak Ridge, Tennessee

ABSTRACT

Processes for the immobilization of waste SiC hulls and fissile particles from reprocessing of HTGR fuels are presented. Compressed cylinders of waste-matrix material were formed under pressures of ~35, 71, or 143 MPa and sintered at temperatures ranging from ~500 to 1025°C for ~1 hr. The cylinders containing 50% SiC–25% soft glass–25% red clay possess the most desirable properties (high mechanical strength, low surface area, and low leachability) of the several different compositions studied. Within the pressure and temperature ranges studied, the pressure of cylinder formation and the sintering temperature appear to have relatively minor effects on those properties except for the initial cesium leachability. Higher pressure and temperature would tend to reduce the initial leachability significantly.

INTRODUCTION

Silicon carbide hulls and waste fissile particles are among the high-level solid waste (HLSW) streams unique to HTGR fuel reprocessing.[1] The SiC hulls are the major portion of the residue discharged from the fissile particle dissolver. They contain small amounts of radionuclides (primarily fission products) that migrated out of the fuel kernel and interacted with the SiC layer during irradiation of fuel particles in the reactor. These radionuclides appear to have formed some stable compounds that resist leaching by HNO_3 and several other mineral acids.

The waste fissile particles result from the head-end processing of 25 W fuel elements[1] up to the secondary crushing step. The outer high-density graphite coating of these particles was removed in the primary burning, but the individual fuel kernels are still protected by two graphite layers and an SiC layer (outermost). Thus, in addition to small amounts of radionuclides in the SiC layer, the waste fissile particles also contain the entire spectrum of fission products and actinides formed during irradiation in the reactor.

The radioactivities of the SiC hulls and the waste fissile particles (both cooled for five years) are estimated at ~1000 Ci/liter and 5000 Ci/liter, respectively. Furthermore, since both types of wastes are fine solids (~80 μm and ~500 μm, respectively) and are readily dispersible, they must be immobilized in a suitable matrix to control and confine the radionuclides.

The objectives of the present experimental program are: (1) to evaluate potential matrix materials for immobilization, (2) to characterize different waste-matrix products, and (3) to identify potential problems relative to the immobilization of SiC hulls and waste fissile particles. The ultimate goal of the program is to generate sufficient technical data for the design of the larger-scale process and equipment. This paper presents the results of the bench-scale experimental study (cold laboratory development) using ^{134}Cs tracers and either nonradioactive SiC powders or SiC hulls from unirradiated fissile fuel particles. Those results are now being verified and refined through the hot-cell experiments based on SiC hulls recovered from actual spent fuel particles discharged from the Peach Bottom HTGR.

POTENTIAL IMMOBILIZATION MEDIA

The basic requirement in immobilization of the HLSW mentioned above is different from that of the soluble high-level liquid waste (HLLW) calcines. Since the radio-

TABLE 1

Characteristics of Clays Used in Immobilization of SiC Hulls

Characteristics	Clay type B	 R
Color	Buff	Indian Red
Size distribution, wt.%		
> 50 μ	8.8	7.0
50–20 μ	6.6	13.0
20–2 μ	38.4	51.0
< 2 μ	44.2	29.0
Total mineral constituents, wt.%		
Quartz	50.0	60.0
Feldspar	<5.0	5.0
Mica	<5.0	1.5
Glauconite		<5.0
Illite	10.0	20.0
Kaolinite	35.0	10.0
Vermiculite		<5.0
Chlorite		<5.0
Free Fe_2O_3	0.24	2.94

nuclides in HLSW are essentially nonleachable, the major requirement is to fix them in place by incorporating the wastes into a matrix material that is chemically and physically stable and does not interact with the wastes. The material should also exhibit a relatively low "melting point" or working temperature, since interactions between SiC hulls and the matrix would tend to become significant as the temperature increases. The high-level radioactivities of the SiC hulls and the waste fissile particles indicate that glass and ceramic would probably be the best materials to use for immobilization. Six different types of glasses were selected for the initial screening tests. Two types of commercially available clay were also used to investigate their effectiveness in retention of key radionuclides, such as cesium and strontium, and to serve as binder materials.

EXPERIMENTAL

Materials and Equipment

Important materials utilized included: (1) SiC powders (~45- and ~115-μm sizes) for the earlier scoping experiments, (2) SiC hulls recovered from unirradiated fissile particles, (3) cesium carbonate and ^{134}Cs tracer for cesium spiking of the SiC hulls, (4) chemicals (C.P.) for preparation of different formulations of glasses, and (5) two types of pottery clay (Buff and Indian Red), the approximate size distributions and mineral compositions of which are shown in Table 1.

Major pieces of equipment employed in immobilization experiments were: (1) a hydraulic press with 24,000-lb/in.^{2} load capacity and (2) a tube furnace with a temperature recorder–controller and the maximum temperature of 1200°C. Special dies for the hydraulic press made of hardened stainless steel 440 were designed to facilitate remote handling in the hot cell. The hydraulic press was used for preparation of the SiC-matrix cylinder samples.

Procedure for Scoping Study

The initial phase of the study used screening tests to select suitable matrix materials from six different types of glasses based mainly on their leachability and approximate melting point. Table 2 indicates the formulations of those glasses.

TABLE 2

Formulations of Glasses for Screening Tests to Select Matrix Material

Type No. or code	Formulations of glass batch (wt.%)
G1	SiO_2, 26.8; CaO, 5.6; PbO, 67.6
G5	SiO_2, 45; B_2O_3, 30; Na_2O, 25
G8	Al_2O_3, 7; P_2O_5, 52; Na_2O, 9; PbO, 32
G9	SiO_2, 54; Al_2O_3, 7.1; B_2O_3, 23.9; Na_2O, 15
G11	SiO_2, 3; Al_2O_3, 3; B_2O_3, 16; PbO, 61.9, ZnO, 10.1; BaO, 3; CuO, 3
K	Commercial soft glass (Kimble)

The chemical constituents for each batch were first blended thoroughly until a homogeneous mixture was obtained. The mixture was then transferred to a muffle furnace and was heated slowly until it was molten (or softened) sufficiently so that it could be poured easily. After the melt was cooled naturally to room temperature, the resulting glass was pulverized to the size range of −230, +325 mesh. One-gram samples of the individual batches were leached at ambient temperature for 65 hr in 20 ml of distilled water in separate sample containers which were tumbled, end over end, at 25 rpm. The result of the scoping study is presented in Table 3.

TABLE 3

Results of Screening Tests for Potential Matrix Materials for Immobilization of SiC Hulls

Type No. or code*	Wt.% loss†	Approximate melting point, (°C)
K	0.22	1000
G1	0.30	800
G11	0.88	600
G9	1.34	800
G8	10.5	700
G5	20.5	700

*See Table 2 for formulations of individual glass types.

†Weight loss of pulverized sample after leaching in distilled water for 65 hr at room temperature.

Methods for Immobilization of SiC Hulls

This phase of study was concerned with development of the immobilization technology for SiC hulls based on the selected matrix materials. Two methods of approach were employed in the study. In the first method, the SiC was mixed with the molten glass in a mold. This method was found to be unsatisfactory. All the experimental results presented in Tables 4 and 5 were based on the second method which consisted of (1) blending the powdered matrix material with the cesium-spiked SiC (50 : 50 by weight), (2) preparation of a cylindrical pellet (~2 cm in diameter by ~2 cm high) in a hydraulic press at a pressure of 35.4, 70.8 or 141.6 MPa (~5130, ~10270, or ~20530 psig), and (3) sintering the cylinder at appropriate temperatures (~500 to 1025°C) for ~1 hr. The cylinder was removed from the furnace immediately after sintering and allowed to cool in air at room temperature.

Methods for Characterization of SiC-Matrix Cylinders

The compressed and sintered cylindrical samples prepared by the preceding method under varying process conditions were evaluated for the following properties:

1. *Leachability (cesium)* was determined by a modified version of the IAEA method.[2] For earlier samples, all the external surfaces of the cylinder were exposed to leachant (water). Later samples had only the top cylindrical surface exposed to the leachant. Total leachability (as a percentage of the total weight loss) was also determined for earlier samples.

2. *Porosity* of each sample was determined by means of the mercury porosimeter with an estimated accuracy within ±3%.

3. *Surface area* of fragmented specimen was determined by the BET method.

4. *Compressive strength* of the sample was determined based on the data obtained by Forney compressive strength tester.

5. *Cesium analysis* was carried out by the single-channel gamma counter as well as by chemical analysis.

RESULTS AND DISCUSSION

Scoping Study

The result of screening tests to select suitable matrix materials for immobilization of SiC hulls appears in Table 3. It is arranged in increasing order of solubility in distilled water. The result indicates that Type G5 glass (high Na_2O borosilicate) was nearly 100 times more soluble than Type K (commercial soft glass), whereas Type G11 (solder glass) was approximately four times more soluble than that of Type K. The approximate melting point ranged from ~600°C for Type G11 to ~1000°C for Type K and did not appear to bear any direct relation to the solubility. Based on these data, Type K glass was selected for the immobilization study.

Immobilization Study

Mixing of the SiC with the molten soft glass in a mold resulted in a SiC-glass product of very high porosity. This was apparently caused by gases produced in the reaction between SiC and the glass constituents. The method was subsequently replaced by the second (three-step) method described in the Experimental section. In the initial study of the three-step method, SiC matrix cylinders containing 50% SiC and different proportions of glass to clay (as matrix material) were evaluated. This led to selection of the composition consisting of 50% SiC 25% soft glass and 25% red clay for further study by comparing it with other compositions, as illustrated in Table 4. Type P glass, which was not tested in the scoping study, is the low melting point (~600°C) lithium zinc phosphate glass with the formulation adapted from Tindyala and Ott[3] (in mole %): Al_2O_3, 5.5; Li_2O, 30; P_2O_5, 40; ZnO, 19.5; PbO, 5.0. The data in Table 4 indicate that the waste SiC-matrix cylinder with the composition of sample No. C-2 has the most desirable characteristics of the four compositions, based on the compressive strength, porosity, and leachability. Table 5 illustrates the results of a more comprehensive investigation of the effects of the immobilization matrix composition, the pressure of cylinder formation, and the sintering temperature on the characteristics of SiC-matrix cylindrical samples.

Immobilization Matrix Composition. As demonstrated in Table 5, so far as the cesium leachability is concerned, the buff (Type B) clay alone (samples H-1 and -2) is just as good an immobilization matrix as the mixture of the clay with Type P glass (samples H-5 and -6). Addition of Type P glass to clay, however, reduced both the porosity and BET surface area considerably. The effect on the compressive strength was not clear based on the data shown. The cesium leachability with the red (Type R) clay matrix was even lower (more than one order of magnitude lower) than that with the buff clay. Type K (soft) glass had a beneficial effect in reducing the cesium leachability when added to either type of clay (samples H-3, -25, -26, and -27). It also drastically reduced the BET surface area and increased the compressive strength of the resulting SiC-matrix cylinders. According to Table 5, variations in the cesium leachability and the BET surface area are more dramatic than changes in either the porosity or the compressive strength. Nevertheless, these variables do not appear to be related by any simple correlation.

Pressure of SiC-Matrix Cylinder Formation. Doubling of pressure from 35.4 MPa to 70.8 MPa (H-25 versus H-26) decreased the initial cesium leachability by an order of magnitude, but no significant difference in leachability could be detected afterward. Only minor effects were observed on other properties listed in Table 5. A further increase in the pressure from 70.8 MPa to 141.6 MPa (H-26

TABLE 4

Selected Characteristics of Waste SiC-Matrix Cylinders of Various Compositions

Sample No.	Composition of matrix,* wt.% Clay	Composition of matrix,* wt.% Glass (type)	Porosity, vol. %	Compressive strength, MPa	Total wt. loss,† %	Incremental Cs leach rate, (frac. cm/day)‡ Initial	Incremental Cs leach rate, (frac. cm/day)‡ Final
C-1	50	0	24.4	37.5	0.21	0.01	5(−4)
C-2	25	25 (K)	22.3	69.4	0.15	0.001	~4(−4)
C-3	0	50 (P)	23.8	32.6	5.01	0.02	0.002
C-4	0	50 (K)	Considerable expansion in volume due to SiC-glass reaction				

*Buff clay was used. Type K, commercial soft glass (Kimble). Type P, low-melting point phosphate glass; cylinder formation pressure was 70.8 MPa for all samples; sintering temperature was ~800°C for C-1, C-2, and C-4 and ~500°C for C-3.

†After 10 days of leaching and drying at 200°C for 24 hr.

‡Initial, rate for first day; final, rate for fourth day; numbers in parentheses represent power of ten. All external surfaces of the cylindrical sample were exposed to leachant (water).

TABLE 5

Characteristics of Waste SiC-Matrix Cylinder Formed Under Different Process Conditions

Sample No.*	Composition of matrix,† wt.% Clay (type)	Composition of matrix,† wt.% Glass (type)	Cylinder formation pressure, MPa	Porosity, vol. %	BET surface area, m²/g	Compressive strength, MPa	Incremental Cs leach rate (frac. cm/day)‡ Initial	Incremental Cs leach rate (frac. cm/day)‡ Final
H-1	50(B)	0	141.6	21.2	9.4	31.2	2.4(−3)	5.8(−4)
H-2	50(B)	0	141.6	19.1	9.9	39.0	2.2(−3)	5.2(−4)
H-3	25(B)	25(K)	141.6	23.1	1.3	47.6	~0	1.0(−4)
H-5	25(B)	25(P)	141.6	16.2	1.0	57.0	2.0(−3)	5.8(−4)
H-6	25(B)	25(P)	141.6	15.0	1.1	35.9	2.3(−3)	6.8(−4)
H-7	50(R)	0	141.6	23.4	7.1	33.6	1.6(−4)	~0
H-8	50(R)	0	141.6	21.6	6.8	32.8	~0	4.4(−5)
H-25	25(R)	25(K)	35.4	29.3	0.50	89.0	4.0(−4)	~0
H-26	25(R)	25(K)	70.8	27.1	0.48	93.7	5.7(−5)	~0
H-27	25(R)	25(K)	141.6	27.6	0.51	70.3	8.2(−5)	~0

*Sintering temperature was 1025°C for all samples except H-25, -26, and -27 (800°C).

†Based on the total weight of waste SiC + matrix; the balance (50%) was always waste SiC. Type B, buff clay; Type R, Indian red clay (see Table 1); Type K, commercial soft glass (Kimble), Type P, low-melting point phosphate glass.

‡Initial, rate for first day; final, rate for 14th day; numbers in parentheses represent power of ten; only the top surface of the cylindrical sample was exposed to the leachant (water). The rate of ~0 implies < 1 × 10^{-5}, the limit of detection.

versus H-27) did not exert any appreciable influence on the characteristics of the SiC-matrix cylinders. A drop in the compressive strength of ~20% was unexpected, but the reasons for this behavior have not yet been determined.

Sintering Temperature. No systematic study was carried out to investigate the effect of the sintering temperature. However, assuming that the effect of the pressure (70.8 MPa versus 141.6 MPa) of cylinder formation may be ignored (based on the preceding discussion on samples H-26 and H-27), the temperature effect could be examined by comparing samples C-1 with H-1 and H-2, and C-2 with H-3. The sintering temperature for both C-1 and C-2 was ~800°C, whereas that for H-1, H-2, and H-3 was 1025°C. A study of the data in Tables 4 and 5 indicates that the higher temperature (1025°C) dramatically reduces the initial cesium leachability. Using clay as the matrix, there seems to be a slight drop in the porosity with an increase in temperature (C-1 versus H-1 and H-2), but the compressive strength was almost unaffected. In the case of the clay–soft-glass matrix (C-2 versus H-3), the porosity was practically unchanged. Reduction in the compressive strength (from 69.4 MPa to 47.6 MPa) at a higher temperature was observed, but it is uncertain that this behavior was caused by the sintering temperature alone.

CONCLUSIONS

The waste SiC hulls (and probably waste fissile particles also) could be immobilized by (a) blending with the powdered matrix material, (b) forming a cylindrical compact by means of a hydraulic press operating at a pressure of ~70 MPa to ~140 MPa, and (c) sintering the resulting compact at ~800°C for ~1 hr.

The SiC-matrix cylinder consisting of 50 wt.% SiC–25 wt.% soft glass–25 wt.% red clay has the most desirable properties (low leachability, low pore surface area, and high mechanical strength). The two types of clay used in the present study appear to be an effective matrix for immobilization of the SiC hulls. They could be utilized without the addition of the glass, but the mechanical strength of the resulting cylinder would be appreciably lower.

The pressure required to form the cylindrical compact of SiC matrix exerts minor effects on the properties of the resulting product in the range of ~35 MPa to ~140 MPa. The higher sintering temperature (i.e., ~1000°C versus ~800°C) seems to reduce the initial cesium leachability remarkably. The temperature effect on other properties was relatively minor between 800 and 1000°C.

ACKNOWLEDGMENT

This work was sponsored by the Nuclear Power Development Division, U. S. Department of Energy under contract W-7405-eng-26 with the Union Carbide Corporation.

REFERENCES

1. K. H. Lin, Radioactive Wastes from Reprocessing of HTGR Fuel --An Overview, *Trans. Am. Nucl. Soc.*, 24: 238 (1976).
2. E. D. Hespe, *At. Energy Rev.*, 9(1): 195 (1971).
3. M. A. Tindyala and W. R. Ott, *Ceramic Bulletin*, 57(4): 432 (1978).

INCORPORATION OF PRECIPITATE FROM TREATMENT OF MEDIUM-LEVEL LIQUID RADIOACTIVE WASTE INTO GLASS MATRIX OR CERAMICS TOGETHER WITH HIGH-LEVEL LIQUID WASTE

M. HUSSAIN* and L. KAHL
Kernforschungszentrum Karlsruhe GmbH, 7500 Karlsruhe, Federal Republic of Germany, and *Pakistan Atomic Energy Commission

ABSTRACT

"MAW-splitting," i.e., precipitation and separation of the radioactive matter from the bulk liquid, has been developed at Kernforschungszentrum Karlsruhe (KfK) as an alternative to direct solidification of MLLW-concentrates by bituminization or cementation. More than 90% of the total radioactivity is removed from MLLW stream by absorbing it on surface rich precipitate, which is ultimately vitrified with HLLW. An addition of MLLW-precipitate to a matrix (glass or glass-ceramic), to which HLLW has already been incorporated, showed no significant decrease in product quality or increase in product amount.

INTRODUCTION

About 1500 m^3 of medium-level-liquid-radioactive-waste-concentrate (MLLW-c) is expected from the future German reprocessing facilities (1500 tons per year LWR fuel), which will be solidified by mixing with cement or hot bitumen in 200 liter drums. For ultimate disposal, these drums will be kept in a salt formation. Annual production of such drums will be about 16,000 with cement (50 Ci/drum) or 4000 with bitumen (200 Ci/drum). Plutonium content will range from 2.5 g to 10 g per drum. Due to radioactivity, the drums will be put in "lost concrete containers" during transportation to the final storage and shall cause an additional cost of $500 per drum and total of $7.5 million per year. Besides higher cost of disposal, limitations such as disintegration of cement blocks caused by radiolysis of water of crystallization or enhancement of heat production due to higher plutonium contents in bitumen resulting in softening of bitumen product and production of gas cannot be ignored.

One can overcome the uncertainties in solidification of MLLW mentioned above if the fission products and actinides from MLLW-c are separated and fixed in a matrix (glass or glass-ceramic) as HLLW. This can be achieved as follows:

1. Evaporation of MLLW-c followed by mixing the solid produced with glass-formers and then melting.
2. Separation of fission products and actinides from MLLW-c and melting them with glass-formers.
3. Separation of fission products and actinides from MLLW-c and melting them together with HLLW and glass-formers.

MAW-SPLITTING

Since 1975, the process "MAW-splitting" has been under development at KfK. By this process more than 90% of the fission products and actinides from MLLW-c are removed by absorbing them on surface rich reagents in the form of precipitate.[1] The precipitate is separated by filtration and the filtrate which is about 80 to 90% of the total volume is treated as low active waste. The filtrate contains 80 to 90% of dissolved inactive salts, mainly $NaNO_3$. The resulting precipitate, after drying, is vitrified by the methods (No. 2 or 3) as mentioned previously.[1-3]

The method for separation of fission products and actinides from simulated MLLW-c is shown in Table 1. Except for $^{134,137}Cs$, the other fission products are absorbed on surface rich hydroxides and oxyhydrates and are coprecipitated. Cesium is attached with $K_4[Fe(CN)_6]$. Actinides are precipitated in an alkaline medium as oxyhydrates.

TABLE 1

Precipitation of Simulated MLLW

Precipitation agent	Amount, g/liter	pH value after dosage
$Al(NO_3)_3 \cdot 9H_2O$	7.0 (Ce, Zr, Nb)	1–2
$SnCl_2$	1.5 (Ru)	
NaOH		Up to 3.5
$TiCl_3$ in HCl	1.0 (Sr)	
NaOH		Up to 4.0
$K_4[Fe(CN)_6] \cdot 3H_2O$	0.5 (Cs)	
NaOH		Up to 7.0
Water glass	16.0 (Sr)	
NaOH		Up to 9.5

Tracer	Df*
^{85}Sr	190
^{95}Zr	1000
^{95}Nb	1000
^{106}Ru	190
^{137}Cs	250
^{144}Ce	1000

*$NaNO_3$ concentration up to 350 g/liter has no influence on Df. Higher concentration decreases the Df.

The chemical composition of the precipitate is given in Table 2. Treatment of one liter MLLW-c produces about 14 to 16 g of precipitate in oxide form. Some of the components present in the precipitate such as SiO_2, TiO_2, Al_2O_3, and Na_2O are also present in the basic glass and glass-ceramic matrices selected for vitrification. Hence the respective amounts of these constituents are reduced from the basic matrix. The precipitate so obtained from the treatment of 10 liter MLLW-c is incorporated in one kg glass or glass-ceramics with HLLW and constitutes only 3 to 4 wt.% of the product. In this work, the precipitate has been vitrified together with HLLW. The objective of the work is to evaluate vitrified products (glass and glass-ceramics) with HLLW and MLLW and to compare them with products obtained only with HLLW and to confirm whether the addition of precipitate is adequate or whether the product becomes less stable. It was seen that addition of the precipitate increased the activity of the HLLW-glass or glass-ceramics only 1% but did not increase the product amount. The vitrification of MLLW-precipitate only will produce about 12 to 16 m^3/yr glass or glass-ceramic product.

SELECTION AND PREPARATION OF A BOROSILICATE GLASS AND GLASS-CERAMIC MATRIX

VG 98/1, a borosilicate glass matrix, and VC 15, a borosilicate glass-ceramic matrix, are the two matrices being investigated in the pilot vitrification facility at KfK for vitrification of HLLW and were taken as basic matrices for the present work. The compositions of these matrices are shown in Tables 3 and 4.

TABLE 2

The Chemical Composition of Precipitate from Treatment of One Liter Simulated MLLW* (As Oxides)

Component	g	wt.%	Component	g	wt.%
SiO_2	4.45	30.48	Cr_2O_3	0.03	0.21
Al_2O_3	0.94	6.44	NiO	0.01	0.07
TiO_2	0.51	3.49	U_3O_8	1.18	8.08
SnO_2	1.19	8.15	CuO	0.05	0.34
Na_2O	4.43	30.34	MnO	0.02	0.14
K_2O	0.30	2.05	PbO	0.09	0.62
CaO	0.28	1.92	ZnO	0.07	0.48
MgO	0.33	2.26	Ru-Ox	0.09	0.62
Fe_2O_3	0.32	2.19	FP-Ox	0.30	2.05

*Total weight = 14.6. The weight may differ with the water content of MLLW precipitate.

During leaching experiments, it was observed that the glass product VG 98/1 with HLLW and MLLW had better leach resistance compared to products with and without HLLW (Fig. 1). It was thought that this is due to the presence of MgO in the precipitate which was confirmed by experiments. This is why borosilicate glass matrix VG 98/3 also contains MgO. A series of three glass matrices also contains Gd_2O_3, an expected neutron poison in the dissolution step of reprocessing.

Simulated HLLW and simulated dried MLLW-c precipitate are thoroughly mixed with frit (glass or glass-ceramic) and heated at 800°C for degasification and then melted at 1200°C for 3 to 4 hr to produce a bubble free melt.[4] The melt is poured into graphite molds, kept at 600°C for two hr, and then cooled to room temperature by switching off the furnace. The glass-ceramic product is kept at 430°C for 24 hr and then at 630°C for 72 hr for complete recrystallization.[5]

PROPERTIES INVESTIGATED

The products with HLLW and HLLW–MLLW-precipitate were investigated for the following properties for comparison purposes. These investigations were selected since they are important from the process development and disposal viewpoint.

1. Viscosity of the melt at 1150°C (melting range 1100 to 1200°C)
2. Volatility of fission products and glass components from the melt
3. Formation of yellow phase
4. Recrystallization tendency (after 360 hr at 800°C) of borosilicate glass products
5. Impact resistance
6. Thermal conductivity at 167°C

TABLE 3

The Chemical Composition (wt.%) of Glass-Ceramic Products

Component	VC 15 (HLLW)	VC 15 (HLLW + MLLW)	VC 15 G (HLLW)	VC 15 G (HLLW + MLLW)
SiO_2	40.000	38.16	35.00	33.16
TiO_2	4.00	3.82	3.50	3.32
Al_2O_3	8.00	7.63	7.00	6.63
B_2O_3	4.00	3.82	3.50	3.32
MgO	4.00	3.82	3.50	3.32
CaO	4.00	3.82	3.50	3.32
Na_2O	4.00	3.82	3.50	3.32
Li_2O	8.00	7.63	7.00	6.63
K_2O	4.00	3.82	3.50	3.32
Gd_2O_3			10.00	10.00
HLLW-Ox	20.00	20.00	20.00	20.00
MLLW-precipitate-Ox		3.68		3.68

TABLE 4

The Chemical Composition of Borosilicate Glasses

	VG 98/1 G						VG 98/2						VG 98/2 G					
	Basic		HAW		HAW + PPT*		Basic		HAW		HAW + PPT*		Basic		HAW		HAW + PPT*	
Component	wt.%	mole%	wt.%	mole%	wt.%	mole%	wt.%	mole%	wt.%	mole%	wt.%	mole%	wt.%	mole%	wt.%	mole%	wt.%	mole%
SiO_2	45.30	51.65	36.30	47.41	36.00	48.19	52.00	53.70	41.60	49.23	40.06	48.72	46.80	52.35	36.44	42.96	35.09	46.39
TiO_2	3.80	3.26	3.00	2.95	3.00	3.02	4.40	3.70	3.52	2.86	3.39	3.09	3.90	3.36	3.12	3.13	3.00	2.97
Al_2O_3	1.30	0.88	1.00	0.77	1.00	0.79	1.40	0.62	1.12	0.71	1.08	0.77	1.20	0.67	0.96	0.78	0.92	0.72
B_2O_3	12.20	11.98	9.80	11.05	9.00	10.40	12.80	11.11	10.24	10.71	9.86	10.27	11.50	11.41	9.20	0.16	8.86	10.03
CaO	2.50	3.05	2.00	2.79	2.00	2.87	2.90	3.09	2.32	2.88	2.23	2.91	2.60	3.36	2.08	3.13	2.00	2.83
Na_2O	24.70	27.26	19.70	24.94	17.20	22.58	24.50	24.69	19.60	22.87	18.87	22.21	22.00	23.49	17.60	21.88	16.95	21.68
Gd_2O_3	10.20	1.92	10.20	2.20	10.20	2.26							10.00	2.00	10.00	2.34	9.63	2.29
MgO					0.33	0.66	2.00	3.09	1.60	2.86	1.54	2.81	2.00	3.36	1.60	3.13	1.54	3.05
HAW-oxide			18.00	7.89	18.00	7.93			20.00	7.88	19.27	8.02			20.00	8.59	19.27	8.73
MAW-precipitate-oxide					3.37	1.30					3.70	1.20					3.70	1.30

*PPT = precipitate.

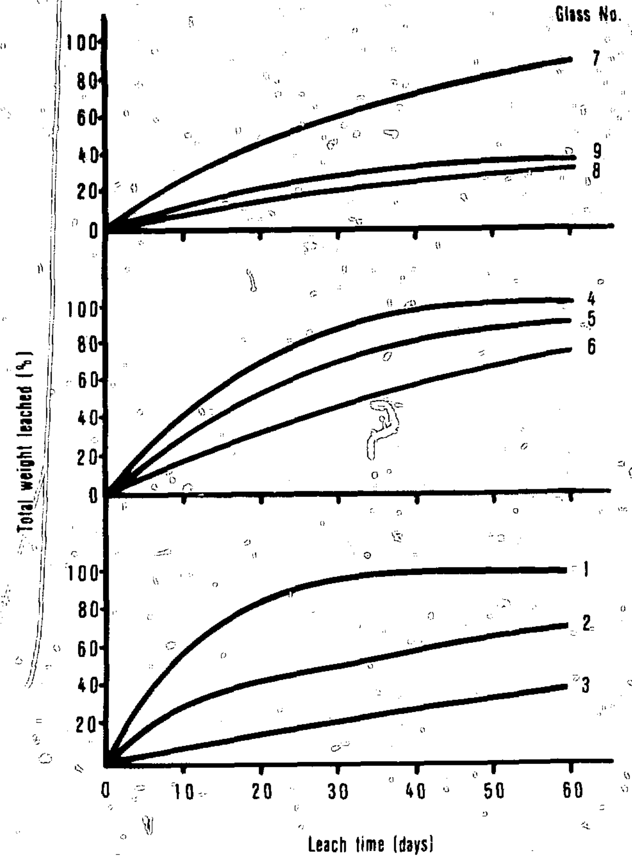

Fig. 1 Weight loss by leaching of borosilicate glass matrices in Soxhlet at 80°C.

7. Leaching behavior of glass (w.r.t. weight and radioactivity in Soxhlet at 80°C and using the IAEA recommended method at room temperature)

8. Leaching behavior of glass-ceramics against water, saturated NaCl solution, and carnallite at boiling and at room temperature

RESULTS AND DISCUSSION

The results obtained appear in Table 5.

1. *Viscosity.* The presence of MgO in borosilicate glass products increases the viscosity. All the matrices have a viscosity at 1150°C < 100 poise and hence cause no problem in the pouring of glass in containers. In the case of glass-ceramics, the addition of MLLW has no remarkable effect. An addition of Gd_2O_3 also has shown an increase in viscosity.

2. *Volatility of fission products.* Volatility was measured by chemical analysis. Ruthenium volatility was not measured. Addition of precipitate showed no significant effect on volatility except 60% volatility of cesium has been observed for the glass and glass-ceramic matrices, due to formation of CsCl. The chloride was present in the precipitate as a precipitating agent. Due to this disadvantage, a precipitation method without chloride is under development. The volatility of some of the components is (average values) B_2O_3 9.5%, Na_2O 1.5%, CaO 10.5%, Cs_2O 10 to 13% (in the absence of Cl^-).

3. *Formation and suppression of yellow phase.* A light, water soluble yellow phase of molybdate and chromate was observed at the surface of glass products. The formation of this phase has been minimized by the addition of 1 to 2% Si. For glass-ceramics it was not remarkable.

4. *Tendency towards devitrification.* Except for glass products 8 and 9, the others had very little or no tendency towards devitrification. Glass product 8 was partially devitrified while 9 was fully devitrified due to the presence of MgO and Gd_2O_3 in the matrix.

5. *Impact resistance.* A test as described by Wallace and Kelley[6] was used only for comparison, although the reproducibility of results is not good.

6. *Thermal conductivity at 167°C.* No significant effect of addition of MLLW-precipitate on thermal conductivity has been observed for glass matrices. In the case of glass-ceramics the effect is irregular.

7. *Leach resistance.* Leach tests for glass products 1–3 indicated better results for products with MLLW-precipitate as compared to others (Fig. 1) due to the presence of MgO in the precipitate and were the basis for use of MgO in other glass matrices with and without Gd_2O_3. Products 8 and 9 with Gd_2O_3 also showed higher leach resistance indicating an increase in hydrolytic resistance of glass products by the addition of Gd_2O_3.

8. *Leach resistance of glass-ceramic products.* Leach resistance of these products against water is lower than against the NaCl solution and carnallite at boiling temperature as indicated in Table 5. Leach resistance of products with HLLW and those with HLLW and MLLW-precipitate is not remarkably different.

CONCLUSIONS

The comparison of products (glass and glass-ceramic) containing HLLW and those containing HLLW and MLLW-precipitate indicates that the addition of precipitate is quite adequate and even improves some properties. The presence of Gd_2O_3 enhances hydrolytic stability, but also increases the tendency towards devitrification. The positive effect of MgO favors its addition of 1 to 2 wt.% in matrices.

ACKNOWLEDGMENT

The authors wish to acknowledge the assistance of Mr. M. Grosse in performing various experiments.

TABLE 5

Results of Properties Investigated

Property	Borosilicate glass matrices and products									Glass-ceramic products			
	1	2	3	4	5	6	7	8	9	1	2	3	4
Density (g cm^{-3})	2.70	3.00	3.01	2.52	2.74	2.78	2.71	3.04	3.03	2.86	3.00	3.09	2.99
Viscosity at 1150°C (poise)	31	37	37	76	56	54	125	55	40	190	255	160	135
Devitrification tendency	No	No	No	No	No	No	No	Partial	Strong				
Impact resistance (cm^2 J^{-1})	6.96	8.78	13.24	5.53	5.97	11.60	5.63	6.61	13.40	4.61	5.07	6.43	12.6
Leach rate (kg m^{-2} s^{-1}).													
Soxhlet, 80°C, 44 days													
Total	2.7×10^{-7}	1.5×10^{-8}	8.6×10^{-9}	1.6×10^{-8}	6.5×10^{-9}	1.4×10^{-9}	2.2×10^{-8}	1.8×10^{-8}	9.0×10^{-9}				
Na	8.7×10^{-8}	6.2×10^{-8}	8.7×10^{-9}	3.5×10^{-8}	1.2×10^{-8}	9.0×10^{-9}	1.2×10^{-8}	5.4×10^{-9}	6.7×10^{-9}				
Cs	6.2×10^{-8}	5.4×10^{-8}	9.2×10^{-9}	5.2×10^{-8}	3.8×10^{-8}	3.1×10^{-9}	8.0×10^{-9}	5.0×10^{-9}	6.5×10^{-9}				
Sr	7.3×10^{-8}	4.0×10^{-8}	2.0×10^{-8}	6.3×10^{-8}	4.0×10^{-8}	5.0×10^{-8}	1.1×10^{-8}	6.2×10^{-9}	2.0×10^{-9}				
Ru	3.5×10^{-8}	3.9×10^{-8}	8.6×10^{-9}	8.9×10^{-9}	6.3×10^{-9}	6.2×10^{-9}	3.5×10^{-9}	1.1×10^{-9}	1.8×10^{-9}				
Ce	2.5×10^{-8}	2.4×10^{-8}	6.4×10^{-8}	7.8×10^{-9}	5.0×10^{-9}	4.3×10^{-9}	7.0×10^{-9}	1.5×10^{-9}	1.1×10^{-9}				
IAEA, 25°C, 41 days (total)	8.3×10^{-11}	1.8×10^{-11}	7.3×10^{-12}	4.2×10^{-11}	1.2×10^{-11}	6.3×10^{-12}	3.9×10^{-11}	9.0×10^{-11}	4.7×10^{-12}				
Water, 7 days (total)													
100°C										1.8×10^{-7}	2.5×10^{-7}	8.4×10^{-8}	3.0×10^{-9}
25°C										3.0×10^{-10}	9.9×10^{-9}	8.9×10^{-9}	
316.5 g NaCl/liter brine, 7 days (total)													
107°C										6.9×10^{-9}	3.5×10^{-8}	2.4×10^{-8}	4.2×10^{-10}
25°C										5.3×10^{-10}	1.1×10^{-9}	1.0×10^{-10}	2.1×10^{-10}
Carnallite solution, saturated, 7 days (total)													
118°C										4.6×10^{-10}	2.7×10^{-9}	1.6×10^{-9}	6.3×10^{-10}
25°C										5.5×10^{-10}	8.0×10^{-10}	1.3×10^{-9}	9.8×10^{-9}

REFERENCES

1. L. Kahl and M. Kelm, *Fixing MAW in an Inorganic Matrix*, KfK-Report 2615, p. 216 (1978).
2. W. Bahr, W. Hild, S. Drobnik, L. Kahl, M. Kelm, W. Kluger, and H. Krause, Recent Experiments on the Treatment of MLW and Spent Solvent and on Fixation into Bitumen, in *IAEA-NEA Symposium on the Management of Radioactive Wastes from the Nuclear Fuel Cycle*, Vienna, p. 133, March 1976.
3. L. Kahl, M. Kelm, and S. Kunze, *Separation and Fixation of the Radioactive Material from Medium Activity Waste Water*, Reaktortagung des Deutschen Atomforums 1978, Hannover, p. 480, April 1978.
4. R. Gasteiger, *Waste [illegible] LWR Fuel Cycle Data Base for Design of a Reprocessing Plant*, KfK-Report 2[illegible] (1976).
5. W. Guber, S. Saidl, P. Dejonghe, and W. Hild, *Thermally Chemically Stable Products for Permanent Storage and Disposal of Highly Radioactive Liquid Wastes*, U.S. Patent No. 4,097,401, June 27, 1978.
6. R. M. Wallace and J. A. Kelley, *[illegible] Waste Forms*, Savannah River Laboratory Report DP-1400, 1975.

CHARACTERISTICS OF STORED HIGH-LEVEL ICPP WASTE CALCINE

B. A. STAPLES, G. S. POMIAK, and E. L. WADE
Allied Chemical Corporation, Idaho Falls, Idaho

ABSTRACT

[illegible]

INTRODUCTION

Spent nuclear fuel is reprocessed at the Idaho Chemical Processing Plant (ICPP) to recover uranium for reuse in fuel fabrication. Highly radioactive waste containing fission products is generated during reprocessing. Since 1963 these liquid wastes have been routinely solidified by a fluidized-bed calcination process in the Waste Calcination Facility (WCF).[1] In this process liquid waste is sprayed by gravity feed directly into the fluidized bed. Originally, heat was supplied to the system indirectly by circulating liquid NaK in pipes through the bed, but since 1971 an in-bed combustion technique has been used in which kerosene is burned in the presence of oxygen.[2] For startup, fission products from the aqueous waste are coated onto a fluidized-bed start-up material. After start-up, the waste forms its own particles. Off-gases are scrubbed in a special cleanup system to remove and recycle all radioactive materials prior to release of the off-gas to the atmosphere. The calcination process results in an eightfold reduction in waste volume, but, most important, it produces a solid waste form which is much safer than the liquid for long-term storage. The process has been successfully applied to the solidification of wastes from the reprocessing of many different types of fuel.

CALCINE SAMPLING

Regulatory criteria may require calcined wastes presently being stored at ICPP to be converted to a less dispersible and more leach-resistant form. Alternative waste forms are being developed should this be necessary.[3,4] Presently, calcined wastes would have to be retrieved if an alternate waste treatment process were necessary.

As part of a solid waste retrieval program, a bin sampling project was performed to determine if the chemical and physical states of calcine stored for 10 to 12 years at ICPP would permit use of a pneumatic removal process. The sampling process basically consisted of driving a string of 28 split-tube samplers into a calcine storage bin using a drill rig and withdrawing the tubes one at a time into a shielded storage cask located directly over the bin.[5] In this manner a bin containing calcined aluminum-clad fuel wastes (alumina calcine) and a bin containing calcined zirconium-clad fuel wastes (zirconia calcine) were sampled. Both sampled bins contained calcine produced by the indirect heating method. The storage casks were removed to a hot cell, and the calcine was removed for analysis. Contents of the samplers were combined to give three composites from each bin. Samples from the alumina calcine bin were designated 3T, 3M, and 3B representing top, middle, and bottom of the bin. Likewise, samples from the zirconia calcine bin were designated 7T, 7M, and 7B.

After combining and mixing, each sample composite was aliquotted through a six-stage splitter.[6] The aliquot obtained, $\frac{1}{64}$ of the original sample, was used for all chemical analyses and all physical analyses except attrition indices, compressibility tests, sieve analyses, shear tests, and wall friction angle tests. These latter tests, performed in the hot cell, required large amounts of material and thus were

TABLE 1

Major Constituents of Retrieved Calcine, Wt.%

Alumina				Zirconia				
Sample	Al	Na	NO_3	Sample	Al	Ca	Zr	F
3T	35.5	3.1	6.0	7T	7.5	25.5	16.9	20.1
3M	35.9	2.0	5.1	7M	7.6	29.1	17.5	20.3
3B	39.8	1.6	4.7	7B	7.6	27.9	17.7	21.1
WCF run, #1 product	40–48	0.9–1.5	2.0	WCF run, #4 product	7.6–9.9	30–36	16–17	8–23

TABLE 2

Minor Constituents of Retrieved Calcine, Wt.%

Alumina

Sample	B	Cu	Fe	Hg	K	Mn	Total rare earths	Total Ru	Zr
3T	0.2	0.9	2.0	1.6	0.5	0.5	0.5	0.04	0.5
3M	0.2	1.1	2.0	1.8	0.5	0.5	0.5	0.04	0.5
3B	0.2	3.5	2.0	1.9	0.5	0.5	0.5	0.04	0.5

Zirconia

Sample	B	Mg	K	Mn	Na	NO_3	Total rare earths	Total Ru
7T	0.60	0.05	0.10	0.05	0.7	1.03	0.5	0.05
7M	0.63	0.02	0.06	0.05	0.5	0.71	0.5	0.04
7B	0.65	0.04	0.08	0.05	0.5	2.88	0.5	0.05
WCF run, #4 product						0.28–11.8		

done on sample composite material less than 106 mm after aliquotting. All chemical tests were done in the analytical laboratories at ICPP. Differential thermal analyses (DTA) and thermal gravimetric analyses (TGA) were done by Rockwell Hanford Company at Richland, Washington.

CHEMICAL PROPERTIES OF RETRIEVED CALCINE

The chemical species determined on the retrieved sample composites are given in Tables 1 through 3. Where possible, comparative results on radioactive samples taken from the WCF at the time of calcine production are included in the tables. In most cases the ranges of values determined for the major constituents of retrieved zirconia samples are similar to those determined for WCF zirconia product. There is some variation in ranges of values determined for major constituents in retrieved alumina and those for WCF alumina product.

Very little information exists on the minor constituents of either alumina or zirconia calcine when originally produced; therefore, comparisons to WCF product at time of production are not possible. In most cases the amounts of minor constituents, including volatile species such as ruthenium and mercury, are relatively constant throughout each bin. Table 3 presents the data obtained from the radiochemical determinations on alumina and zirconia calcine. The fission products and their concentration in stored calcine depend on the fuel processed as well as the age of calcine. Thus meaningful comparisons of fission product contents in stored calcine can be made only when these contents at time of production are known. This information is not available at the time of production for the retrieved calcine samples. However, the contents of the liquid waste tanks are known; therefore fission product contents could be estimated by determining the contents of the tanks which were calcined and sent to the sampled bins.

The determination of uranium and transuranic contents is important for determining presently unknown quantities of these elements in stored calcine. The contents are of particular interest because they reflect the efficiency of the uranium recovery process.

Spectrochemical and X-ray diffraction analyses were performed on the retrieved calcine samples to determine crystalline and amorphous components. Both fines (less than U. S. Standard No. 140 mesh) and product (greater than U. S. Standard No. 140 mesh) materials were ana-

TABLE 3

Radioactive Species in Retrieved Calcine

	Major fission products*		Uranium		Transuranics	
Sample	Nuclide	µg/g	Mass, µg/g	Isotope	Nuclide	µg/g
			Alumina			
3T	^{90}Sr	38.7	59.3	234 5.0	^{238}Pu	0.10
	^{137}Cs	73.5		235 65.0	^{239}Pu	2.96
				236 6.7	^{240}Pu	0.32
				238 23.3	^{241}Am	0.09
3M	^{90}Sr	40.5	53.16	234 1.1	^{238}Pu	0.10
	^{137}Cs	73.8		235 69.9	^{239}Pu	2.98
				236 3.7	^{240}Pu	0.32
				238 25.8	^{241}Am	0.09
3B	^{90}Sr	132.7	37.82	234 3.8	^{238}Pu	0.10
	^{137}Cs	60.0		235 67.1	^{239}Pu	2.33
				236 5.0	^{240}Pu	0.27
				238 24.2	^{241}Am	0.11
			Zirconia			
7T	^{90}Sr	15.2	51.10	234 3.4	^{238}Pu	1.11
	^{137}Cs	21.7		235 68.9	^{239}Pu	3.89
				236 6.0	^{240}Pu	0.98
				238 21.7	^{241}Am	0.32
7M	^{90}Sr	17.8	13.20	234 6.8	^{238}Pu	0.86
	^{137}Cs	22.5		235 59.8	^{239}Pu	3.38
				236 6.7	^{240}Pu	0.96
				238 26.7	^{241}Am	0.24
7B	^{90}Sr	15.0	28.36	234 3.9	^{238}Pu	1.00
	^{137}Cs	22.4		235 62.9	^{239}Pu	3.26
				236 6.5	^{240}Pu	0.87
				238 26.6	^{241}Am	0.18

*Determined on September 15, 1978.

lyzed. These analyses indicate that there is little difference in the types and amounts of crystalline and amorphous components between the retrieved alumina and zirconia calcine and WCF alumina and zirconia product.

PHYSICAL PROPERTIES OF RETRIEVED CALCINE

Table 4 summarizes composition and structural properties of the retrieved calcine. Entries for the WCF alumina product are unpublished data from the second and third processing campaigns. Bulk density and MMPD entries for the WCF zirconia product are unpublished data from the fourth campaign. Sieve analyses of retrieved samples were obtained by dividing each entire composite, minus the aliquot removed for physical and chemical analyses, by a screen sequence in the sonic sifter into seven sieve fractions. The results of the sieve analyses are given in Table 5.

Comparison of sieve analyses for WCF alumina product and retrieved alumina calcine given in Table 5 shows little change in weight distribution on various screens. A sieve analysis has not been performed on WCF zirconia product. However, the data in Table 5 indicate that sample 7B (from the bottom of bin 7) contains considerably more fines than samples from the top and middle of the bin. These fines from 7B were analyzed by X-ray diffraction and were determined to contain 20% dolomite. Storage and flow properties were determined on the fines portion of the retrieved calcine on an instantaneous basis (no waiting period under a compacting load before samples are sheared by a horizontal force) for comparison to those of simulated calcine. The results of these tests are given in Table 6.

The property F is a measure of the cohesive strength a material gains when subjected to a compacting load V_1 (Ref. 8). The wall friction angle, ϕ', of a material is a measure of its ability to adhere to the wall of its storage container.[8] The data in Table 6 indicate that there is little significant change in these properties between retrieved and simulated calcines. Likewise, the results of compressibility

TABLE 4

Compositional and Structural Properties of Retrieved Calcine Samples

	Alumina			
	3T	**3M**	**3B**	**WCF alumina product**
Bulk density, g/cm³	0.89	1.12	1.00	0.6-1.6
Packed density, g/cm³	0.98	1.17	1.11	
MMPD,* mm	0.625	0.59	0.620	0.3-0.6
Product : fines ratio†	3.68 : 1	4.37 : 1	5.33 : 1	~7.13 : 1
Calcine dissolution‡ (wt% dissolved)	95.27	89.22	94.77	
Attrition indices§	76	68	62	

	Zirconia			
	7T	**7M**	**7B**	**WCF zirconia product**
Bulk density, g/cm³	1.71	1.62	1.56	1.01-1.78
Packed density, g/cm³	1.74	1.71	1.71	
MMPD,* mm	0.426	0.399	0.404	0.31-0.44
Product : fines ratio†	42.5	32.3	10.5	
Calcine dissolution‡ (wt% dissolved)	95.06	92.57	95.50	94.50-96.60
Attrition indices§	80	68	72	

*MMPD is mass mean particle diameter.

†Ratio of calcine sample material greater than U. S. Std. sieve No. 140 to material less than U. S. Std. sieve No. 140.

‡Percent of one gram dissolved in 10 ml of 8*M* HNO_3 at 90°C for 30 min (Ref. 7).

§Loss in wt.% of 425 to 500 µm material in standardized fluidization test.

TABLE 5

Sieve Analysis on Retrieved Calcine Sample Composites (Weight Fraction Retained on Each Sieve)

Alumina						Zirconia				
U. S. sieve No.	Size (μm)	3T	3M	3B	WCF alumina product	U. S. sieve No.	Size (μm)	7T	7M	7B
+35	>500	0.478	0.511	0.461	0.490	+35	500	0.142	0.104	0.146
+50	300	0.220	0.223	0.200	0.210	+50	300	0.466	0.515	0.424
+70	212	0.042	0.037	0.130	0.090	+70	212	0.339	0.314	0.284
+100	150	0.026	0.027	0.025	0.049	+100	150	0.020	0.039	0.061
+140	106	0.021	0.015	0.026	0.038	+140	106	0.013	0.014	0.053
+200	75	0.025	0.025	0.023	0.030	+200	75	0.010	0.016	0.053
200	<75	0.189	0.161	0.135	0.093	200	<75	-		0.028
Total sample weight, kg		2.512	3.628	3.502		Total sample weight, kg		2.670	4.516	5.962

TABLE 6

Properties in Retrieved and Simulated Calcines

Sample	Cohesive strength F, kg	Compacting load V_p, kg	V_1/F	Wall friction angle ϕ', degrees
3T	13.6	150.0	11	30
3M	13.9	138.6	10	28
3B	20.2	149.4	7.4	28
Simulated alumina calcine	35.6	149.4	4.2	30
7B	20.7	143.0	6.9	29
Simulated zirconia calcine	25.3	149.1	7.1	31

tests, performed on the fines portions of the composites (Table 6) indicate little change in that property between retrieved and simulated calcines. These similarities suggest that these materials would behave almost identically during pneumatic transfer.

DTA and TGA analyses were performed on the retrieved calcine to determine amounts of volatiles present and to attempt to identify the volatile components. The analyses were performed by the Rockwell Hanford Operations Analytical Group. The results of these analyses are presented in Table 7.

The reactions detected by DTA analysis on the retrieved calcine were minor, while those detected on the WCF product were significant. This suggests that the loss of volatile components or crystalline transitions are greater in fresh calcine than in more aged radioactive calcine.

The TGA analyses indicate:

1. A weight loss in all retrieved alumina calcine samples between 750 and 890°C, probably caused by nitrate volatilization.
2. An additional weight loss for retrieved alumina calcine sample 3T between 650 and 750°C, possibly from nitrate volatilization.
3. A 2% weight loss at 50 to 150°C in retrieved zirconia calcine sample 3T is probably from water volatilization. A weight loss at 450 to 530°C from this sample is possibly from nitrate volatilization.
4. No weight losses were detected from retrieved zirconia sample 7T and 7B.
5. The WCF zirconia product samples both underwent weight losses greater than 5% between 550 and 700°C from calcium nitrate dissociation.

With respect to retrieved alumina calcine, DTA analyses indicate endothermic reactions between 400 and 580°C,

TABLE 7

DTA and TGA Analyses on Retrieved Calcine and WCF 8th Campaign Product

	DTA analysis		TGA analysis	
Sample	Endotherm locations, °C	Possible reaction	Loss, wt.%	Temp., °C
3T	N. D.*		3.1	650-750
	400-580	Crystalline transition or nitrate loss	1.0	810-890
	700	Nitrate loss	5.0	750-860
3B	250-429	Crystalline transition or nitrate loss		
7T	460-560	Nitrate loss	2.0	50-100
7M	N. D.		N. D.	
7B	N. D.		N. D.	
78-4204†	690-720	Calcium nitrate dissociation with nitrate loss	5.4	600-700
78-4864‡	660-770	Calcium nitrate dissociation with nitrate loss	5.3	540-700

*N. D., none detected.

†WCF 8th campaign zirconia product sampled on August 20, 1978.

‡WCF 8th campaign zirconia product sampled on September 11, 1978.

although the TGA curves indicate no weight loss at that temperature range. This suggests crystalline transitions rather than volatilization. For the retrieved zirconia calcine sample 7T, the endotherm at 450 to 560°C from DTA analysis correlates to the 1.9% weight loss by TGA analysis suggesting volatilization. Both WCF zirconia product samples show endothermic reactions between 490 and 770°C by DTA analysis. These correlate with weight loss greater than 5% by TGA analysis suggesting nitrate volatilization or dissociation reactions.

CONCLUSION AND SUGGESTIONS FOR FUTURE WORK

The most significant determination of the testing program is that the sampled bins can be emptied pneumatically. This is a necessary condition of stored calcine for postcalcination treatment or for shipment to a federal repository. The results of this testing program indicate that most physical and chemical properties of radioactive alumina and zirconia calcine produced by use of a liquid-metal heat transfer system do not change substantially over several years of storage. Solidification of liquid wastes using the current method of in-bed combustion of kerosene is expected to exhibit similar properties after prolonged storage.

Where comparisons could be made, the chemical properties of retrieved calcine were determined to be similar to those measured at the time of production. Information is lacking on the behavior of the important minor species. Analytical procedures for water, chloride, radioiodine, and sulfate were not available for the retrieved samples. Analyses for the potentially volatile species mercury and ruthenium were performed; however, the amounts of these elements in freshly prepared WCF product have not been determined. The crystalline structure of both types of calcine remains unchanged, and no detectable additional crystalline species results from storage. The results of actinide analyses on the sample composites can be used to construct material balances of these species for the overall waste processing operation and are important input for the actinide removal processes being developed at the ICPP. Although little information is available for comparison, most physical properties appear to be similar between simulated and radioactive calcine. Thus many of the physical properties of stored calcine can be extrapolated from those determined on simulated calcine.

ACKNOWLEDGMENT

This study was performed under Department of Energy Contract No. DE-AM07-76IDO1540.

REFERENCES

1. R. F. Commander, G. F. Lohse, D. E. Black, et al., *Operation of the Waste Calcining Facility with Highly Radioactive Aqueous Waste*, IDO-14662, Idaho Chemical Processing Plant, Idaho Falls, June 1966.
2. J. A. Wielang, G. E. Lohse, and M. P. Hales, *The Fourth Processing Campaign in the Waste Calcining Facility*, ICP-1004, Idaho Chemical Processing Plant, Idaho Falls, May 1971.
3. D. Gombert II, H. S. Cole, and J. R. Berreth, *Vitrification of High-Level ICPP Calcined Wastes*, ICP-1177, Idaho Chemical Processing Plant, Idaho Falls, February 1979.
4. K. M. Lamb and H. S. Cole, *Development of a Pelletized Waste Form for High-Level ICPP Zirconia Wastes*, ICP-1185, Idaho Chemical Processing Plant, Idaho Falls, February 1979.
5. J. S. Schofield, A. G. Westra, S. J. Horn, et al., *Sampling of Stored High-Level Radioactive Calcined Waste at ICPP*, ICP-1186, Idaho Chemical Processing Plant, Idaho Falls, March 1979.
6. R. R. Suchomel and W. J. Lackey, *Device for Sampling HTGR Recycle Fuel Particles*, ORNL/TM-5739, Oak Ridge National Laboratory, March 1977.
7. C. M. Slansky (Ed.), *Technical Division Quarterly Progress Report for October 1 December 31, 1977*, ICP-1141, p. 39, Idaho Chemical Processing Plant, Idaho Falls, February 1978.
8. A. W. Jenike, *Storage and Flow of Solids*, Bulletin 123, Engineering Experiment Station, University of Utah, November 1964.

STABILIZATION OF HIGH-LEVEL WASTE FROM A CHLORIDE VOLATILITY NUCLEAR FUEL REPROCESSING SYSTEM

L. A. SMITH and T. A. THORNTON
Babcock & Wilcox Company, Lynchburg Research Center, Lynchburg, Virginia

ABSTRACT

Methods for stabilizing high-level waste from a chloride volatility thorium-based fuel coprocessing system have been studied. The waste, which is present as chloride salts, is combined with SiO_2 or Al_2O_3 and pyrohydrolyzed to remove the chloride ions. The resulting solid is then combined with a flux and glassified.

INTRODUCTION

Pyrochemical and dry processing methods (PDPM) can be used as alternatives to the common Purex method for reprocessing spent nuclear fuels to improve proliferation resistance. The chloride volatility method for reprocessing thoria–urania fuels is one such proliferation resistant process. A rudimentary block flow diagram of the chloride volatility coprocess is shown in Fig. 1. The concern of this paper is the fission product dechlorination by pyrohydrolysis and conversion of the resulting oxides to borosilicate glass. The pyrohydrolysis reaction for fission product dechlorination would be of the form:

$$MCl_2 + H_2O = MO + 2\,HCl \qquad (1)$$

For many fission products, this reaction has large positive values of ΔG_r, so conversion to the oxide will be difficult in many cases. However, previous work showed that SiO_2 or Al_2O_3 aid in removing chlorides.[1]

The crystalline silicate or aluminates thus formed may be sufficiently stable to be acceptable for disposal. However, we have assumed that borosilicate glass will be the reference material, so the conversion of the pyrohydrolized fission product chlorides to borosilicate glass was tested. It is probable that at least some chloride will remain in the fission products. For example, lanthanum and yttrium have been shown to have very stable oxychlorides.[2,3] These will not completely dechlorinate even with SiO_2 or Al_2O_3 present and will, therefore, cause some chloride to remain in the fission product oxide. For this reason, tests of glassification of fission product oxides with low levels of chloride contamination were done. An experimental program was performed to investigate the feasibility of all aspects of chloride volatility coprocessing. This paper discusses that portion of the program which demonstrated the borosilicate glass stabilization of the fission products. This work was divided into three segments: conversion of the chlorides to oxides by pyrohydrolysis, glassification of the oxides, and leach testing of the resulting glass.

PYROHYDROLYSIS

The pyrohydrolysis gas, moist air, was created by drawing (with a downstream vacuum) air at 1500 SCCM through a rotameter and a water bubbler where it becomes saturated at a controlled 94°C. This resulted in a steam flow of 1.7 g/min. The chloride sample was held in a platinum boat inside an electrically heated quartz tube furnace. A condenser at the furnace outlet was used to condense the steam in the exiting gas stream. A three-way valve allowed sampling of this condensate without interrupting the pyrohydrolysis in the furnace.

Nine pyrohydrolysis experiments were completed. The sample composition, size, operating temperature, and run time are shown in Table 1. The pyrohydrolysis temperature was chosen to be slightly lower than the melting point or sublimation point of the chloride compound. This limit was selected because it is probable that a full-scale system would not be able to operate above the melting point due

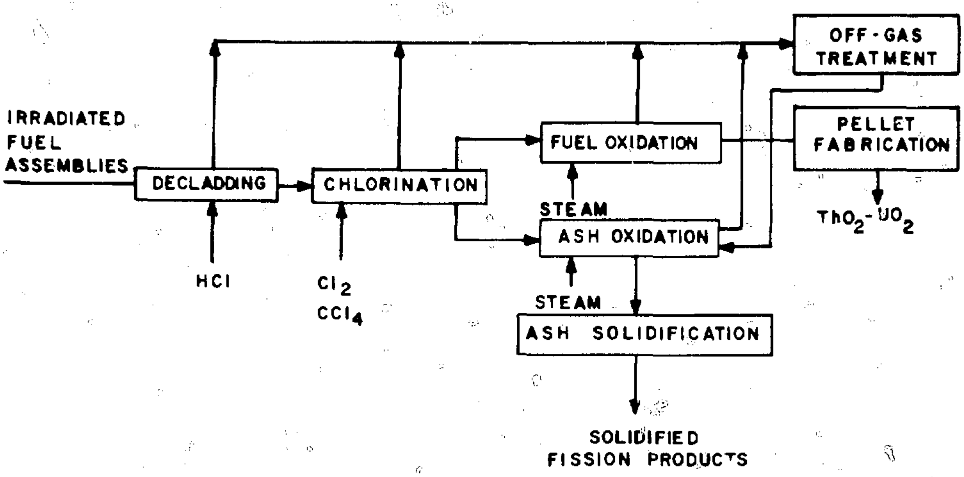
OFF-GAS TREATMENT
IRRADIATED FUEL ASSEMBLIES
FUEL OXIDATION
PELLET FABRICATION
DECLADDING
CHLORINATION
STEAM
ASH OXIDATION
ThO_2-UO_2
HCl
Cl_2
CCl_4
STEAM
ASH SOLIDIFICATION
SOLIDIFIED FISSION PRODUCTS

Fig. 1 Chloride volatility coprocessing system.

TABLE 1

Pyrohydrolysis Experimental Conditions

Experiment	Type of material	Sample size, g	Pyrohydrolysis temperature, °C	Pyrohydrolysis time, min.
1(Ba)	50% $BaCl_2 \cdot 2H_2O$ 50% Al_2O_3	0.26	900	60
2(Ba)	$BaCl_2 \cdot 2H_2O$	0.23	900	60
3(Ba)	50% $BaCl_2 \cdot 2H_2O$ 50% Al_2O_3	0.41	900	75
4(Ba)	50% $BaCl_2 \cdot 2H_2O$ 50% SiO_2	0.41	900	60
5(Cs)	50% CsCl 50% Al_2O_3	0.39	900	60
6(Cs	50% CsCl 50% SiO_2	0.39	900	60
7(La)	$LaCl_3 \cdot 6H_2O$	0.38	800	61
8(La)	54% $LaCl_3 \cdot 6H_2O$ 45% SiO_2	0.67	800	42
9(Zr)	$ZrCl_4$	0.21	300	25

to particle agglomeration or above the boiling point due to volatilization. With a mixture of fission products, pyrohydrolysis would be started at a low temperature to convert the low boiling chlorides to oxides. The temperature would then be increased to convert the remaining chlorides.

The results of the pyrohydrolysis experiments are given in Table 2. The chloride removal rate as a function of time for the barium chloride samples is plotted in Fig. 2. The low initial chloride evolution rate in experiment 1(Ba) was due to low steam flow at the beginning of that experiment. Experiments 1(Ba) and 3(Ba) are duplicates except for the low steam flow and the sample size. The sample size in experiment 3(Ba) was about 60% larger. However, the chloride evolution rate in experiment 1(Ba) actually starts out about the same rate as experiment 3(Ba). The larger sample in experiment 3(Ba) resulted in a deeper bed in the boat. It is probable that reaction of the material at the

TABLE 2

Pyrohydrolysis Experimental Results

Experiment	Measured weight loss, mg	Calculated weight loss, mg	Initial chloride content, mg	Chloride removed, %	Residual chloride, %
1(Ba)	60 ± 5	47 ± 5	38	84 ± 1	16 ± 1
2(Ba)	39 ± 1	44 ± 5	66	20 ± 1	79 ± 1
3(Ba)	75 ± 1	71 ± 5	59	92 ± 1	6 ± 3
4(Ba)	75 ± 1	71 ± 5	59	92 ± 1	4 ± 3
5(Cs)	98 ± 1	*	42	*	*
6(Cs)	195 ± 1	*	42	*	*
7(La)	183 ± 1	175 ± 5	114	68 ± 1	27 ± 3
8(La)	ND†	ND	108	60 ± 1	ND
9(Zn)	90 ± 5	111 ± 10	127	99 ± 1	ND

*Invalid due to cesium volatility.
†Not determined.

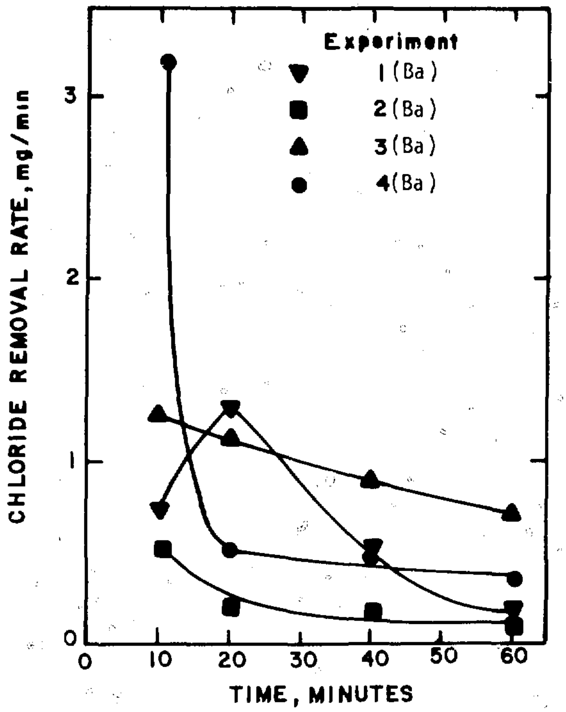

Fig. 2 Chloride removal rate during pyrohydrolysis.

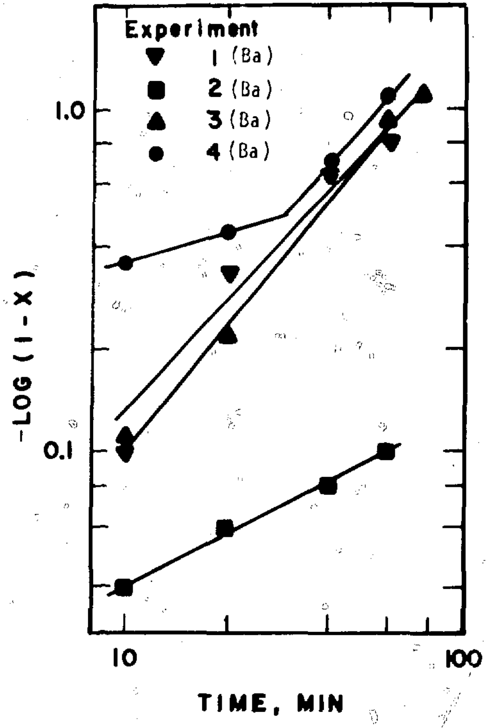

Fig. 3 Erofeev equation plot.

bottom was inhibited by the shielding effect of the material above it.

It is reasonable to expect that the oxidation reaction would follow topochemical kinetics. The interaction of oxygen and steam with barium chloride occurs at a solid interface. The reaction rate depends upon the rate of H_2O diffusion into the crystal lattice and upon the rate of crystal-chemical conversion. The thickness of the layer of solid reaction products increases continuously and hinders the diffusion of H_2O into the reaction zone and the diffusion of HCl out of that zone.

Teterevkov[4] studied the oxidation of $FeCl_2$ with dry air and found that an Erofeev equation applies. It has the form:

$$x = 1 - e^{(-kt^n)}$$

where x = weight percent conversion; t = time, minutes; and k and n = constants. Taking logarithms twice gives:

$$\log - \log(1-x) = \log k/2.303 + n \log t$$

Therefore, if the logarithm of $1 - x$ is plotted as a function of time on log-log paper, a straight line will be the result. Any change in slope will indicate a change in the reaction mechanism. The results of experiments 1(Ba), 2(Ba), 3(Ba), and 4(Ba) are shown on this type of plot in Fig. 3. The mechanism for pyrohydrolysis of $BaCl_2$ with SiO_2 as accelerator is much more rapid than $BaCl_2$ with Al_2O_3 in the early stages but then slows when the last traces of chloride are being removed. The solids from experiments 3(Ba) and 4(Ba) were characterized by X-ray diffraction patterns. The $BaCl_2$ and Al_2O_3 resulted in $BaAl_2O_4$ and Al_2O_3. The $BaCl_2$ and SiO_2 gave Ba_2SiO_4.

Following the $BaCl_2 \cdot 2H_2O$ runs, two runs were made with 0.2 grams CsCl. In one case, 0.2 gram Al_2O_3 was used as an accelerator and in the other, 0.2 gram SiO_2 was substituted for the alumina. In both cases, more than 90% of the cesium volatilized. About 50% of the volatilized material was collected in the condensate during the first 20 minutes, and 2% collected in the condensate in the following 40 minutes. A trace was found in the bubblers. A deposit was noted near the furnace outlet. It was determined to contain cesium, but the exact quantity could not be determined. Provision for collecting the volatilized cesium would be required in the plant off-gas system.

A 0.38 gram sample of $LaCl_3 \cdot 6H_2O$ and a 0.67 gram sample containing 54% $LaCl_3 \cdot 6H_2O$ were pyrohydrolyzed. In both cases, a temperature of 800°C was used. As expected, in both cases LaOCl formed. The compound was identified by X-ray diffraction. The reaction was essentially complete in five minutes making it impossible to plot rate data as a function of time. The chloride removal rate during the first five minutes was ~10 mg/Cl/min. The condensate was not analyzed for lanthanum, but carry-over is expected to be small. One sample with 0.21 gram $ZrCl_4$ was pyrohydrolyzed at 310°C. Chloride evolution was very rapid. The chloride removal was 99%. Less than 0.03% of the zirconium volatilized.

GLASS FORMATION

Since complete removal of chloride is not possible, the effect of chloride on the waste glass was tested. Melts with and without chlorides were prepared. The samples were (a) pure frit; (b) 63% frit plus 37% BaO; (c) 70% frit, 19% BaO, plus 11% $BaCl_2 \cdot 2H_2O$; (d) 65% frit plus 35% fission product simulation mix; and (e) 65% frit, 20% fission product simulation mix, plus 15% $ZrCl_4$. Table 3 shows the frit composition, and in Table 4 the product simulation mix composition is shown. These samples were prepared as 20 gram melts by grinding to less than 200 mesh and then heating in air at 900°C for three hours in alumina crucibles. The samples were furnace cooled. The pure frit formed a clear, homogeneous light green glass which fractured on cooling. The color change is probably due to impurities from the grinder. The frit plus BaO formed a microcrystalline solid which was determined by X-ray diffraction to be $Ba_2ZnSi_2O_7$. Samples c, d, and e formed solid opaque glasses which appeared homogeneous when fractured prior to grinding. Samples d and e contained a large quantity of bubbles.

TABLE 3

Glass Frit Composition

	Wt.%
SiO_2	37
B_2O_3	15
ZnO	29
Na_2O	19
	100

TABLE 4

Fission Product Simulation Mix Composition

	Wt.%
BaO	26.2
ZrO_2	21.7
La_2O_3	18.1
CeO_2	14.9
Nd_2O_3	12.1
Pr_2O_3	5.8
Sm_2O_3	1.2
	100.0

LEACH TESTING

Leach resistance of glass samples was tested by an accelerated Soxhlet extraction method. The glass was ground and sieved to give about a three-gram sample which lies between 45 and 60 mesh. The powder is contained in a 100-mesh stainless steel screen envelope. The sample was exposed to the condensed leachant at 80°C. The test was carried out for 24 hours. The results are reported as wt.% loss per day. Sample *a*, pure frit, lost 3.8%; sample *d*, frit with fission product oxide, lost 1.0%; sample *c*, frit with fission product oxides and chlorides, lost 4.3%. The leach test result for the glass with fission product oxides is in good agreement with values reported in the literature. Leach resistance is measurably reduced by the presence of chloride. However, it is not so poor as to make the chloride volatility waste totally unacceptable for burial.

CONCLUSIONS

The disposal of the high-level wastes from a dry chloride volatility coprocessing system was studied. The objective was to briefly assess the feasibility of a process to convert the fission product chloride waste to borosilicate glass. This was done by converting several representative fission product chlorides to oxides by pyrohydrolysis. A problem with cesium volatility during pyrohydrolysis was encountered. It is probable that a cesium collection process would be required in the off-gas system. Since complete chloride removal during pyrohydrolysis was not accomplished in all cases, a glass sample containing 9% chloride was made and leach tested. The leach resistance was poorer than the comparable fission product oxide glass but was still reasonably good.

Further testing of pyrohydrolysis with a wider variety of fission product chlorides, glassification of the chloride contaminated silicates and aluminates, and alternatives to borosilicate glass are required to fully prove that solidification of chloride volatility wastes is possible. However, this project demonstrated the initial feasibility of a process to solidify chloride volatility reprocessing wastes.

REFERENCES

1. J. C. Warf, W. D. Cline, and R. D. Tevebaugh, Pyrohydrolysis in the Determination of Fluoride and Other Halides, *Anal. Chem.*, 26: 342 (1954).
2. G. P. Dudchik, O. G. Polyachenok, and G. I. Novikov, Thermodynamics of Lanthanide and Yttrium Oxide Chlorides, *Russ. J. Phys. Chem.*, 45: 409 (1971).
3. C. W. Koch, A. Broido, and B. B. Cunningham, The Vapor Phase Hydrolysis of Rare Earth Halides, *J. Am. Chem. Soc.*, 74: 2349 (1952).
4. A. I. Teterevkov, Ya. E. Vil'Nyaskii, and M. V. Lapkina, Action of Oxygen on Ferrous Chloride at High Temperatures, *J. Appl. Chem. (USSR)*, 43: 487 (1970).

GLASS-CRYSTALLINE MATERIALS FOR ACTIVE WASTE INCORPORATION

V. V. KULICHENKO, N. V. KRYLOVA, V. I. VLASOV, and A. S. POLYAKOV
State Committee for the Utilization of Atomic Energy, Moscow, USSR

ABSTRACT

This paper presents the results of investigations into the possibility and conditions for using glass-crystalline materials for the incorporation of radionuclides. Materials of a cast pyroxene type that are obtained by smelting calcinated wastes with acid blast furnace slags are described. A study was also made of materials of a basalt type prepared from wastes with and without alkali metal salts. Changes in the structure and properties of materials in the process of storage at different temperatures have been studied.

INTRODUCTION

Currently in the USSR and abroad there has been large progress in the development of technological processes for production of glass-like materials of borosilicate or phosphate types to be used in the solidification of highly active wastes.[1] Along with the production of these materials, methods are being developed for incorporating wastes into glass-crystalline materials and solidified wastes into metallic matrices.[1]

Apart from the localization of radioactive nuclides, one of the requirements is to decrease waste volumes which permits reduction in the area to be used for burial grounds. The storage arrangement is facilitated when the chemical and thermal stability of materials to be buried is increased. This particularly applies to the storage of wastes which may attain a specific activity of 30,000 Ci/liter and higher (e.g., wastes from reprocessing fast reactor fuel elements).

Therefore it is of interest to study glass-crystalline materials of a basalt type. The major crystalline phase of basalt-base materials is pyroxenes, and this ensures the main properties of the materials—high chemical stability and mechanical strength. From the point of view of crystal chemistry, pyroxenes may be considered to be a diopside ($CaO \cdot MgO \cdot 2SiO_2$) in which silicon is partially substituted (while calcium and magnesium are partially or fully substituted by other elements.[2]

RESULTS AND DISCUSSION

Production of high-quality chemically stable basalt-like acid-proof materials has been adequately studied,[3,4] permitting the use of acid blast-furnace slags for the preparation of pyroxene materials for the incorporation of highly active wastes. The major constituents of acid blast-furnace slags are SiO_2, Al_2O_3, CaO, Fe_2O_3, and MgO. Depending on the relation between the contents of major slag oxides, different compounds such as monticellite ($CaMgSiO_4$), diopside ($CaMgSi_2O_6$), fayalite ($2FeO \cdot SiO_2$), and others may form on crystallization.

The quality of materials produced from slag melts depends on the chemical composition and viscosity of the starting material as well as on the structure and phase composition of the material prepared. Since pyroxenes constitute the main mineral phase of basalts and determine their principal technical properties, it is possible by adjusting the chemical composition to prepare slag materials having properties close to those of basalts (Table 1).

The adjustment of a slag composition is aimed at introducing all the slag components into the composition of pyroxenes. The amount of unbound oxides and the amount of SiO_2 addition required to bind them into diopside or other minerals of a pyroxene group have been calculated.[3,4] Such a correction results in a reduction of the basicity modulus (the ratio between the sum of acid oxides and that of basic ones) of the matrix material to 0.5 to 0.6. The

TABLE I

Properties of Cast Basalt and Slag

Materials	Chemical stability: Acid resistance	Chemical stability: Alkali resistance	Compressive strength, kg/cm²
Basalt	98.5	99.4	4000–6000
Slag compositions	95.4–98.4	99.6–100	4500–5800

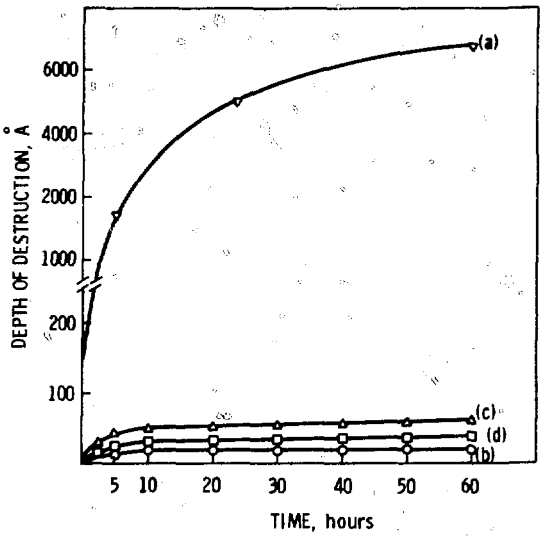

Fig. 1 Depth of water destruction of samples based on slag and wastes containing ferrous oxide. (a) Slag. (b) Slag-based pyroxene material. (c) Pyroxene : calcined wastes = 30 : 70. (d) Pyroxene : calcined wastes 40 : 60.

melting of a charge corrected in this way leads to pyroxene materials which have a chemical stability two orders of magnitude higher than that of the starting slag (Fig. 1).

The low content of alkali metal compounds (<0.5%) in acid slags permits the incorporation of significant amounts of calcined wastes into a pyroxene matrix. The co-melting of a pyroxene composition charge and calcined wastes in a weight ratio of 30 : 70 and 40 : 60 at a temperature of ~1350°C results in a fine crystal material of high strength and chemical stability, characterized by sodium and cesium leach rates of ~10^{-6} g/cm² · day and a strontium leach rate of 10^{-7} g/cm² · day with a depth of attack of 22 to 25 Å on contact with distilled water (Fig. 1).

Prolonged annealing at 900°C of prepared materials results in decreased chemical stability during the first hours of annealing; however, further heat treatment of samples again improves their chemical stability (Fig. 2). No changes in strontium leaching were observed. An alteration of chemical stability of samples as a result of heat treatment is likely to be due to restructuring to form new mineral phases and compounds.

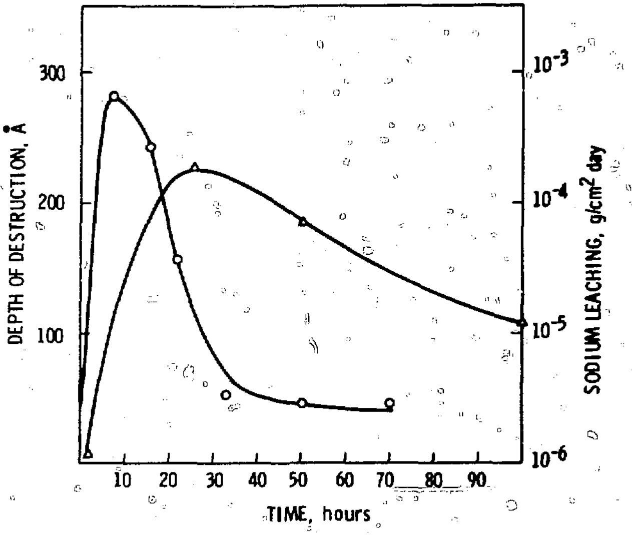

Fig. 2 Effect of annealing duration at 900°C on the depth of water destruction of samples and sodium leaching.

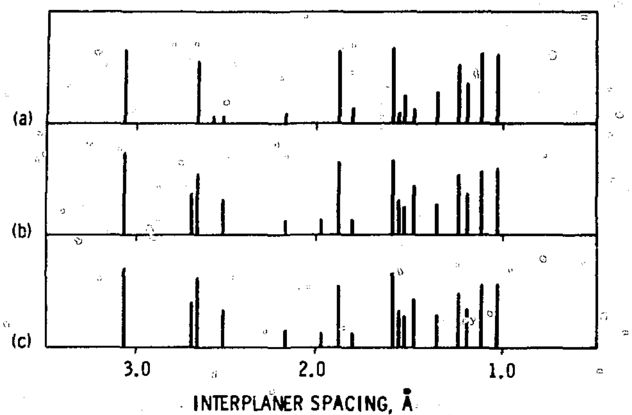

Fig. 3 X-ray patterns of pyroxene samples. (a) Without annealing. (b) Following 50-hr annealing at 900°C. (c) Following 100-hr annealing at 900°C.

As shown in Fig. 3, along with the lines of the basic phase, additional reflections appear in X-ray patterns. The intensity of the additional reflections grows with increased heat treatment time, which points to an increased amount of a new phase. The appearance of this phase is likely to be responsible for the improved chemical stability of an annealed material. As pointed out above, to incorporate wastes into pyroxene materials, temperatures above 1250°C are required. It is clear that these materials cannot be prepared in equipment developed at present for the solidification of highly active wastes. It is thought that induction furnaces can be used to prepare such materials.

Similar properties are characteristic of basalt-like materials prepared by solidification of wastes using the heat of chemical reactions.[5-7] In processes of this type, exothermic reactions of interaction between components of thermite additions, such as ferrous oxide–aluminum and sodium nitrate–aluminum mixtures, are a source of heat. The distinguishing feature of a chemothermal process is its high temperature (1600 to 1900°C) which basically depends on waste composition, process specific capacity, and heat losses.

The materials prepared contain up to 30 to 35% of calcined residue of wastes and 65 to 70% of fluxing additions and are a glass-crystalline substance with the crystal phase prevailing. The chemical stability of these materials hardly varies with annealing time at 550°C, has a complex dependency at 900°C, and increases at 1100°C (Fig. 4).

The X-ray analysis (Fig. 5) shows that the structure of a sample is not significantly changed at a temperature of 550°C but varies appreciably with annealing time at 900 and 1100°C. It is likely that with an increase of the extent of crystallization the process of forming thermodynamically stable fine crystals similar to glass-ceramics takes place and this leads to a marked increase in chemical stability.

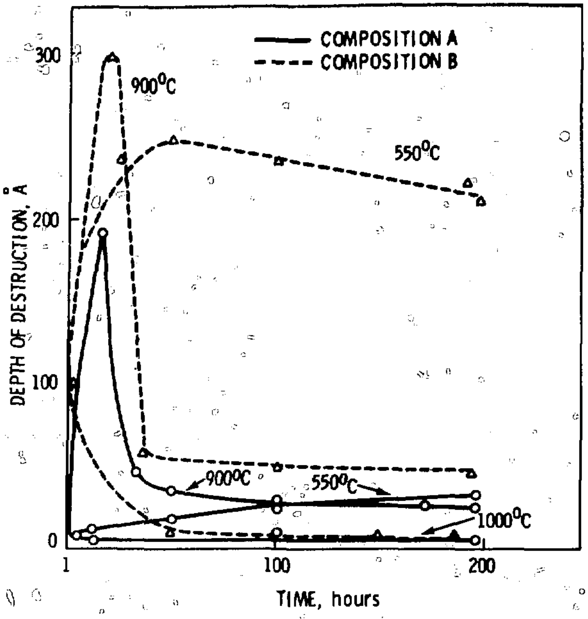

Fig. 4 Effect of annealing time on samples at different temperatures on the depth of their destruction with water. Sample A composition: 35% SiO_2, 9% Al_2O_3, 16% CaO, 13% MgO, 20% $Fe_2O_3 \cdot Cr_2O_3 \cdot Mn_3O_4$, and 7% balance. Sample B composition: 33% SiO_2, 37% Al_2O_3, 12% Na_2O, and 18% CaO.

CONCLUSIONS

The high chemical stability of the above glass-crystalline materials and their chemical stability are likely to permit a

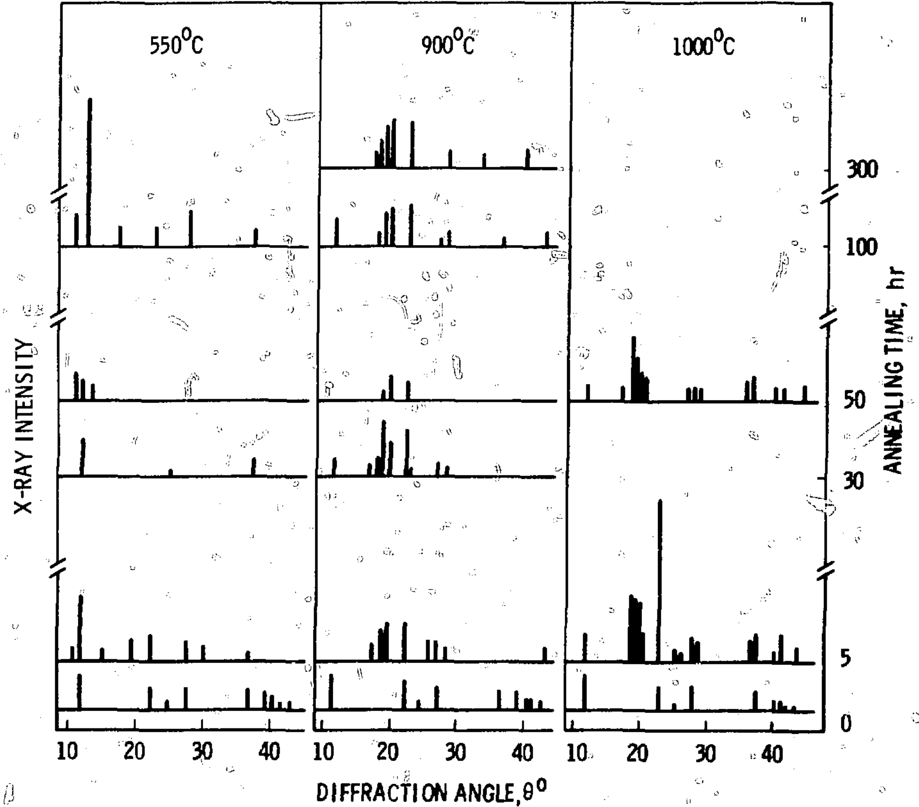

Fig. 5 X-ray patterns of samples prepared by chemothermal reactions. At 1000°C, X-ray patterns for 30, 100, and 300 hours were not taken.

more economical arrangement of their storage as compared to storage of silicate and phosphate glass materials being developed at present. Thus, as compared to glass materials, the use of pyroxene materials permits a twofold decrease in the volume of solidified materials and an eightfold increase in material loading per unit storage volume through an increase of allowable storage temperature.

REFERENCES

1. *Management of Radioactive Wastes from the Nuclear Fuel Cycle*, Vols. I and II, IAEA, Vienna, 1979.
2. V. V. Lapin, *Proceedings of the Institute of Geological Sciences*, Vol. 77, AN USSR, 1945.
3. A. G. Kotlova, Results on Crystallization of Basalt and Pyroxene in Melting Glass, *Proceedings of IGEM*, Vol. 30, 1958.
4. V. D. Krychinin and V. V. Bazarov, Acid-Based and Wear-Based Castings Based on Furnace Slag, *Pererabotha*, Kiev, 1965.
5. K. P. Zakharova, G. M. Ivanov, V. V. Kylichenko, N. V. Kryilova, V. V. Sorokin, and M. N. Federova, On Use of Heat of Chemical Reactions for Thermal Rework of Liquid Radioactive Wastes, *Atomic Energy*, 24(5): 475 (1968).
6. V. G. Vereskynov, K. P. Zakharova, P. V. Zimakov, V. V. Kylichenko, V. P. Martyinov, and U. V. Sorokin, *On the Possibility and Expediency of Processing Calcined Radioactive Wastes in the Ground*, p. 445, IAEA, Vienna, 1967.
7. V. V. Kylichenko, F. S. Gykhovich, N. V. Kryilova, K. P. Zakharova, B. H. Volkova, I. I. Kriukov, V. P. Martyihov, and R. N. Sherbakova, Report on Contract with MAGATE No. 340/RL/RB, *Study of Physico-Chemical Properties of Different Types of Hard Materials with Goal of Determining the Possibility and Expediency of Using These Materials for Attaching Radioisotopes During Processing of Radioactive Wastes.*